



Out of the twilight zone: phylogeny and evolutionary morphology of the orb-weaving spider family Mysmenidae, with a focus on spinneret spigot morphology in symphytognathoids (Araneae, Araneoidea)

LARA LOPARDO* and GUSTAVO HORMIGA

Department of Biological Sciences, The George Washington University, 2023 G Street NW, Washington DC, WA 20052, USA

Received 21 March 2014; revised 23 July 2014; accepted for publication 28 July 2014

This paper provides the first comprehensive comparative morphological study of symphytognathoid spiders, with an emphasis on the family Mysmenidae. Hypotheses of primary homology, particularly at the level of male genitalia, are proposed for a total of 65 taxa (42 mysmenids), compiled into a morphological data set of more than 350 characters. Male palpal structures (paracymbium and tegular conductor), considered absent for the family by previous workers, are actually present in Mysmenidae. The pattern of interfamilial relationships based on the morphological data differs from the hypothesis based on the total evidence (morphology plus multigene sequence data) in the placement of Theridiosomatidae. We have based all formal taxonomic and nomenclatural decisions on the results of analysis of the total evidence from a previous study, except in the cases in which only morphological information was available. Based on such phylogenetic results, the following generic transfers from Mysmenidae are proposed: *Crassignatha*, *Iardinis* (to Symphytognathidae); *Leviola* (to Zodariidae); and *Phricotelus* (Araneoidea *incertae sedis*). Mysmenidae is redelimited to include at least eight genera: *Mysmena*, *Microdipoena*, *Maymena*, *Trogloneta*, *Isela*, *Mysmenopsis*, *Brasilionata*, and *Mysmeniola*, which are re-diagnosed. *Mysmenella* and *Anjouanella* are synonymized with *Microdipoena*. *Calodipoena*, *Itapua*, *Calomyspoena*, *Tamasesia*, and *Kekenboschiella* are synonymized with *Mysmena*. Two mysmenid subfamilies are here proposed: **Mysmenopsinae subf. nov.** and Mysmeninae. In addition, diagnostic features for all symphytognathoid families are provided. One significant outcome of this comparative review is the entelegyne internal genitalic conformation for the family Anapidae (as opposed to haplogyne): all anapid representatives examined possess fertilization ducts. We provide some comments on the evolution of the morphology of spinneret spigots in symphytognathoids.

© 2015 The Linnean Society of London, *Zoological Journal of the Linnean Society*, 2015, 173, 527–786.
doi: 10.1111/zoj.12199

ADDITIONAL KEYWORDS: Anapidae – cladistics – comparative morphology – Micropholcommatinae – Mysmeninae – Mysmenopsinae – Symphytognathidae – Synaphridae – taxonomy – Theridiosomatidae.

The group [Mysmenidae] lies in a twilight zone between families and presents such diluted morphological characters that placement and relationships become uncertain.

Willis J. Gertsch (1960a: 1)

*Corresponding author. Current address: Zoologisches Institut und Museum, Ernst-Moritz-Arndt-Universität, J.-S.-Bach-Str. 11/12, D-17489 Greifswald, Germany.
E-mail: lalarlopardo@gmail.com

INTRODUCTION

Orbiculariae, the orb-weaving spiders (Araneoidea, Deinopoidea, and Nicodamidae), include 21 families and approximately one-quarter of the described species in the order Araneae. The exact limits and the familial composition of Orbiculariae have been the focus of numerous studies and have often been intensively debated (Griswold *et al.*, 1998, 2005; Schütt, 2000; Rix, Harvey & Roberts, 2008; Blackledge *et al.*, 2009; Miller *et al.*,

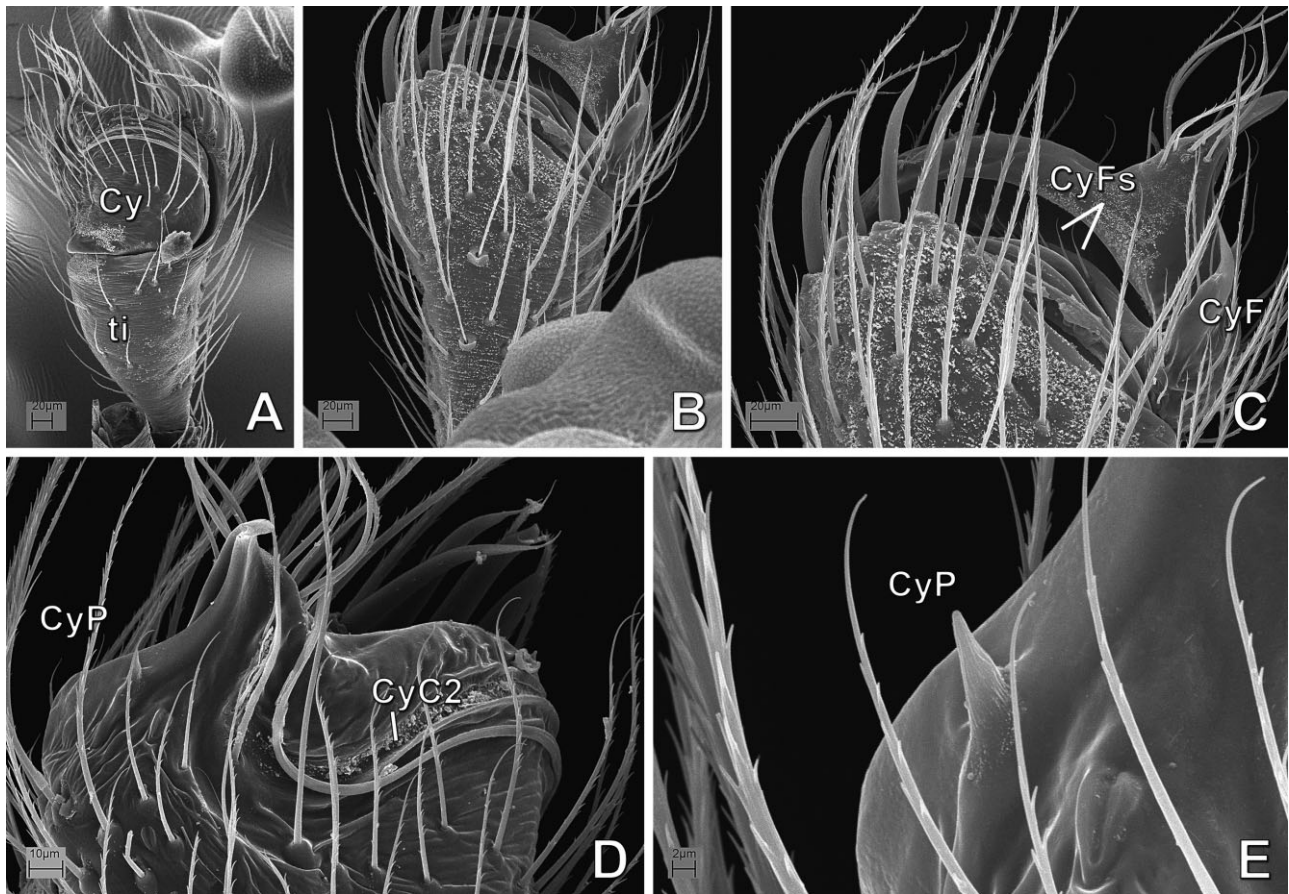


Figure 1. *Isela okuncana* (Mysmenidae), male left palp: A, D, E, ventral view; B, C, dorsal view; C, D, detail of tip of palp; E, detail of cymbial process. See Appendix 3 for the list of abbreviations.

2010; Hormiga & Griswold, 2014). Although the most exhaustive (in terms of taxon sampling) molecular analysis of Orbiculariae published to date (Dimitrov *et al.*, 2012) has recovered the monophyly of orbicularians, taxonomically expanded versions of these data (Dimitrov *et al.*, 2013) refute orbicularian monophyly. Our more recent work (Fernández, Hormiga & Giribet, 2014) using a transcriptomic approach (2637 genes and 791 793 amino acids) has also revealed the non-monophyly of Orbiculariae (for a similar study using 327 genes, see also Bond *et al.* 2014). The phylogenomic data place the Deinopoidea (the cribellate orb weavers) with other groups and not with Araneoidea (the ecribellate orb weavers), implying either independent origins of both types of orb webs or a much more ancient origin of the orb with subsequent losses in lineages such as the RTA clade. Thus, as Hormiga & Griswold (2014) had anticipated in light of Dimitrov *et al.*'s (2013) findings, 'the evolution of the whole RTA clade from an orbicularian ancestor is thus conceivable'. These results clearly require a major reevaluation of our current understanding of the spider evolutionary chronicle.

Nonetheless, the monophyly of Araneoidea (the ecribellate orb weavers) is well supported by both morphological and molecular data (Fernández *et al.*, 2014; Hormiga & Griswold, 2014).

Mysmenidae, a small family of minute araneoids (23 genera, 131 species; Platnick, 2014) (see Table 1 hereafter for authorship of taxa), are one of the least studied family-level groups of orb weavers, mainly because of their small size (0.7–3 mm) and cryptic lifestyle. Until recently (Lopardo, Giribet & Hormiga, 2011), no modern phylogenetic research has been performed in this araneoid group, and its monophyly has never been robustly established (but see below). Mysmenids belong to the so-called 'symphytognathoid' clade: minute orb weavers that build highly modified orb webs. This clade was originally delimited to include the families Anapidae, Mysmenidae, Symphytognathidae, and Theridiosomatidae (Fig. 150A; as delimited by Griswold *et al.* 1998; see also Coddington (1990). The composition and the familial relationships within symphytognathoids, as well as the relationships of the whole Araneoidea, have been recently challenged and

Table 1. Author names and list of taxa referred to in the text, matrix, and figures

Taxa	Author and year	Family placement	Observations
Anapidae	Simon, 1895(a)		
Mysmenidae	Petrunkévitch, 1928		
Symphytognathidae	Hickman, 1931		
Synaphridae	Wunderlich, 1986		
Theridiosomatidae	Simon, 1881		
<i>Acrobleps</i>	Hickman, 1979	Anapidae	
<i>Acrobleps hygrophilus</i>	Hickman, 1979	Anapidae	
<i>Anapisona</i>	Gertsch, 1941	Anapidae	
<i>Anapisona kethleyi</i>	Platnick & Shadab, 1979	Anapidae	
<i>Comaroma simoni</i>	Bertkau, 1889	Anapidae	
<i>Crassanapis</i>	Platnick & Forster, 1989	Anapidae	
<i>Crassanapis chilensis</i>	Platnick & Forster, 1989	Anapidae	
<i>Elanapis</i>	Platnick & Forster, 1989	Anapidae	
<i>Elanapis aisen</i>	Platnick & Forster, 1989	Anapidae	
<i>Epecthina</i>	Simon, 1895(a)	Anapidae	Synonym of <i>Anapis</i>
<i>Epecthinula</i>	Simon, 1903	Anapidae	Synonym of <i>Anapis</i>
Micropholcommatinae	Hickman, 1944	Anapidae	After Lopardo <i>et al.</i> (2011), but see Rix & Harvey (2010)
<i>Minanapis casablanca</i>	Platnick & Forster, 1989	Anapidae	
<i>Minanapis palena</i>	Platnick & Forster, 1989	Anapidae	
<i>Taphiassa</i>	Simon, 1880	Anapidae	After Lopardo <i>et al.</i> (2011), but see Rix & Harvey (2010)
<i>Taphiassa punctata</i>	(Forster, 1959)	Anapidae	After Lopardo <i>et al.</i> (2011), but see Rix & Harvey (2010)
<i>Tasmanapis</i>	Platnick & Forster, 1989	Anapidae	
<i>Tasmanapis strahan</i>	Platnick & Forster, 1989	Anapidae	
<i>Teutoniella cekalovici</i>	Platnick & Forster, 1986	Anapidae	After Lopardo <i>et al.</i> (2011), but see Rix & Harvey (2010)
<i>Phricotelus</i>	Simon, 1895(a)	Araneoidea <i>incertae sedis</i>	This study
<i>Phricotelus stelliger</i>	Simon, 1895(a)	Araneoidea <i>incertae sedis</i>	This study
<i>Linyphia triangularis</i>	(Clerck, 1757)	Linyphiidae	
<i>Anjouanella comorensis</i>	Baert, 1986	Mysmenidae	
<i>Brasilionata</i>	Wunderlich, 1995	Mysmenidae	
<i>Brasilionata arborensis</i>	Wunderlich, 1995	Mysmenidae	
<i>Calodipoena</i>	Gertsch & Davis, 1936	Mysmenidae	
<i>Calodipoena conica</i>	(Simon, 1895)(b)	Mysmenidae	
<i>Calodipoena dumoga</i>	Baert, 1988	Mysmenidae	
<i>Calodipoena incredula</i>	Gertsch & Davis, 1936	Mysmenidae	
<i>Calodipoena mooatae</i>	Baert, 1988	Mysmenidae	
<i>Calodipoena tarautensis</i>	Baert, 1988	Mysmenidae	
<i>Calomyspoena santaacruzi</i>	Baert & Maelfait, 1983	Mysmenidae	
<i>Dominicanopsis grimaldii</i>	Wunderlich, 2004	Mysmenidae	Fossil species
<i>Eomysmenopsis spinipes</i>	Wunderlich, 2004	Mysmenidae	Fossil species
<i>Isela</i>	Griswold, 1985	Mysmenidae	
<i>Isela okuncana</i>	Griswold, 1985	Mysmenidae	
<i>Itapua</i>	Baert, 1984(b)	Mysmenidae	
<i>Itapua tembei</i>	Baert, 1984(b)	Mysmenidae	
<i>Kekenboschiella</i>	Baert, 1982	Mysmenidae	
<i>Kekenboschiella awari</i>	Baert, 1984(a)	Mysmenidae	
<i>Kekenboschiella marijkeae</i>	Baert, 1982	Mysmenidae	
<i>Kilifina</i>	Baert & Murphy, 1987	Mysmenidae	

Table 1. Continued

Taxa	Author and year	Family placement	Observations
<i>Kilifina inquilina</i>	Baert & Murphy, 1987	Mysmenidae	
<i>Lucarachne</i>	Bryant, 1940	Mysmenidae	Synonym of <i>Mysmenopsis</i>
<i>Maymena</i>	Gertsch, 1960a	Mysmenidae	
<i>Maymena ambita</i>	(Barrows, 1940)	Mysmenidae	
<i>Maymena mayana</i>	(Chamberlin & Ivie, 1938)	Mysmenidae	
<i>Maymena misteca</i>	Gertsch, 1960a	Mysmenidae	
<i>Maymena rica</i>	Platnick, 1993	Mysmenidae	in Eberhard, Platnick & Schuh (1993)
<i>Microdipoena</i>	Banks, 1895	Mysmenidae	
<i>Microdipoena elsae</i>	Saaristo, 1978	Mysmenidae	
<i>Microdipoena guttata</i>	Banks, 1895	Mysmenidae	
<i>Microdipoena nyungwe</i>	Baert, 1989	Mysmenidae	
<i>Mysmena</i>	Simon, 1894	Mysmenidae	
<i>Mysmena dominicana</i>	Wunderlich, 1998	Mysmenidae	Fossil species
<i>Mysmena fossilis</i>	Petrunkévitch, 1971	Mysmenidae	Fossil species
<i>Mysmena groehni</i>	Wunderlich, 2004	Mysmenidae	Fossil species
<i>Mysmena grotae</i>	Wunderlich, 2004	Mysmenidae	Fossil species
<i>Mysmena leichhardtii</i>	Lopardo & Michalik, 2013	Mysmenidae	As <i>Mysmena</i> -MYSM-017-AUST in Lopardo <i>et al.</i> (2011)
<i>Mysmena leucoplagiata</i>	(Simon, 1879)	Mysmenidae	
<i>Mysmena phyllicola</i>	(Marples, 1955)	Mysmenidae	
<i>Mysmena tasmaniae</i>	Hickman, 1979	Mysmenidae	
<i>Mysmena vitiensis</i>	Forster, 1959	Mysmenidae	
<i>Mysmena woodwardi</i>	Forster, 1959	Mysmenidae	
<i>Mysmenella</i>	Brignoli, 1980	Mysmenidae	
<i>Mysmenella illectrix</i>	(Simon, 1895b)	Mysmenidae	
<i>Mysmenella jobi</i>	(Kraus, 1967)	Mysmenidae	
<i>Mysmenella samoensis</i>	(Marples, 1955)	Mysmenidae	
Mysmeninae	Petrunkévitch, 1928	Mysmenidae	
<i>Mysmeniola</i>	Thaler, 1995	Mysmenidae	
<i>Mysmeniola spinifera</i>	Thaler, 1995	Mysmenidae	
Mysmenopsinae		Mysmenidae	New rank, this study
<i>Mysmenopsis</i>	Simon, 1897	Mysmenidae	
<i>Mysmenopsis cidrelicola</i>	(Simon, 1895b)	Mysmenidae	
<i>Mysmenopsis dipluramigo</i>	Platnick & Shadab, 1978	Mysmenidae	
<i>Mysmenopsis furtiva</i>	Coyle & Meigs, 1989	Mysmenidae	
<i>Mysmenopsis gamboa</i>	Platnick & Shadab, 1978	Mysmenidae	
<i>Mysmenopsis ischnamigo</i>	Platnick & Shadab, 1978	Mysmenidae	
<i>Mysmenopsis lissycoleyae</i>	Penney, 2000	Mysmenidae	Fossil species
<i>Mysmenopsis monticola</i>	Coyle & Meigs, 1989	Mysmenidae	
<i>Mysmenopsis palpalis</i>	(Kraus, 1955)	Mysmenidae	
<i>Mysmenopsis penai</i>	Platnick & Shadab, 1978	Mysmenidae	
<i>Mysmenopsis tengellacompa</i>	Platnick, 1993	Mysmenidae	in Eberhard, Platnick & Schuh (1993)
<i>Palaeomysmena hoffeinsorum</i>	Wunderlich, 2004	Mysmenidae	Fossil species
<i>Tamasesia</i>	Marples, 1955	Mysmenidae	
<i>Tamasesia acuminata</i>	Marples, 1955	Mysmenidae	
<i>Tamasesia rotunda</i>	Marples, 1955	Mysmenidae	
<i>Trogloneta</i>	Simon, 1922	Mysmenidae	
<i>Trogloneta cantareira</i>	Brescovit & Lopardo, 2008	Mysmenidae	
<i>Trogloneta granulum</i>	Simon, 1922	Mysmenidae	

Table 1. Continued

Taxa	Author and year	Family placement	Observations
<i>Trogloneta paradoxa</i>	Gertsch, 1960a	Mysmenidae	
<i>Crassignatha</i>	Wunderlich, 1995	Symphytognathidae	Miller <i>et al.</i> (2009), also this study
<i>Crassignatha haeneli</i>	Wunderlich, 1995	Symphytognathidae	Miller <i>et al.</i> (2009), also this study
<i>Iardinis</i>	Simon, 1899	Symphytognathidae	This study
<i>Iardinis martensi</i>	Brignoli, 1978	Symphytognathidae	This study
<i>Iardinis mussardi</i>	Brignoli, 1980	Symphytognathidae	This study
<i>Symphytognatha picta</i>	Harvey, 1992	Symphytognathidae	
<i>Cepheia</i>	Simon, 1894	Synaphridae	
<i>Cepheia longiseta</i>	(Simon, 1881)	Synaphridae	
<i>Synaphris</i>	Simon, 1894	Synaphridae	
<i>Synaphris saphrynis</i>	Lopardo <i>et al.</i> , 2007	Synaphridae	
<i>Tengella</i>	Dahl, 1901	Tengellidae	
<i>Leucauge venusta</i>	(Walckenaer, 1841)	Tetragnathidae	
<i>Tetragnatha versicolor</i>	Walckenaer, 1841	Tetragnathidae	
<i>Asagena americana</i>	(Emerton, 1882)	Theridiidae	Previously on <i>Steatoda</i> , see Wunderlich (2008)
<i>Steatoda</i>	Sundevall, 1833	Theridiidae	
<i>Steatoda bipunctata</i>	(Linnaeus, 1758)	Theridiidae	
<i>Steatoda grossa</i>	(C.L. Koch, 1838)	Theridiidae	
<i>Theonoe</i>	Simon, 1881	Theridiidae	
<i>Coddingtonia euryopoides</i>	Miller, Griswold & Yin, 2009	Theridiosomatidae	See also Labarque & Griswold, 2014
<i>Theridiosoma gemmosum</i>	(L. Koch, 1877)	Theridiosomatidae	
<i>Akytara</i>	Jocqué, 1987	Zodariidae	
<i>Diores</i>	Simon, 1893	Zodariidae	
<i>Leviola</i>	Miller, 1970	Zodariidae	Presumably, this study
<i>Leviola termitophila</i>	Miller, 1970	Zodariidae	Presumably, this study

Taxa names are sorted by family. Familial placement refers to taxonomic changes from this study and Lopardo *et al.* (2011) (noted under 'Observations', see Appendix 5), or are otherwise taken from Platnick (2014).

are currently under debate (Figs 150B, 151A, B; Schütt, 2003; Lopardo & Hormiga, 2008; Rix *et al.*, 2008; Rix & Harvey, 2010; Lopardo *et al.*, 2011; Dimitrov *et al.*, 2012; Wood, Griswold & Gillespie, 2012; Wood *et al.*, 2013; Hormiga & Griswold, 2014).

The monophyly of symphytognathoids has not been supported by analyses based exclusively on DNA sequence data using a sufficiently dense taxon sample (reviewed in Hormiga & Griswold, 2014). The recent work on the phylogenetics of symphytognathoids has been driven by studies on micropholcommatine anapids (Rix *et al.*, 2008, 2010; Rix & Harvey, 2010) and on mysmenids (Lopardo *et al.*, 2011). These studies have used both morphological and molecular data. Rix & Harvey (2010) revised micropholcommatine classification and phylogeny, erecting and describing many new taxa. In our recent molecular study (Lopardo *et al.*, 2011), only after the inclusion of an extensive morphological and behavioural character matrix that we present and discuss here in more detail, was symphytognathoid

monophyly supported. Dimitrov *et al.*'s (2012) multigene analyses of orbicularians, using a much denser taxon sampling, suggest that Lopardo *et al.*'s (2011) results might not simply be artefacts of outgroup sampling. In Dimitrov *et al.*'s (2012) results only Symphytognathidae (represented by four species) were recovered as monophyletic. Theridiosomatidae and Anapidae came out as polyphyletic, although the support values of most of the nodes involved in their polyphyly are very low. Mysmenidae, represented in their analysis by 15 species, were not monophyletic, but this was the result of a single species (*Trogloneta* sp.) moving out of an otherwise relatively well-supported lineage with all other mysmenids. The analysis of Rix & Harvey (2010) using 18S and 28S rRNA sequences, and a smaller taxon sample, did not resolve this problem either. The results of Lopardo *et al.*'s (2011) combined analysis also support in part the monophyly and the relationships of 'symphytognathoids' proposed by Griswold *et al.* (1998), as modified by Schütt (2003).

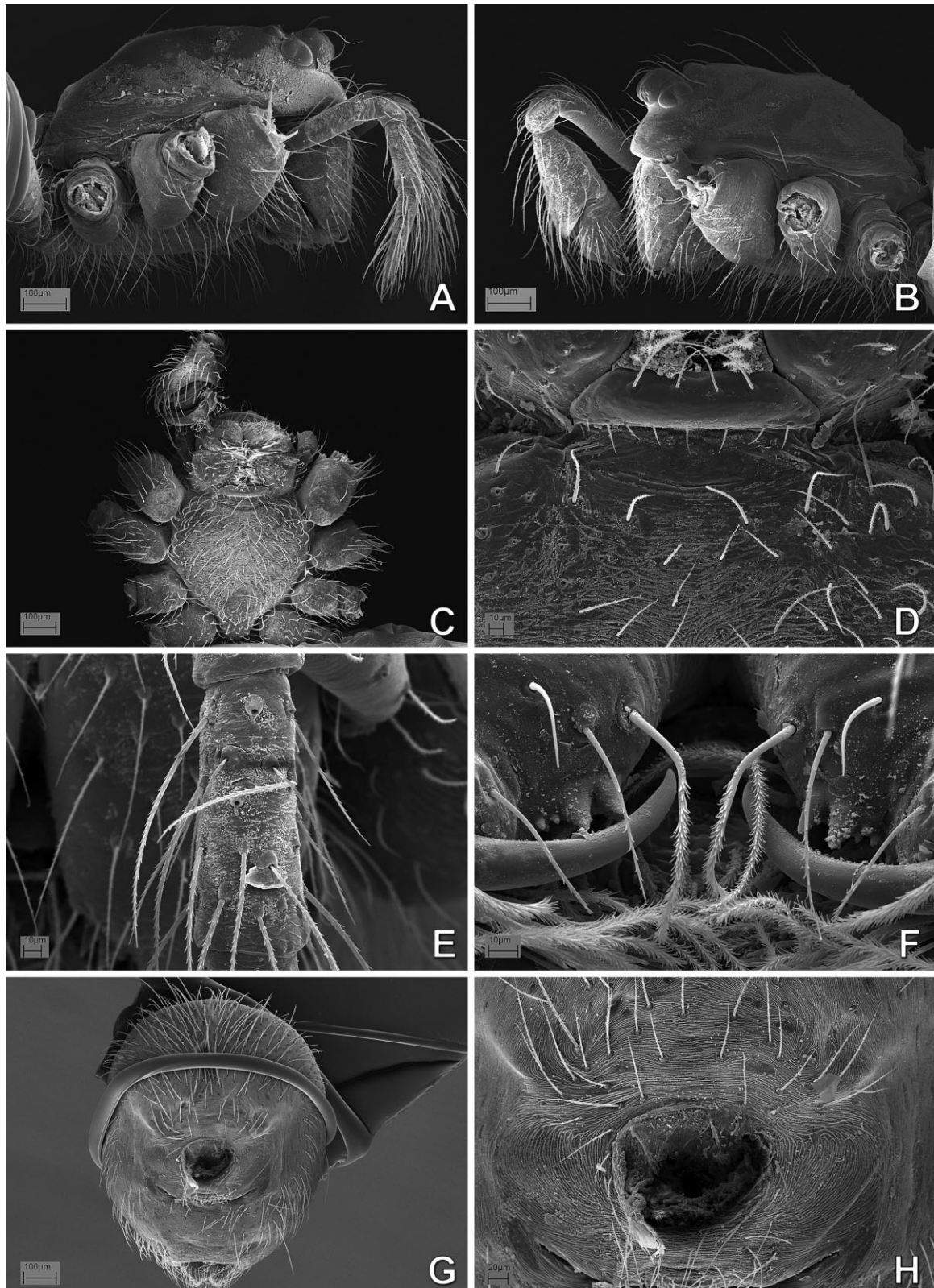


Figure 2. *Isela okuncana* (Mysmenidae): A, D–F, female; B, C, G, H, male. A, B, carapace, lateral view; C, carapace, ventral view; D, same, detail of labium–sternum junction; E, detail of female palpal tibia; F, detail of mouthparts; G, abdomen, ventral view; H, same detail of pedicel area.

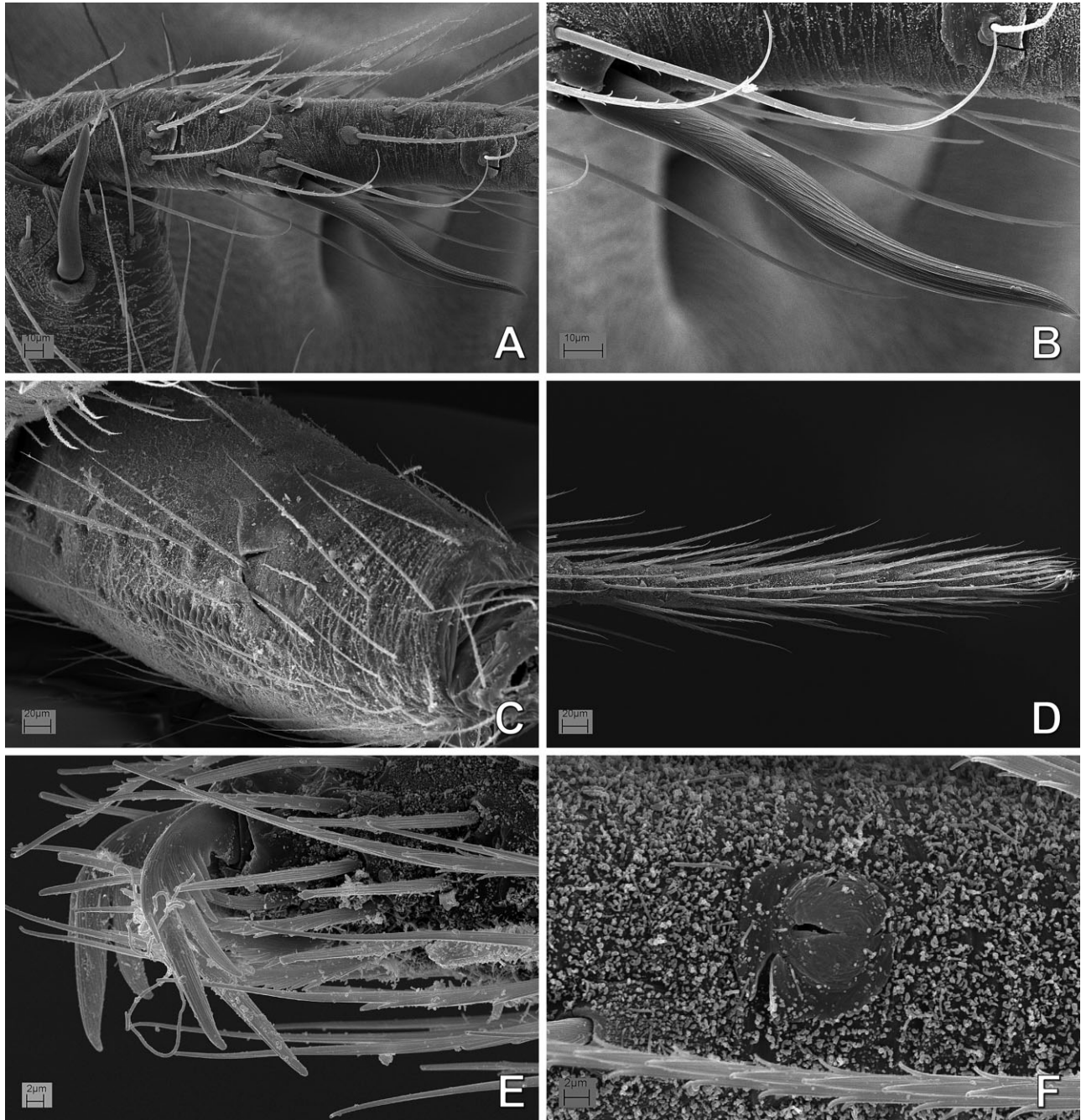


Figure 3. *Isela okuncana* (Mysmenidae), legs: A, B, male; C–F, female; A, left leg I, prolateral view, tibia–metatarsus junction bearing clasp spines; B, detail of metatarsal clasp spine; C, right leg I, femur, ventral surface; D, left leg IV, tarsus, prolateral view; E, right leg I, prolateral view, detail of claws; F, right leg I, prolateral view, detail of tarsal organ.

Mysmenids are distributed worldwide, but remain poorly studied from all aspects. About half of the described mysmenid genera (ten out of 23) are monotypic. The taxonomic diversity of mysmenids is grossly understudied. For example, no mysmenid species has ever been described from Argentina or Chile, just seven

species have been described from Brazil (Banks, 1895; Platnick & Shadab, 1978; Wunderlich, 1995; Brescovit & Lopardo, 2008), the family was first reported in Hispaniola in 2007 (Hormiga, Álvarez-Padilla & Benjamin, 2007), and only two species of mysmenid has been described from Australia (Hickman, 1979; Lopardo &

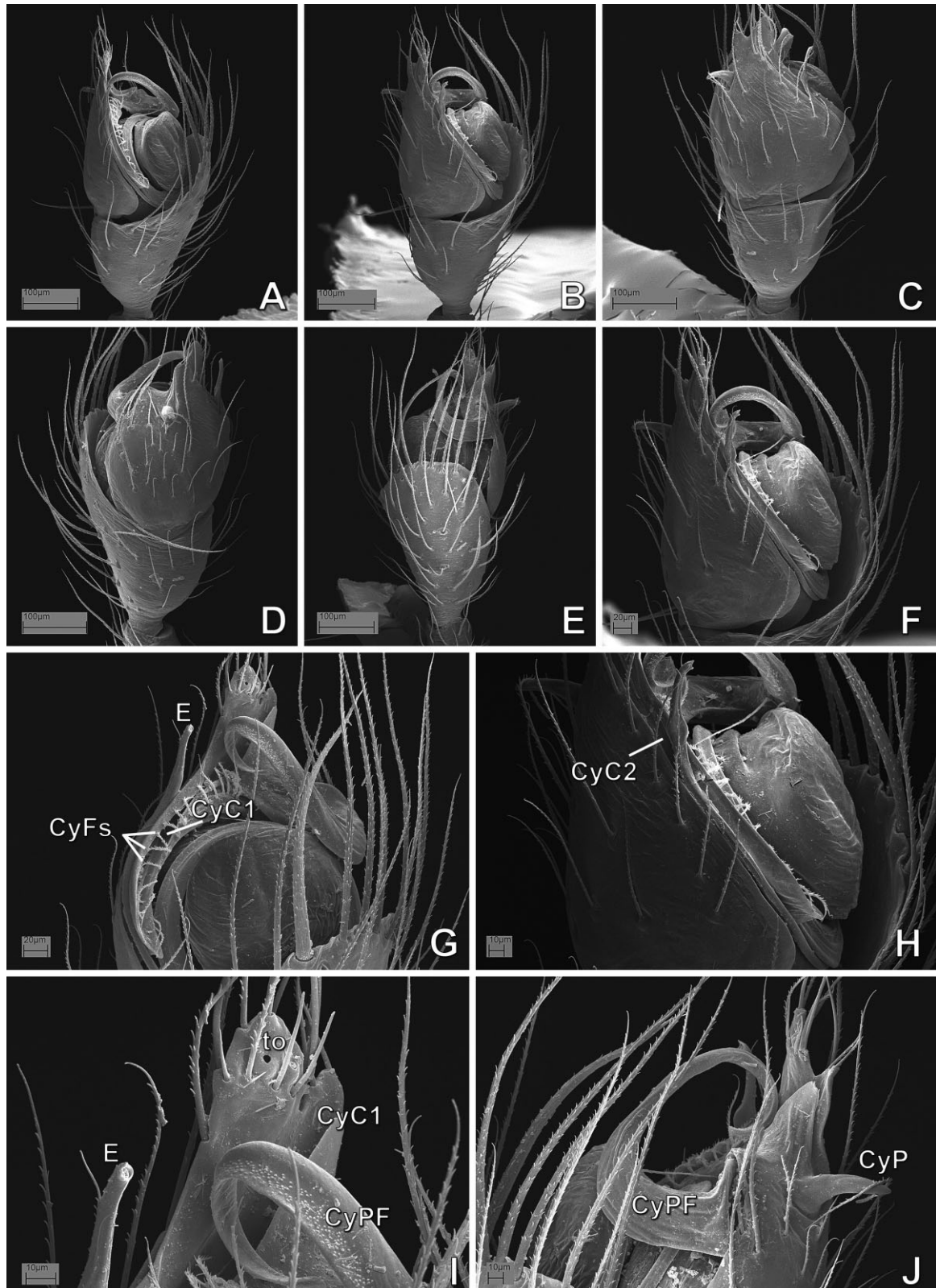


Figure 4. *Kilifina*-MYSM-002-KENYA (*Isela* sp., Mysmenidae) from Kwale, Kenya, male left palp: A, B, F, prolateral view; C, dorsal view; D, retrolatero-dorsal view; E, J, retrolateral view; G, I, ventral view; F, detail from figure B; I, detail from figure G. See Appendix 3 for the list of abbreviations.

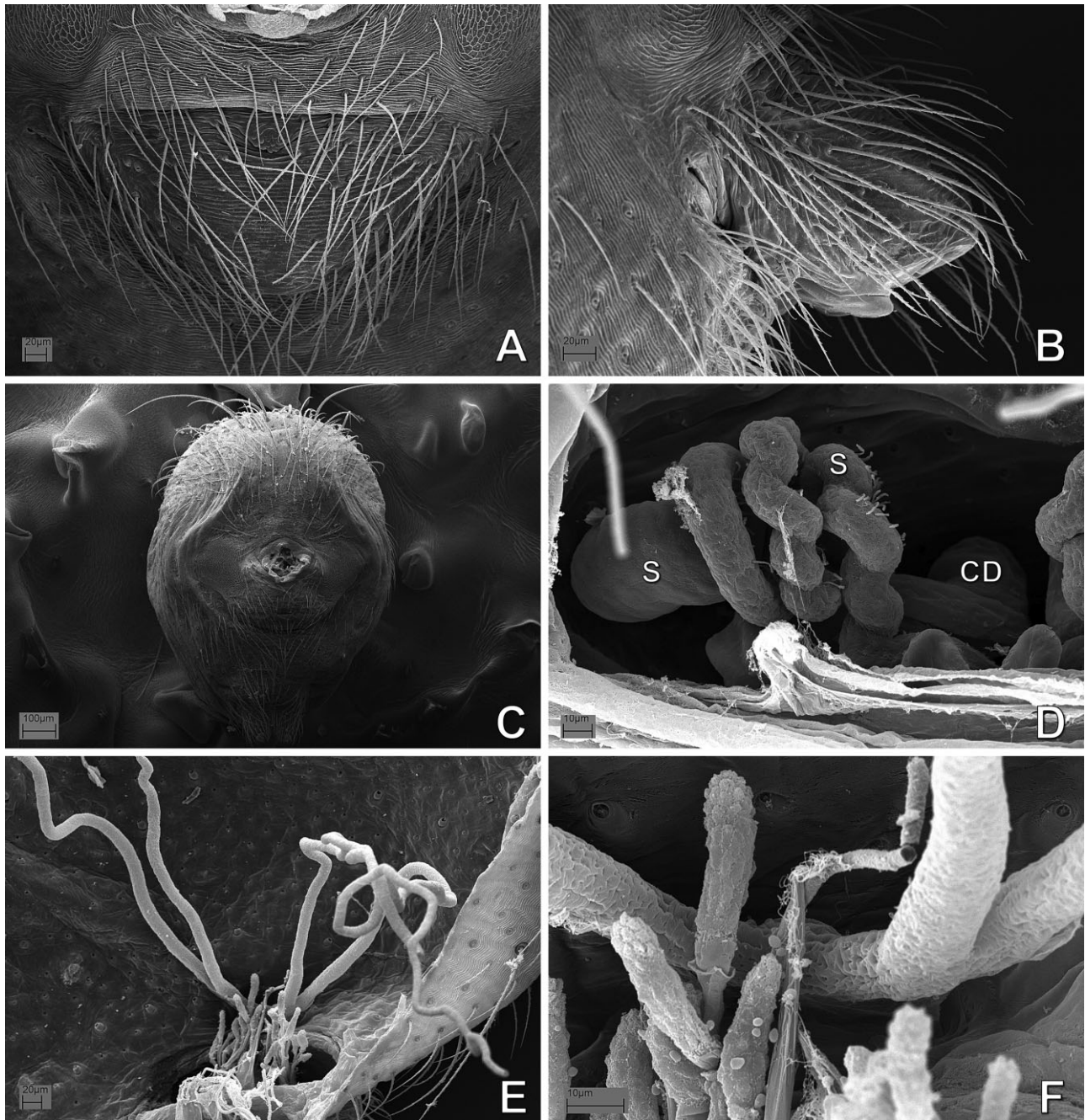


Figure 5. *Kilifina*-MYSM-002-KENYA (*Isela* sp., Mysmenidae) from Kwale, Kenya; opisthosoma: A, B, D–F, female; C, male. A, B, epigynum; A, ventral view; B, lateral view. C, abdomen, ventral view; D–F, digested abdomen; D, detail of vulva; E, posterior respiratory system; F, detail of internal posterior tracheae on spiracular area. See Appendix 3 for the list of abbreviations.

Michalik, 2013), although numerous undescribed specimens of this family have been collected and/or exist in some museum collections in the aforementioned and other countries. Traditionally, mysmenids have been distinguished from other orbicularians by: the presence of at least one prolateral clasp spine on the

male metatarsus or tibia I, or both (Figs 3A, 26C, 57G, 140C, E, J, K, 141K–O, 142G); a ventral, subapical, sclerotized spot on the femur of at least leg I on most females and some males (Figs 34A, 39D, 141C, 143N); the ‘apically twisted’ cymbium (Figs 14A, D, 17C, 22F, 30D) (Platnick & Shadab, 1978; Brignoli, 1980;

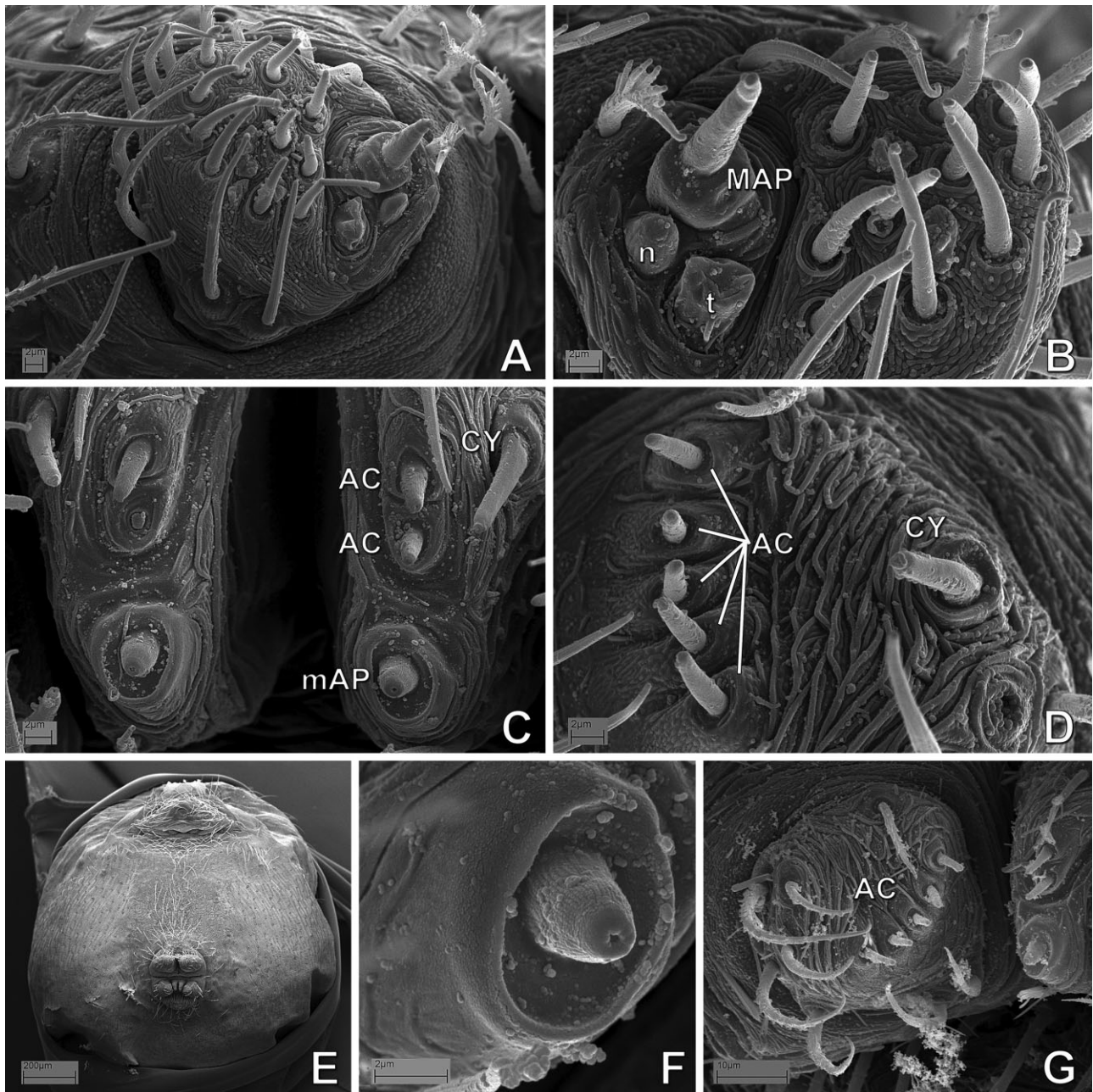


Figure 6. *Kilifina*-MYSM-002-KENYA (*Isela* sp., Mysmenidae) from Kwale, Kenya; opisthosoma: A–F, female; G, male. A, right anterior lateral spinneret; B, same, left, detail; C, posterior median spinnerets; D, G, posterior lateral spinnerets; E, abdomen, posterior view; F, detail of minor ampullate spigot.

Wunderlich, 1995; Griswold *et al.*, 1998; Schütt, 2003); and the highly elevated carapace on males of some species (compare Figs 27F, G, 63G, 64E, 141M, N) (Lopardo & Coddington, 2005). Although some of the modern descriptions of mysmenids are greatly detailed in terms of genital morphology, most of the species have been insufficiently described, and have been diagnosed by the general appearance of the geni-

talia, by measurements of eyes, and their interdistances, or by the somatic coloration patterns. Furthermore, there has been no monographic work for the family and most taxonomic work on this family has been regionally focused. Differential diagnoses of mysmenid genera are almost non-existent, generic circumscriptions are vague, and some of the current genera share the same diagnostic features (but see below).

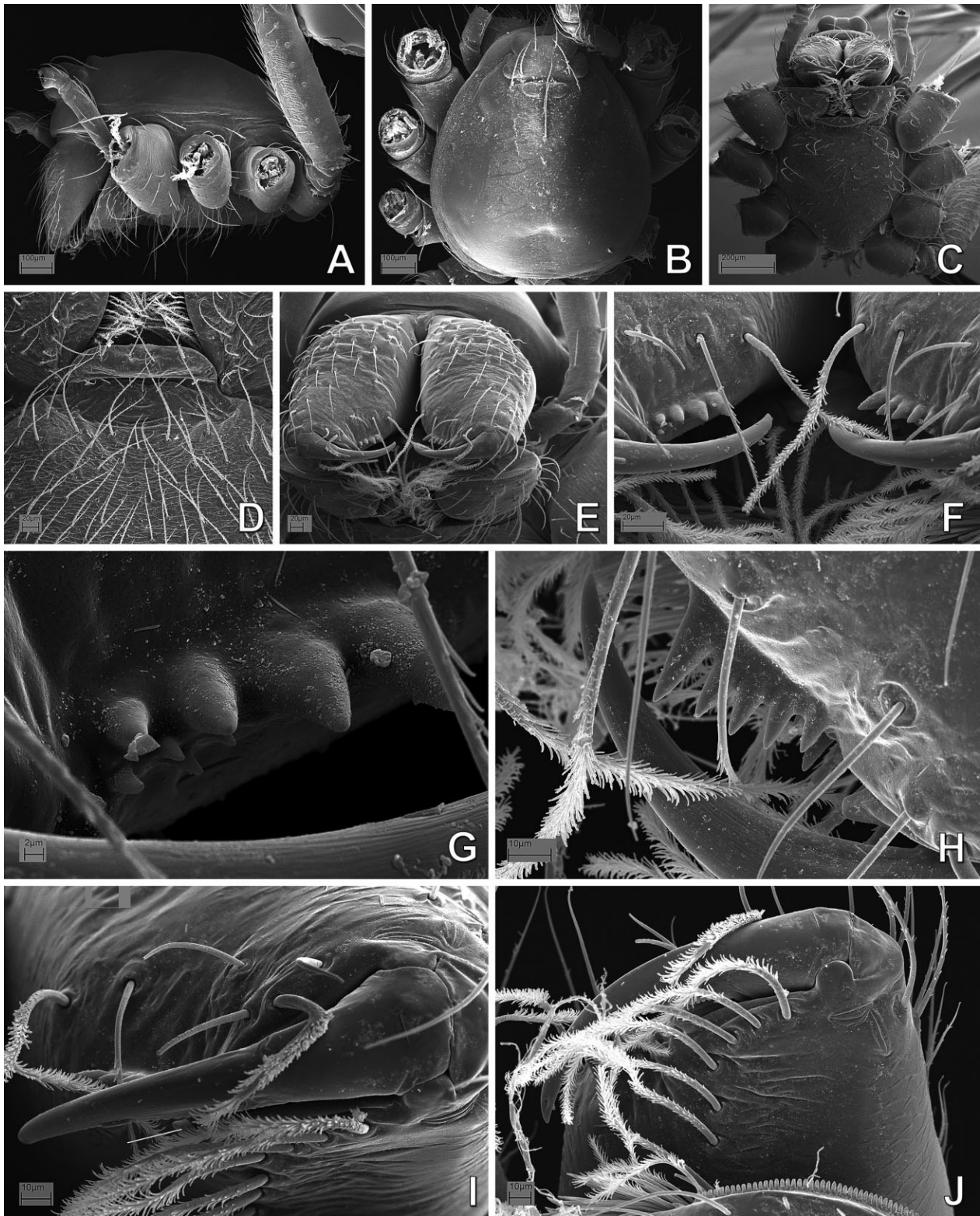


Figure 7. *Kilifina*-MYSM-002-KENYA (*Isela* sp., Mysmenidae) from Kwale, Kenya; prosoma: A, C, E–J, female; B, D, male. A, lateral view; B, dorsal view; C, ventral view; D, same, detail of labium–sternum junction; E, mouthparts, anteroventral view; F, same, detail of cheliceral fangs and promarginal teeth; G, same, detail of cheliceral denticles; H, detail of promarginal teeth; I, cheliceral fang and surrounding setae; J, cheliceral retromargin. See Appendix 3 for the list of abbreviations.

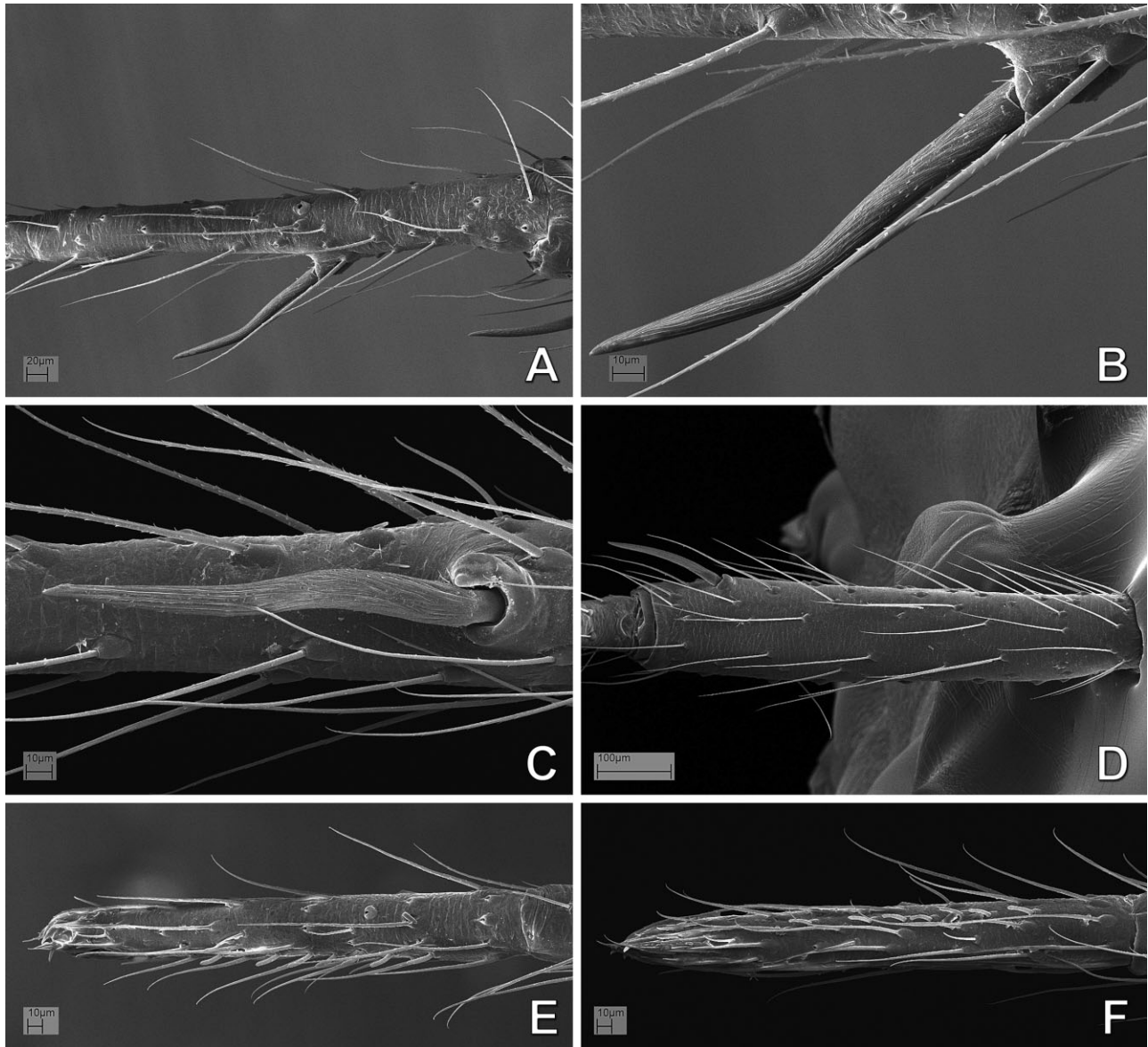


Figure 8. *Kilifina*-MYSM-002-KENYA (*Isela* sp., Mysmenidae) from Kwale, Kenya; male right leg I: A, metatarsus, dorsal view; B, same, detail of clasp spine; C, same prolateral view; D, tibia, ventral view; E, tarsus, dorsal view; F, same prolateral view.

Mysmenids live mainly in leaf litter, caves, and other cryptic places in highly humid habitats (Banks, 1895; Bishop & Crosby, 1926; Barrows, 1940; Levi, 1956; Gertsch, 1960a; Lopardo & Coddington, 2005; Miller, Griswold & Yin, 2009; Lopardo & Michalik, 2013; also L. Lopardo and G. Hormiga, pers. observ.). Web-spinning mysmenids usually prefer the interstices of leaf litter or small cavities created by the top layer of leaves (~5–15 cm in diameter, depending on the size of the spider). They can be collected by beating foliage, pitfall traps, Berlese funnels, Winkler extractors, by fogging the tree canopy with insecticides, or just manu-

ally (see above, see also Wunderlich, 1995; Lin & Li, 2008). Little is known about the biology and natural history of mysmenids, with few exceptions (e.g. *Mysmena tasmaniae*; see Hickman, 1979; and *Trogloneta granulum*; see Fage, 1931; Gertsch, 1960a; Hajer, 2000, 2002; Hajer & Reháková, 2003). In addition, 11 species in three mysmenid genera have been reported to be kleptoparasites on the webs of other spiders (Platnick & Shadab, 1978; Griswold, 1985; see also Baert & Murphy, 1987; Eberhard, Platnick & Schuh, 1993; reviewed in Lopardo *et al.*, 2011). It has been recently hypothesized that the kleptoparasitic lifestyle has a

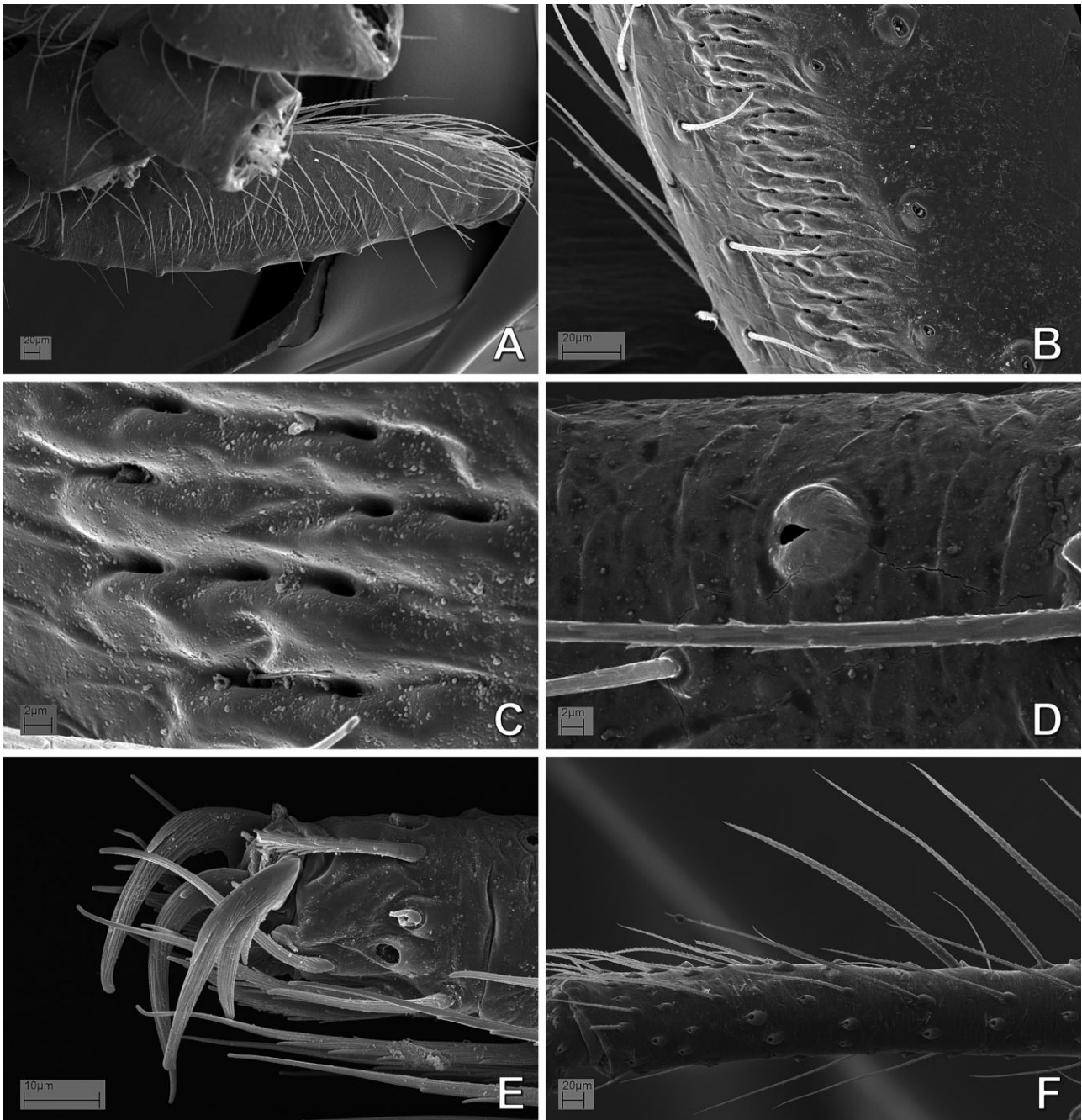


Figure 9. *Kilifina*-MYSM-002-KENYA (*Isela* sp., Mysmenidae) from Kwale, Kenya; legs: A–C, E, female; D, F, male. A–C, E, left leg IV; D, right leg I; F, right leg IV. A, femur, prolateral view; B, same, detail of stridulatory area, C, same, close up; D, tarsus, dorsal view, tarsal organ; E, claws, retrolateral view; F, tibia, prolateral view.

single origin within mysmenids (Lopardo *et al.*, 2011). Furthermore, kleptoparasitic mysmenids are not known to build webs of their own, and some have even lost the ability to spin the sticky silk that is characteristic of orb-weaving spiders (Griswold *et al.*, 1998; Lopardo *et al.*, 2011). Mysmenid web architecture has been documented for a few species of *Maymena*, *Microdipoena*,

Mysmena, and *Trogloneta*, and recently for the Chinese genera *Simaoa* and *Gaoligonga* (reviewed in Lopardo *et al.*, 2011). Two main types of webs are built by different mysmenid genera: a three-dimensional orb web with a proliferation of out-of-plane radii that result in a unique spherical-shaped web (Fig. 147A–C), or a mainly planar orb web with the hub distorted upwards

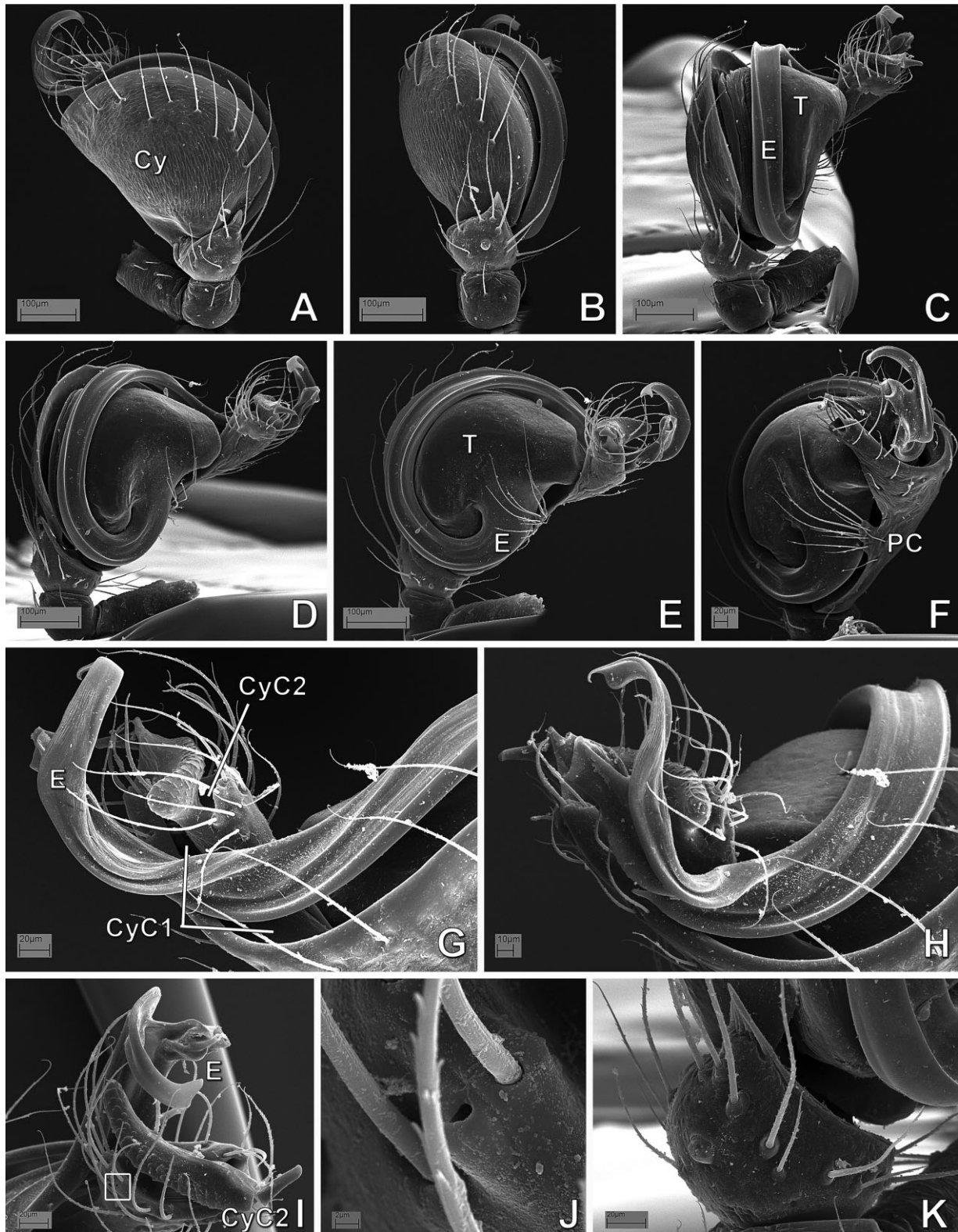


Figure 10. *Maymena ambita* (Mysmenidae), male left palp: A, dorsal view; B, prolateral–dorsal view; C, prolateral view; D, prolateral–ventral view; E, ventral view; F, retrolateral–ventral view; H, retrolateral view, detail of tip of embolus and housing cymbial conductors; G, same, retrolateral–dorsal view; I, same, retrolateral–dorsal view; J, detail of squared area from I; K, detail of tibia from C. See Appendix 3 for the list of abbreviations.

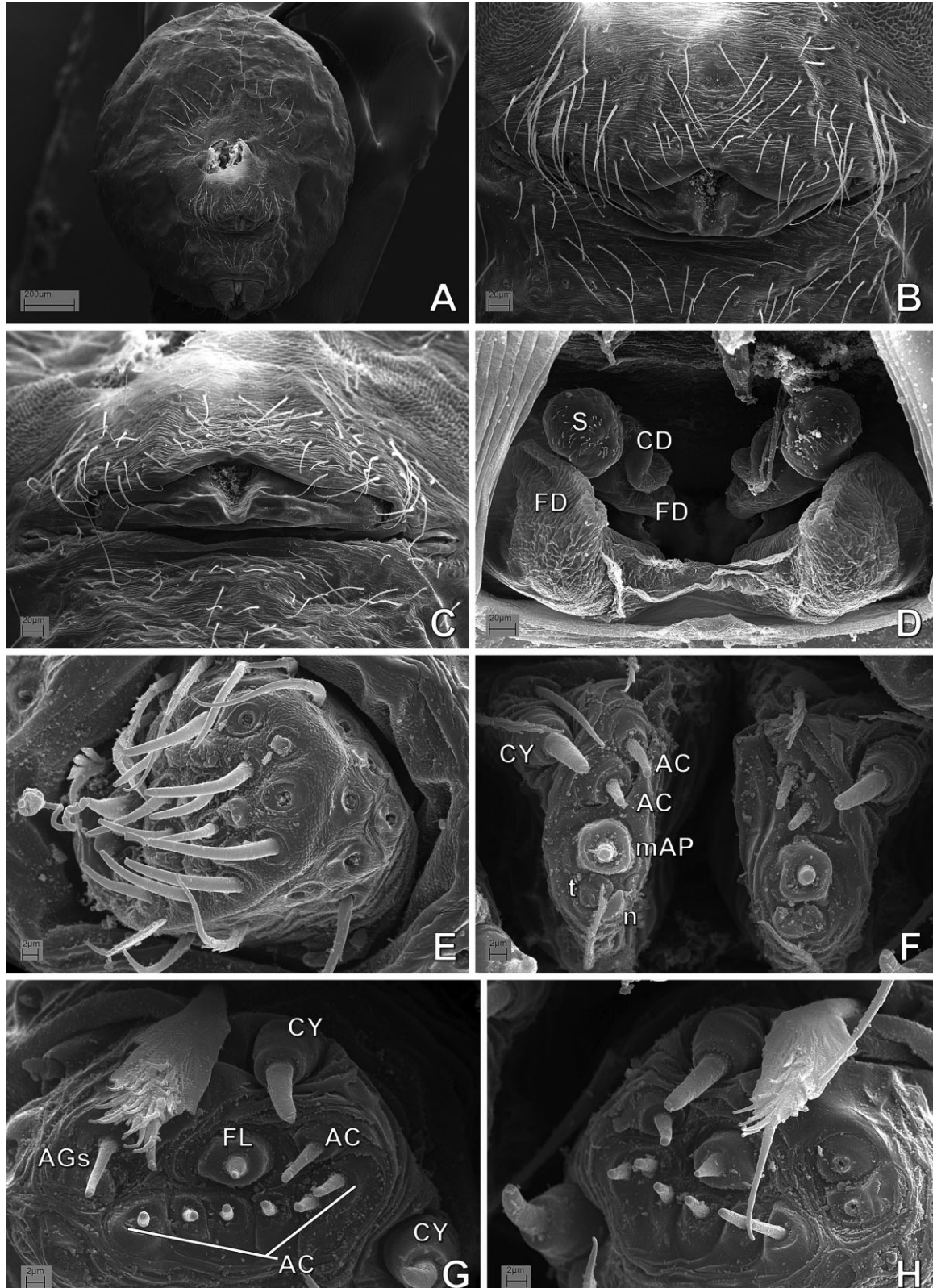


Figure 11. *Maymena ambita* (Mysmenidae), female: A, abdomen, ventral view; B, same, detail of epigynum; C, same, posterior view; D, digested abdomen, vulva; E, left anterior lateral spinneret; F, posterior median spinnerets; G, H, posterior lateral spinnerets (PLS); G, right PLS; H, left PLS. See Appendix 3 for the list of abbreviations.

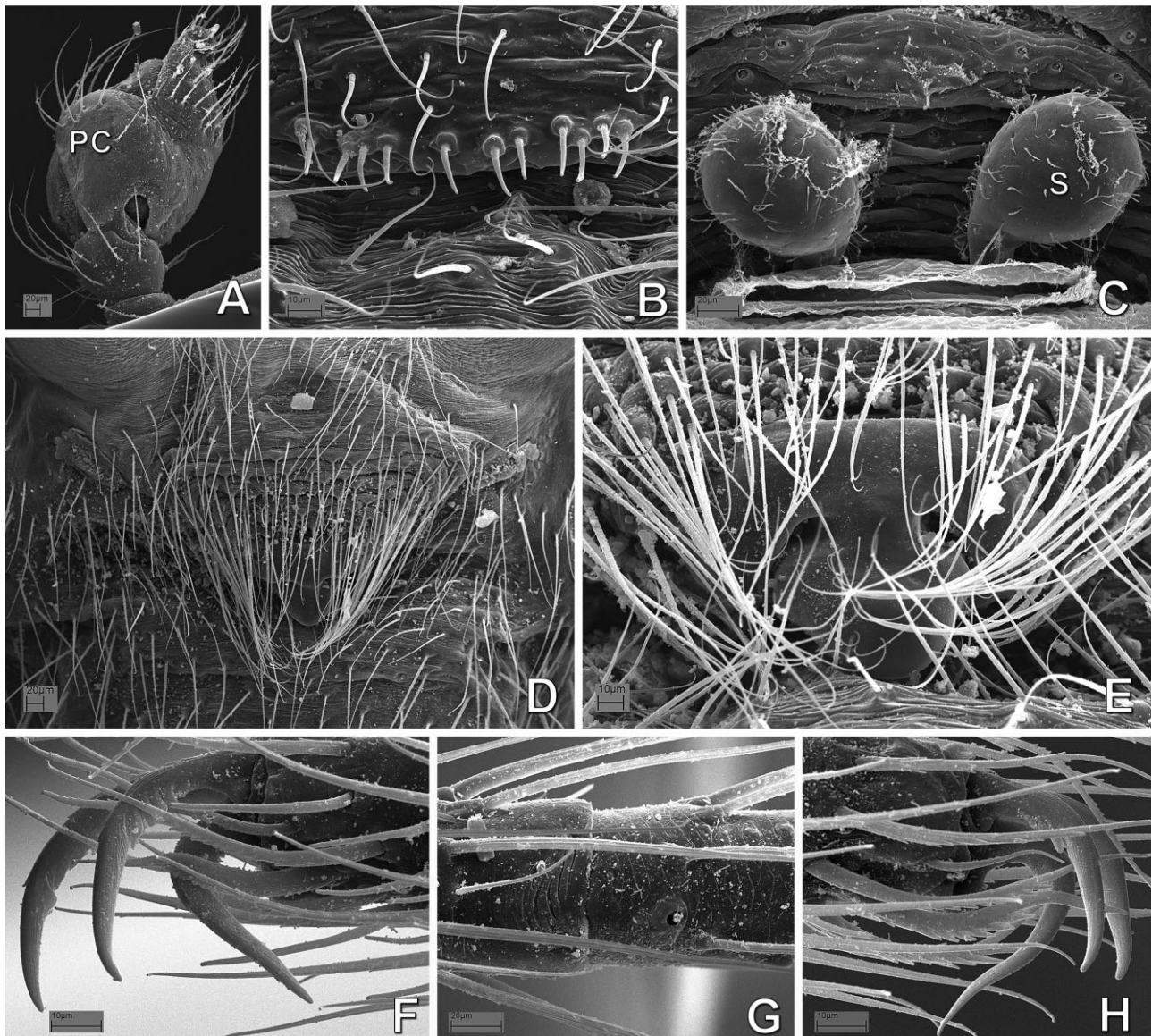


Figure 12. *Maymena mayana* (Mysmenidae): A, B, male; C–H, female. A, left palp, dorsal–retrolateral view; B, abdomen, detail of epiandrous spigots; C, digested abdomen, detail of spermathecae; D, epigynum, ventral view; E, same, detail of copulatory openings; F, G, right leg I; F, claws; G, tarsus–metatarsus junction; H, left leg IV, claws. See Appendix 3 for the list of abbreviations.

by between one and several out-of-plane radial lines that attach to substrate above the web (Fig. 147D, E).

The respiratory system of Mysmenidae, as well as other members of the symphytognathoids, is greatly diverse, but also remains relatively poorly studied (e.g. Forster, 1959, 1980; Gertsch, 1960a; Levi, 1967; Levi & Kirber, 1976). No detailed comparative study of either female or male mysmenid genitalia exists, and the homologies of male palpal sclerites are poorly understood. Mysmenids are entelegynes: their epigyna can be weakly sclerotized (e.g. *Microdipoena*, *Brasilionata*, *Itapua*, *Mysmenella*, and *Calodipoena*), or can have a

sclerotized and protruding epigynal plate (e.g. *Trogloneta*, *Mysmenopsis*, and *Maymena*). In some species a finger-like scape extends posteriorly (e.g. the species in the genera *Calodipoena* and *Mysmenella*). The morphology of the male palp is highly intricate. The embolus can be long and straight, long and coiled, short, bifid, and/or with apophyses, and it can also be distally twisted. The cymbium is highly complex, with lobes or apophyses related to the embolus, forming an apical cymbial ‘conductor’. Although the details of the male palp morphology have been insufficiently studied, the conductor, median apophysis, and paracymbium appear

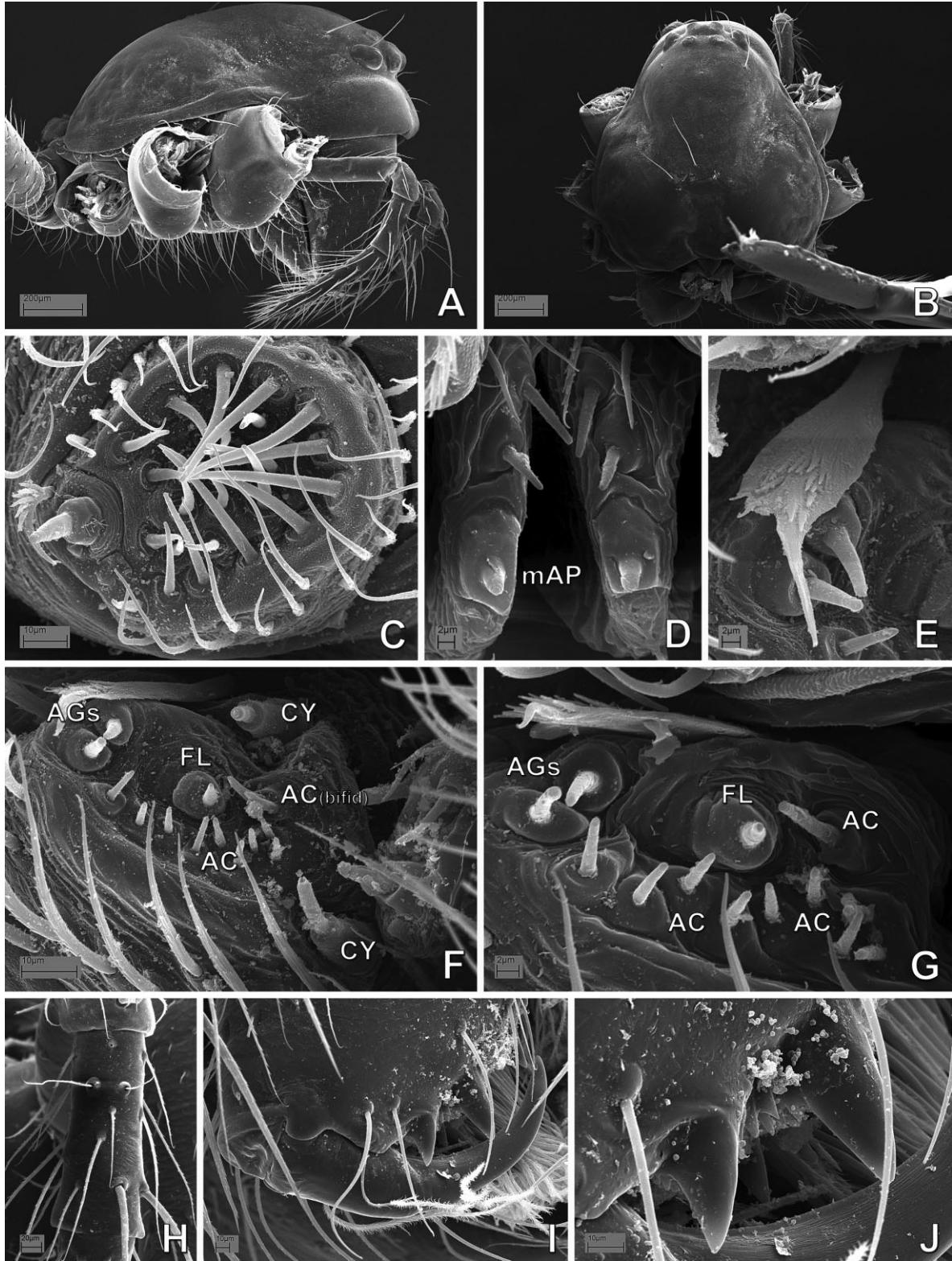


Figure 13. *Maymena mayana* (Mysmenidae): A–C, E, F, H–J, female; D, G, male. A, prosoma, lateral view; B, same, dorsal view; C, left anterior lateral spinnerets; D, posterior median spinnerets; E–G, right posterior lateral spinnerets; E, detail of modified spatulate seta and aggregate spigots; H, detail of female palpal tibia; I, mouthparts, distal right palpal tibia; J, same, detail of promarginal teeth. See Appendix 3 for the list of abbreviations.

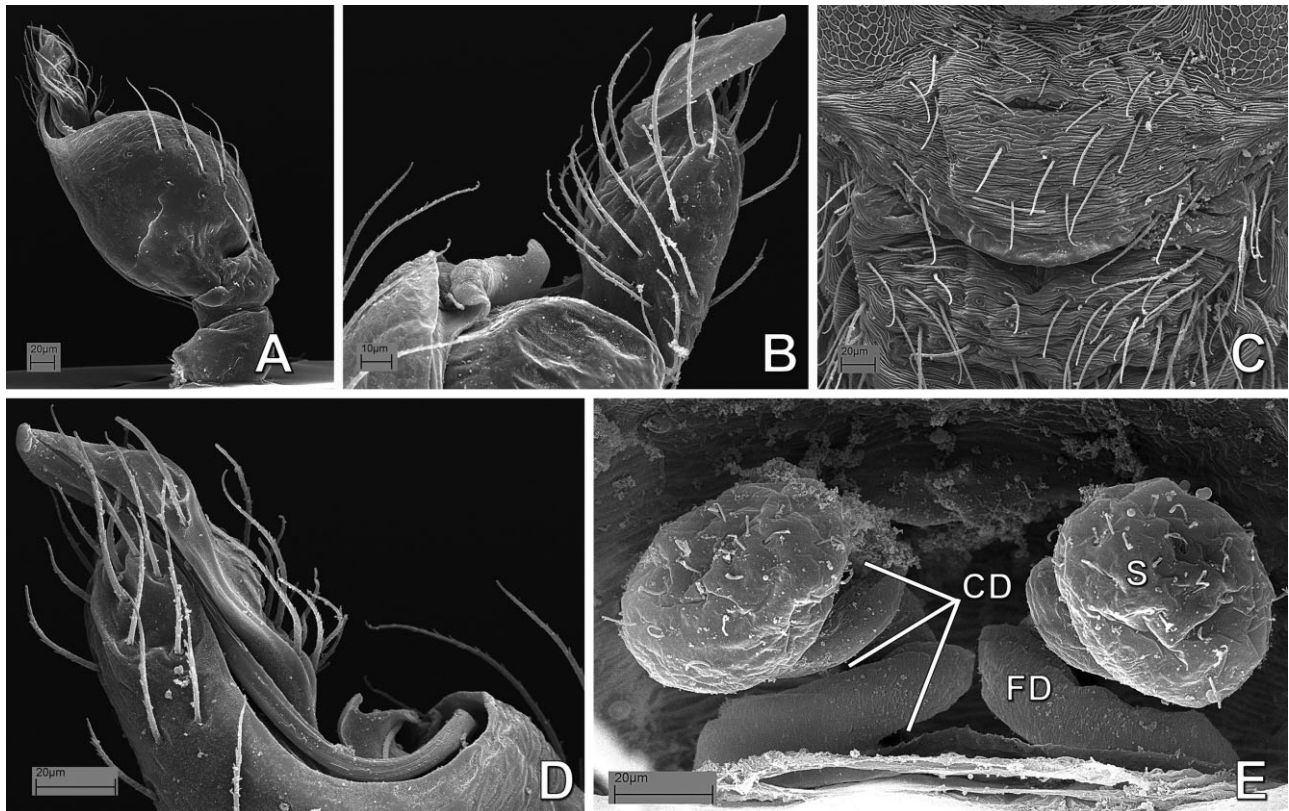


Figure 14. *Maymena rica* (Mysmenidae): A, B, D, male left palp; C, E, female. A, dorsal view; B, same, prolateral view, detail of tip of embolus and housing cymbial conductors; C, epigynum, ventral view; D, same as B, dorsal view; E, digested abdomen, detail of vulva. See Appendix 3 for the list of abbreviations.

to be absent (Coddington, 1990; Griswold *et al.*, 1998). In addition, the spinning organs of Mysmenidae have been studied in only a few species (Griswold, 1985; Griswold *et al.*, 1998; Brescovit & Lopardo, 2008; Miller *et al.*, 2009). Mysmenidae seem to possess the typical symphytognathoid and higher araneoid gland spigot conformation. The anterior lateral spinnerets (ALS, see Appendix 3 for abbreviations) have few piriform gland spigots (with small bases) and a deep groove between the major ampullate and the piriform field. The posterior spinnerets (PMS and PLS) have few aciniform gland spigots. No additional data are available on the spinning organs of mysmenids.

Ten mysmenid species in five genera have been reported from the fossil record (all of them described from Cenozoic amber; Dunlop, Penney & Jekel, 2014). Five of the oldest fossil species have been reported from the Eocene (Palaeogene; 44 Mya): three species from Baltic amber (*Mysmena grotae*, *Mysmena curvata*, and *Palaeomysmena hoffeinsorum*) and two species from Baltic and Bitterfeld ambers (*Eomysmenopsis spinipes* and *Mysmena groehni*) (Wunderlich, 2004, 2011). One species has been reported from the Miocene–Oligocene (Neogene and Palaeogene; 19–27 Mya), from Chiapas

amber: *Mysmena fossilis* (see Petrunkevitch, 1971). Two species have been reported from the Miocene (Neogene; 15–20 Mya), from Dominican amber: *Dominicanopsis grimaldii* and *Mysmenopsis lissycoleyae* (see Penney, 2000; Wunderlich, 2004). Two relatively young fossil species, *Mysmena dominicana* and *Mysmena (s.l.) copalis*, were described by Wunderlich (1998, 2011) from Madagascan copal (a semi-fossilized resin of less than two million years old), dating to Early Pleistocene (Neogene).

TAXONOMIC HISTORY

Mysmenidae were proposed by Simon in 1922 as a group within Theridiidae, under the name ‘Mysmeneae’ (Simon, 1922, 1926). The elusive circumscription of this family is illustrated by the fact that several species originally placed in Mysmenidae have now been transferred to a diverse array of families, such as Tetragnathidae, Theridiidae, Anapidae, Symphytognathidae, Synsphyridae, and Theridiosomatidae, and one species was even transferred to Acari! The following quotations of Mysmenidae, as well as the one preceding the Introduction, illustrate the traditionally obscure

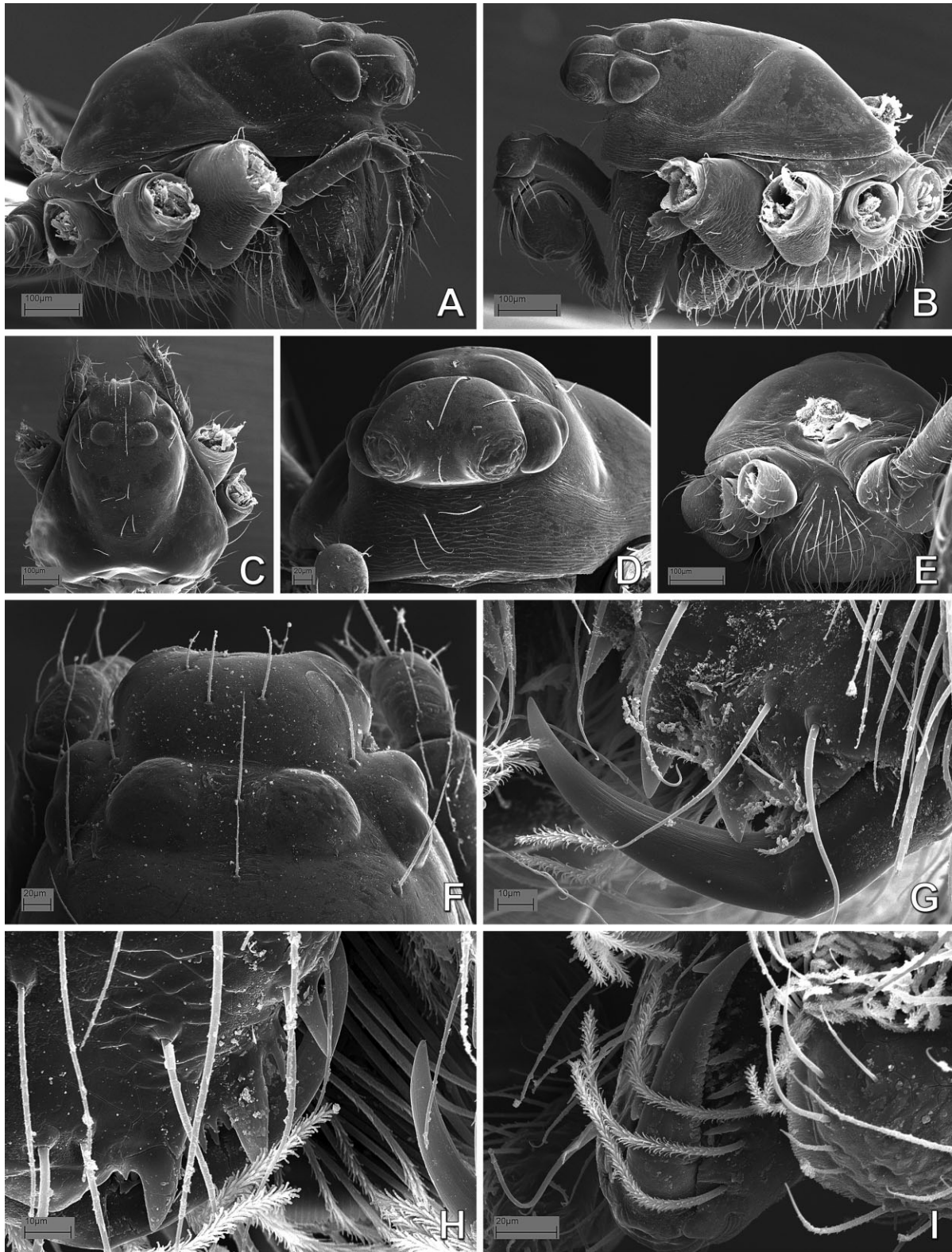


Figure 15. *Maymena rica* (Mysmenidae), prosoma: A, C, F, G, female; B, D, E, H, I, male. A, B, lateral view; C, dorsal view; D, carapace, frontal view; E, prosoma, posterior view; F, ocular area, detail from panel C; G–I, mouthparts, detail of cheliceral fang and teeth; G, distal promargin of left chelicera; H, distal promargin of right chelicera; I, distal right chelicera.

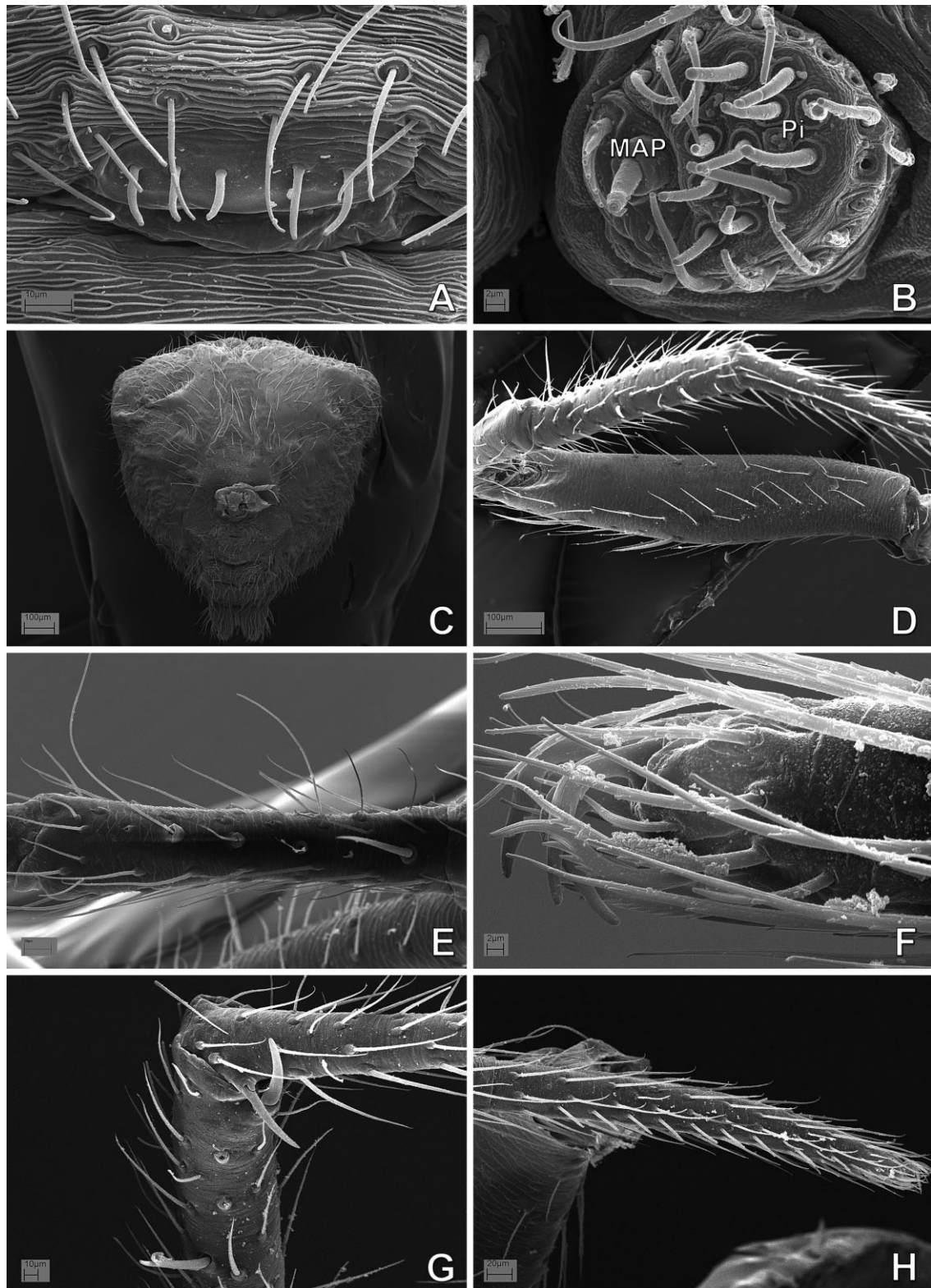


Figure 16. *Maymena rica* (Mysmenidae), abdomen and legs: A, B, G, H, male; C–F, female. A, epiandrous spigots; B, left anterior lateral spinnerets; C, abdomen, ventral view. D, G, H, left leg I; E, F, left leg IV. D, femur, ventral view; E, tibia, dorsal view; F, claws, retrolateral view; G, tibia–metatarsus junction, prolaterodorsal view; H, tarsus, prolaterodorsal view. See Appendix 3 for the list of abbreviations.

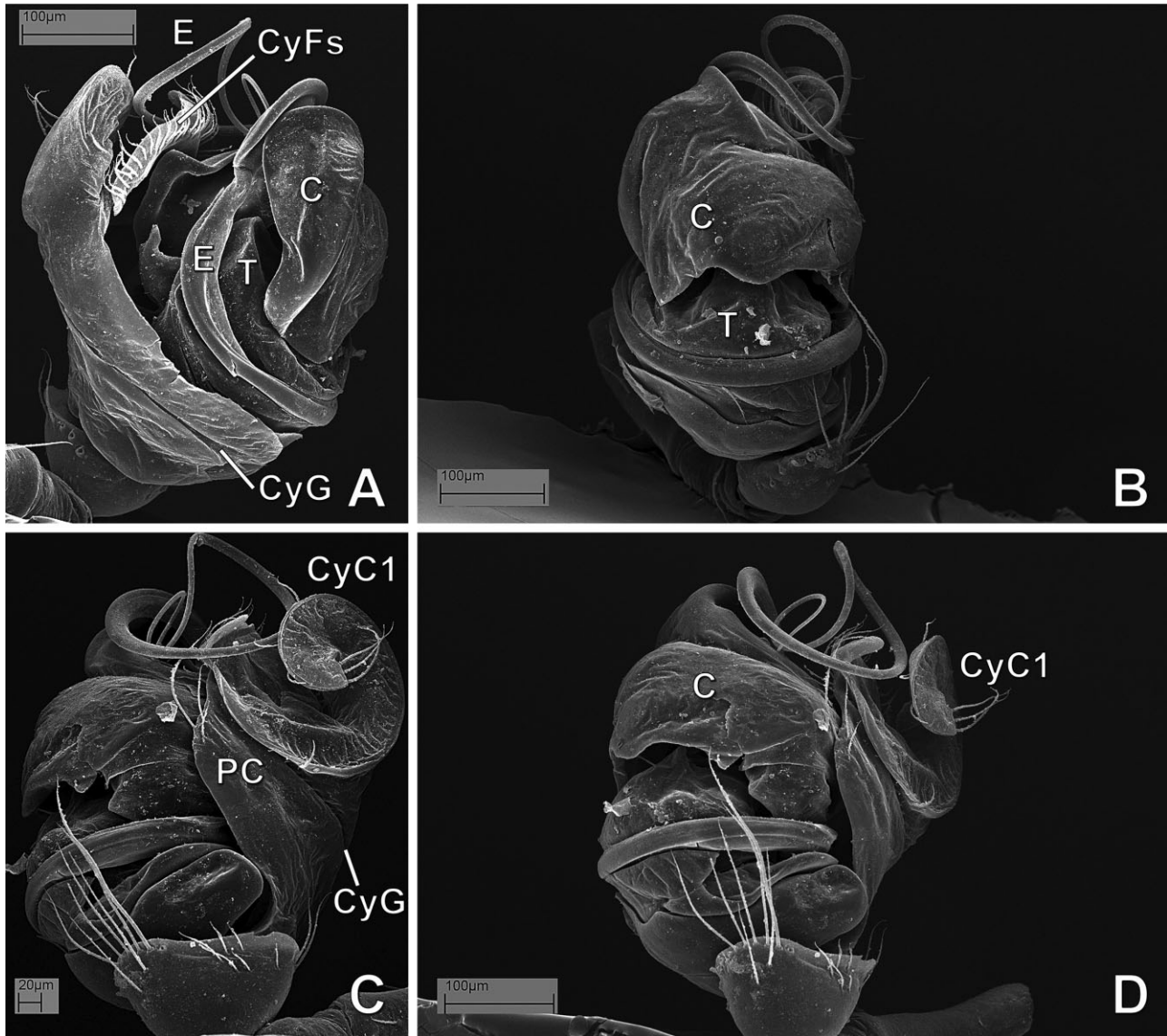


Figure 17. *Microdipoena elsae* (Mysmenidae), male right palp, inverted images: A, prolateral view; B, ventral view; C, retrolateral view; D, retroventral view. See Appendix 3 for the list of abbreviations.

status of mysmenids. Concerning the monophyly of the family, Paolo Brignoli (1980: 727) stated that

... what we call Mysmenidae is equal to what has remained of the ‘Symphytognathidae’ (sensu Forster 1959 and Levi & Levi, 1962) after the removal of the Anapidae, Tetricellidae and Symphytognathidae s.s.

Also, as Karin Schütt (2003: 137) declared,

Every large taxon seems to have a polyphyletic waste disposal group. In the case of symphytognathoids, the family Mysmenidae, into which all unassignables are swept together, has apparently been used for this purpose.

Simon’s ‘Mysmeneae’ (Simon, 1922, 1926) included five genera: *Mysmena*, *Mysmenopsis*, *Cepheia*, *Synaphris*, and *Trogloneta* (Simon, 1926: 315). ‘Mysmeneae’ was diagnosed mainly based on the absence of the female palpal claws, the presence of a voluminous male bulb with a long embolus, the globular or conical abdomen with sparse, rather long hairs, and the median tarsal claw being as long as the superior claws. In a revision of Theridiidae, Petrunkevitch (1928) elevated the group to the subfamily level. He united Simon’s Mysmeneae and Theonoeae in the theridiid subfamily Mysmeninae, thus adding four genera to the original group: *Epecthina*, *Epecthinula*, *Iardinis*, and *Theonoe*.

Table 2. Generic list and information of mysmenid described species included in the morphological data set

Genus	Total species	Total species scored for morphology	Species included	Species excluded	Reason for exclusion
<i>Anjouanella</i> (= <i>Microdipoena</i>)	1	1	<i>A. comorensis</i> *		
<i>Brasilionata</i>	1	1	<i>B. arborensis</i> *		
<i>Calodipoena</i> (= <i>Mysmena</i>)	10	3	<i>C. incredula</i> *, <i>C. mooatae</i> , <i>C. tarautensis</i>	1 (<i>C. tarautensis</i>)	No detailed observation, > 78% missing data
<i>Calomyspoena</i> (= <i>Mysmena</i>)	1	1	<i>C. santacruzii</i> *		Type and only specimen not available, > 78% missing data
<i>Crassignatha</i> (Symphytognathidae)†	8	1	<i>C. haeneli</i> *	1	Type and only specimen lost, > 78% missing data
<i>Iardinis</i> (Symphytognathidae)	3 (2)‡	2	<i>I. martensi</i> , <i>I. mussardi</i>	1 (<i>I. martensi</i>)	Type and only specimen lost, > 78% missing data
<i>Isela</i>	1	1	<i>I. okuncana</i> *		
<i>Itapua</i> (= <i>Mysmena</i>)	1	1	<i>I. tembei</i> *		
<i>Kekenboschiella</i> (= <i>Mysmena</i>)	4	2	<i>K. awari</i> , <i>K. marijkeae</i> *		
<i>Kilifina</i> (= <i>Isela</i>)	1	(1)			
<i>Leviola</i> (Zodariidae)	1	1	<i>L. termitophila</i> *	1	Type and only specimen not available, > 78% missing data
<i>Maymena</i>	13	3	<i>M. ambita</i> , <i>M. mayana</i> *, <i>M. rica</i>		
<i>Microdipoena</i>	4	3	<i>M. elsaе</i> , <i>M. guttata</i> *, <i>M. nyungwe</i>		
<i>Mysmena</i>	26	3	<i>M. leichhardtii</i> , <i>M. leucoplagiata</i> *, <i>M. tasmaniae</i>		
<i>Mysmenella</i> (= <i>Microdipoena</i>)	11	3	<i>M. illectrix</i> *, <i>M. jobi</i> , <i>M. samoensis</i>		
<i>Mysmeniola</i>	1	1	<i>M. spinifera</i> *		
<i>Mysmenopsis</i>	27	4	<i>M. cidrelicola</i> , <i>M. dipluramigo</i> , <i>M. palpalis</i> , <i>M. penai</i>		
<i>Phricotelus</i> (Araneoidea <i>incertae sedis.</i>)	1	1	<i>P. stelliger</i> *	1	No detailed observation, > 78% missing data
<i>Tamasesia</i> (= <i>Mysmena</i>)	3	2	<i>T. acuminata</i> , <i>T. rotunda</i> *		
<i>Trogloneta</i>	11	2	<i>T. cantareira</i> , <i>T. granulum</i> *		

*Type species.

†Currently under Symphytognathidae, see Miller *et al.* (2009) and this study.‡Type and only specimen of type species lost: *nomen dubium*.

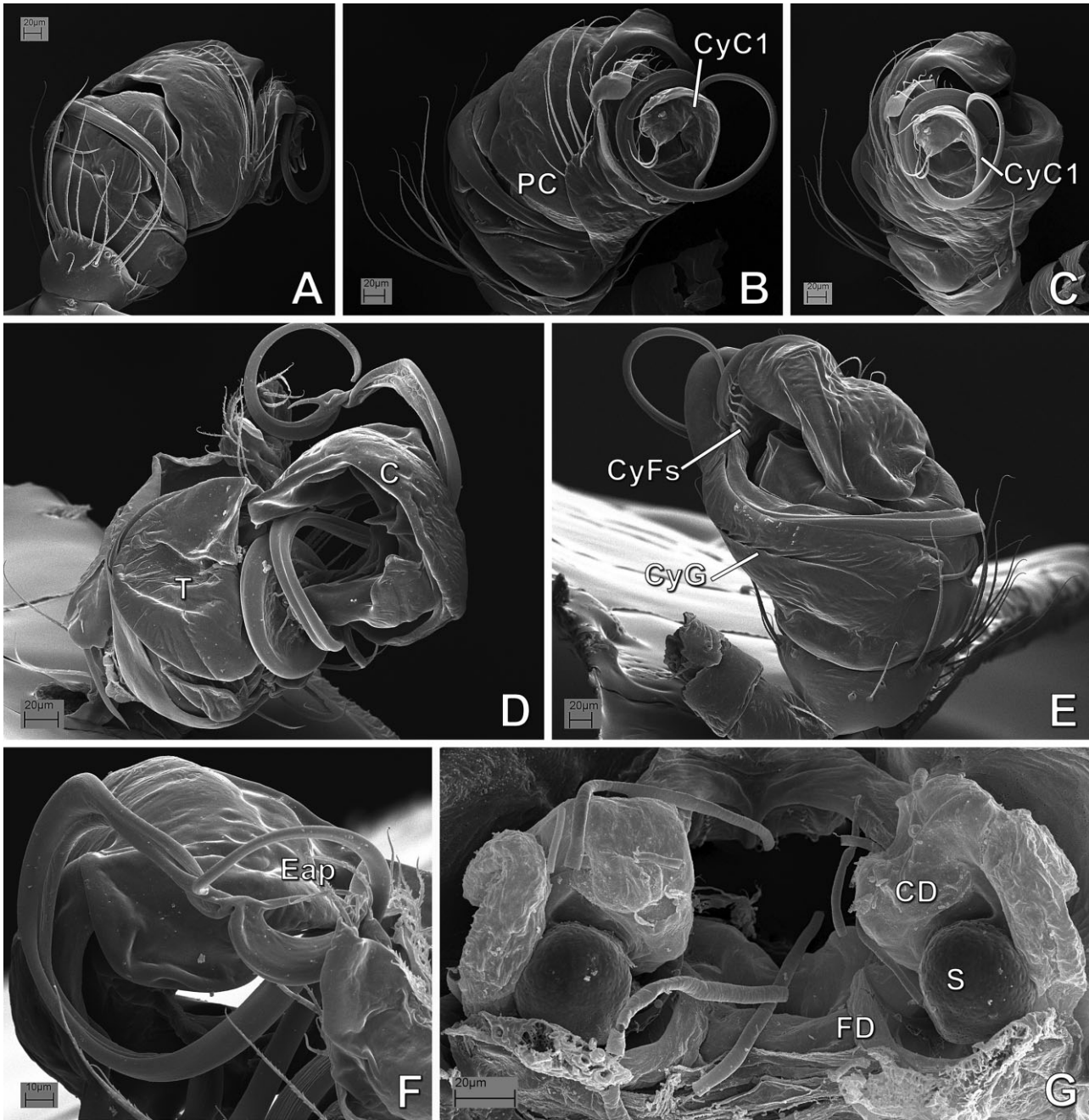


Figure 18. *Microdipoena guttata* (Mysmenidae): A–F, male left palp; G, female. A, ventral–proximal view; B, retrolateral–distal view; C, dorsal–retrolateral view; D, expanded bulb, prolateral view; E, prolateral view; F, expanded bulb, detail of tip of embolus, retrolateral–distal view; G, digested abdomen, detail of vulva. See Appendix 3 for the list of abbreviations.

In a revision of Symphytognathidae *s.l.* (with Anapidae, ‘Micropholcommatidae’, ‘Textricellidae’, Mysmenidae, and Symphytognathidae *s.s.* as subfamilies), Forster (1959) transferred *Mysmena* and consequently the entire subfamily from Theridiidae to Symphytognathidae, and described the respiratory

system of many *Mysmena* species, some of them considered to now belong to *Mysmena* itself (*Microdipoena*, *Calodipoena*, *Tamasesia*, and *Mysmenella*). Gertsch (1960a) summarized the taxonomic revisions of Symphytognathidae by Forster (1959) and of *Mysmena* by Levi (1956), and proposed new diagnostic features

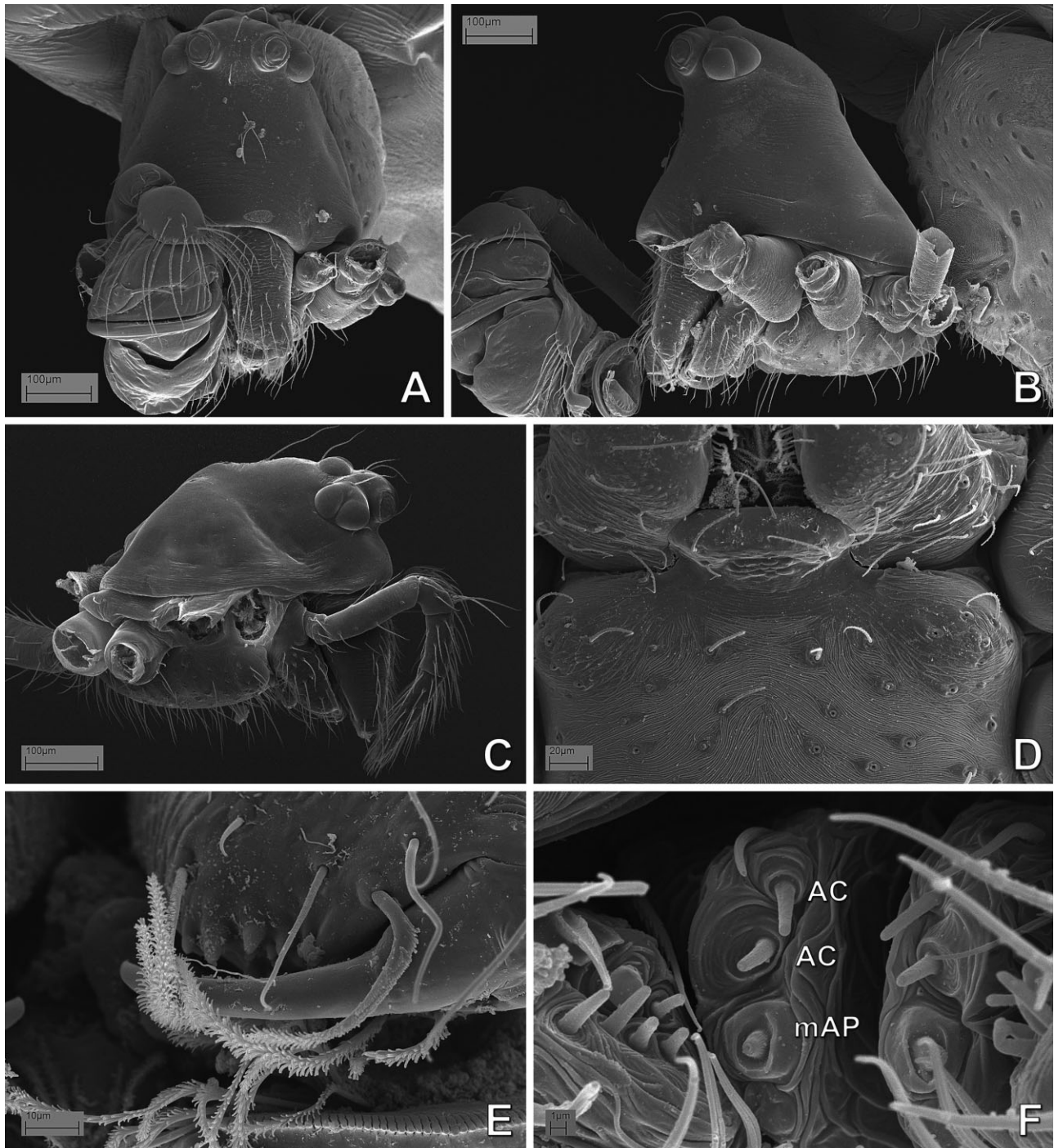


Figure 19. *Microdipoena guttata* (Mysmenidae). A, B, D–F, male; C, female. A, prosoma, frontal view; B, C, same, lateral view; D, same, ventral view, detail of labium–sternum junction; E, mouthparts, detail of tip of left chelicera; F, posterior median spinnerets. See Appendix 3 for the list of abbreviations.

for mysmenines, currently shared by many other symphytognathoid species (e.g. their small to minute size, with or without book lungs, pedipalps present and of normal size in females, lack of comb in the hind tarsi, and metatarsi longer or of equal size than tarsi).

Gertsch (1960a) transferred *Lucarachne*, *Mysmenopsis*, *Iardinis*, and *Trogloneta* from Theridiidae to Symphytognathidae, and stated that Mysmeninae comprised the following genera: *Mysmena*, *Mysmenopsis*, *Lucarachne*, *Maymena*, *Cepheia*, *Synaphris*, *Iardinis*,

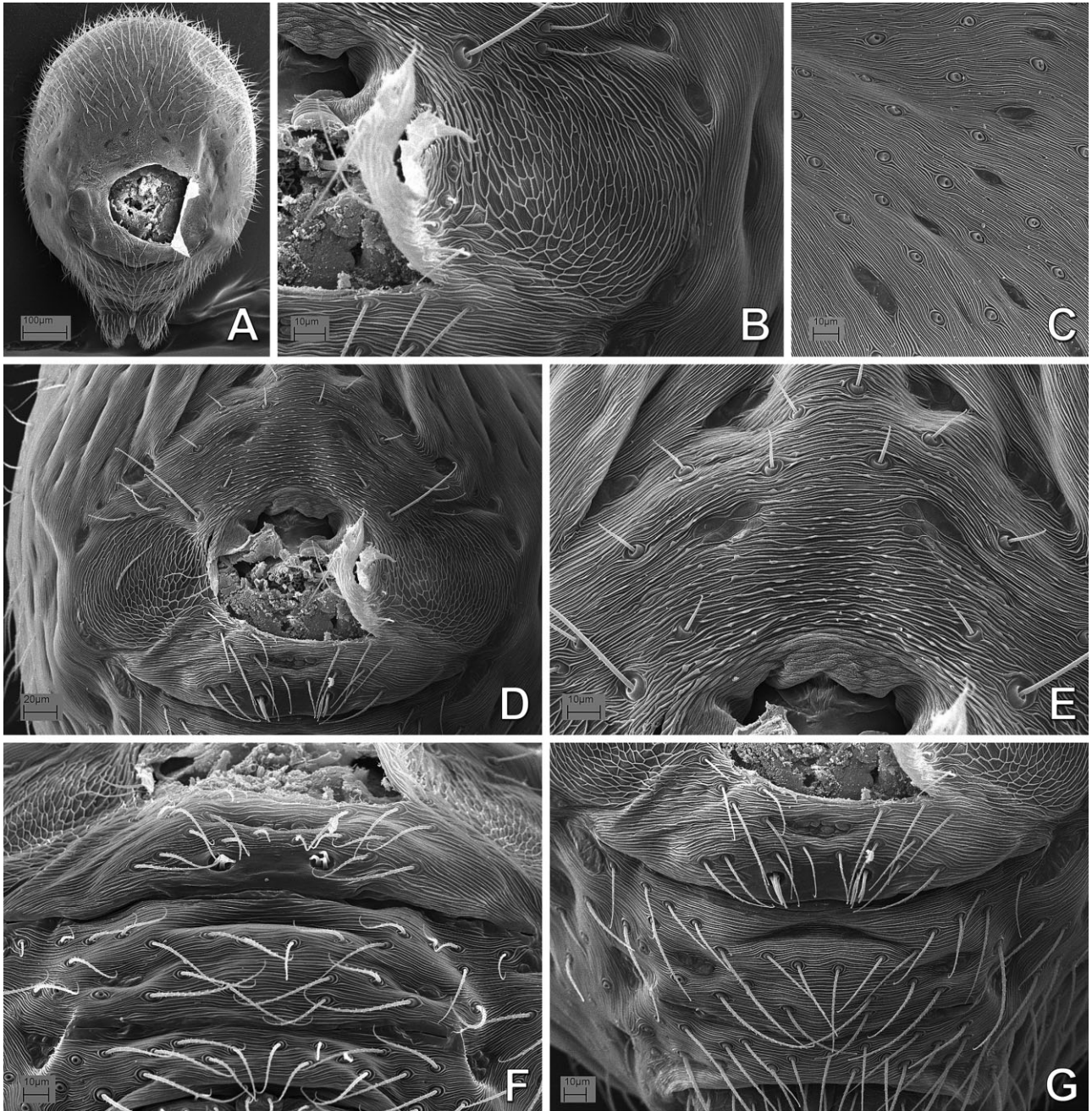


Figure 20. *Microdipoena guttata* (Mysmenidae), abdomen: A, female; B–G, male. A, ventral view; B, detail of booklung cover; C, detail of abdominal cuticular pattern; D, pedicel area and booklung covers; E, detail of area above pedicel; F, posterior–ventral view, detail of epigastric furrow, epiandrous spigots and spiracular openings; G, same, ventral view.

and *Trogloneta*. Levi & Levi (1962), in a generic revision of Theridiidae, transferred *Taphiassa* to Symphytognathidae s.l. and placed *Iardinis* as *incertae sedis* within the latter family.

Forster & Platnick (1977) concluded that mysmenids were sufficiently distinct from Symphytognathidae to warrant family rank, without providing further justification. A year later, Platnick & Shadab (1978), in

a revision of the genus *Mysmenopsis*, provided an explicit, although tentative, diagnosis of Mysmenidae, based only on New World genera. According to Platnick & Shadab (1978), four features diagnosed Mysmenidae: a clasping spur on the male metatarsus I (occasionally also on tibia I), the presence of lobes or apophyses on the cymbium, a ventral sclerotized spot on distal femur I of females, and a series of tiny denticles

Table 3. List of described and undescribed outgroup (i.e. non-mysmenid) taxa

Family	Species
Anapidae	<i>Acroleps hygrophilus</i> <i>Anapisona kethleyi</i> <i>Crassanapis chilensis</i> <i>Comaroma simoni</i> <i>Elanapis aisen</i> <i>Minanapis casablanca</i> <i>Minanapis palena</i> <i>Tasmanapis strahan</i>
(Micropholcommatinae)	<i>Taphiassa punctata</i> <i>Teutoniella cekalovici</i>
Linyphiidae	<i>Linyphia triangularis</i>
Symphytognathidae	<i>Crassignatha haeneli</i> Patu-SYMP-001-DR SYMP-002-MAD SYMP-006-AUST SYMP-007-AUST <i>Symphytognatha picta</i>
Synaphridae	<i>Cepheia longiseta</i> <i>Synaphris saphrynis</i>
Tetragnathidae	<i>Leucauge venusta</i> <i>Tetragnatha versicolor</i>
Theridiidae	<i>Steatoda</i>
Theridiosomatidae	<i>Theridiosoma gemmosum</i> <i>Coddingtonia euryopoides</i>

scattered between the cheliceral teeth. Brignoli (1980) questioned the validity of the new family rank of Mysmenidae and its diagnosis, and reviewed some of its genera, revalidating some, creating others, and thus splitting the genera previously placed in the family. Still, Brignoli accepted the group diagnosis. He revalidated *Microdipoena* (previously revalidated by Saaristo, 1978), *Calodipoena*, and *Tamasesia*, and erected the genus *Mysmenella*. Wunderlich (1986; contra Forster & Platnick, 1977) defended the monophyly of Symphytognathidae *s.l.* (i.e. *sensu* Forster, 1959), thus reverting Mysmenidae to subfamily level, and splitting this subfamily into two: Mysmeninae and Synaphrinae. Synaphrinae included the mysmenid genera *Synaphris*, *Iardinis*, and *Cepheia*. Furthermore, Wunderlich (1986) proposed a hypothesis of relationships between symphytognathoid families (as Anapidae *s.l.*), although no data set or thorough and explicit phylogenetic rationale for inferring such relationships was provided (as discussed by Schütt, 2002).

More than 90 years after its erection, and despite the many arguments about its circumscription and phylogenetic placement, Mysmenidae still lack a modern phylogenetic morphological revision. Only recently the monophyly of Mysmenidae has been robustly tested in a comprehensive combined phylogenetic analysis of

symphytognathoid spiders using morphological and molecular data (Lopardo *et al.*, 2011, and see references therein for a review of previous phylogenetic analysis including mysmenid representatives; see also Dimitrov *et al.*, 2012 for a comprehensive orbicularian analysis and the problematic monophyly of symphytognathoids).

GOALS

The goals of this study are several. First, to perform the first comparative morphological study of mysmenids and their close relatives, and to propose and test hypotheses of primary homology. These primary homology hypotheses have been compiled as characters into a morphological data set. Second, to explore the phylogenetic signal of the morphological (and behavioural) data partition by means of a generic-level cladistic analysis of Mysmenidae, to test the monophyly of the family and its genera, and to place Mysmenidae within symphytognathoids. The morphological characters were also included as part of a larger, combined analysis of mysmenid and other symphytognathoids elsewhere, and therefore proper taxonomic and nomenclatorial actions from the phylogenetic classification for the family are based on the results of our combined analyses, which have been presented and discussed elsewhere (Figs 160, 161; see also Lopardo *et al.*, 2011: fig. 12). Thirdly, to discuss the evolutionary implications for the spinneret silk gland spigot conformations in Mysmenidae and other symphytognathoids, based on the evolutionary and comparative framework provided by the total-evidence phylogenetic hypothesis of the combined analysis (Fig. 160; see also Lopardo *et al.*, 2011, fig. 12).

MATERIAL AND METHODS

SPECIMENS

Taxon sampling

Specimens for this study were borrowed from museum collections, kindly loaned or donated by colleagues, or collected in the field (see Acknowledgements). See Appendix 1 for a list of material examined and voucher information.

Ingroup

The ingroup for the morphological and behavioural data set (hereafter referred to as 'morphological' data set) consists of 47 mysmenid species: 36 species belong to described taxa, representing 18 of the 23 mysmenid genera as currently defined (see Table 2). Described species (see Table 1 for authorship of taxa) scored in this data set include *Anjouanella comorensis*,

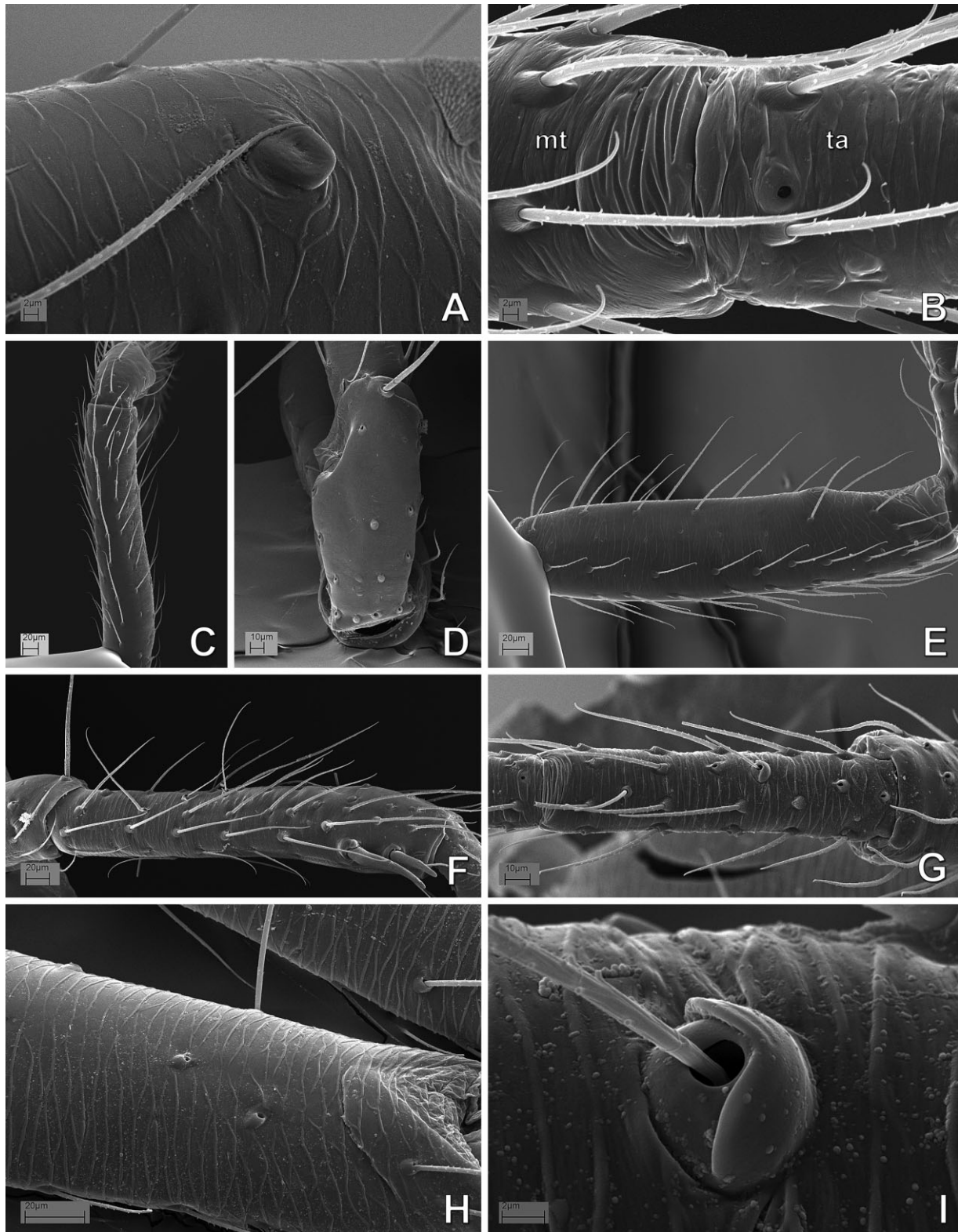


Figure 21. *Microdipoena guttata* (Mysmenidae), legs: A, D, F–I, male; B, C, E, female. A, left leg I, detail of femoral spot; B, right leg I, metatarsus–tarsus junction; C, right femur II, dorsal view; D, left patella I, dorsal view; E, right femur II, prolateral view; F, left tibia I, prolateral view; G, right metatarsus III, dorsal view; H, right femur II, ventral view; I, right leg III, metatarsal trichobothrium.

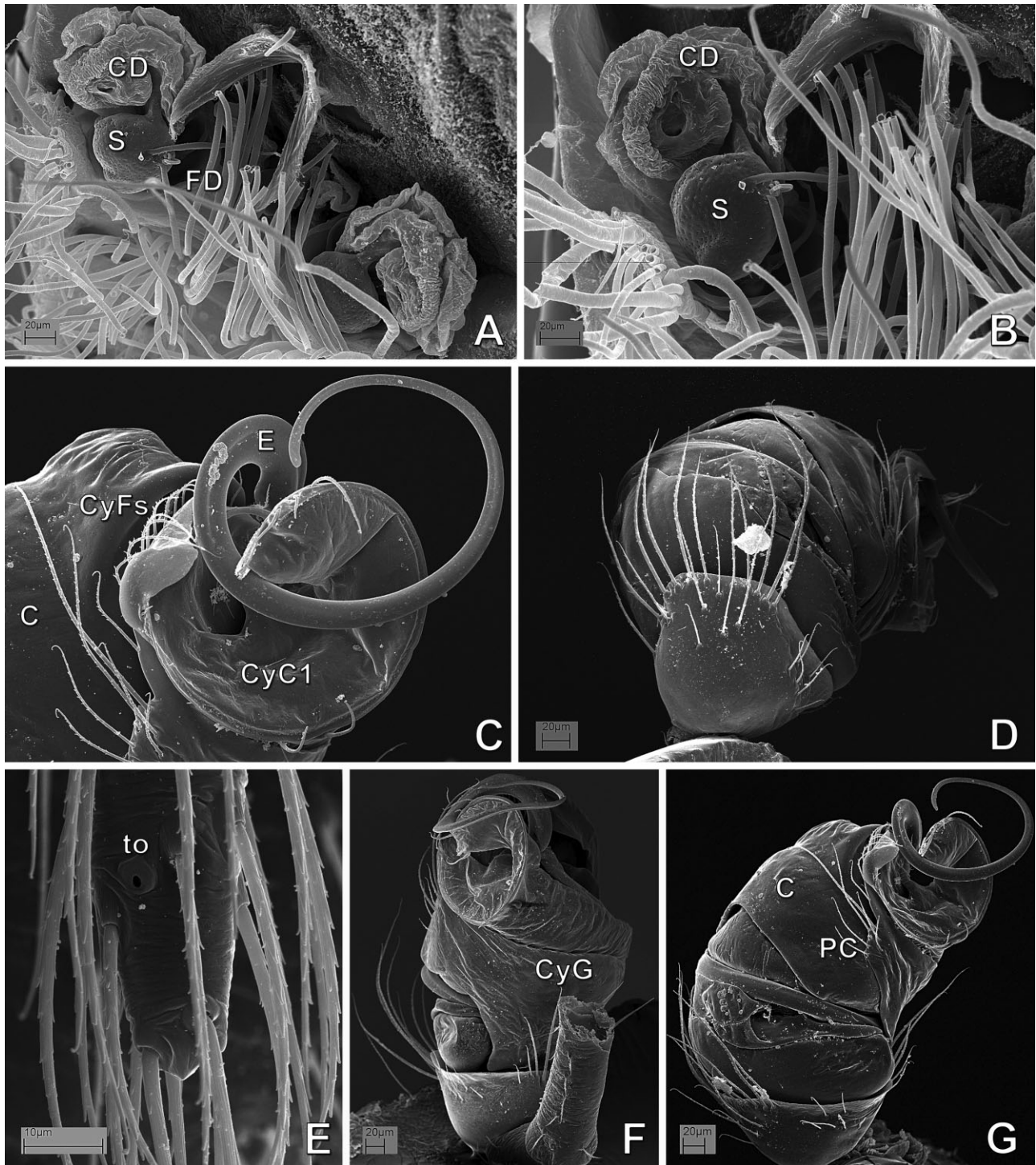


Figure 22. *Microdipoena nyungwe* (Mysmenidae): A, B, E, female; C, D, F, G, male left palp. A, digested abdomen, respiratory system and vulva; B, same, detail of vulva; C, distal-retrolateral view, detail of tip of embolus and primary cymbial conductor; D, ventral-proximal view; E, tip of palp and tarsal organ; F, dorsal view; G, retrolateral view. See Appendix 3 for the list of abbreviations.

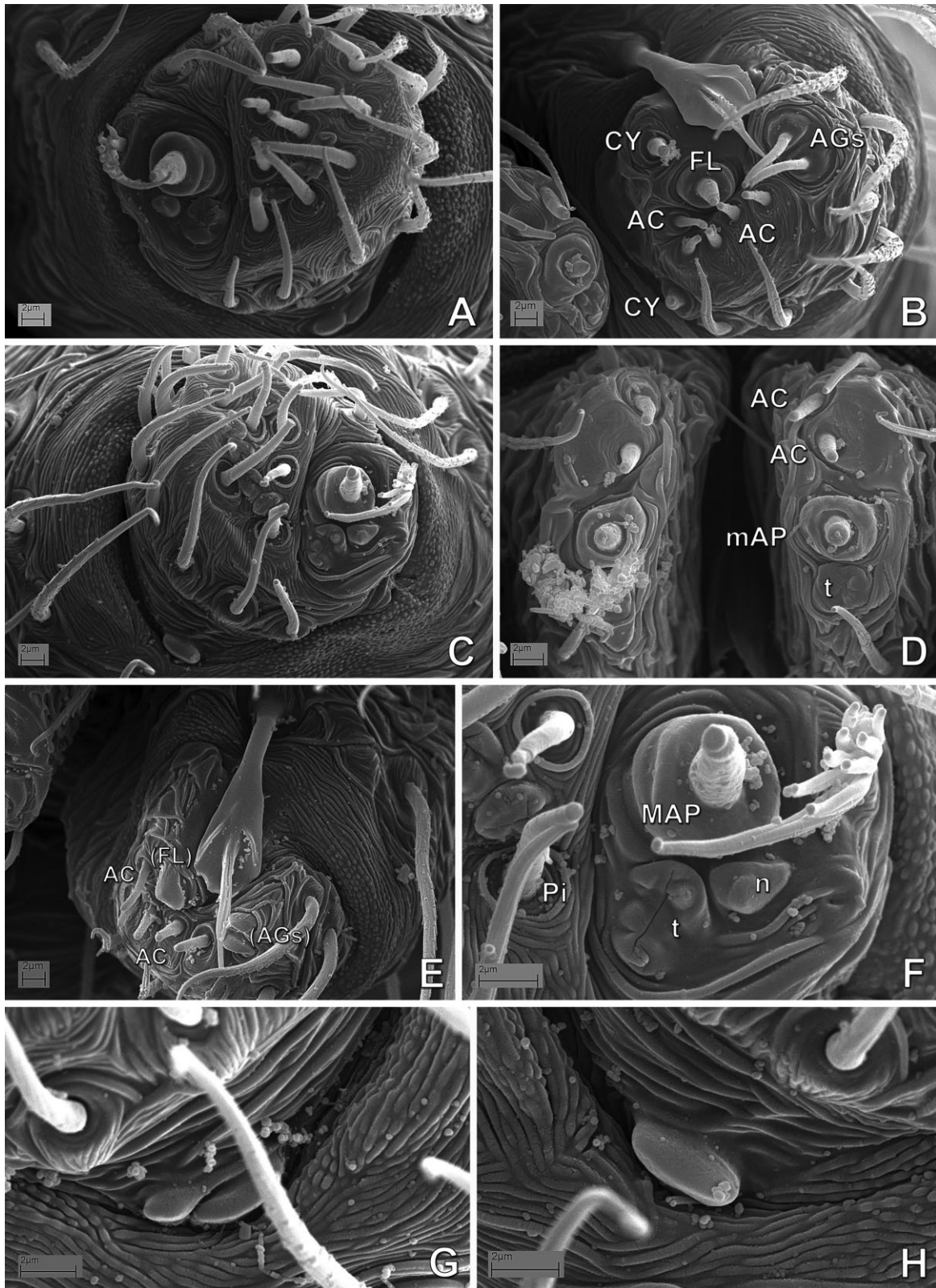


Figure 23. *Microdipoena nyungwe* (Mysmenidae), spinnerets: A, B, female; C–H, male. A, C, anterior lateral spinnerets (ALS); B, E, left posterior lateral spinnerets; D, posterior median spinnerets; F, ALS, detail of major ampullate field; G, H, ALS, detail of intersegmental lobe. See Appendix 3 for the list of abbreviations.

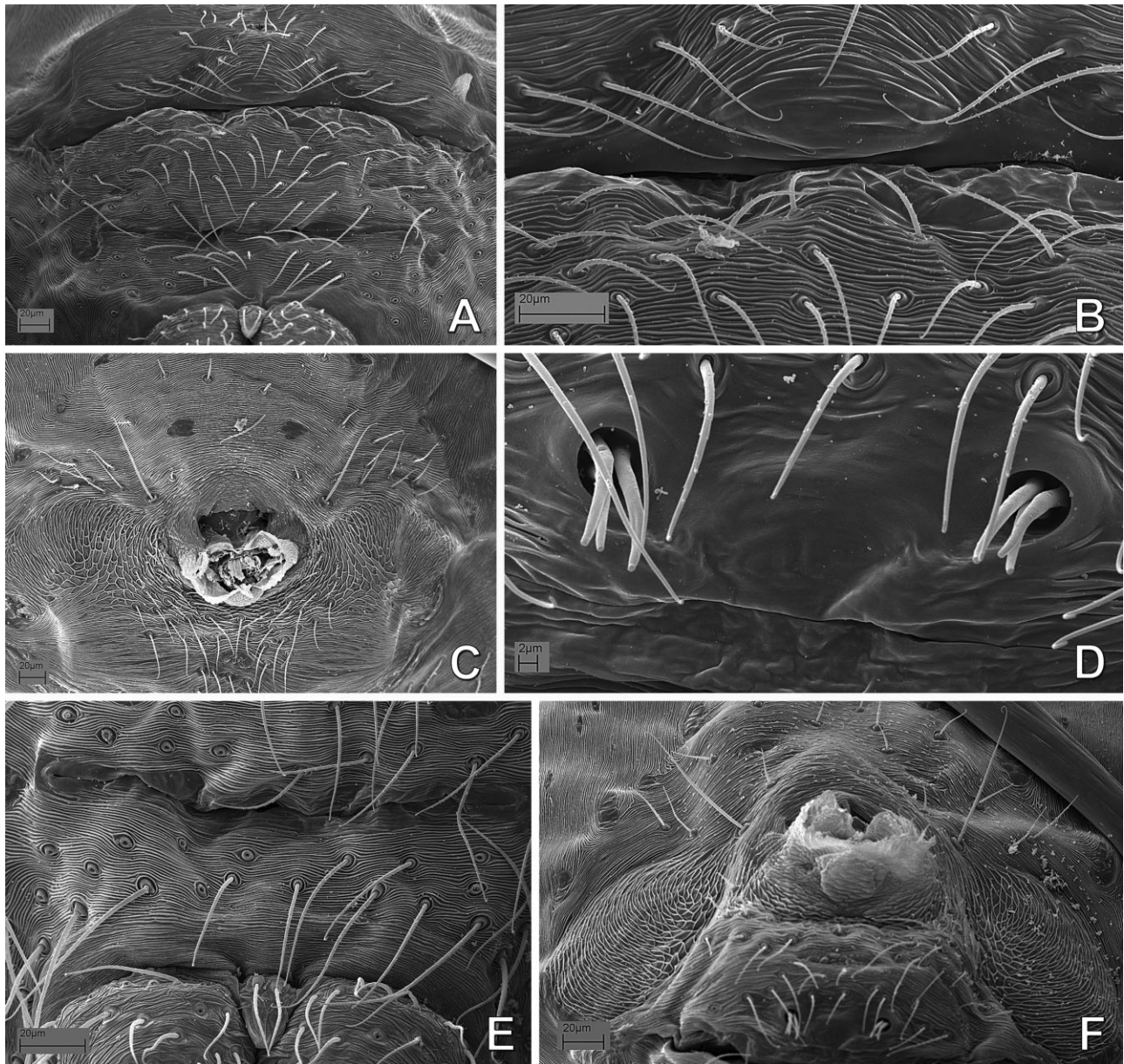


Figure 24. *Microdipoena nyungwe* (Mysmenidae), abdomen: A–D, female; E–G, male. A, epigastric furrow, epigynal area and spiracular openings, posterior–ventral view; B, same, detail of epigynal area; C, pedicel area and booklung covers; D, epiandrous spigots, detail from figure F; E, posterior respiratory spiracle and colulus, ventral view; F, pedicel area, booklung covers and epiandrous spigots.

Brasilionata arborens, *Calodipoena incredula*, *Calodipoena mooatae*, *Calodipoena tarautensis*, *Calomyspoena santacruzii*, *Crassignatha haeneli* (but see below), *Iardinis martensi*, *Iardinis mussardi*, *Isela okuncana*, *Itapua tembei*, *Kekenboschiella awari*, *Kekenboschiella marijkeae*, *Leviola termitophila*, *Maymena ambita*, *Maymena mayana*, *Maymena rica*, *Microdipoena elsa*, *Microdipoena guttata*, *Microdipoena nyungwe*, *Mysmena leichhardti*, *Mysmena leucoplagiata*, *Mysmena tasmaniae*, *Mysmenella illectrix*, *Mysmenella*

jobi, *Mysmenella samoensis*, *Mysmeniola spinifera*, *Mysmenopsis cidrelicola*, *Mysmenopsis dipluramigo*, *Mysmenopsis palpalis*, *Mysmenopsis penai*, *Phricotelus stelliger*, *Tamasesia acuminata*, *Tamasesia rotunda*, *Trogloneta cantareira*, and *Trogloneta granulum*. The currently monotypic genus *Kilifina* was represented by an undescribed species sharing apomorphies with the type species *Kilifina inquilina*, also from Kenya, the country from which the type species was collected. This undescribed species has also been collected

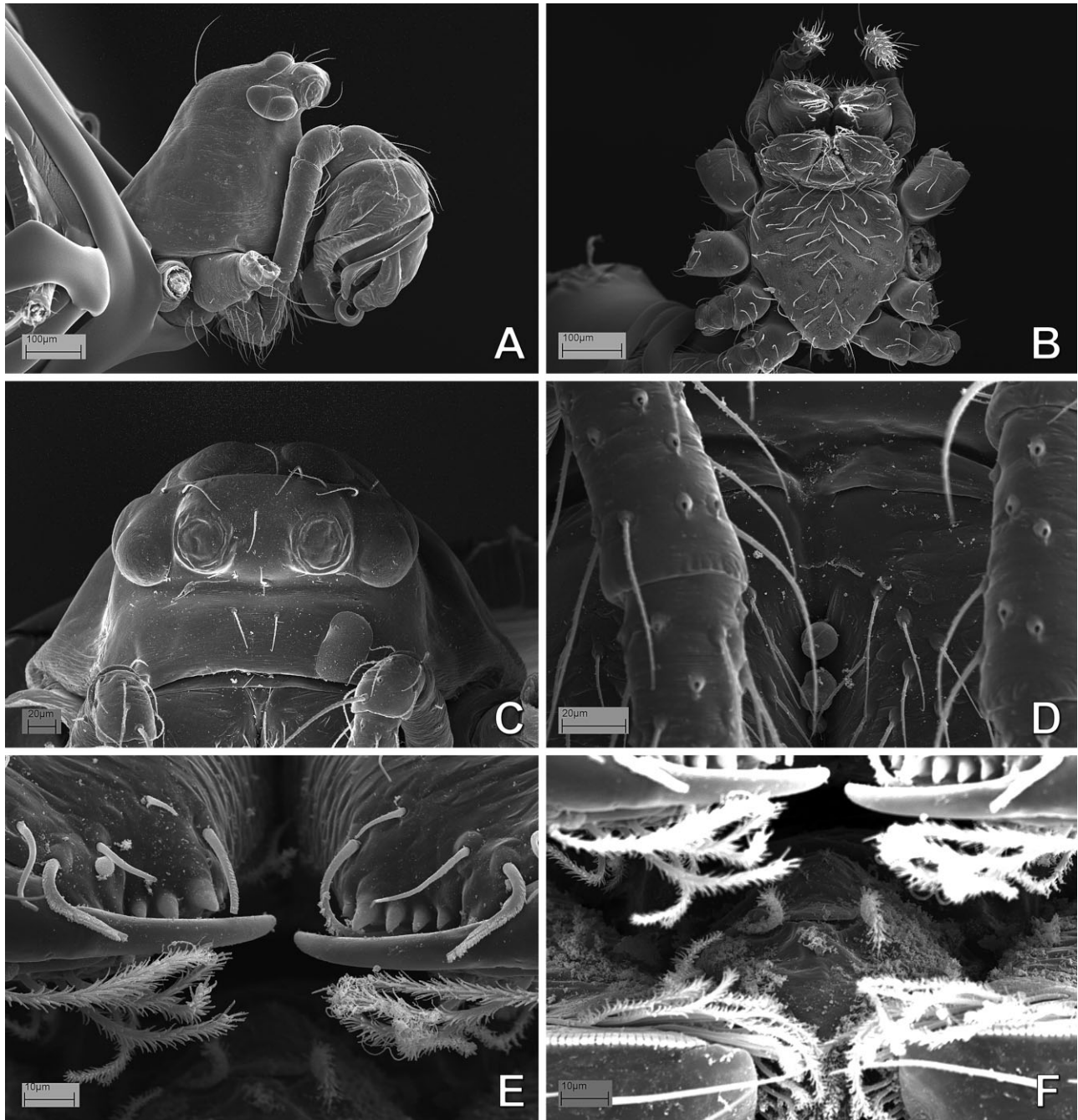


Figure 25. *Microdipoena nyungwe* (Mysmenidae), prosoma: A, male; B–F, female. A, lateral view; B, ventral view; C, ocular area, frontal view; D, cheliceral bases, frontal view; E, distal chelicerae; F, labrum.

in Cameroon and São Tomé (C. Griswold, pers. comm.). The monotypic genus *Crassignatha* was recently transferred from Mysmenidae to Symphytognathidae based on morphology by Miller *et al.* (2009), and this newly proposed familial placement is tested in the present study. The remaining ten taxa correspond to undescribed mysmenid species (see Appendix 1). When possible, undescribed species were identified (i.e. tentatively

assigned to a genus) so that generic (and familial) membership could also be tested. The exemplar approach was followed as much as possible when scoring characters (i.e. morphological characters were scored following direct observation of specimens). When specimens from described species were not available for study, or insufficient material existed or was suitable for detailed and thorough comparative observations, scoring

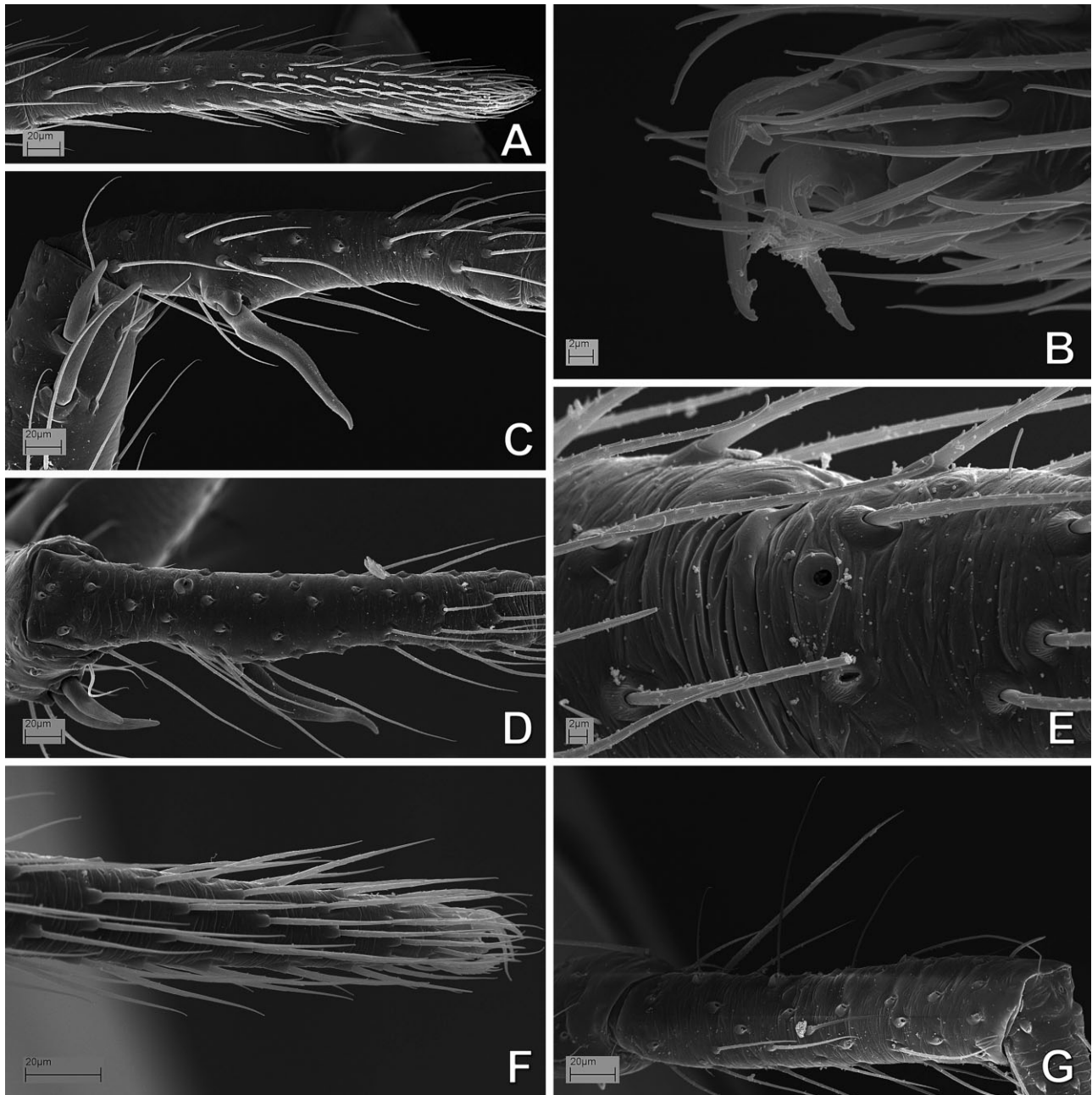


Figure 26. *Microdipoena nyungwe* (Mysmenidae), left legs: A, C, D, G, male; B, E, F, female. A, tarsus I, prolateral view; B, claws I, retrolateral view; C, leg I, tibia-metatarsal junction, prolateral view; D, metatarsus I, dorsal view; E, leg I, metatarsus-tarsus junction, dorsal view; F, tarsus IV, prolateral view; G, tibia IV, prolateral view.

was based on the original species descriptions or other descriptive literature, or on previous phylogenetic work. As a result of a lack of detailed observations, the level of missing data for five of the 'literature-based taxa' was higher than 78% in the current data set, and they were not included in the final analyses. Instead, these five species were included in a preliminary analysis comprising all taxa to test their familial placement (for

the inclusion/exclusion of taxa and reasons for exclusion, see Table 2). The five taxa removed from the final analyses include three species not available for study, and scored entirely from the literature (*Crassignatha haeneli*, *Iardinis martensi*, and *Leviola termitophila*), and two species without adequate material for direct detailed observation, and therefore scored mainly from literature (*Phricotelus stelliger* and *Calodipoena*

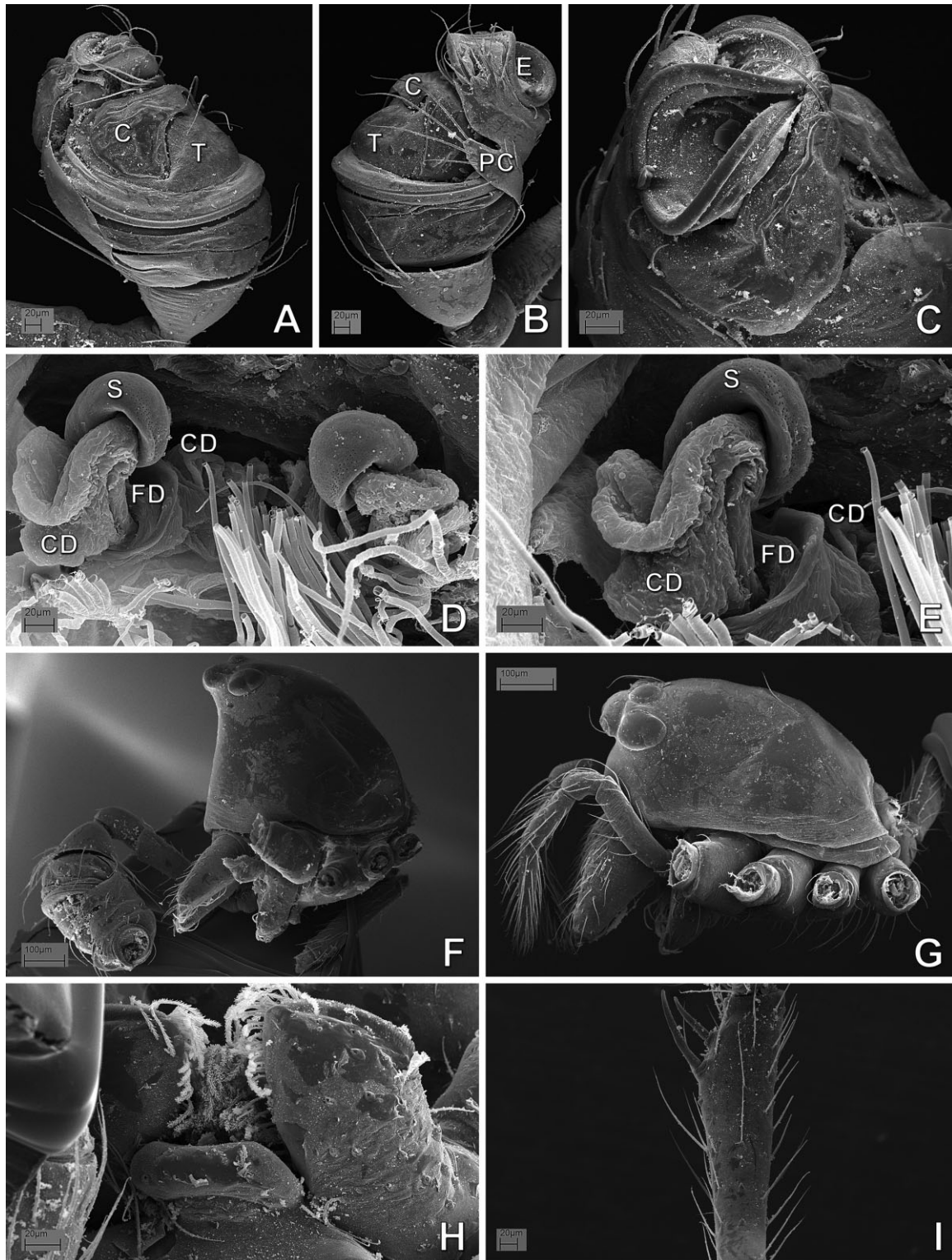


Figure 27. *Microdipoena* (= *Mysmenella*) *samoensis* (Mysmenidae), syntypes: A–C, F, H, I, male; D, E, G, female. A, left palp, prolateral–ventral view; B, same, retrolateral–ventral view; C, same, detail of tip of embolus and interaction with primary cymbial conductor, prolateral view; D, digested abdomen, vulva, and part of respiratory system; E, same, detail of vulva; F, G, prosoma, lateral view; H, mouthparts, ventral view, detail of retromargin of chelicerae and labium; I, left tibia I, dorsal view. See Appendix 3 for the list of abbreviations.

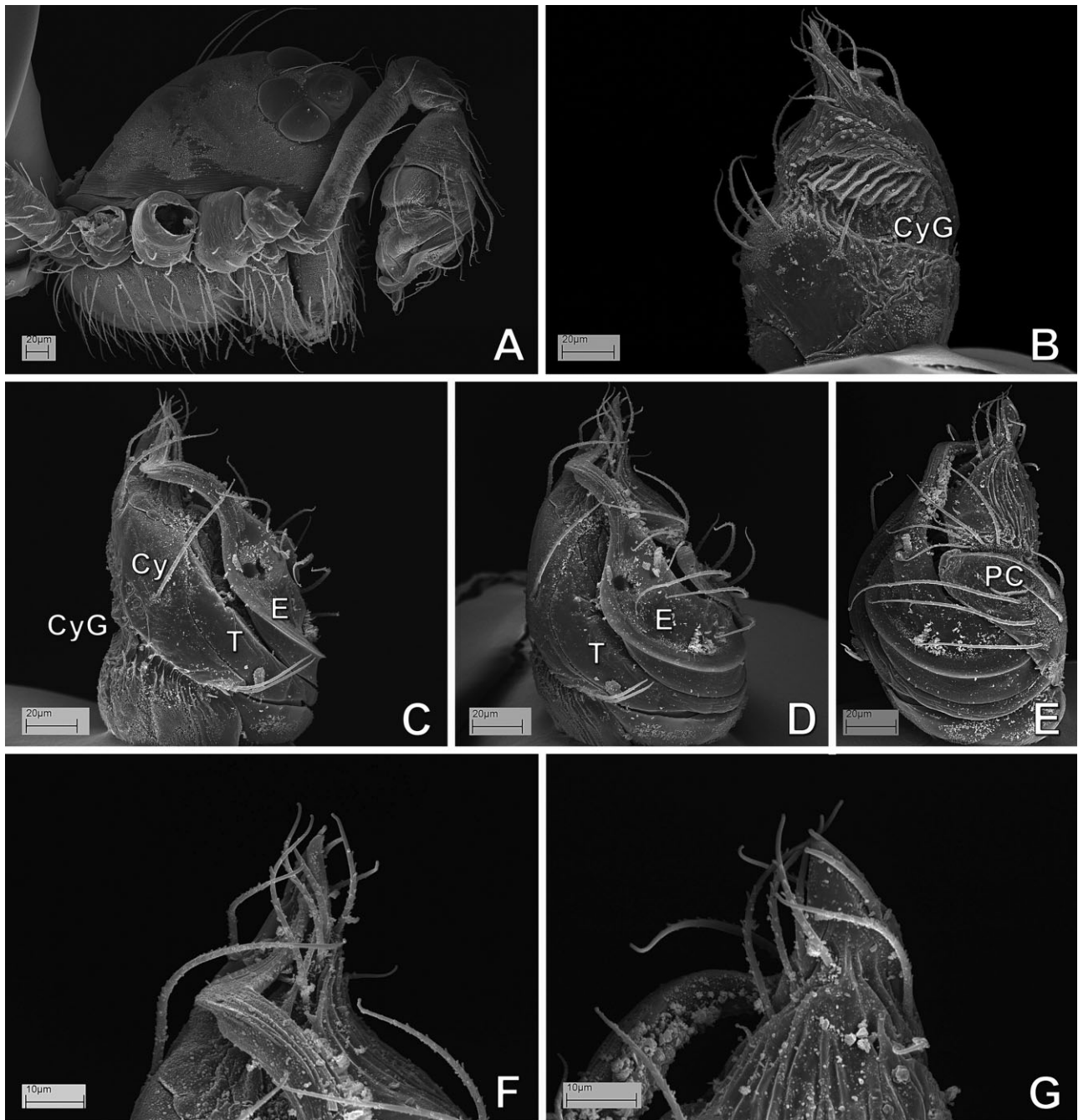


Figure 28. MYSM-005-ARG (*Mysmena*, Mysmenidae) from Misiones, Argentina; male. A, prosoma, lateral view; B–G, left palp. B, dorsal view; C, prolateral view; D, prolateral–ventral view; E, retrolateral–ventral view; F, detail of embolus tip, ventral view; G, same, retrolateral view. See Appendix 3 for the list of abbreviations.

tarautensis). The ingroup includes the type species of most genera, plus up to three other described species for those non-monotypic genera. Although the representative ingroup species were initially selected taking into account the morphological diversity of each genus, the availability of material is always the final arbiter for the taxon selection used. The final ingroup sample

includes 42 mysmenid species representing 16 genera (see Appendix 1 for a list of studied specimens).

Outgroups

The phylogenetic relationships among araneoid families have yet to be satisfactorily resolved (Hormiga & Griswold, 2014), and thus when designing the

Table 4. List of character sets reporting number of corresponding characters and their relative proportions (see Fig. 152)

Character set	Number of characters	Percentage	Number of continuous characters in the set
Abdomen (including respiratory system)	35	9.80%	1
General body	1	0.28%	
Cephalothorax	20	5.60%	
Egg sacs	1	0.28%	
Epiandrous spigots	3	0.84%	
Epigynum (internal and external female genitalia)	29	8.12%	
Eyes	9	2.52%	
Legs	58	16.25%	4
Male palp	111	31.09%	
Mouthparts	35	9.80%	
Palp (female)	7	1.96%	
Spinnerets	39	10.92%	2
Web building (and other behavioural characters)	9	2.52%	
Total	357	100.00%	7

out-group sampling it is very difficult, if not impossible, not to fall down the slippery slope that brings the study into the orbicularian phylogeny abyss. The choice of which families to represent quickly becomes a question of which families will not be represented in the analysis. Our taxon selection has emphasized the symphytognathoid families, and is largely based on the phylogenetic hypotheses of Coddington (1990), Griswold *et al.* (1998), Schütt (2003), and Lopardo & Hormiga (2008; for a detailed rationale for outgroup taxon sampling, see also Lopardo *et al.*, 2011). Cyatholipidae were not represented; retrospectively, their inclusion along with Synotaxidae would have been relevant to the problem finding the closest relatives of symphytognathoids. But ultimately a line must be drawn across this slippery slope, otherwise our study would grow out of proportion to become an analysis of the araneoid families. Although Mysmenidae seem to be related to other symphytognathoid families, the limits and diagnoses of these families appear problematic, except for Theridiosomatidae (see Coddington, 1986a; Labarque & Griswold, 2014; see also Lopardo *et al.*, 2011, for current re-delimitation and diagnoses of symphytognathoid families). The choice of outgroup taxa therefore focused on symphytognathoid representatives, in particular Symphytognathidae and Anapidae, and was also based on, and limited by, specimen availability. The outgroup taxon partition consists of 23 species representing seven araneoid families (18 species correspond to described taxa, see Table 3): Anapidae [ten species: *Acroleps hygrophilus*, *Anapisona kethleyi*, *Crassanapis chilensis*, *Comaroma simoni*, *Elanapis aisen*, *Minanapis casablanca*, *Minanapis palena*, and *Tasmanapis strahan*, plus two species of the subfamily Micropholcommatinae *sensu* Lopardo *et al.*

(2011), *Taphiassa punctata* and *Teutoniella cekalovici*], Symphytognathidae [five species: *Symphytognatha picta* plus four undescribed species and *Crassignatha haeneli*, see Ingroup above), Theridiosomatidae (two species: *Theridiosoma gemmosum* and *Coddingtonia euryopoides*), Synaphridae (two species: *Cepheia longiseta* and *Synaphris saphrynis*); and the non-symphytognathoid families Theridiidae (*Steatoda*, see below), Linyphiidae (*Linyphia triangularis*), and Tetragnathidae (two species: *Leucauge venusta* and *Tetragnatha versicolor*) (see Table 3). Most of the observations are based on our study of the relevant specimens, using an exemplar approach (e.g. Prendini, 2001), rather than inferring basal states for genera; otherwise the scoring was based on the literature. The theridiid genus *Steatoda* is the only chimeric taxon in this data set. This genus has also been included as a single chimeric representative in previous studies, including a phylogenetic analysis of the same Theridiidae (see also Griswold *et al.*, 1998; Agnarsson, 2004), where more than one species was examined. The general morphology of *Steatoda* appears to be sufficiently invariable, and following Agnarsson's (2004) approach, a combination of species was included to represent the groundplan character vector of the genus (*Steatoda americana*, *Steatoda bipunctata*, and *Steatoda grossa*). Specimens of *S. americana* were examined here, although the character scoring was complemented with information from the data sets of Griswold *et al.* (1998; *S. grossa*) and Agnarsson (2004; *S. americana*, *S. bipunctata*, and *S. grossa*) (but see Wunderlich, 2008 for the transfer of *S. americana* to *Asagena*). All resulting trees were rooted using the tetragnathid *Tetragnatha versicolor*. See Appendix 1 for a list of all examined material.

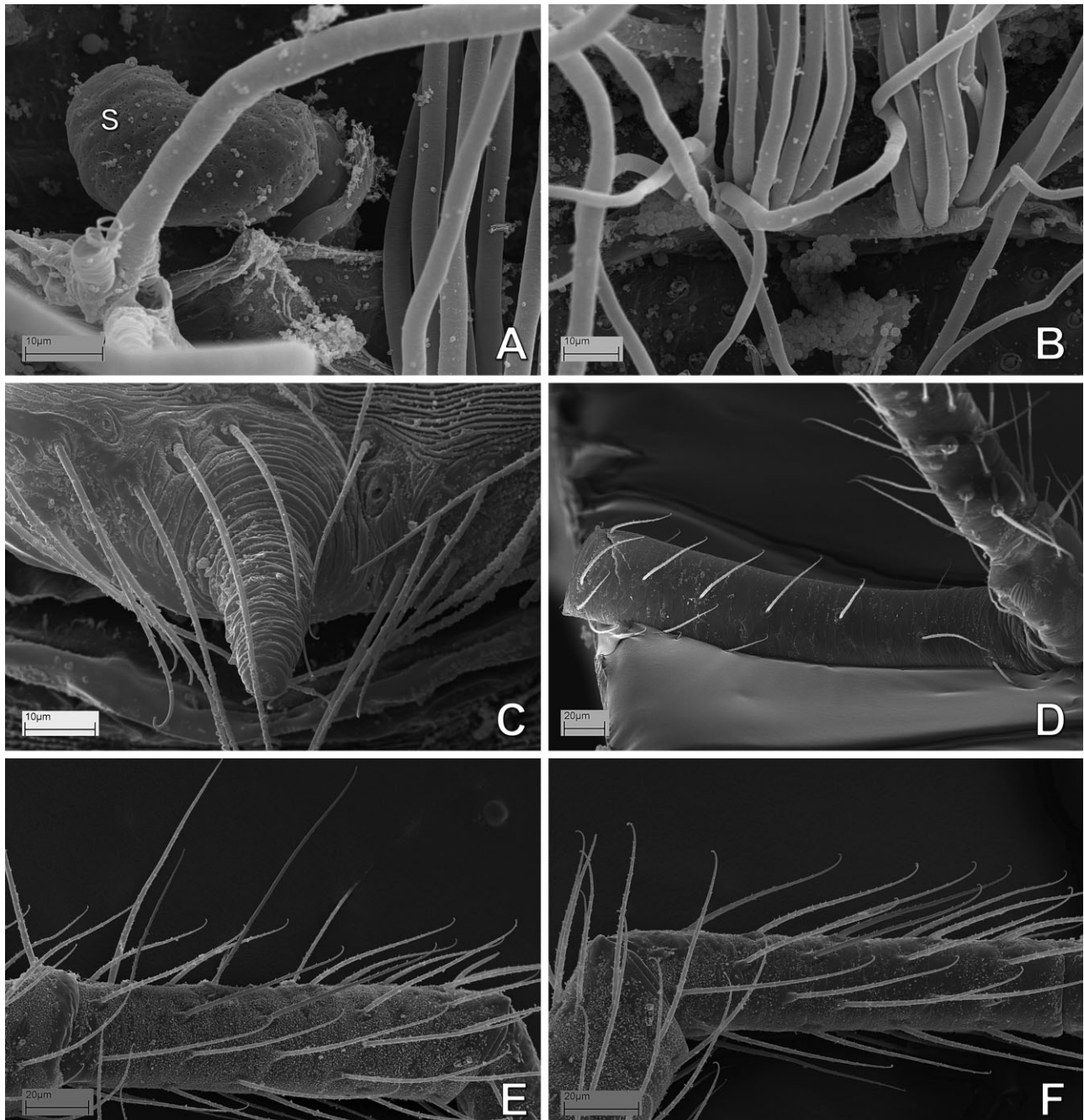


Figure 29. MYSM-005-ARG (*Mysmena*, Mysmenidae) from Misiones, Argentina. A–C, E, F, female; D, male. A, digested abdomen, detail of left spermatheca; B, same, detail of posterior tracheal system; C, epigynal area and scapus; D, left femur I, retrolateral view; E, left tibia IV, prolateral view; F, left metatarsus IV, prolateral view. See Appendix 3 for the list of abbreviations.

METHODS OF STUDY

Morphological and behavioural methods

Specimens were studied using standard morphological techniques in arachnology. Morphological methods of study follow Lopardo (2005) and Lopardo, Hormiga

& Melic (2007). Specimens were initially examined in 80% ethanol using Leica MZAPO or MZ16A stereomicroscopes. Because of their minute size, further detailed observations and illustrations were performed using a Leica DMRM compound microscope with a drawing tube, and Scanning Electron Microscopy

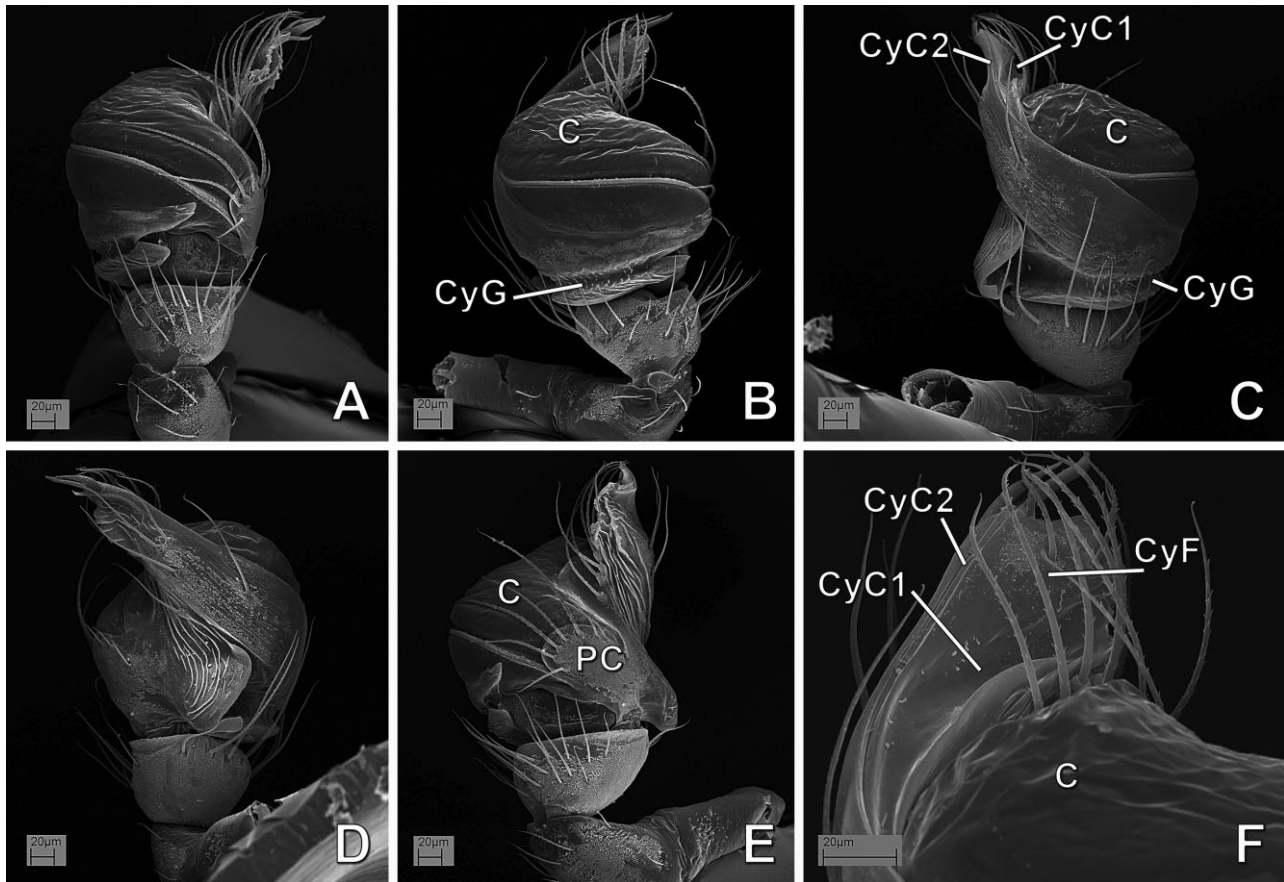


Figure 30. MYSM-007-MEX (*Mysmena*, Mysmenidae) from Chiapas, Mexico; male left palp. A, retroventral view; B, ventral view; C, prolateral view; D, dorsal view; E, retrolateral view; F, detail of tip of palp, ventral–prolateral view. See Appendix 3 for the list of abbreviations.

(SEM; see below). Measurements are in millimetres. Carapace height was measured at the highest point, from carapace lateral edge. Carapace length and height were measured in lateral view; carapace width was taken at its widest point in dorsal view. Abdominal length and height were measured in lateral view, and width at widest point in dorsal view. In most symphytognathoids the abdomen is globular and the position of the pedicel seems to have advanced towards the spinnerets (or *vice versa*), so the length of the abdomen is measured here from the spinnerets to the opposite point in the abdomen, and height is measured as the longest section perpendicular to the length (for a detailed explanation, see characters related to the abdominal morphology in Appendix 2). Leg article lengths were mostly measured using SEM microscopy, and measurements were taken in lateral or dorsal views. Left structures (mostly male palps) are depicted unless otherwise stated. If right palps were used and/or illustrated, images were reversed to facilitate comparisons (and noted in the figure legend). Most hairs and macrosetae are usually not depicted in final palp

and epigynum drawings, unless they provide putative phylogenetic information. As a convention, relative position of sclerites in male palp is stated as if the cymbium were dorsal, regardless of the relative position of the cymbium to the whole palp or the prosoma.

For observation of respiratory structures and female internal genitalia, we used the method of Álvarez-Padilla & Hormiga (2008). Abdomens were bisected horizontally and digested with SIGMA Pancreatin P1750 enzyme complex, in a solution of sodium borate prepared using the concentrations described by Dingerkus & Uhler (1977), as modified by Álvarez-Padilla & Hormiga (2008). Bisected abdomens were left in this solution at room temperature (i.e., 20–25°C) overnight or for a few hours. After enzymatic digestion, abdomens were transferred to distilled water, and then to ethanol.

Digital images of spider habitus and other details were taken with a Leica DFC 500 camera. A composite of multiple digital images taken at varying focal lengths along the *z*-axis was assembled using the software package Leica Application Suite. Most

Table 5. Continued

	0	1	2	3	4	5	6
<i>Brasilionata arborensis</i>	1.3	?	?	?	?	?	?
<i>Calodipoena incredula</i>	?	1.21	0.79	1.97	?	?	?
<i>Calodipoena moootae</i>	1.4	1.23	0.96	1.83	1.3	5.0	?
<i>Calodipoena tarautensis</i>	1.0	1.26	1.04	1.7	1.17	?	?
<i>Calomyspoena santacruxi</i>	1.1	1.16	0.9	1.78	1.19	?	?
<i>Crassignatha haeneli</i>	1.0	?	?	?	1.33	?	?
<i>Iardinis martensi</i>	?	?	?	?	?	?	?
<i>Iardinis mussardi</i>	?	?	?	?	?	?	?
<i>Isela okuncana</i>	1.4	1.04	1.05	1.7	?	?	?
<i>Itapua tembei</i>	?	1.04	0.76	2.0	1.33	5.0	10.0
<i>Kekenboschiella awari</i>	1.1	?	?	?	1.23	3.0	7.0
<i>Kekenboschiella marijkeae</i>	1.2	?	?	?	?	?	?
<i>Leviola termitophila</i>	?	0.86	1.03	1.37	?	?	?
<i>Maymena ambita</i>	1.2	1.71	1.22	1.97	1.09	?	?
<i>Maymena mayana</i>	1.3	1.5	1.21	1.51	1.44	7.0	14.0
<i>Maymena rica</i>	1.3	1.46	1.08	?	1.21	10.0	22.0
<i>Microdipoena elsae</i>	1.1	1.27	0.89	1.94	1.45	7.0	14.0
<i>Microdipoena guttata</i>	1.1	1.19	0.86	1.94	1.26	5.0	11.0
<i>Microdipoena nyungwe</i>	1.1	1.15	0.9	1.67	1.18	5.0	11.0
<i>Kilifina-MYSM-002-KENYA</i>	?	?	?	?	1.15	5.0	12.0
<i>MYSM-005-ARG</i>	1.1	1.1	0.84	1.86	?	5.0	12.0
<i>MYSM-007-MEX</i>	1.0	1.13	0.87	1.8	1.18	4.0	7.0
<i>Mysmena-MYSM-015-MAD</i>	1.2	1.09	0.85	1.82	1.19	4.0	9.0
<i>Mysmena-MYSM-018-MAD</i>	1.2	1.33	0.86	2.01	1.06	3.0	9.0
<i>MYSM-019-MAD</i>	1.3	1.24	0.98	1.87	1.44	5.0	8.0
<i>MYSM-020-MAD</i>	1.5	?	?	?	1.56	5.0	11.0
<i>MYSM-023-MAD</i>	1.0	1.2	0.88	2.13	?	5.0	?
<i>MYSM-028-MAD</i>	?	?	1.04	1.9	1.35	5.0	11.0
<i>MYSM-029-MAD</i>	1.1	1.17	0.79	1.61	1.37	5.0	10.0
<i>MYSM-034-MAD</i>	1.2	1.2	0.91	1.69	1.2	5.0	11.0
<i>Mysmena leichhardtii</i>	1.3	?	0.95	1.7	1.15	4.0	9.0
<i>Mysmena leucoplagiata</i>	1.1	1.09	0.83	2.16	1.17	4.0	10.0
<i>Mysmena tasmaniae</i>	1.2	1.09	0.95	1.83	1.32	?	?
<i>Mysmenella illectrix</i>	?	?	?	?	1.28	?	7.0
	?	?	?	?	?	?	?

Table 5. Continued

	0	1	2	3	4	5	6
<i>Mysmenella jobi</i>	1.1	1.13	0.83	1.95	1.25	?	?
<i>Mysmenella samoensis</i>	?	1.21	1.02	1.8	1.19	6.0	11.0
<i>Mysmeniola spinifera</i>	1.4	?	?	?	?	?	?
<i>Mysmenopsis cidrelicola</i>	1.2	1.1	0.92	1.67	1.35	6.0	?
<i>Mysmenopsis dipluramigo</i>	?	1.21	1.1	2.06	1.53	6.0	15.0
<i>Mysmenopsis palpatis</i>	?	1.2	1.25	1.59	1.04	6.0	11.0
<i>Mysmenopsis penai</i>	1.2	1.31	1.06	1.39	1.13	6.0	11.0
<i>Phricotellus stelliger</i>	1.1	?	?	?	?	?	?
<i>Tamasesia acuminata</i>	1.1	1.44	1.08	1.74	1.3	?	?
<i>Tamasesia rotunda</i>	1.1	1.28	1.09	1.63	1.21	4.0	9.0
<i>Trogloneta cantareira</i>	1.3	1.0	1.11	1.76	1.32	?	11.0
<i>Trogloneta granulum</i>	1.4	1.0	1.22	1.55	0.96	3.0	11.0
SYMPHYTOGNATHIDAE							
<i>Patu-SYMP-001-DR</i>	1.2	1.25	0.67	?	1.28	3.0	9.0
<i>SYMP-002-MAD</i>	1.2	?	0.83	1.93	1.28	3.0	5.0
<i>SYMP-006-AUST</i>	1.1	1.17	0.81	2.05	1.39	3.0	8.0
<i>SYMP-007-AUST</i>	1.1	1.11	0.8	2.01	1.37	3.0	8.0
<i>Symphytognatha picta</i>	?	0.95	0.94	1.81	1.0	3.0	?
SYNAPHRIDAE							
<i>Cepheia longiseta</i>	1.2	0.97	0.91	1.65	1.2	?	4.0
<i>Synaphris saphrynis</i>	?	?	?	?	?	?	?
THERIDIIDAE							
<i>Steatoda americana</i>	1.5	1.02	1.7	1.33	1.12	5.0	20.0
THERIDIOSOMATIDAE							
<i>Theridiosoma gemmosum</i>	1.3	1.32	1.66	1.62	1.16	8.0	19.0
<i>Coddingtonia euryopoides</i>	?	1.27	1.12	1.86	1.15	4.0	16.0
TETRAGNATHIDAE							
<i>Leucauge venusta</i>	1.8	1.35	2.92	1.11	1.05	15.0	63.0
<i>Tetragnatha versicolor</i>	2.8	?	3.2	?	?	22.0	65.0

First 350 characters correspond to discrete characters, last seven characters are continuous. Polymorphic terminals are coded as follows: a = (01); b = (02); c = (03); d = (04); e = (12); f = (13); g = (14); h = (23); i = (34). Inapplicable characters are scored as '-'; missing data as '?'. To facilitate matrix exploration, discrete character scoring is highlighted in bold every tenth character.

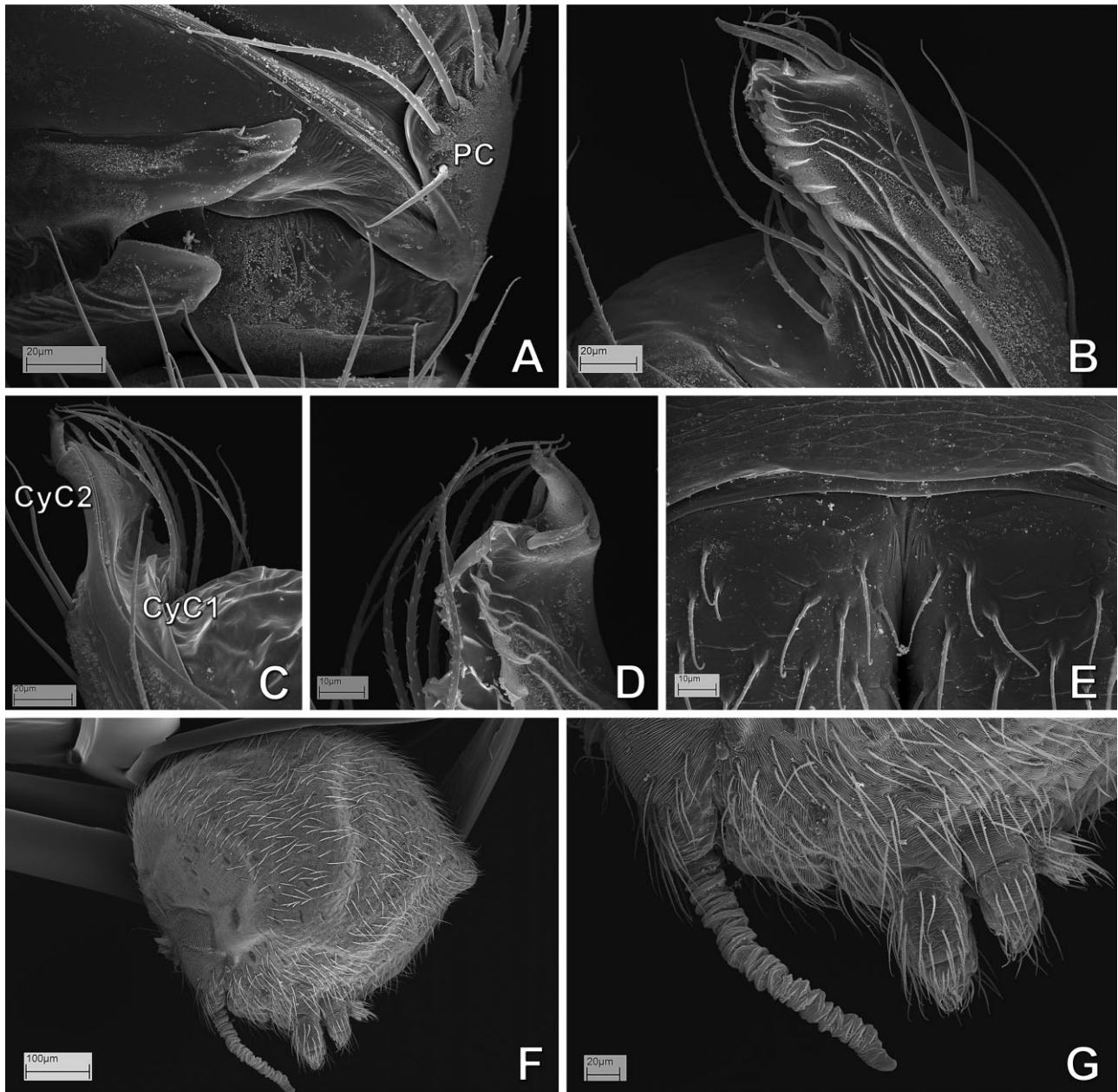


Figure 31. MYSM-007-MEX (*Mysmena*, Mysmenidae) from Chiapas, Mexico; A–D, male left palp; E–G, female. A, detail of proximal palp, prolateral basal expansion and paracymbium, retroventral view; B, detail of dorsal–retrolateral tip of cymbium; C, same, prolateral view; D, same, retrolateral view; E, cheliceral bases, frontal view; F, abdomen, lateral view; G, abdomen, lateral view, detail of scapus and spinnerets. See Appendix 3 for the list of abbreviations.

morphological data used for character scoring was gathered by means of SEM observations. More than 7000 SEM images were taken for all ingroup and most outgroup taxa (~120 images/species). For SEM study, the specimens were dissected; all structures including female digested abdomens were dried using an Autosamdri-815 (Tousimis®, Rockville, MD) critical-point drier. To avoid damage to tracheal and internal

female genitalia, digested abdomens were critical-point dried in separate porous capsules. Specimens were then mounted on aluminum rivets with adhesive copper conductive tape. If the preparation was relatively large, it was attached to the tape with the help of a surrounding fine thread of glue made of an acetone solution of polyvinyl resin (as also explained in Álvarez-Padilla & Hormiga, 2008), and then

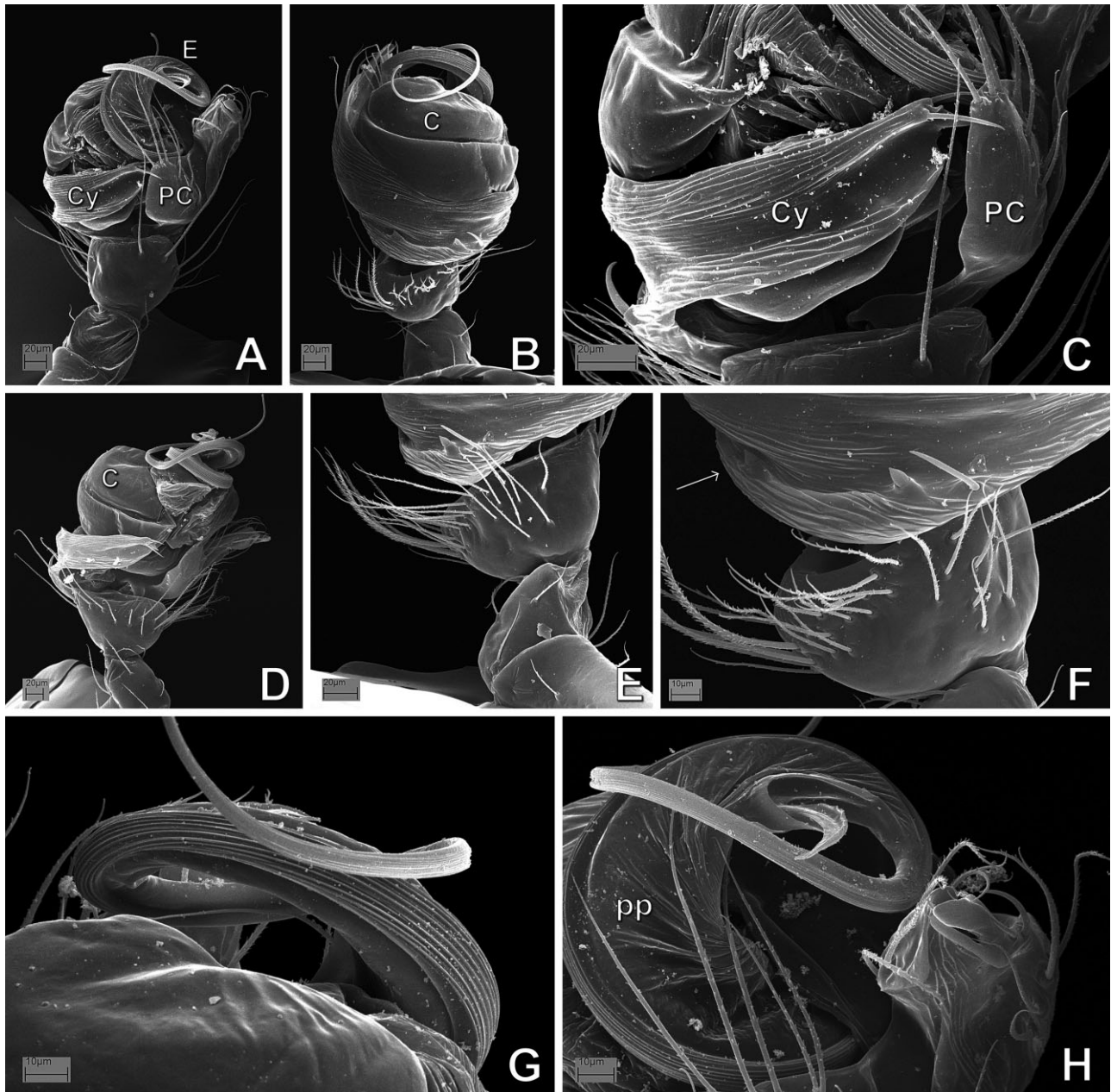


Figure 32. *Mysmena* (= *Calodipoena*) *incredula* (Mysmenidae); male palp. A–C, E–H, left palp; D, right palp, subtly expanded, inverted. A, D retrolateral view; B, ventral–prolateral view; C, detail of proximal palp, retrolateral view; E, detail of tibia and prolateral basal expansion, ventral view; F, same, close up; G, detail of tip of palp, ventral view; H, same, retrolateral view. See Appendix 3 for the list of abbreviations.

sputter-coated with gold-palladium using a Desk II LLC Cold Sputter Coater (Denton Vacuum, Moorestown, NJ, USA). Usually, a maximum of eight preparations (i.e. rivets) were made for each species: four for females (digested abdomen, abdomen, cephalothorax, left legs I + IV) and four for males (abdomen, cephalothorax with right palp attached, left palp, left legs I + IV) (see Appendix 1). Images were taken with a LEO

1430VP scanning microscope at the Department of Biological Sciences SEM facility (George Washington University, GWU).

About 190 camera lucida schematic drawings of female and male genitalia, representing most taxa, were produced in order to visualize complex structures, internal ducts, and to propose hypotheses of primary homology. For observation of internal genitalia, male palps

Table 6. Summary of analyses performed in this study

	Morphological data set	Discrete morphological data set	Morphological data set (including taxa with 78% missing data)
Root	<i>T. versicolor</i>	<i>T. versicolor</i>	<i>T. versicolor</i>
Number of characters	357	350	357
Number of taxa	65	65	70
Number of MPTs	3	3835	3
MPT length	1.512.169	1323	1.545.559
CI	0.366	0.349	0.36
RI	0.666	0.663	0.664
Hits	300	895	21
Informative characters	311	304	312
% informative characters	87.1%	86.9%	87.4%
% uninformative characters	0.0%	0.0%	0.0%
% autapomorphic characters	12.9%	13.1%	12.6%

Composition, resulting statistics, as well as informative character proportions are reported for each data set. Abbreviations: CI, consistency index; MPT, most-parsimonious tree; RI, retention index. 'Informative characters' and their percentages exclude autapomorphic characters; 'Uninformative characters' refer to characters only scored for one constant state.

and female epigyna were dissected and/or digested, and observed under clove oil. Interpretation and drawing of genitalic structures was also facilitated after observation of the same structures under SEM. The presence and details of respiratory systems were directly observed in digested abdomens, preferably under SEM, or when no sufficient material was available, through compound microscopy.

Behavioural data are limited to a few field observations and data from the literature, except for the genus *Synaphris* (Synaphridae). The web architecture of only one synaphrid species is known (*Synaphris lehtineni*). This Ukrainian species builds a small, thin sheet web underneath stones in hollow depressions (Marusik, Gnelitsa & Kovblyuk, 2005: 129). In order to account for web architecture in at least one synaphrid genus (the web of *Cepheia* remains unknown), we scored the web of *Synaphris saphrynis* to be like that of *S. lehtineni*, even though the web architecture of the former species is not known. The web-building behaviour of synaphrids is still unknown. For photography, and to facilitate detailed observations in the field, contrast was increased by dusting webs with cornstarch (Eberhard, 1976; Carico, 1977). Drawing and production of images were performed in Adobe PHOTOSHOP. For definitions of the abbreviations used throughout the figures and text, see Appendix 3.

Morphological and behavioural data

The morphological data set combines 101 new characters proposed here with 256 characters used in five previous studies (in chronological order): Griswold *et al.*

(1998), hereafter referred to as G98 (93 characters); Schütt (2002), hereafter referred to as S02 (156 characters); Schütt (2003), hereafter referred to as S03 (120 characters); Agnarsson (2004), hereafter referred to as A04 (241 characters); and Griswold *et al.* (2005), hereafter referred to as G05 (154 characters). Our selection of previously published data sets was guided mainly by two criteria: a relevant taxonomic sample and a detailed and extensive morphological examination of the study taxa. Two morphological phylogenetic studies included at least two representatives of each symphytognathoid family: Griswold *et al.* (1998) and Schütt (2003). The matrix of the latter study is essentially a subset of the author's previous work on Araneoidea (Schütt, 2002), and therefore all characters investigated by this author were included. As symphytognathoids are of fairly small size (on the order of 1 mm), traditional morphological characters (i.e. at stereomicroscope and compound microscope levels) were not comprehensive enough to encompass their morphological diversity, especially for genitalic features. Only recently has the number of phylogenetic analyses that rely extensively on SEM data been increasing for representatives across spider families. Among those, the data matrix of theridiid spiders by Agnarsson (2004) comprises a large number of characters that focus on spider morphology at the SEM level. Griswold *et al.* (2005) focuses on spinneret gland spigot morphology for a wide variety of entelegyne families. The detailed study of Rix & Harvey (2010) on micropholcommatine anapids was published after the completion of our analyses, and it largely relied on Griswold

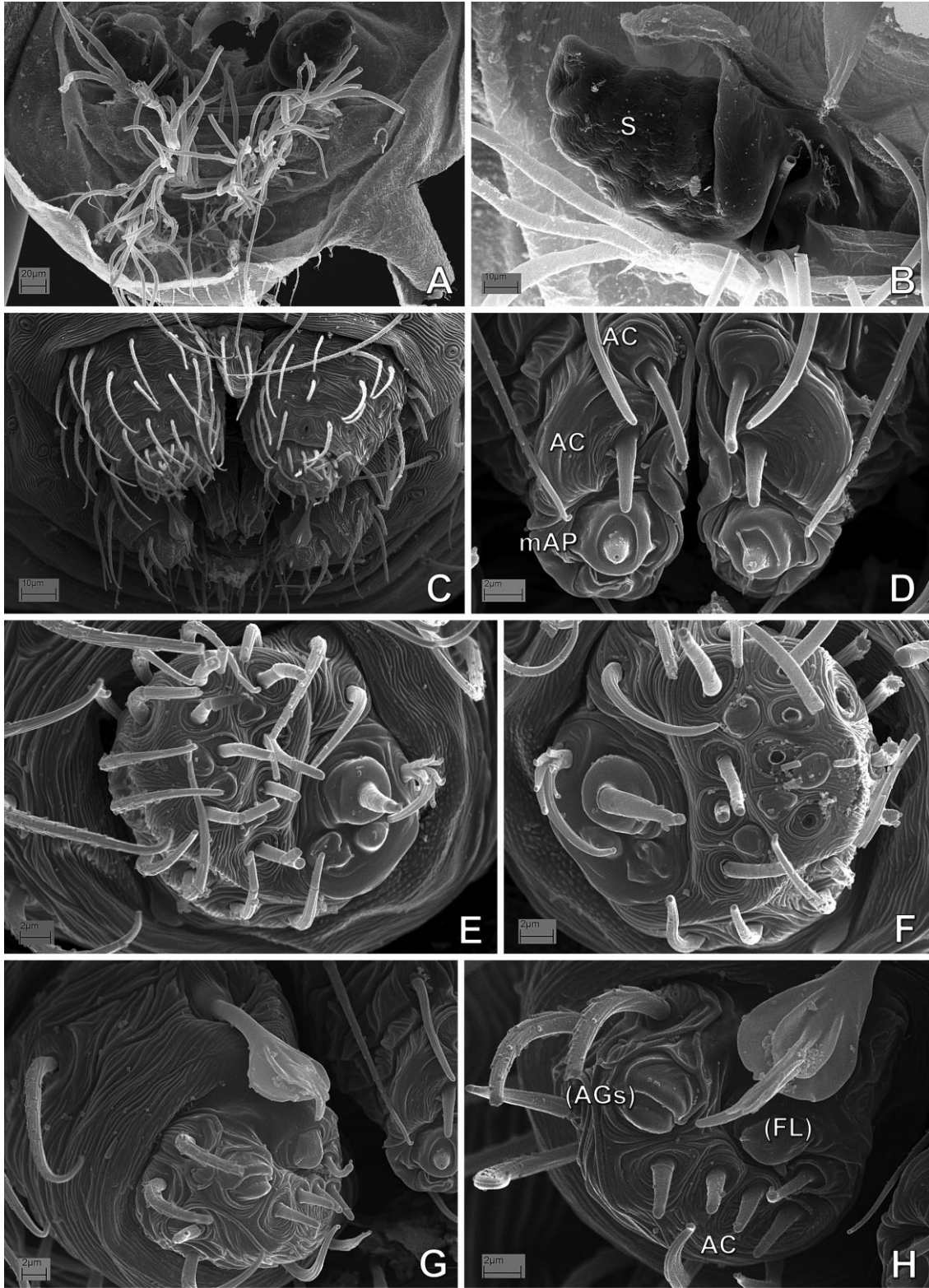


Figure 33. *Mysmena* (= *Calodipoena*) *incredula* (Mysmenidae); abdomen. A, B, female digested abdomen; C–H, male spinnerets. A, tracheal system and vulva; B, same, detail of vulva; C, spinning field, ventral–posterior view; D, posterior median spinnerets; E, right anterior lateral spinnerets (ALS); F, left ALS; G, right posterior lateral spinnerets; H, same, detail. See Appendix 3 for the list of abbreviations.

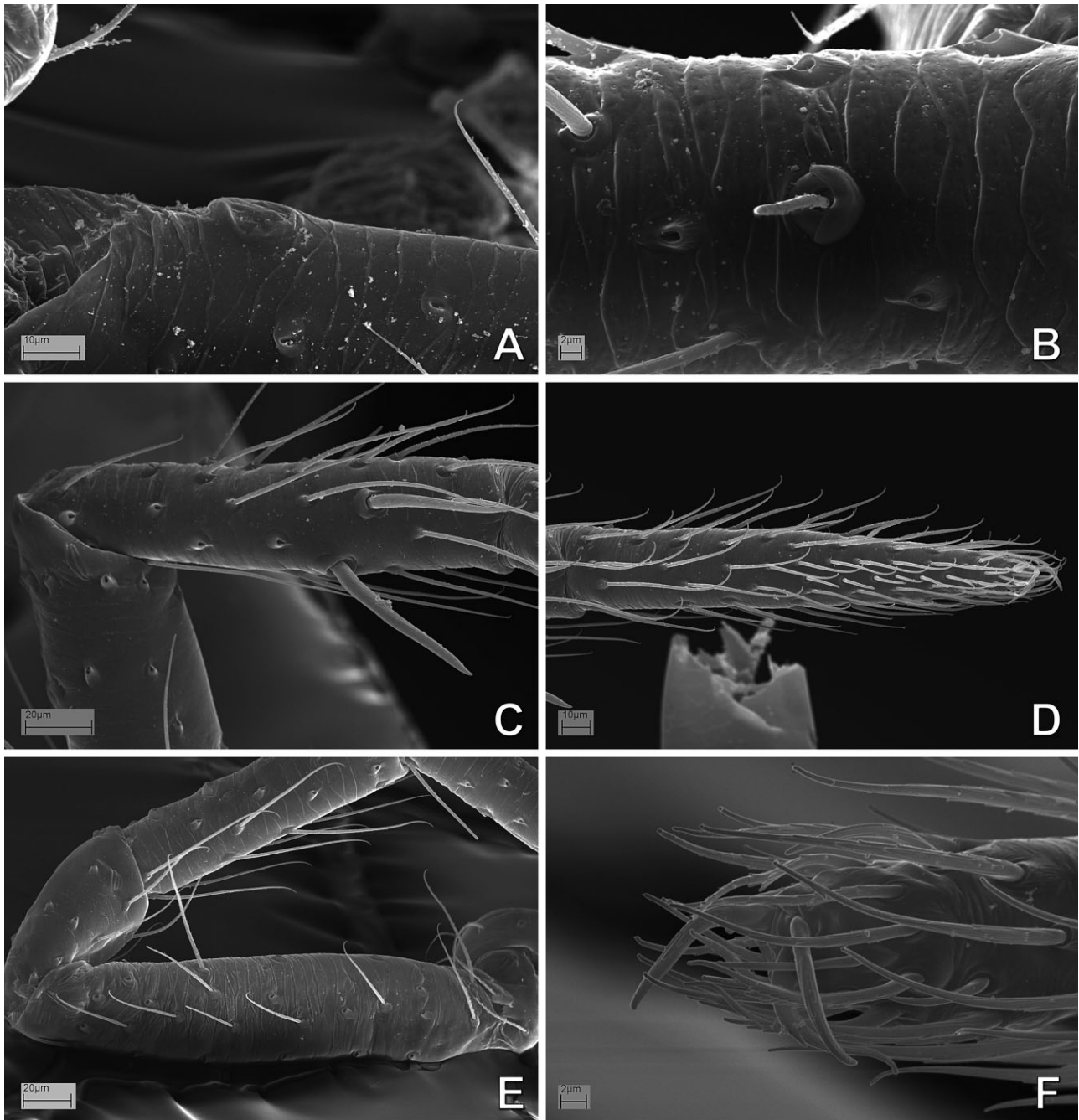


Figure 34. *Mysmena* (= *Calodipoena*) *incredula* (Mysmenidae); legs. A, B, female right leg I; C–F, male left legs. A, femoral spot, retrolateral view; B, metatarsal trichobothrium, dorsal view; C, metatarsus I, prolateral view; D, tarsus I, prolateral view; E, femur IV, prolateral view; F, claws IV, retrolateral view.

et al. (1998) and Lopardo & Hormiga (2008) for characters addressing non-micropholcommatine symphytognathoid relationships.

As most of these five published data sets include taxa not represented in the current study, all published characters (764 characters in total) were evaluated in order to assess their relevance to our taxon sampling. Char-

acter overlap among matrices decreased the number of characters to 530: 256 of those were relevant (i.e. phylogenetically informative or autapomorphic) for our taxonomic sample, including (some with modifications) 249 discrete and seven continuous characters. The remaining 274 characters were inapplicable or uninformative, and are not reported here. In summary,

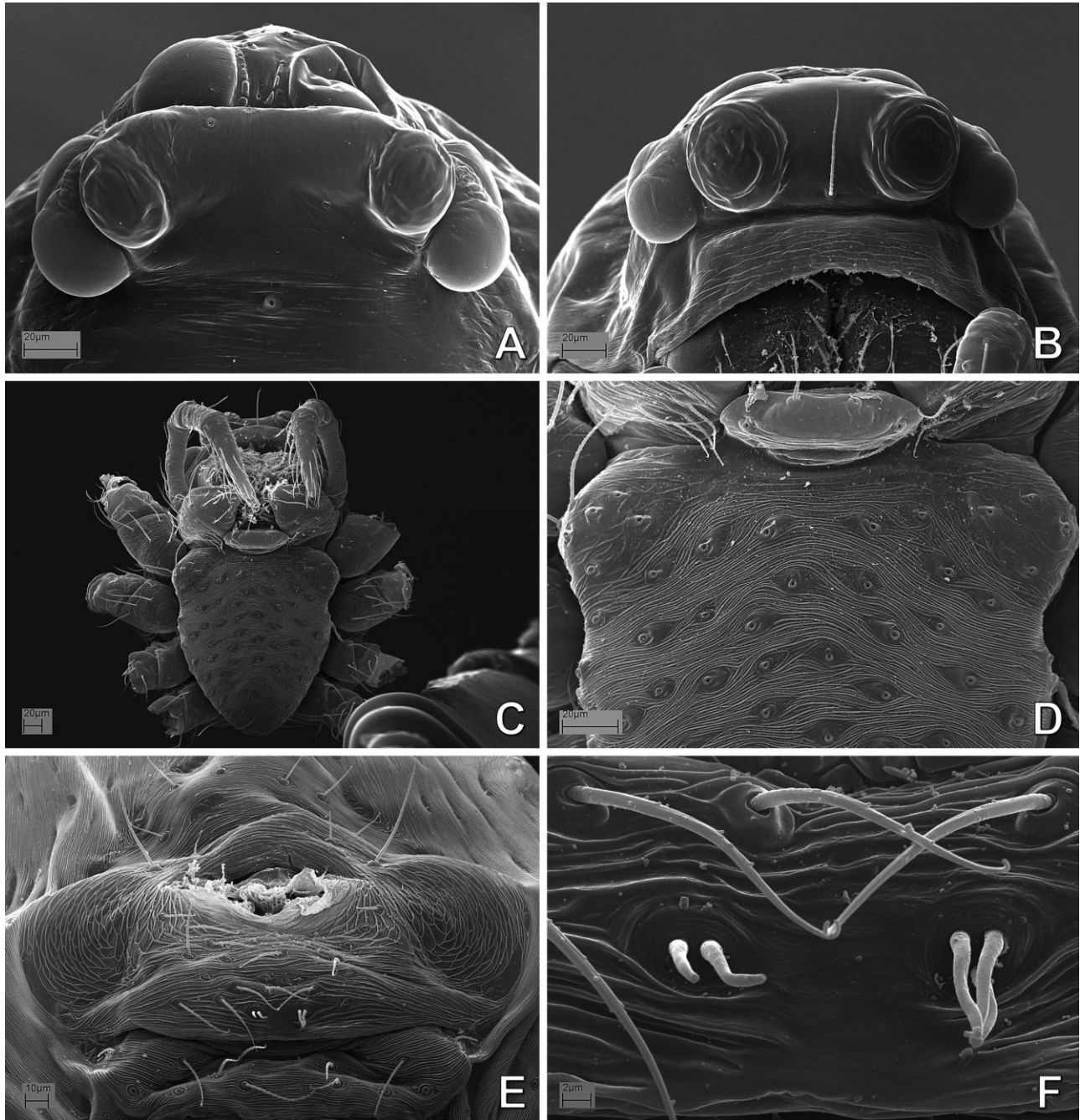


Figure 35. *Mysmena* (= *Calodipoena*) *incredula* (Mysmenidae): A, E, F, male; B–D, female; A, B, ocular area, frontal view; C, prosoma, ventral view; D, same, detail of anterior sternum and labium; E, abdomen, pedicel area and epigastric furrow; F, epiandrous spigots.

the morphological matrix presented here includes 357 characters: 101 new hypotheses of homology plus 256 previously published ones, some of them modified to describe symphytognathoid diversity. All characters comprise features related to the somatic morphology of males and females, internal anatomy, internal and external genitalic structures, and natural history. Char-

acters were grouped into 13 non-overlapping sets: abdomen (including respiratory system); general somatic morphology; cephalothorax; egg sacs; epiandrous fusules; epigynum (internal and external female genitalia); eyes; legs; male palp; mouth parts; palp (female); spinnerets; and web building and other behavioural characters. The morphological data set is summarized in Table 5.

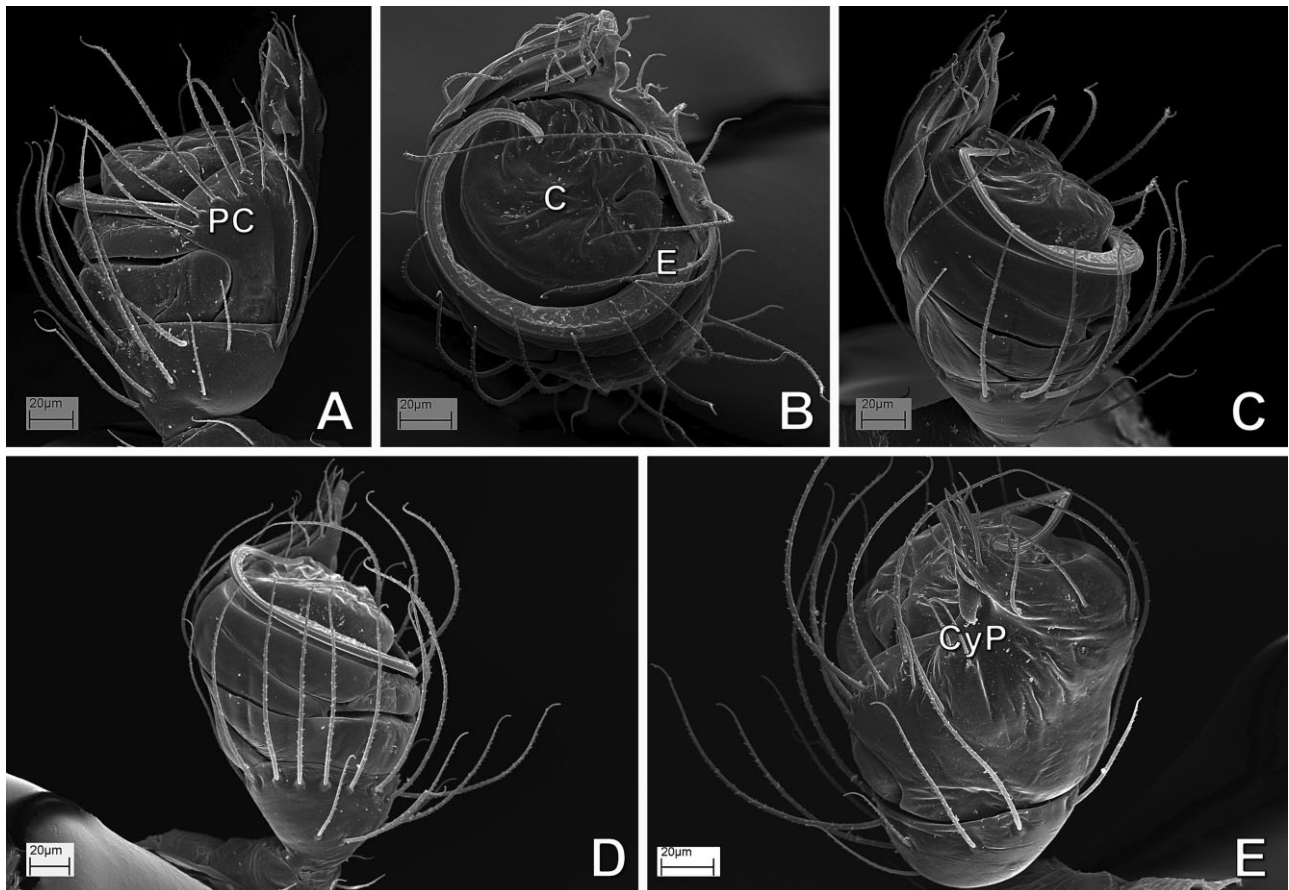


Figure 36. *Mysmena*-MYSM-015-MAD (*Mysmena*, Mysmenidae) from Antananarivo, Madagascar; male left palp; A, retrolateral view; B, distal view; C, prolateral view; D, ventral view; E, dorsal view. See Appendix 3 for the list of abbreviations.

All morphological and behavioural character state definitions used in this study are listed and summarized in Appendix 2, with a brief description of their evolution based on the total-evidence phylogenetic hypothesis. See also Table 4 and Figure 152 for the number of characters for each set and their relative proportions.

PHYLOGENETIC ANALYSES

Evaluation of cladistic hypotheses: search for most-parsimonious trees

Three different phylogenetic analyses were performed. First, the morphological data set (65 taxa and 357 characters) was analysed performing heuristic searches with parsimony under equal weights using TNT 1.1 (Goloboff, Farris & Nixon, 2003b, 2008). The shortest trees were found using the parsimony ratchet (Nixon, 1999a), as implemented in TNT (Goloboff *et al.*, 2003b: program documentation). Heuristic searches consisted of 1000 replicates of random-addition sequences (RASs), followed by 500 iterations of tree bi-

section and reconnection branch swapping (TBR) and the parsimony ratchet (alternating search and perturbation phases, with periodic rounds of original weights), retaining ten trees per replication (commands *ratchet: iter 500 equal; mult = ratchet repl 1000 tbr hold 10;*). To evaluate the familial placement of taxa with more than 78% of missing data in the morphological partition (see Ingroup above), a second analysis was performed, with all scored taxa included into a complete morphological data set (70 taxa, 357 characters). This complete data set was analysed under the same parameters as above, and both resulting phylogenetic hypotheses were compared.

Morphological continuous characters in this data set were treated as ordered, and analysed as such (Goloboff, Mattoni & Quinteros, 2006) with the algorithms recently incorporated into TNT. Continuous characters carry phylogenetic information (e.g. Thiele, 1993; Rae, 1998; Wiens, 2001; Humphries, 2002; Goloboff *et al.*, 2006; González-José *et al.*, 2008), and this treatment avoids the problems with discretization (e.g. loss of information; assignment of different discrete states to

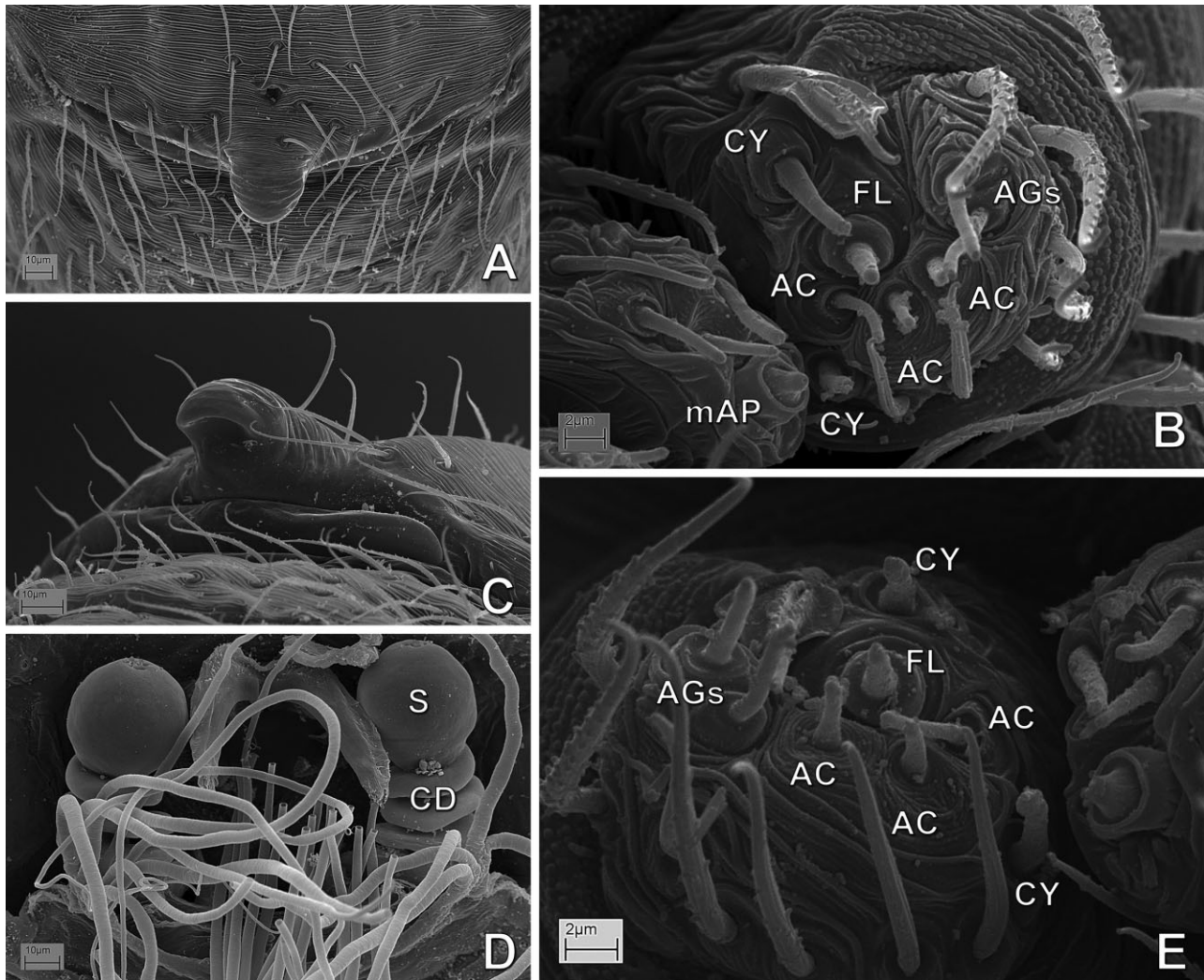


Figure 37. *Mysmena*-MYSM-015-MAD (*Mysmena*, Mysmenidae) from Antananarivo, Madagascar; female abdomen; A, epigynal area and scapus, ventral view; B, left posterior spinnerets (PS); C, same as A, posterolateral view; D, digested abdomen, detail of vulva; E, right PS. See Appendix 3 for the list of abbreviations.

taxa that do not differ significantly and/or vice versa; difficulty of state delimitation with overlapping distributions of measurements) (e.g. Farris, 1990; Wiens, 2001; Humphries, 2002; Clouse, de Bivort & Giribet, 2009; de Bivort, Clouse & Giribet, 2010). Measurements used in the morphological data set appear to correlate well with taxonomic groups (see Fig. 155A–G); they were taken from one specimen and assumed to represent the species, although when available, several specimens of each species were compared in order to ensure the constancy of measurements. The data set includes seven continuous characters, all of them originally proposed as discrete. Two continuous characters represent meristic counts of large ranges (original character A04 – 211, 205); and the remaining five characters correspond to ratio characters (i.e.

not direct measurements; original characters S02 – 61, 64, 89; S03 – 27, 29; and A04 – 184, 185, 186, 187). Scoring of characters based on ratios is problematic as they may conceal information about which of the two features measured is actually undergoing change (i.e. changes in either feature can produce identical ratios, and therefore similar ratios may originate in different ways; e.g. Hormiga, Scharff & Coddington, 2000). As identical ratios may require different evolutionary explanations, each of the measured features should ideally be evaluated independently. In addition, all five ratio characters in this data set are related to shape or size (as either abdominal shape or leg segment lengths). Our taxon sample varies greatly in body size, from 7 mm to less than 1 mm (body length scored in character 34), and therefore all features

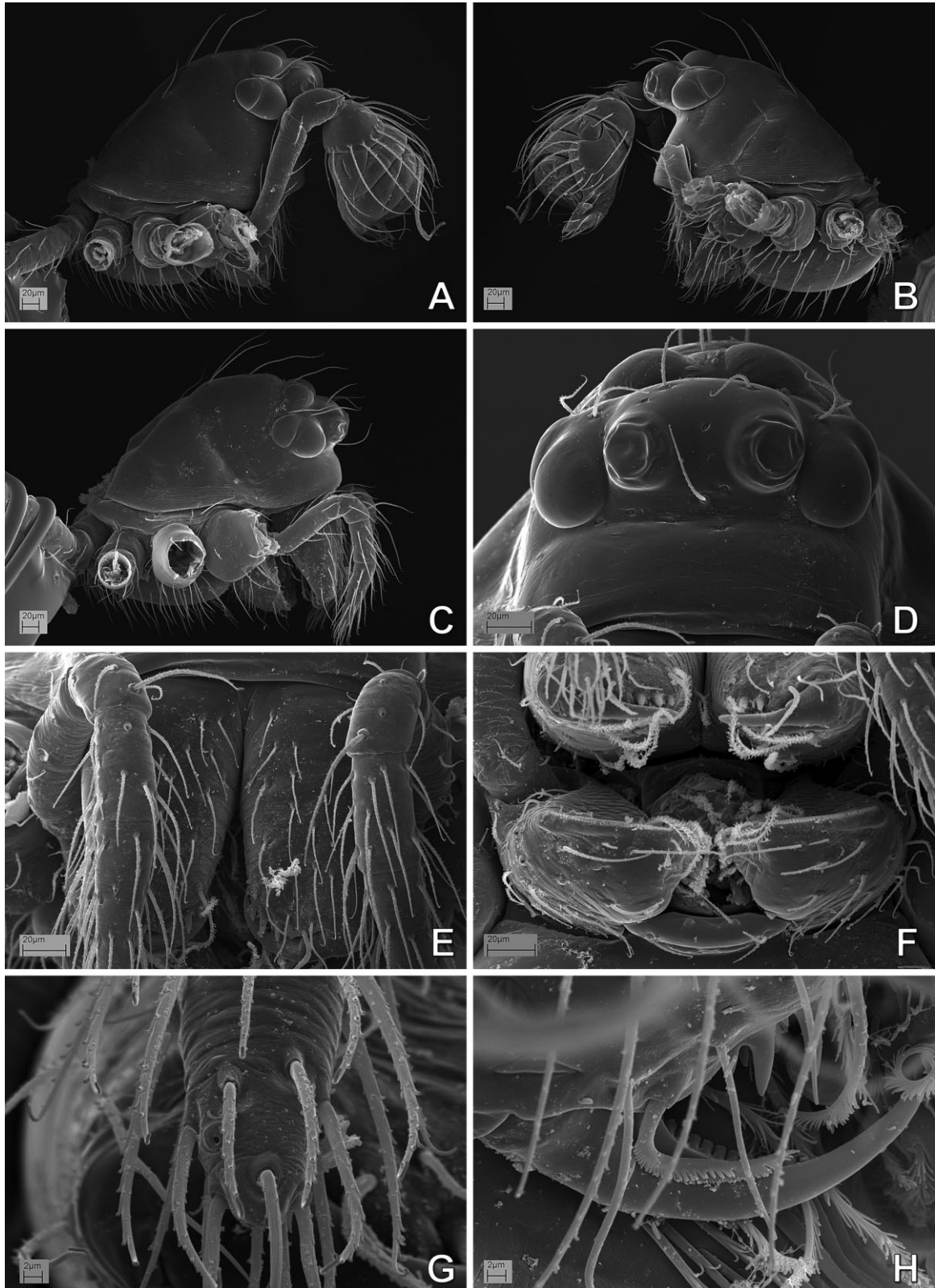


Figure 38. *Mysmena*-MYSM-015-MAD (*Mysmena*, Mysmenidae) from Antananarivo, Madagascar; prosoma: A, B, male; C–H, female; A–C, lateral view; D, carapace, frontal view; E, chelicerae and palps, frontal view; F, mouthparts, ventral view; G, right palp, detail of palpal tip; H, distal promargin of right chelicera.

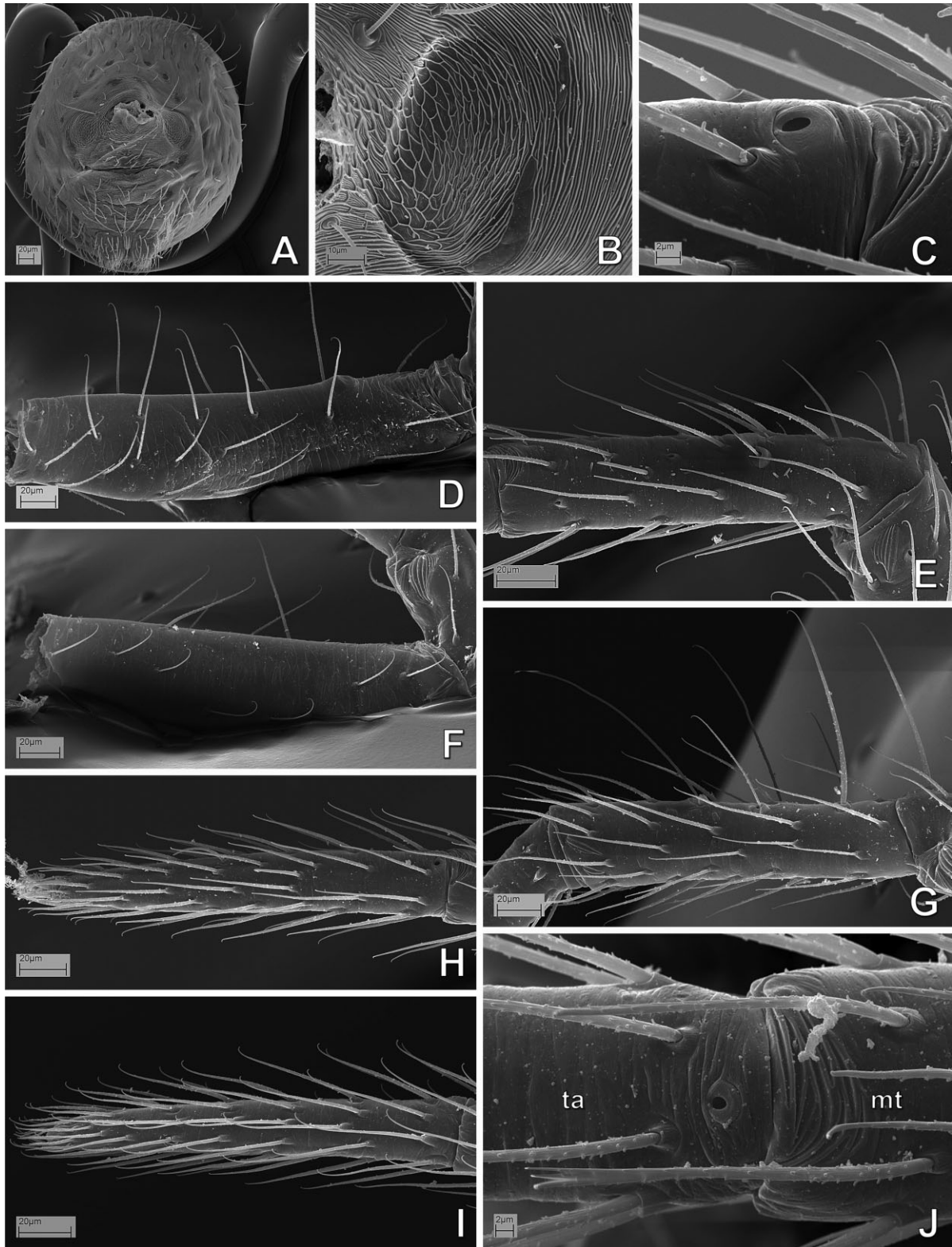


Figure 39. *Mysmena*-MYSM-015-MAD (*Mysmena*, Mysmenidae) from Antananarivo, Madagascar; abdomen and left legs: A, C, male; B, D–J, female. A, abdomen, ventral view; B, booklung cover; C, leg I, tarsal organ, retrolateral view; D, femur I, retrolateral view; E, metatarsus I, retrolateral view; F, femur IV, retrolateral view; G, tibia IV, retrolateral view; H, tarsus I, retrolateral view; I, tarsus IV, retrolateral view; J, leg IV, metatarsus–tarsus junction, dorsal view.

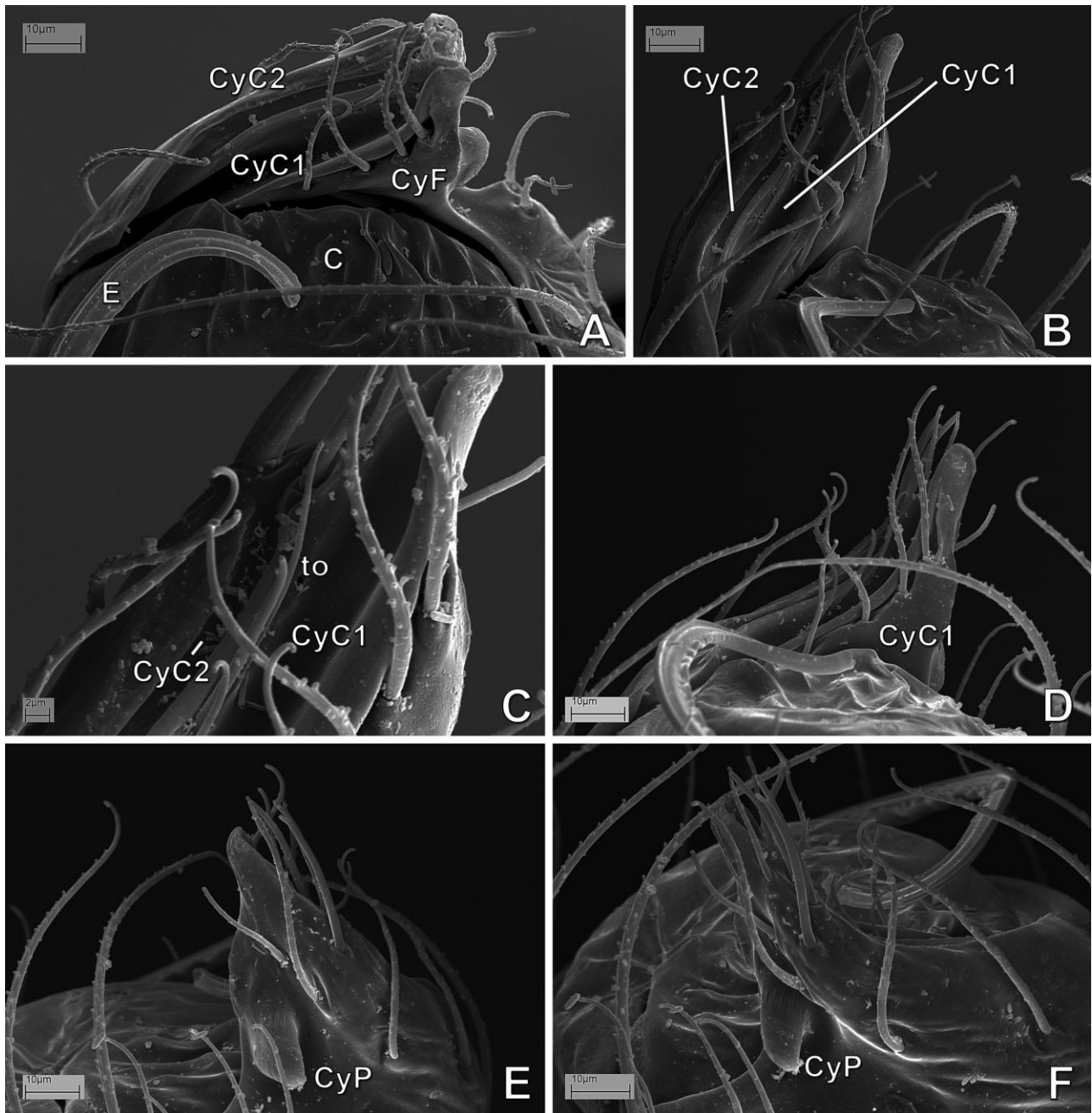


Figure 40. *Mysmena*-MYSM-015-MAD (*Mysmena*, Mysmenidae) from Antananarivo, Madagascar; male left palp, details. A, ventral-distal view; B, prolateral view; C, same, close up; D, ventral view; E, retrolateral view; F, dorsal view. See Appendix 3 for the list of abbreviations.

measured in ratio characters are dependent on body size, but not on their ratios. If measurements scored in each of the ratio characters are included as separate characters, then these characters would be highly correlated and size variation would be scored many times under different names. Consequently, these measurements are included here as ratio characters, in spite of missing evolutionary information. Given the

subjectivity of the discretization and the lack of state definitions in the original discrete ratio characters, this coding represents an improvement in the objectivity of their definition, and can further elucidate a tendency (if any) of change in proportion throughout the phylogenetic history of these features. We carried out a third phylogenetic analysis to explore the influence of the phylogenetic signal of the seven continuous

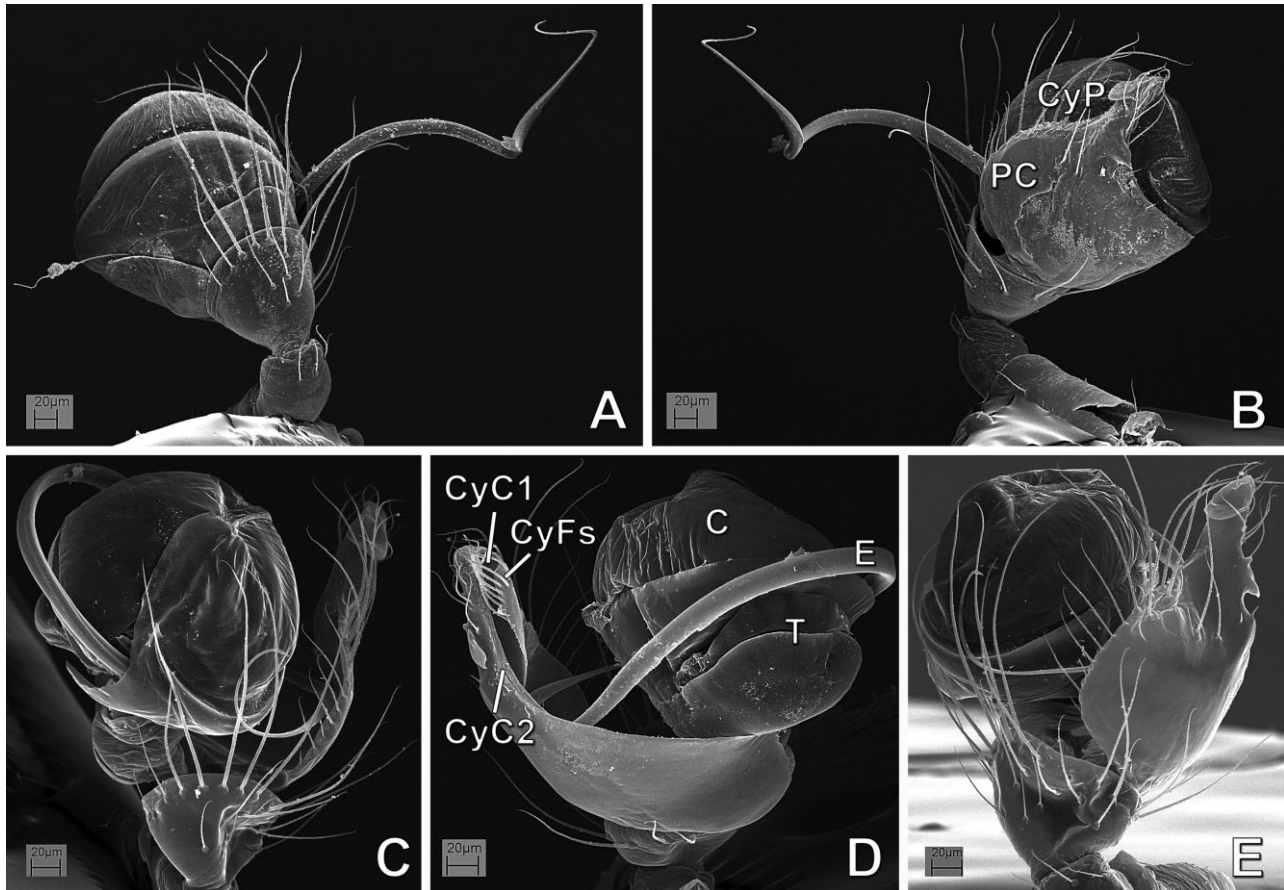


Figure 41. *Mysmena leichhardti* (Mysmenidae) from Queensland, Australia; male left palp. A, prolateral–ventral view; B, dorsal view; C, retrolateral–ventral view; D, prolateral view; E, retrolateral view. See Appendix 3 for the list of abbreviations.

characters by removing them from the original morphological data set. The modified data set containing only discrete characters (65 taxa, 350 characters) was analysed under the same heuristic search parameters. In addition, we compared the changes in the symmetric resampling frequencies (see below) for the clades shared between the resulting cladograms from both analyses (Goloboff *et al.*, 2006).

Internal branches were considered unsupported and collapsed during searches if they were supported ambiguously (when some optimization lacks support, ‘rule 1’ of TNT; i.e. the minimum length is zero; see discussion in Coddington & Scharff, 1994). All discrete multistate characters were treated as unordered (non additive; Fitch, 1971). For complex characters, reductive (binary) coding was maximized as much as possible in the data set. In this coding, a multistate character is usually split into a number of characters, where generally absence and presence are treated separately from the remaining qualities. This method introduces inapplicable scores in the matrix (which are

treated as missing data by the current phylogenetic software), with the known risk associated with inapplicable characters for optimization (see Maddison, 1993). Nevertheless, it minimizes redundancy and dependency among characters (Maddison, 1993; for a review and discussion of coding methods and the problem of inapplicable character states, see also Strong & Lipscomb, 1999). State transformations are considered synapomorphies for a given node only if they are unambiguous and shared by all dichotomous most-parsimonious trees; however, comments on putative (i.e. ambiguously optimized) synapomorphies for clades and for taxa are also discussed. Putative synapomorphies may result from inapplicable scoring, from abundant missing information, or simply from ambiguity resulting from scoring of different states around the node of interest. Nevertheless, when these features occur exclusively within a clade of interest (or at least in most of its representatives), they are reported here as putative synapomorphies. Resulting cladograms are summarized in strict

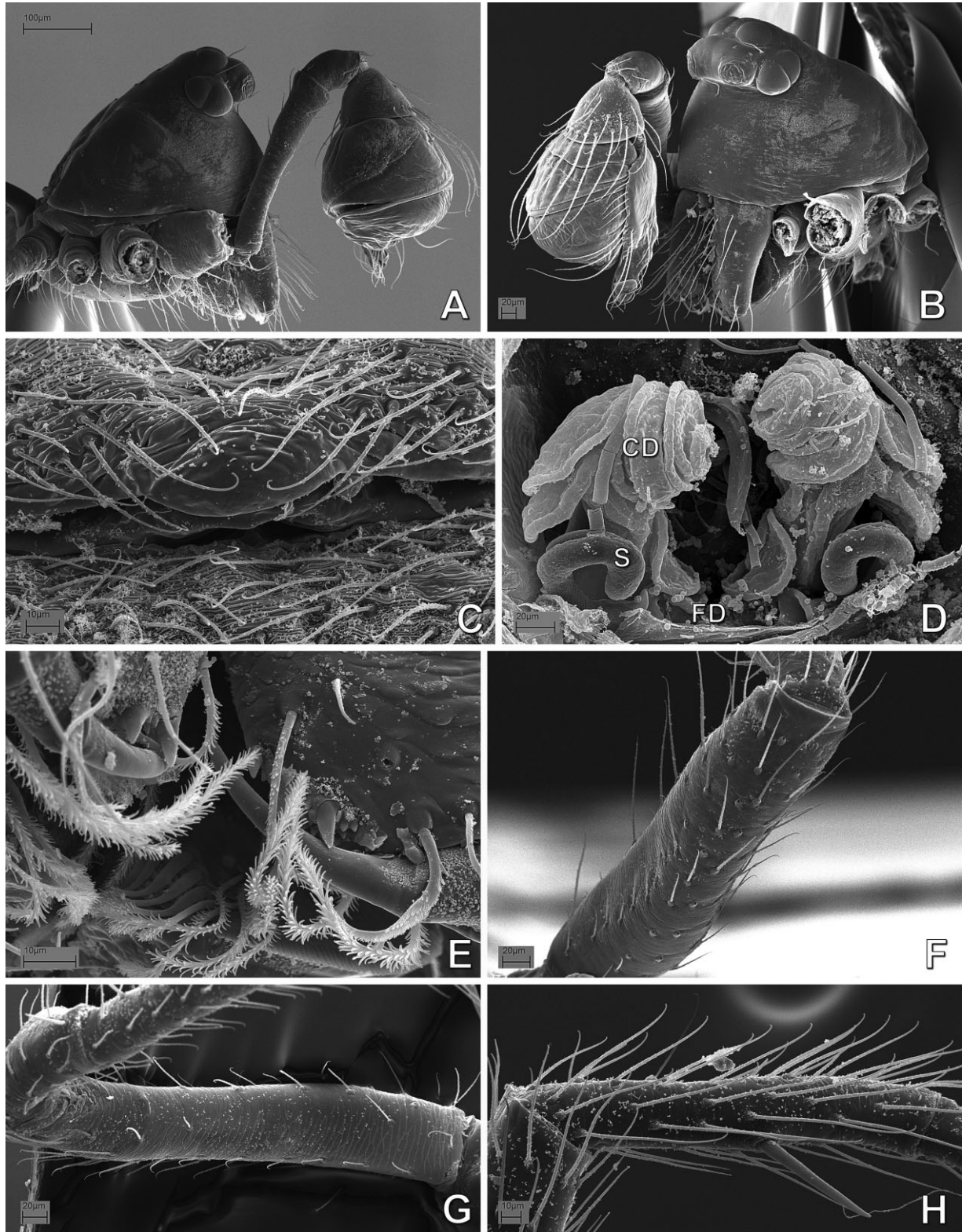


Figure 42. *Mysmena leichhardti* (Mysmenidae) from Queensland, Australia: A, B, E, G, H, male; C, D, F, female. A, prosoma, lateral view; B, same, lateral–frontal view; C, epigynal area and scapus, ventral view; D, digested abdomen, detail of vulva, tracheae removed; E, mouthparts, distal view; right femur I, prolateral–dorsal view; G, left femur I, ventral view; H, left metatarsus I, prolateral view. See Appendix 3 for the list of abbreviations.

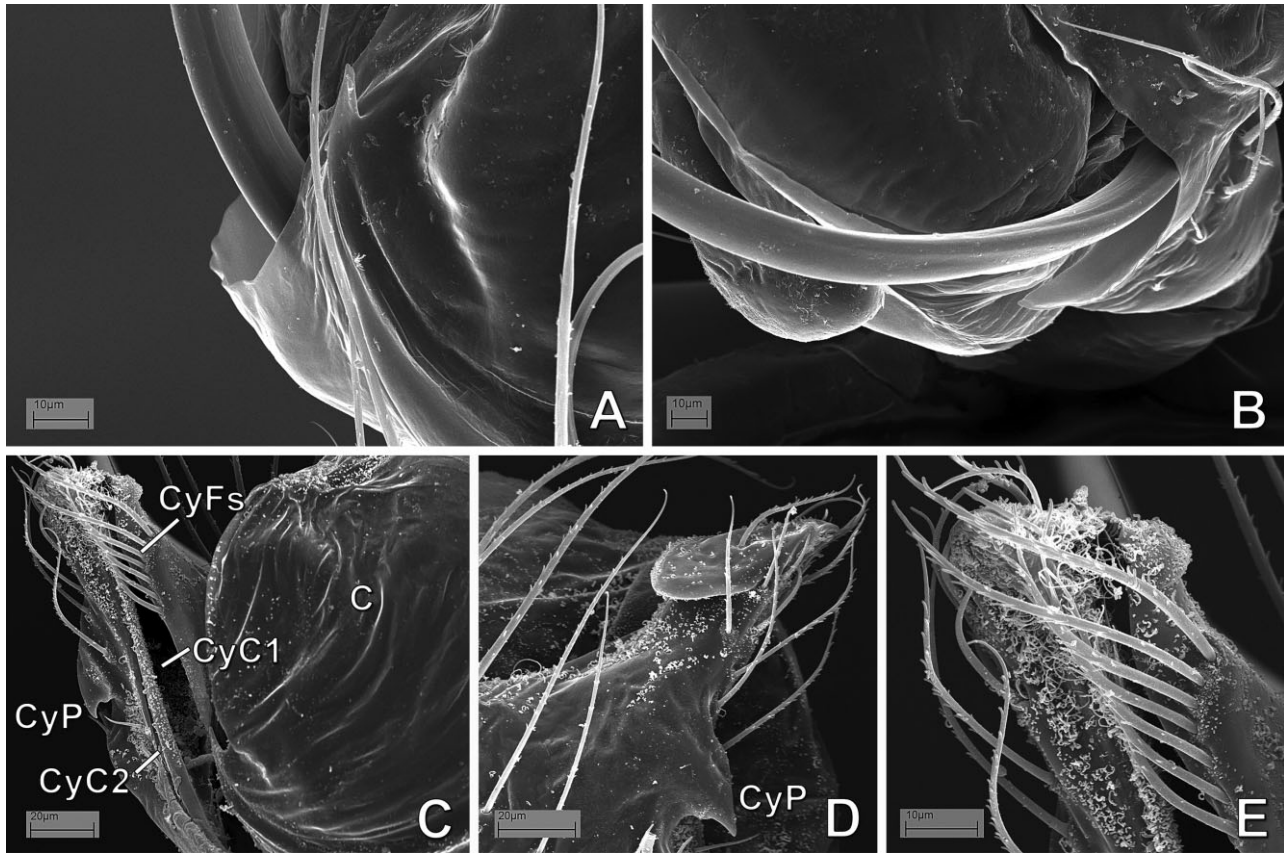


Figure 43. *Mysmena leichhardti* (Mysmenidae) from Queensland, Australia; male left palp, details. A, B, embolus–conductor interaction; C, distal palp, distal–prolateral view; D, dorsal cymbial tip; E, ventral–prolateral cymbial tip. See Appendix 3 for the list of abbreviations.

consensus for each analysis. The character matrix (Table 5) was edited and managed using MES-QUITE 2.01 (Maddison & Maddison, 2007). Character state optimizations and tree editing were performed in WINCLADA (Nixon, 1999b).

SENSITIVITY ANALYSES

To explore the sensitivity of the data to variation in analytical parameters, i.e. the effect of data perturbation on phylogenetic results ('sensitivity analysis' *sensu* Wheeler, 1995; see also Giribet, 2003), the morphological data set (65 taxa, 357 characters) was analysed under parsimony using differential character-weighting schemes. Although the analyses were performed here solely to explore the stability of relationships proposed in the preferred phylogenetic hypotheses, the sensitivity of groups to changes in the analytical parameters might also provide an insight to the support of groups (Giribet, 2003). Stable clades and taxa relationships remain invariable under a wide range of parameters, whereas unstable relationships remain only under fewer particular parameters. The

data set was analysed under different weighting regimes against homoplasy, using implied weighting (Goloboff, 1993). Sensitivity of the results to variations in the strength of the weighting function was assessed performing heuristic searches (same commands as above) using integer values of the constant of concavity (k). The selection of 11 different concavities representing a range of 100 values was based on preliminary analyses of the morphological data set under all concavities (1–100, not shown). The k values chosen were: 1, 2, 3, 6, 8, 10, 12, 20, 35, 50, and 99. We plotted the stability of clades as 'Navajo rugs' (sensitivity plots; Giribet & Edgecombe, 2006) at the nodes in the strict consensus of the equal-weights hypotheses.

SUPPORT VALUES: CLADE SUPPORT

We calculated three clade support measures using TNT: Bremer support, relative Bremer support, and symmetric resampling frequencies.

Bremer support measures

The Bremer support (BS; Bremer, 1988, 1994) of a clade represents the number of extra steps a

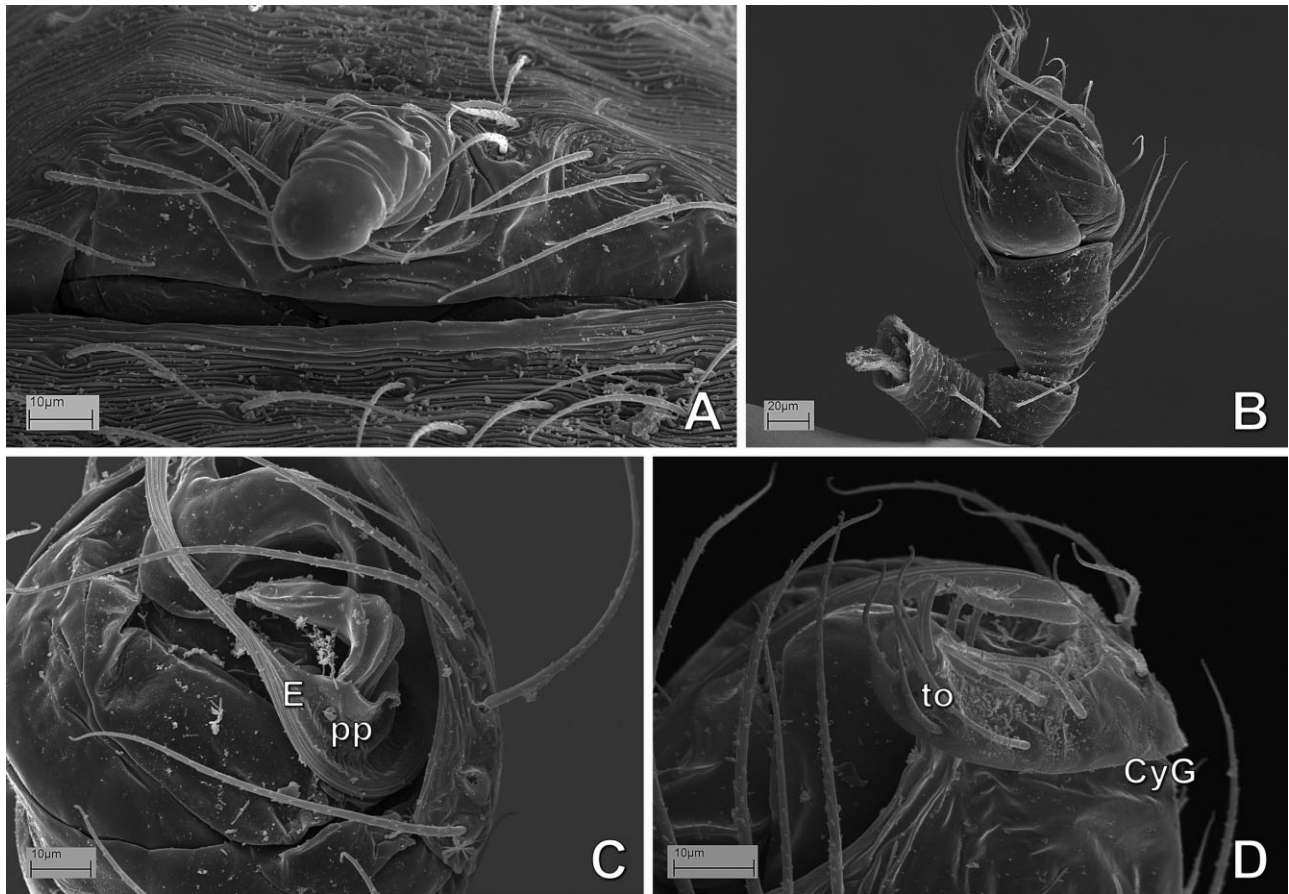


Figure 44. *Mysmena*-MYSM-018-MAD (*Mysmena*, Mysmenidae) from Mahajanga, Madagascar: A, female epigynal area and scapus, ventral–posterior view; B–D, male left palp; B, prolateral view; C, detail of embolus and pars pendula, retrolateral–ventral view; D, cymbial distal tip. See Appendix 3 for the list of abbreviations.

most-parsimonious tree requires to collapse the monophyly of that clade. BS was calculated heuristically searching for suboptimal trees using the optimal trees as a starting point. TBR branch swapping was performed until the tree-buffer was filled, gradually increasing the number of steps of suboptimals by one (from 1 to 12) then by two (from 12 to 22), expanding the numbers of retained trees in intervals of 3000 each time, (from 2000 to 50 000, with a series of commands similar to *sub 1 hold 2000; bb = tbr fillonly; sub 2 hold 5000; bb = tbr fillonly;*). The lowest values of BS are reported. The relative Bremer support (relative fit difference, RFD; Goloboff & Farris, 2001), takes into account the relative levels of evidence, contradictory and favourable, for a clade (ranging from 0 to 100%, for highly contradicted and highly supported groups, respectively). The RFD was calculated in the same manner as the BS using only suboptimal values in a number of steps no greater than the BS of the group (i.e. only suboptimal trees within absolute support; command *bsupport;*).

Symmetric resampling frequencies

Absolute symmetric resampling frequencies (SFqs) were calculated by computing 4000 pseudoreplicates (probability of character elimination: 0.33), performing heuristic searches consisting of ten random-addition sequences (RASs), followed by ten iterations of TBR, holding one tree (commands *mult: noratchet repl 10 tbr hold 1; resample sym repl 4000 freq from 0 [mult];*). SFq and frequency differences (GC, Goloboff *et al.*, 2003a) are reported in the strict consensus of Figs 154, 157, and 158. The GC is the absolute frequency of a group, minus the frequency of the most frequent contradictory group (ranging from 100 to –100% for best to worst support, respectively). Both GC and absolute symmetric frequencies have been shown to be less biased than traditional bootstrap or jackknifing estimations (Goloboff *et al.*, 2003a). In addition to symmetric resampling, we also calculated group frequencies under traditional bootstrap (Felsenstein, 1985) and jackknife (Farris *et al.*, 1996; Farris, 1997; Goloboff *et al.*, 2003a) resampling schemes (same search strategies,

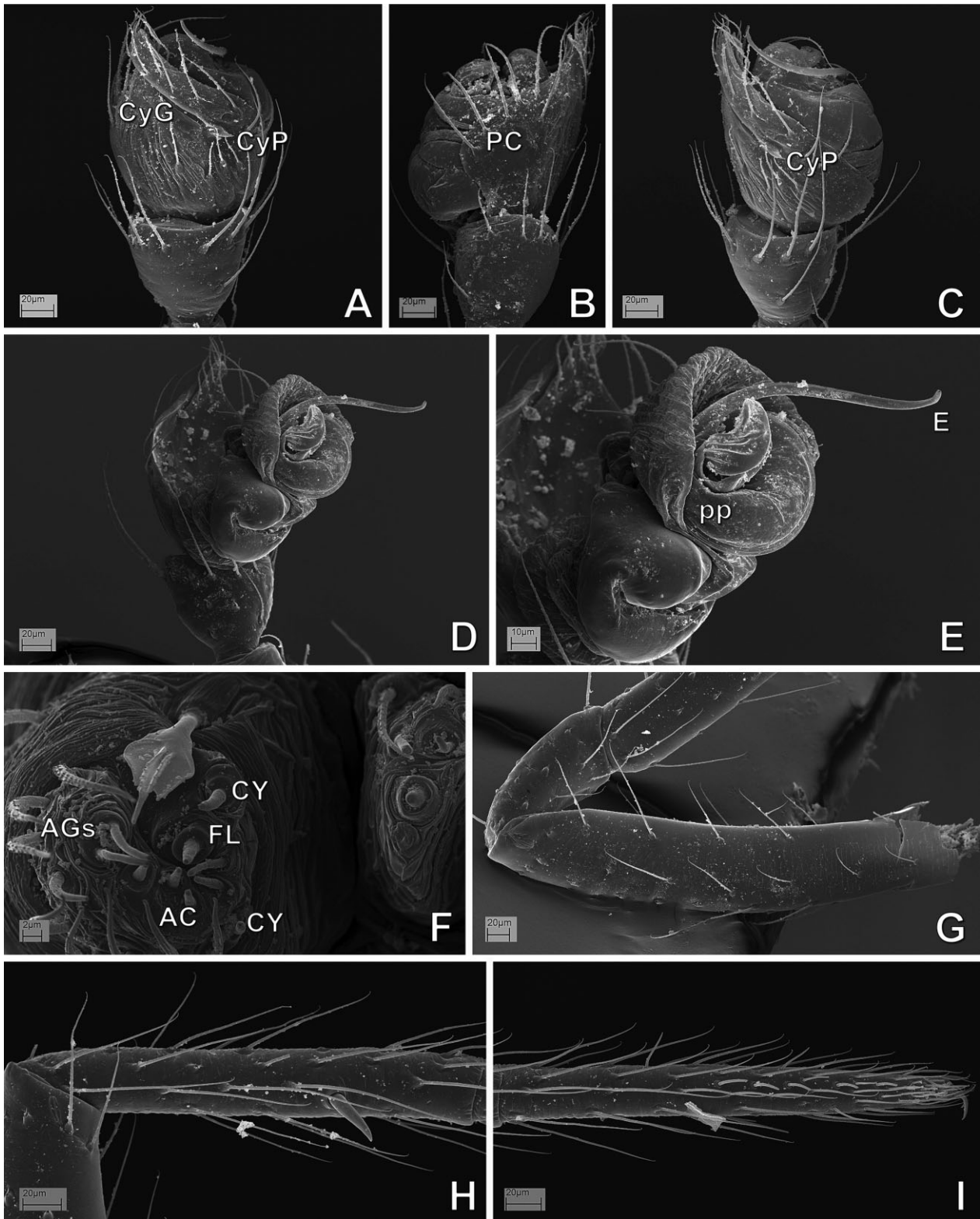


Figure 45. MYSM-019-MAD (Mysmeninae, Mysmenidae) from Toliara, Madagascar. A–C, male right palp, inverted; A, dorsal view; B, retrolateral view; C, prolateral view. D, E, male left palp, expanded; D, prolateral–ventral view; E, same, detail of embolus and pars pendula; F, female posterior spinnerets; G–I, male left leg I, prolateral view; G, femur and patella; H, metatarsus; I, tarsus. See Appendix 3 for the list of abbreviations.

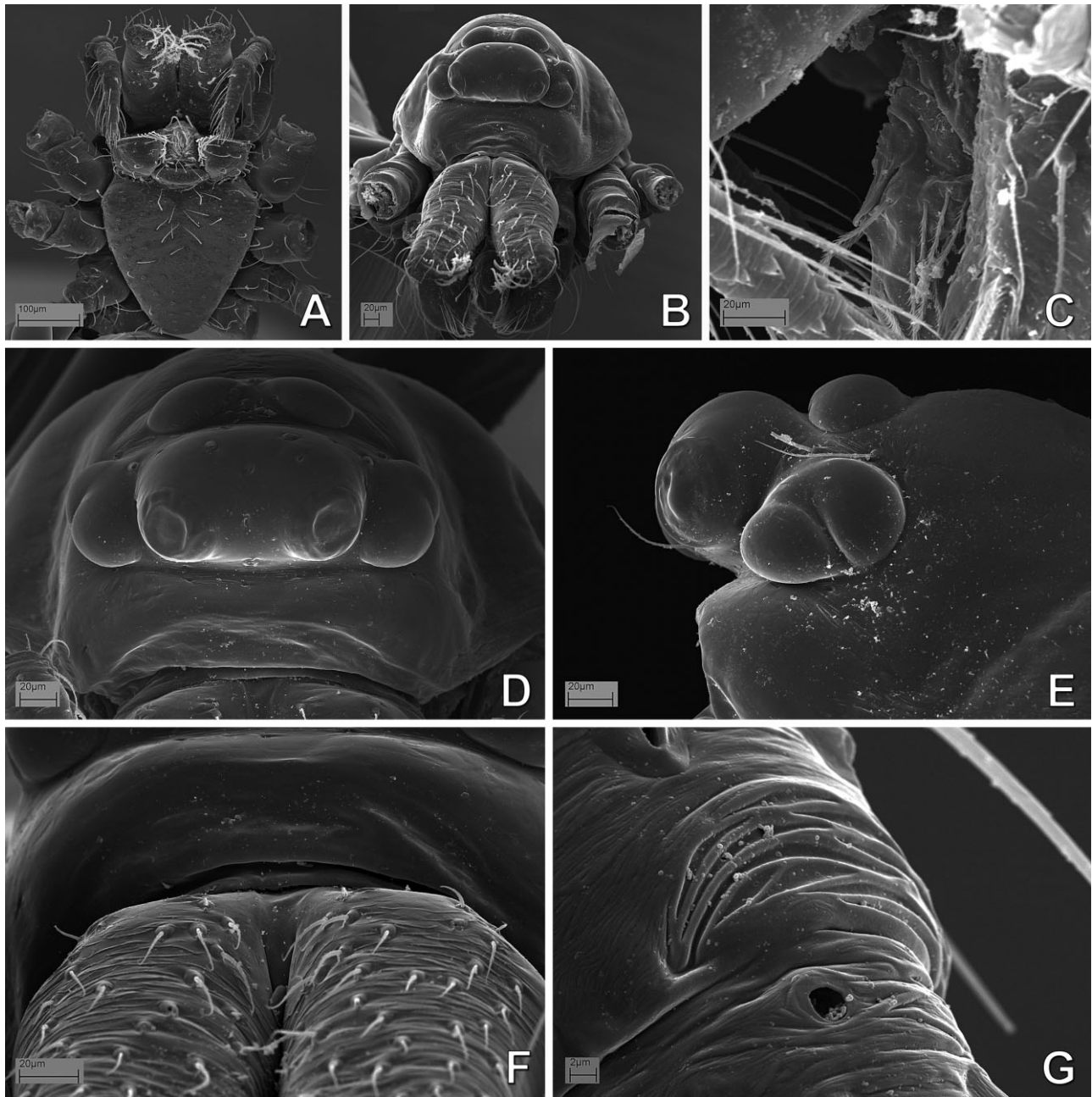


Figure 46. MYSM-019-MAD (Mysmeninae, Mysmenidae) from Toliara, Madagascar. A, C, D, F, G, female; B, E, male. A, prosoma, ventral view; B, same, frontal view; C, labrum, lateral view; D, ocular area, frontal view; E, same, lateral view; F, cheliceral bases, frontal view; G, right leg I, tarsal organ and tarsus–metatarsus junction.

with commands *boot* or *jak* instead of *sym* for bootstrap or jackknife resampling, respectively), expressed as absolute frequencies or frequency differences (not shown). Because all values were highly correlated, we only report the symmetric resampling values.

For the support values calculated in the analyses and reported below, we refer to low support for values 0.01–2.50 (BS), 0–39 (RFD), and 50–73% (SFq); inter-

mediate support for values 2.51–8 (BS), 40–79 (RFD), and 74–85% (SFq); and high support for values 8.01 or higher (BS), 80–100 (RFD), and 86–100% (SFq).

RESULTS

The following section reports the results of all morphological cladistic analyses performed in this study.

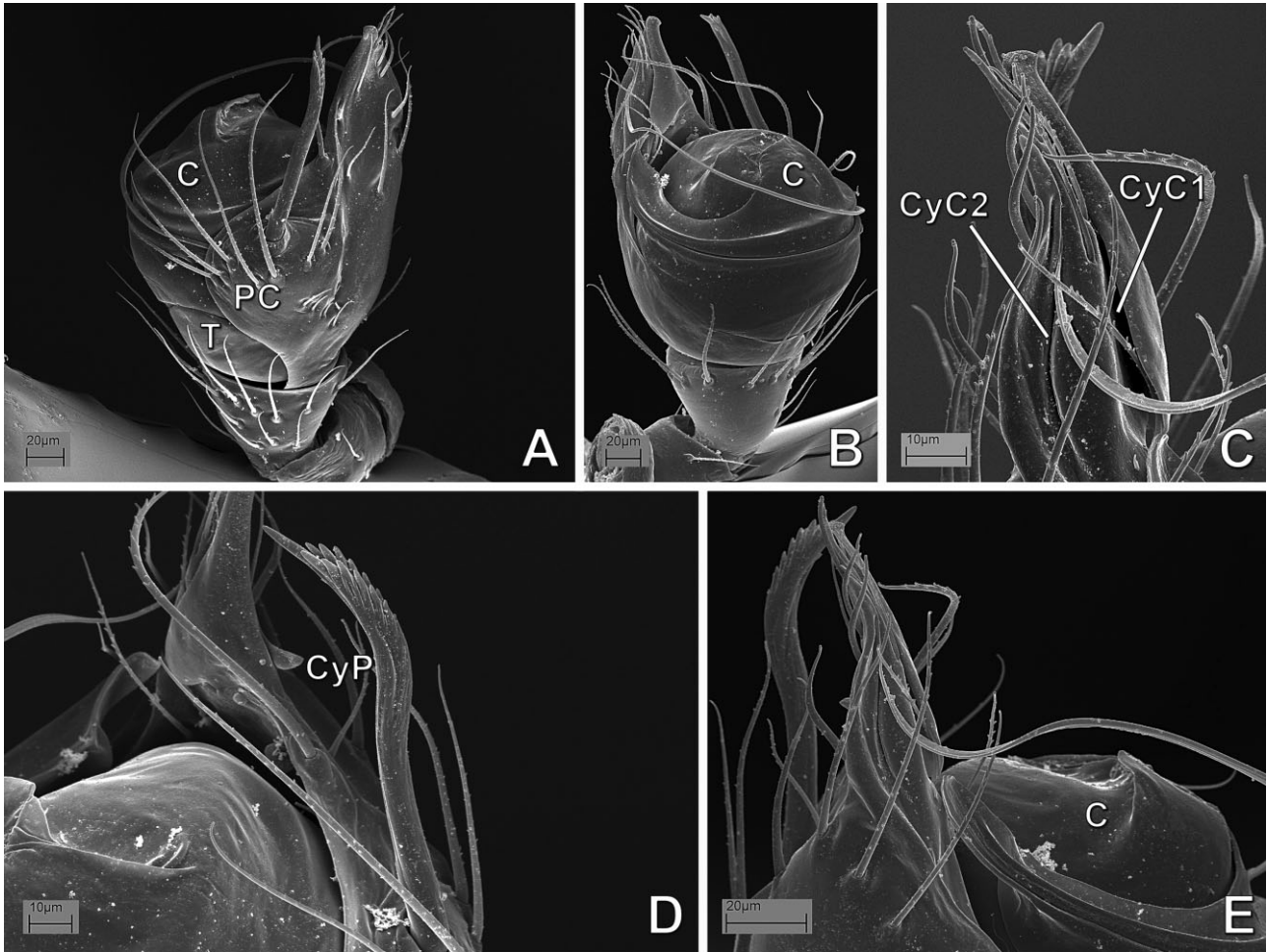


Figure 47. MYSM-020-MAD (Mysmeninae, Mysmenidae) from Toamasina, Madagascar, male. A–E, left palp; A, retrolateral view; B, prolateral–ventral view; C, same, detail of tip of embolus and cymbial conductors; D, same, ventral–retrolateral view; E, same, prolateral view. F, digested abdomen, tracheal system, dorsal view; G, same, detail of posterior tracheal system. See Appendix 3 for the list of abbreviations.

Names of taxa refer to taxonomic or nomenclatural decisions from the classification based on the preferred total-evidence hypothesis of relationships (Lopardo *et al.*, 2011, fig. 12; see Figs 160, 161B, Appendix 5, and below). Node numbers from the phylogenetic hypothesis based on morphological data (Fig. 153) begin with ‘M’; nodes from the combined total-evidence hypothesis (Figs 160, 161) begin with ‘C’.

MORPHOLOGICAL DATA SET (65 TAXA,
357 CHARACTERS)

The cladistic analysis of the morphological data set of 65 taxa (357 characters) resulted in three most-parsimonious trees (MPTs) of 1512.169 steps (consistency index, CI = 0.366; retention index, RI = 0.666; see strict consensus in Figs 153, 154). A total of 311 characters (87.1%) are phylogenetically informative, the re-

maining 12.9% characters are autapomorphic (for a summary of analysis of statistics and character composition, see Table 6). Conflicting relationships caused one node within Anapidae to collapse in the strict consensus. Major clades, and support and stability values, are reported below. Synapomorphies for clades (except for Mysmenidae, see below), and the description and images of characters and character states, are listed in Appendices 2 and 4.

‘Symphytognathoids’ (node M69) and clades within symphytognathoids

Results of the morphological analysis support the composition of symphytognathoids as proposed by Griswold *et al.* (1998), and modified in Schütt (2003). That is, it includes Anapidae, Mysmenidae, Symphytognathidae, Theridiosomatidae, and also Synaphridae and Micropholcommatinae *sensu* Lopardo *et al.* (2011).

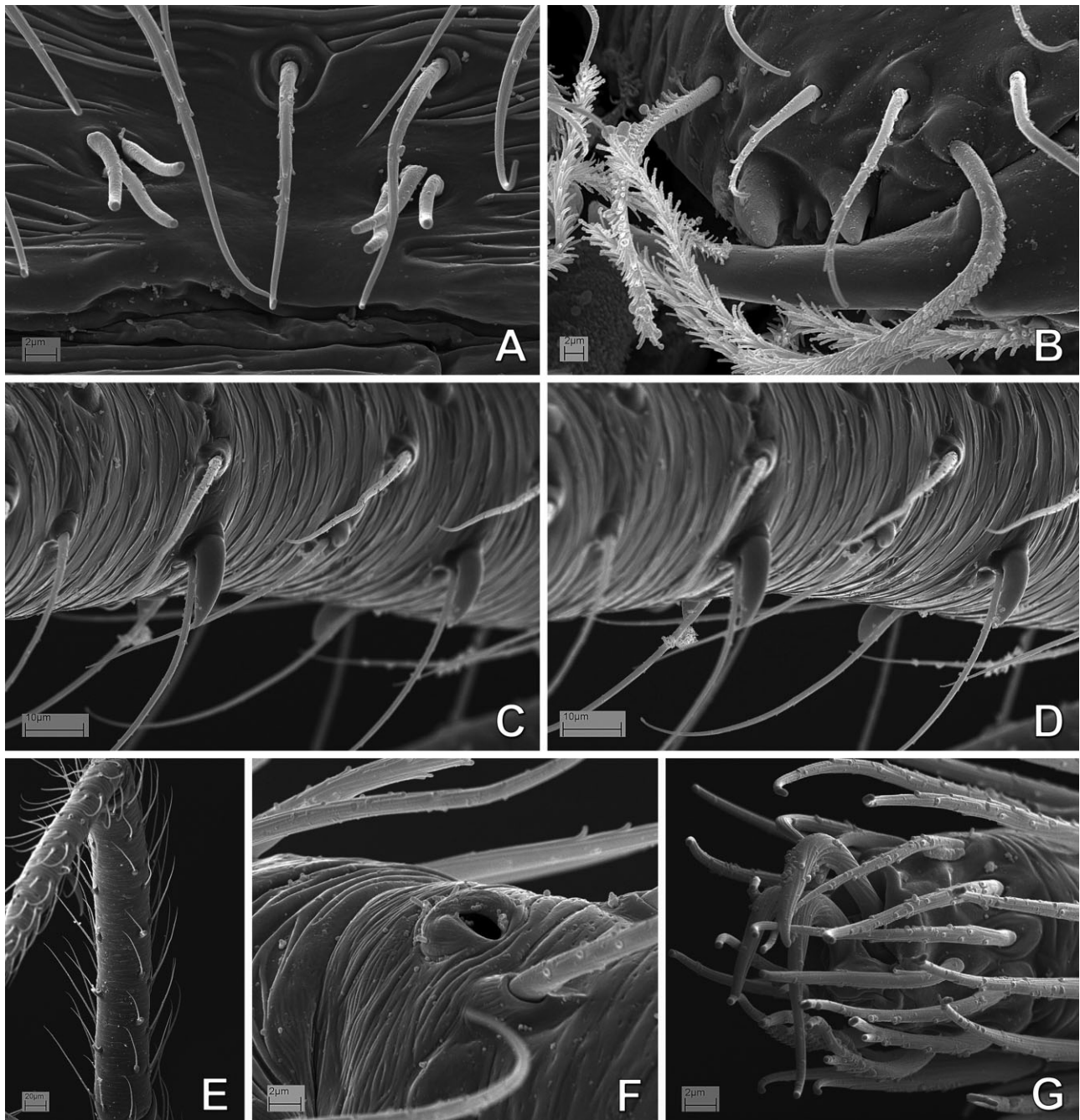


Figure 48. MYSM-020-MAD (Mysmeninae, Mysmenidae) from Toamasina, Madagascar, male: A, epiandrous spigots; B, cheliceral teeth and fang; C, D, right tibia I, detail of ventral paired setae with protruded bases, prolateral view; E, right tibia I, ventral view; F, right tarsus I, detail of tarsal organ, retrolateral view; G, right leg IV, claws.

Although the implied weighting sensitivity analysis recovered symphytognathoids as a natural group under all concavities studied, group support values are intermediate to low (BS 4.560; SFq 68%; RFD 20%; GC 45%). Interfamilial relationships are stable except for the position of Synaphridae, with an alternative placement as sister to all other symphytognathoid families (see

below). Two main symphytognathoid clades resulted from the analysis.

First, a re-delimited Mysmenidae (see below) sister to Theridiosomatidae (node M95). Both theridiosomatid and mysmenid representatives in this data set grouped together, although with low support values (BS 0.960; SFq 38%; RFD 10%; GC 7%). Mysmenidae are sister

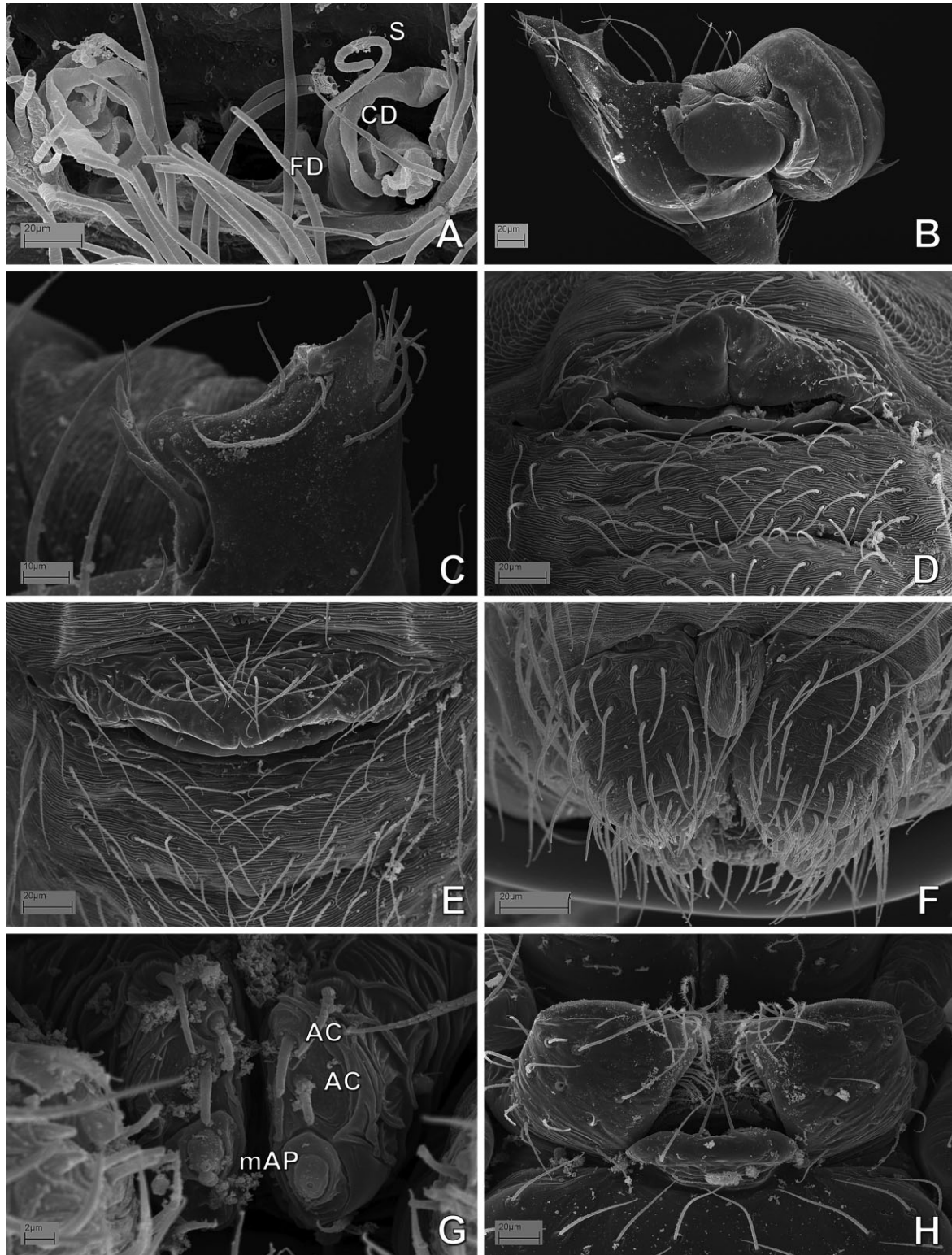


Figure 49. MYSM-023-MAD (Mysmeninae, Mysmenidae) from Antananarivo, Madagascar: A, D, E, female; B, C, F–H, male. A, digested abdomen, detail of vulva; B, left palp, prolateral view, bulb displaced; C, same, detail of cymbial tip, retrolateral–dorsal view; D, abdomen, detail of epigynal area and respiratory spiracles, posterior view; E, same, ventral view; F, colulus and spinnerets, ventral view; G, posterior median spinnerets; H, prosoma, detail of sternum, labium and maxillae, ventral view. See Appendix 3 for the list of abbreviations.

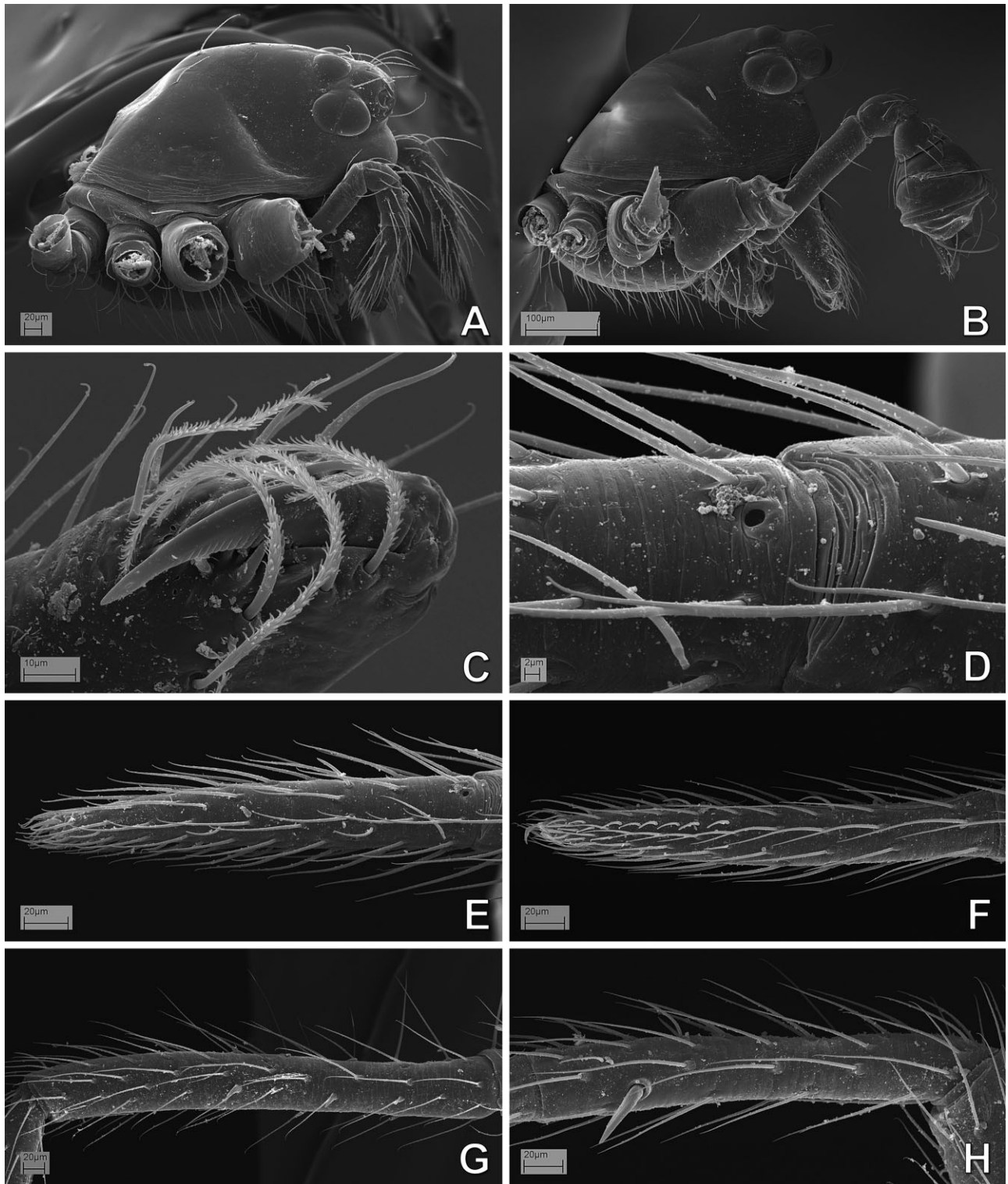


Figure 50. MYSM-023-MAD (Mysmeninae, Mysmenidae) from Antananarivo, Madagascar: A, D, E, female; B, C, F–H, male. A, B, prosoma, lateral view; C, left chelicera, retromarginal view. D–H, right leg I, prolateral view; D, tarsus–metatarsus junction, prolateral–dorsal view; E, F, tarsus; G, tibia; H, metatarsus.

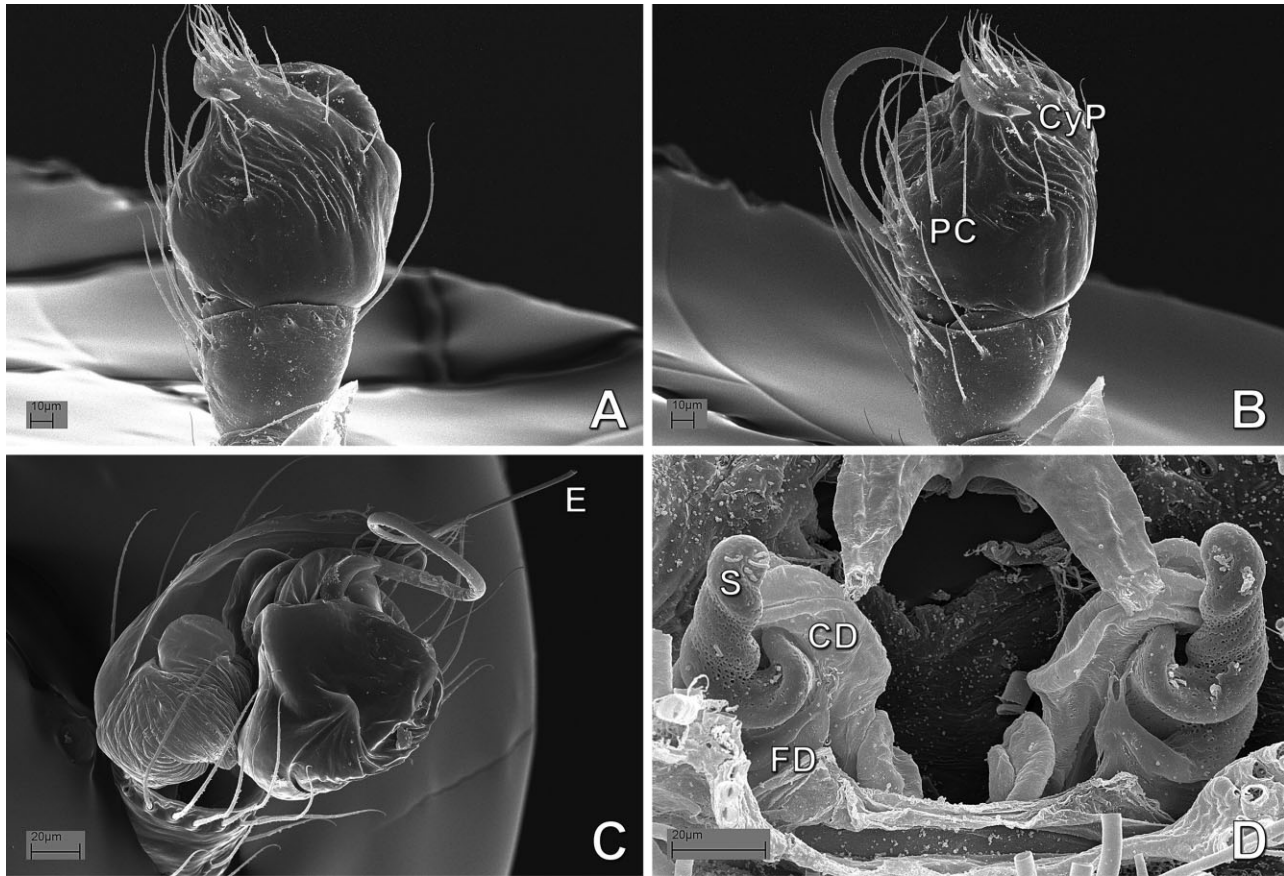


Figure 51. *Mysmena tasmaniae* (Mysmenidae). A–C male left palp; A, dorsal view; B, retrolateral–dorsal view; C, expanded palp, distal–ventral view. D, female digested abdomen, detail of vulva, tracheae removed. See Appendix 3 for the list of abbreviations.

to Theridiosomatidae under all implied weighting concavities, except $k = 1$. Within this group, Theridiosomatidae (node M127) have intermediate to low support values (BS 3.410; SFq 79%; RFD 20%; GC 73%), but appears highly stable (monophyletic under all implied weighting concavities).

The second clade comprises Synaphridae sister to Anapidae + Symphytognathidae (node M68), with intermediate to low support values (BS 4.160; SFq 65%; RFD 34%; GC 44%). This clade is one of the most unstable (at the interfamilial level) within symphytognathoids, recovered by two weighting schemes (EW and IW at $k = 99$). Synaphridae (node M126), a highly supported and stable family (BS 13.000; SFq 100%; RFD 76%; GC 100%; recovered under all implied weighting concavities), are alternatively placed as sister to all other symphytognathoids (recovered by all other concavities). Support values for the clade comprising Anapidae and Symphytognathidae (node M67) are intermediate to low (BS 3.170; SFq 67%; RFD 51%; GC 56%), with all concavities recovering this clade.

Symphytognathidae (node M103) are relatively well supported (intermediate support) and stable, and comprise all representatives in this data set, including the enigmatic *Jardinis mussardi* (see below) (BS 6.000; SFq 79%; RFD 60%; GC 70%). Symphytognathidae are monophyletic under all implied weighting concavities. The resulting pectinated pattern of relationships encumbers the proposal of groups within the family.

Anapidae (node M66) include all its representatives. In addition, the analysis places all micropholcommatine representatives within this family (*Taphiassa* and *Teutoniella*, node M79), which group together distally within the family, sister to the controversial *Comaroma* (node M76, recovered under all concavities, see below). This hypothesis (i.e. Micropholcommatinae as a subfamily of Anapidae) is not new (Brignoli, 1970; Schütt, 2003), and is in agreement with the hypothesis rendered by the morphological and molecular combined analysis (Fig. 160; Lopardo *et al.*, 2011; but see Rix & Harvey, 2010). Although seemingly stable, Micropholcommatinae is weakly supported (BS 1.800;

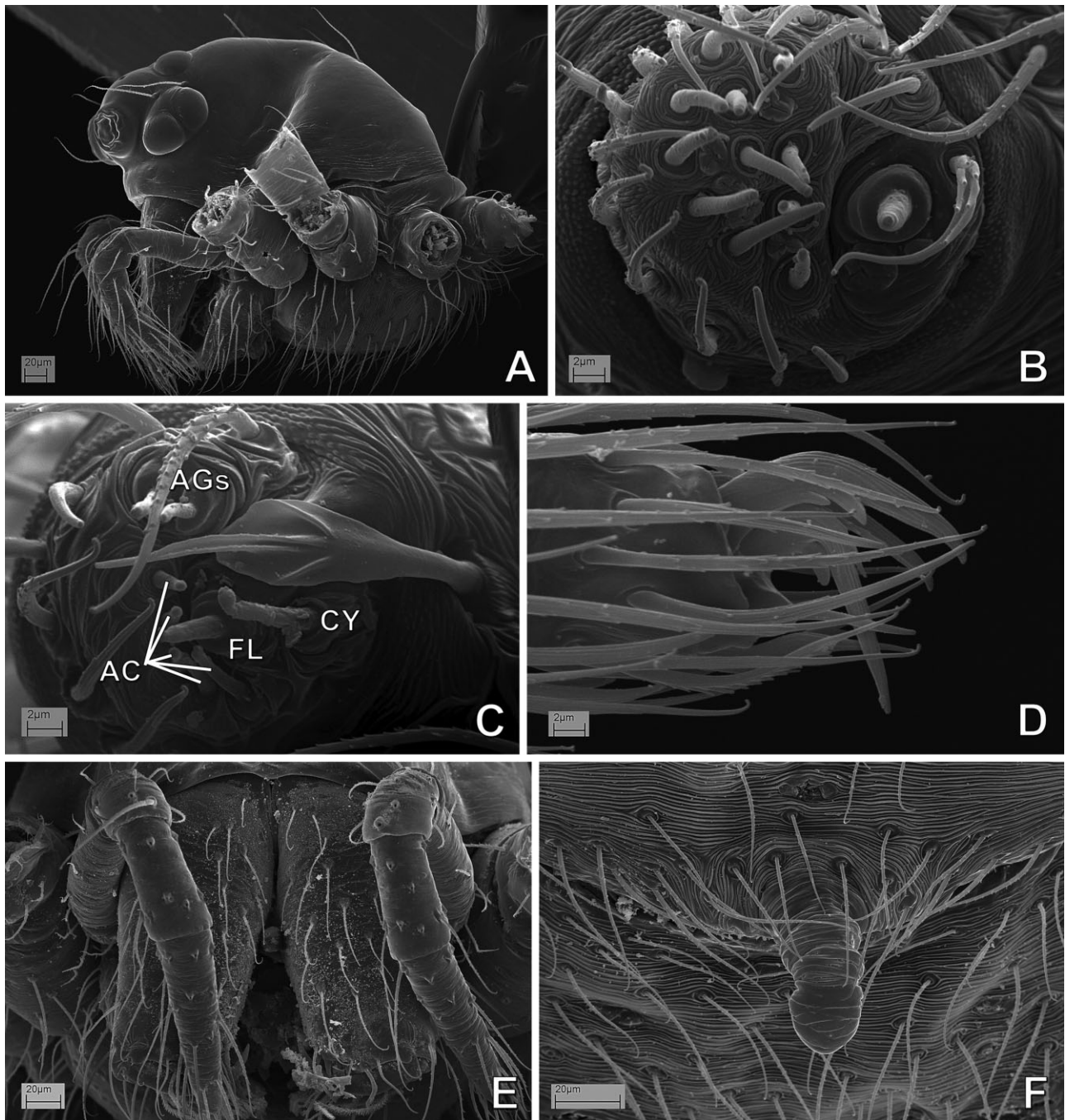


Figure 52. A, MYSM-034-MAD (*Mysmena*, Mysmenidae), female; B–D, MYSM-029-MAD (Mysmeninae, Mysmenidae), female; E, F, MYSM-028-MAD (*Mysmena*, Mysmenidae), female. A, prosoma, lateral view; B, right anterior lateral spinneret; C, right posterior lateral spinneret; D, right leg I, claws, retrolateral view; E, chelicerae and palps, frontal view; F, epigynal area, ventral view. See Appendix 3 for the list of abbreviations.

SFq 67%; RFD 18%; GC 54%; recovered under all implied weighting concavities). Support and stability values for Anapidae (including Micropholcommatinae) are intermediate to relatively high (BS 6.500; SFq 90%; RFD 42%; GC 87%; all implied weighting concavities recover

this clade). Relationships within Anapidae are mostly unresolved and have relatively low support (except *Minanapis*). The familial placement of the controversial genus *Acrobleps* as an anapid is corroborated (as hypothesized in Lopardo & Hormiga,

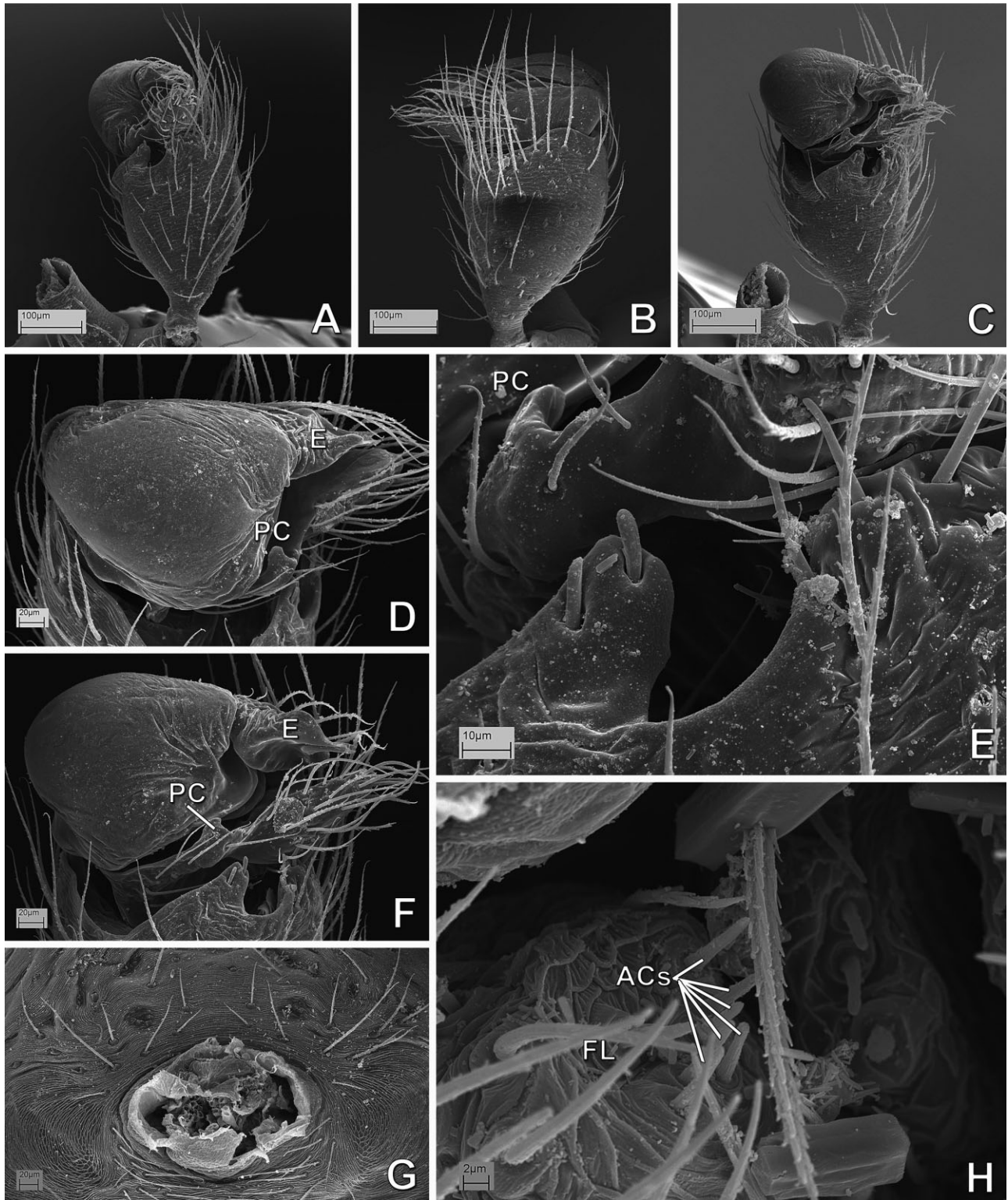


Figure 53. *Mysmenopsis cidrelicola* (Mysmenidae), male paralectotype. A–F, left palp; A, retrolateral view; B, dorsal view; C, retrolateral–ventral view; D, bulb and cymbium, ventral view; E, detail of tibial hollow area; F, bulb and cymbium, retrolateral–ventral view. G, abdomen, pedicel area; H, posterior spinnerets. See Appendix 3 for the list of abbreviations.

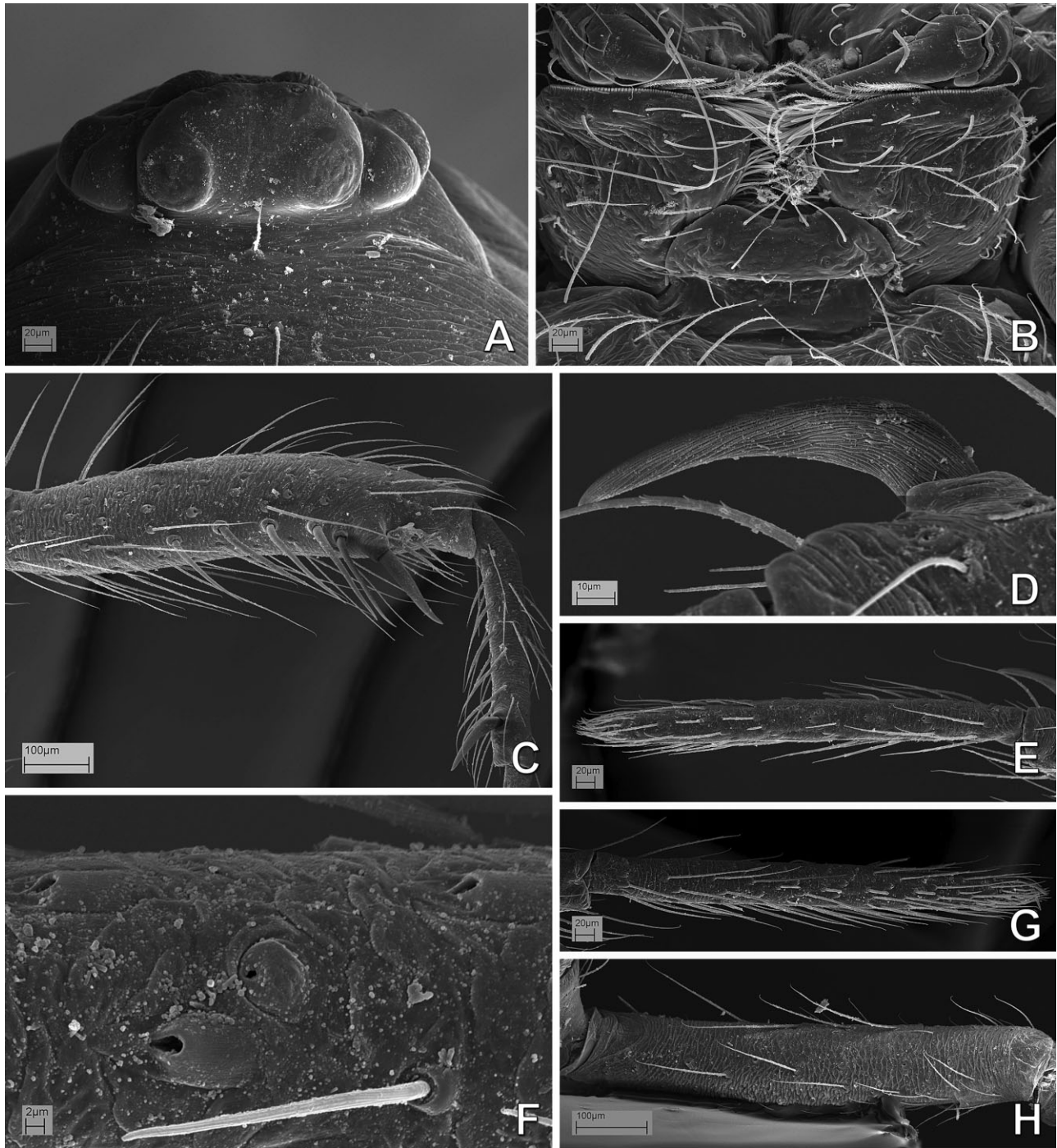


Figure 54. *Mysmenopsis cidrelicola* (Mysmenidae), male paralectotype. A, ocular area, frontal view; B, mouthparts, ventral view. C–G, left leg I; C, tibia and metatarsus, prolateral view; D, metatarsal clasp spine, dorsal view; E, tarsus, dorsal view; F, same, detail of tarsal organ; G, tarsus, prolateral view. H, femur, prolateral–ventral view.

2008; also recovered by Lopardo *et al.*, 2011). *Acrobleps* is placed basally in Anapidae, sister to the remaining family representatives. *Minanapis* is monophyletic.

Mysmenidae (node M94)

The results of this analysis support the monophyly of Mysmenidae, which are here re-delimited to exclude the genus *Jardinis*, an enigmatic taxon of uncertain

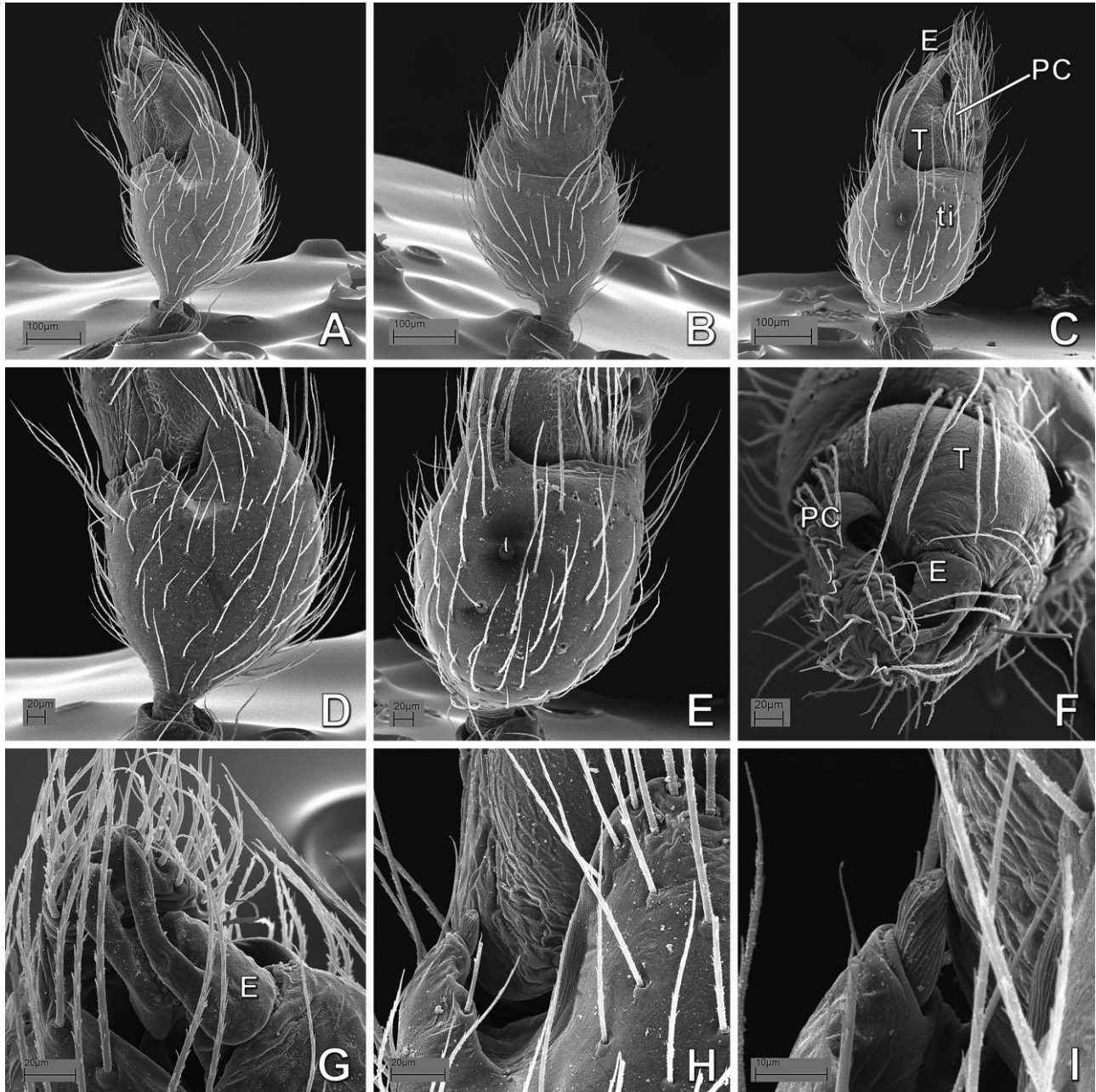


Figure 55. *Mysmenopsis dipluramigo* (Mysmenidae), male left palp. A, prolateral view; B, dorsal view; C, retrolateral view; D, tibia, detail from figure A, prolateral view; E, same, detail from figure C, retrolateral view; F, distal view; G, embolus and tip of cymbium, detail from figure A, prolateral view; H, detail of tibial hollow area, ventral view; I, same, detail of spur. See Appendix 3 for the list of abbreviations.

familial placement, recently disputed between Mysmenidae and Synsphyridae (Gertsch, 1960a; Levi & Levi, 1962; Forster & Platnick, 1977; Brignoli, 1978, 1980; Wunderlich, 1986; Schütt, 2003; Miller, 2007; Platnick, 2014). *Iardinis mussardi*, our study species, is placed within Symphytognathidae in a distal clade of relatively high support and stability. As a result, a redefinition of Mysmenidae to exclude *Iardinis* is needed.

Mysmenidae, comprising all current mysmenid genera included in this analysis, with the exception of *Iardinis*, form a monophyletic group. Support for the family is intermediate to low (BS 4.010; SFq 58%; RFD 57%; GC 31%); however, Mysmenidae are monophyletic under 11 out of the 12 implied weighting concavities explored (all concavities except the most severe weighting, $k = 1$).

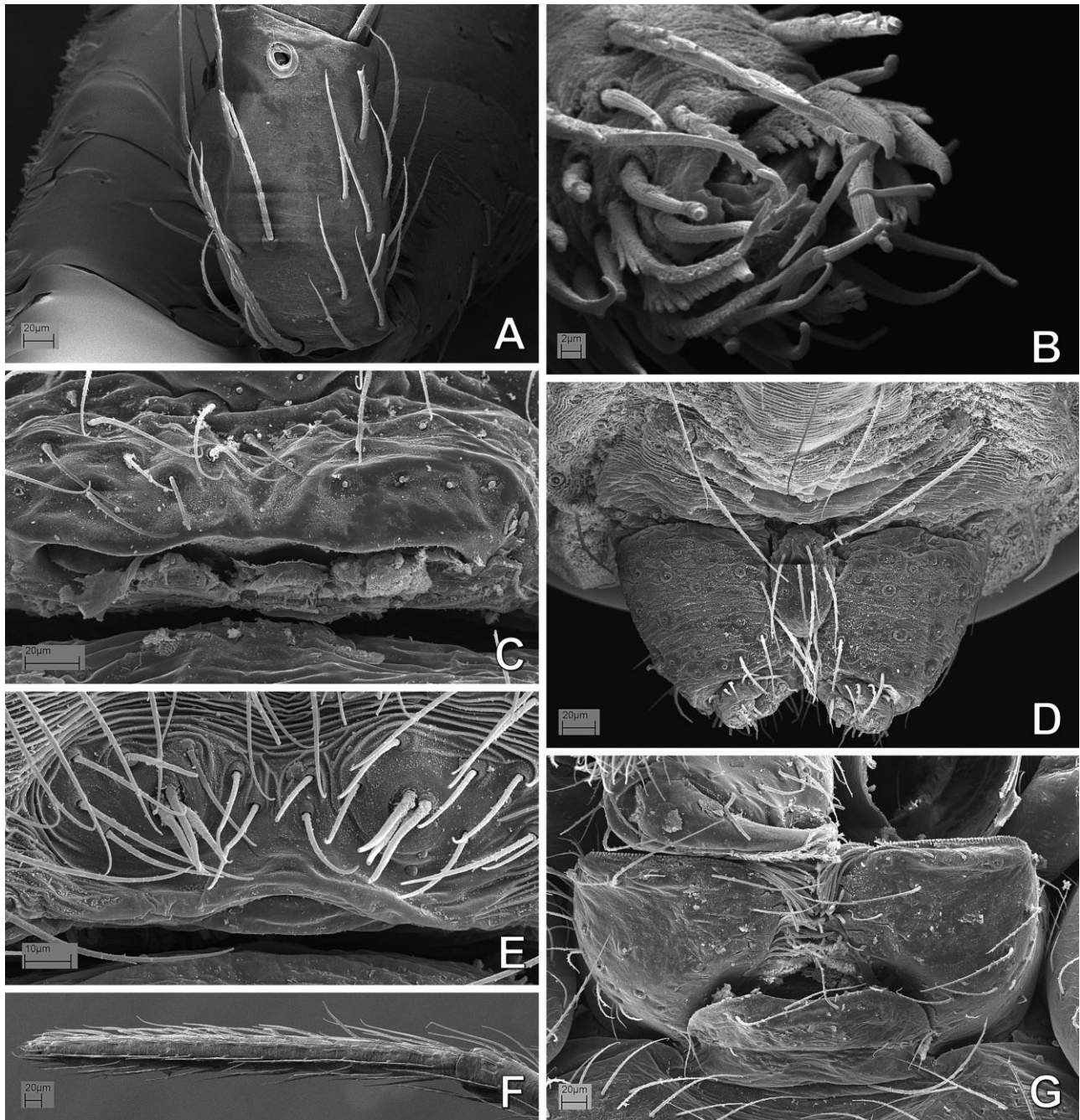


Figure 56. *Mysmenopsis dipluramigo* (Mysmenidae): A, B, E–G, male; C, D, female. A, left patella III, dorsal view; B, left leg II, claws; C, abdomen, epigynal area, ventral view; D, same, colulus, posterior respiratory spiracle and spinnerets, ventral view; E, epiandrous spigots; F, left tarsus I, dorsal view; G, mouthparts, ventral view.

Under the phylogenetic hypothesis based on morphological data, Mysmenidae are diagnosed by the following combination of unambiguous synapomorphies, present in most of their representatives (but see Appendix 5 and Figs 160, 161B for the diagnosis and taxonomic decisions of the family based on the combined total-evidence hypothesis; see also Lopardo *et al.*, 2011

for the diagnosis of Mysmenidae based on total-evidence analyses): cymbium oriented ventrally or prolatero-ventrally (character 163, state 1; retrolateral-dorsal or fully prolateral in few mysmenid taxa); cymbium with a distinct prolateral and apical internal cymbial conductor (CyC1; characters 175, state 1; 176, state 0; strictly apical in Mysmeninae, absent in

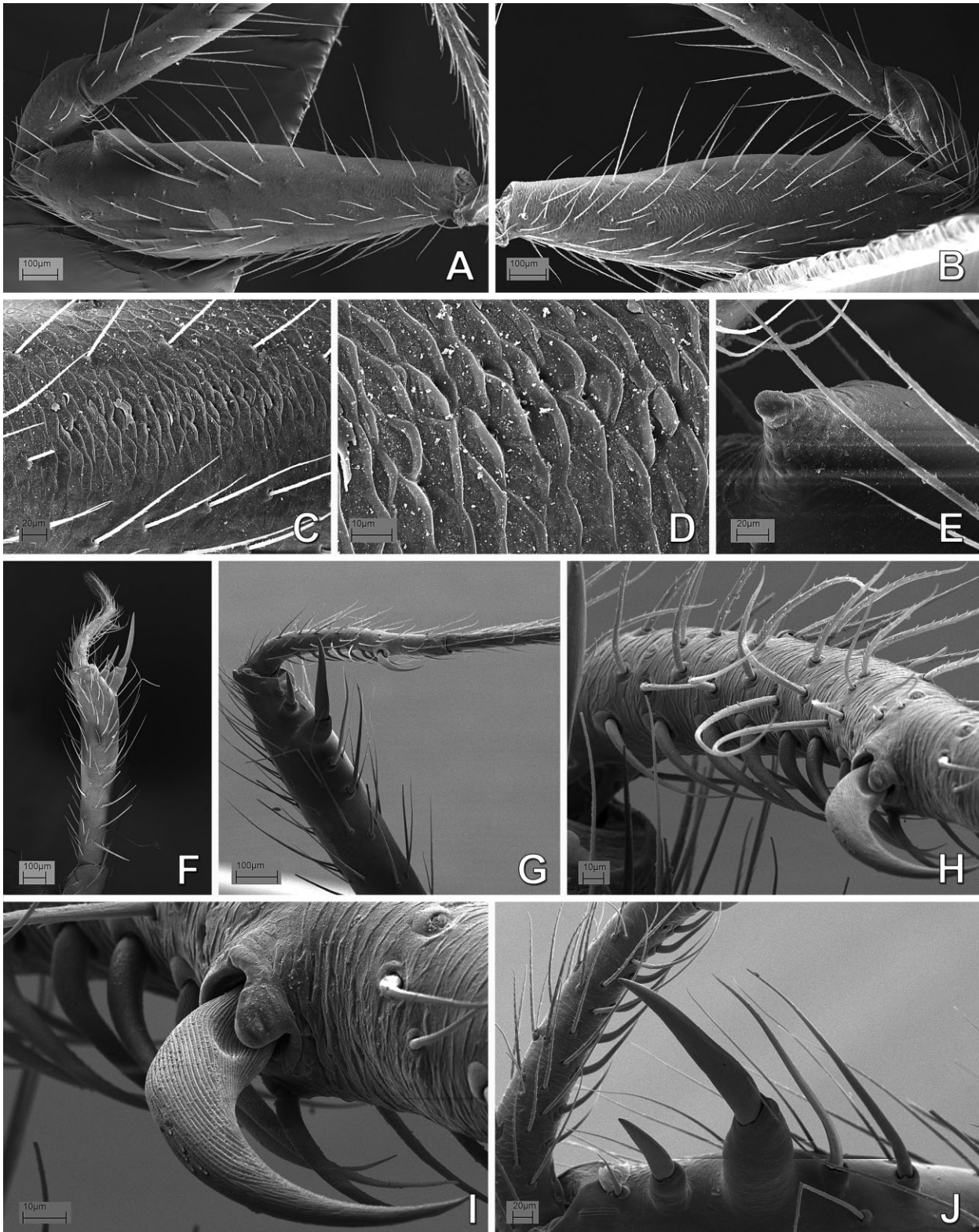


Figure 57. *Mysmenopsis dipluramigo* (Mysmenidae), left legs I: A–E, female; F–J, male. A, femur, prolateral view; B, same, retrolateral view; C, same, detail of stridulatory area; D, same, detail from panel C; E, femoral projection, detail from panel A; F, dorsal view; G, tibial and metatarsal clasp spines, prolateral view; H, metatarsal clasp spines; I, same, detail of strongest clasp spine; J, tibial clasp spines.

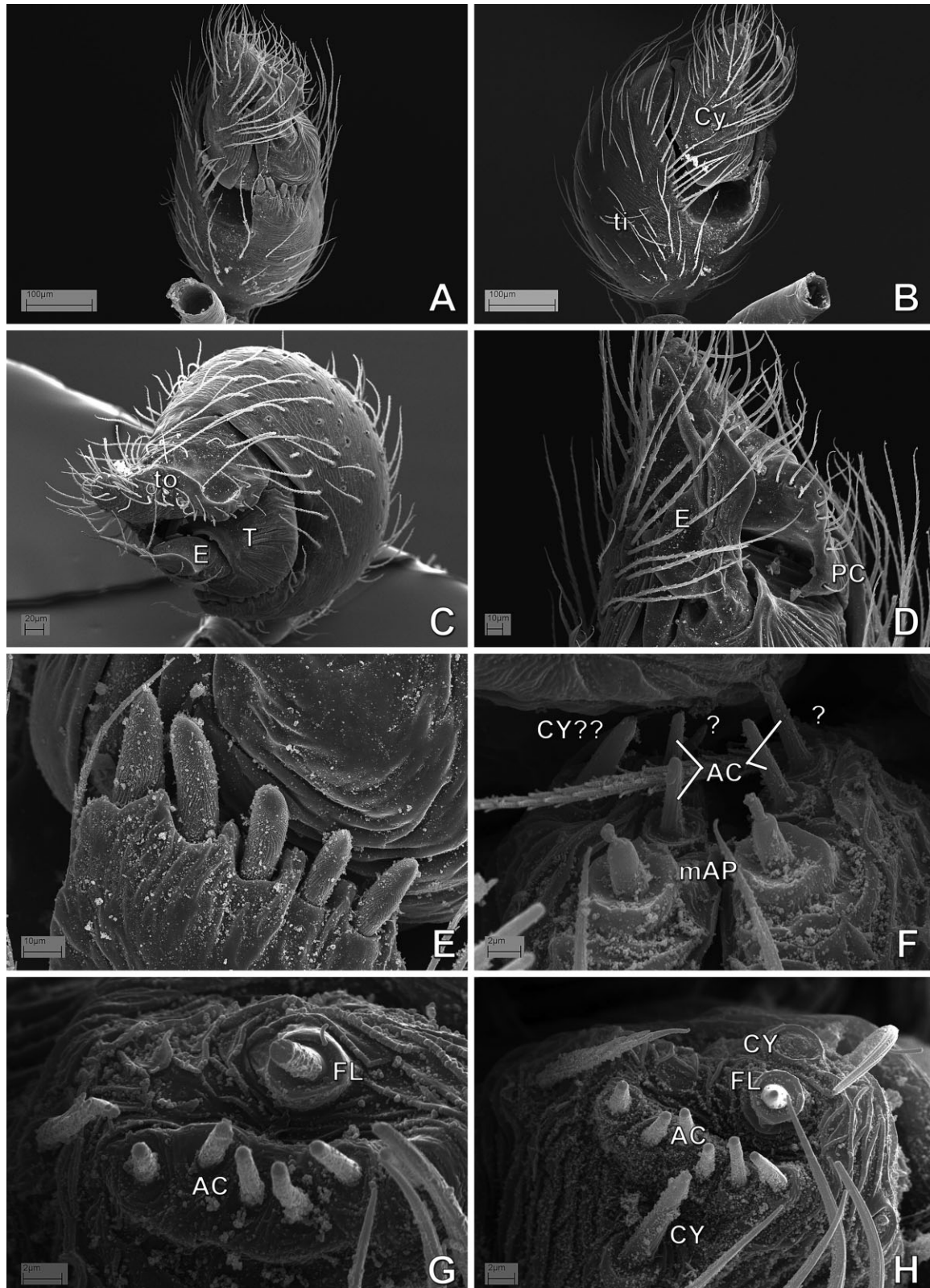


Figure 58. *Mysmenopsis palpalis* (Mysmenidae): A–G, male; H, female. A–E, left palp; A, prolateral view; B, dorsal view; C, distal view; D, embolus and distal cymbium, ventral view; E, detail of tibial spurs. F, posterior median spinnerets; G, H, posterior lateral spinneret. See Appendix 3 for the list of abbreviations.

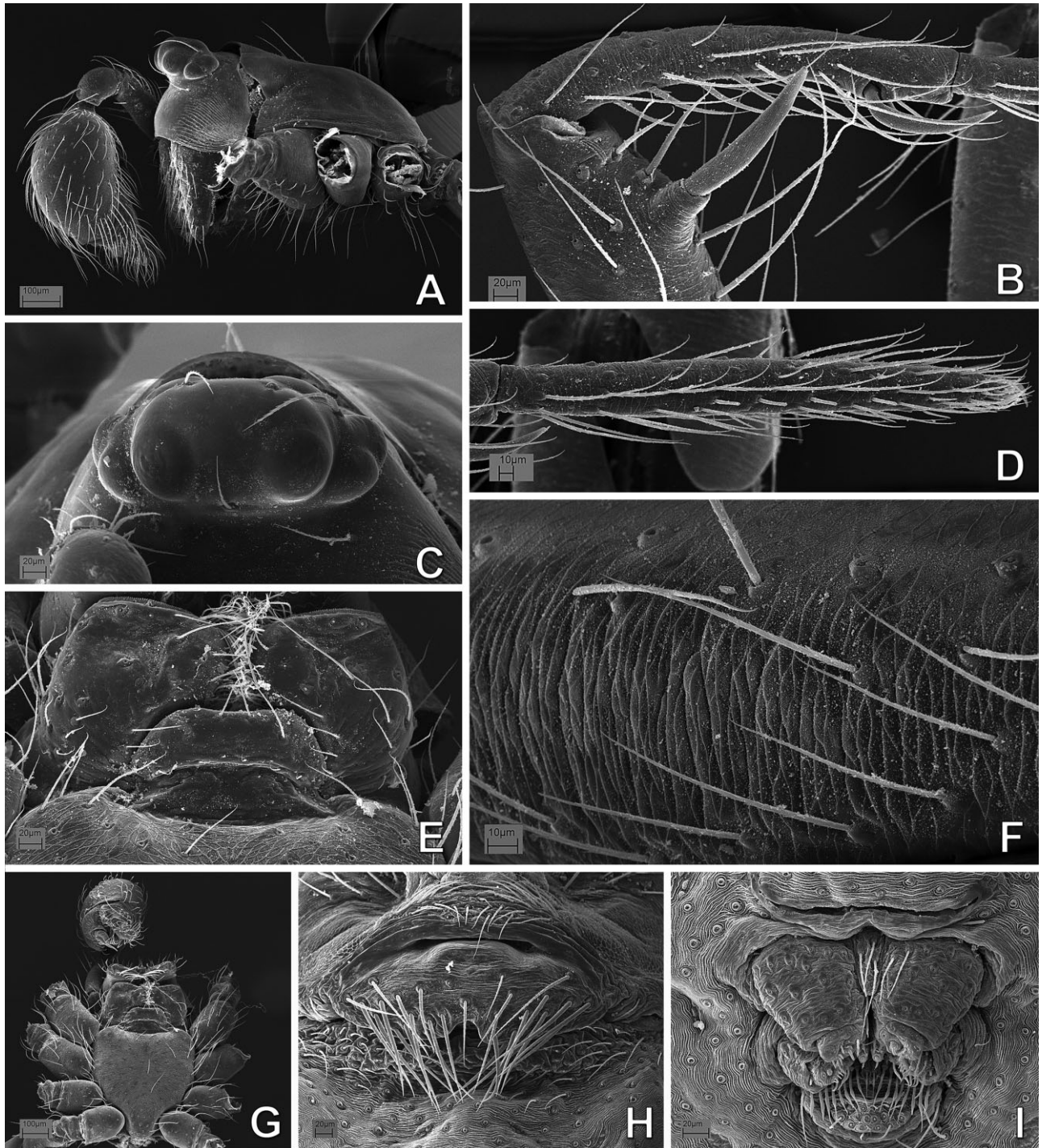


Figure 59. *Mysmenopsis palpalis* (Mysmenidae): A–G, male; H–I, female. B, D, F, left legs, prolateral view. A, prosoma, lateral view; B, tibial and metatarsal clasp spines, leg I; C, ocular area, frontal view; D, tarsus I; E, mouthparts, detail from figure G, ventral view; F, femur IV, detail of stridulatory area; G, prosoma, ventral view; H, epigynum, ventral view; I, spinning field and posterior respiratory spiracle, posterior view.

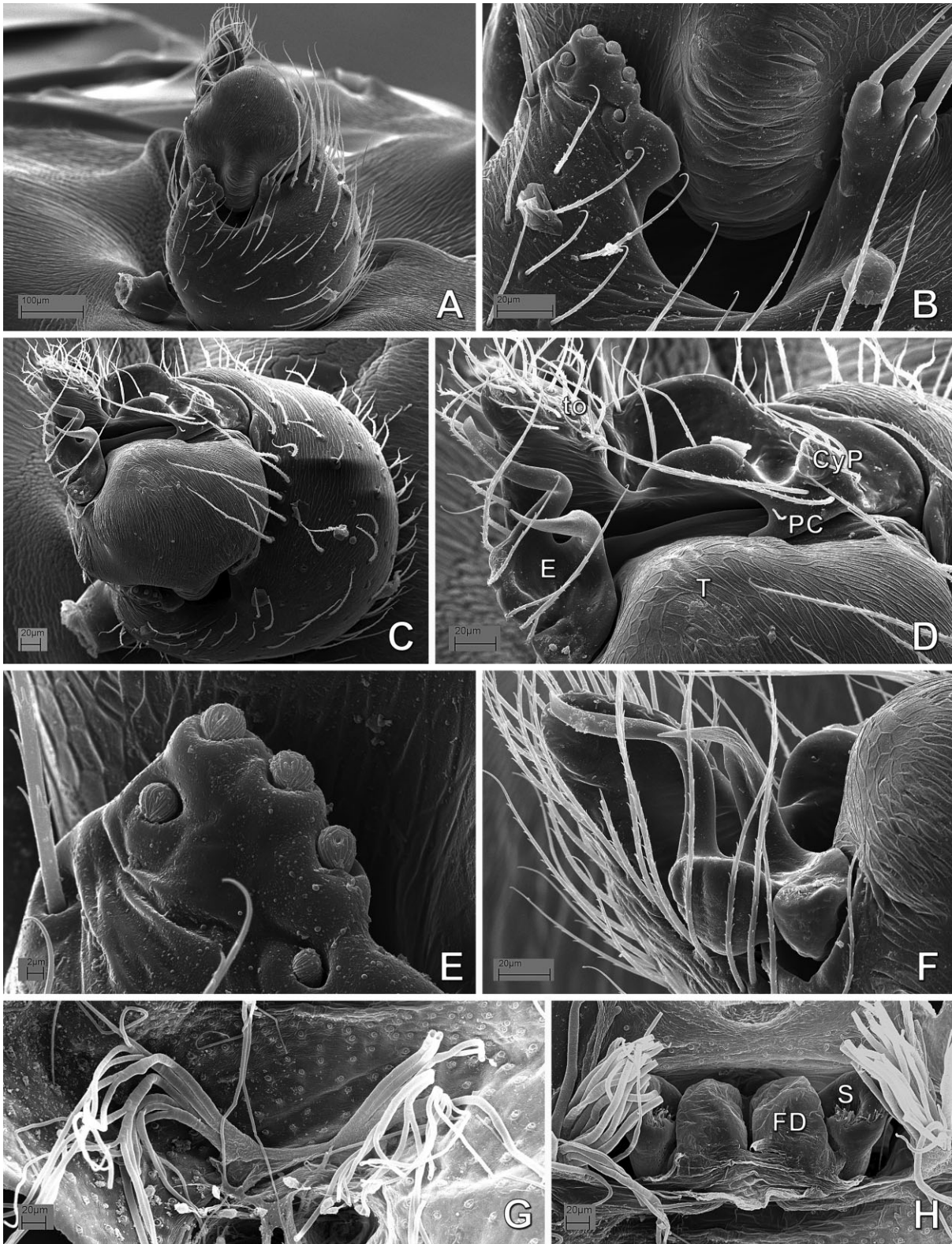


Figure 60. *Mysmenopsis penai* (Mysmenidae): A–F, male right palp, inverted; G, H, female digested abdomen. A, ventral view; B, same, detail of tibial hollow area; C, distal view; D, same, detail of embolus and cymbium; E, tibial spurs, detail from panel B; F, embolus and distal cymbium; G, posterior tracheal system; H, anterior tracheal system and vulva. See Appendix 3 for the list of abbreviations.

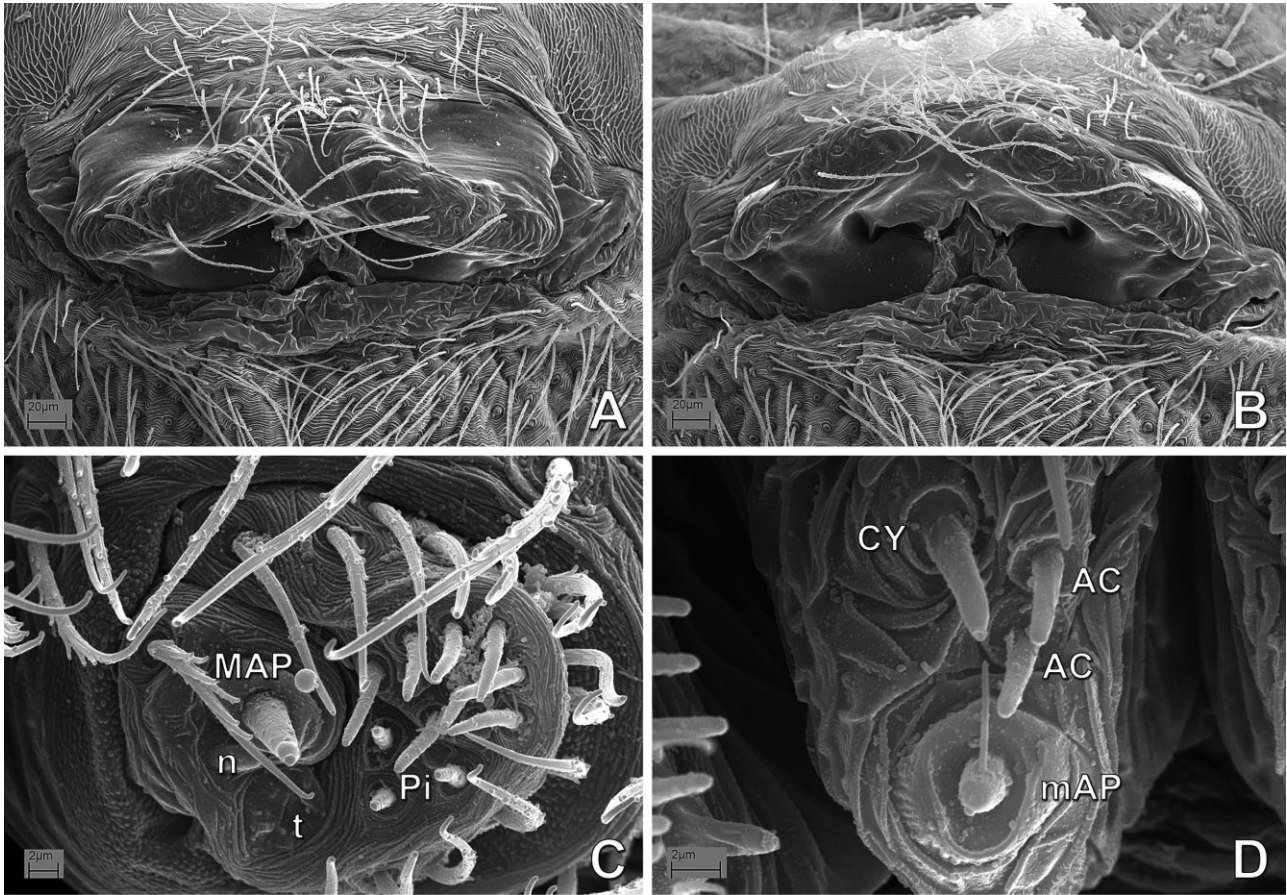


Figure 61. *Mysmenopsis penai* (Mysmenidae), female. A, epigynum, ventral view; B, same, posterior view; C, left anterior lateral spinneret; D, right posterior median spinneret. See Appendix 3 for the list of abbreviations.

Mysmenopsis), and a flat, rounded paracymbium (character 239, state 3; hook-shaped in *Mysmenopsis*). Mysmenid females have a distinct structure on the apical ventral surface of at least femur I, either a sclerotized spot or a projection (character 101, state 1; absent in some *Mysmenopsis* species and MYSM-005-ARG). Other unambiguous synapomorphies for the family include a lobe on the intersegmental groove of the anterior lateral spinnerets (ALS; character 309, state 1; convergently present in few anapid representatives); abdomen with fingerprint cuticle pattern (character 4, state 1; independently synapomorphic for Symphytognathidae, imbricate in *Maymena ambita*); and cheliceral promargin with three teeth (character 278, state 1, although either four or two teeth can occur within the family). Putative synapomorphies for Mysmenidae (see Discussion below for details in the evolution of these characters): intermediate sternum posterior margin (character 53, state 2; pointed in some *Maymena* species); prolateral row of modified setae on tarsus I (character 138, state 1); sparse imbricate cuticular pattern on carapace border (character 47, state 0;

smooth in *Maymena mayana*); two aciniform gland spigots on posterior median spinnerets (PMS AC; character 305, state 1); male palpal tibial rim setae longer than remaining tibial setae and arranged distally in a row or two (character 255, state 1; equally short and of irregular conformation arising convergently in *Trogloneta* and few other mysmenid taxa); medial paracymbium (PC; character 241, state 1; basal in *Trogloneta* and in Theridiosomatidae; median also in Synaphridae); cymbial fold (character 187, state 1; absent in *Maymena mayana* and *Mysmenopsis*); metatarsal clasping spine in males (character 115, state 1; the presence of this distinct metatarsal structure – character 114, state 1 – optimized as ambiguous in Mysmenidae because of the absence of such structure in *Maymena mayana*); female ventral distal spot (character 102, state 0; projection in *Mysmenopsis*) on femora I and II (character 103, state 1; on femur I in *Mysmenopsis*, *Trogloneta*, and node M96); epigynal median plate projecting from epigastric furrow (character 70, state 1; ambiguously optimized because of unknown information in theridiosomatids, some

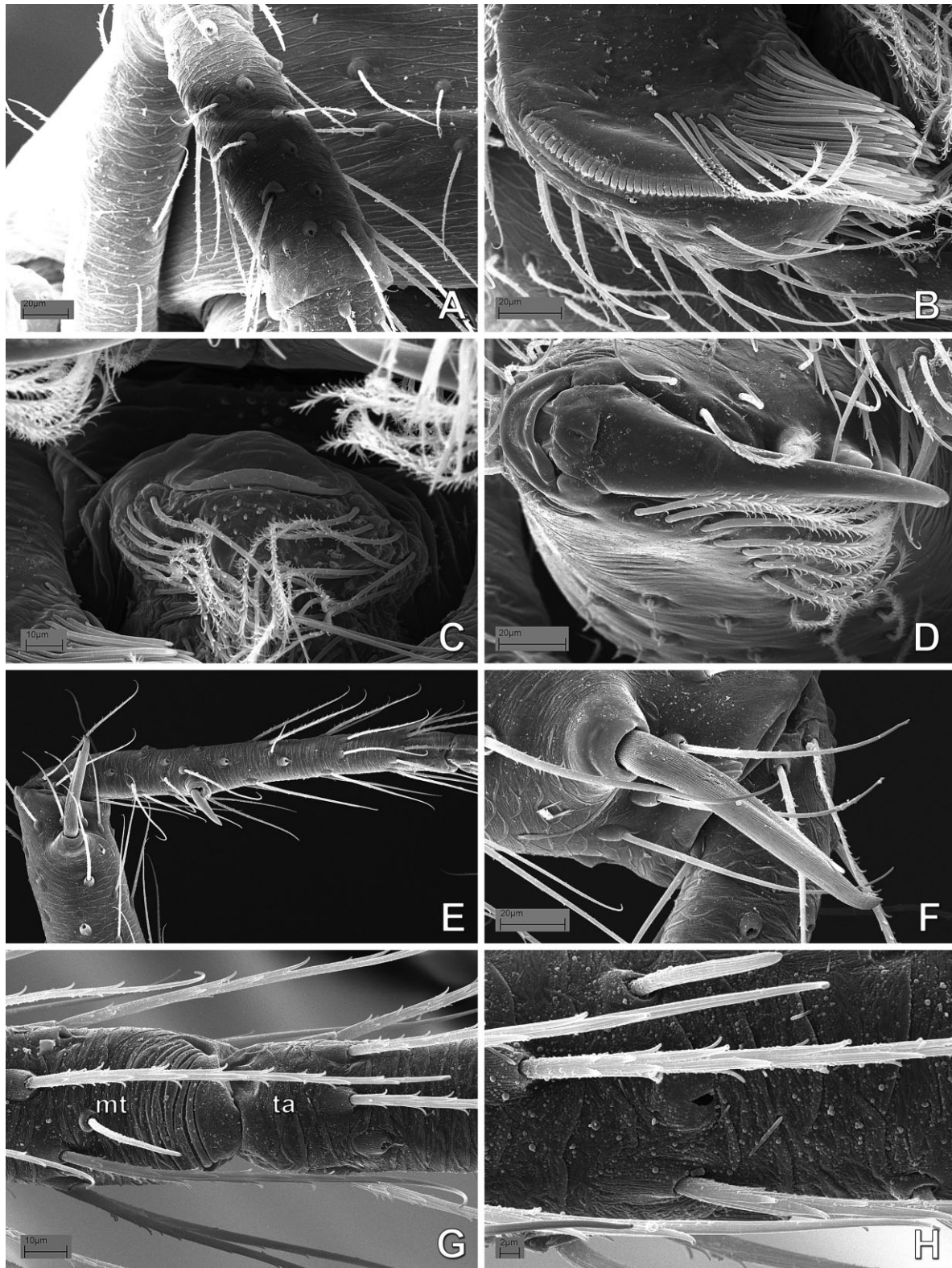


Figure 62. *Mysmenopsis penai* (Mysmenidae): A–D, female; E–H, male left leg I. A, right palpal tibia, dorsal view; B, right maxilla; C, labrum; D, right chelicera, distal view. E, tibial and metatarsal clasp spines, prolateral view; F, same, detail of tibial clasp spine; G, metatarsus–tarsus junction, dorsal view; H, tarsal organ. See Appendix 3 for the list of abbreviations.

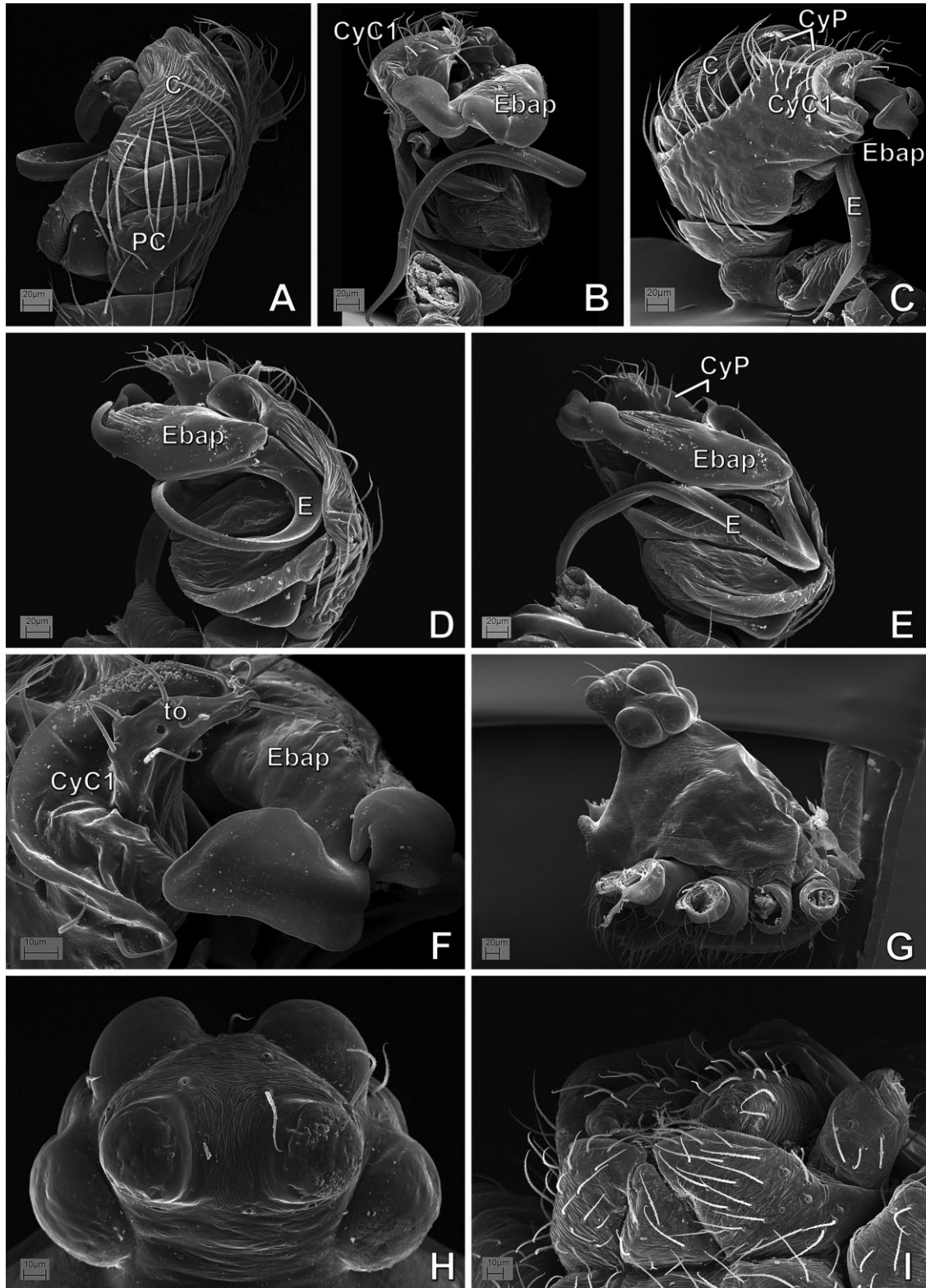


Figure 63. *Trogloneta cantareira* (Mysmenidae), male. A–F, right palp, inverted; A, retrolateral view; B, prolateral view; C, dorsal view; D, ventral–retrolateral view; E, ventral view; F, detail of embolic base and primary cymbial conductor. G, prosoma, lateral view; H, ocular area, frontal view; I, mouthparts, lateral–ventral view. See Appendix 3 for the list of abbreviations.

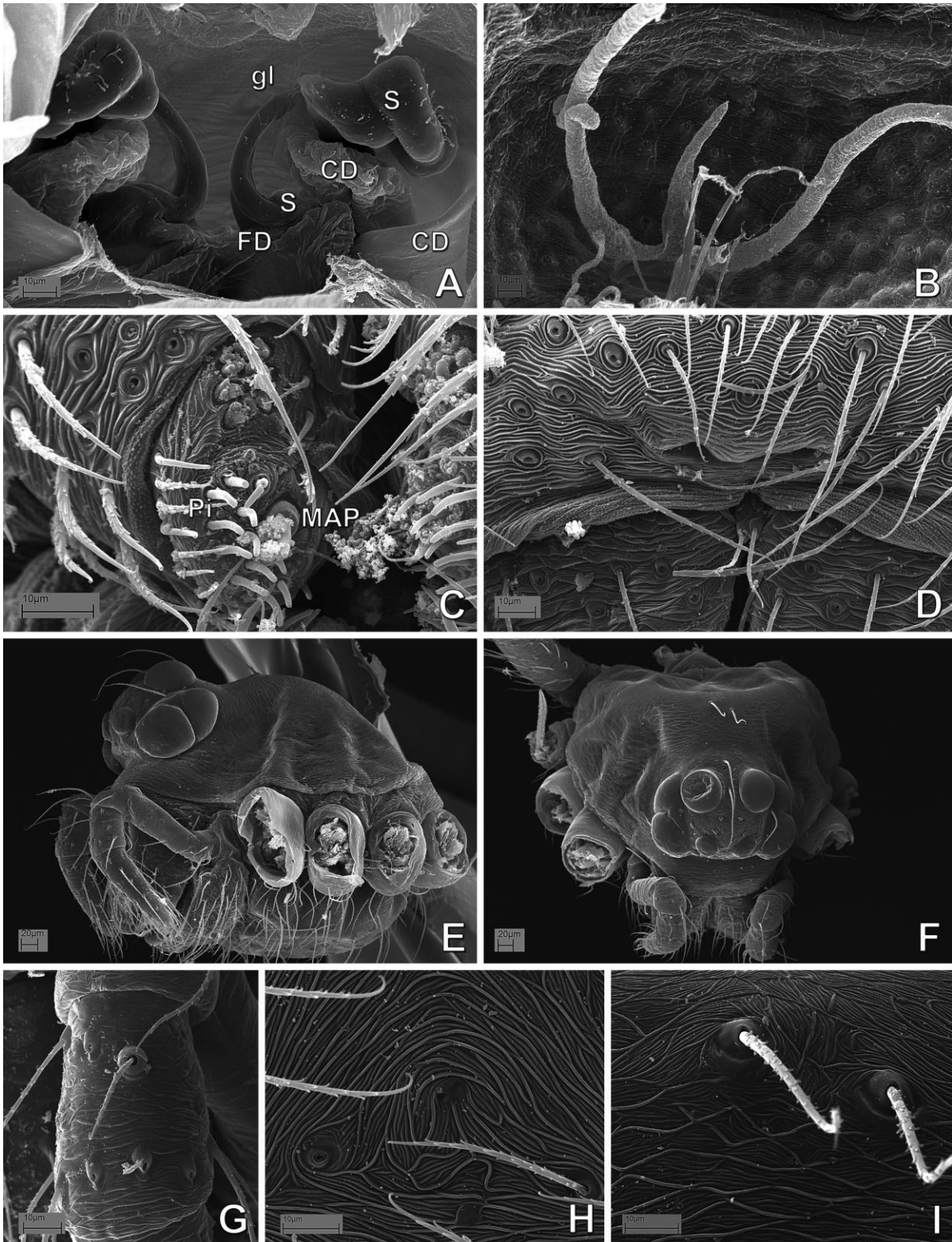


Figure 64. *Trogloneta cantareira* (Mysmenidae), female: A, digested abdomen, detail of vulva; B, same, detail of posterior respiratory system; C, right anterior lateral spinneret; D, abdomen, detail of colulus and posterior respiratory spiracle; E, prosoma, lateral view; F, same, anterodorsal view; G, left palpal tibia, dorsal view; H, sternal cuticular pattern; I, carapace dorsal cuticular pattern, detail from panel F. See Appendix 3 for the list of abbreviations.

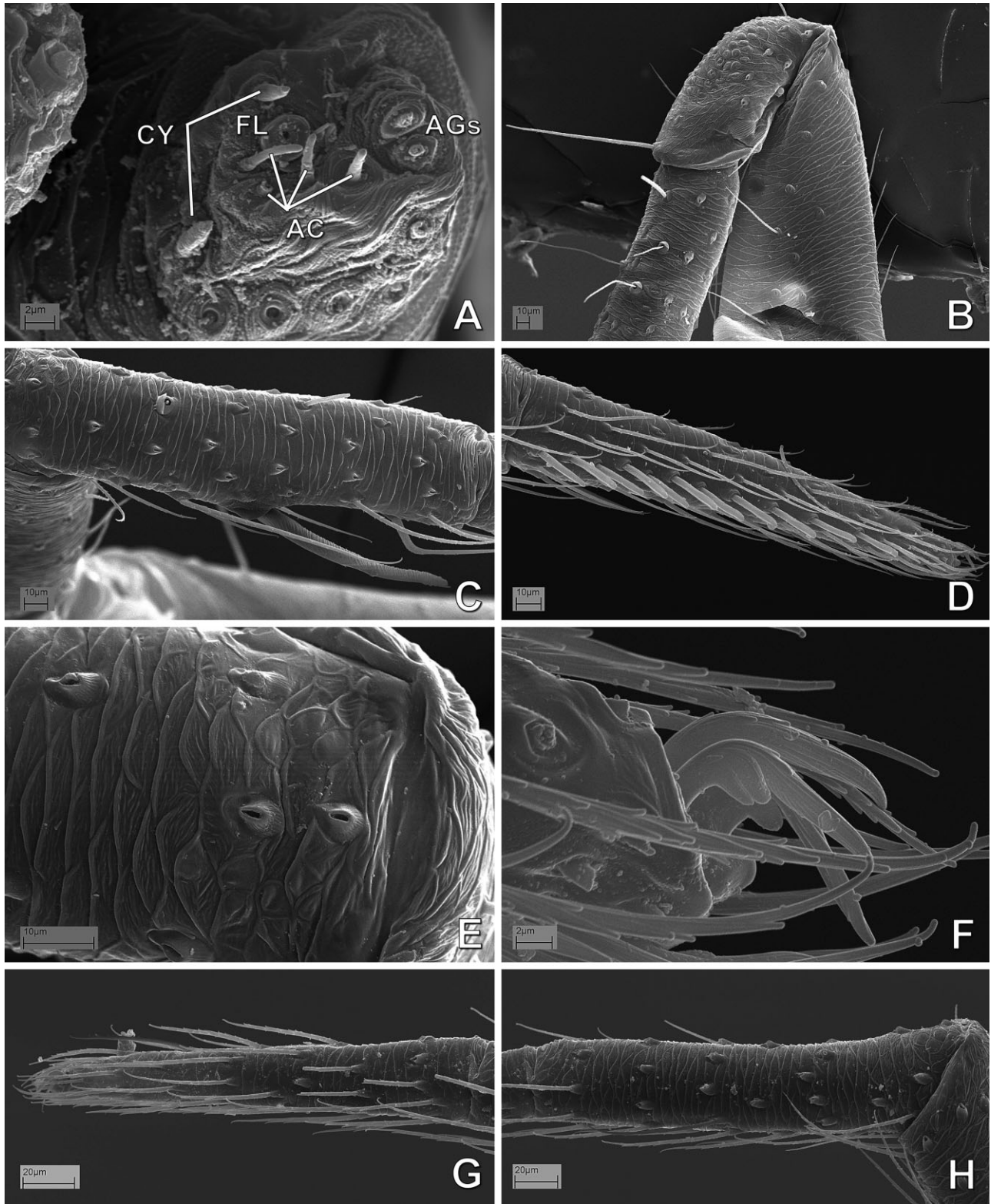


Figure 65. A, *Mysmena* (= *Tamasesia*) *rotunda* (Mysmenidae), female syntype, left posterior lateral spinneret. B–H, *Trogloneta cantareira* (Mysmenidae). B, female left leg I; C–F, male left leg I; G, H, female left leg IV. B, femur, patella and tibia; C, metatarsus, dorsal view; D, tarsus, prolateral view; E, proximal metatarsal cuticular pattern, dorsal view; F, claws, prolateral view; G, tarsus, retrolateral view; H, metatarsus, retrolateral view. See Appendix 3 for the list of abbreviations.

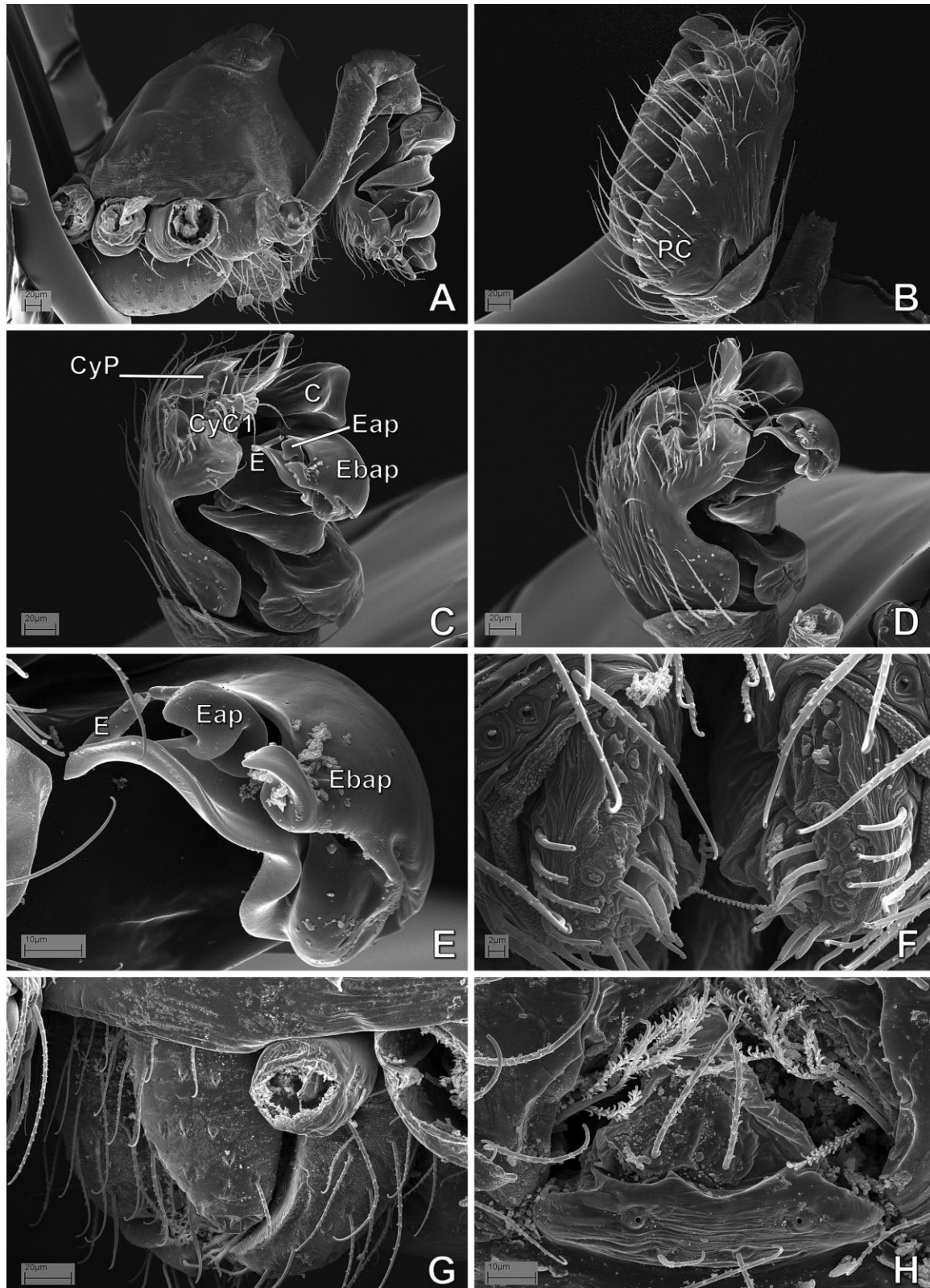


Figure 66. *Trogloneta granulatum* (Mysmenidae), male. A, prosoma, lateral view. B–E, left palp; B, retrolateral view; C, prolateral view; D, prolateral–dorsal view; E, embolus. F, anterior lateral spinnerets; G, mouthparts, lateral view; H, labium, ventral view. See Appendix 3 for the list of abbreviations.

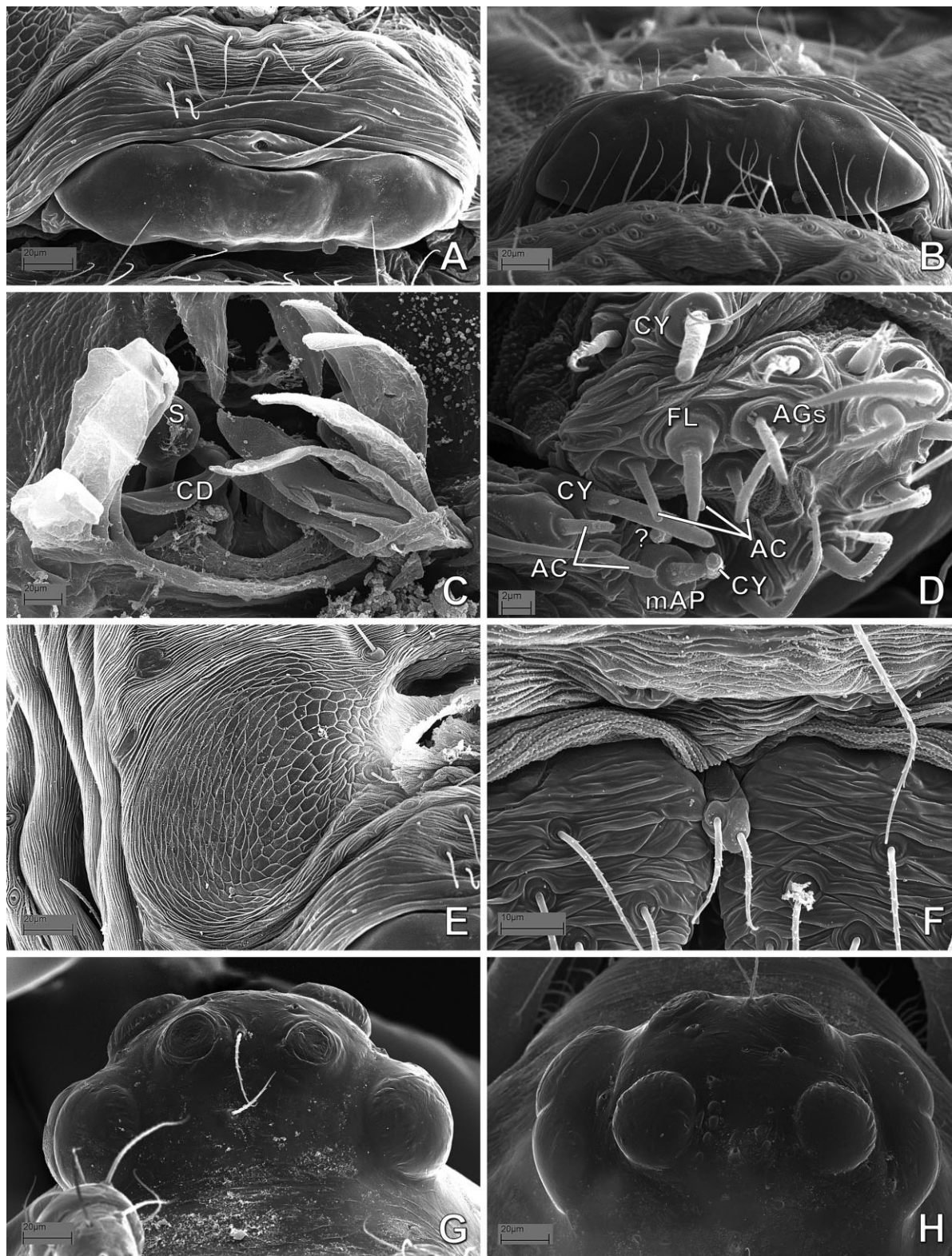


Figure 67. *Trogloneta granulum* (Mysmenidae), female. A, epigynum, ventral view; B, same, posterior view; C, digested abdomen, anterior respiratory system and vulva; D, left posterior spinnerets; E, booklung cover; F, abdomen, detail of colulus and posterior spiracle, ventral view; G, ocular area, frontal view; H, same, dorsal view. See Appendix 3 for the list of abbreviations.

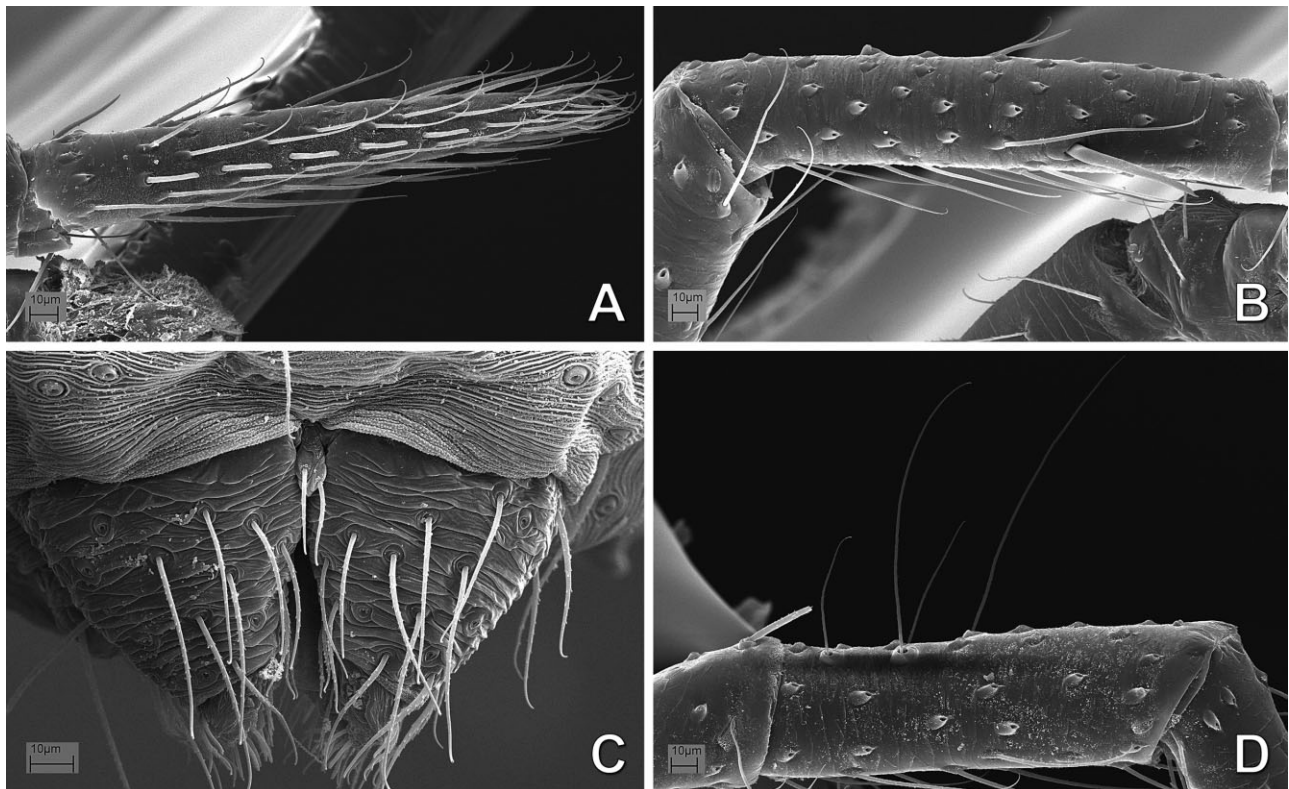


Figure 68. *Trogloneta granulatum* (Mysmenidae), male. A, left tarsus I, prolateral view; B, left metatarsus I, prolateral view; C, abdomen, detail of colulus, posterior spiracle and spinnerets, ventral view; D, left tibia III, prolateral view.

reversions within the family); and either a more or less straight trajectory or a convoluted trajectory of the copulatory ducts (character 78, states 0 and 2, highly homoplastic basally).

Clades within Mysmenidae

Mysmenidae are fully resolved in the consensus of the MPTs. Monophyletic genera include: *Kekenboschiella*, *Microdipoena*, *Maymena*, *Mysmenopsis*, and *Trogloneta*, whereas non-monophyletic mysmenid genera include *Calodipoena*, *Mysmenella*, *Tamasesia*, and the type genus *Mysmena* (but see Appendix 5 for generic synonymies). Below we report major clades within Mysmenidae in reference to the strict consensus of Figures 153, 154. For a complete list of unambiguous synapomorphies for each node and taxa, see Appendix 4. See Appendix 5 for taxonomic changes and generic diagnoses based on the hypothesis of the combined total-evidence analysis from Lopardo *et al.* (2011; refer to Fig. 161B).

Maymena (node M110) is monophyletic, sister to the remaining mysmenid representatives (BS 3.070; SFq 58%; RFD 22%; GC 32%). In the implied weighting sensitivity analysis, the genus is monophyletic under all concavities except the most extreme ($k = 1$; see Fig. 154). The clade comprising all remaining mysmenid

representatives (node M93, excluding *Maymena*) is one of the few clades diagnosed by several unambiguous and non-homoplastic synapomorphies (see Appendix 4); however, support values for this node are relatively intermediate to low (BS 3.050; SFq 46%; RFD 25%; GC 31%). The implied weighting sensitivity scheme, however, consistently recovers this clade under all but the two most extreme concavities ($k = 1$ and 2).

Trogloneta (node M123) is monophyletic; support values for this genus are among the highest for this data set (BS 13.000; SFq 100%; RFD 93%; GC 100%). Accordingly, the implied weighting sensitivity scheme recovers *Trogloneta* under all concavities explored. The clade comprising the remaining mysmenids, excluding both *Maymena* and *Trogloneta* (i.e. node M92), includes the subfamilies Mysmenopsinae (node M105) and Mysmeninae (node M91) (see Appendix 5). This clade has support values among the lowest for this data set (BS 0.040; SFq 35%; RFD 1%; GC -8%). In the implied weighting sensitivity scheme, however, this group is consistently monophyletic under all but the two most extreme concavities ($k = 1$ and 2).

The subfamily Mysmenopsinae (node M105; see Appendix 5) comprises all studied kleptoparasitic mysmenids. This subfamily is monophyletic under all

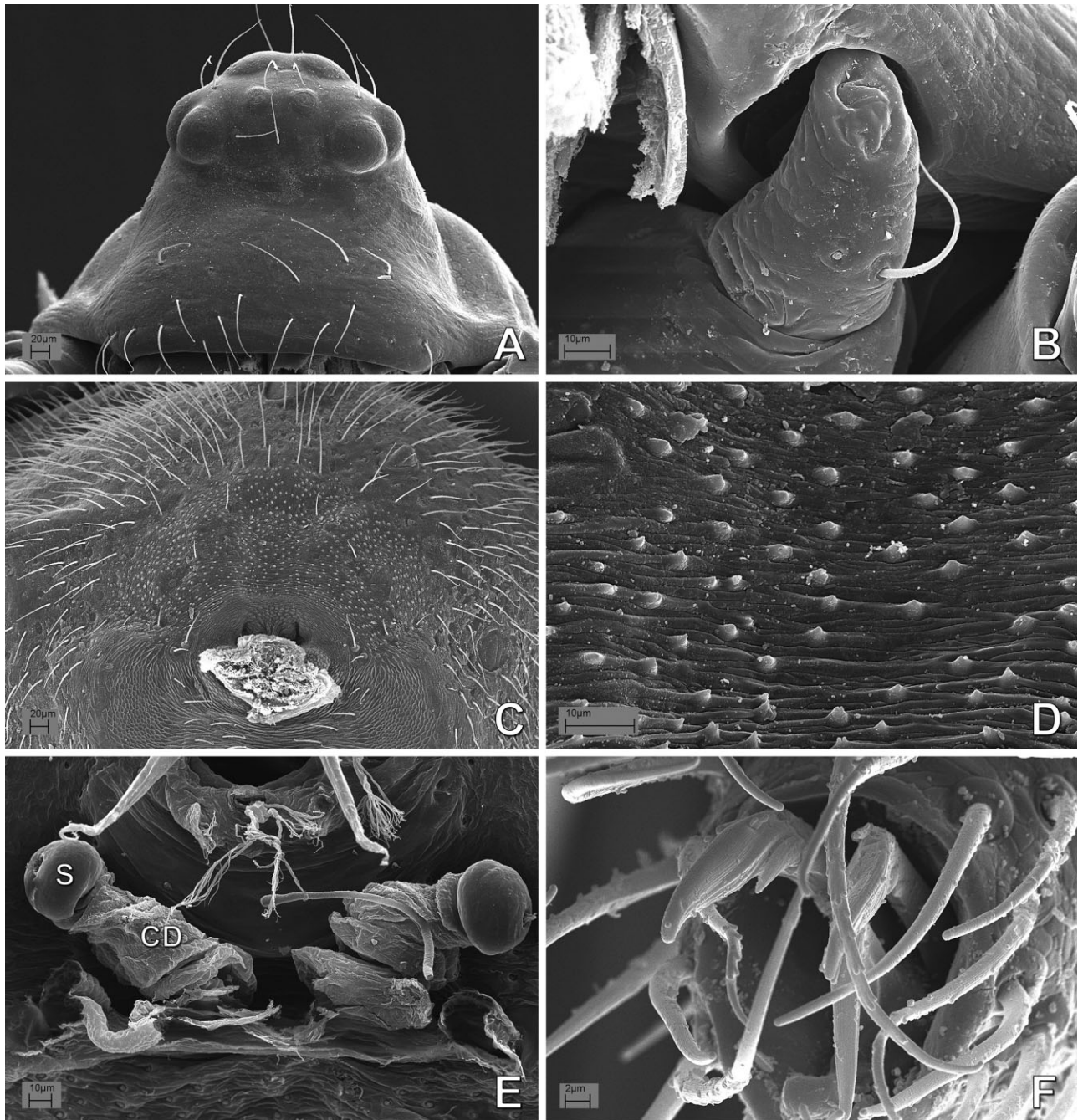


Figure 69. *Acrobleps hygrophilus* (Anapidae), female. A, carapace, frontal view; B, left palp and carapace lateral depression; C, abdomen, pedicel area, ventral view; D, same, detail of suprapedicellate nubbins; E, digested abdomen, detail of vulva, tracheae removed; F, right leg II, claws. See Appendix 3 for the list of abbreviations.

concavities explored, and support values for this node are fairly high (BS 7.020; SFq 98%; RFD 50%; GC 98%). *Isela* (node M104), including the *Kilifina* representative (*Kilifina*-MYSM-002-KENYA) is monophyletic under all concavities explored (not shown; see Appendix 5 for generic synonymy). Frequency values for this genus are high (SFq 95%; GC 92%) although Bremer support

is low (BS 1.990; RFD 33%). *Mysmenopsis* (node M121) has the highest clade support within symphytognathoids (BS 14.160; SFq 100%; RFD 67%; GC 100%). Accordingly, the implied weighting sensitivity scheme recovers this node under all concavities explored (not shown).

The subfamily Mysmeninae (node M91; see Appendix 5) comprises the remaining mysmenid

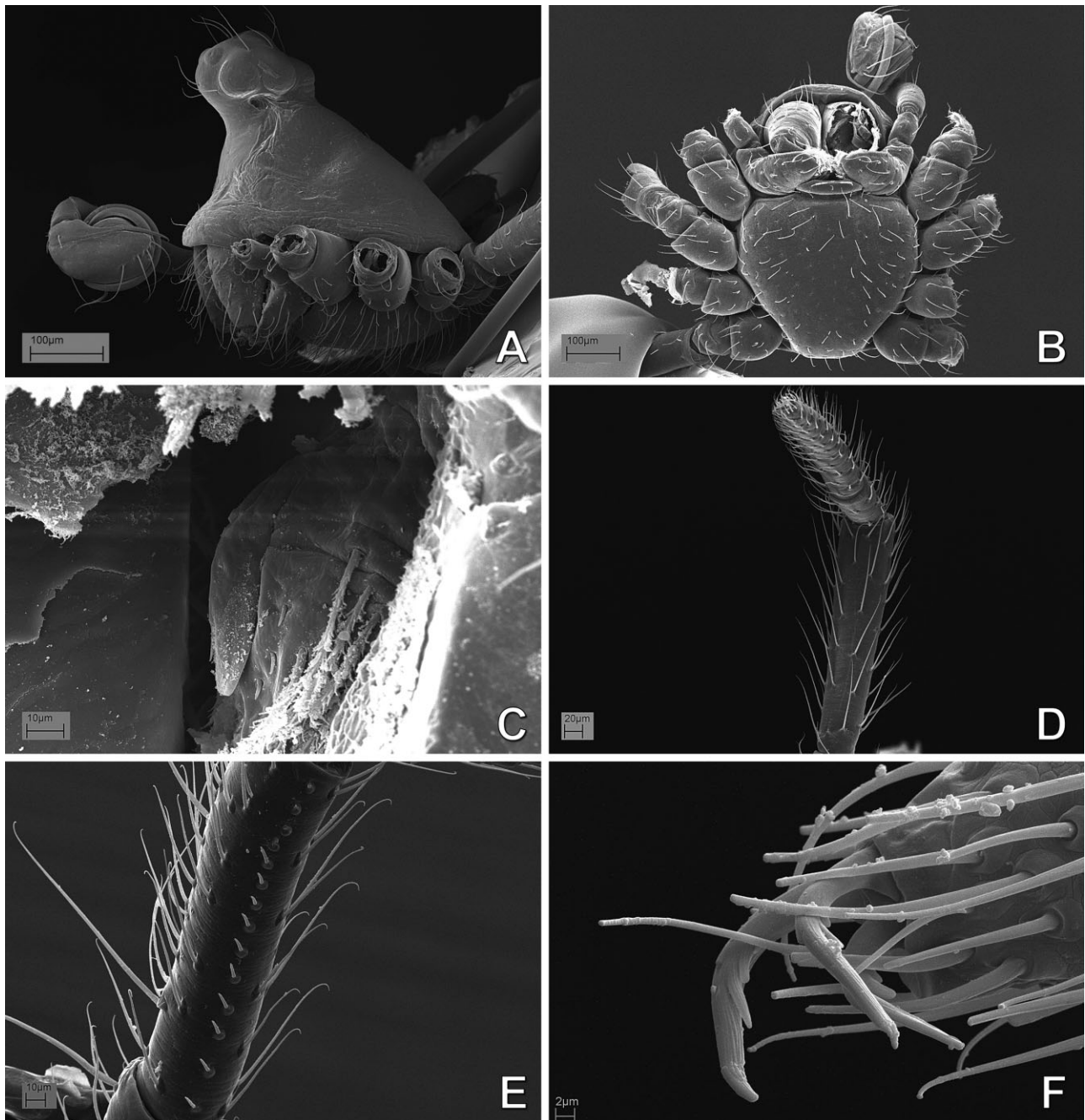


Figure 70. *Acrobleps hygrophilus* (Anapidae), male: A, prosoma, lateral view; B, same, ventral view; C, labrum, lateral view; D, left tibia I, ventral view; E, left tibia II, prolateral, view; F, right leg II, claws.

representatives studied here (that is, all mysmenids except *Maymena*, *Trogloneta*, *Isela*, and *Mysmenopsis*, BS 5.000; SFq 87%; RFD 83%; GC 83%). The implied weighting sensitivity analysis recovers the subfamily as monophyletic under all concavities. Two main clades resulted from the analysis. A distinct basal clade (node M118: MYSM-020-MAD and MYSM-023-MAD) is characterized by a particular male palpal morphology, among

other features, and has intermediate to low support (BS 6.120; SFq 70%; RFD 67%; GC 70%). Additionally, the implied weighting sensitivity analysis recovers this group under all concavities explored. The clade comprising the remaining lineages within Mysmeninae (node M90) has contradicting support values (BS 3.000; SFq of 27%, RFD 100%; GC 7%). The stability of this group is fairly high: it is monophyletic under nine

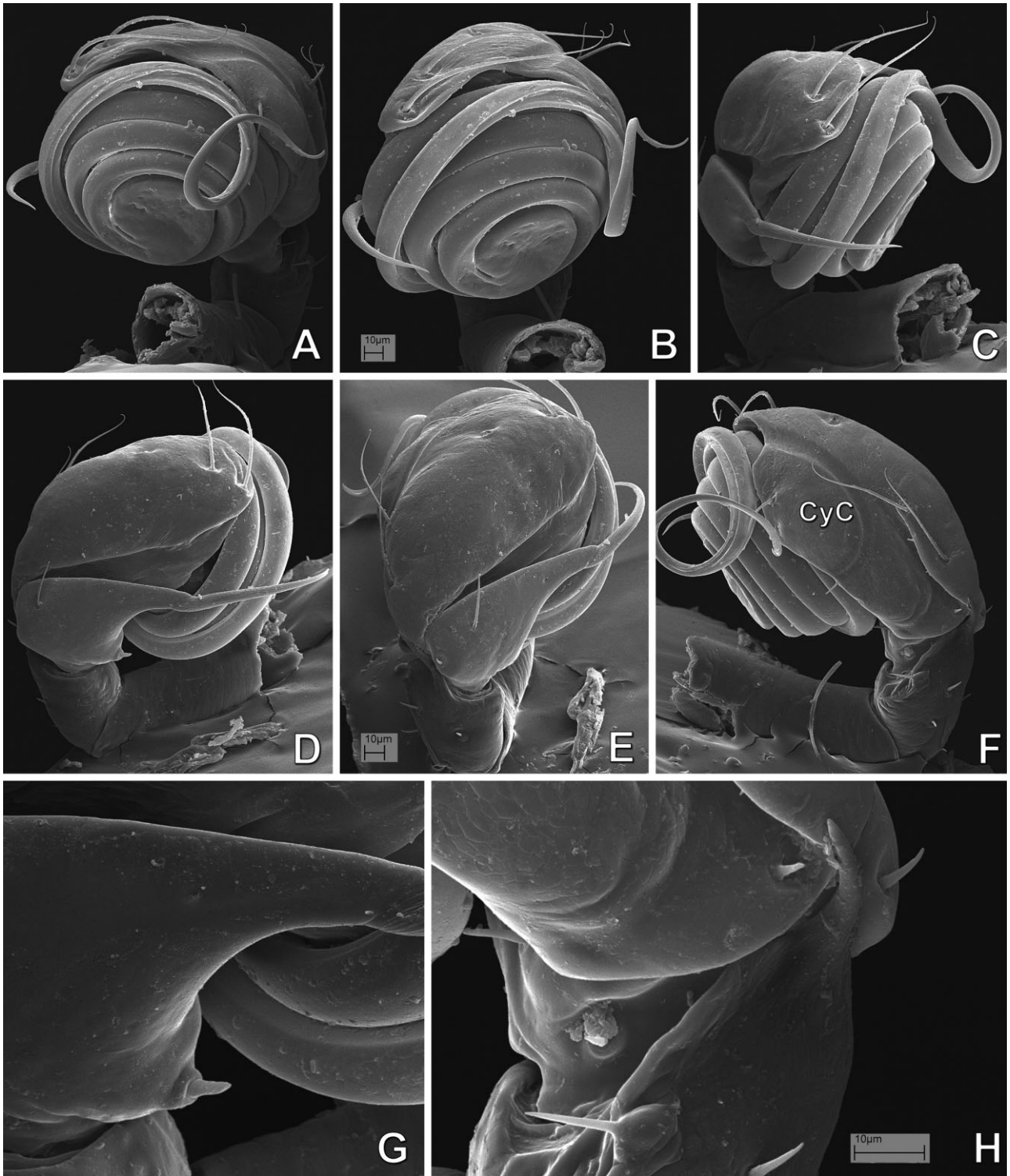


Figure 71. *Acrobleps hygrophilus* (Anapidae), male left palp: A, ventral view; B, ventral–prolateral view; C, prolateral view; D, prolaterodorsal view; E, dorsal view; F, retrolateral view; G, detail of tibial structures, detail from panel D; H, detail of patellar apophyses, retrolateral view, detail from panel F. See Appendix 3 for the list of abbreviations.

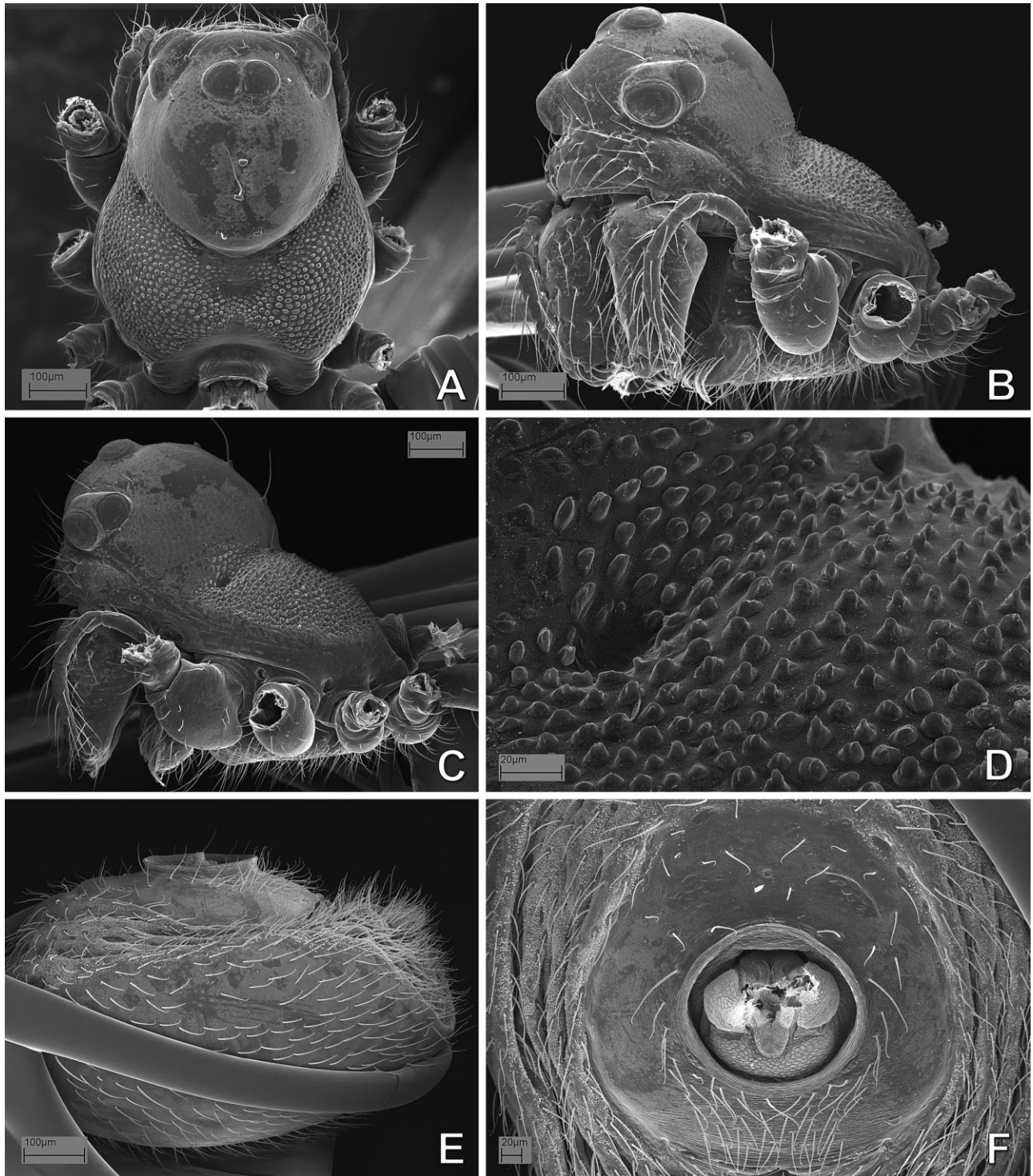


Figure 72. *Anapisona kethleyi* (Anapidae): A–D, female; E, F, male. A, prosoma, dorsal view; B, same, frontal–lateral view; C, same, lateral view; D, same detail of carapace cuticular pattern; E, abdomen, lateral view; F, same, detail of pedicel area, ventral view.

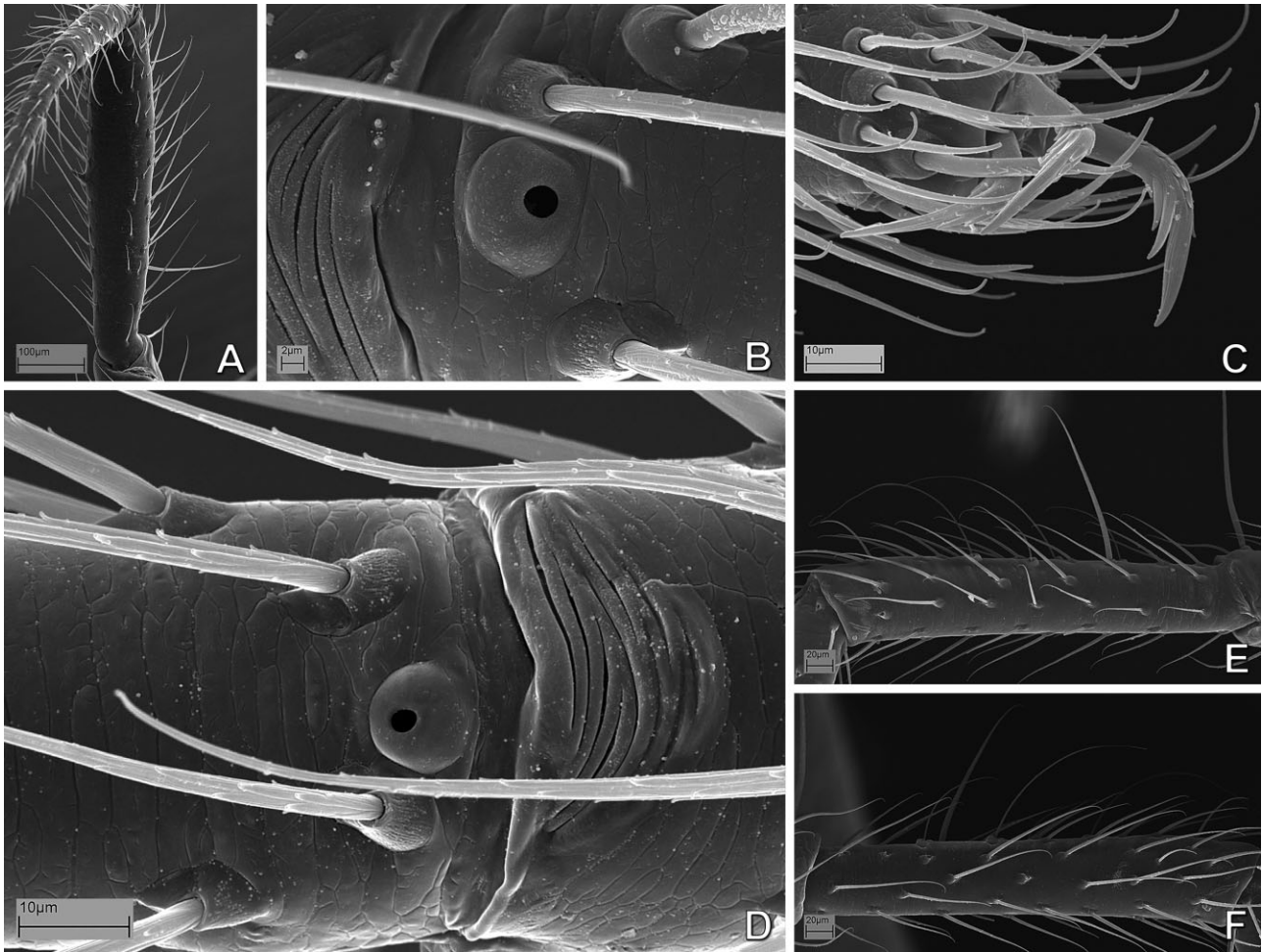


Figure 73. *Anapisona kethleyi* (Anapidae), left legs: A, male; B–F, female. A, tibia I, ventral view; B, leg I, tarsal organ, dorsal view; C, same, claws, prolateral view; D, leg IV, metatarsus–tarsus junction; E, tibia IV, retrolateral view; F, same, prolateral view.

concavities (all concavities except $k = 3, 6,$ and 8). In addition, low support and low stability values occur in most of the internal nodes of this clade.

DISCRETE MORPHOLOGICAL DATA SET
(65 TAXA, 350 CHARACTERS)

The cladistic analysis of the discrete morphological data set (65 taxa scored for 350 characters: i.e. excluding all seven continuous characters) resulted in 3835 MPTs of 1323 steps (CI = 0.349; RI = 0.663; see strict consensus in Fig. 157; see Table 6 for summary of analysis statistics and character composition). The family-level signal of the discrete characters analysed alone is essentially identical to the combined data set including continuous characters: each family represented by more than one taxon is monophyletic, and Mysmenidae are monophyletic excluding *Iardinis* (which falls within Symphytognathidae). Relation-

ships among families and among mysmenid genera differ slightly from the analysis of the complete data set, as follows. Synaphridae are no longer sister to the Anapidae + Symphytognathidae clade. Instead, Synaphridae are placed basally, sister to all other symphytognathoids, a relationship recovered under most concavity values in the implied weighting sensitivity analyses of the complete morphological data set. As in the complete analysis, Mysmenidae and Theridiosomatidae are sister taxa. Within Mysmenidae, clades (and correspondent subclades) common to both analyses include (node numbers refer to consensus of the complete morphological analysis, Fig. 153): *Maymena*, *Mysmenopsis*, *Isela*, Mysmenopsinae, *Trogloneta*, Mysmeninae, *Kekenboschiella*, and node M118 (compare Figs 153, 157). *Trogloneta* is sister to Mysmeninae when continuous characters are excluded. Few clades within Mysmeninae are recovered. MYSM-005-ARG is the basal taxon, sister to all

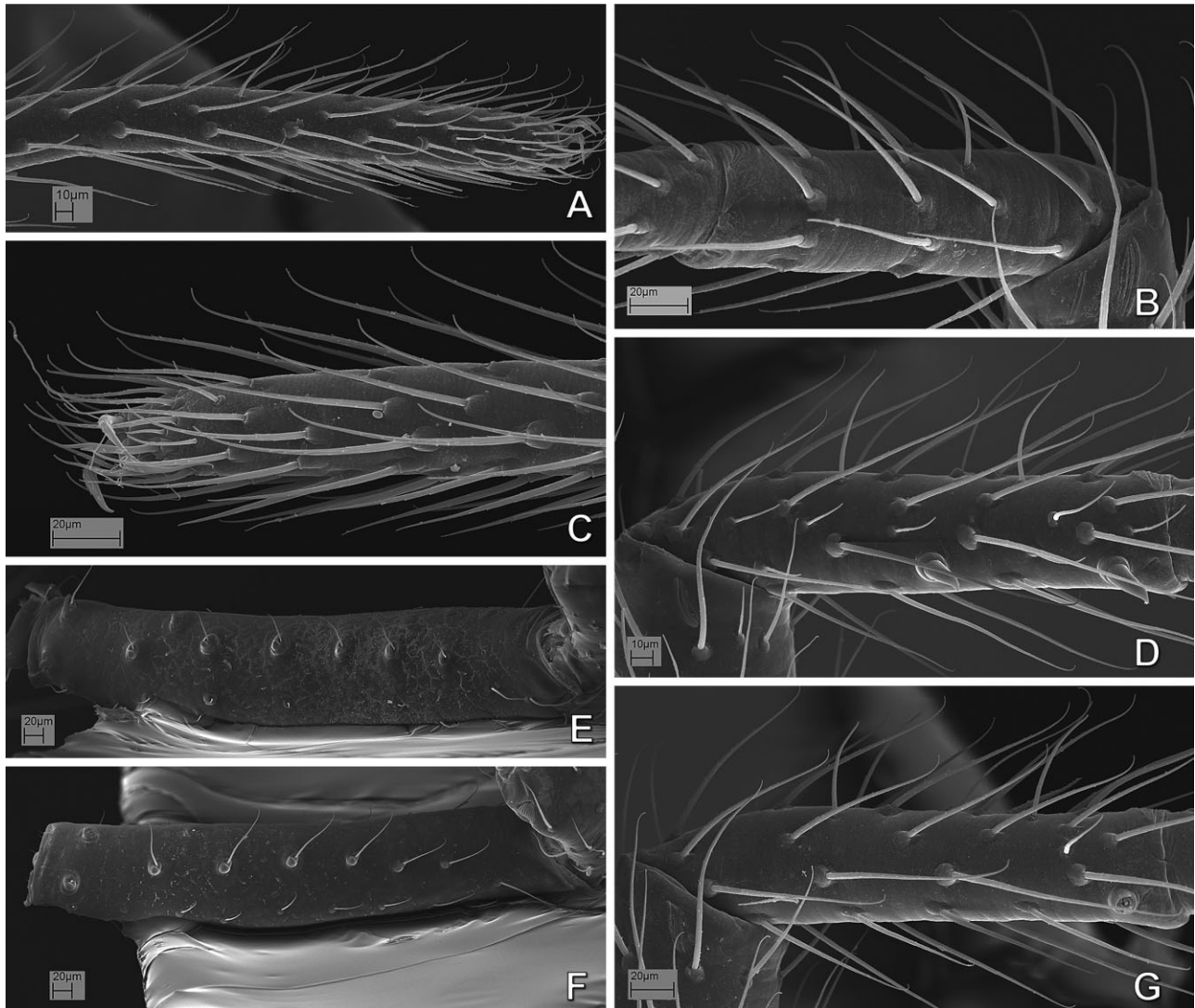


Figure 74. *Anapisona kethleyi* (Anapidae), left legs: A, B, D, E, male; C, F, G, female. A, tarsus I, prolateral view; B, metatarsus IV, retrolateral view; C, tarsus IV, retrolateral view; D, G, metatarsus I, prolateral view; E, F, femur I, retrolateral view.

remaining mysmenines, which comprise a mostly unresolved clade.

In order to assess the effect of continuous characters on the phylogenetic signal of the discrete characters alone (i.e. conflict or agreement between the two subsets of data), support differences for common clades between the discrete and the complete morphological data sets were examined (see also Goloboff *et al.*, 2006). Differences on the symmetric resampling frequencies and GC were compared and plotted on the consensus of the discrete analysis (Fig. 158, compare values on Figs 154, 157). Out of a total of 27 common clades between the two consensus trees, support when including the continuous characters decreased in 14 groups for GC (13 groups for absolute frequencies), with a sum

of support differences of 254 and 144 (respectively); increased in nine groups for GC (eight groups for absolute frequencies), with a sum of support differences of 118 and 77 (respectively); and remained unchanged in four groups for GC (six groups for absolute frequencies). Unexpectedly, it appears that in our analyses the tendency when adding continuous characters is an overall decrease in support of approximately 50%.

FAMILIAL PLACEMENT OF TAXA OF UNCERTAIN AFFINITIES (70 TAXA, 357 CHARACTERS)

The cladistic analysis of the complete morphological data set, including five taxa with more than 78% of

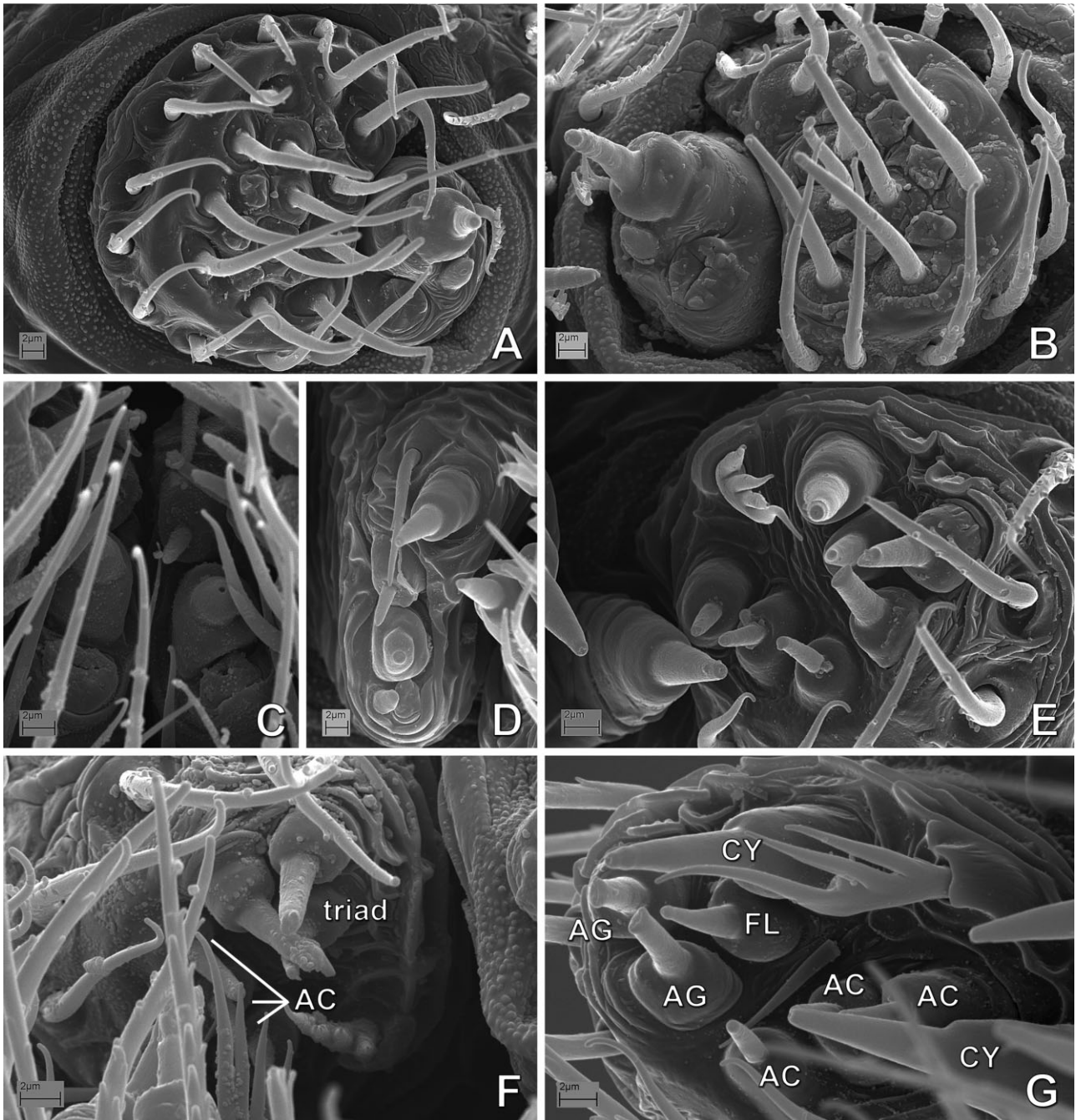


Figure 75. *Anapisona kethleyi*, spinnerets: A, D, E, G, female; B, C, F, male. A, B, anterior lateral spinnerets; C, D, posterior median spinnerets; E–G, posterior lateral spinnerets. See Appendix 3 for the list of abbreviations.

missing data (i.e. *Calodipoena tarautensis*, *Crassinatha haeneli*, *Iardinis martensi*, *Leviola termitophila*, and *Phricotelus stelliger*; 70 taxa, 357 characters) rendered three MPTs of 1545.559 steps (CI = 0.360; RI = 0.664; see strict consensus in Fig. 159). A total of 312 characters (87.4%) are phylogenetically informative, and the remaining 12.6% characters are autapomorphic (for a summary of the analysis of sta-

tistics and character composition, see Table 6). Overall, the resulting pattern of relationships is essentially similar to that of the complete morphological data set including 65 taxa. Each family represented by more than one taxon is monophyletic and, as previously found, *Iardinis mussardi* is placed within Symphytognathidae. All three MPTs support the symphytognathoids interfamilial relationships, with Theridiosomatidae sister

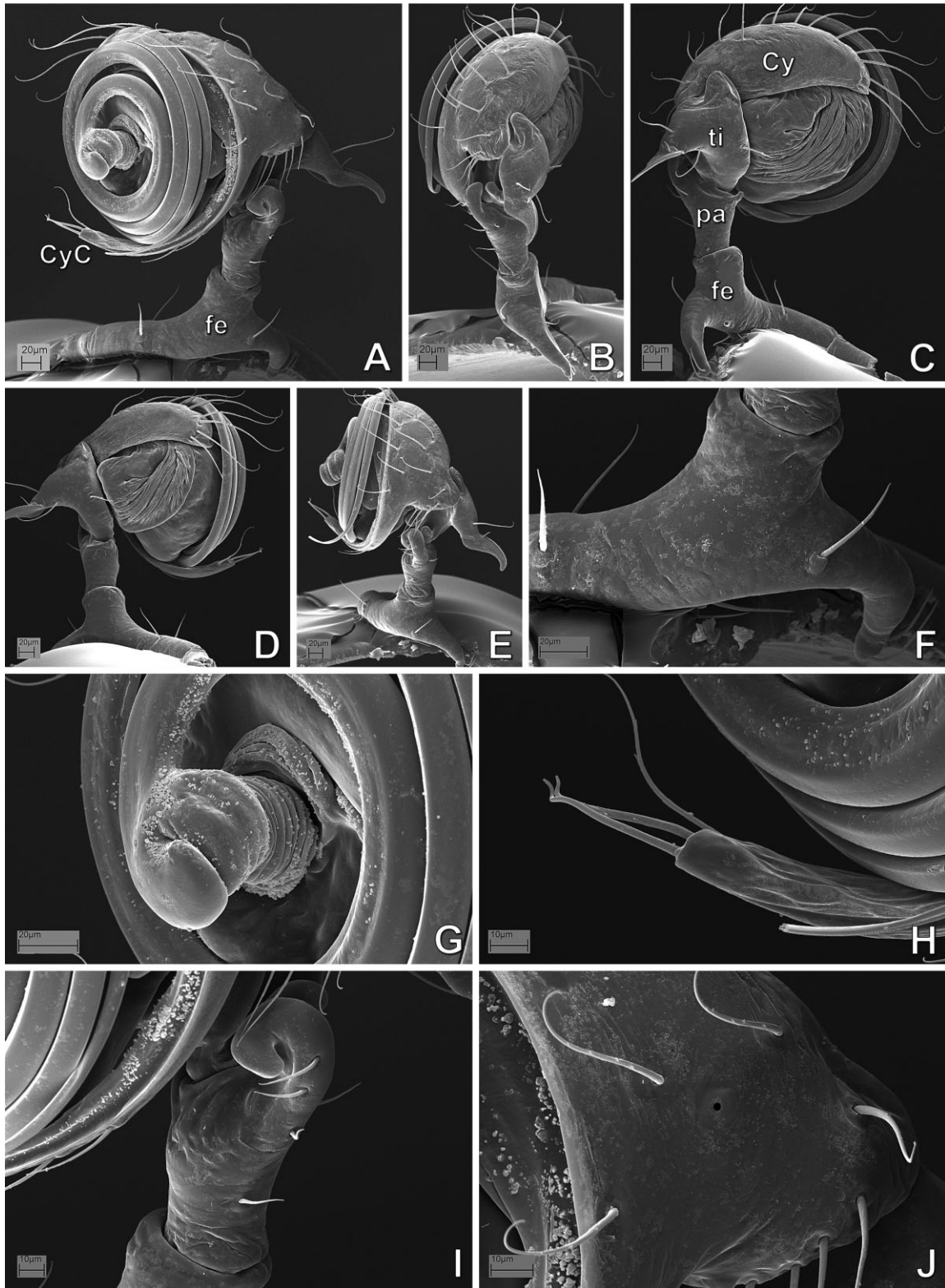


Figure 76. *Anapisona kethleyi* (Anapidae), male right palp, inverted. A, retrolateral view; B, dorsal view; C, prolateral-dorsal view; D, prolateral view; E, retrolateral-dorsal view; F, detail of femur, retrolateral view; G, detail of embolic base, retrolateral view; H, detail of tip of cymbial conductor; I, detail of patella, retrolateral view; J, cymbial tarsal organ, retrolateral view. See Appendix 3 for the list of abbreviations.

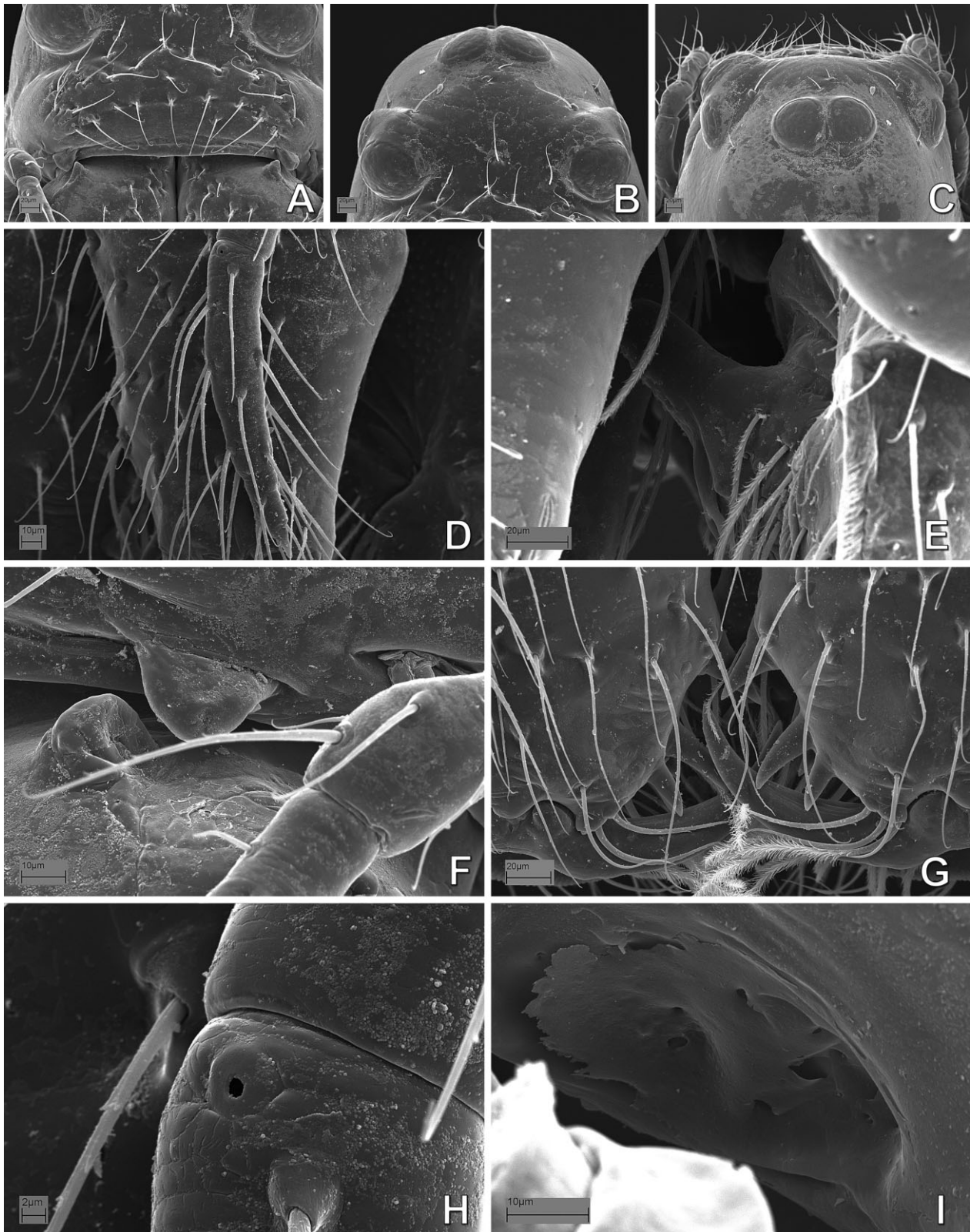


Figure 77. *Anapisona kethleyi* (Anapidae), female prosoma: A, clypeus and cheliceral bases, frontal view; B, ocular area, frontal view; C, same, dorsal view; D, left palpal tarsus; E, labrum, lateral view; F, detail of cheliceral lateral condyle-boss; G, distal chelicerae, cheliceral fang and teeth; H, palpal tarsal organ; I, carapace lateral depression.

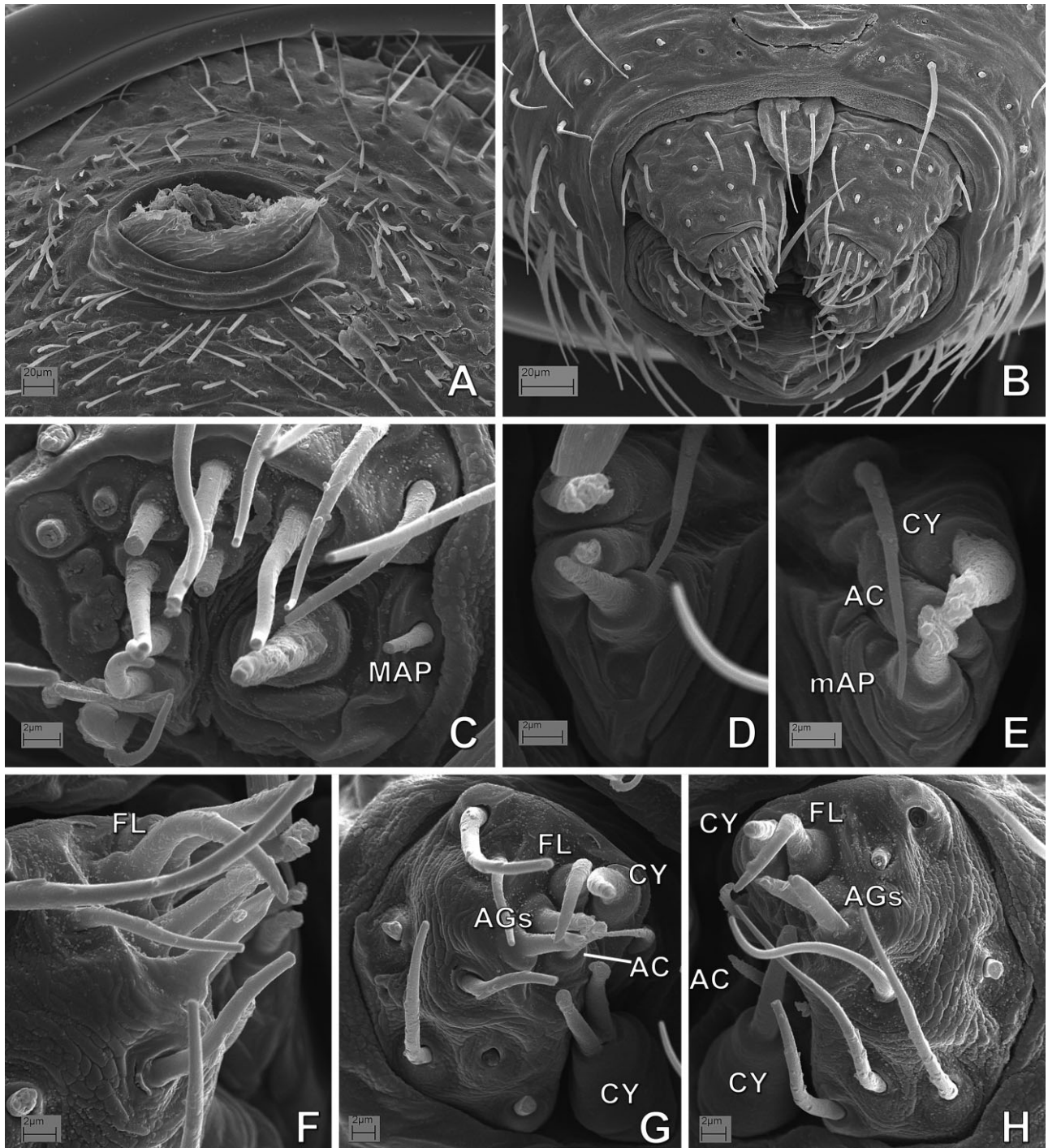


Figure 78. *Comaroma simoni* (Anapidae), female abdomen: A, pedicel area, ventral–posterior view; B, spinning field, colulus, and posterior spiracle, ventral–posterior view; C, right anterior lateral spinneret; D, right posterior median spinneret (PMS); E, left PMS; F, right posterior lateral spinneret (PLS), lateral view; G, same, posterior view; H, left PLS. See Appendix 3 for the list of abbreviations.

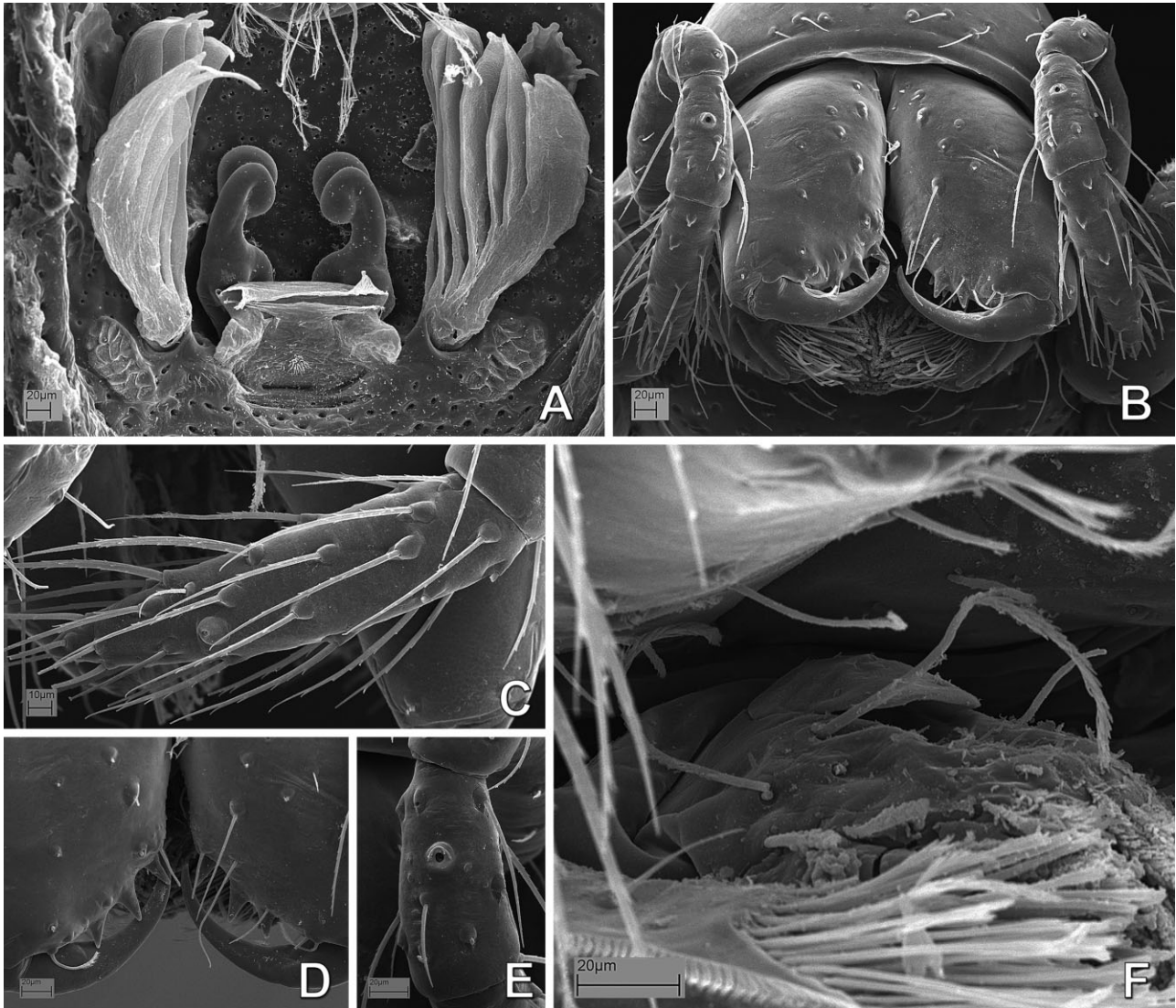


Figure 79. *Comaroma simoni* (Anapidae), female. A, digested abdomen, anterior respiratory system and vulva; B, mouthparts, ventral–frontal view; C, right palpal tarsus, retrolateral view; D, distal chelicerae, frontal view; E, left palpal tibia, dorsal view; F, labrum.

to Mysmenidae, Anapidae sister to Symphytognathidae, and Synaphridae sister to (Anapidae + Symphytognathidae); however, because of the alternative placements of *Phricotelus* (see below), relationships among the latter three families are unresolved. Regarding the familial placement of taxa with a high proportion of missing data, we suggest the following:

CALODIPOENA TARAUTENSIS BAERT 1988 (FIG. 130A)

Calodipoena tarautensis Baert, 1988: 17, fig. 21 [female holotype and female paratype from Sulawesi (Indonesia), Sulawesi Utara, Dumoga Bone National Park, Toraut, Grassland, 200 m, 27.x.1985, R. Bosman &

J. Van Stalle, in IRSN (no. IG 26977), male unknown, female paratype examined].

Familial placement: Mysmenidae. As expected, this species grouped within one of the largest clades within Mysmeninae, which includes *Calodipoena mootae*, *Mysmena leichhardti*, *Anjouanella*, *Microdipoena s.s.*, *Mysmenella*, and three undescribed species [*Mysmena*-MYSM-015-MAD, MYSM-(029 034)-MAD]. *Calodipoena tarautensis* is known only from females, and shares with mysmenines several features, such as femoral spots on legs I and II, wide posterior tracheal spiracle, anterior tracheae, absence of epigynal plate, long scape, highly membranous and complex pattern of ducts in

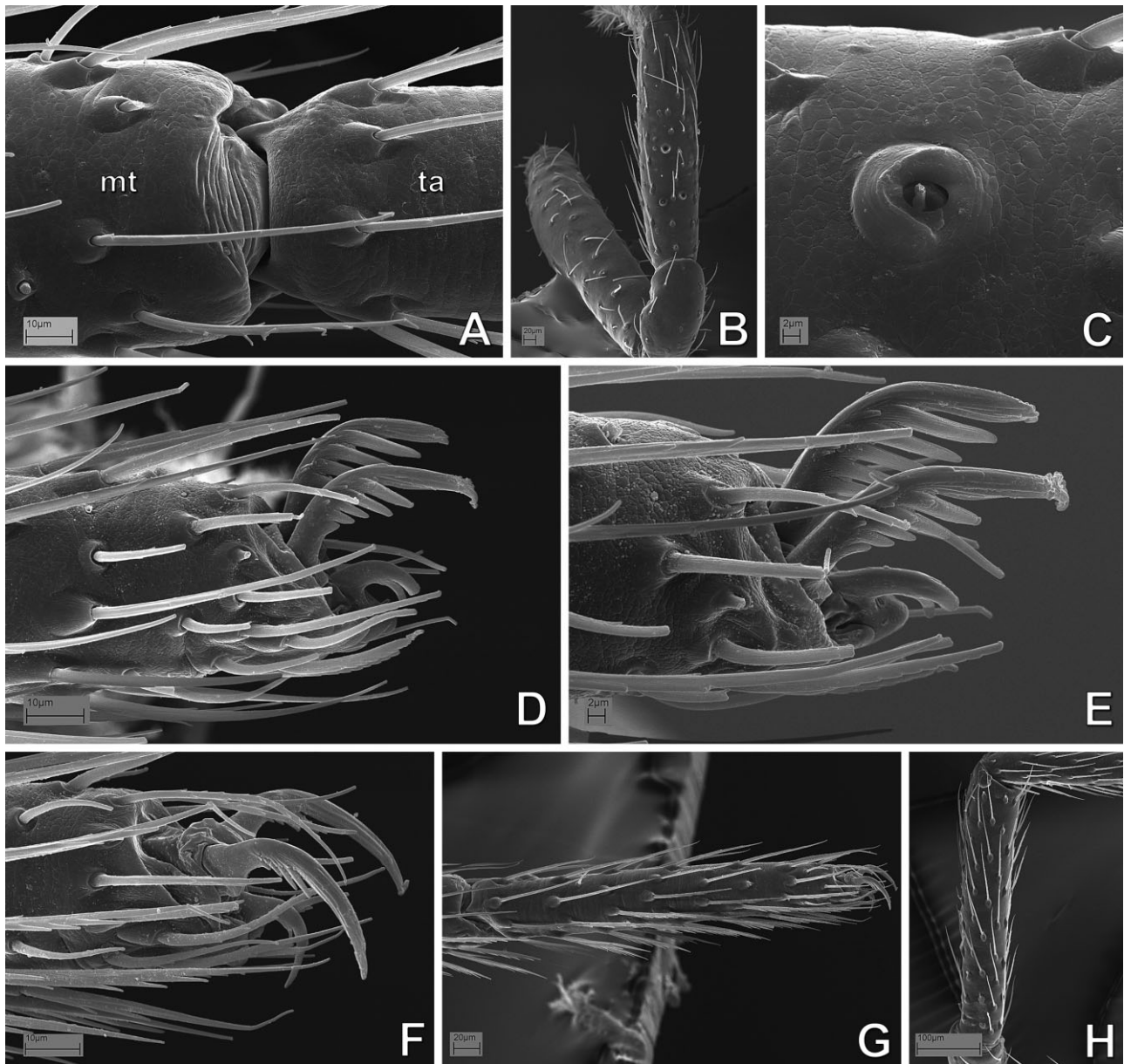


Figure 80. *Comaroma simoni* (Anapidae), female left legs: A–E, left leg I; F–H, left leg IV. A, metatarsus–tarsus junction, dorsal view; B, patella, tibia, dorsal view; C, metatarsal trichobothrial base; D–F, claws, prolateral view; G, tarsus, prolateral view; H, tibia, prolateral view. See Appendix 3 for the list of abbreviations.

the vulva, absence of palpal claw but palp with all segments, and absence of pore-bearing depressions.

GENUS *CRASSIGNATHA* WUNDERLICH 1995

Crassignatha Wunderlich, 1995: 546. Type species by original designation and monotypy: *Crassignatha haeneli* Wunderlich 1995: 547 (type and only specimen not examined, scored from literature). Miller *et al.* 2009: 68 (transfer from Mysmenidae to Symphytognathidae).

Familial placement: Symphytognathidae. The placement of this genus within Symphytognathidae was recently proposed by Miller *et al.* (2009) based exclusively on morphological comparative observations (as here, the type species was also not examined). This placement is corroborated by the results of our phylogenetic analysis. *Crassignatha* nested within Symphytognathidae as sister to a distal clade comprising three undetermined symphytognathid species (SYMP-002-MAD, SYMP-006-AUST, and SYMP-007-AUST). The

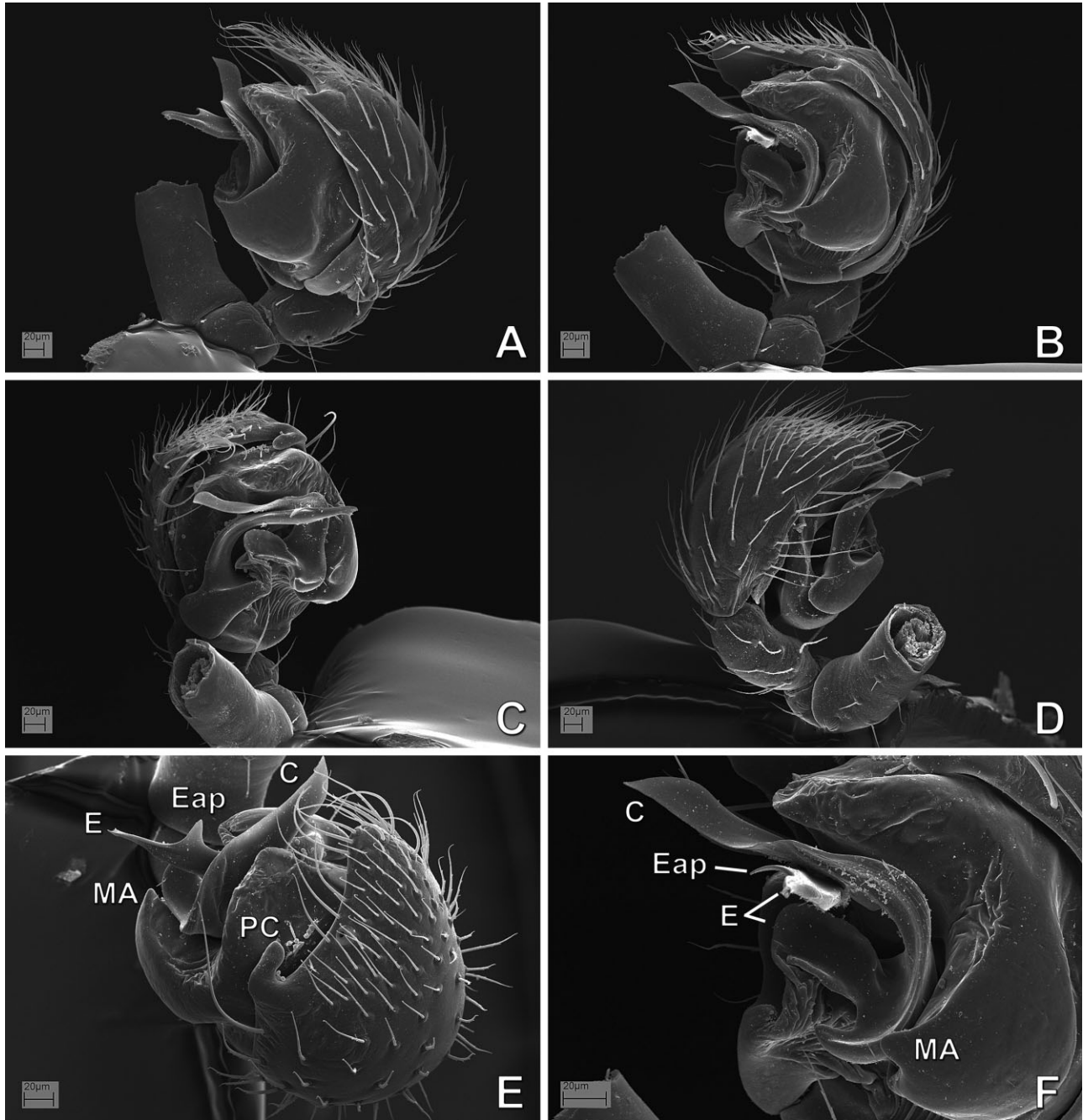


Figure 81. *Comaroma simoni* (Anapidae), male left palp: A, retrolateral view; B, ventral view; C, ventral–distal view; D, prolateral view; E, distal view; F, bulb, detail from panel B. See Appendix 3 for the list of abbreviations. See Appendix 3 for the list of abbreviations.

type species of *Crassignatha*, *Crassignatha haeneli*, is known only from a male specimen (holotype), has none of the synapomorphic features of Mysmenidae, and consequently its placement in a different family is hardly surprising. It differs from Mysmenidae in the absence of femoral spots, absence of tibial or metatarsal clasping spines on leg I, prolateral (instead of ventral)

cymbium, absence of cymbial structures (e.g. primary conductor, process, and paracymbium), absence of pars pendula, and presence of median apophysis. In addition, *Crassignatha* shares with Symphytognathidae the loss of the anterior median eyes, promarginal cheliceral teeth originating from a common base or raised plate, and loss of the colulus. It also shares with several

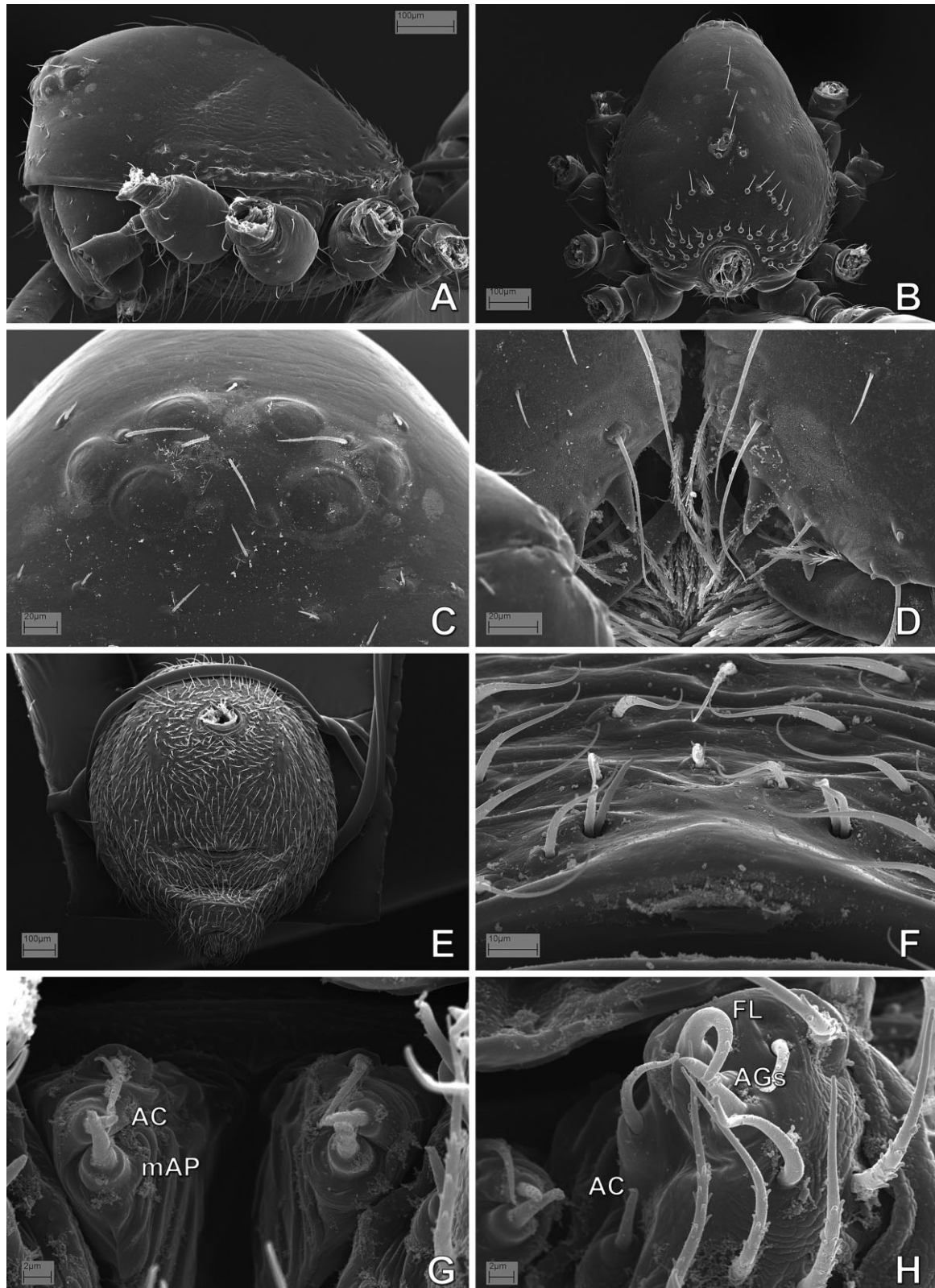


Figure 82. *Comaroma simoni* (Anapidae), male: A, prosoma, lateral view; B, same, dorsal view; C, ocular area, frontal view; D, distal chelicerae, frontal view; E, abdomen, ventral view; F, epiandrous spigots; G, posterior median spinnerets; H, left posterior lateral spinneret. See Appendix 3 for the list of abbreviations.

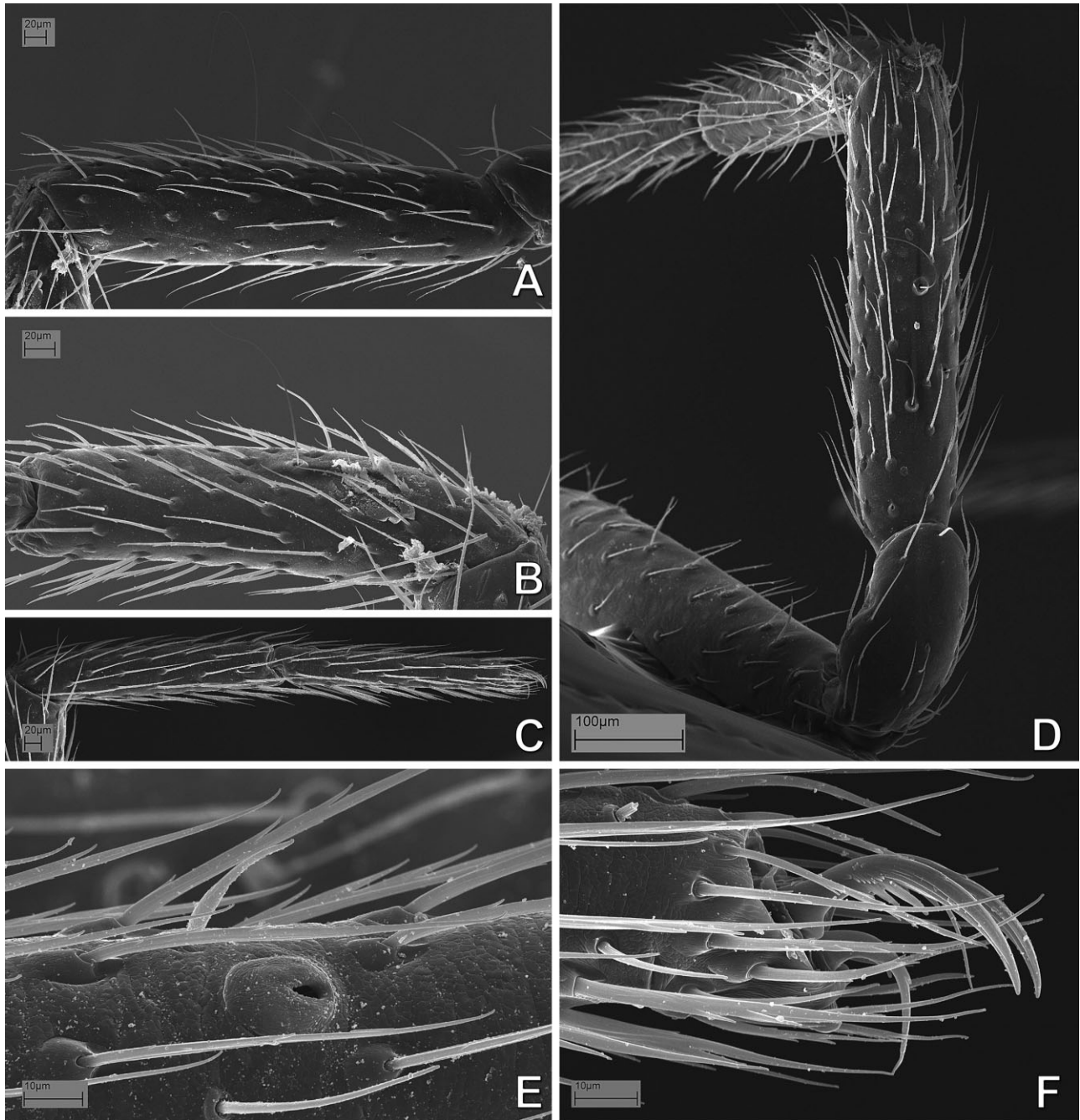


Figure 83. *Comaroma simoni* (Anapidae), male left legs: A, tibia I, retrolateral; B, metatarsus I, retrolateral; C, metatarsus, tarsus IV, prolateral; D, patella, tibia I, prolaterodorsal; E, leg I, tarsal organ; F, leg IV, claws, prolateral.

symphytognathids in this data set a clasping spine located ventrally on tibia II and the absence of palpal patellar or tibial apophyses.

GENUS *IARDINIS* SIMON 1899 (FIGS 135A, B, 144C)
Iardinis Simon, 1899: 87. Type species by original designation: *Iardinis weyersi* Simon 1899: 87 (*nomen*

dubium, female type and only specimen lost); Levi & Levi, 1962: 22 (considered *incertae sedis*); Forster & Platnick, 1977: 5 (considered *nomen dubium*); Brignoli, 1970: 1426; 1978: 250; 1980: 731 (provisional transfer to Mysmenidae).

Iardinus, Gertsch, 1960a: 8 (*lapsus calami*, transferred from Theridiidae to Symphytognathidae s.l.).

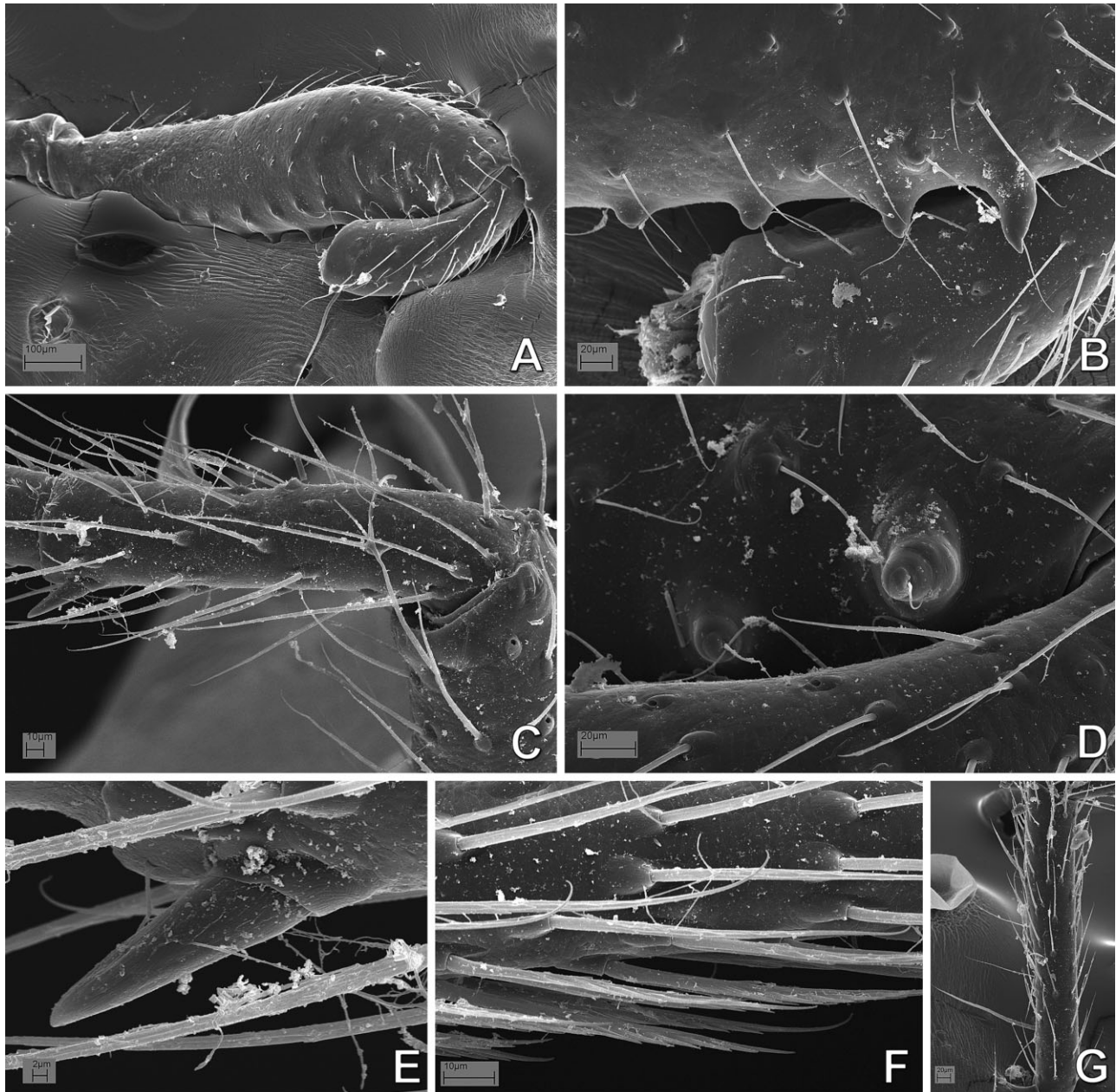


Figure 84. *Crassanapis chilensis* (Anapidae), right legs: A–E, right legs I; F, G, right legs IV. A, B, D, G, male; C, E, F, female. A, femur and patella, retrolateral; B, same, detail; C, metatarsus, prolateral; D, detail of setal bases on ventral femur; E, metatarsal clasp spur, detail from panel C; F, detail of tarsal ventral setae, retrolateral view; G, tibia, retrolateral view.

Familial placement: Symphytognathidae. The type and only specimen of the type species (*Iardinus weyersi*) from Sumatra was described by Simon in 1899, but has been considered lost by the arachnologists that have tried to examine the type material (Gertsch, 1960a; Levi & Levi, 1962; Brignoli, 1970, 1978, 1980; Forster & Platnick, 1977). The vial from the Paris Museum (MNHN) with the original label that

should have housed the type material is actually empty (L. Lopardo & G. Hormiga, pers. observ.). Nevertheless, two additional species have been described for the genus: *Iardinus martensi* Brignoli, 1978 from Nepal, and *Iardinus mussardi* Brignoli 1980 from India (holotype examined, see also Figs 135A, B, 144C). Both species are exclusively known from their male type specimens. To add to the enigmatic status of

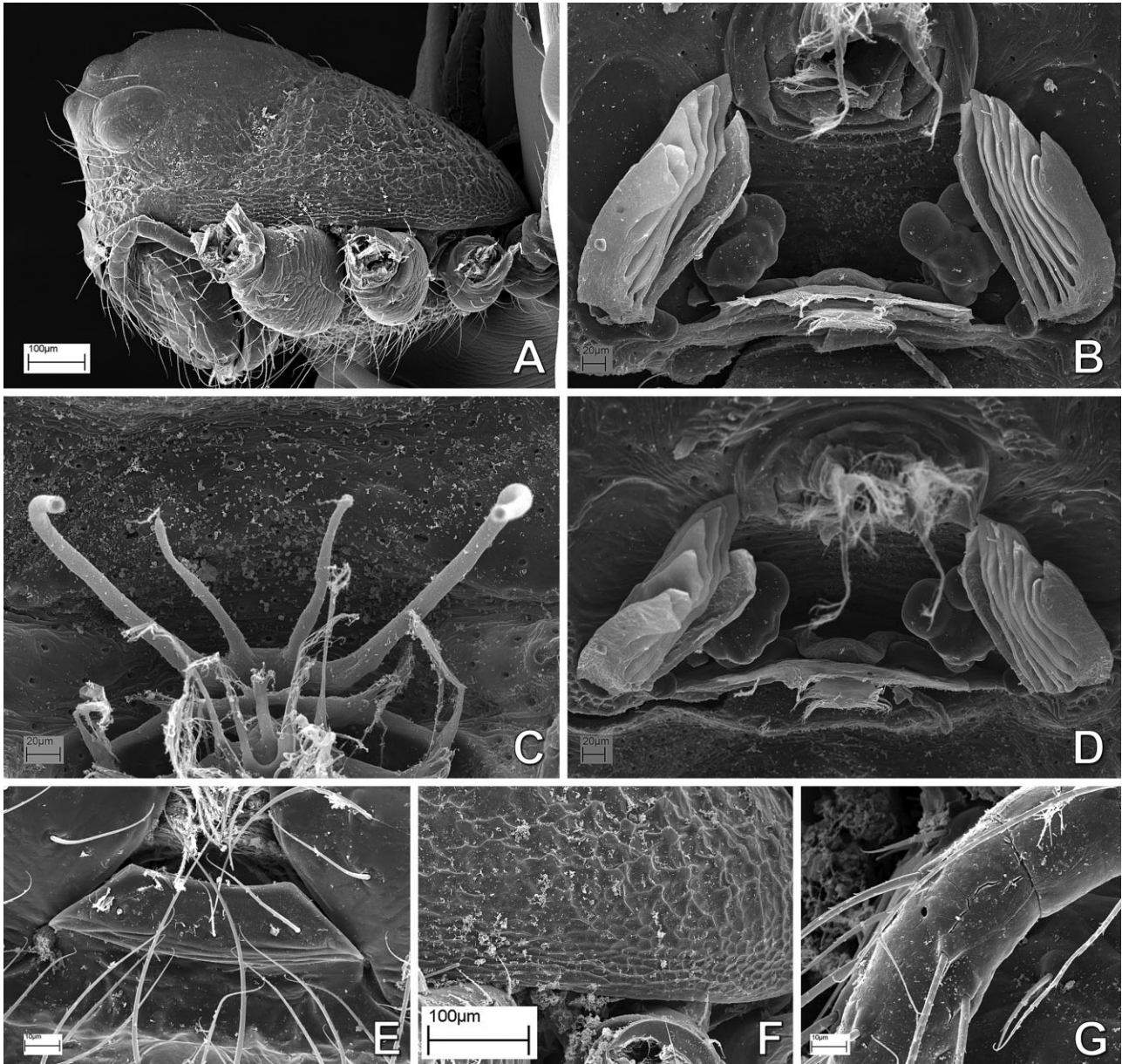


Figure 85. *Crassanapis chilensis* (Anapidae), female: A, prosoma, lateral view; B, digested abdomen, anterior respiratory system and vulva, dorsal view; C, same, posterior respiratory system; D, same, anterior respiratory system and vulva, dorsal–anterior view; E, labium, ventral view; F, carapace, lateral cuticular pattern; G, left palpal tarsus.

the genus, the original vial containing the type and only specimen of *I. martensi* instead contained a female anapid (L. Lopardo & G. Hormiga, pers. observ.), and therefore its morphology had to be scored from the literature.

Nonetheless, both *Iardinis* species included in the 65- and 70-taxa data sets (i.e. *I. martensi* and *I. mussardi*) are more closely related to Symphytognathidae than to Mysmenidae. Morphologically these species have none of the synapomorphic features of Mysmenidae, and thus, as with *Crassignatha*, their

placement in a different family was expected. They differ from Mysmenidae in the absence of femoral spots (at least in *I. mussardi*), absence of tibial or metatarsal clasping spines on leg I, dorsal (instead of ventral) cymbium, absence of cymbial structures (e.g. primary conductor, process, and paracymbium), and presence of median apophysis. They further share with Symphytognathidae the loss of anterior median eyes, thick setae on the dorsal part of the abdomen, absence of cheliceral denticles, loss of colulus, and absence of palpal patellar or tibial apophyses.

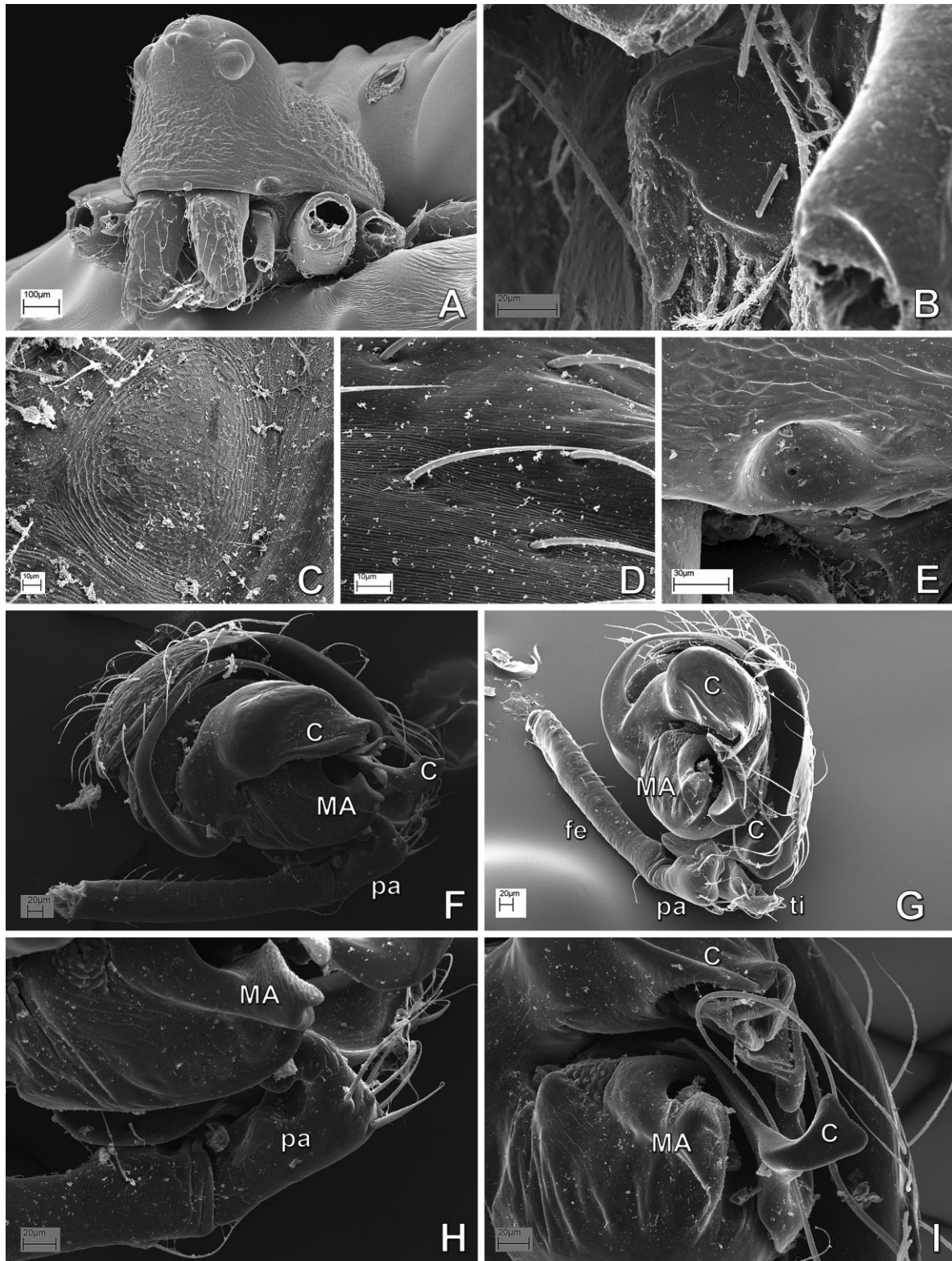


Figure 86. *Crassanapis chilensis* (Anapidae), male: A, prosoma, frontal-lateral view; B, labrum, lateral view; C, booklung cover; D, abdominal cuticle; E, carapace lateral depression. F, H, right palp, inverted; G, I, left palp. F, ventral view; G, ventral-proximal view; H, detail of patella and median apophysis; I, detail of median apophysis, conductor, and tip of embolus. See Appendix 3 for the list of abbreviations.

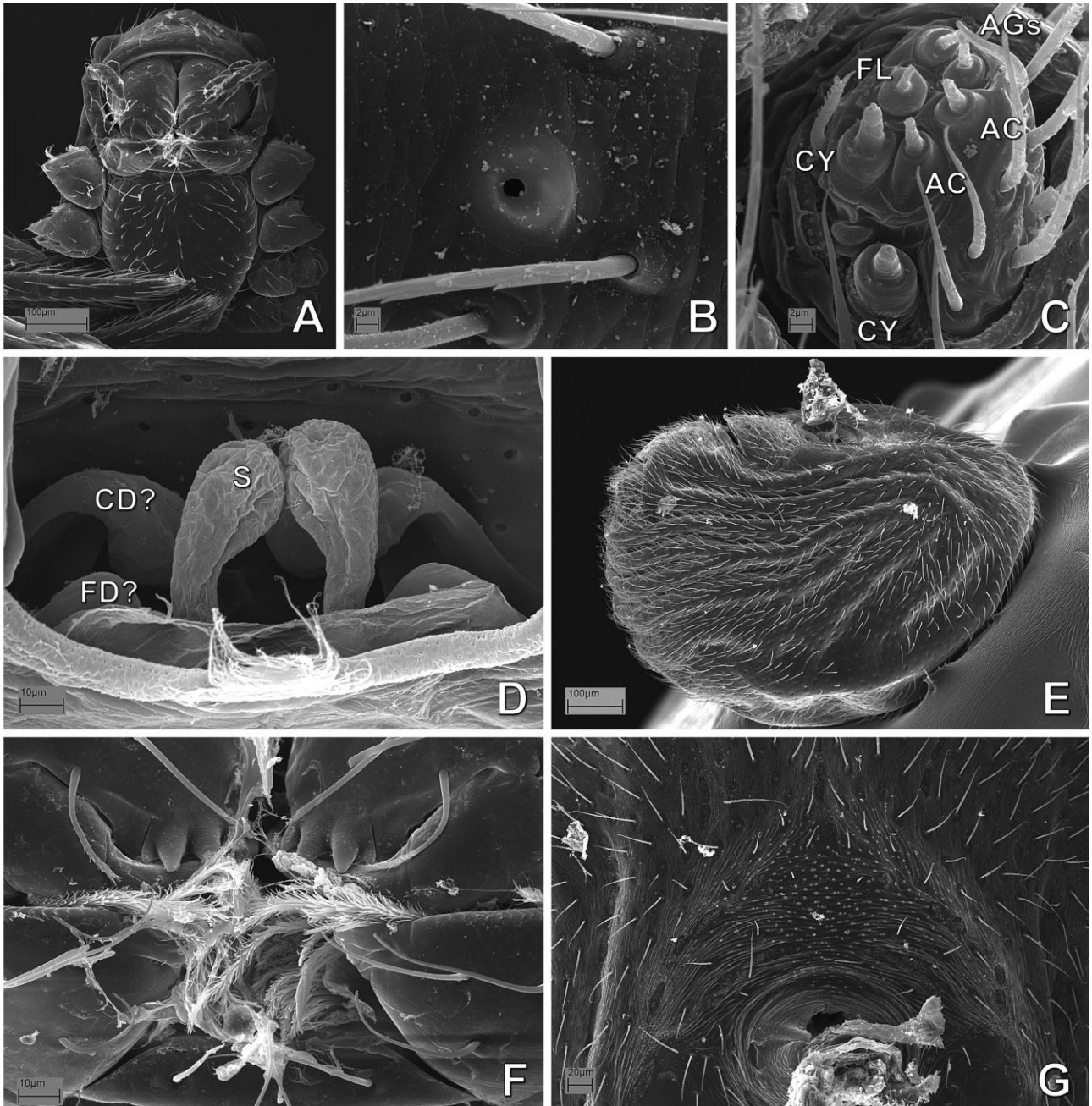


Figure 87. *Elanapis aisen* (Anapidae), female: A, prosoma, ventral view; B, left tarsus I, detail of tarsal organ; C, left posterior lateral spinneret; D, digested abdomen, detail of vulva; E, abdomen, lateral view; F, mouthparts, ventral view; G, abdomen, anterior pedicel area, ventral view. See Appendix 3 for the list of abbreviations.

GENUS *PHRICOTELUS* SIMON, 1895
(FIGS 135C, 144B)

Phricotelus Simon, 1895a: 919. Type species by original designation and monotypy: *Phricotelus stelliger* Simon, 1895a: 919 (type specimen examined); Levi, 1972: 534 (transferred from Theridiosomatidae to Symphytognathidae); Brignoli, 1980: 731, 1981: 14 (provisional transfer to Mysmenidae).

Familial placement: Araneoidea incertae sedis. Alternative equally parsimonious placements of *Phricotelus* imply various relationships to Synsphyridae, Anapidae, or Symphytognathidae; therefore, its placement becomes unresolved in the strict consensus cladogram. In the resulting three MPTs, *Phricotelus* is placed as the most basal species of Anapidae, Anapidae + Symphytognathidae, or Synsphyridae. Although much of the morphology for *P. stelliger* needs to be properly

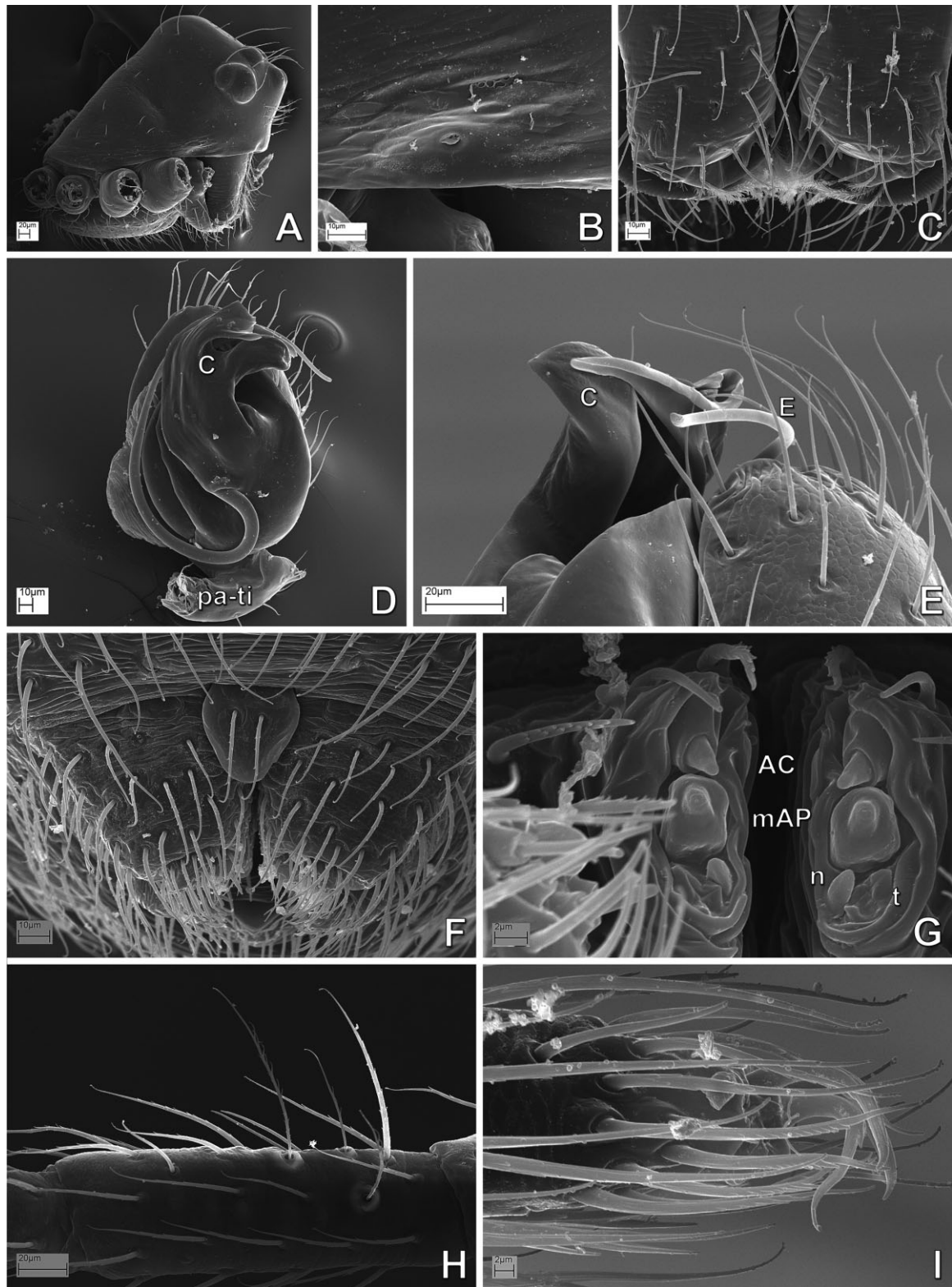


Figure 88. *Elanapis aisen* (Anapidae), male: A, prosoma, lateral view; B, detail of carapace lateral depression; C, chelicerae, frontal view; D, right palp, inverted, ventral view; E, same, detail of tip of palp, retrolateral view; abdomen, detail of colulus, posterior spiracle and spinnerets, ventral view; G, posterior median spinnerets; H, tibia III; I, leg IV, claws. See Appendix 3 for the list of abbreviations.

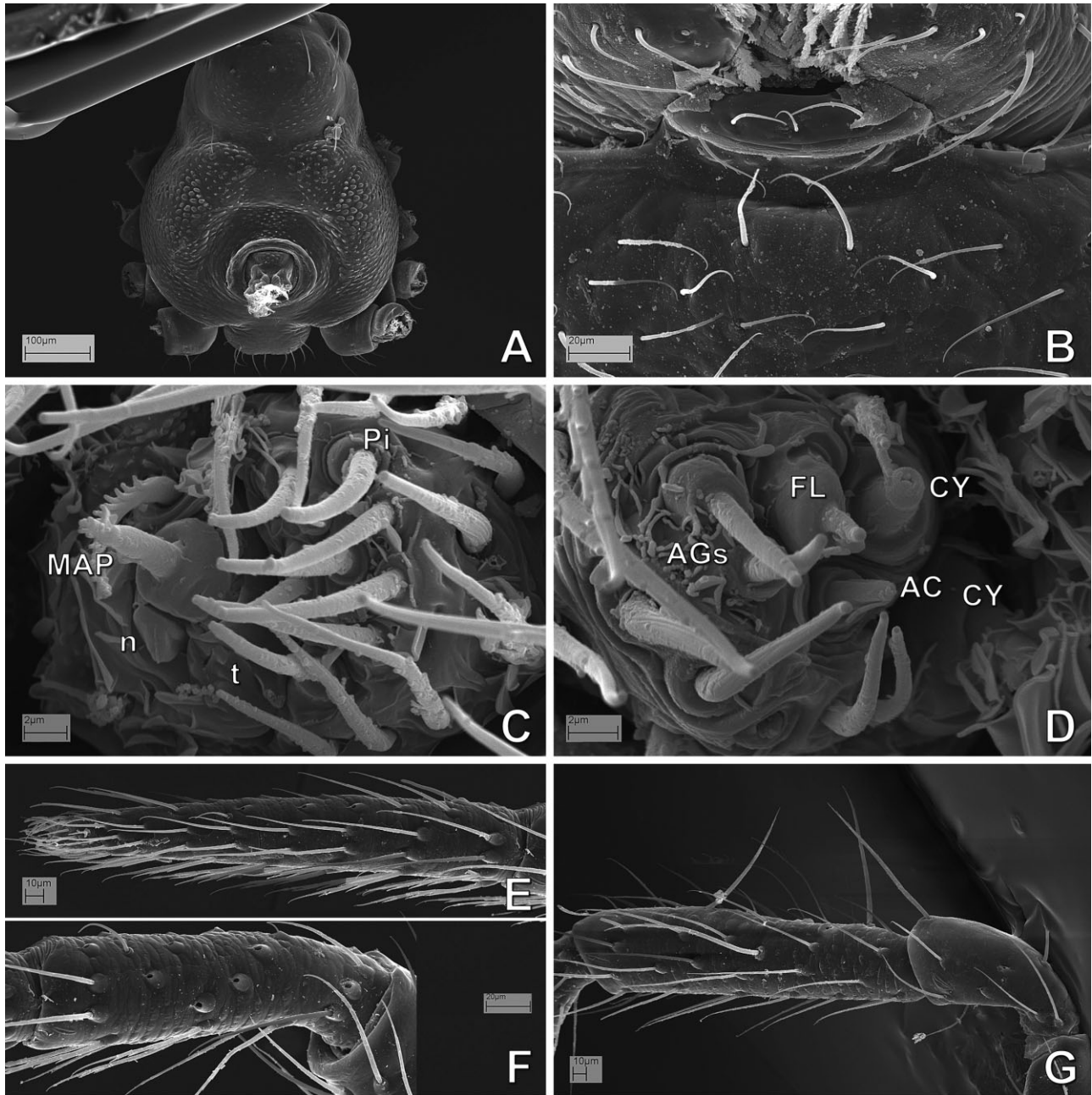


Figure 89. *Minanapis casablanca* (Anapidae), female: A, prosoma, dorsal view; B, labium–sternum junction, ventral view; C, left anterior lateral spinneret; D, right posterior lateral spinneret. E–G, right leg I, prolateral view; E, tarsus; F, meta-tarsus; G, tibia and patella. See Appendix 3 for the list of abbreviations.

scored, the type species of this genus, only known by females, was not placed within or closely related to Mysmenidae. Furthermore, its placement within symphytognathoids also remains uncertain. Morphologically, *Phricotelus* has none of the synapomorphic features that diagnose Mysmenidae, and thus its placement in a different family was expected. Although females have long scape, no

epigynal plate (Fig. 135C), no pore-bearing depression on lateral edges of the carapace, and a narrow posterior respiratory spiracle located in front of the spinnerets, the species differs from Mysmenidae in the absence of femoral spots, two pairs of spermathecae, and abdomen extremely projected posteriorly (see Figs 135C, 144B; further morphological details not observed).

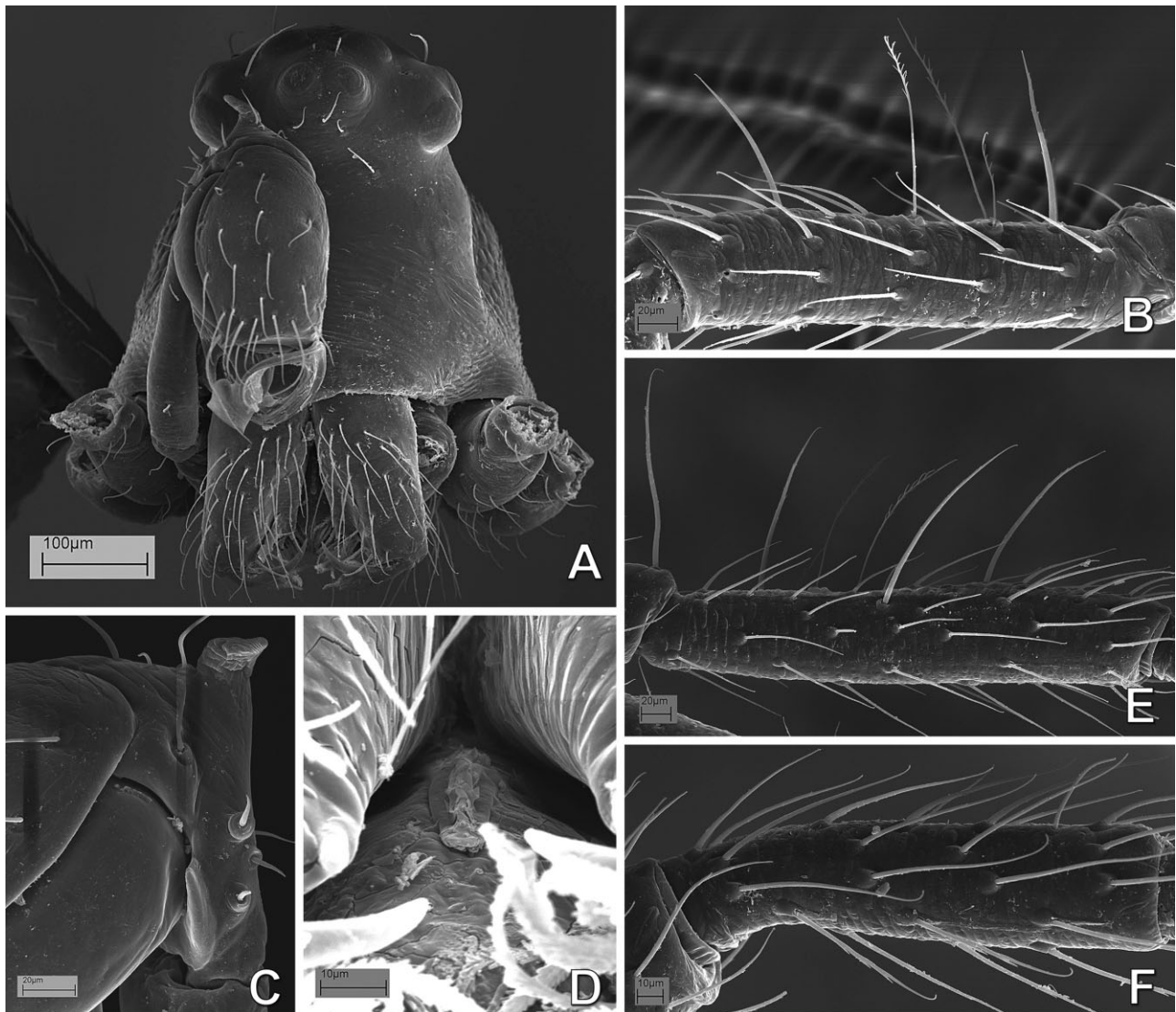


Figure 90. *Minanapis casablanca* (Anapidae), male: A, prosoma, frontal view; B, left tibia IV, retrolateral view; C, left palp, detail of fused tibia–patella, retrolateral view; D, labrum; E, left tibia I, prolateral view; F, left metatarsus I, prolateral view.

GENUS *LEVIOLA* MILLER, 1970

Leviola Miller, 1970: 155. Type species by original designation and monotypy: *Leviola termitophila* Miller 1970 (female type and only specimen not examined, presumably lost or in Museu do Dundo, Angola; scored from literature). Levi, 1972: 534 (transfer from Theridiidae to Symphytognathidae); Brignoli, 1980: 731 (provisional transfer from Symphytognathidae to Mysmenidae).

Familial placement: Zodariidae. The placement of this enigmatic genus, known only from females, has been controversial, and the rationale for its various family placements tenuous at best. Based on the original de-

scription (Miller, 1970), the morphology of *L. termitophila* is highly different from that of symphytognathoids (or even araneoids), including features such as: presence of a palpal claw, which is flat and comb-like; large anterior median eyes; lateral eyes not juxtaposed, tarsal and metatarsal trichobothrium in all legs, etc. (see Griswold *et al.*, 1998). Furthermore, its peculiar morphology resembles that of a few zodariid genera, such as the African genera *Akyttara* or *Diores*. *Leviola* shares with the latter zodariid genera (and with the family Zodariidae in general) robust chelicerae, large anterior median eyes, female palpal claw with roughly ten teeth on the prolateral side, comb-like teeth arising from the side on the lateral tarsal claws, minute median

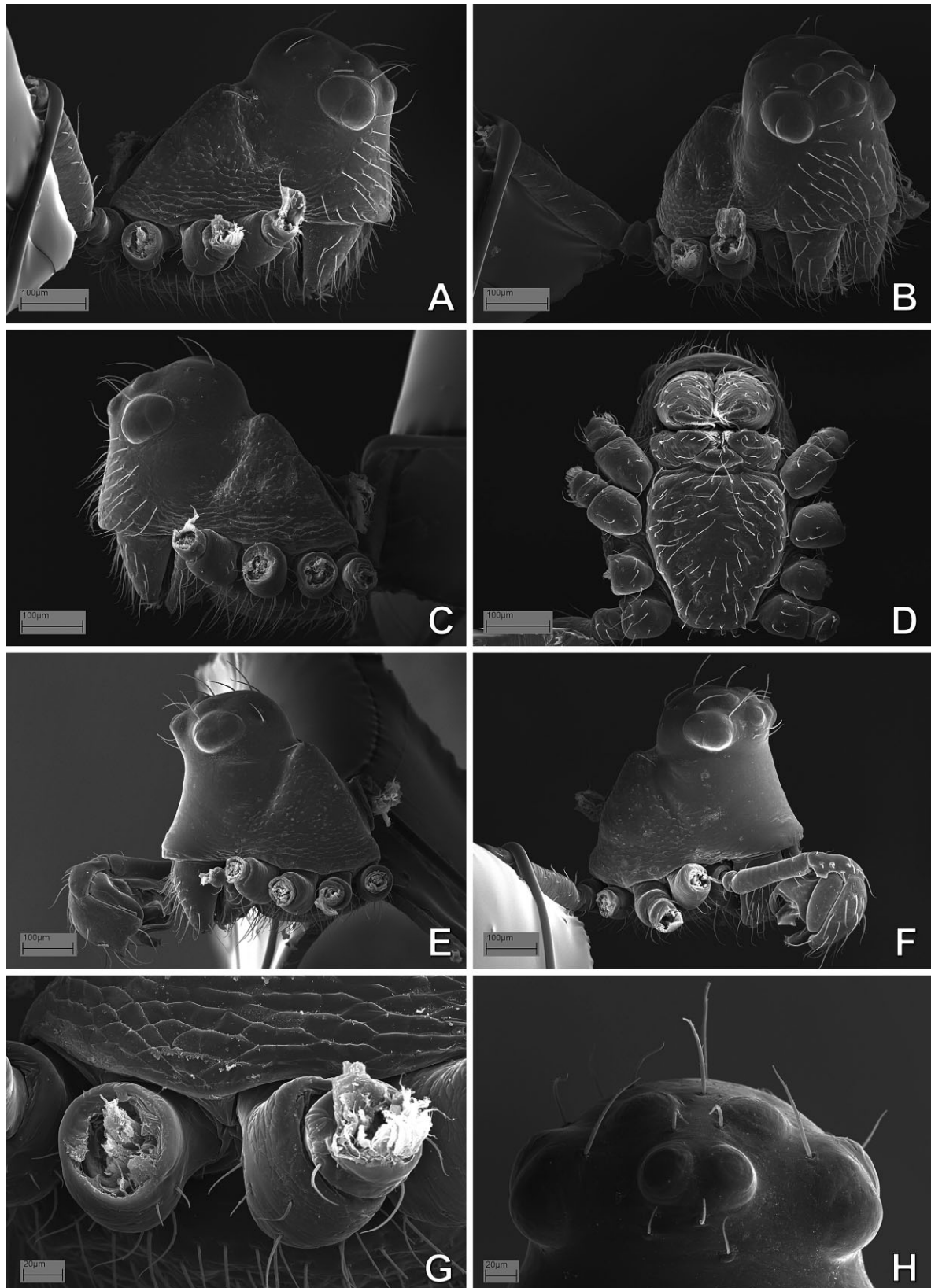


Figure 91. *Minanapis palena* (Anapidae), prosoma: A–D, G, female; E, F, H, male. A, C, E, lateral view; B, F, lateral–frontal view; D, ventral view; G, detail of lateral prosoma; H, ocular area, frontal view.

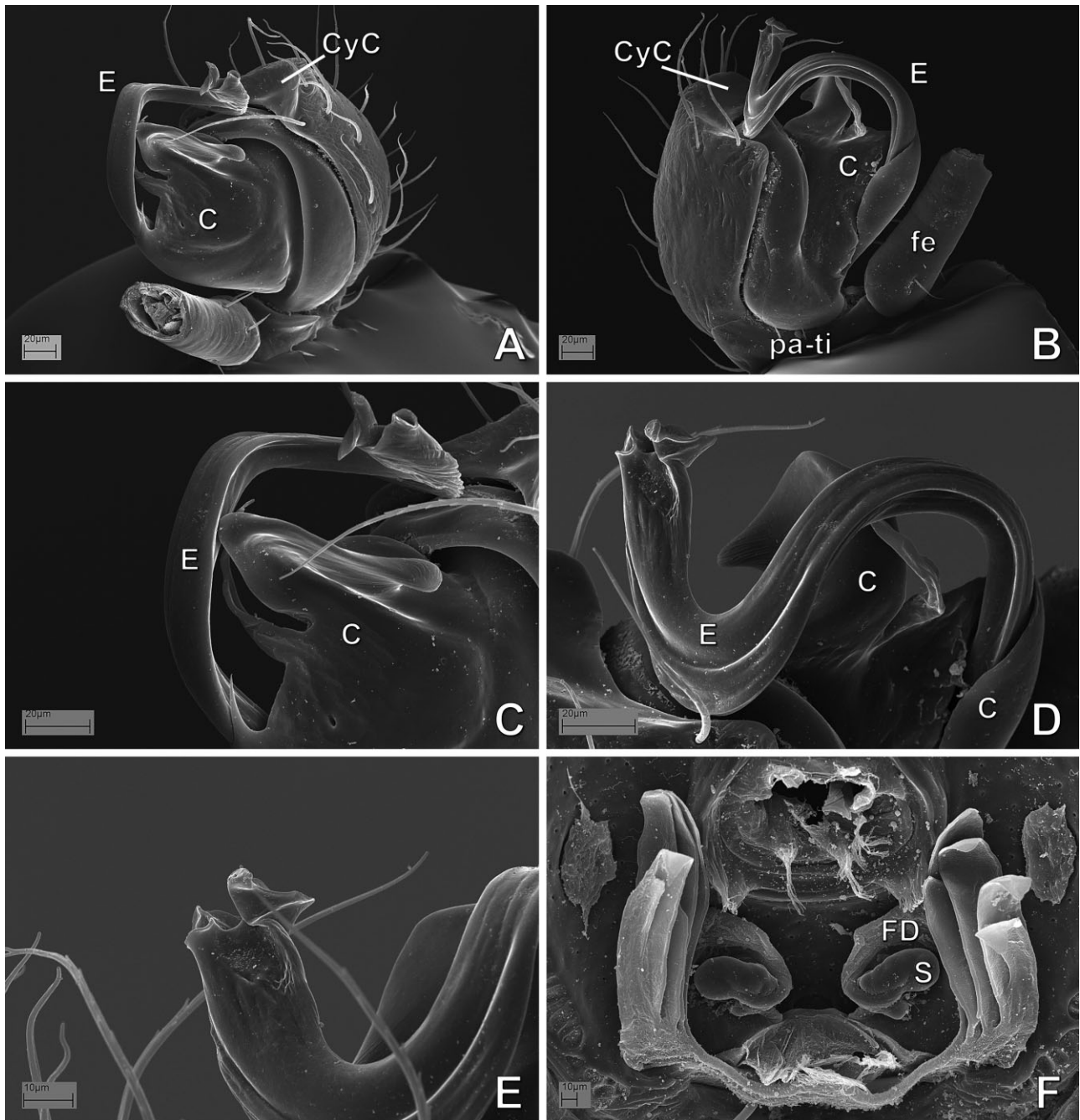


Figure 92. *Minanapis palena* (Anapidae): A–E, male left palp; A, retrolateral–ventral view; B, prolateral view; C, conductor and distal embolus, detail from panel A; D, same, detail from panel B; E, detail of tip of embolus. F, female digested abdomen, anterior respiratory system, and vulva. See Appendix 3 for the list of abbreviations.

claw, trichobothrium on all tarsi and metatarsi, colulus imperceptible, strongly serrated setae on tarsi, metatarsi and tibiae on all legs, and dorsal abdominal scutum (e.g. Jocqué, 1987, 1991; Dippenaar-Schoeman & Jocqué, 1997). Details of the general morphology of the spinnerets and female genitalia are lacking. The species

has been collected in termite nests in Angola, an association previously reported in some zodariines as well (see Jocqué, 1991; Dippenaar-Schoeman & Jocqué, 1997, and references therein), which lends further support to our conjecture that *Leviola* is in fact a member of the family Zodariidae.

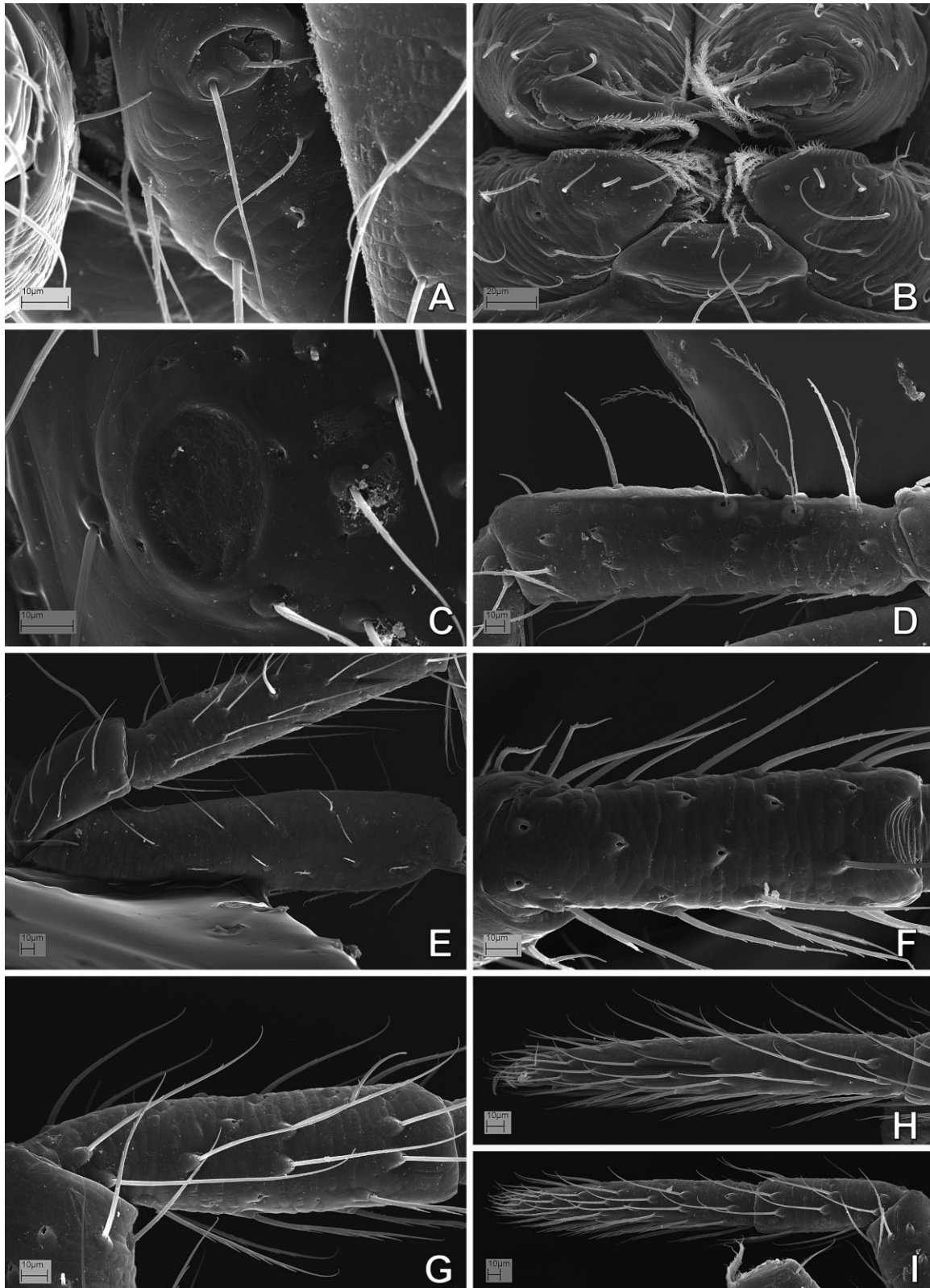


Figure 93. *Minanapis palena* (Anapidae): A, B, D, I, female; C, E–H, male. D–I, left legs. A, reduced right palp; B, mouthparts, ventral view; C, booklung cover; D, tibia IV, retrolateral view; E, leg I, prolateral view; F, metatarsus IV, dorsal view; G, metatarsus I, prolateral view; H, tarsus IV, retrolateral view; I, tarsus, metatarsus IV, retrolateral view.

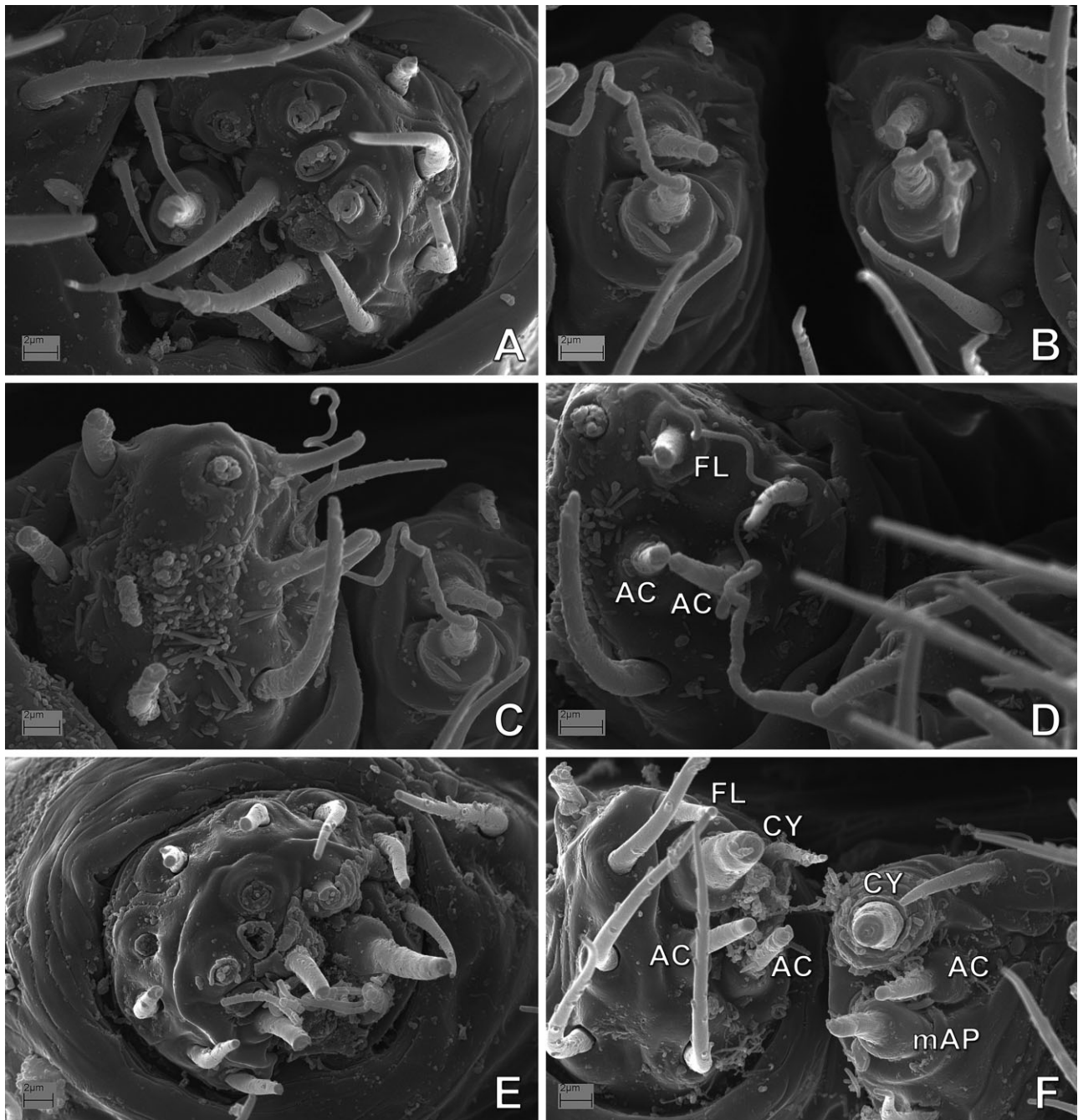


Figure 94. *Taphiassa punctata* (Anapidae), spinnerets: A, E, F, female; B–D, male. A, E, anterior lateral spinnerets; B, posterior median spinnerets; C, F, posterior spinnerets; D, right posterior lateral spinneret. See Appendix 3 for the list of abbreviations.

Given the high proportion of missing data for *Leviola* (84%) and the limited (and symphytognathoid-biased) taxon sample in this data set, the position of *Leviola* cannot be rigorously tested in a quantitative cladistic context. Furthermore, its placement within symphytognathoids

should be interpreted as an artefact caused by the aforementioned factors. A re-analysis of the complete data set excluding *Leviola* (i.e. 69 taxa and 357 characters, results not shown) rendered an identical pattern of relationships as explained above.

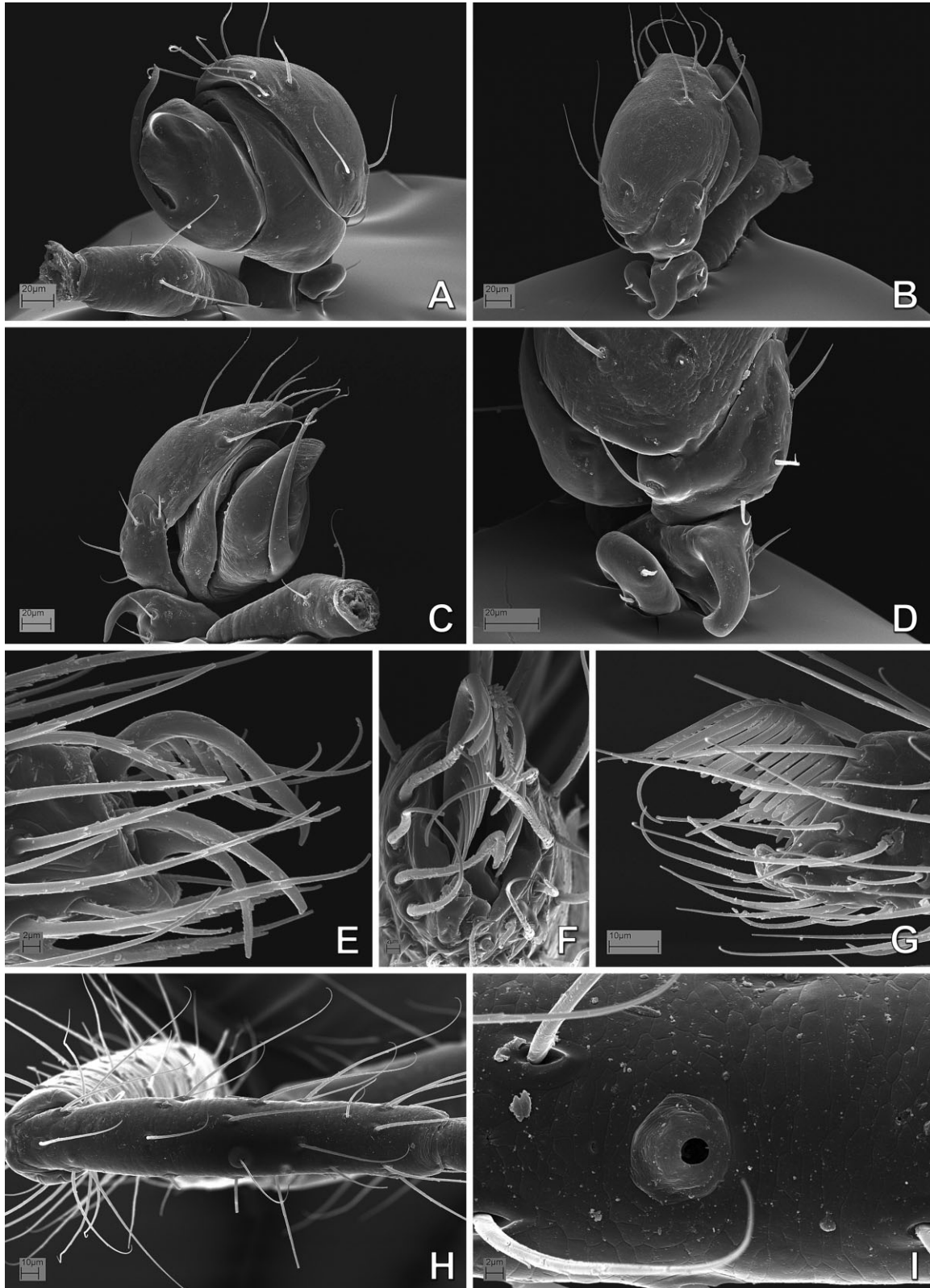


Figure 95. *Taphiassa punctata* (Anapidae), male. A–D, left palp; A, ventral–retrolateral view; B, dorsal view; C, prolateral view; D, detail of palpal patella and tibia. E, right leg IV, claws, retrolateral view. F–I, right leg I; F, claws, distal view; G, same, prolateral view; H, metatarsus, dorsal view; I, detail of tarsal organ.

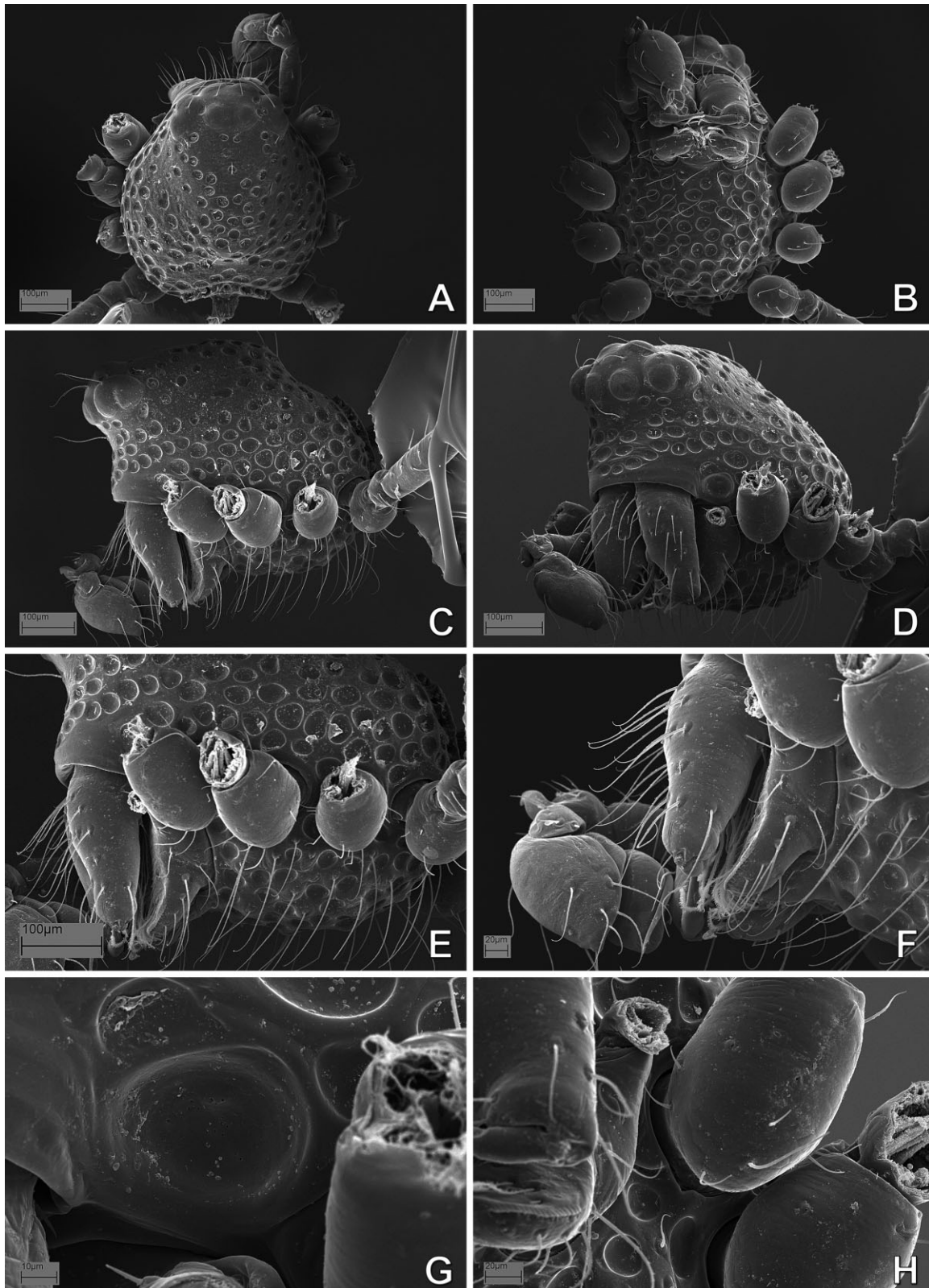


Figure 96. *Taphiassa punctata* (Anapidae), male prosoma: A, dorsal view; B, ventral view; C, lateral view; D, lateral-frontal view; E, detail of prosoma, lateral view; F, detail of anterior prosoma, ventral-lateral view; G, detail of carapace lateral depression; H, detail of sternal edge.

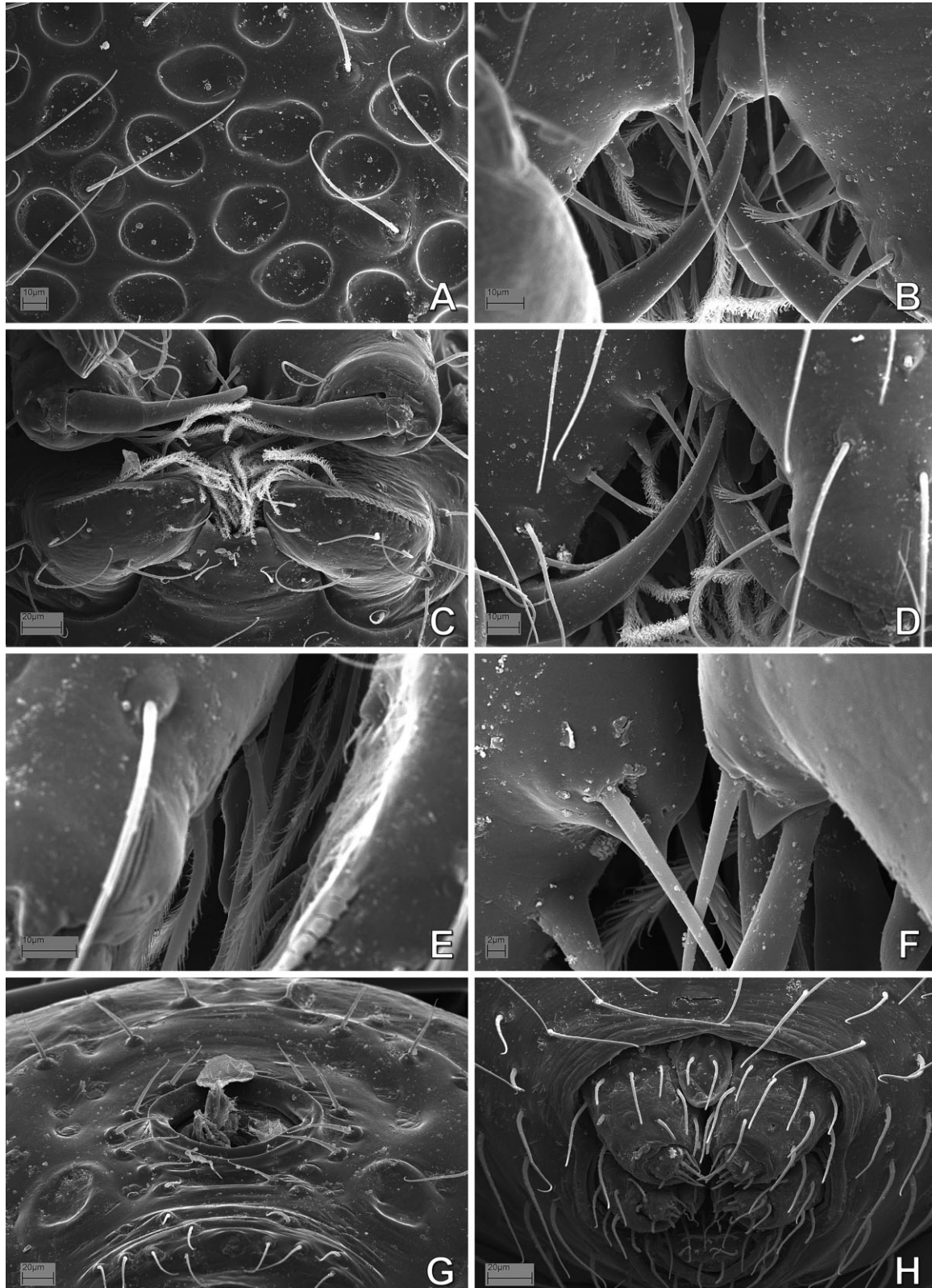


Figure 97. *Taphiassa punctata* (Anapidae), male: A, sternal cuticle; B, detail of distal chelicerae, frontal view; C, mouthparts, ventral view; D, detail of distal chelicerae, frontal-lateral view; E, labrum, lateral view; F, detail of gland mound, from panel D; G, abdomen, pedicel area; H, spinning field.

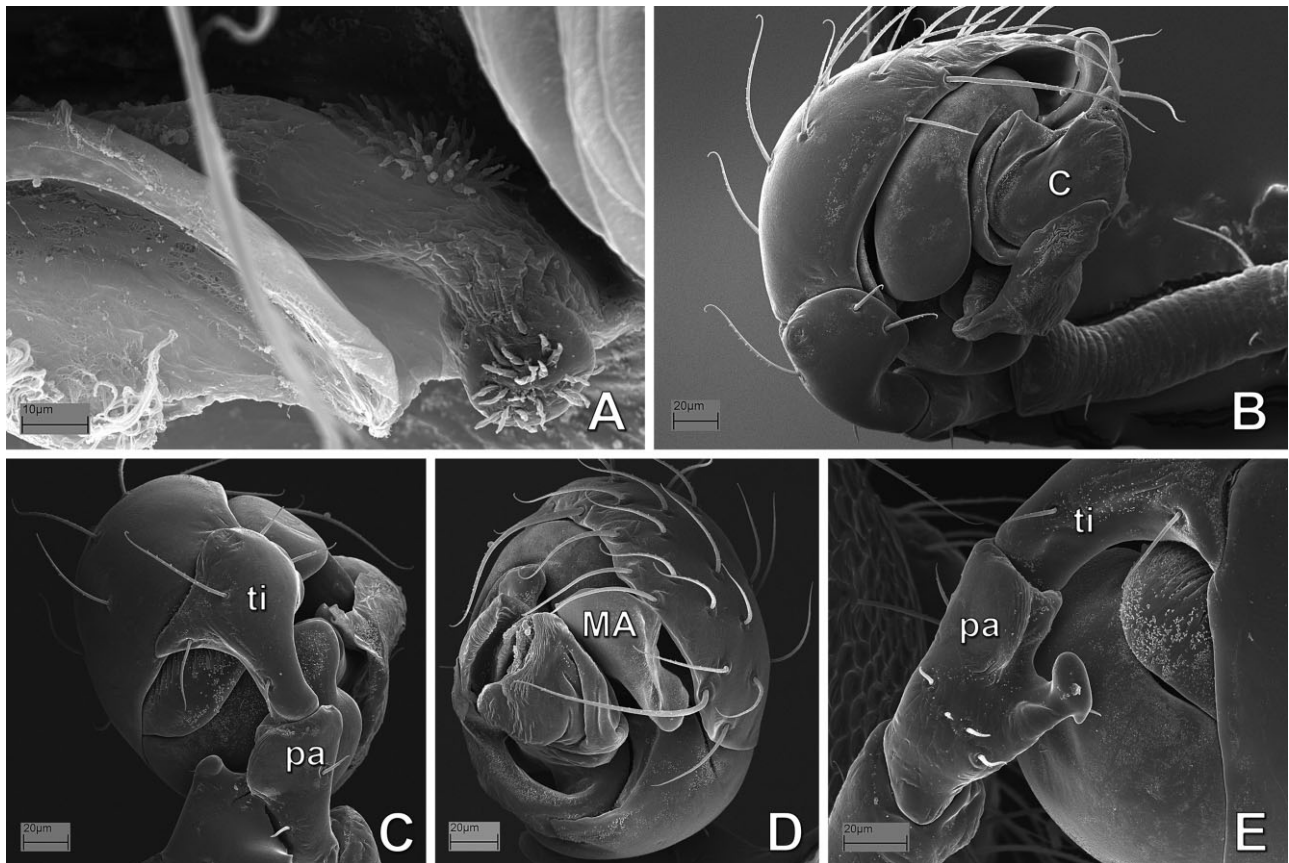


Figure 98. *Tasmanapis strahan* (Anapidae). A, female; B–E, male. A, digested abdomen, detail of vulva, anterior view; B–D, left palp; B, prolateral view; C, dorsal-proximal view; D, distal view; E, right palp, retrolateral view (image not inverted). See Appendix 3 for the list of abbreviations.

DISCUSSION

MORPHOLOGICAL PARTITION: PHYLOGENETIC PLACEMENT AND COMPOSITION OF MYSMENIDAE

Although ultimately we base our phylogenetic conclusions on the results of the total-evidence analysis (morphological plus sequence data; see next section and Lopardo *et al.*, 2011), we think that it is important to examine in detail the phylogenetic signal of each data partition. One of the main goals of this paper is to study the morphological partition and its phylogenetic signal. Although nucleotide data plays an increasingly important role in orbicularian systematics (for a review of the advances in the last decade, see Hormiga & Griswold 2014), much of the diversity of this group as represented in museum collections is not accessible to genetic sampling analysis (because of age and/or state of preservation of the specimens). Consequently, morphological data remain critical for phylogenetic inference and for comparative biology. The results of the cladistic analysis of the morphological data set alone (65 taxa, 357 characters) provide the basis for an ex-

plicit phylogenetic re-circumscription of Mysmenidae, a family that had been previously considered a ‘polyphyletic waste disposal group’ (Schütt, 2003: 137). *Calodipoena tarautensis* was placed within the subfamily Mysmeninae and possesses several of the proposed synapomorphies for the family. *Crassignatha* and *Iardinis*, on the other hand, are both excluded from Mysmenidae and placed within Symphytognathidae. The type species of *Iardinis*, *I. weyersi*, is lost and therefore the transfer suggested here is preliminary, although it is objectively based on a cladistic analysis of the remaining species in the genus. The placement of the peculiar *Leviola termitophila* in Mysmenidae is erroneous and the genus is transferred to Zodariidae. *Phricotelus stelliger* is also removed from Mysmenidae and placed in Araneoidea as *incertae sedis* until a thorough morphological study can be carried out and its placement more rigorously tested.

Previous morphological phylogenetic analyses hypothesized Mysmenidae monophyly based on two or three synapomorphies: the ‘distally twisted and notched cymbium’, the sclerotized spot subapically on ventral

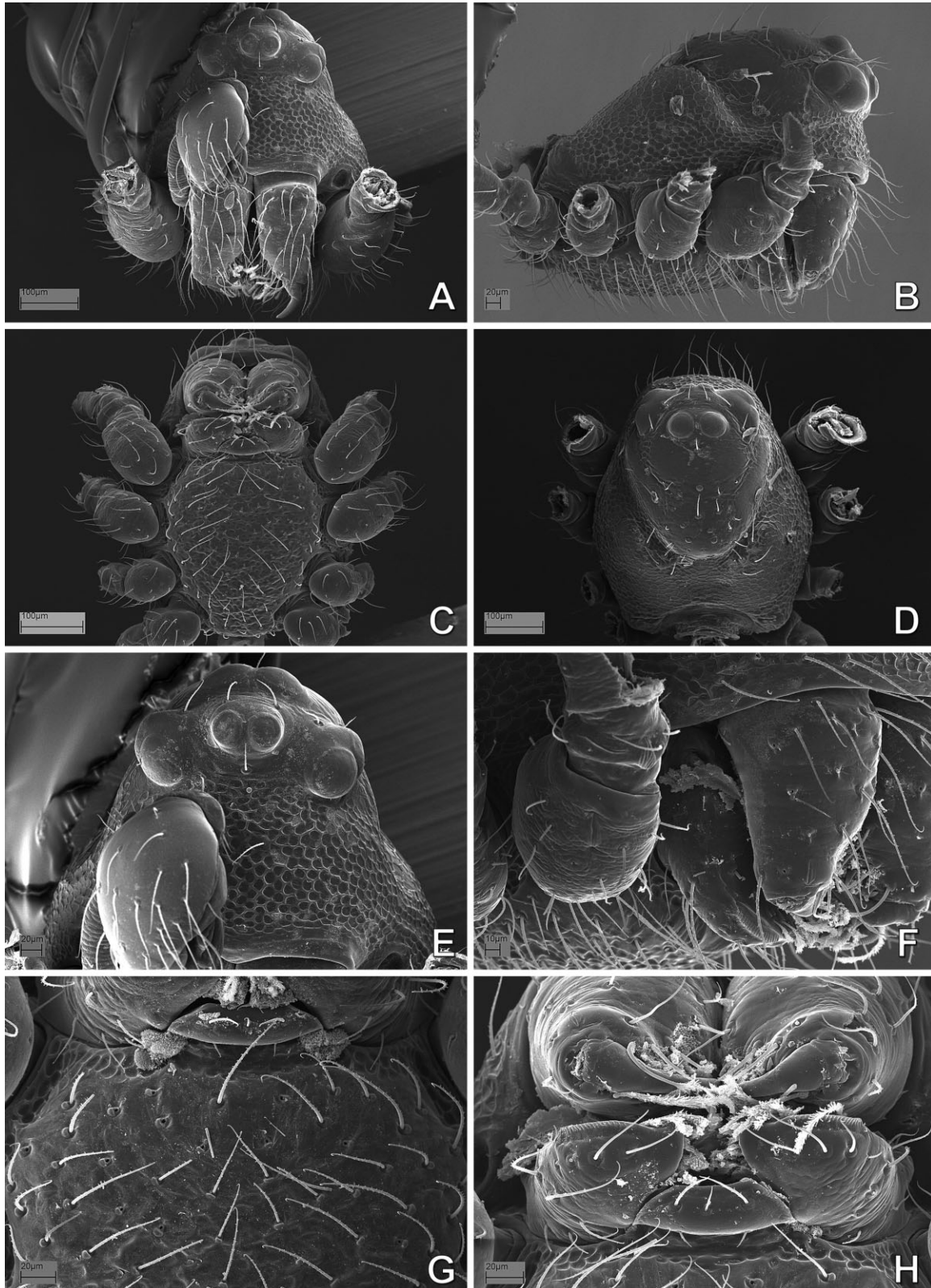


Figure 99. *Tasmanapis strahan* (Anapidae), prosoma: A, E, G, male; B–D, F, H, female. A, frontal view; B, lateral view; C, ventral view; D, dorsal view; E, ocular area and clypeus, frontal view; F, mouthparts, lateral–frontal view; G, detail of sternum and labium, ventral view; H, mouthparts, ventral view.

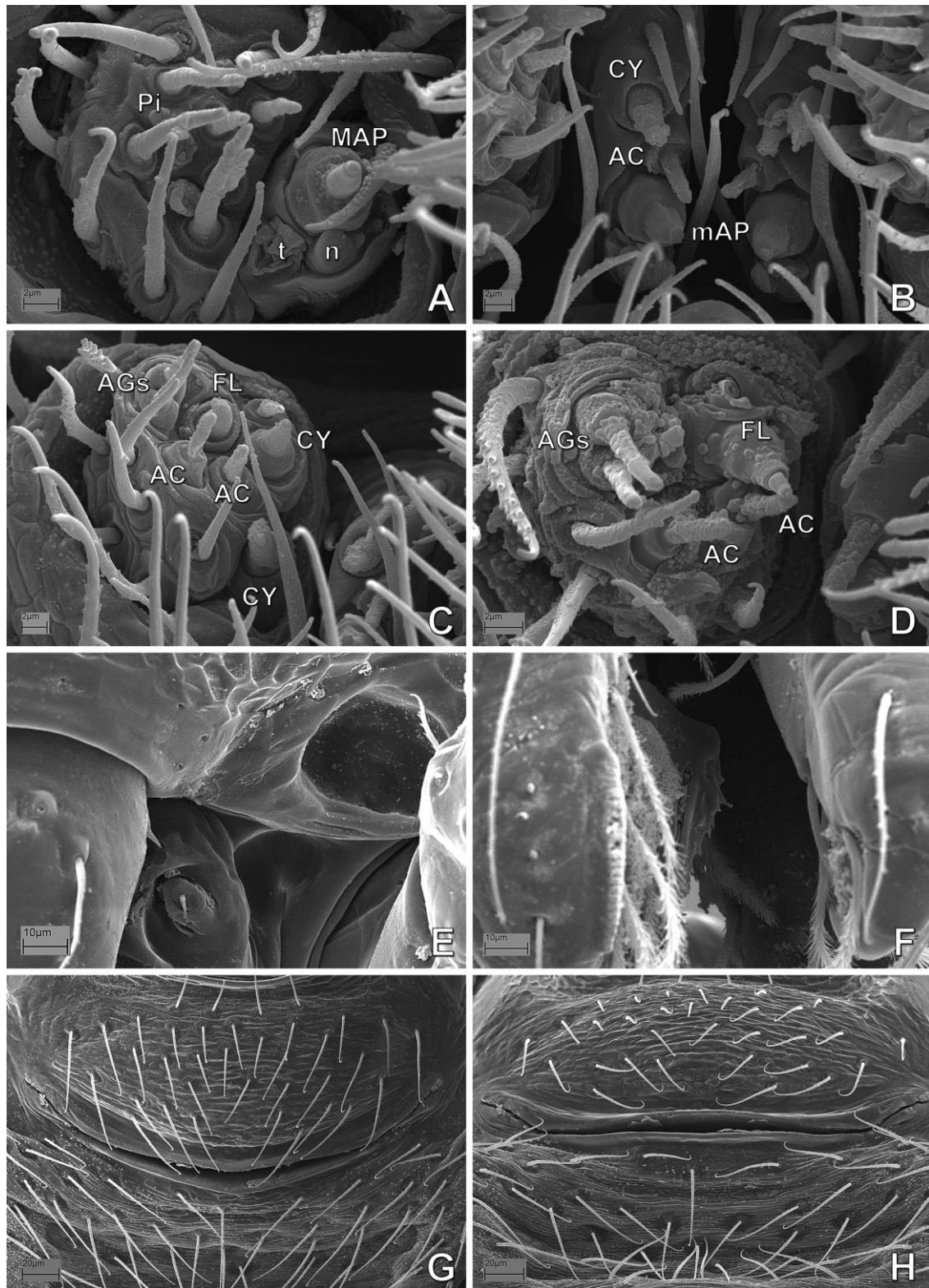


Figure 100. *Tasmanapis strahan* (Anapidae): A–C, E, female; D, F–H, male. A, right anterior lateral spinneret; B, posterior median spinnerets; C, D, right posterior lateral spinneret; E, reduced palp and carapace lateral depression; F, labrum, lateral view; G, abdomen, epigastric furrow area, ventral view; H, same, posterior view. See Appendix 3 for the list of abbreviations.

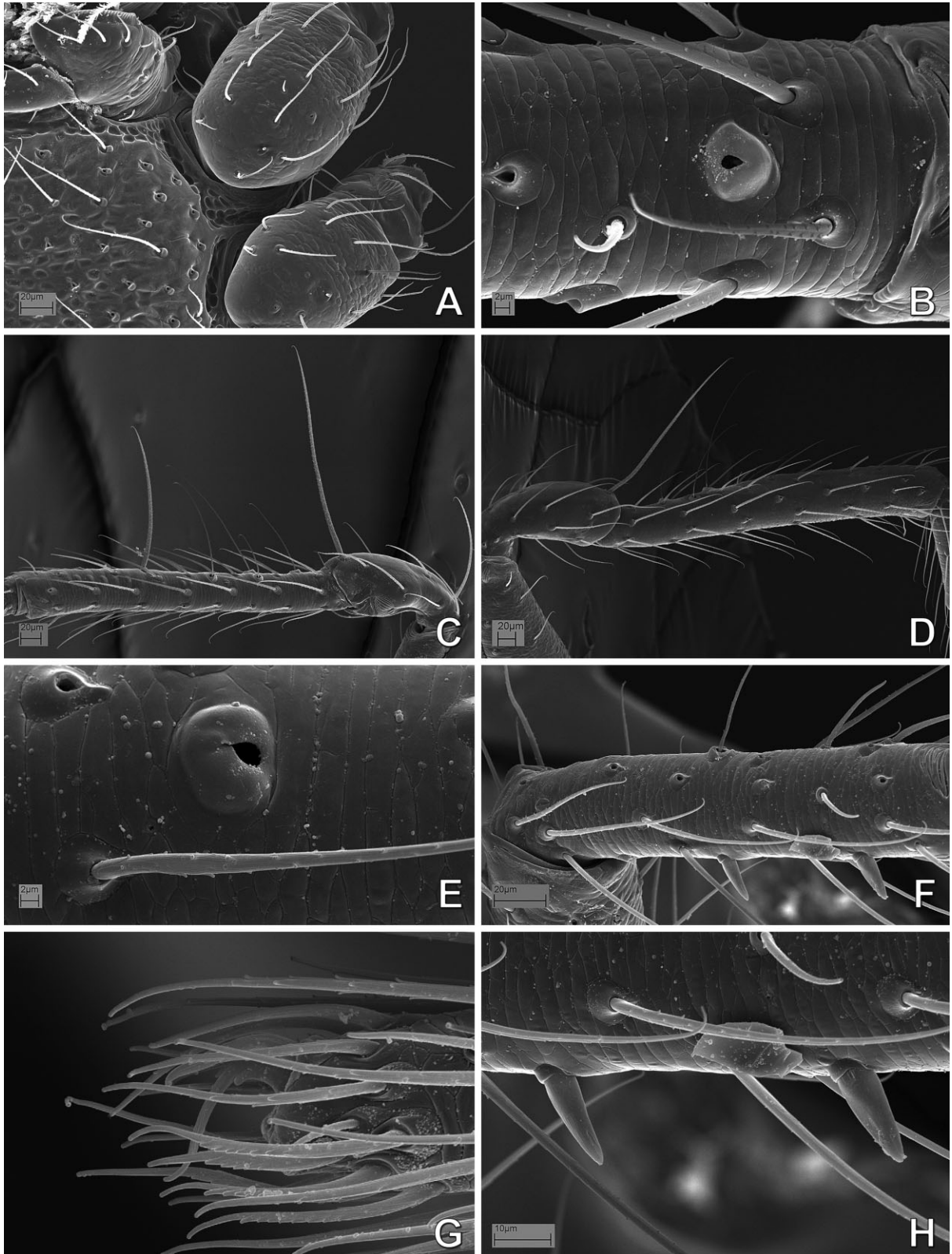


Figure 101. *Tasmanapis strahan* (Anapidae): A, B, D, female; C, E–H, male. A, sternum, detail of sternal edge. B–H, left legs; B, leg IV, tarsal organ; C, patella–tibia IV, retrolateral view; D, patella–tibia I, prolateral view; leg I, tarsal organ; F, metatarsus I, prolateral view; G, leg IV, claws, retrolateral view; H, clasp spurs, detail from panel F.

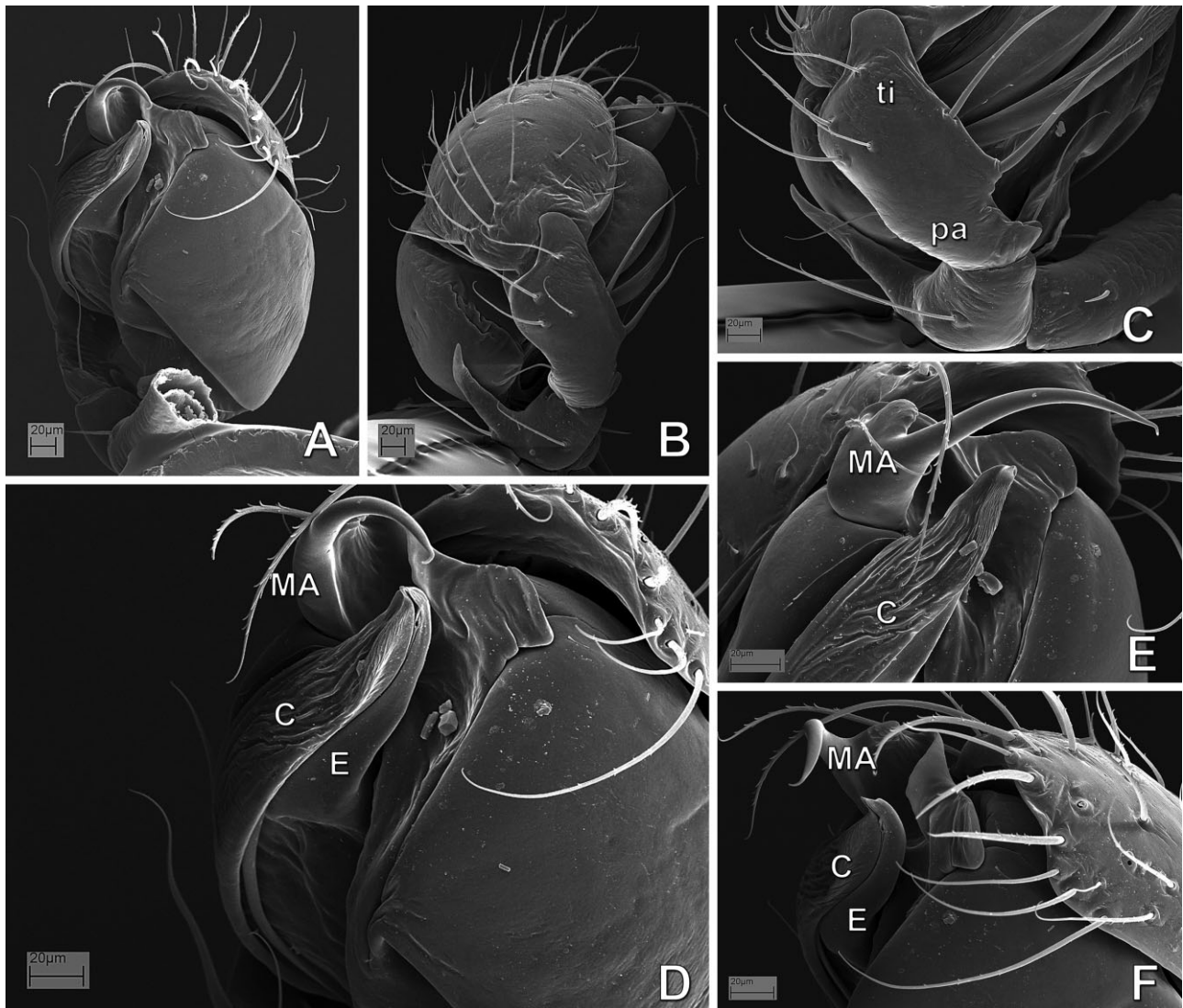


Figure 102. *Teutoniella cekalovici* (Anapidae), male left palp: A, ventral view; B, dorsal–proximal view; C, detail of dorsal tibia and patella; D, detail of apical palp, ventral view; E, same, prolateral view; F, same, retrolateral–distal view. See Appendix 3 for the list of abbreviations.

femur I and II, and the male metatarsus I clasping spine (Griswold *et al.*, 1998), or just the ‘apical lobes on the cymbium of the male palp and femoral spots on the first or first two pairs of legs’ (Schütt, 2003: 134). Our study provides a more in depth understanding of the primary homology hypotheses of structures such as ‘lobes, twists, or notches’ of the cymbium (see below and Appendix 2). Mysmenidae are here diagnosed by seven unambiguous and twelve ambiguously optimized synapomorphies not only related to legs and male palp, but also related to female genitalia, spinnerets, cuticle patterns, chelicerae, and sternum morphology (see Results above; see also Lopardo *et al.*, 2011).

The morphological data set places Mysmenidae as sister to Theridiosomatidae, a relationship recovered

in only one recent study performing a modified phylogenetic analysis of a previous data set (see Fig. 151B; Lopardo & Hormiga, 2008). Previous phylogenetic hypotheses have placed Mysmenidae as sister to a clade comprising Anapidae and Symphytognathidae s.s. (Fig. 150A, B; Griswold *et al.*, 1998; Lopardo & Hormiga, 2008), or a redelimited Mysmenidae sister to Symphytognathidae s.s. (Fig. 151A; Schütt, 2003; but for the best-informed phylogenetic placement of Mysmenidae based on a total-evidence approach, see Lopardo *et al.*, 2011). Also, the pattern of familial relationships within symphytognathoids agrees with that proposed by Griswold *et al.* (1998), but circumscribed as in Schütt (2003), with two main symphytognathoid clades resulting from the

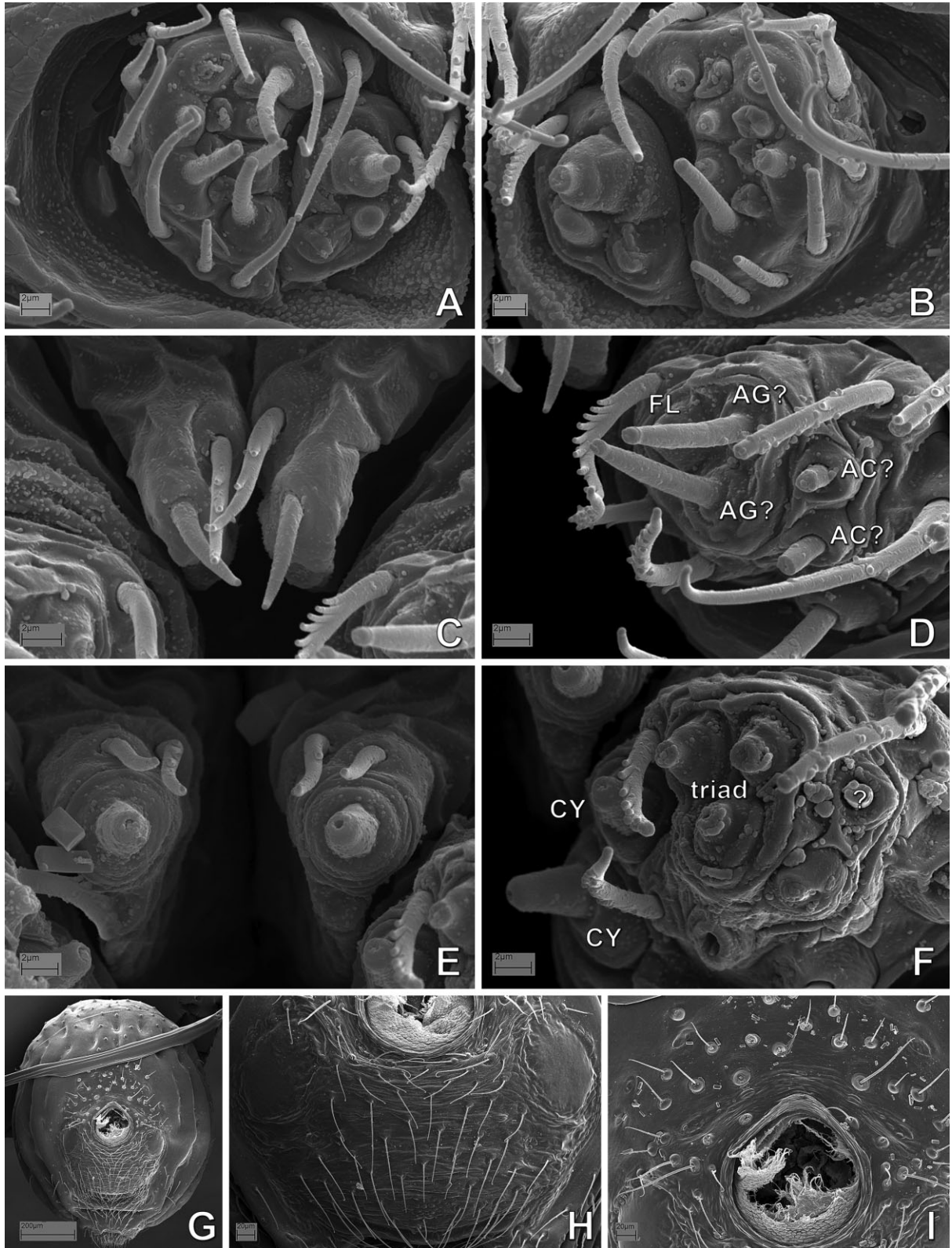


Figure 103. *Teutoniella cekalovici* (Anapidae), abdomen: A–D, H, male; E–G, I, female. A, B, anterior lateral spinnerets; C, E, posterior median spinnerets; D, F, posterior lateral spinnerets; G, abdomen, ventral view; H, abdomen, detail of epigastric area, ventral view; I, same as H, detail of pedicel area. See Appendix 3 for the list of abbreviations.

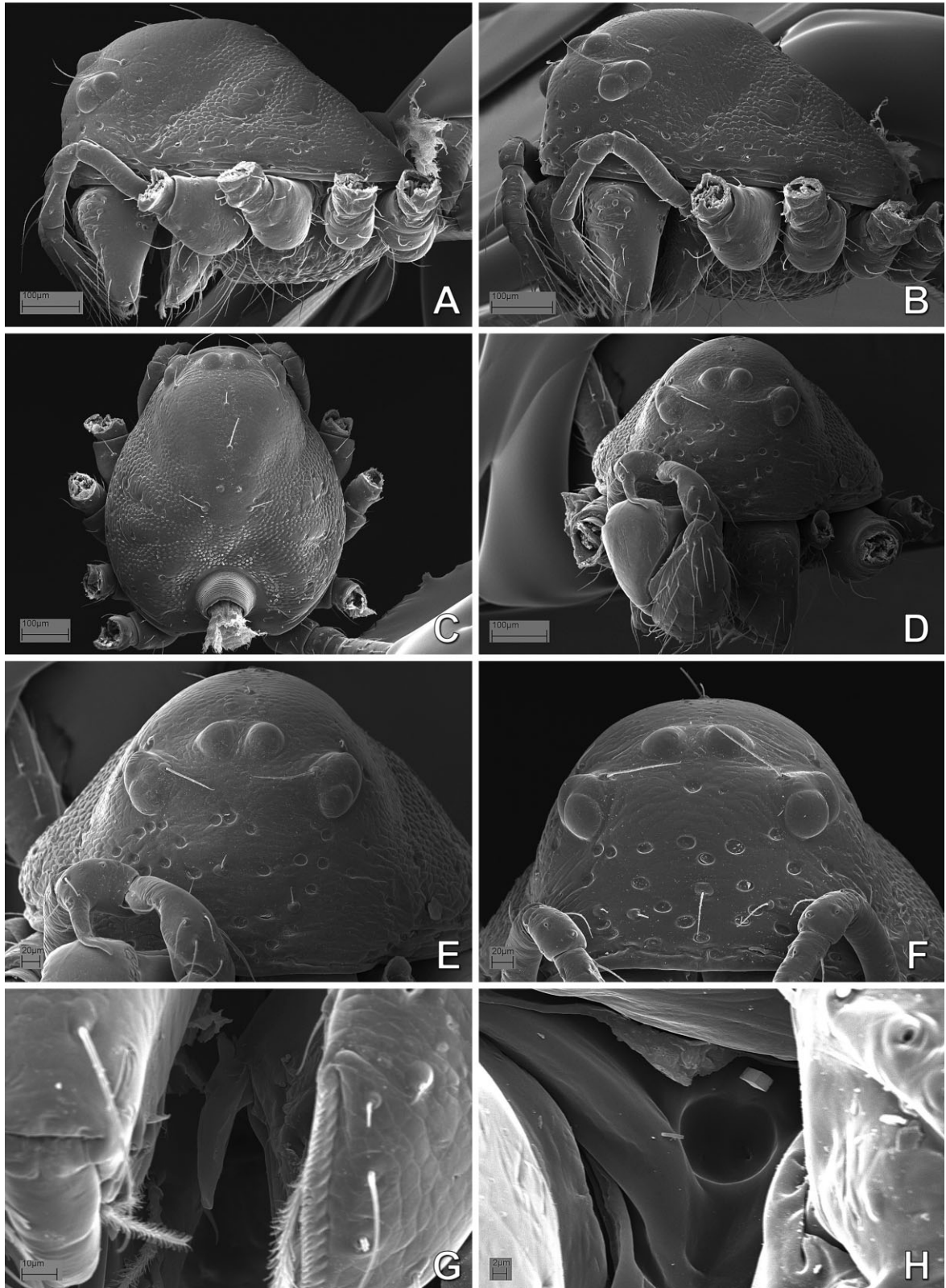


Figure 104. *Teutoniella cekalovici* (Anapidae), prosoma: A–C, F–H, female; D, E, male. A, lateral view; B, lateral-frontal view; C, dorsal view; D, frontal view; E, F, carapace, frontal view; G, labrum, lateral view; H, detail of prosomal depression between coxae II and III.

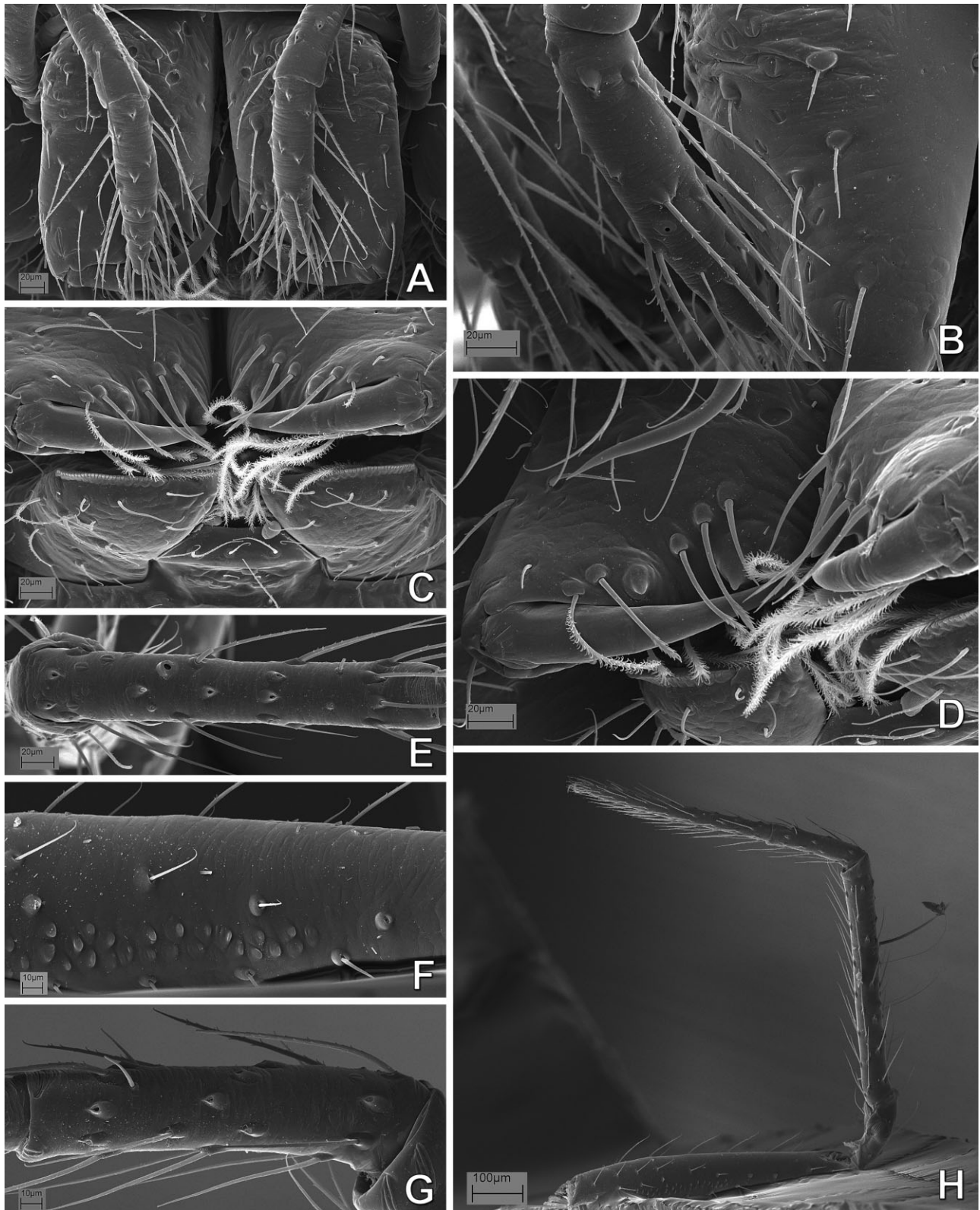


Figure 105. *Teutoniella cekalovici* (Anapidae): A, B, E–H, female; C, D, male. A, chelicerae and palps, frontal view; B, same, lateral view; C, mouthparts, ventral view; D, same, lateral–ventral view; E, left metatarsus I, dorsal view; F, left femur IV, retrolateral view; G, left metatarsus IV, retrolateral view; H, left leg IV, retrolateral view.

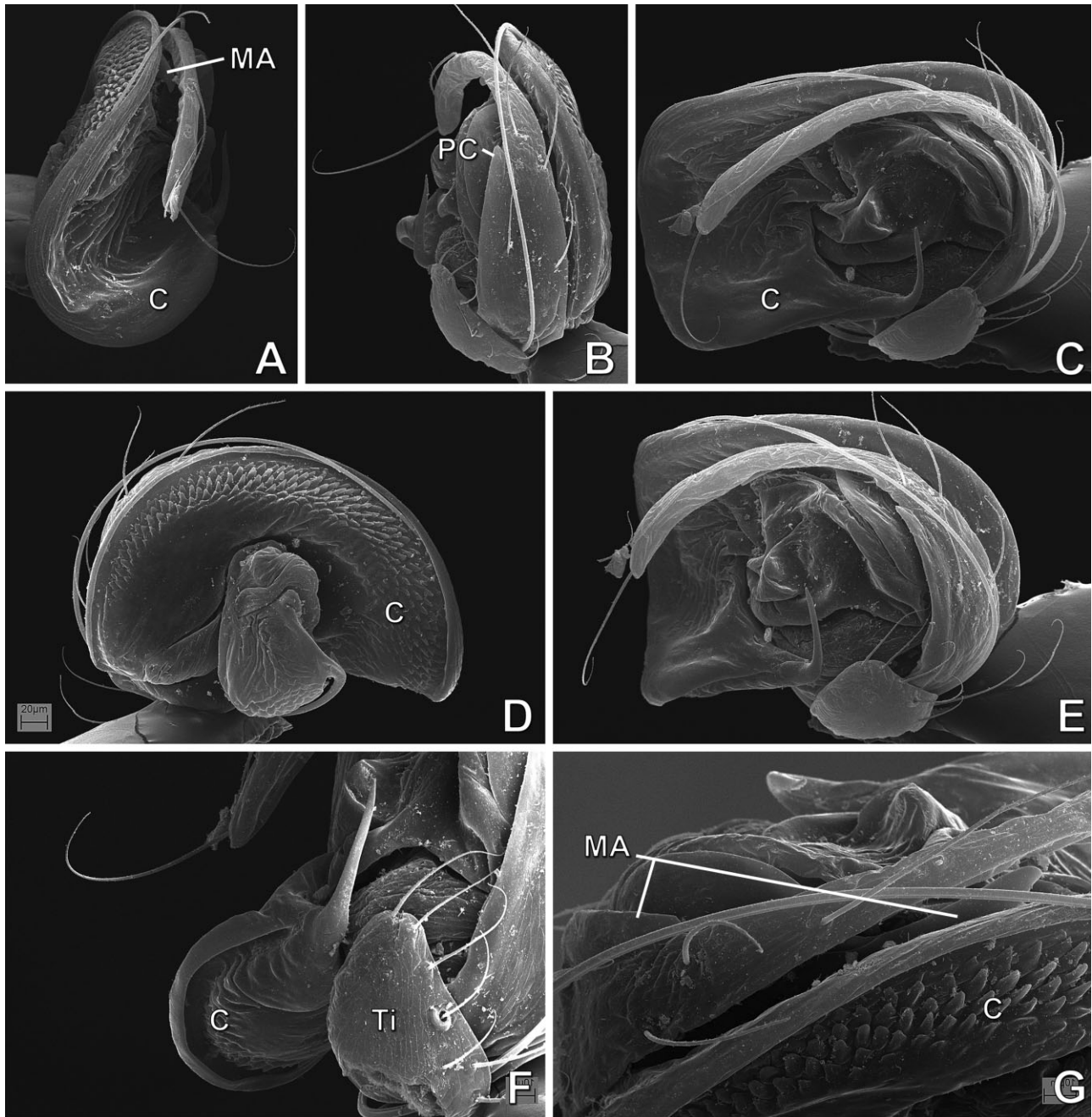


Figure 106. *Cepheia longiseta* (Synaphridae), male paralectotype, right palp, inverted: A, apical view; B, dorsal view; C, retrolateral view; D, prolateral view; E, retrolateral–dorsal view; F, detail of palpal tibia and tip of conductor; G, detail of dorsal–apical view. See Appendix 3 for the list of abbreviations.

analysis. Mysmenidae are sister to Theridiosomatidae, and Synaphridae are sister to Anapidae + Symphytognathidae. Symphytognathidae are here re-delimited to include the enigmatic mysmenid genus *Iardinis*. The family Anapidae includes a basal *Acrobleps* and a distal clade comprising *Comaroma simoni* sister to the remaining micropholcommatine taxa (node M76, see Lopardo *et al.*, 2011). The monophyly of

Micropholcommatinae (formally ranked as a subfamily by Lopardo *et al.*, 2011) has already been recovered in a previous analysis (Schütt, 2003), although its placement within Anapidae has been questioned in a catalogue, rooted on the opinion that those results ‘were based on analyses of very few genera’ (Platnick, 2014). It should be noted, however, that Lopardo *et al.* (2011) studied other taxa relevant to the monophyly

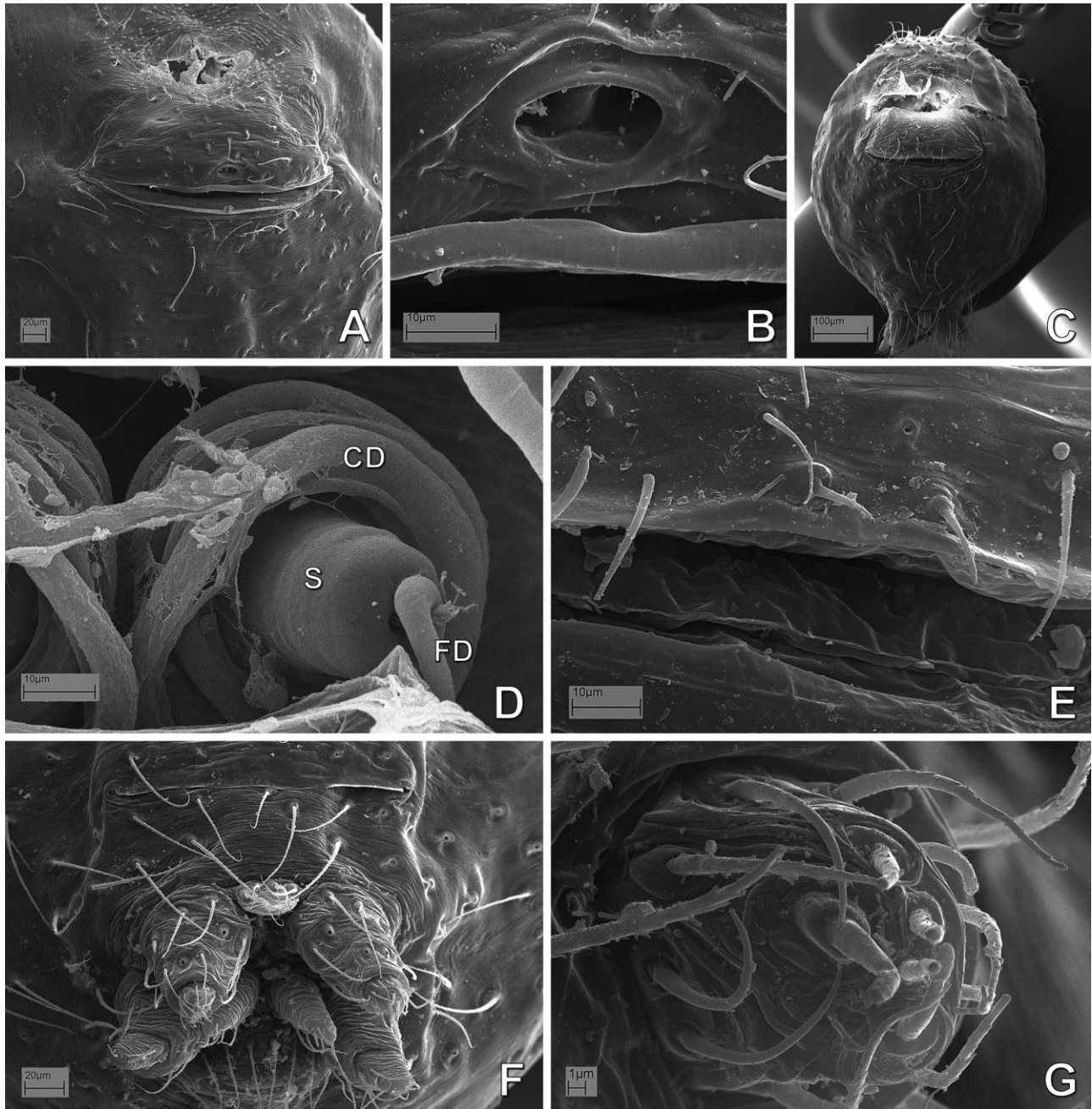


Figure 107. *Cepheia longiseta* (Synaphridae), paralectotypes, abdomen: A, B, D, F, G, female; C, E, male. A, pedicel and epigastric area; B, E, detail of epigastric–genital area; C, abdomen, ventral view; D, digested abdomen, detail of vulva; F, spinning field, colulus and posterior spiracle; G, left anterior lateral spinneret. See Appendix 3 for the list of abbreviations.

issue that had not been included in their character matrix: ‘... based on the results of our study, published descriptions of other micropholcommatines (e.g. Hickman, 1944, 1945; Forster, 1959; Rix, 2008) show no character evidence that contradicts our hypothesis’. The results of the current analysis involve a much more comprehensive taxon sampling of

symphytognathoids in general, and support the placement of the subfamily Micropholcommatinae as a distal clade within Anapidae, challenging the monophyly of Anapidae exclusive of micropholcommatines (Forster, 1959; Brignoli, 1970; but see Forster & Platnick, 1984; Platnick *et al.*, 1991; Schütt, 2003; Rix *et al.*, 2008; Rix & Harvey, 2010). Whereas our classification is based

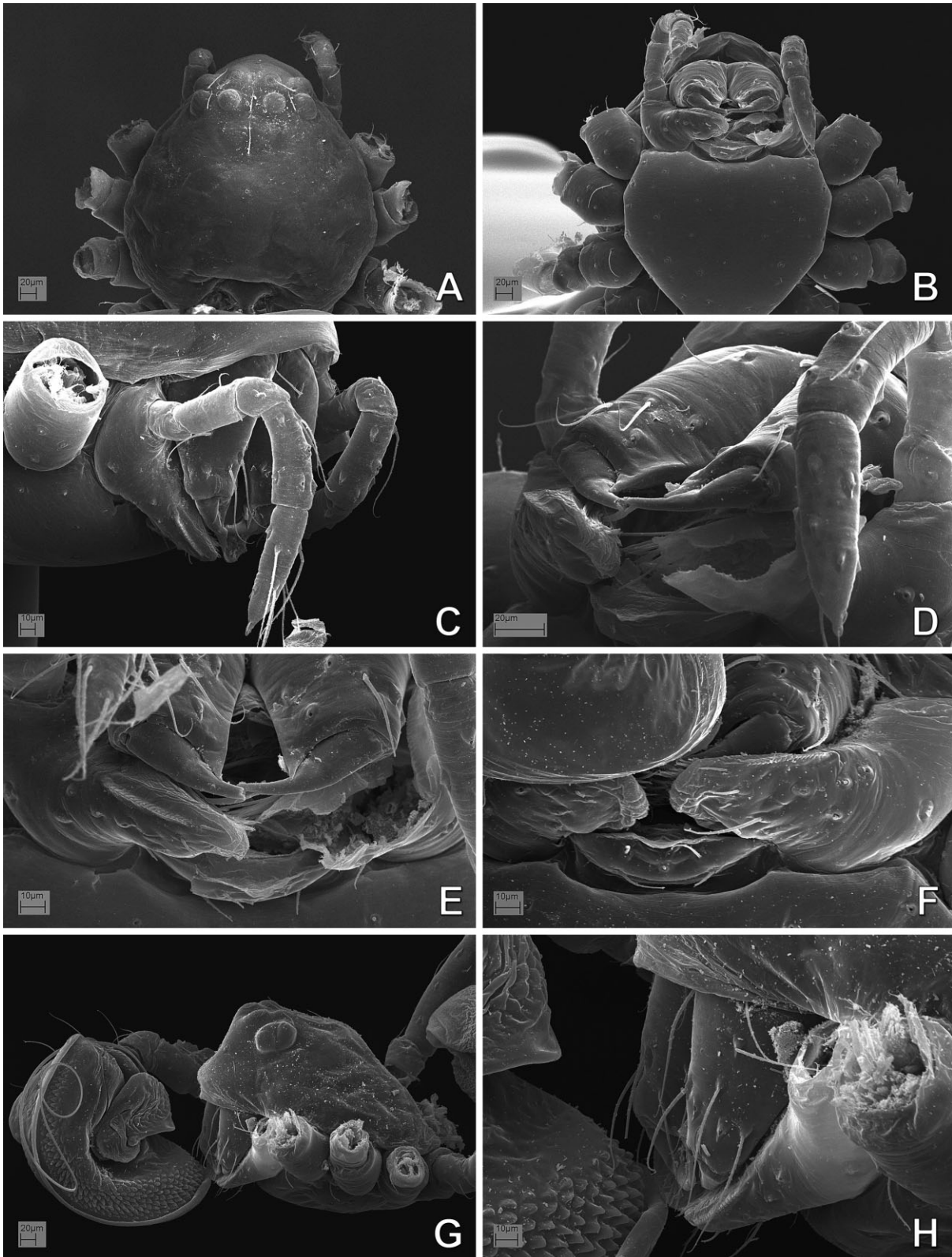


Figure 108. *Cepheia longiseta* (Synaphridae), paralectotypes, prosoma: A–E, female; F–H, male. A, dorsal view; B, ventral view; C, mouthparts and palp, lateral view; D, same, lateral–ventral view; E, same, ventral–frontal view; F, detail of maxilla and labium; G, prosoma, lateral view; H, same, detail of mouthparts.

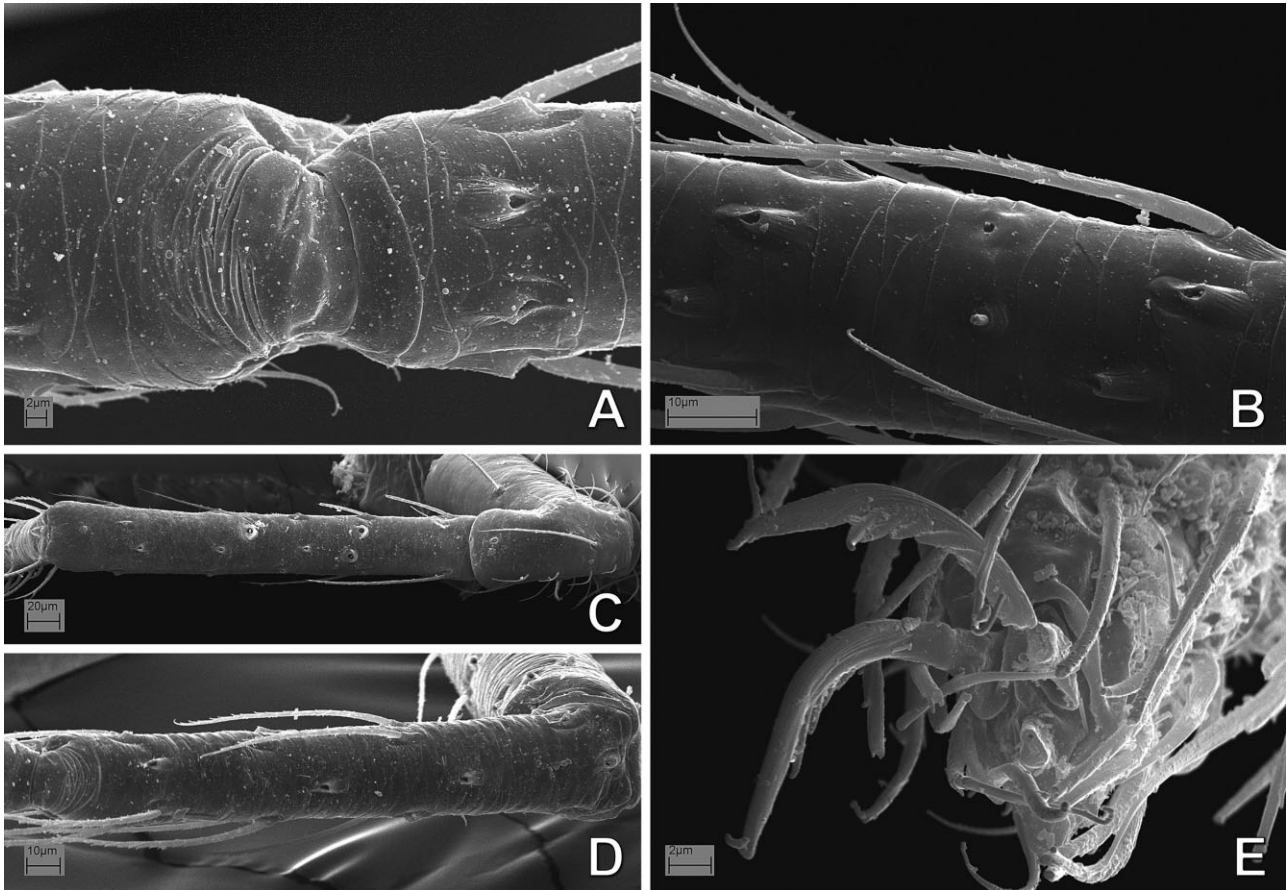


Figure 109. *Cepheia longiseta* (Synaphridae), paralectotypes, legs: A, B, female left legs; C–E, male right legs. A, leg II, metatarsus–tarsus junction, dorsal view; B, leg I, tarsal organ, lateral view; C, leg I, tibia–patella, dorsal view; D, metatarsus III, dorsal view; E, leg I, claws.

on the data at hand, it seems clear that further research is required to further test the phylogeny of the extremely diverse Anapidae, using a still wider selection of taxa from across the world.

Given the nature of measurements (i.e. decimal numbers) as characters and the concomitant treatment of such continuous characters as additive in the phylogenetic analyses, an increase in the resolution of the phylogenetic hypothesis was expected (compare cladograms from Figs 154, 157, see optimization of the seven continuous characters into the most parsimonious cladogram in Fig. 155A–G). Our results show a tendency towards an overall decrease in clade support of approximately 50% when continuous characters are included in the analyses (Fig. 158). Cladogram length and continuous character changes are consequently measured not as entire ‘steps’, but as fractions of steps. Support values calculated based on step numbers (e.g. absolute Bremer support, BS) can therefore yield decimal numbers as total clade support values. Typically in analyses with exclusively discrete char-

acters, the minimum BS value for a clade is one step, meaning that only one extra step is required by that hypothesis to collapse the monophyly of that clade. The meaning of decimal values in Bremer support calculations is not entirely clear, especially when such values are close to zero (see Fig. 154), even though such clades can be supported by two or more discrete changes. Decimal BS values are the result of subtle changes in the continuous characters. If all clades with BS lower than 0.95 are collapsed, the loss of resolution is distributed in three main clades within Mysmenidae (Fig. 156): relationships within *Mysmenopsis* collapse, as well as within clades M86 (including all its internal nodes) and M93. Even though the phylogenetic hypothesis from the complete morphological analysis contains unstable clades and decreased support, when compared with a discrete-only analysis, the overall homoplasy in the discrete characters alone is also relatively high, and we see no epistemological reason to exclude such continuous characters (see also Rae, 1998; Humphries, 2002).

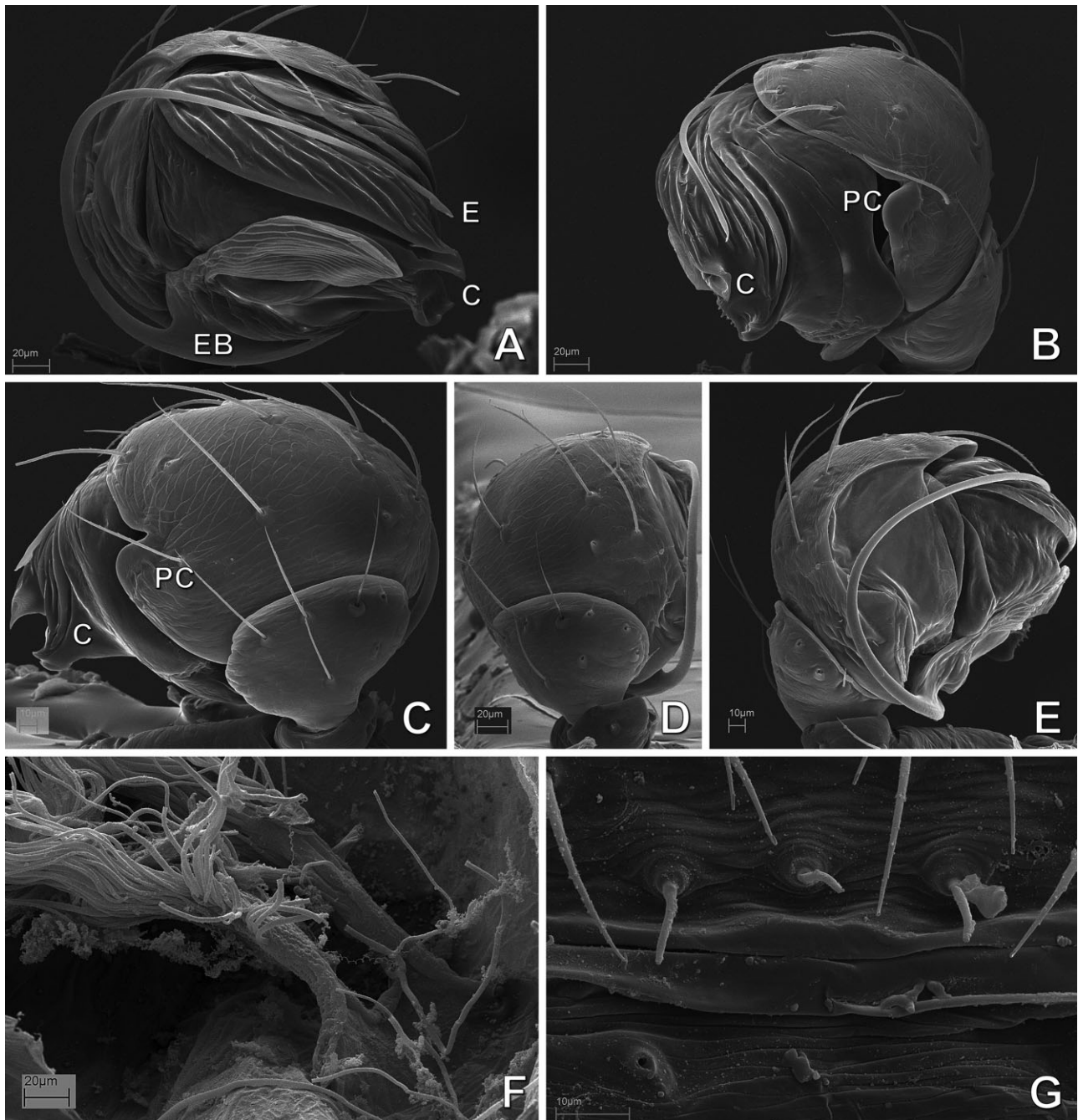


Figure 110. *Synaphris saphrynis* (Synaphridae), male paratype. A–E, left palp; A, prolateral–apical view; B, apical view; C, retrolateral view; D, dorsal–proximal view; E, prolateral–proximal view. F, digested abdomen, detail of posterior respiratory atrium and tracheae; G, epiandrous spigots. See Appendix 3 for the list of abbreviations.

COMBINED ANALYSIS: PHYLOGENETIC IMPLICATIONS
AND EVOLUTIONARY MORPHOLOGY

To study and report morphological and behavioural character evolution in Mysmenidae (below) and

symphytognathoids (in part below, see Appendix 2), we use the preferred optimal tree that results from the total evidence analysis, which combines morphology, behaviour, and multigene sequence data (see Figs 160, 161, and Appendices 2, 5; see also Lopardo *et al.*, 2011).

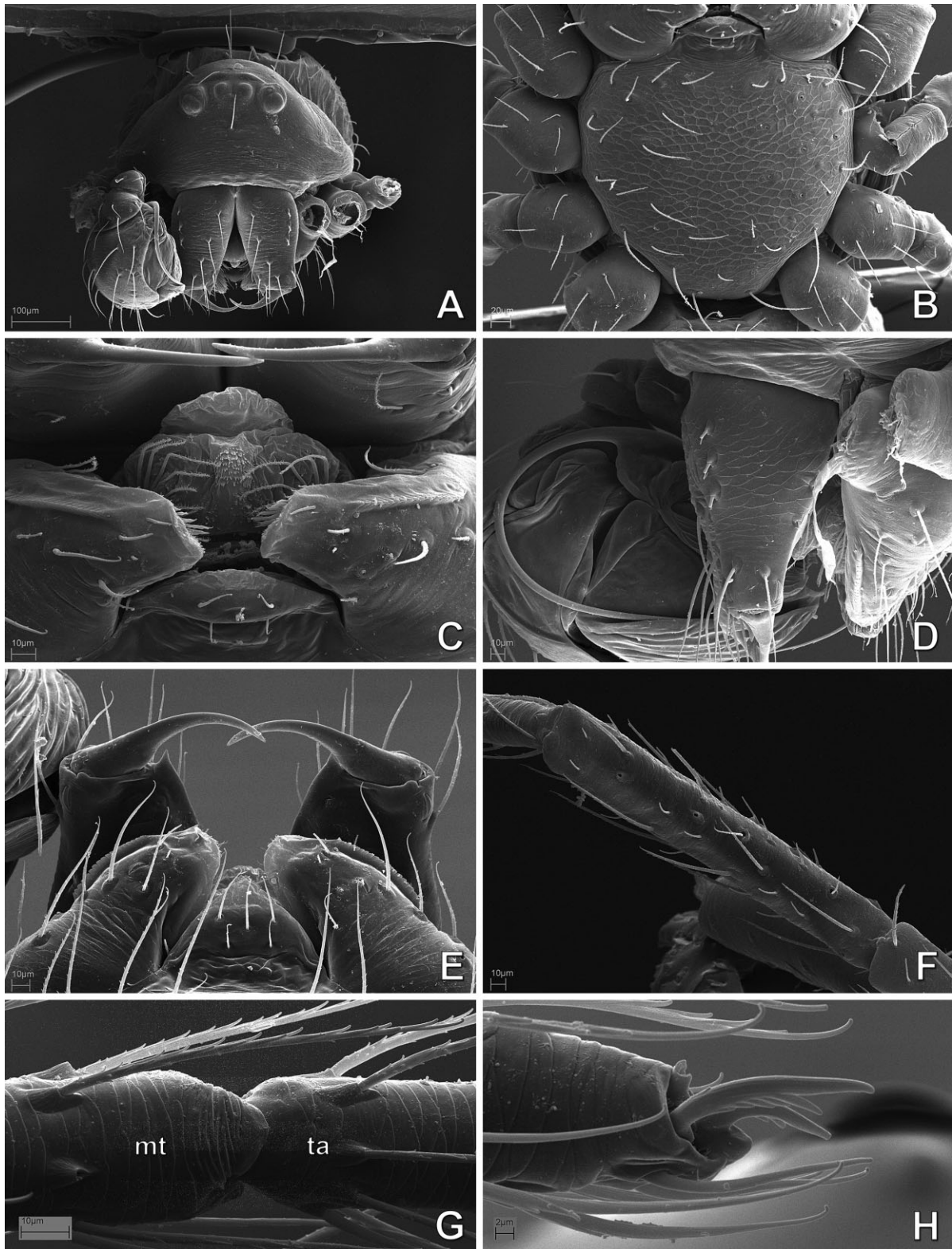


Figure 111. *Synaphris saphrynis* (Synaphridae), male paratype: A, prosoma, frontal view; B, sternum, ventral view; C, mouthparts, ventral view; D, mouthparts, lateral view; E, mouthparts, posterior view; F, right tibia I, dorsal view; G, left leg I, metatarsus–tarsus junction, dorsal view; H, right leg I, claws, retrolateral view. See Appendix 3 for the list of abbreviations.

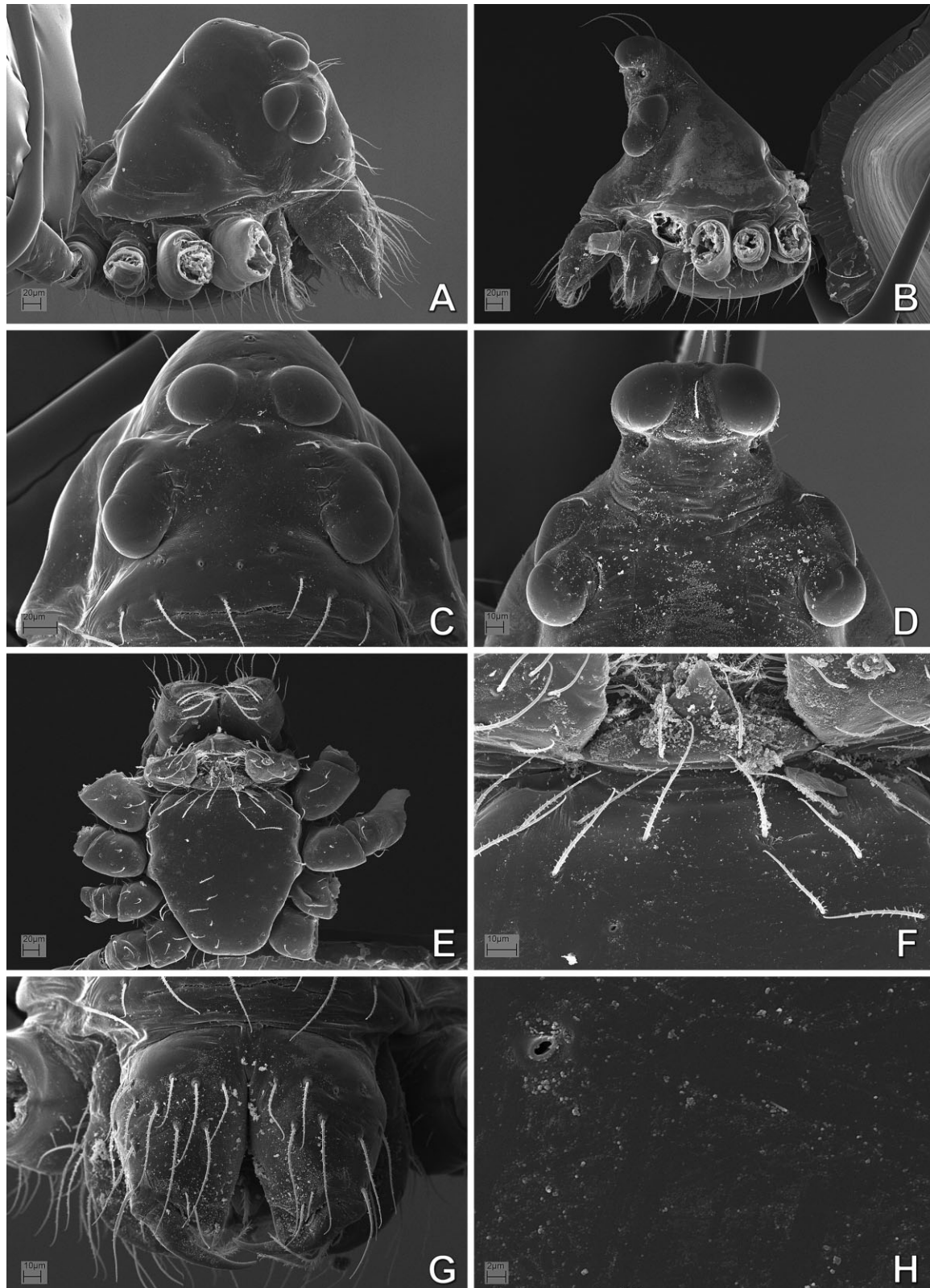


Figure 112. *Patu*-SYMP-001-DR (Symphytognathidae), from Barahona, Dominican Republic; prosoma: A, C, E–H, female; B, D, male. A, B, lateral view; C, D, ocular area, frontal view; E, ventral view; F, same, detail of labium–sternum junction; G, mouthparts, frontal view; H, sternal cuticular pattern, detail from panel F.

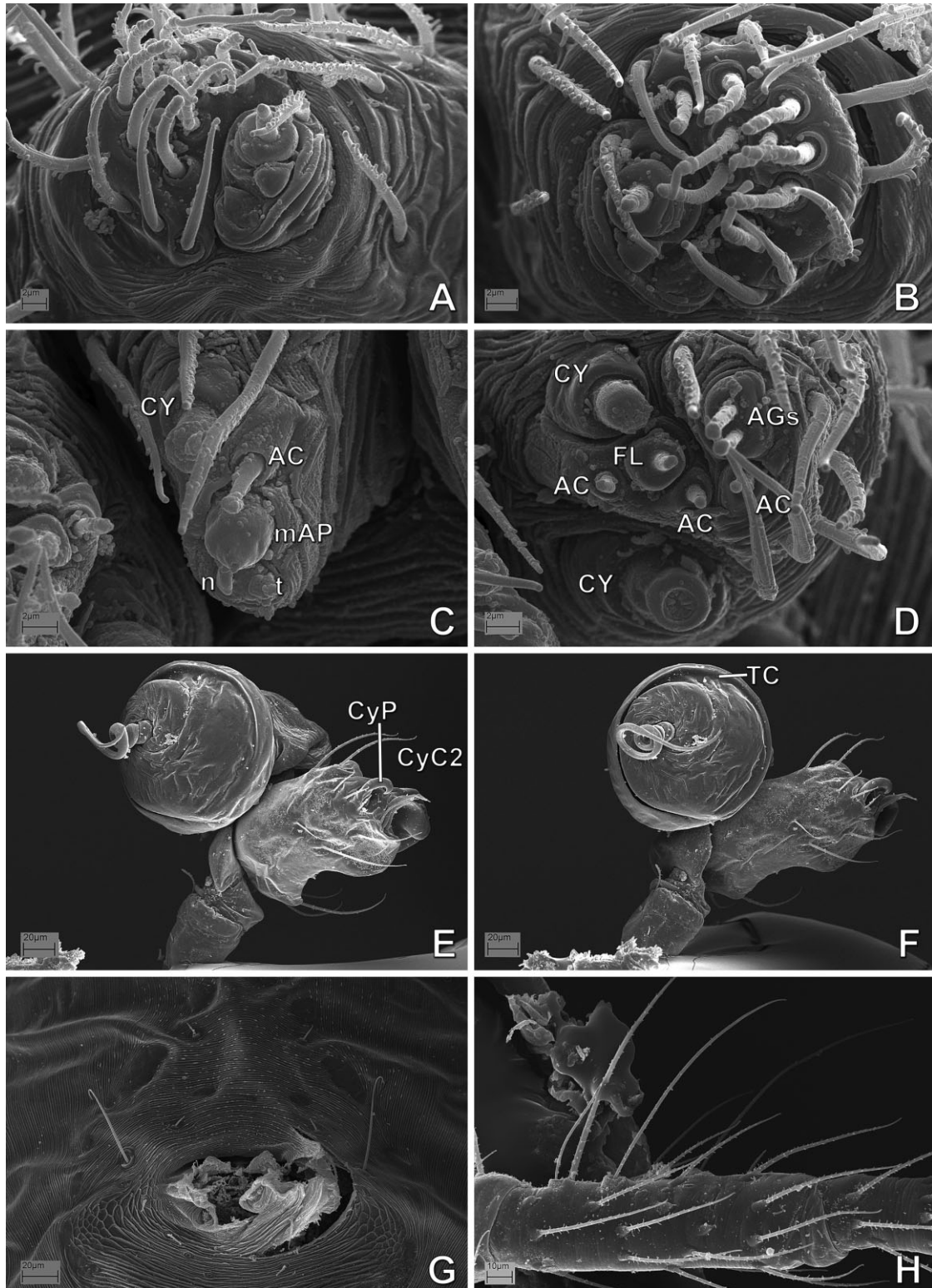


Figure 113. *Patu*-SYMP-001-DR (Symphytognathidae), from Barahona, Dominican Republic: A–D, G, female abdomen; E, F, H, male. A, right anterior lateral spinneret (ALS); B, left ALS; C, right posterior median spinneret; D, left posterior lateral spinneret. E, right palp, inverted, bulb detaching from cymbium, retrolateral–ventral (bulb) and apical (cymbium) views; F, same, ventral (bulb) and dorsal (cymbium) views. G, pedicel area; H, left tibia IV, retrolateral view. See Appendix 3 for the list of abbreviations.

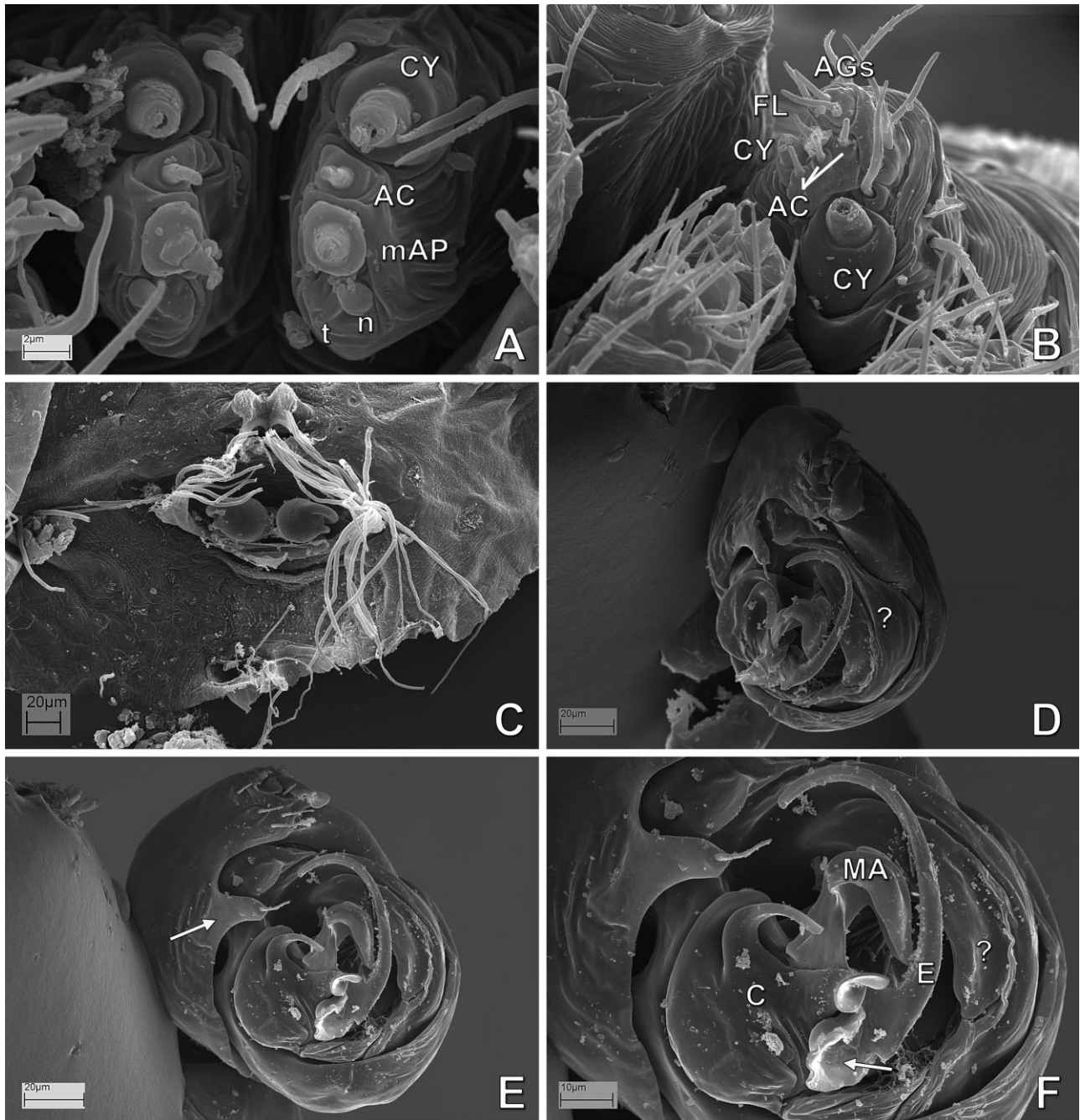


Figure 114. SYMP-002-MAD (Symphytognathidae), from Mahajanga, Madagascar: A–C, female abdomen; D–F, male left palp. A, posterior median spinnerets; B, left posterior lateral spinneret; C, digested abdomen, showing respiratory system and vulva; D, left palp, ventral–apical view; E, same, prolateral view, arrow to prolateral distal expansion; F, same, detail from panel E, arrow to embolic basal expansion. See Appendix 3 for the list of abbreviations.

Taxon names used throughout the discussion include the taxonomic decisions reported in Appendix 5. We will discuss the comparative morphology of the respiratory system in mysmenids, and its evolutionary implications within symphytognathoids, in a separate paper.

MYSMENIDAE COMPARATIVE MORPHOLOGY

Male palp (refer to characters 151–261)

The diversity and sclerite homologies of mysmenid male palps are only superficially understood. Mysmenidae have been recognized and even diagnosed by the

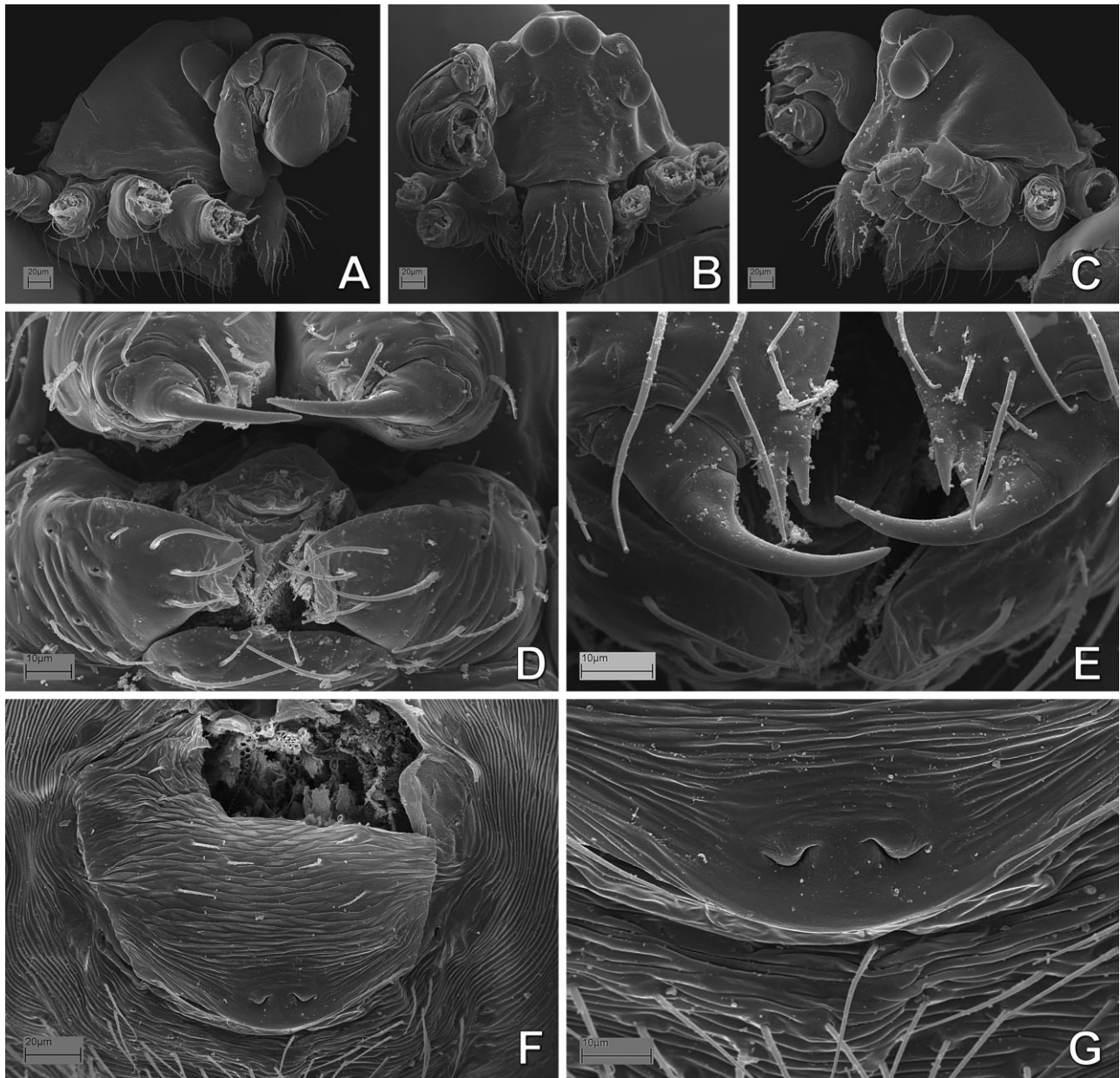


Figure 115. SYMP-002-MAD (Symphytognathidae), from Mahajanga, Madagascar: A–C, male prosoma; D–G, female. A, C, lateral views; B, frontal view. D, mouthparts, ventral view; E, same, detail of cheliceral fangs and teeth. F, pedicel and epigynal areas; G, same, detail of epigynal area.

generalized shape of the cymbium, described as ‘apically twisted and with lobes’ (Platnick & Shadab, 1978; Brignoli, 1980; Coddington, 1990; Wunderlich, 1995; Griswold *et al.*, 1998; Schütt, 2003). Despite the fact that several relatively modern descriptions of mysmenids have included detailed illustrations of genitalic morphology (e.g. Kraus, 1967; Thaler, 1975, 1995; Saaristo, 1978; Baert & Maelfait, 1983; Baert, 1984a, 1990; Lin & Li, 2008; Miller *et al.*, 2009), most mysmenid species remain poorly described. The details of the palp mor-

phology are also insufficiently studied, especially in terms of explicit hypotheses of homology. For example, it has been suggested that a tegular conductor, median apophysis, and paracymbium are absent (Coddington, 1990; Griswold *et al.*, 1998; Miller *et al.*, 2009); however, a paracymbium had previously been identified in Mysmenidae (Kraus, 1967). The mysmenid male palp appears highly complex and morphologically variable, and in most species it is greatly translucent, so that the cymbium, conductor, and other sclerites are

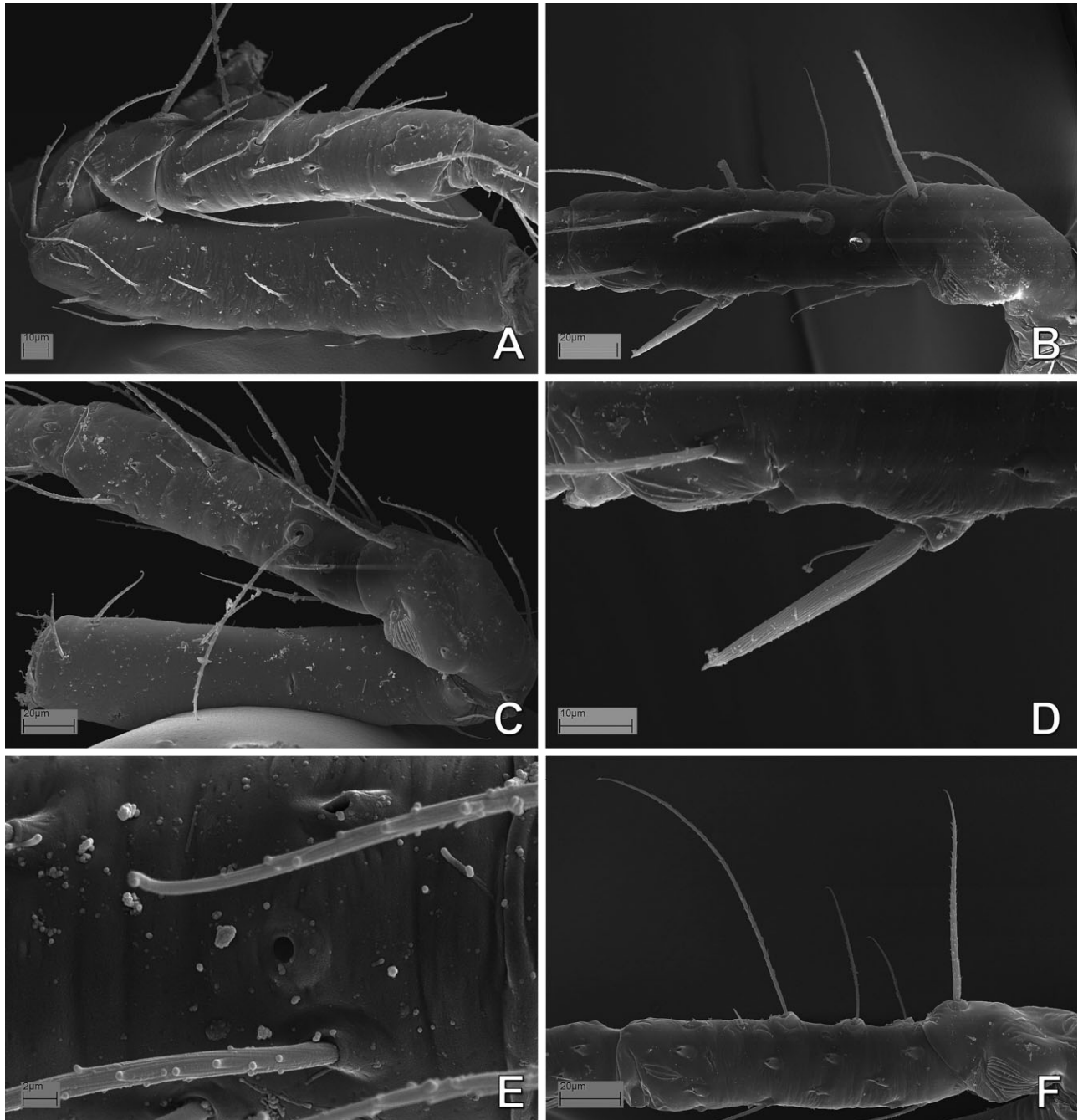


Figure 116. SYMP-002-MAD (Symphytognathidae), from Mahajanga, Madagascar, left legs. A, C, E, female; B, D, F, male. A, femur, patella and tibia I, prolateral view; B, patella and tibia II, retrolateral view; C, femur, patella and tibia I, retrolateral view; D, detail of tibia II clasp spine, from panel B; E, leg I, tarsal organ; F, patella and tibia IV, retrolateral view.

difficult to distinguish and to delineate precisely under light microscopy. In summary, mysmenid male palps have distinct cymbial structures, including a paracymbium, and can also have a tegular conductor. A median apophysis or any other tegular sclerites are lacking, however. As in the details of the differ-

ent respiratory organs in Mysmenidae, the diversity of palpal structures is great within the family, although each particular arrangement seems characteristic at the genus or sometimes subfamily level (this is simply a consequence of how taxonomists have circumscribed higher taxa in Mysmenidae). In the

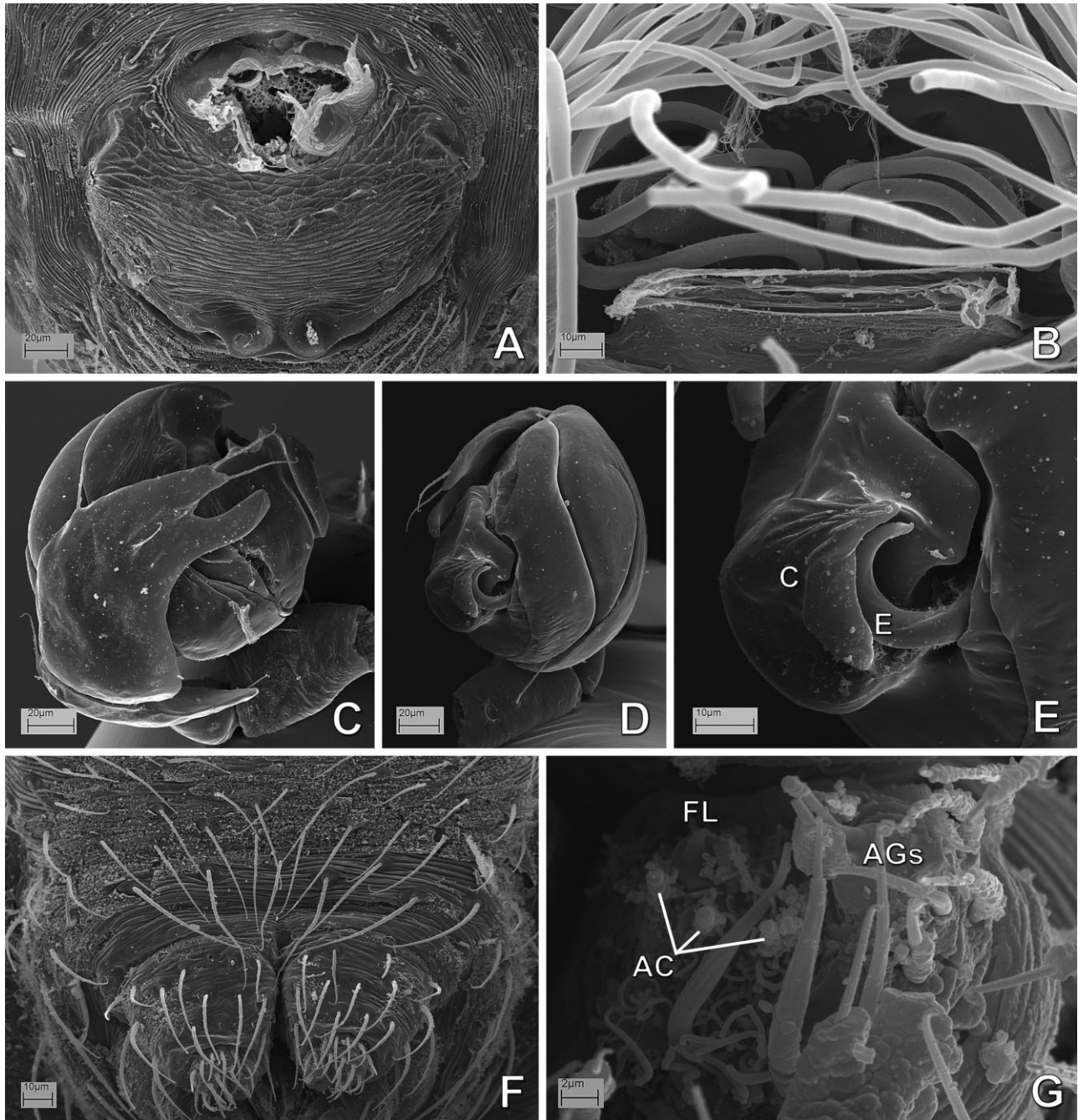


Figure 117. SYMP-006-AUST (Symphytognathidae), from Queensland, Australia: A, B, F, female; C–E, G, male. A, pedicel and epigynal areas; B, digested abdomen, detail of vulva. C, left palp, dorsal view; D, same, ventral-apical view; E, same, detail of embolus and conductor. F, ventral abdomen and anterior spinnerets, note absence of colulus and posterior spiracle; G, left posterior lateral spinneret. See Appendix 3 for the list of abbreviations.

sections below, we address the large diversity of mysmenid palpal morphology.

Palpal femur, patella and tibia

Mysmenids lack any modifications on the palpal femur and patella. Conversely, and across symphytognathoids,

varying shapes of the male palpal tibia can be found. A distally broad tibia (i.e. wider distally, usually more than two times its basal width) may be symplesiomorphic for symphytognathoids, as it also occurs in Theridiidae. Distally broad tibiae occur in Theridiosomatidae, Synsphyridae, and most Mysmenidae

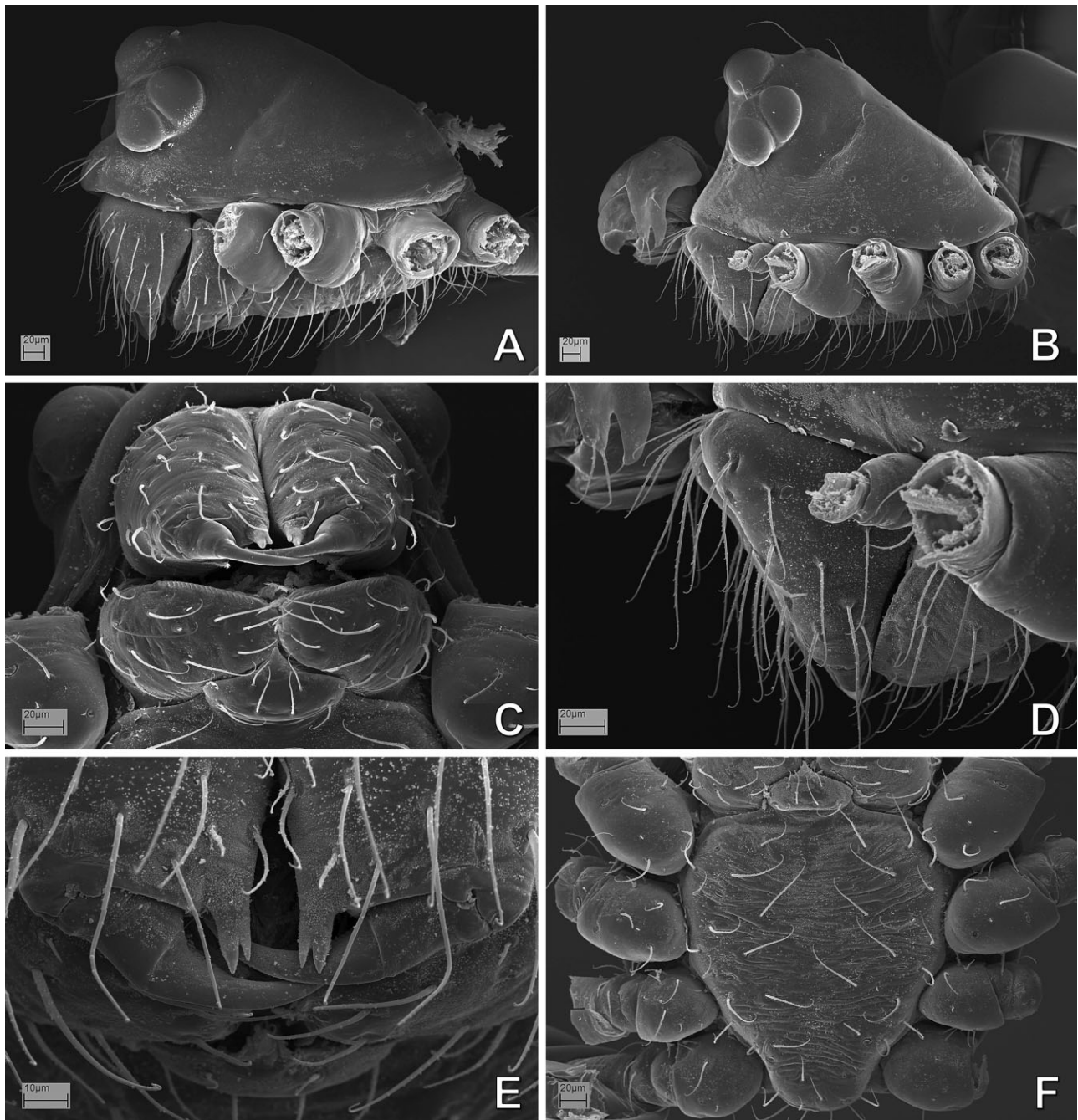


Figure 118. SYMP-006-AUST (Symphytognathidae), from Queensland, Australia, prosoma: A, C, female; B, D–F, male. A, B, lateral view; C, mouthparts, ventral view; D, same, lateral view, detail from panel B; E, detail of cheliceral fangs and teeth; F, sternum and labium, ventral view.

(Figs 4A, 17D, 28A, 30E, 32E, 38A, 42A, 47B, 63C). Within symphytognathoids, a flat tibia (i.e. flattened from the base, and usually with irregular, not circular, distal section outline) is synapomorphic for the clade comprising Symphytognathidae plus Anapidae (Figs 91F, 95C, D, 102C). Within Mysmenidae, broad male palpal tibiae are widespread, occurring

in *Trogloneta*, *Isela*, and all Mysmeninae. Moreover, a cylindrical tibia (distal width similar to or less than two times proximal width) is synapomorphic for *Maymena*, and convergently present in *Comaroma* and *Tasmanapis* (Figs 10A, 81D, 98B,C). A globose tibia is a synapomorphy of *Mysmenopsis* (Figs 55A, C, 58A, 60A).

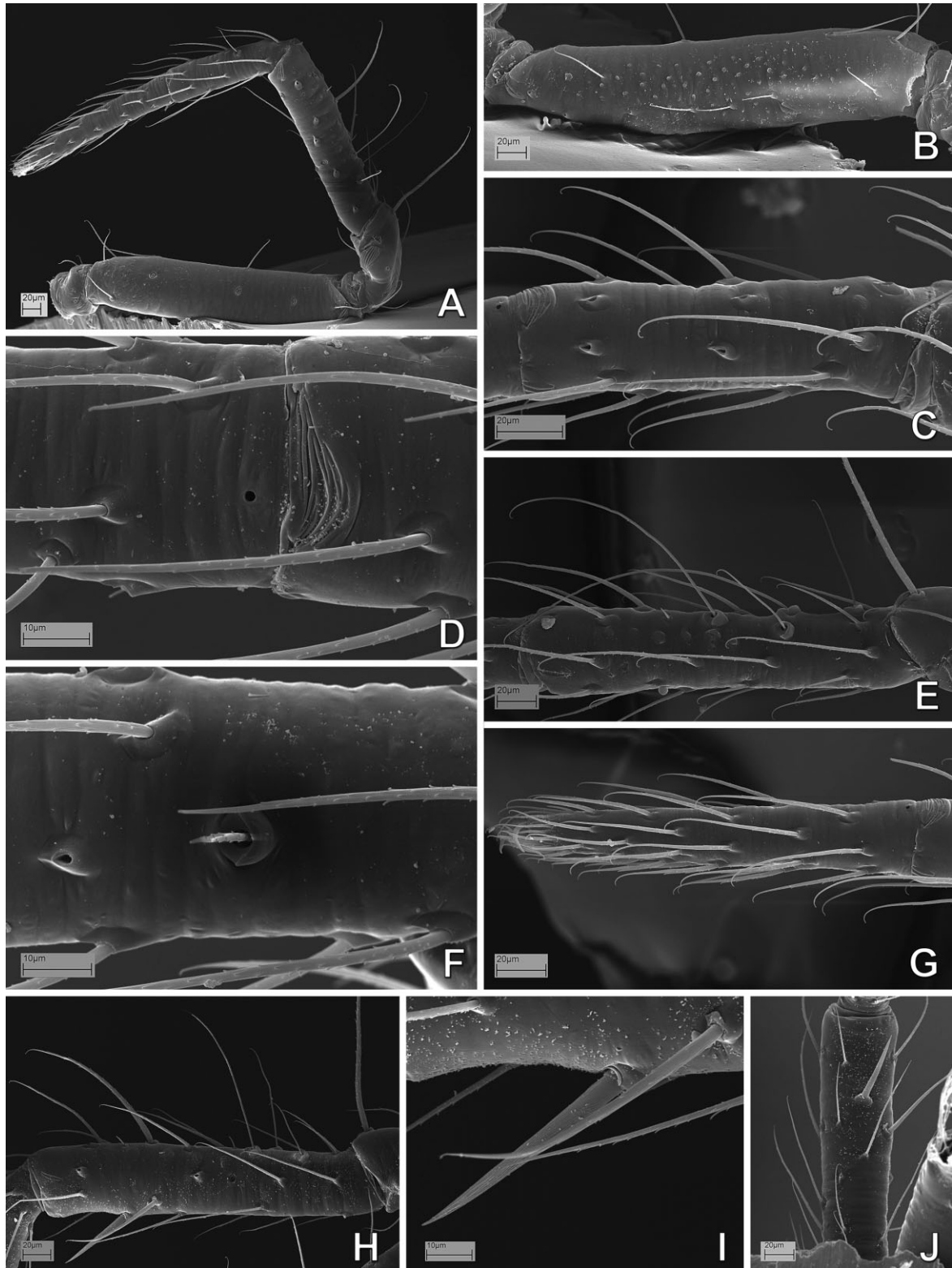


Figure 119. SYMP-006-AUST (Symphytognathidae), from Queensland, Australia, left legs. A–G, female; H–J, male. A, leg I, retrolateral; B, femur I, prolateral; C, metatarsus IV, retrolateral; D, leg I, tarsal organ and metatarsus–tarsus junction, dorsal; E, tibia IV, retrolateral; F, metatarsus I, detail of trichobothrial base, dorsal; G, tarsus IV, retrolateral; H, tibia II, retrolateral view; I, same, detail of clasp ing spine; J, same, ventral view.

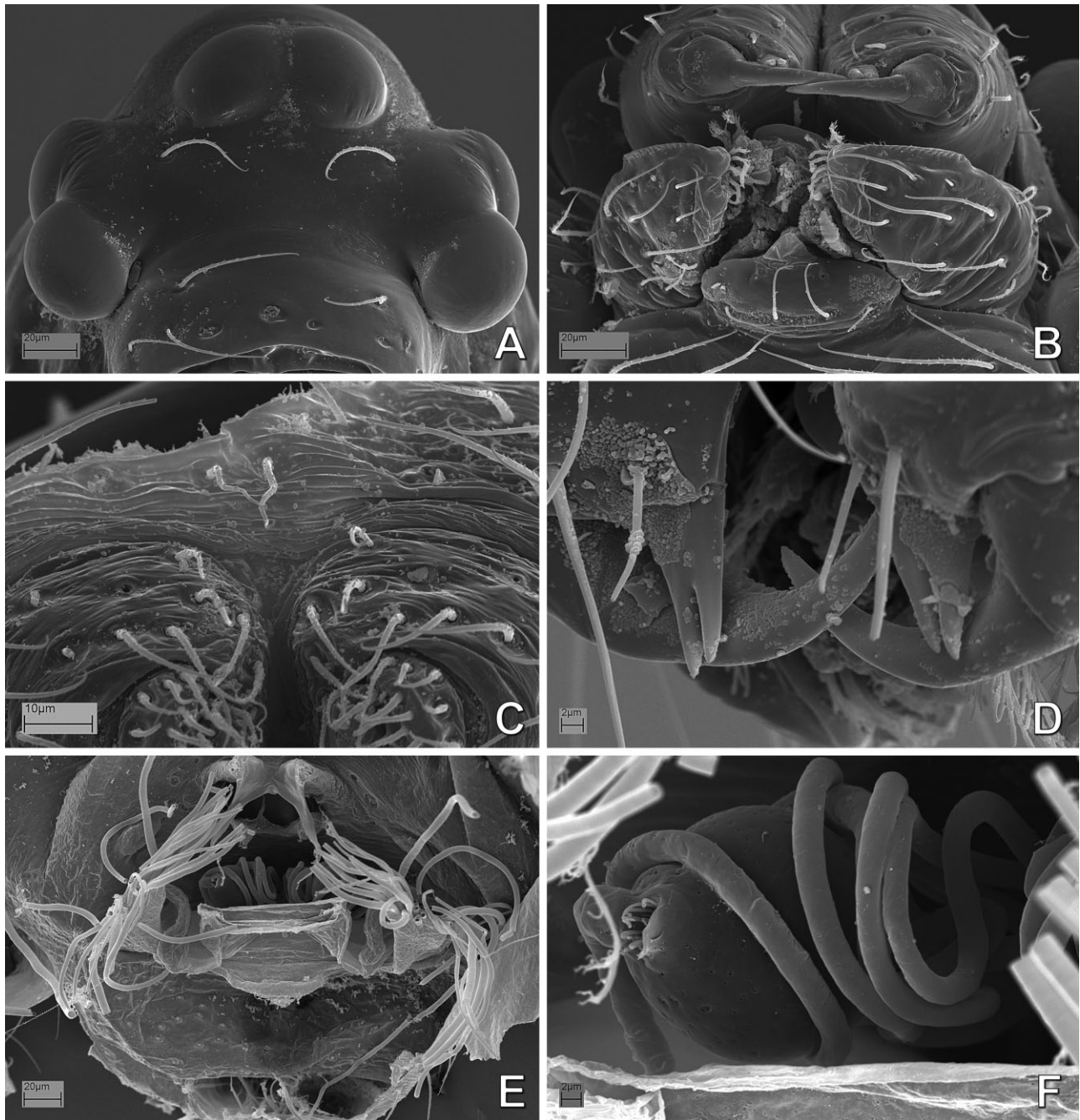


Figure 120. SYMP-007-AUST (Symphytognathidae), from Queensland, Australia, female. A, ocular area, frontal view; B, mouthparts, ventral view; C, spinning field, details to absence of colulus; D, mouthparts, detail of cheliceral fangs and teeth; E, digested abdomen, respiratory system and vulva; F, same, detail of vulva.

Most mysmenid palpal tibiae are small, shorter than cymbium, as in other symphytognathoids (Figs 10A, 27B, 30D, 47A, B, 63B, C, 71D, 106C, 110E). A large tibia is synapomorphic for Mysmenopsinae (Figs 1A, 4A, 55A, C). In addition, no distinct tibial processes occur in Mysmenidae, except for a prolateral extension in *Mysmeniola* (Fig. 134D; see also Thaler, 1995:

figs 5, 7) and an apical ventral (sometimes ventroretrolateral) excavation usually bearing spurs in *Mysmenopsis* (Figs 53A, 58A, 60A). Mysmenopsines have modified setae distally on the tibiae, such as spurs in *Mysmenopsis* (as mentioned above, Figs 53E, 55H, 58E, 60B), or spine-like, strong setae in *Isela* (Figs 1A, B, 4A, E). Mysmenid tibial rim setae are longer than

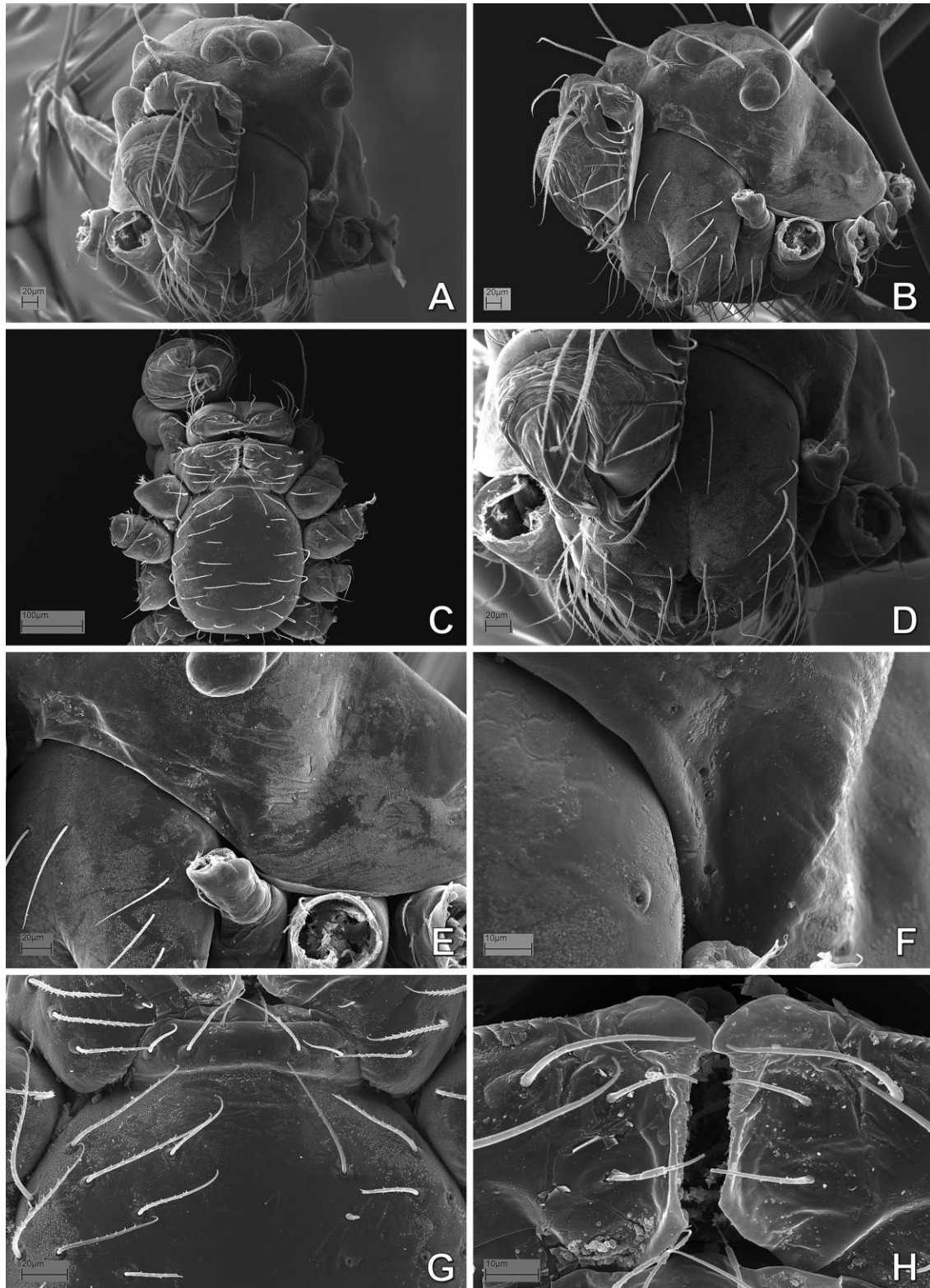


Figure 121. *Symphytognatha picta* (Symphytognathidae), from Western Australia, Australia, male prosoma: A, frontal view; B, lateral–frontal view; C, ventral view; D, chelicerae, ventral view, detail from panel A; E, detail anterior prosoma, lateral view; F, carapace lateral depression, detail from panel B; G, labium–sternum junction, detail from panel C; H, maxillae, ventral view.

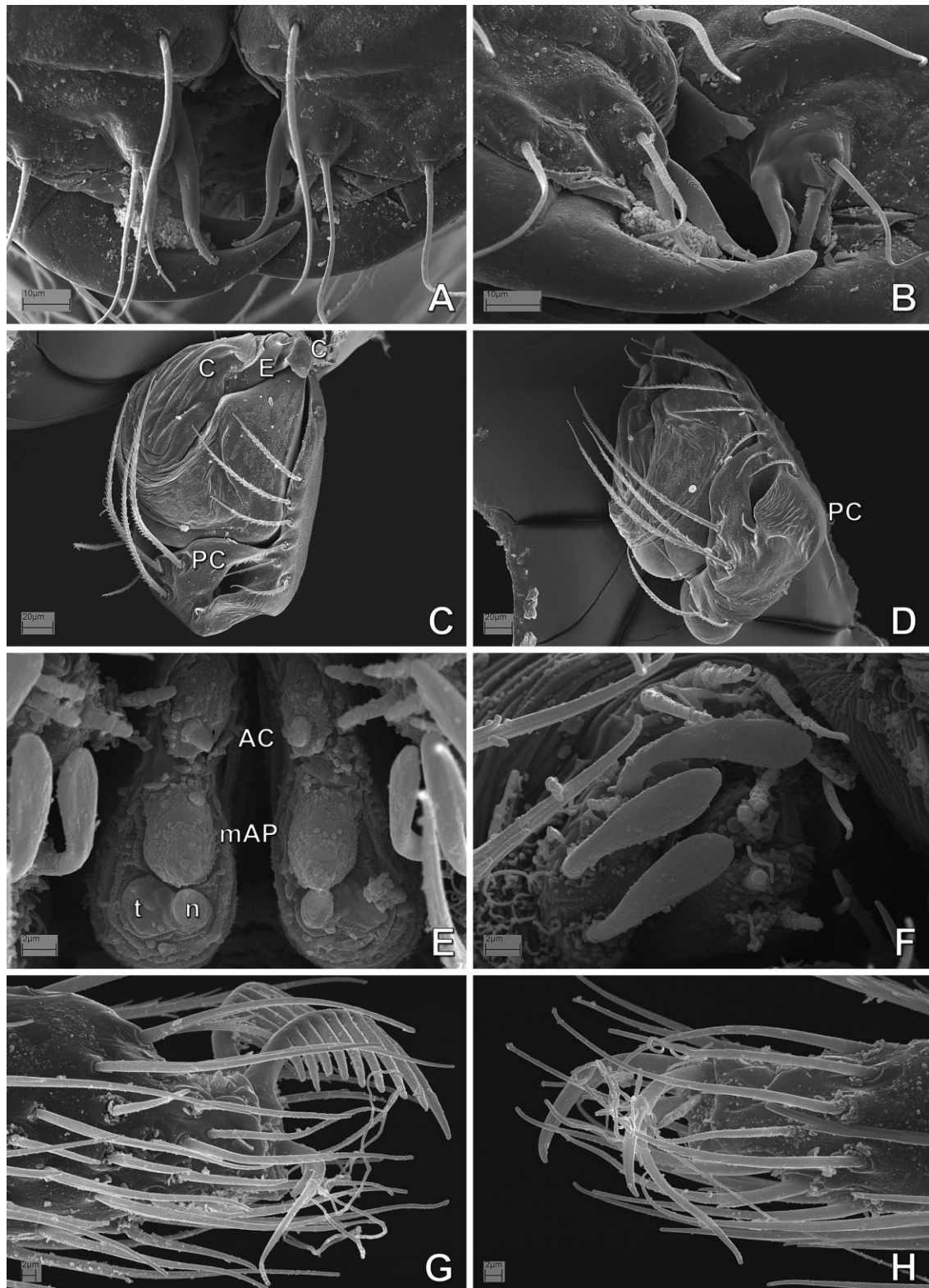


Figure 122. *Symphytognatha picta* (Symphytognathidae), from Western Australia, Australia, male: A, cheliceral fangs and teeth, frontal view; B, same, lateral view; C, left palp, retrolateral–ventral view; D, same, retrolateral view; E, posterior median spinnerets; F, right posterior lateral spinneret; G, left leg I, claws, prolateral view; H, left leg IV, claws, retrolateral view. See Appendix 3 for the list of abbreviations.

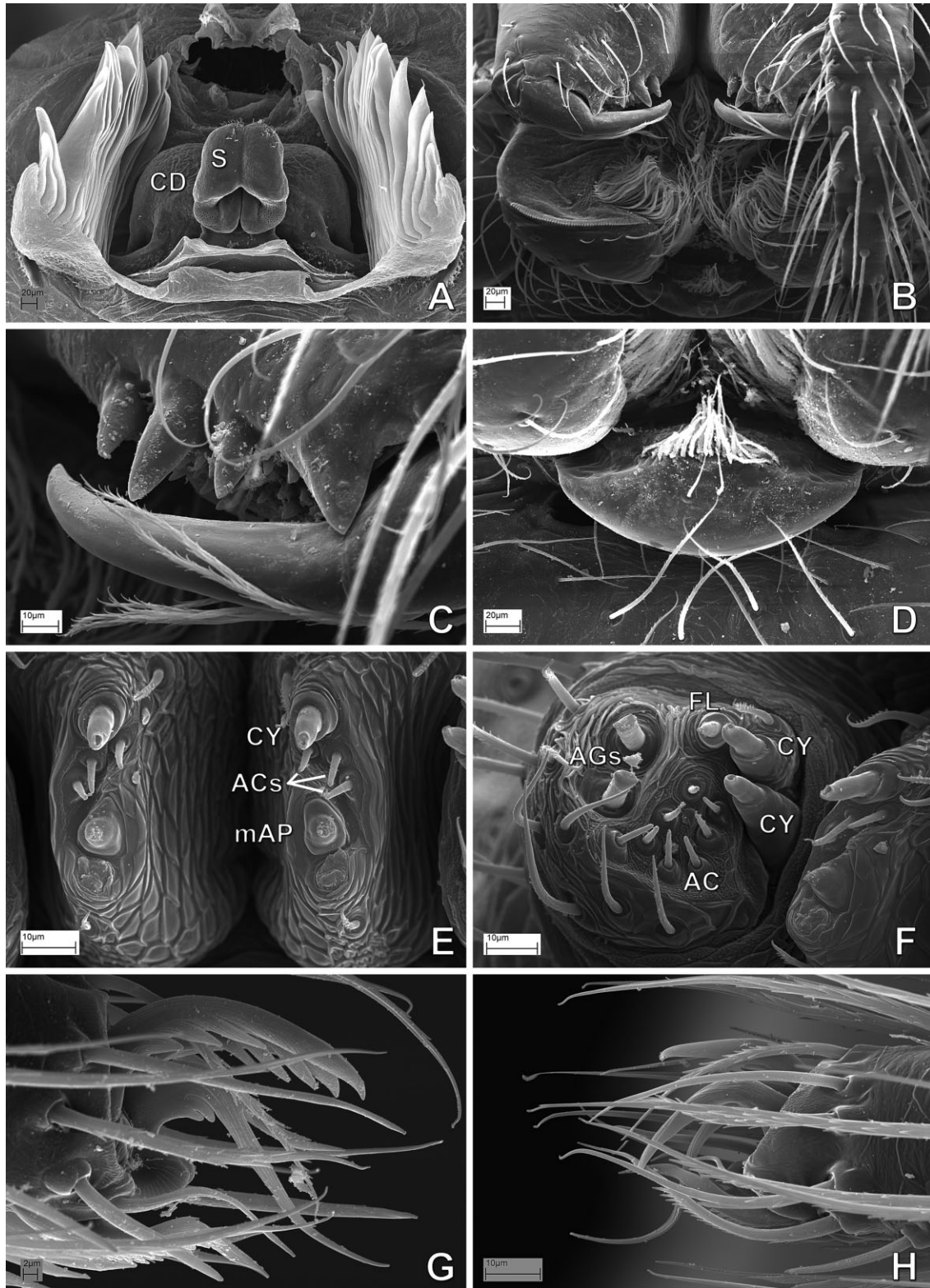


Figure 123. *Theridiosoma gemmosum* (Theridiosomatidae), female: A, digested abdomen, detail of anterior respiratory system and vulva; B, mouthparts, ventral–frontal view; C, same, detail of cheliceral fang and teeth; D, labium, ventral view; E, posterior median spinnerets; F, right posterior lateral spinneret; G, left leg I, claws, prolateral view; H, left leg IV, claws, retrolateral view. See Appendix 3 for the list of abbreviations.

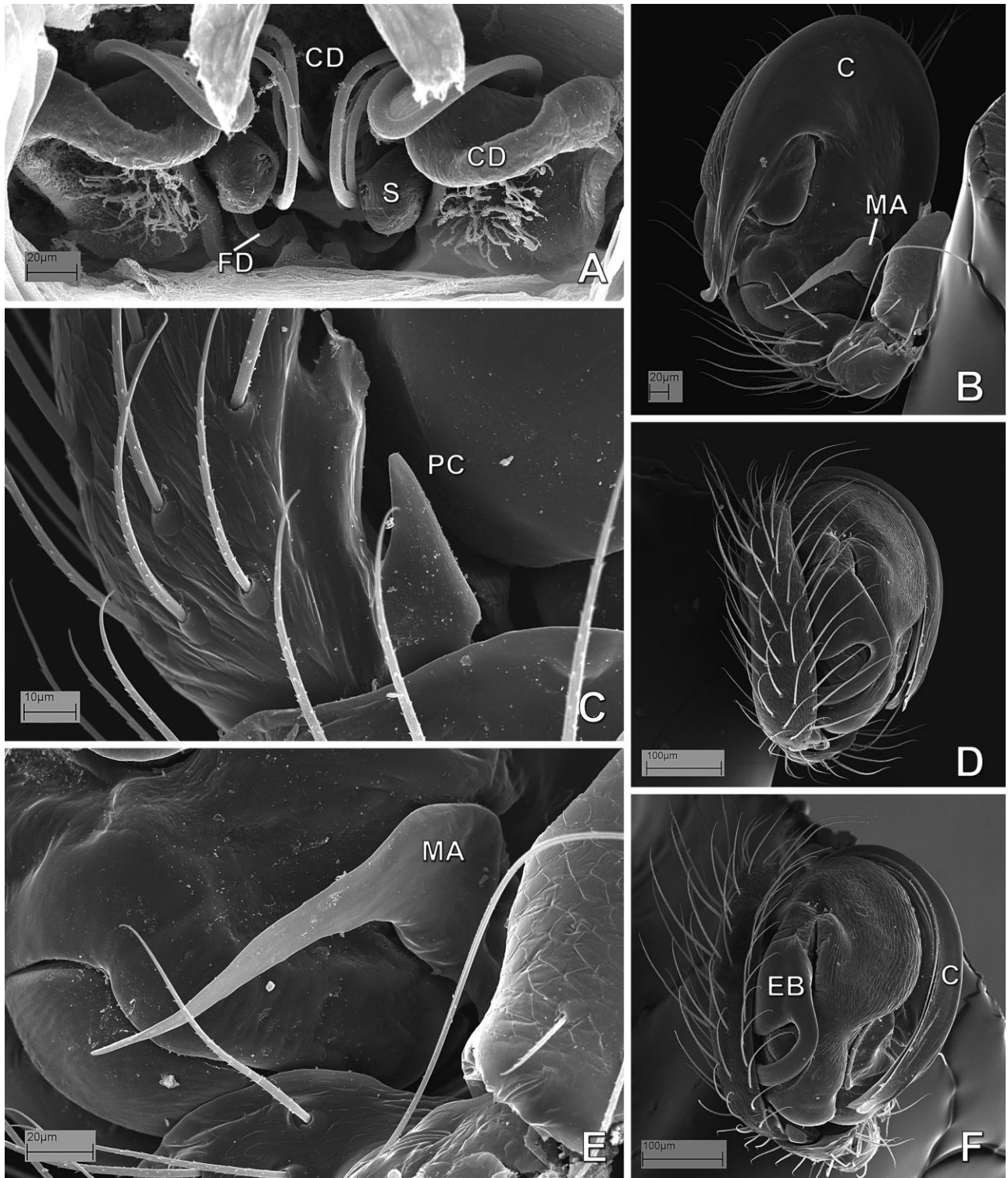


Figure 124. *Coddingtonia euryopoides* (Theridiosomatidae) from Chiang Mai, Thailand. A, female digested abdomen, vulva, anterior view. B–F, male right palp, images not inverted; B, ventral view; C, detail of paracymbium; F, palp, retrolateral view; D, palp, dorsal view; E, detail of median apophysis, from panel B. See Appendix 3 for the list of abbreviations.

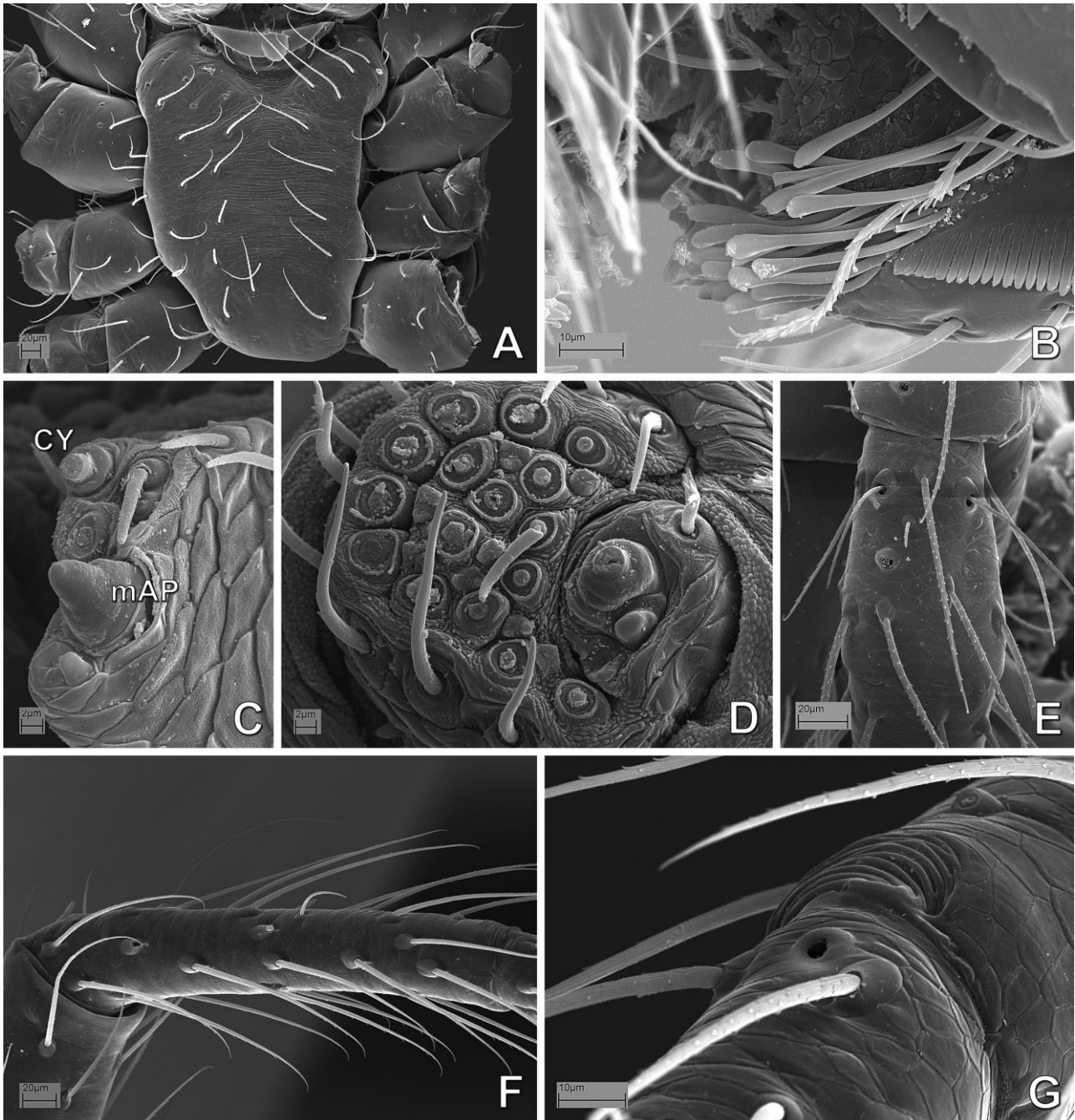


Figure 125. *Coddingtonia euryopoides* (Theridiosomatidae) from Chiang Mai, Thailand; female: A, sternum and labium, ventral view; B, mouthparts, detail of maxillary setae; C, right posterior median spinneret; D, right anterior lateral spinneret; E, palpal tibia, dorsal view; F, left metatarsus I, prolateral view; G, leg I, tarsal organ. See Appendix 3 for the list of abbreviations.

remaining tibial setae, and are arranged distally in one or two rows (Figs 4E, 10D, 18A, 32E, 36D, 42B, 45C, 53B, 55C), except in *Trogloneta* and a few other mysmenids where the setae are equally short and dispersed in an irregular conformation (Figs 63C, 66A).

Cymbium: general morphology
(see Fig. 126 for reference)

The size of the cymbium and bulb (relative to the size of the carapace, in lateral view) varies across mysmenid taxa. Although small male palps are common in adult

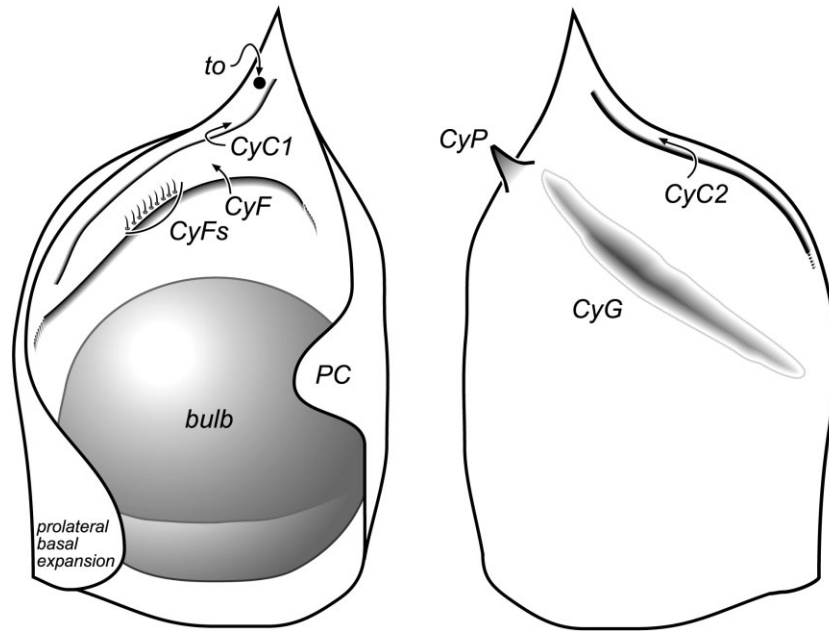


Figure 126. Schematic drawings showing cymbial structures on the male palp of Mysmenidae. Left cymbium is depicted: A, ventral view; B, dorsal view. See Appendix 3 for the list of abbreviations.

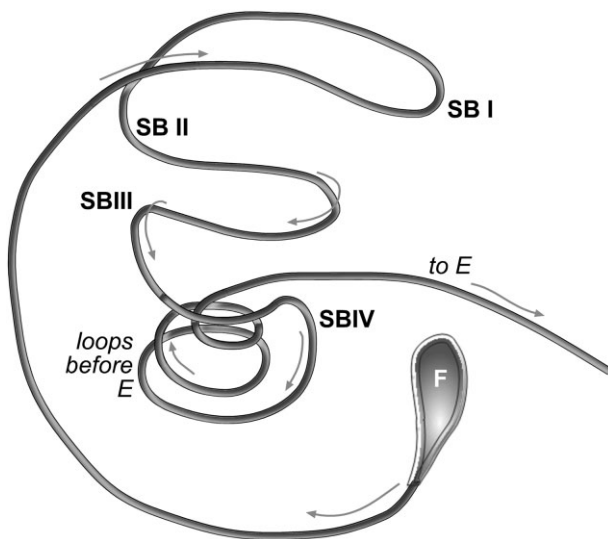


Figure 127. Schematic drawing of the trajectory of the spermatid duct on male left palp, in prolateral view. See Appendix 3 for the list of abbreviations.

spiders, medium-sized palps are widespread within symphytognathoids, including mysmenids (i.e. the cymbium-bulb complex is about half the size of the carapace; Figs 27F, 66A, 141K). The cymbium bulb becomes secondarily small (about one-fifth the size of the carapace) in *Maymena mayana* and mysmenopsines, however (Figs 2B, 140E, 141D). A very large cymbium-

bulb complex (i.e. as large as the prosoma) has evolved independently in some distal clades within *Microdipoena* and *Mysmena*, including *Mysmena leucoplagiata* (Figs 19B, 142A), in Theridiosomatidae, and the synphrid genus *Cepheia*. Superficially, there appears to be a tendency towards an increase in palpal size, which suggests a correlation with the reduction of body size in symphytognathoids; however, most symphytognathoids are equally minute in body size, regardless of their familial placement or size of the palp. For example, most *Microdipoena* species (and also theridiosomatids) with huge palps are as small as any other mysmenine or even larger than members of Symphytognathidae, which possess medium-sized palps. *Taphiassa*, a small micropholcommatine anapid, also has small palps.

The cymbium in most mysmenids is uniquely oriented ventrally or prolatero-ventrally in the palp (Figs 38A,B, 42B, 66A). The cymbium evolved independently to a prolateral position in *Mysmenopsis*, *Mysmeniola*, and the mysmenine MYSM-023-MAD (Fig. 50B), or to a retrolateral-dorsal position in some *Maymena* species (Fig. 15B).

In some symphytognathoids the cymbium is sometimes modified relative to the typical cymbium of most araneoids, which is scoop-shaped and round to oval in dorsal view (e.g. Griswold *et al.*, 1998: figs 16A, 18F). This is especially so in mysmenids. Without taking into account any other cymbial structures (such as cymbial conductors, apophyses, paracymbia, expansions, etc.; see comments below), an oval cymbium is plesiomorphic

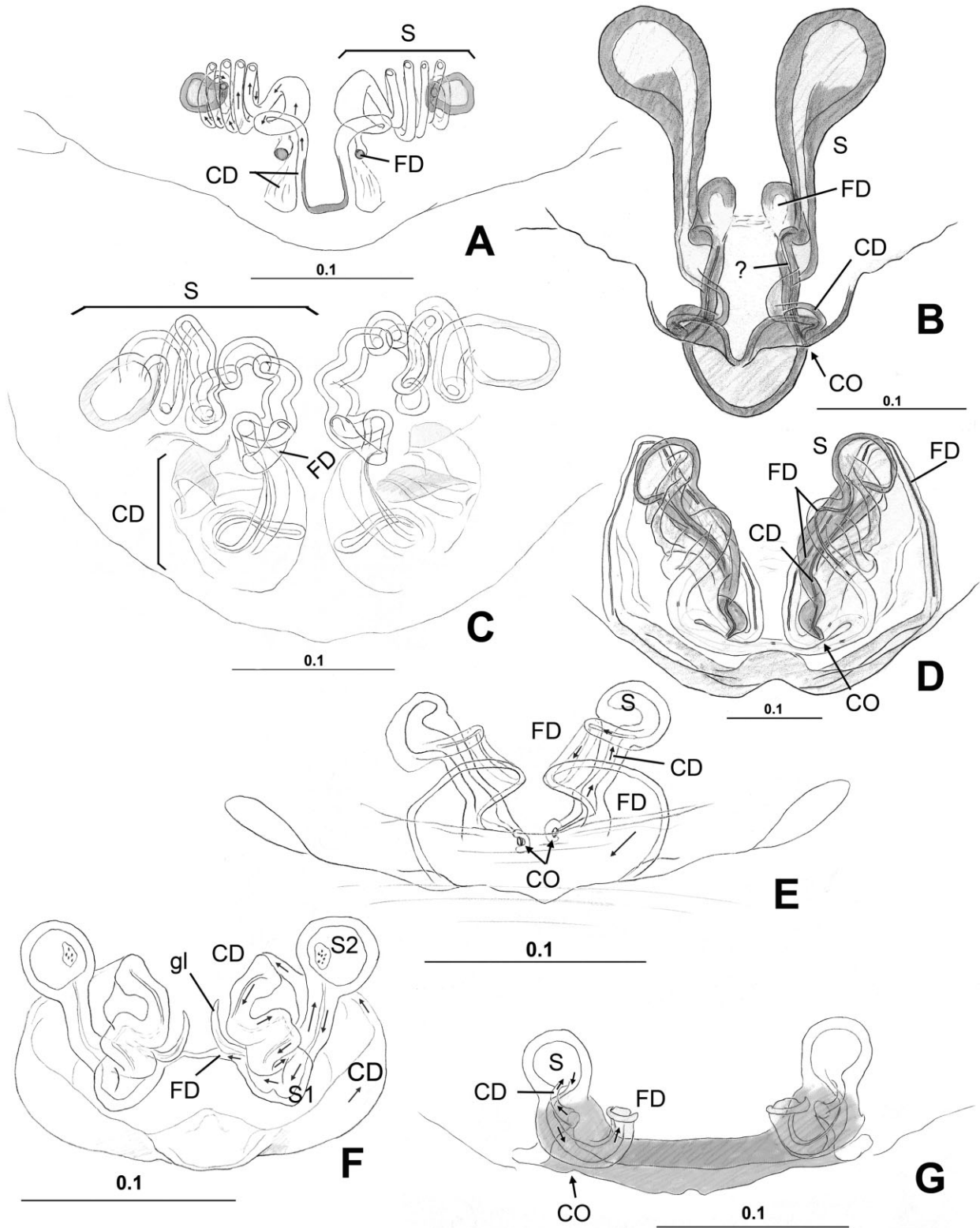


Figure 128. Mysmenidae female genitalia, cleared: A, *Isela okuncana*, dorsal view; B, *Maymena mayana*, dorsal view; C, *Kilifina*-MYSM-002-KENYA (*Isela* sp.), from Kwale, Kenya, dorsal view; D, *Maymena ambita*, ventral view; E, *Maymena rica*, dorsal view; F, *Trogloneta granulum*, ventral view; G, *Mysmenopsis dipluramigo*, dorsal view. See Appendix 3 for the list of abbreviations.

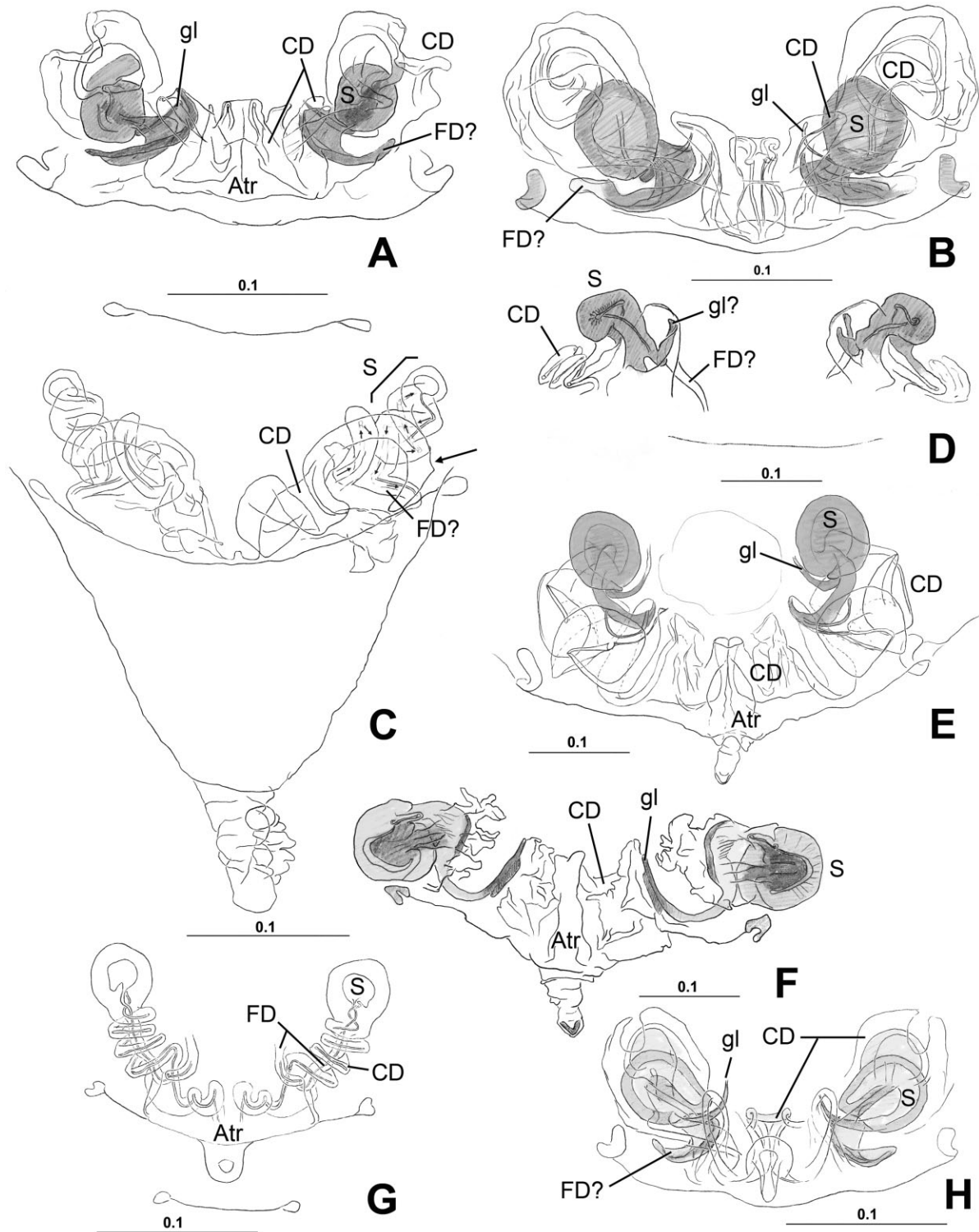


Figure 129. Mysmenidae female genitalia, cleared: A, *Microdipoena guttata*, ventral view; B, *Microdipoena nyungwe*, ventral view; C, MYSM-007-MEX (*Mysmena*), from Chiapas, Mexico, ventral view, arrow to diverticle of copulatory duct; D, *Microdipoena elsaе*, ventral copulatory duct; E, *Microdipoena* (= *Mysmenella*) *samoensis*, syntype, ventral view; F, *Microdipoena* (= *Mysmenella*) *jobi*, paratype, ventral view; G, *Mysmena*-MYSM-015-MAD (*Mysmena*), from Antananarivo, Madagascar, dorsal view; H, MYSM-029-MAD (*Mysmeninae*), from Antsiranana, Madagascar, ventral view. See Appendix 3 for the list of abbreviations.

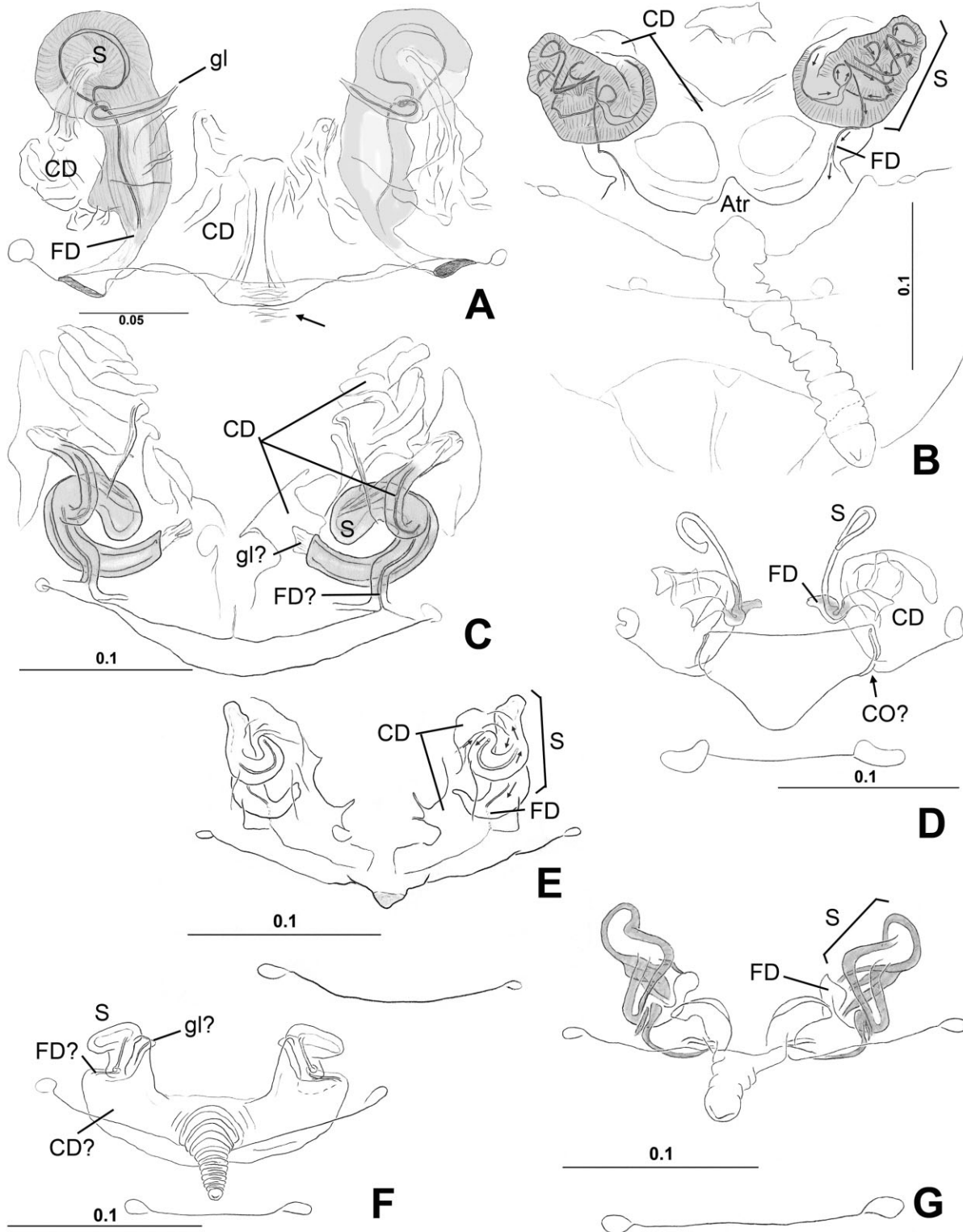


Figure 130. Mysmenidae female genitalia, cleared. A, *Mysmena* (= *Calodipoena*) *tarautensis*, paratype, dorsal view, arrow to broken scapus; B, *Mysmena* (= *Calodipoena*) *incredula*, dorsal view; C, *Mysmena leichhardti*, from Queensland, Australia, ventral view; D, MYSM-023-MAD (Mysmeninae), from Antananarivo, Madagascar, ventral view; E, *Mysmena tasmaniae*, ventral view; F, MYSM-005-ARG (*Mysmena*), from Misiones, Argentina, ventral view; G, MYSM-019-MAD (Mysmeninae), from Toliara, Madagascar, ventral view. See Appendix 3 for the list of abbreviations.

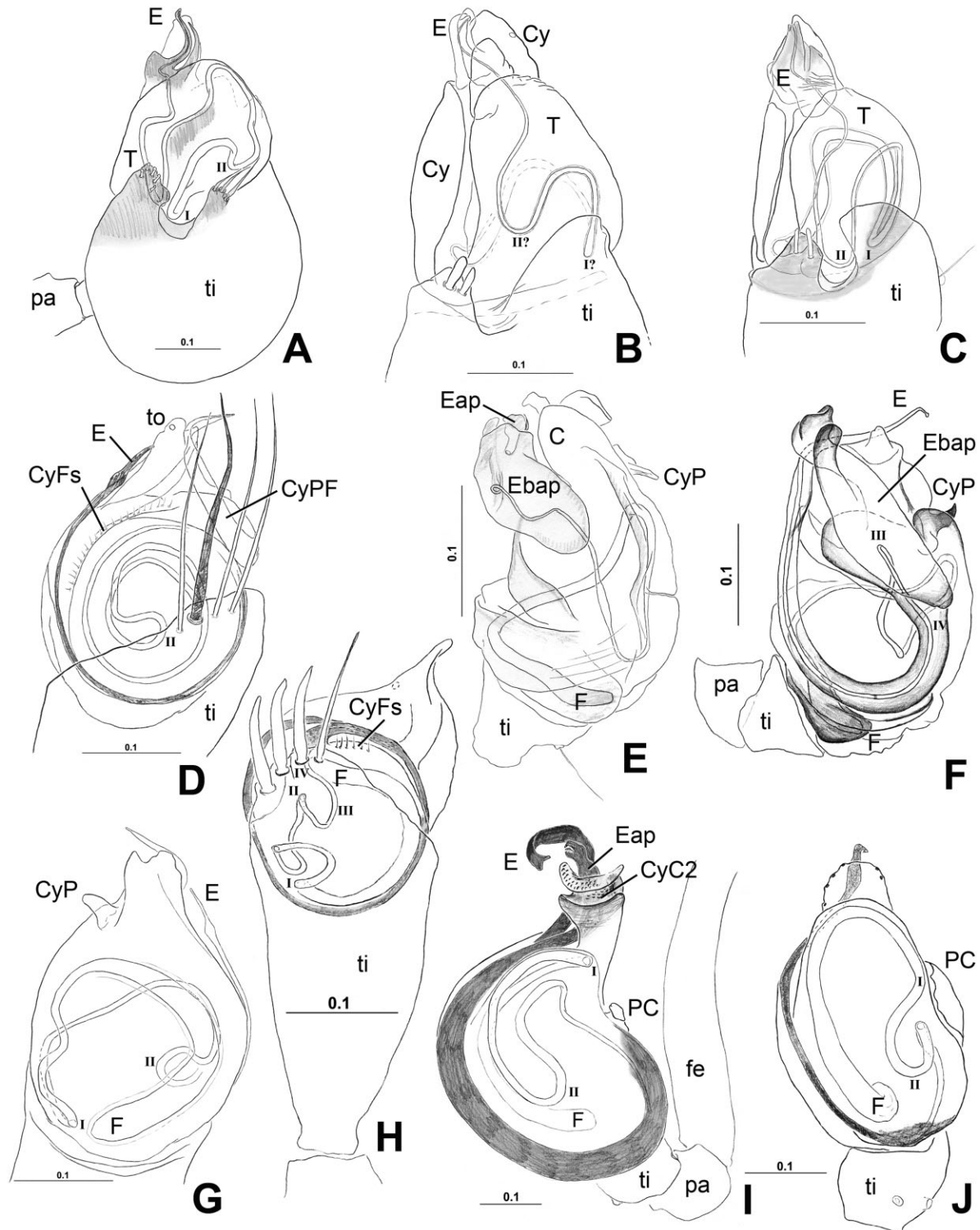


Figure 131. Mysmenidae male left palp (unless otherwise stated), cleared: A, *Mysmenopsis penai*, retrolateral view, right palp, inverted; B, *Mysmenopsis dipluramigo*, retrolateral view; C, *Mysmenopsis cidrelicola*, presumably paralectotype, retrolateral view, right palp, inverted; D, *Kilifina*-MYSM-002-KENYA (*Isela* sp.), from Kwale, Kenya, ventral view, right palp, inverted; E, *Trogloneta granulum*, ventral view; F, *Trogloneta cantareira*, ventral view; G, *Kilifina*-MYSM-002-KENYA (*Isela* sp.), from Kwale, Kenya, dorsal view, right palp, inverted; H, *Isela okuncana*, ventral view; I, *Maymena ambita*, ventral view; J, *Maymena mayana*, ventral view. See Appendix 3 for the list of abbreviations.

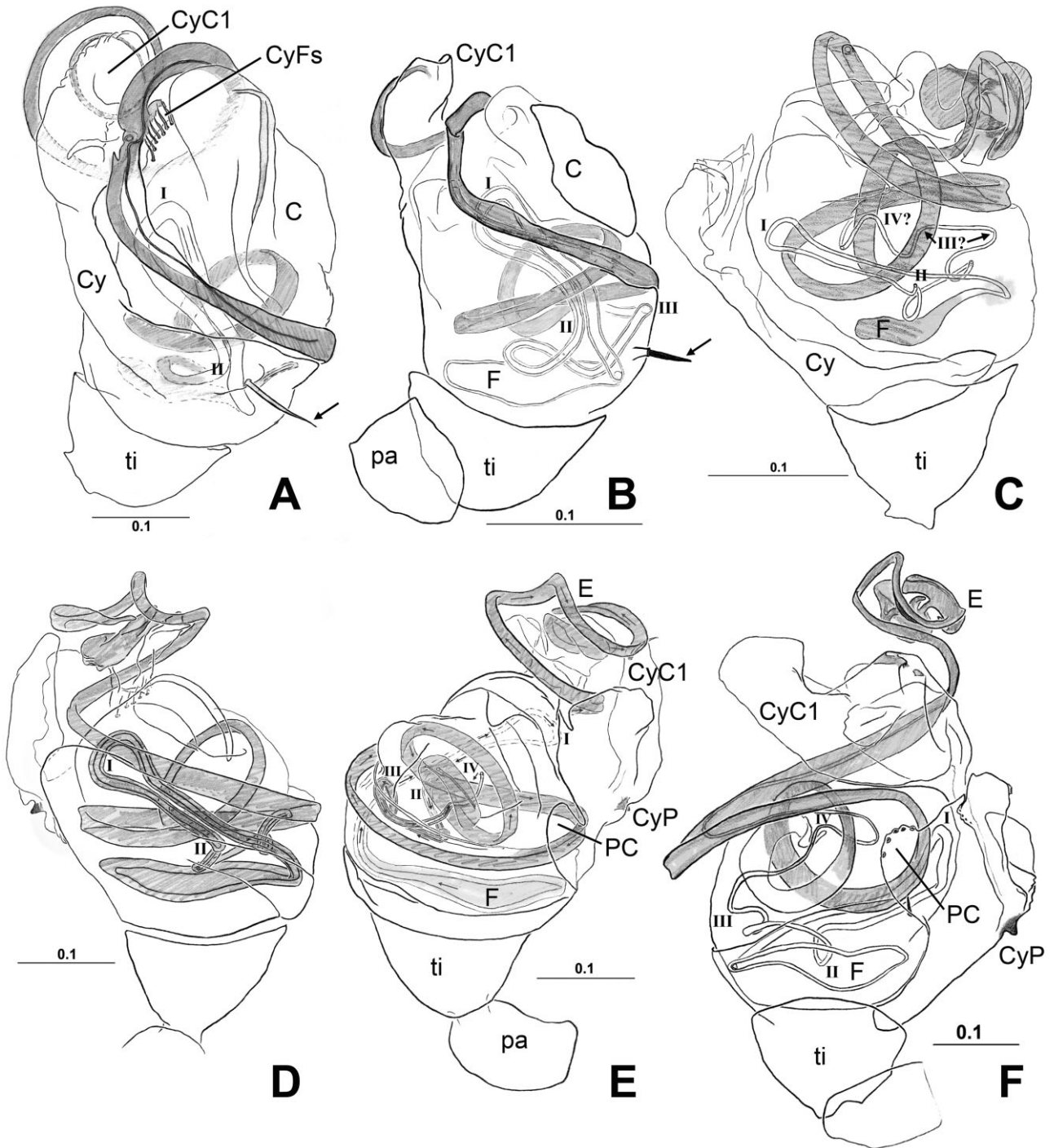


Figure 132. Mysmenidae male left palp, cleared: A, *Microdipoena elsaе*, prolateral view, arrow to spine of basal prolateral cymbial expansion; B, *Microdipoena guttata*, prolateral view, arrow to spine of basal prolateral cymbial expansion; C, *Microdipoena* (= *Mysmenella*) *illectrix*, type, prolateral view; D, *Microdipoena* (= *Mysmenella*) *samoensis*, syntype, prolateral view; E, same, retrolateral view; F, *Microdipoena* (= *Mysmenella*) *jobi*, holotype, retrolateral view. See Appendix 3 for the list of abbreviations.

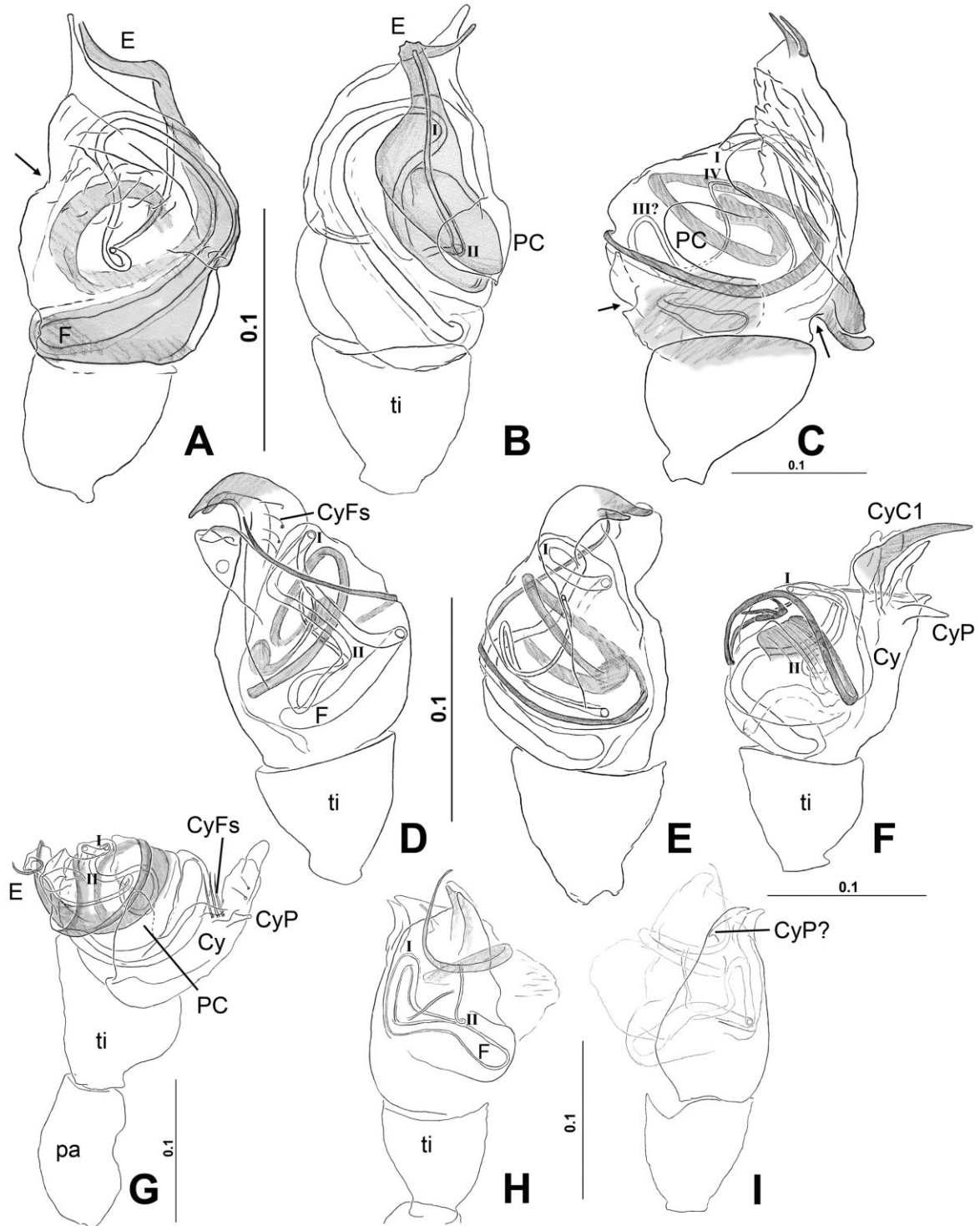


Figure 133. Mysmenidae male left palp (unless otherwise stated), cleared. A, MYSM-005-ARG (*Mysmena*), from Misiones, Argentina, dorsal view, right palp, inverted, arrow to cymbial groove (CyG); B, same, ventral view; C, MYSM-007-MEX (*Mysmena*), from Chiapas, Mexico, retrolateral view, arrows to CyG; D, *Mysmena* (= *Kekenboschiella*) *awari*, paratype, prolateral view; E, same, dorsal-retrolateral view; F, *Mysmena* (= *Kekenboschiella*) *marijkeae*, holotype, retrolateral view, right palp, inverted; G, *Brasilionata arborensae*, holotype, retrolateral view, right palp, inverted; H, *Mysmena* (= *Tamasesia*) *rotunda*, type, prolateral view; I, same, retrolateral view, schematic drawing. See Appendix 3 for the list of abbreviations.

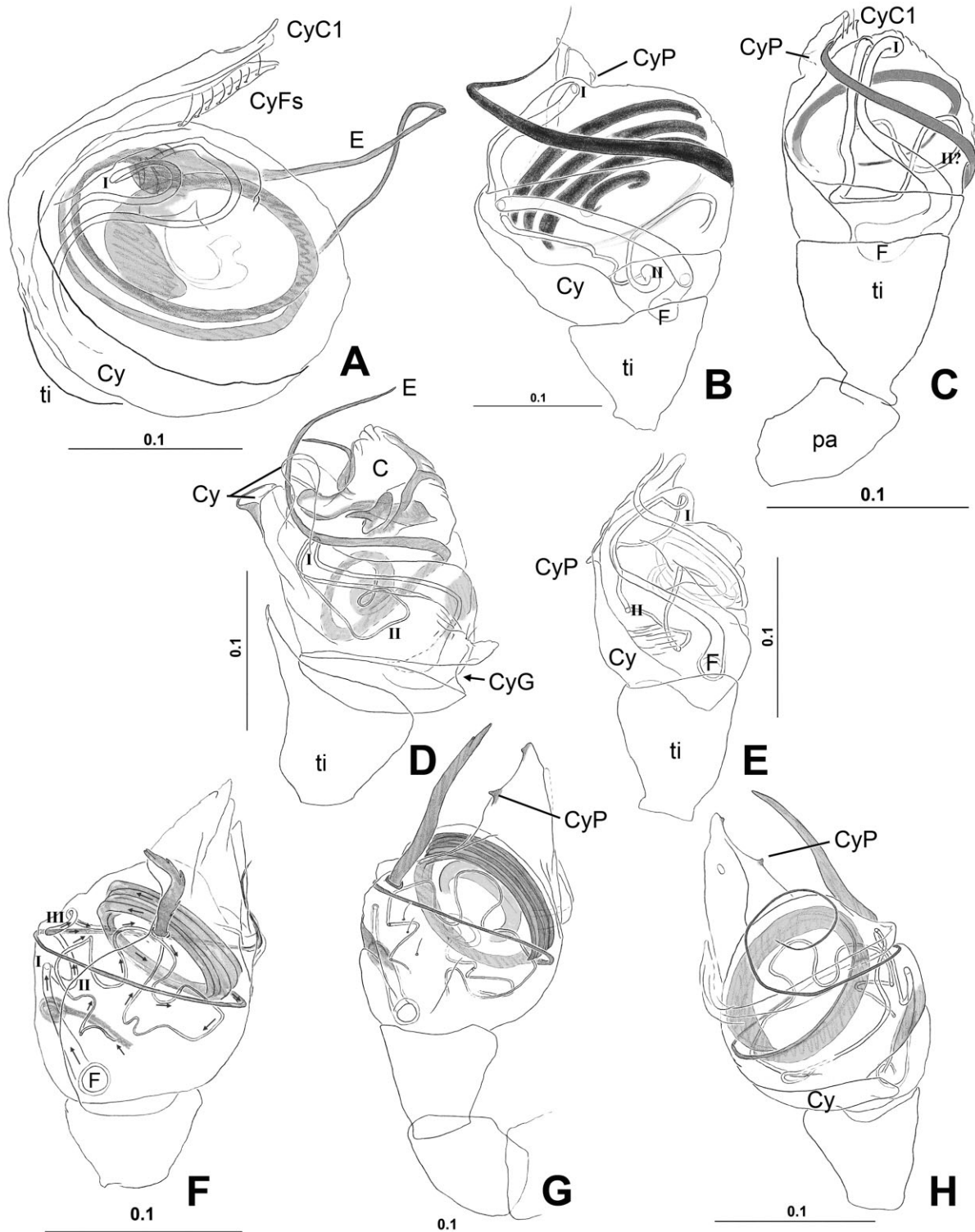


Figure 134. Mysmenidae male left palp (unless otherwise stated), cleared: A, *Mysmena leucoplagiata*, type, prolateral view, right palp, inverted; B, *Mysmena leichhardti*, from Queensland, Australia, prolateral-ventral view; C, *Mysmena tasmaniae*, prolateral-ventral view, right palp, inverted; D, *Mysmeniola spinifera*, holotype, prolateral view, right palp, inverted; E, MYSM-019-MAD (Mysmeninae), from Toliara, Madagascar, prolateral view; F, MYSM-023-MAD (Mysmeninae), from Antananarivo, Madagascar, retrolateral view, right palp, inverted; G, MYSM-020-MAD (Mysmeninae), from Toamasina, Madagascar, dorsal view, right palp, inverted; H, same, ventral view. See Appendix 3 for the list of abbreviations.

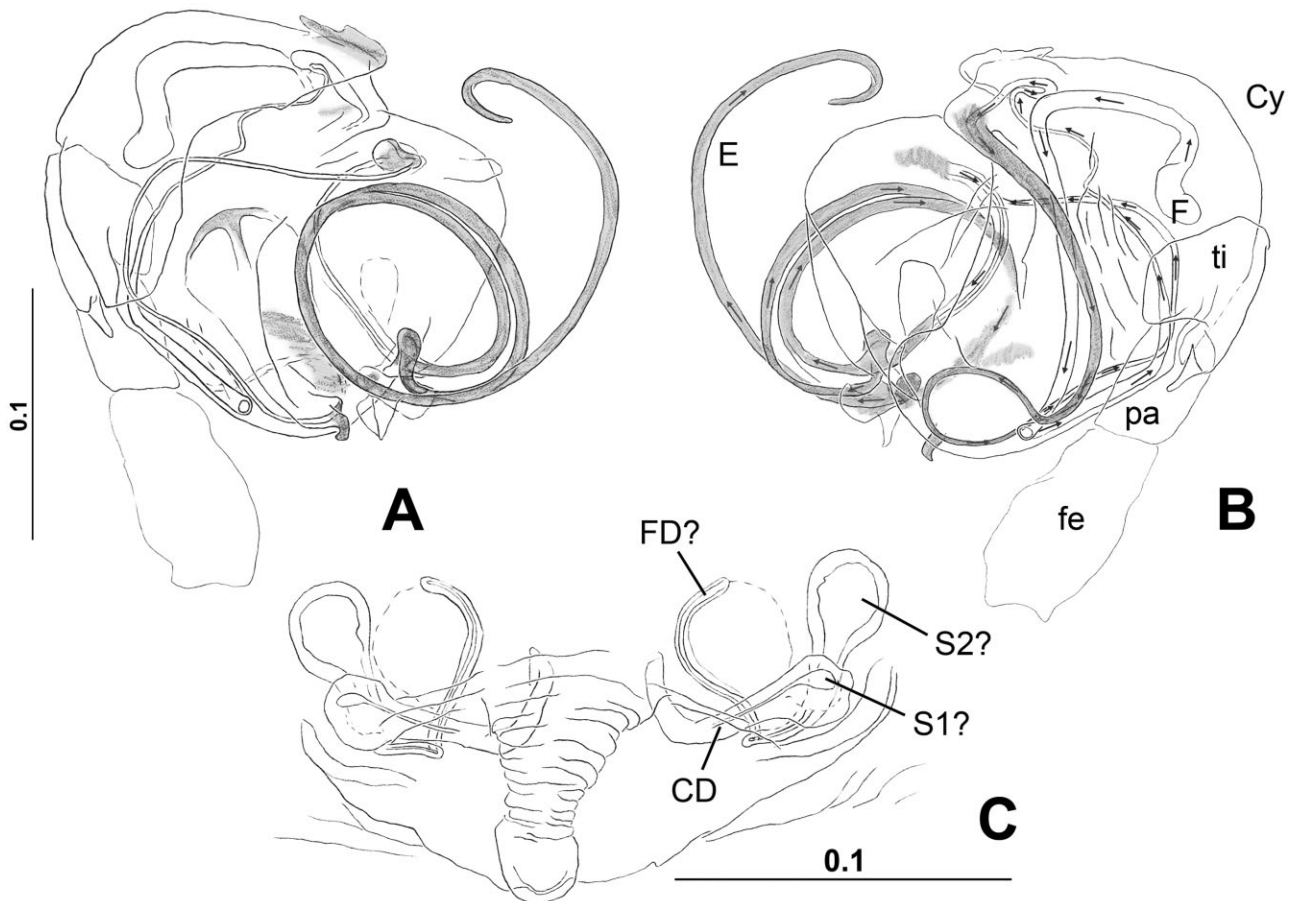


Figure 135. Cleared genitalia: A, *Iardinis mussardi* (Symphytognathidae) male holotype, right palp, inverted, prolateral view; B, same, retrolateral view, same scale as in panel A; C, *Phricotelus stelliger* (symphytognathoid) female type, cleared epigynum, ventral view. See Appendix 3 for the list of abbreviations.

in Mysmenidae (Figs 10A, 14A), and it has independently evolved in MYSM-005-ARG (*Mysmena*; Fig. 28B). A cymbium as long as wide occurs in mysmenopsines and independently in a clade comprising most mysmenines (Figs 1A, 4C, 22F, 30D, 41B, 55B), whereas a distinctly flat and tapering cymbium is unique to *Trogloneta* (Fig. 63C; convergent in some symphytognathids).

The cymbium of mysmenids is greatly modified when compared with other symphytognathoids. There seems to be a pattern of shared modifications, such as grooves, processes, and modified setae, which can be recognized in the cymbium (Fig. 126). Not all mysmenids have all the cymbial structures that we describe. Furthermore, different combinations of these features usually vary among (and are distinctive of) each genus. A summary of these cymbial features is presented below (refer to Fig. 126).

Primary and secondary cymbial conductors (CyC1 and CyC2): Up to two apical grooves, which seemingly interact with the distal portion of the embolus, can occur in mysmenid cymbia. Both structures are here considered cymbial conductors.

The ‘primary cymbial conductor’ (CyC1) is located internally (i.e. closer to the bulb; Figs 4G, 10C, G, 14A, B, D, 22C, 27A, 30F, 43C, 47C, 63B, C), and it can bear the cymbial fold (CyF, see below). This internal conductor is a synapomorphy of Mysmenidae, although it is secondarily absent in *Mysmenopsis* (Figs 53D, 60D). Usually, the CyC1 is pointed apically, which is the plesiomorphic condition in Mysmenidae (Figs 4G, 30F, 40B, 43C, 47C); however, the CyC1 evolved independently into different shapes. A ‘half-circle’ shaped conductor is characteristic of *Trogloneta* (Fig. 63B, C, F). A CyC1 consisting of prolateral, retrolateral, and apical projections occurs

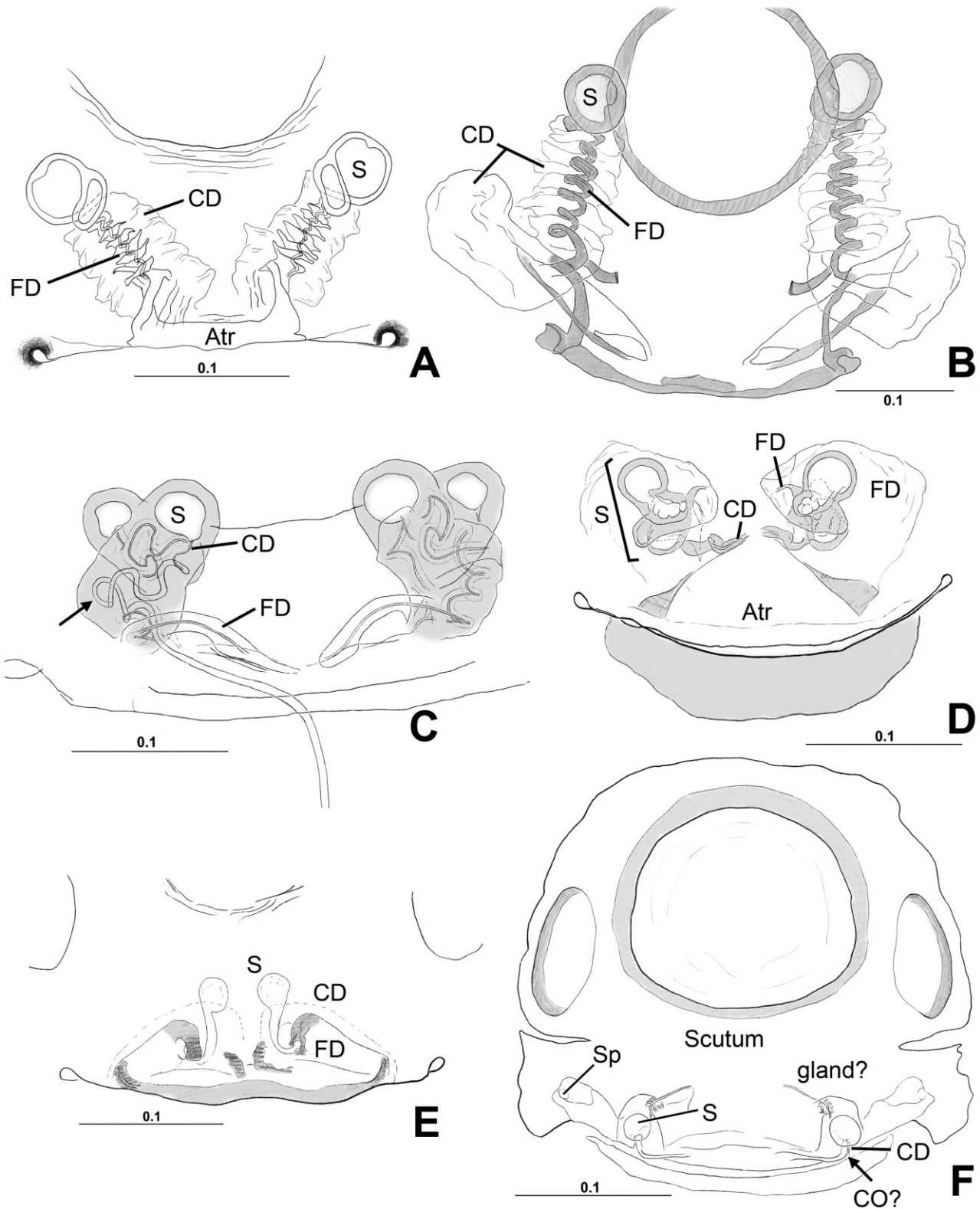


Figure 136. Anapidae female genitalia, cleared. A, *Acrobleps hygrophilus*, ventral view; B, *Anapisona kethleyi*, dorsal view; C, *Crassanapis chilensis*, dorsal view, arrow to broken inserted embolus; D, *Minanapis palena*, dorsal view; E, *Elanapis aisen*, dorsal view; F, *Tasmanapis strahan*, dorsal view. See Appendix 3 for the list of abbreviations.

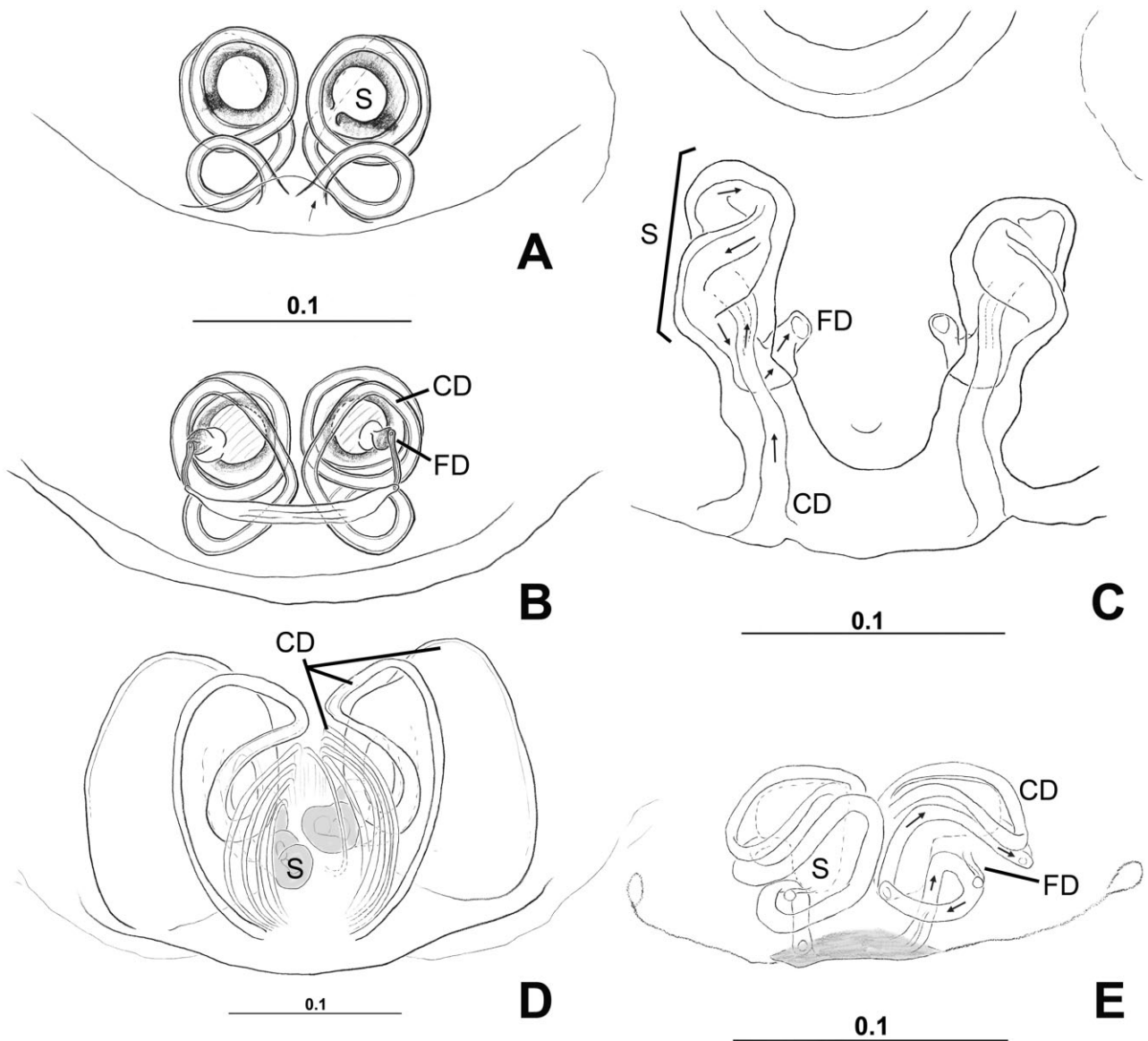


Figure 137. Female genitalia, cleared: A, *Cepheia longiseta* (Synaphridae) paralectotype, ventral view; B, same, dorsal view, same scale as in panel A; C, *Taphiassa punctata* (Anapidae), ventral view; D, *Coddingtonia euryopoides* (Theridiosomatidae), from Chiang Mai, Thailand, ventral view; E, SYMP-006-AUST (Symphytognathidae), from Queensland Australia, dorsal view. See Appendix 3 for the list of abbreviations.

in the clade comprising *Microdipoena* and *Mysmeniola*, independently occurring in *Mysmena* (= *Calomyspoena*) *santacruzii* (Fig. 27A). A spiral cymbial conductor occurs in *Microdipoena* s.s. (Fig. 22C). In *Maymena*, the characteristic CyC1 comprises a particular apical cymbium that is bent over the ventral side (Fig. 10D, G).

The 'secondary cymbial conductor' (CyC2) is external, located on the edge or dorsally on the cymbium (e.g. Figs 30F, 31C, 43C). This external conductor is plesiomorphically absent in *Trogloneta*, *Maymena mayana*, and in most *Mysmenopsis* species (Fig. 63C). Within Mysmenidae, the CyC2 has evolved convergently

in *Maymena* (excluding *M. mayana*), *Isela*, *Mysmenopsis penai*, and Mysmeninae (Figs 4G, 10G, 31C, 40A, 41D, 43C, 60D). The CyC2 has been secondarily lost in the clade comprising *Microdipoena* and MYSM-019-MAD (Fig. 22F).

Cymbial fold (CyF): The external cuticle of the cymbium is usually hirsute, the internal one is glabrous. Although the external cuticle can also cover the internal side of the cymbium, both cuticles are delimited by a well-defined border (e.g. Figs 86G, 102D). In some mysmenids the delimitation or border between

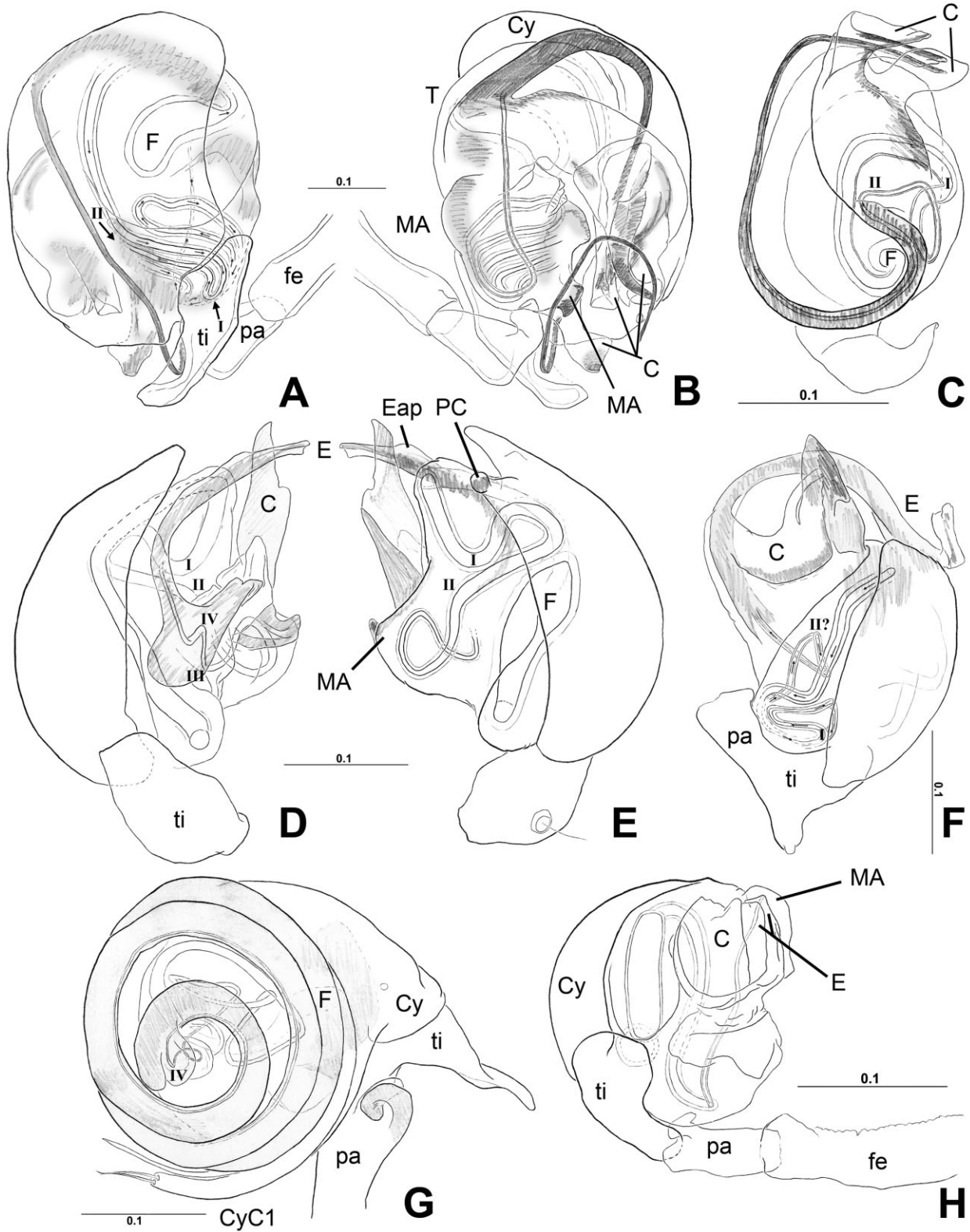


Figure 138. Anapidae male left palp, cleared. A, *Crassanapis chilensis*, dorsal view; B, same, ventral view, same scale as in panel A; C, *Elanapis aisen*, ventral view; D, *Comaroma simoni*, prolateral view; E, same, retrolateral view, same scale as in panel D; F, *Minanapis casablanca*, retrolateral view; G, *Anapisona kethleyi*, retrolateral view; H, *Tasmanapis strahan*, prolateral view. See Appendix 3 for the list of abbreviations.

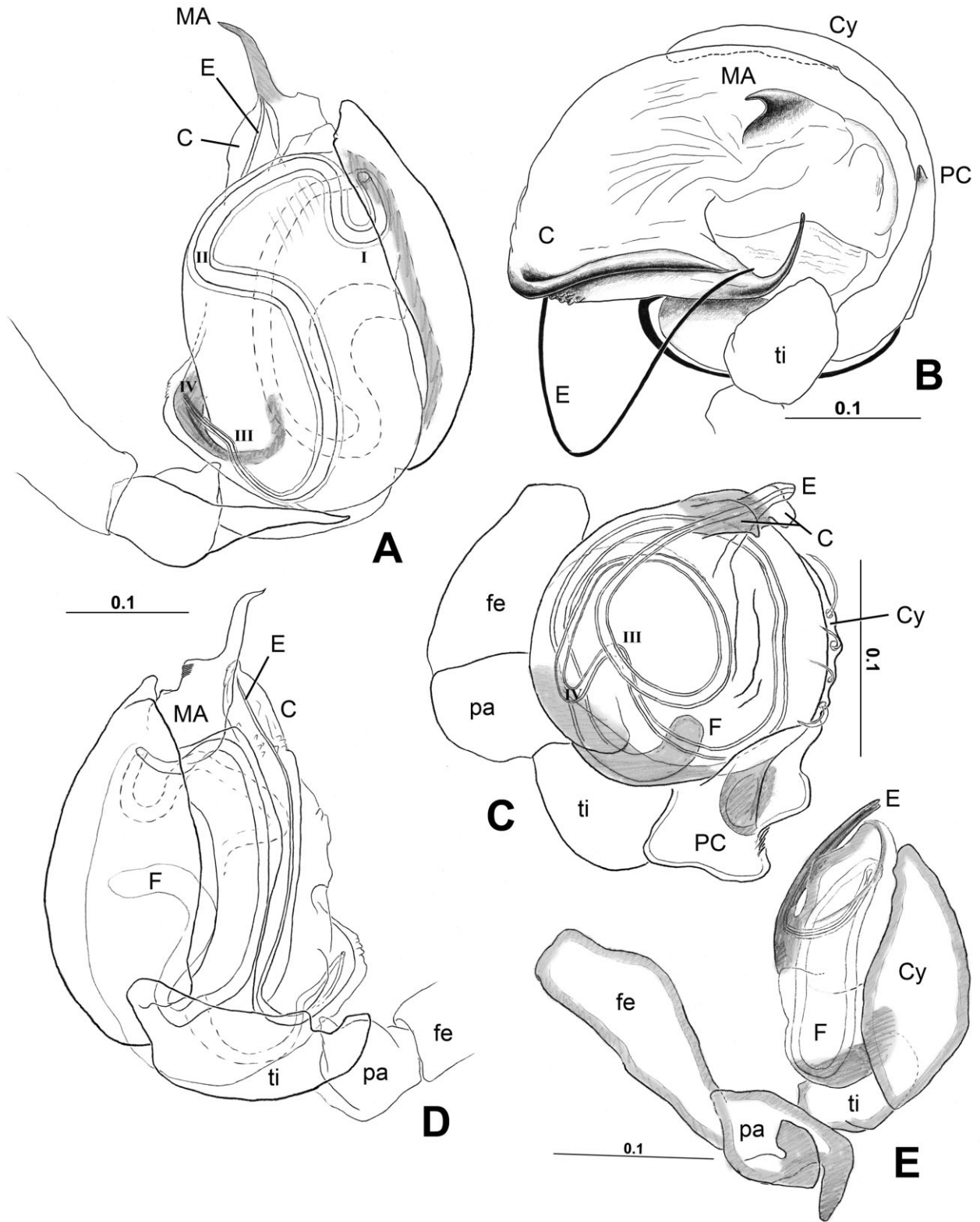


Figure 139. Male left palp, cleared. A, *Teutoniella cekalovici* (Anapidae), retrolateral view; B, *Cepheia longiseta* (Synaphridae), paralectotype, retrolateral view; C, *Symphytognatha picta* (Symphytognathidae), ventral view; D, *Teutoniella cekalovici* (Anapidae), prolateral view, same scale as A; E, *Taphiassa punctata* (Anapidae), retrolateral view. See Appendix 3 for the list of abbreviations.



Figure 140. Composite images of Mysmenidae species: Mysmenopsinae and *Maymena*. A–C, *Isela okuncana*; A, female, lateral view; B, female, ventral view; C, male, ventral view. D–F, *Kilifina*-MYSM-002-KENYA (*Isela* sp.), from Kwale, Kenya; D, female, lateral view; E, male, lateral view; F, male, ventral view. G, H, *Mysmenopsis dipluramigo*; G, female, lateral view; H, male, lateral view. I, *Mysmenopsis palpalis*, female, ventral view. J, K, *Mysmenopsis cidrelicola*, male paralectotype; J, lateral view; K, ventral view. L, *Mysmenopsis penai*, female, dorsal view. M–O, *Maymena ambita*; M, male, lateral view; N, female, lateral view; O, female, dorsal view. Scale bars: A–I, L–O, 0.5 mm; J, K, 1 mm.



Figure 141. Composite images of Mysmenidae species: *Maymena* and Mysmeninae. A, B, *Maymena rica*, female allotype; A, lateral view; B, dorsal view. C–F, *Maymena mayana*; C, female, frontal view; D, male, lateral view; E, male, dorsal view; F, male, ventral view. G–I, *Maymena* species, female, abdomen ventral; G, *Maymena ambita*; H, *Maymena mayana*; I, *Maymena rica*, female allotype. J–L, *Microdipoena* (= *Anjouanella*) *comorensis*; J, female paratype, lateral view; K, male holotype, lateral view; L, male holotype, ventral view. M, N, *Microdipoena elsae*; M, male holotype, lateral view; N, female allotype, lateral view. O, *Microdipoena* (= *Mysmenella*) *illectrix*, male, ventral view. Scale bars: A, B, G, I–O, 0.5 mm; C–F, H, 1 mm.

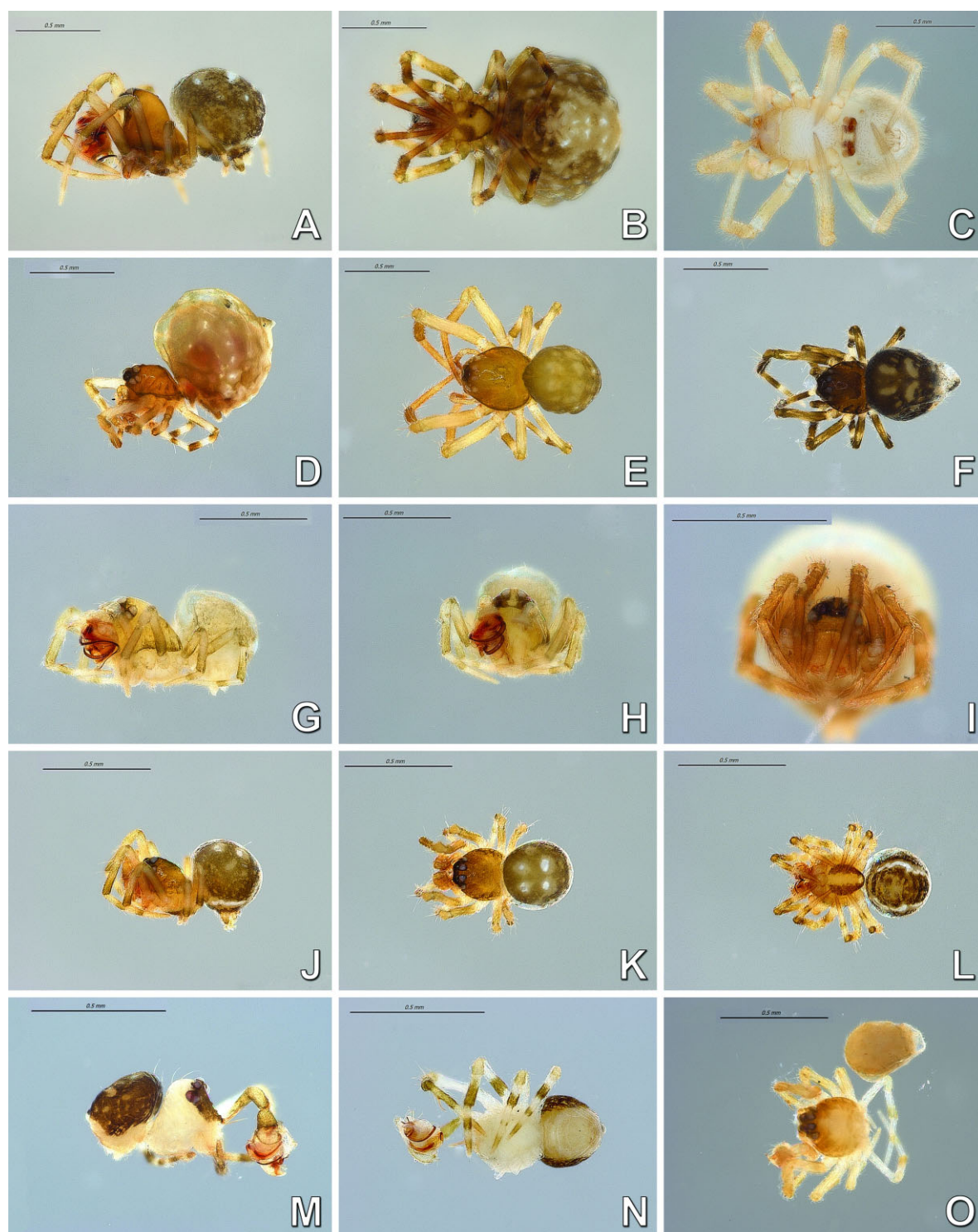


Figure 142. Composite images of Mysmenidae species: Mysmeninae and *Trogloneta*. A, B, *Microdipoena nyungwe*; A, male, lateral view; B, female, ventral view. C, *Trogloneta granulum*, female, ventral view. D, *Mysmena* (= *Calodipoena*) *incredula*, female, lateral view, inverted. E, *Mysmena* (= *Calodipoena*) *mootae*, female holotype, dorsal view. F, *Mysmena* (= *Calomyspoena*) *santacruzii*, female paratype, dorsal view. G–I, *Mysmena* (= *Itapua*) *tembei*; G, male holotype, lateral view, inverted; H, male holotype, frontal view; I, female paratype, frontal view. J–L, *Mysmena* (= *Kekenboschiella*) *awari*, male paratype; J, lateral view; K, dorsal view; L, ventral view. M, N, *Mysmeniola spinifera*, male holotype; M, lateral view; N, ventral view. O, *Brasilionata arborensis*, male holotype, dorsal view, abdomen detached. Scale bars: 0.5 mm.



Figure 143. Composite images of Mysmeninae species. A–C, *Mysmena tasmaniae*; A, female, lateral view; B, female, ventral view; C, male, ventral view. D–F, MYSM-019-MAD (Mysmeninae); D, female, lateral view; E, female, ventral view; F, male, lateral view. G–I, MYSM-005-ARG (*Mysmena*), female; G, lateral view; H, dorsal view; I, ventral view. J–L, MYSM-007-MEX (*Mysmena*); J, female, lateral view; K, female, dorsal view; L, male, ventral view. M, *Mysmena*-MYSM-015-MAD (*Mysmena*), female, lateral view. N, *Mysmena leichhardti*, female, lateral view. O, MYSM-028-MAD (*Mysmena*), female prosoma, ventral view. Scale bars: 0.5 mm.

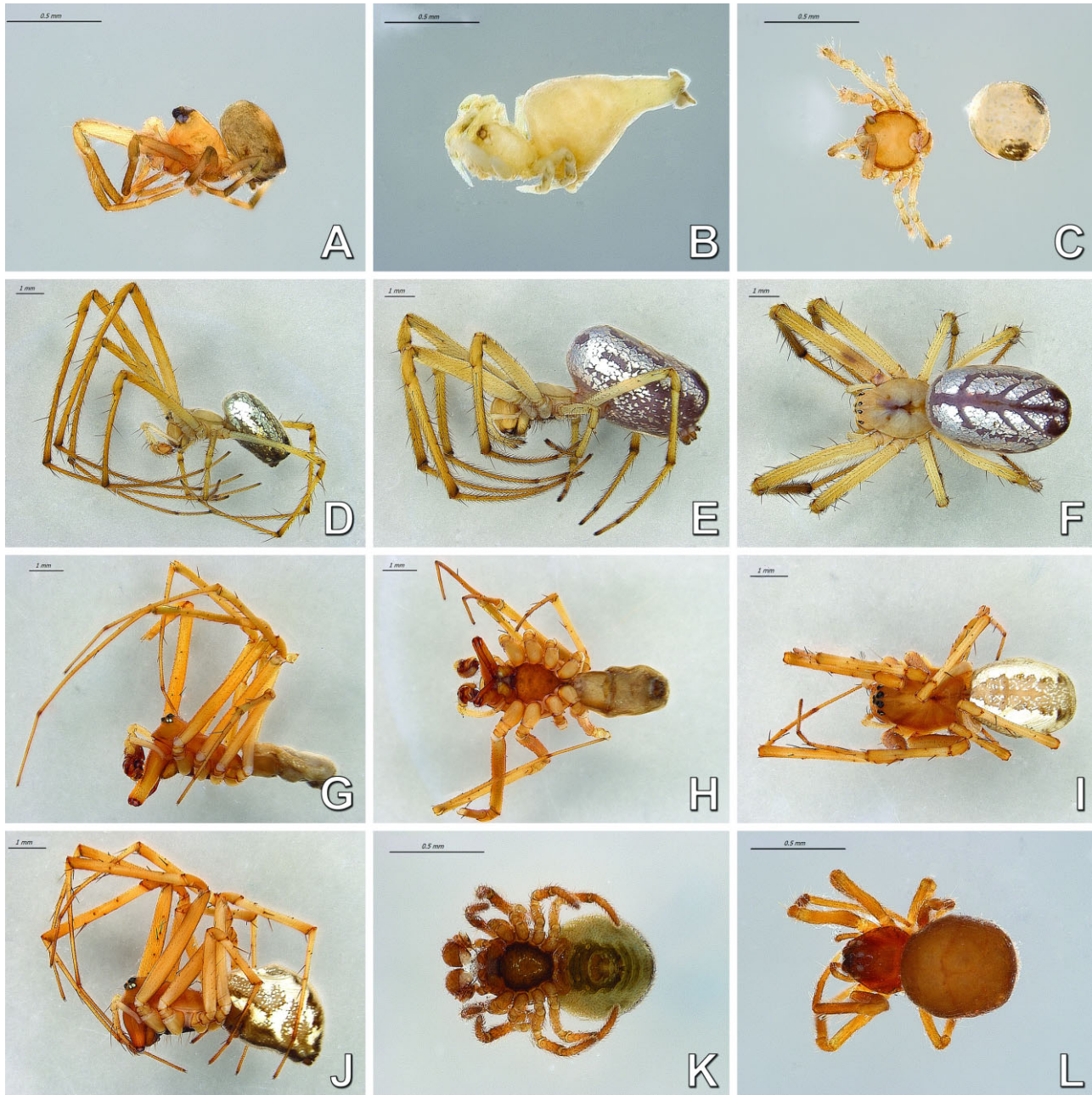


Figure 144. Composite images of Mysmenidae species and outgroups. A, MYSM-023-MAD (Mysmeninae, Mysmenidae), male, lateral view. B, *Phricotelus stelliger* (Araneoidea), female, type, lateral view. C, *Iardinis mussardi* (Symphytognathidae), male holotype, dorsal view. D–F, *Leucauge venusta* (Tetragnathidae); D, male, lateral view; E, female, lateral view; F, female, dorsal view. G–J, *Linyphia triangularis* (Linyphiidae); G, male, lateral view; H, male, ventral view; I, female, dorsal view; J, female, lateral view. K, *Elanapis aisen* (Anapidae), male, ventral view; L, *Mysmena* (= *Tamasesia*) *rotunda*, female, dorsal view. Scale bars: A–C, K, 0.5 mm; D–J, 1 mm.

external and internal cuticles (or cymbial areas) is rather clear, often corresponding to the outline of the cymbium; however, the internal cuticle on the tip of the cymbium bears setae (and can also bear the tarsal organ), and it frequently appears flattened against the outer cuticle.

The internal cuticle can also be modified into a primary cymbial conductor. This suggests that the inner cymbium, at least apically, might be composed of part of the external cuticle. This condition is here referred to as a ‘fold’, and it is different from a twisted



Figure 145. Composite images of Anapidae species. A–D, *Anapisona kethleyi*; A, female, lateral view; B, female, ventral view; C, male prosoma, frontal–lateral view; D, male prosoma, lateral view. E, F, *Tasmanapis strahan*; E, female, lateral view; F, male, lateral view. G–I, *Comaroma simoni*, female; G, lateral view; H, dorsal view; I, ventral view. J–L, *Crassanapis chilensis*; J, female, lateral view; K, male, lateral view; L, male, ventral view. M–O, *Minanapis palena*; M, female, lateral view; N, female, dorsal view; O, male, ventral view. Scale bars: 0.5 mm.



Figure 146. Composite images of other symphytognathoid species. A, B, *Taphiassa punctata* (Anapidae); A, female, lateral view; B, male, lateral view. C, *Teutoniella cekalovici* (Anapidae), male, dorsal view. D, E, *Cepheia longiseta* (Synaphridae), female paralectotype; D, lateral view; E, dorsal view. F, *Synaphris saphrynis* (Synaphridae), male holotype, lateral view. G, *Patu-SYP-001-DR* (Symphytognathidae), female, lateral view. H, I, *Symphytognatha picta* (Symphytognathidae), male prosoma; H, frontal view; I, ventral view. J, SYMP-006-AUST (Symphytognathidae), female, lateral view. K, L, SYMP-007-AUST (Symphytognathidae), female; K, lateral view; L, dorsal view. Scale bars: 0.5 mm.

tip of the cymbium, where the same external cuticle is bent inwards, i.e. ventrally (compare with Figs 10G, 14B). The ‘cymbial fold’ is a synapomorphy of Mysmenidae (Figs 4G, 18E), secondarily and independently lost in *Maymena mayana*, *Mysmenopsis*, and *Microdipoena* (= *Mysmenella*) *illectrix* (Fig. 60D).

On the cymbial fold cuticle, a distinct row of setae can be present, usually associated with the primary cymbial conductor (CyFs). Fold setae arise independently in *Isela*, the clade comprising *Brasilionata* and *Microdipoena*, and in a large clade within *Mysmena* (Figs 4G, 43E). The row setae can be similar to the

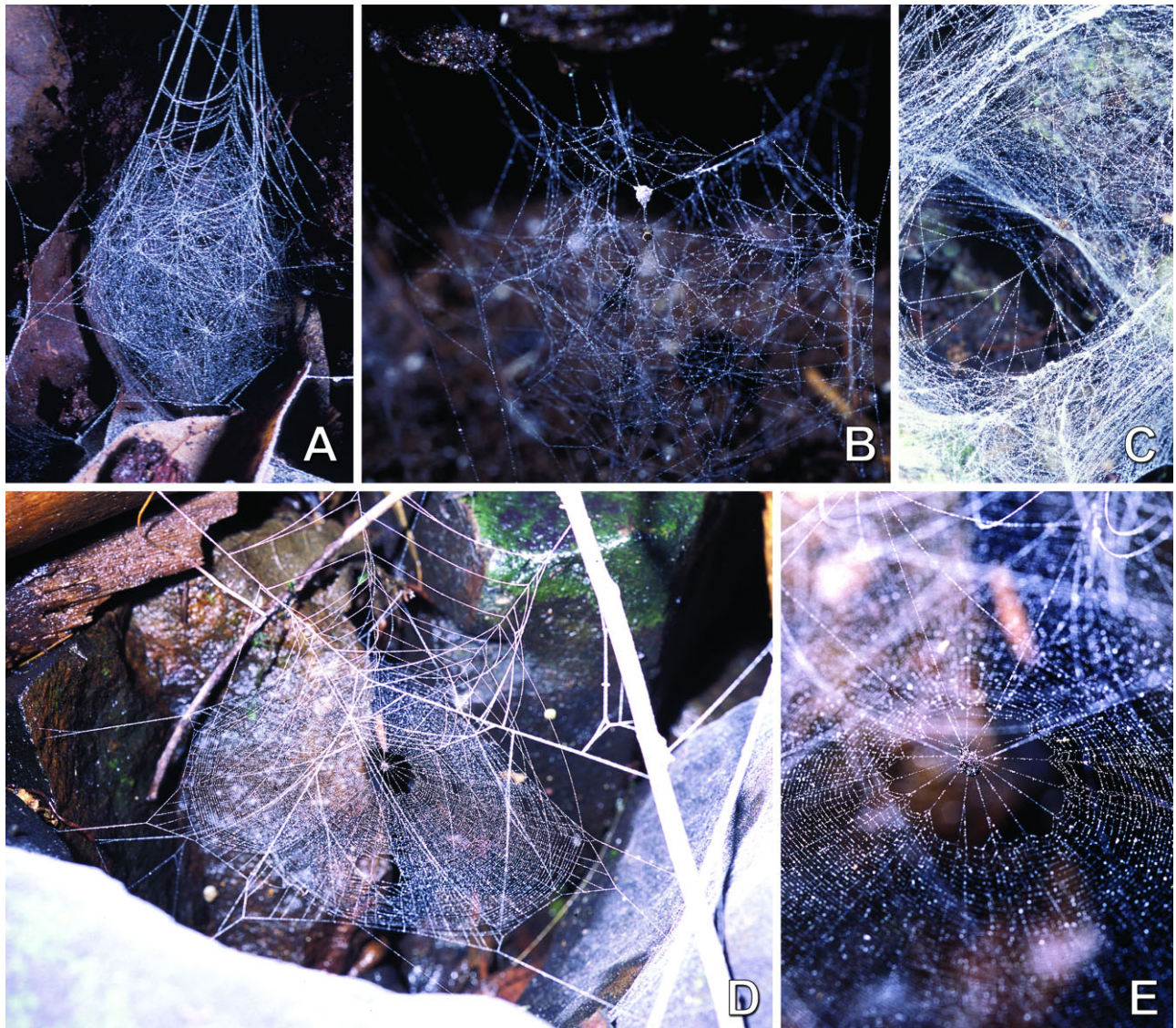


Figure 147. Webs of Mysmenidae: A, *Mysmena tasmaniae*, B, MYSM-005-ARG (*Mysmena*), from Misiones, Argentina, female with egg sac; C, Mysmenidae from Chiapas, Mexico, detail of centre of web, external threads removed to expose the hub; D, *Maymena* sp. from Misiones, Argentina; E, same, detail of centre of web.

surrounding setae at the tip of the cymbium (Figs 40D, 43E), or can be distinctly minute (Figs 4G, 17A, 18E, 22C, 132A, D, 134A).

Cymbial tarsal organ (to): In most spiders, and basally in Mysmenidae, the tarsal organ is located externally on the cymbium (e.g. Figs 10I, J, 44D, 58C). An internal tarsal organ, located within the cymbial fold, optimizes as independently synapomorphic in *Trogloneta*, *Isela*, *Mysmena*-MYSM-015-MAD (*Mysmena*), and the mysmenine MYSM-020-MAD (Figs 4I, 40B, C, 63B, F).

Cymbial groove (CyG): A diagonal groove of varying depth can occur dorsally on the cymbium of some mysmenids (Fig. 126). The cymbial groove can be either a shallow and wide irregular depression (Figs 36E, 51A, B) or a narrow and deep furrow (Figs 18E, 22F, 28B, 30B, C, 45A, 134D). Besides the depth and width of this groove, its position and length appear to be correlated: apical grooves are always shorter than medial or basal grooves (Figs 36E, 45A). The latter are longer, extending sometimes into the prolatateral basal expansion of the cymbium (Figs 18E, 22F, 28B, 30A, C; see below).

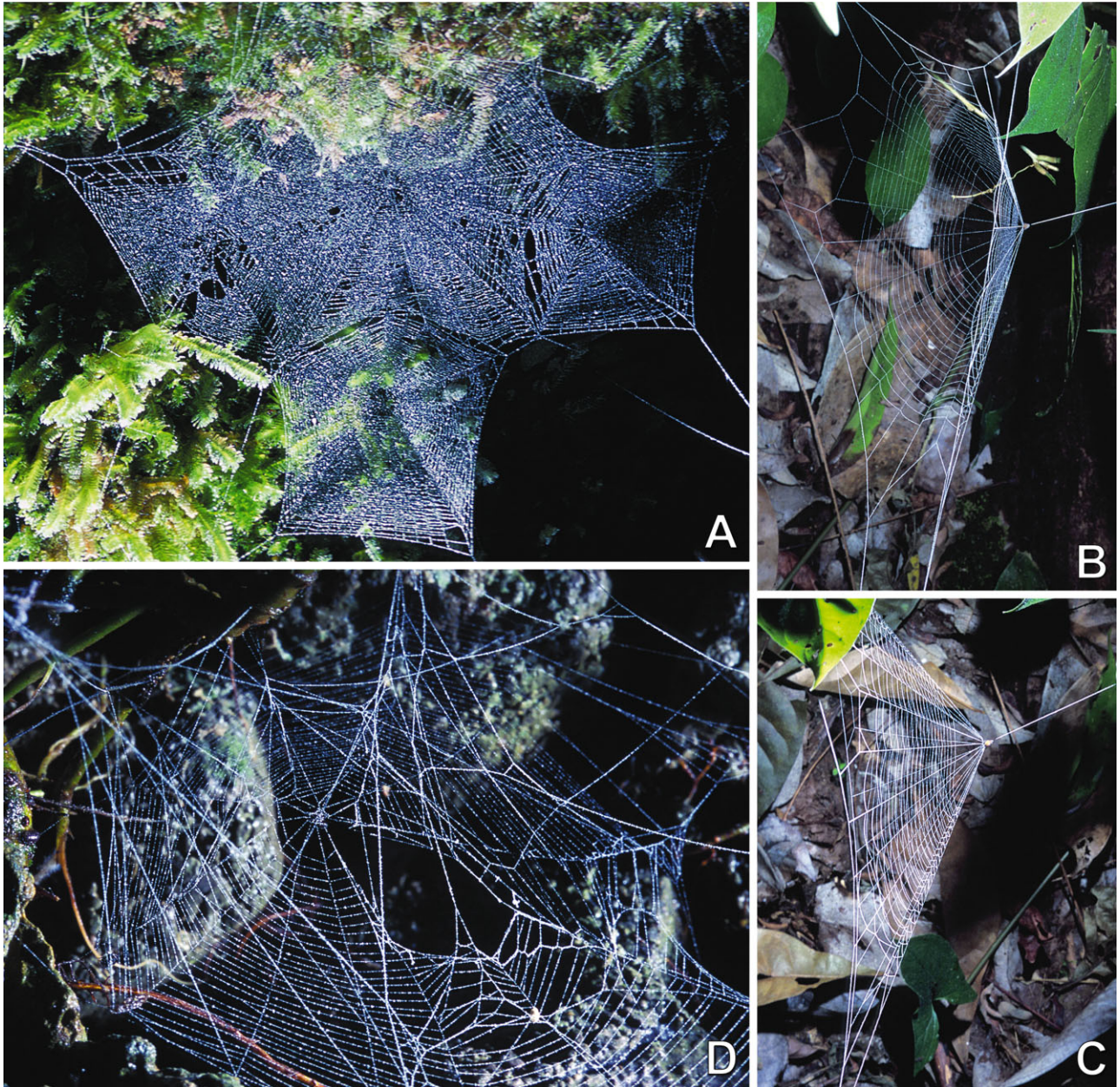


Figure 148. Symphytognathoids webs. A, *Tasmanapis strahan* (Anapidae), spider not collected; B, C, Theridiosomatidae from Mexico; D, *Anapisona kethleyi* (Anapidae), male; E, potential web and egg sac of a *Symphytognatha* species (Symphytognathidae), from Tasmania, Australia, spider not collected.

Cymbial process (CyP) (Kraus, 1967: 'Kegeldorn des paracymbium'; Baert & Maelfait, 1983: 'cymbial thorn'): In most mysmenids there is a process, often pointed, on the dorsal surface of the cymbium. The process is located often apically, retrolateral to the cymbial tip (Figs 1A, E, 4C, 40F, 51A, 63C, 133G, 134G, H), or basally and prolaterally, at the end of the cymbial groove (Figs 45A, 132D, E), or it can be located apically, but prolateral to the cymbial tip (Fig. 43C, D).

Paracymbium (PC): As in most araneoids (except Theridiidae), a retrolateral paracymbium is present in all symphytognathoid families, except for Anapidae (Figs 71F, 92A). Although the loss of the paracymbium is synapomorphic for Anapidae, it has secondarily evolved in *Comaroma* (Fig. 81B). Almost all mysmenids have a paracymbium; within this data set, it is secondarily absent in *Maymena rica* and *Isela* (Fig. 4D, E). Although in recent studies the paracymbium was



Figure 149. Webs of Symphytognathidae from Tasmania, Australia: A, SYMP-006-AUST, female with egg sacs; B, same, detail of edge of web where egg sacs are attached, note female spider close to one of the egg sacs; C, SYMP-007-AUST, female?; D, same, detail of hub.

considered to be absent in mysmenids (Coddington, 1990; Griswold *et al.*, 1998; Miller *et al.*, 2009), it had been previously reported as present by some authors (e.g. Kraus, 1967).

Our phylogenetic hypothesis suggests that the mysmenid paracymbium evolved from a basal hook-shaped paracymbium into a characteristic shape and position (e.g. as in *Mysmena tasmaniae*, Fig. 51B). In mysmenids the paracymbium is flat and rounded, with a uniform transition to the cymbium, and it is located medially, not basally (i.e. as a medial flat extension of cymbial edge; Figs 18B, 22G, 27B, 30E, 32A, 36A, 45B, 63A). A flat, rounded paracymbium evolved independently as synapomorphic for Mysmenidae, but also in *Iardinis mussardi* and in *Synaphris*. The paracymbium becomes secondarily basal in *Trogloneta* (Fig. 63A), and secondarily hook-shaped in *Mysmenopsis*, where it is a thick (i.e. not flat), short distinct process, usually as long as wide (Figs 53D, 60D). Furthermore, in *Mysmenopsis*, the paracymbium is bent inwards

and is seemingly interacting with a tegular groove located dorsally on the bulb (Figs 53F, 55F, 58D, 60D). The interaction is here considered tentative. The dorsal tegular groove does not appear to have a 'conductor' function related to the embolus, and the paracymbium–bulb interaction as a locking mechanism is not evident, as in the case of theridiids (Levi, 1961; Saaristo, 1978; Agnarsson, 2004; and references therein).

Prolateral basal expansion: This prolonged cuticle on the prolateral basal edge of the cymbium was originally observed in Theridiosomatidae, and has been termed the 'prolateral basal paracymbium' by Schütt (2003). The term 'paracymbium', however, has been proposed and long used for the classical araneoid retrolateral process on the cymbium (e.g. Comstock, 1910; Coddington, 1986b, 1990; Griswold *et al.*, 1998; and references therein). Here, this prolateral structure is simply referred to as 'prolateral basal expansion'. Furthermore, both the paracymbium and the

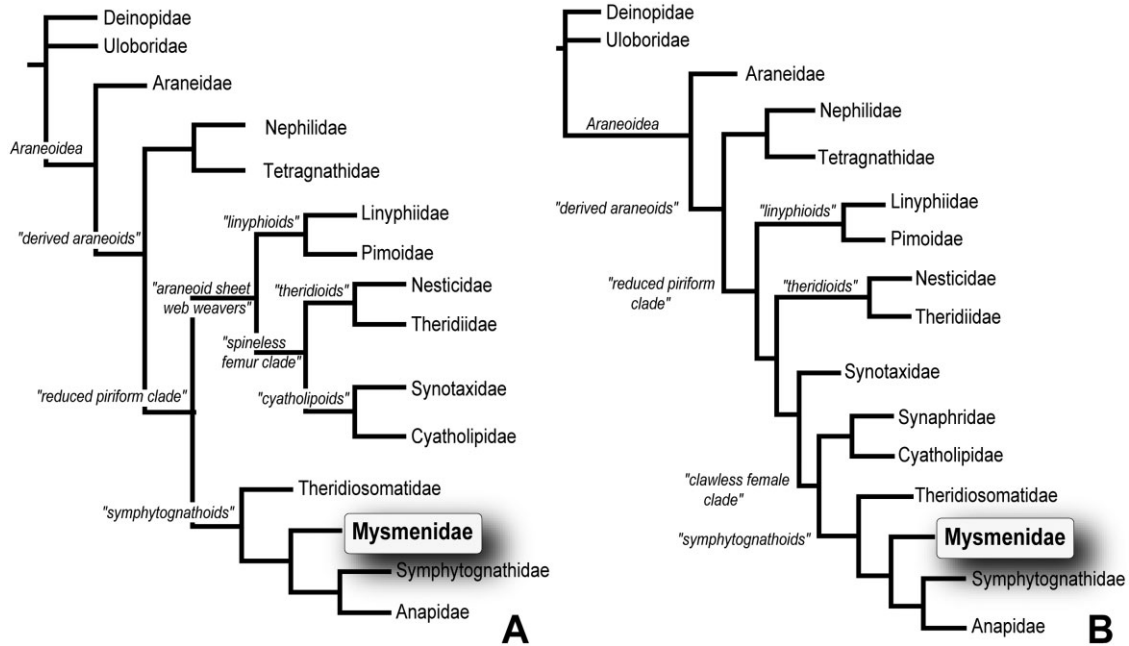


Figure 150. A, summary of the original phylogenetic hypothesis for Orbiculariae, showing the position of Araneoidae, ‘symphytognathoids’, and Mysmenidae (from Griswold *et al.* 1998). Only family names are shown, not actual representatives. B, summary of the current phylogenetic hypothesis for Orbiculariae, showing the position of Araneoidae, ‘symphytognathoids’, Synaphridae, and Mysmenidae (from Lopardo & Hormiga 2008; as modified from Griswold *et al.* 1998). Only family names are shown, not actual representatives.

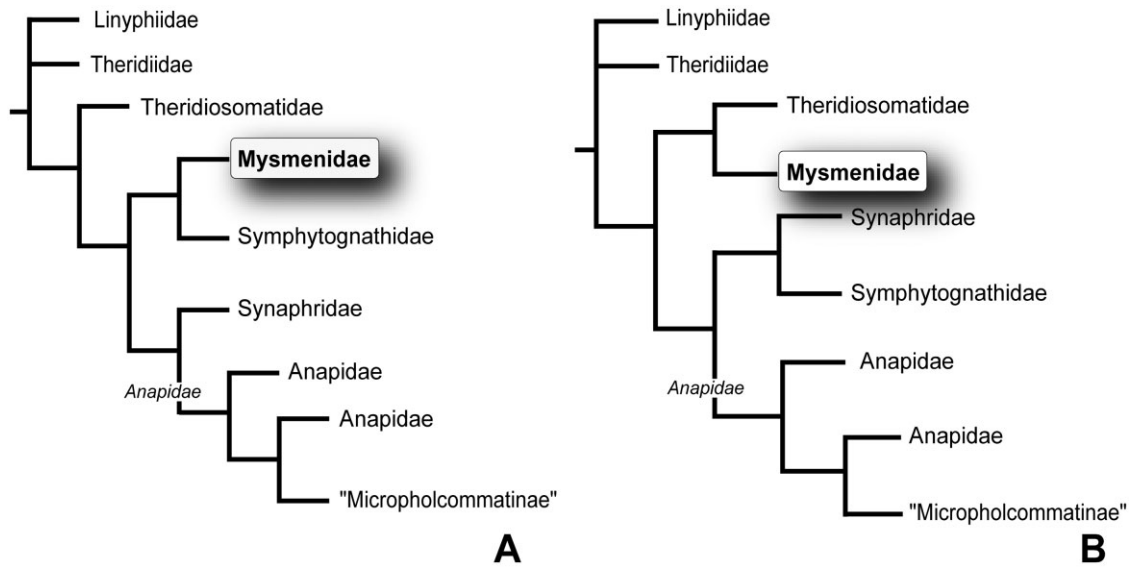


Figure 151. A, summary of the original phylogenetic hypothesis for ‘symphytognathoids’, showing the position of Mysmenidae (from Schütt 2003). Only family names are shown, not actual representatives. B, summary of the current phylogenetic hypothesis for ‘symphytognathoids’, showing the position of Mysmenidae (from Lopardo & Hormiga 2008; as modified from Schütt 2003). Only family names are shown, not actual representatives.

prolateral basal expansion can co-occur in the palp of some species. Such conjunction refutes the homology statement among the two structures. The prolonged cuticle of the basal expansion surrounds the bulb

ventrally in varying degrees and occurs in theridiosomatids and most mysmenids (Figs 4B, 27A, 30B, C, 36C, 47B, 66D), but is absent in *Maymena* and most mysmenopsines (Figs 10B, C, 55A).

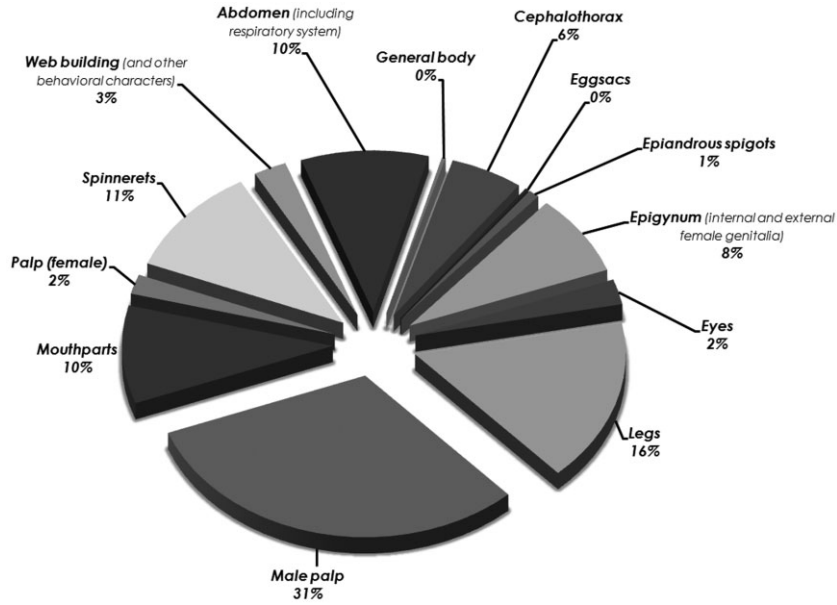


Figure 152. Chart representing the proportion of each of the thirteen characters sets (see Table 4).

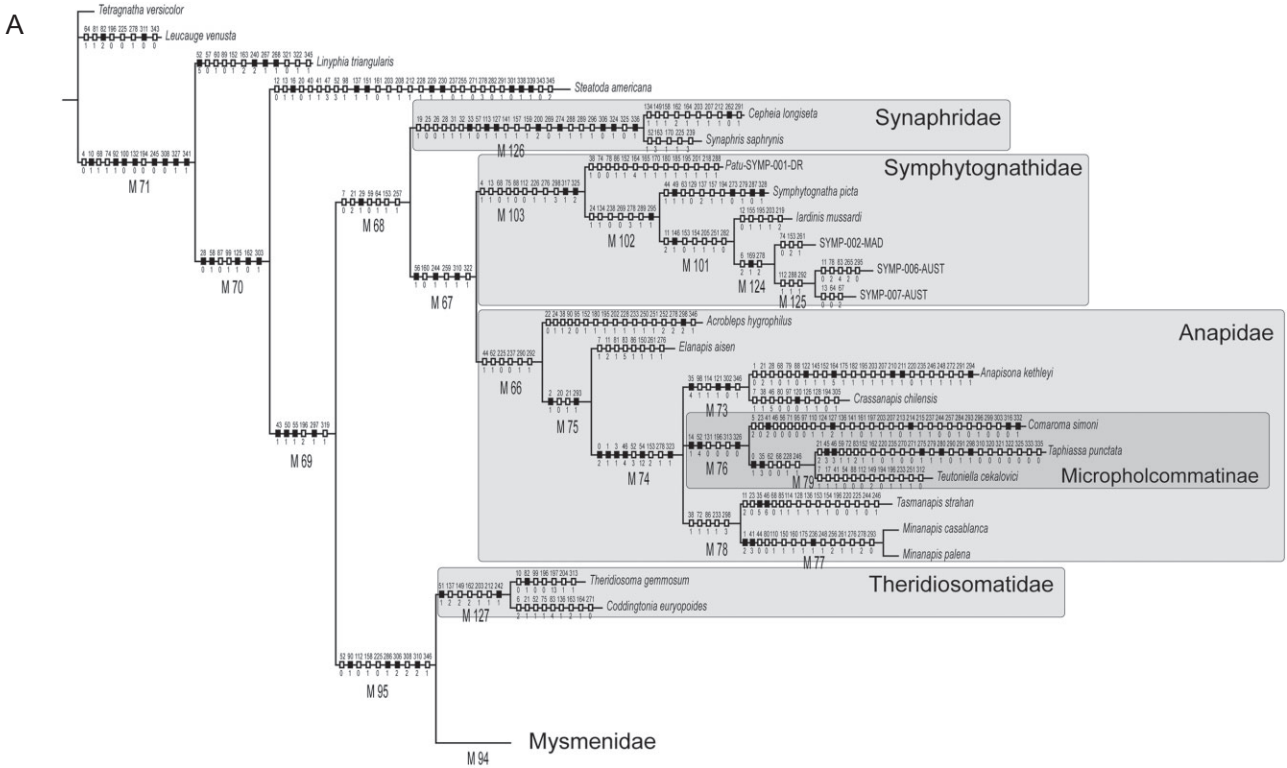


Figure 153. Strict consensus of the three most-parsimonious trees (MPTs) that resulted from the analysis of the morphological data set. See tree statistics in Table 6. Unambiguous character optimizations are shown for every branch in the tree. Numbers below each node indicate node numbers. Empty and filled boxes represent homoplasious and non-homoplasious transformations, respectively. Family codes used for unidentified species are as follows: MYSM, Mysmenidae; SYMP, Symphytognathidae; TSMD, Theridiosomatidae.

Downloaded from https://academic.oup.com/zoolinnean/article/173/3/527/2449763 by guest on 19 April 2024



Figure 153. Continued.

Mysmenid bulb: general morphology

The median apophysis is absent in all mysmenids. In *Trogloneta* and independently in the clade comprising *Brasilionata*, *Mysmeniola*, and *Microdipoena*, a tegular groove housing the embolus can occur (Figs 27A, 63E, 66C; see below).

Embolus: The general shape of the embolus varies greatly within Mysmenidae, and no general pattern can be proposed. The embolus of mysmenids can be thin (or filiform) and coiled (Figs 47B, 134G), or thick (and flattened) and either coiled (Figs 4H, 27A, 36B, 131H, 132B, D, E), or straight (Figs 10E, 28D, 60F,

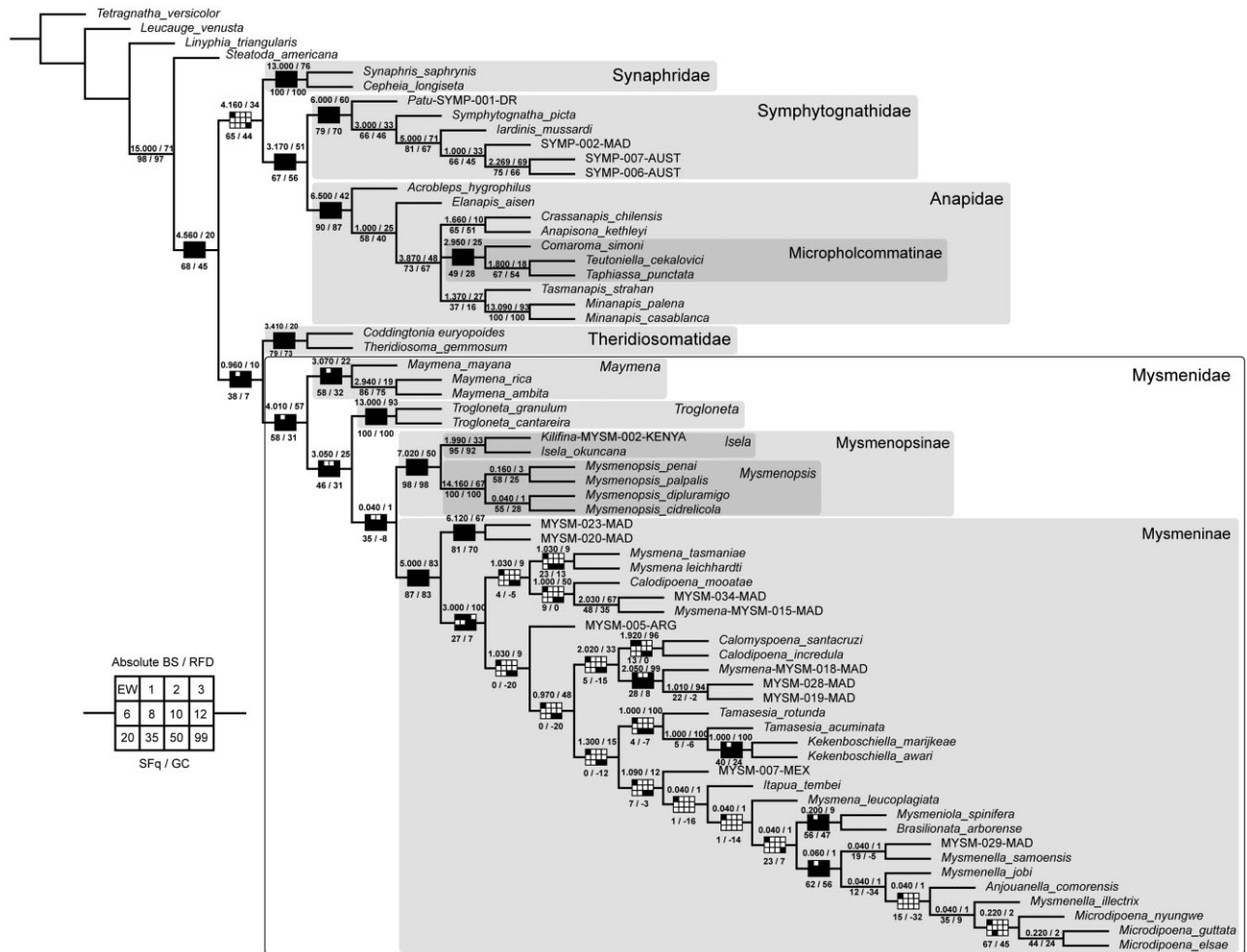


Figure 154. Strict consensus of the three most-parsimonious trees (MPTs) that resulted from the analysis of the morphological data set. See tree statistics in Table 6. Numbers before and after the slash above each node indicate absolute Bremer support (BS) and relative BS (RFD) values, respectively. Numbers before and after the slash below each node indicate absolute symmetric frequencies (SFq) and frequency differences (GC), respectively. Filled spaces on Navajo rugs indicate groups recovered by the sensitivity scheme performed under different implied weighting concavities (see reference rug beside tree, and also see text for an explanation). Family codes used for unidentified species are as follows: MYSM, Mysmenidae; SYMP, Symphytognathidae; TSMD, Theridiosomatidae.

63B, E, 131A). Thick and straight emboli occur in *Trogloneta*, *Maymena*, and *Mysmenopsis*, whereas thick and coiled emboli occur in *Microdipoena*, *Isela*, and some *Mysmena* species. An apical switch in the coiling direction of the embolus is characteristic of the clade comprising *Brasilionata* and *Microdipoena* [secondarily absent in *Microdipoena* (= *Anjouanella*) *comorensis*] (Figs 18C, F, 27C, 132A–F). In addition, the embolus surface can be smooth (Figs 10H, 18F, 27C, 60F) or ridged (Figs 28C, 32G).

As in most symphytognathoids, the embolus of mysmenids is often long (i.e. much longer than the bulb, Figs 4A, 10E, 27A, 63E, 132E), usually tapering apically without further modifications (Figs 1D, 36B, 60F, 63B). Short emboli occur in *Mysmenopsis* (Figs 60F,

131A–C) and in *Trogloneta granulum*. In some *Maymena*, *Trogloneta*, and a few other mysmenids, distal modifications of the embolus can occur, such as a distal apophysis (Figs 10H, 18F) or a distal irregular membrane (Fig. 27A, C).

The embolic base can be simple, or it can be lobed and bearing an apophysis, as in *Mysmenopsis* and *Trogloneta* (Figs 55G, 60F, 63E, 66E, 131A). In Mysmeninae, the basal or medial embolic trajectory has a pars pendula (Comstock, 1910), a membrane that houses the spermatid duct before entering to the embolus (Figs 32H, 36B, 132C, E, F, 133C). Therefore, the spermatid duct enters the embolus not at its origin but further distally, meaning also that the embolus is actually longer than the embolic portion of the

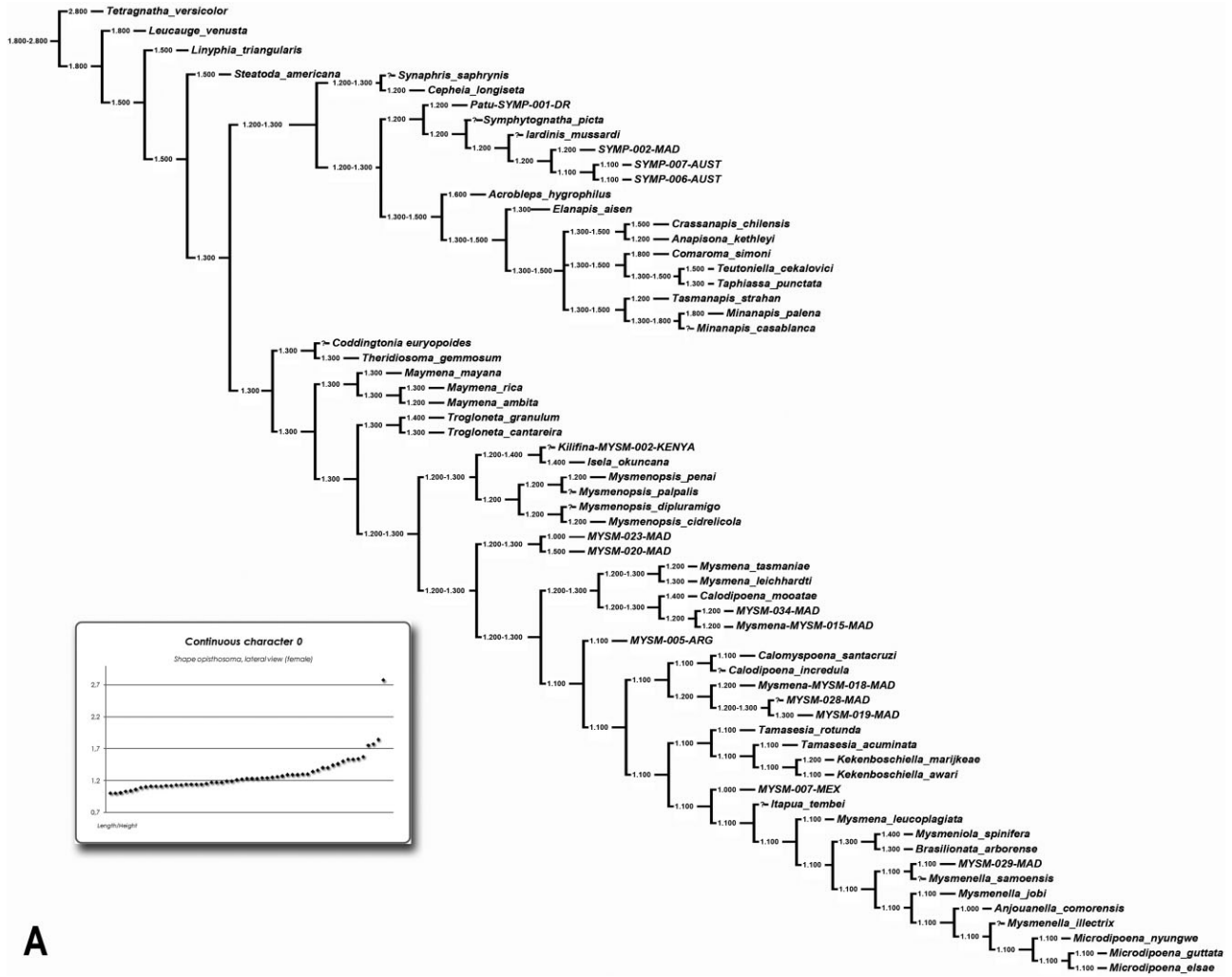


Figure 155. A, strict consensus of the three most-parsimonious trees (MPTs) that resulted from the analysis of the morphological data set. Continuous character optimization. Character 0: shape opisthosoma, lateral view. Family codes used for unidentified species are as follows: MYSM, Mysmenidae; SYMP, Symphytognathidae; TSMD, Theridiosomatidae.

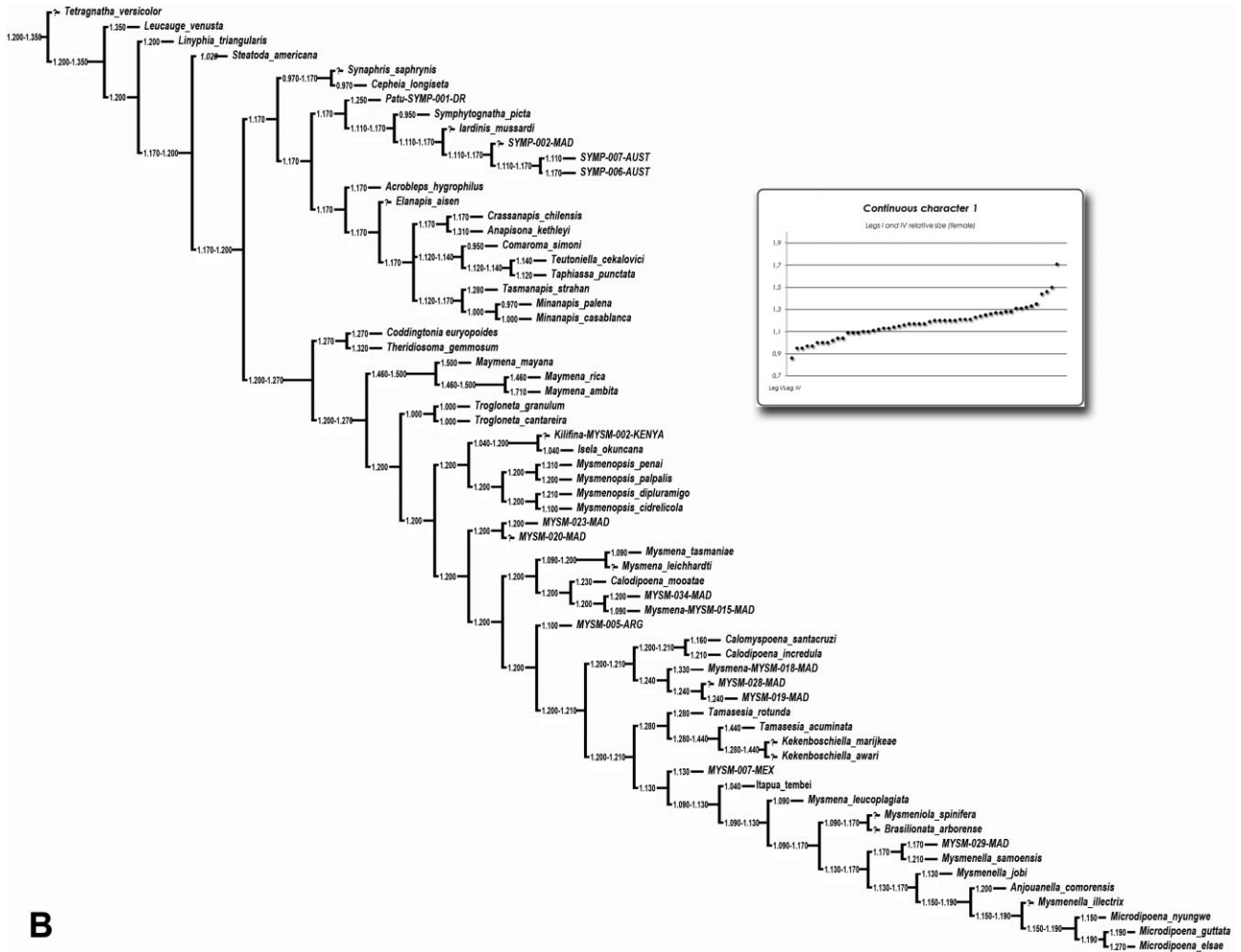


Figure 155. B, strict consensus of the three MPTs that resulted from the analysis of the morphological data set. Continuous character optimization. Character 1: legs I and IV relative size. Family codes used for unidentified species are as follows: MYSM, Mysmenidae; SYMP, Symphytognathidae; TSMD, Theridiosomatidae.

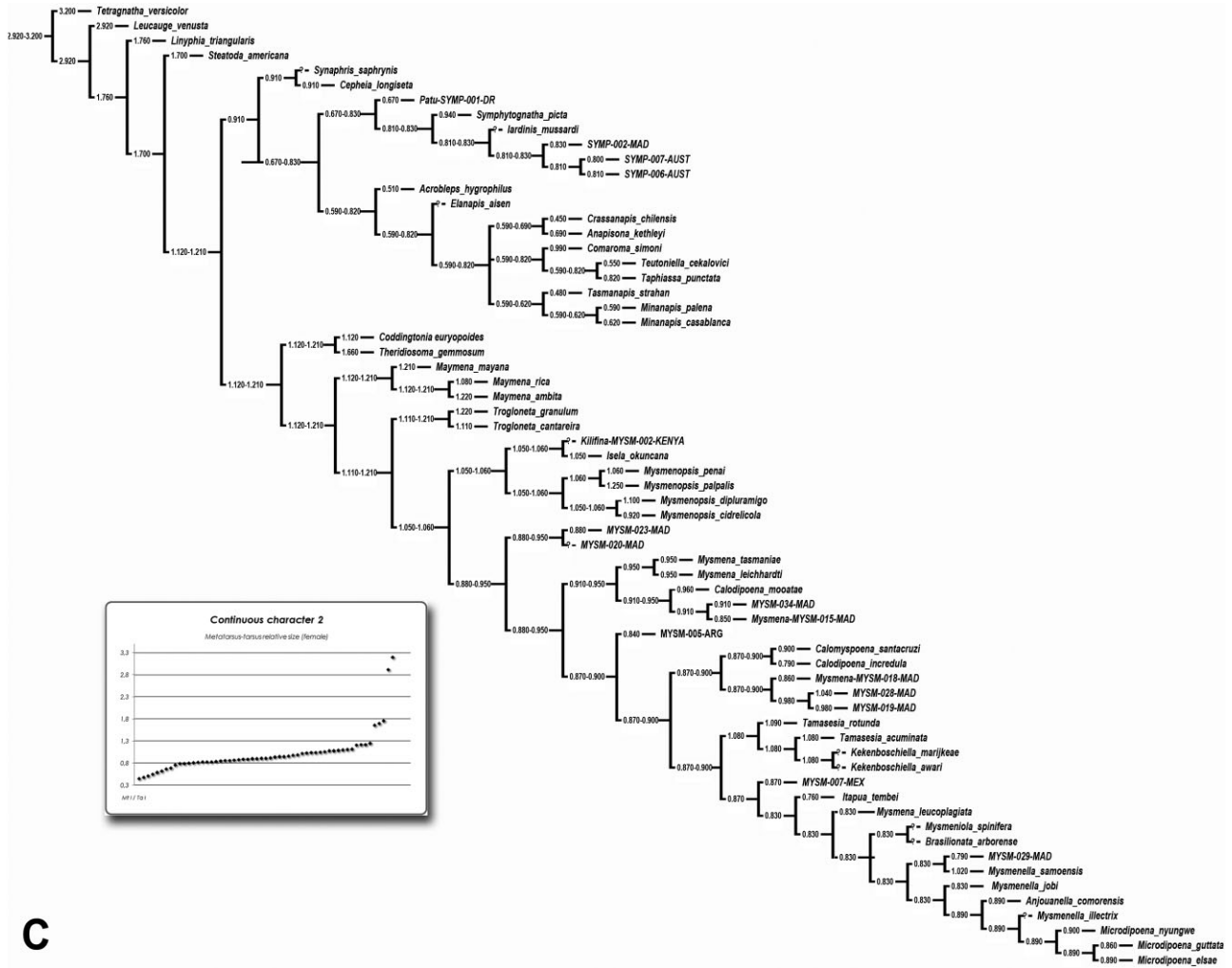


Figure 155. C, strict consensus of the three MPTs that resulted from the analysis of the morphological data set. Continuous character optimization. Character 2: metatarsus–tarsus relative size. Family codes used for unidentified species are as follows: MYSM, Mysmenidae; SYMP, Symphytognathidae; TSMD, Theridiosomatidae.

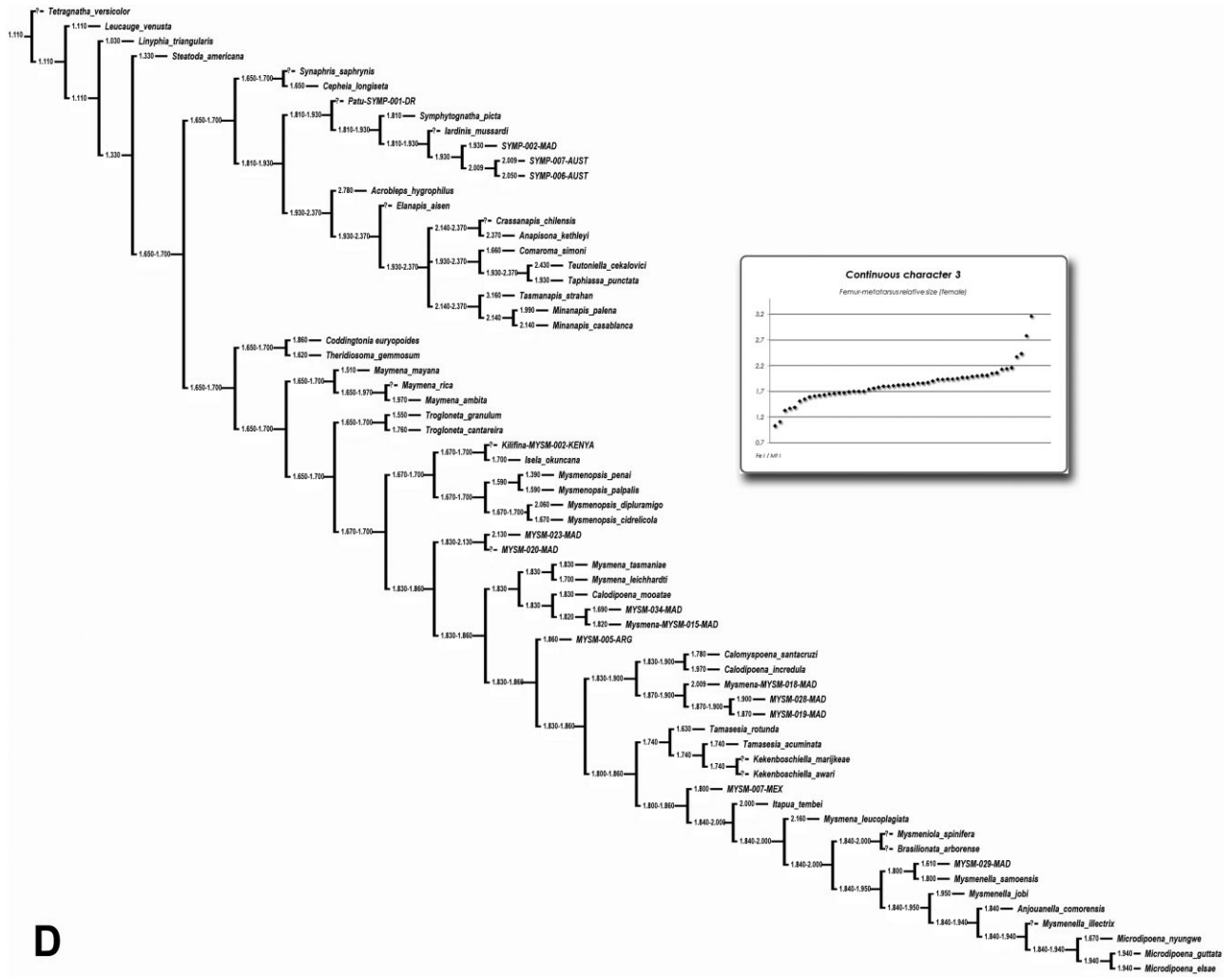


Figure 155. D, strict consensus of the three MPTs that resulted from the analysis of the morphological data set. Continuous character optimization. Character 3: femur–metatarsus relative size. Family codes used for unidentified species are as follows: MYSM, Mysmenidae; SYMP, Symphytognathidae; TSMD, Theridiosomatidae.

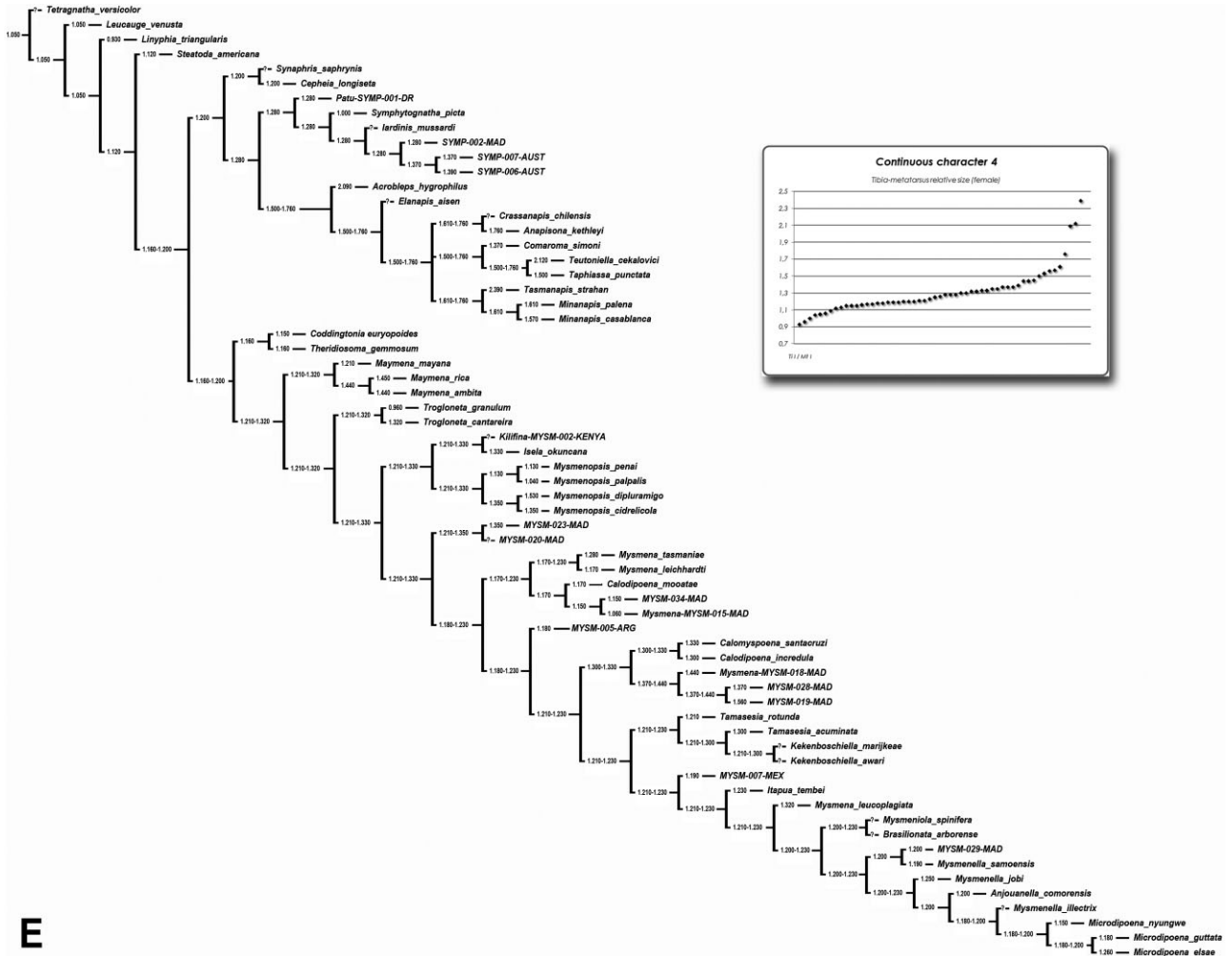


Figure 155. E, strict consensus of the three MPTs that resulted from the analysis of the morphological data set. Continuous character optimization. Character 4: tibia–metatarsus relative size. Family codes used for unidentified species are as follows: MYSM, Mysmenidae; SYMP, Symphytognathidae; TSMD, Theridiosomatidae.

Downloaded from https://academic.oup.com/zoolinnean/article/173/3/527/2449763 by guest on 19 April 2024

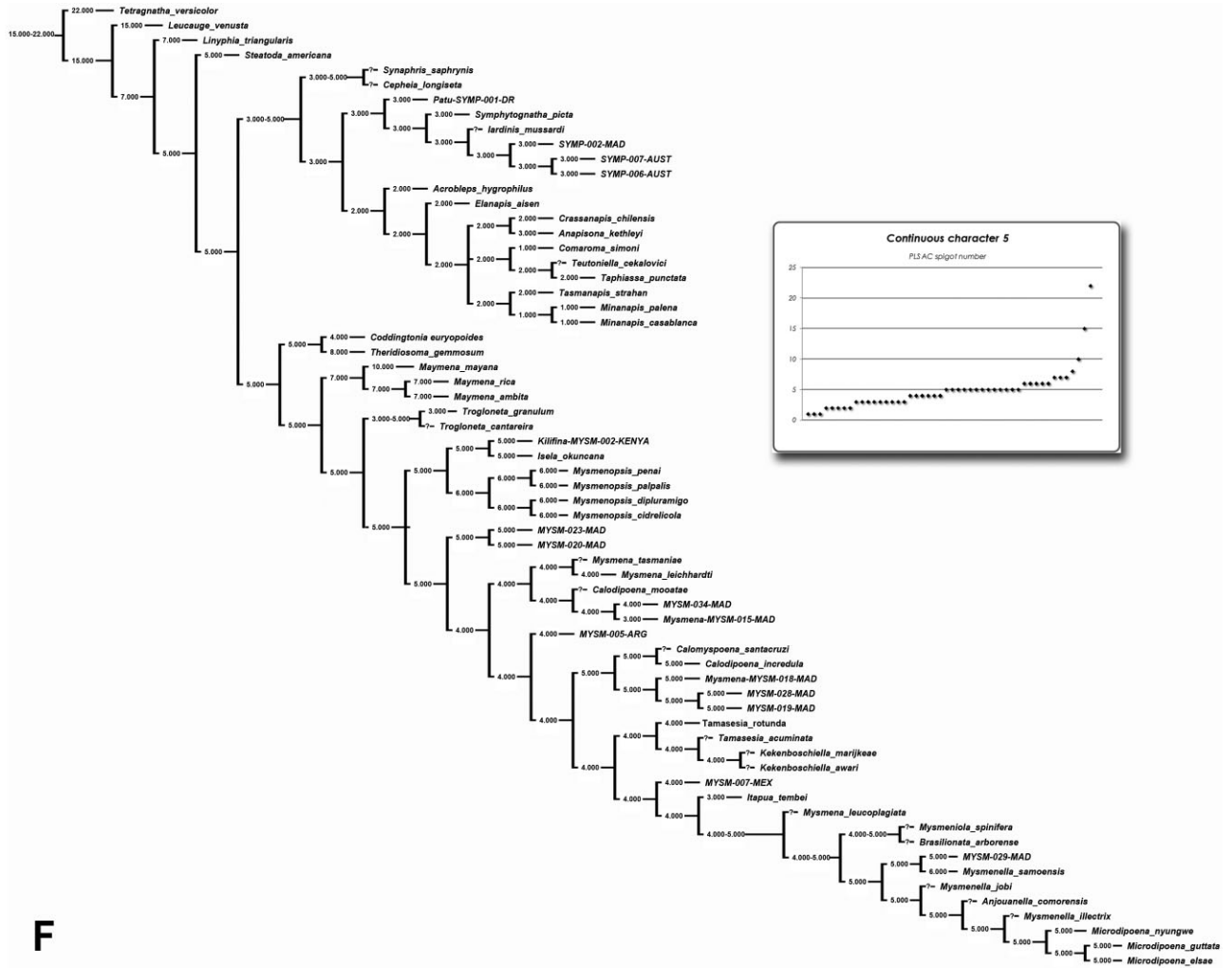


Figure 155. F, strict consensus of the three MPTs that resulted from the analysis of the morphological data set. Continuous character optimization. Character 5: posterior lateral spinnerets aciniform gland spigot number. Family codes used for unidentified species are as follows: MYSM, Mysmenidae; SYMP, Symphytognathidae; TSMD, Theridiosomatidae.

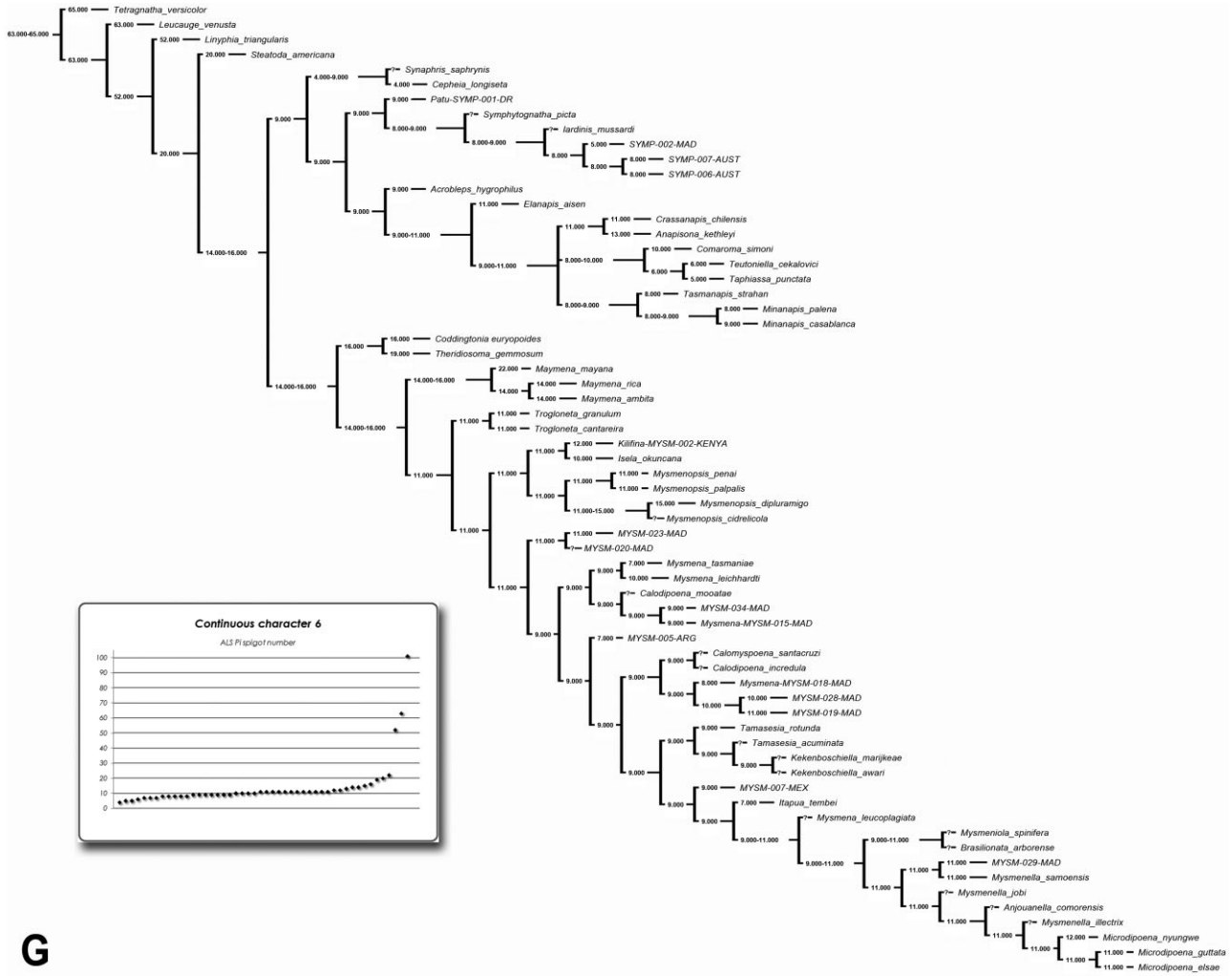


Figure 155. G, strict consensus of the three MPTs that resulted from the analysis of the morphological data set. Continuous character optimization. Character 6: anterior lateral spinnerets piriform spigot number. Family codes used for unidentified species are as follows: MYSM, Mysmenidae; SYMP, Symphytognathidae; TSMD, Theridiosomatidae.

Downloaded from https://academic.oup.com/zoolinnean/article/173/3/527/2449763 by guest on 19 April 2024

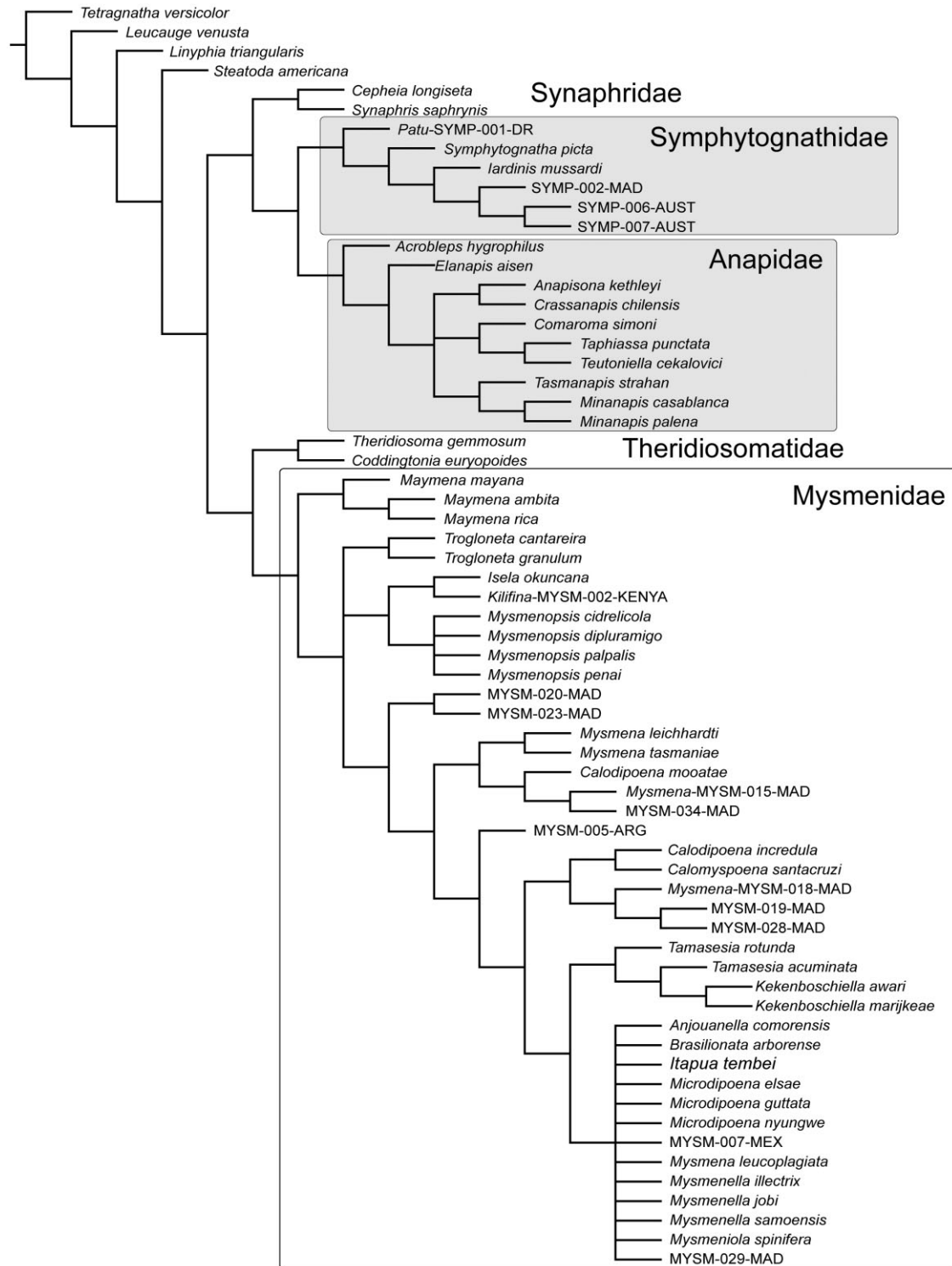
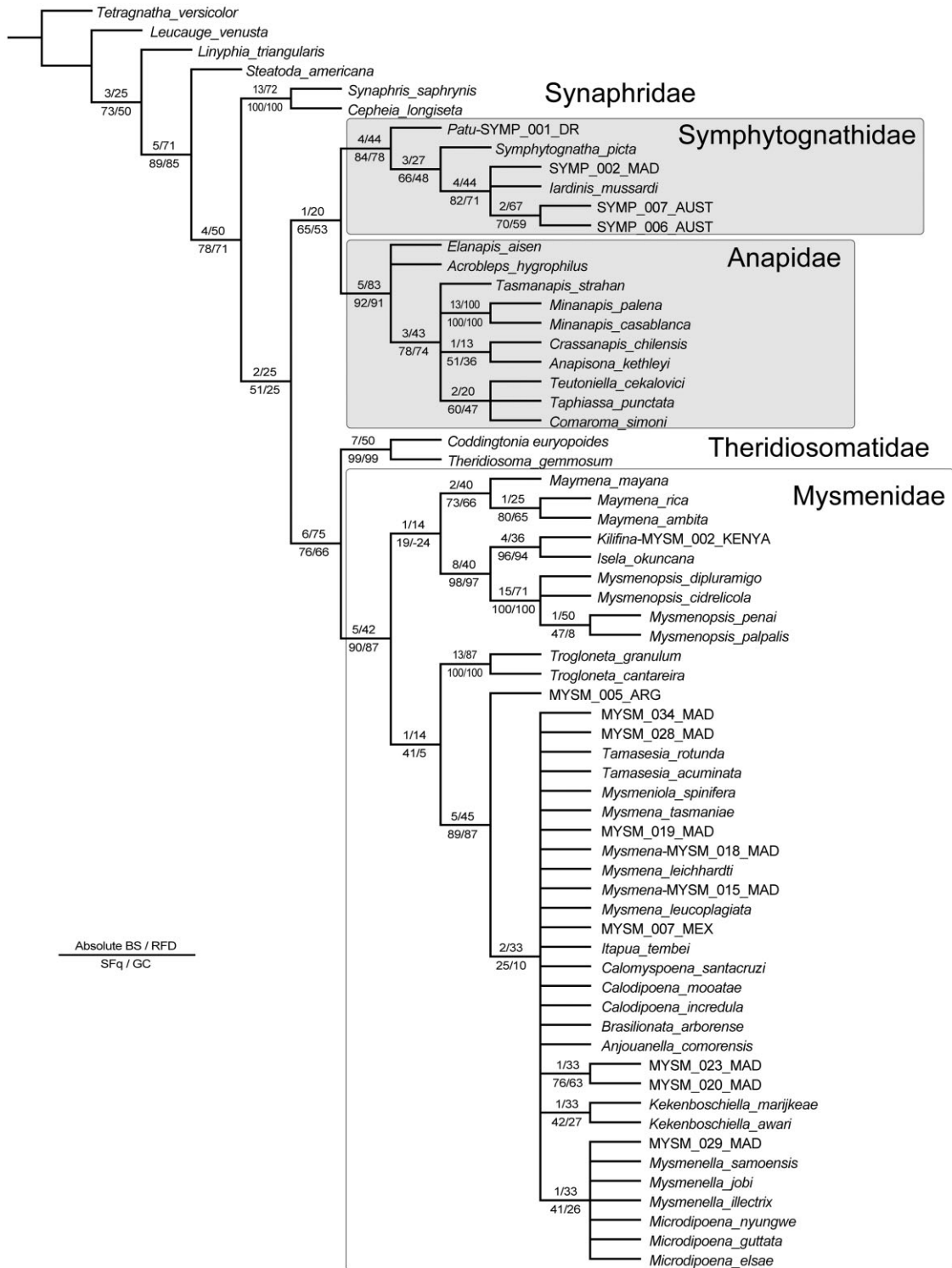


Figure 156. Strict consensus of the three most-parsimonious trees (MPTs) that resulted from the analysis of the morphological data set. Nodes collapsed if Bremer support values are smaller than 0.95 steps. Family codes used for unidentified species are as follows: MYSM, Mysmenidae; SYMP, Synphytognathidae; TSMD, Theridiosomatidae.



Downloaded from https://academic.oup.com/zoolinnean/article/173/3/527/2449763 by guest on 19 April 2024

Figure 157. Strict consensus of 3835 most-parsimonious trees (MPTs) that resulted from the analysis of the morphological data set including only discrete characters. See tree statistics in Table 6. Numbers before and after the slash above each node indicate absolute Bremer support (BS) and relative BS (RFD) values, respectively. Numbers before and after the slash below each node indicate absolute symmetric frequencies (SFq) and frequency differences (GC), respectively. Family codes used for unidentified species are as follows: MYSM, Mysmenidae; SYMP, Symphytognathidae; TSMD, Theridiosomatidae.

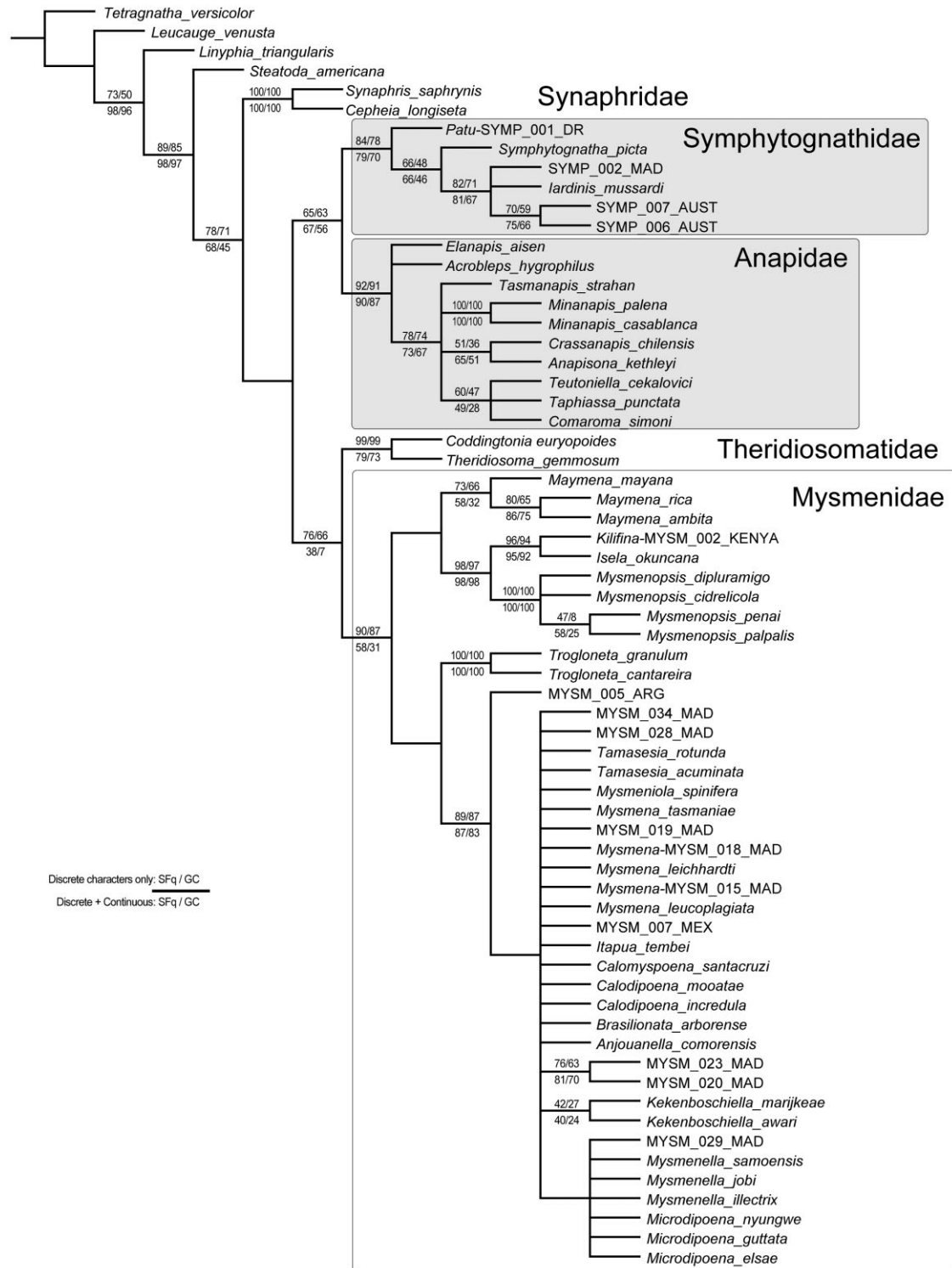
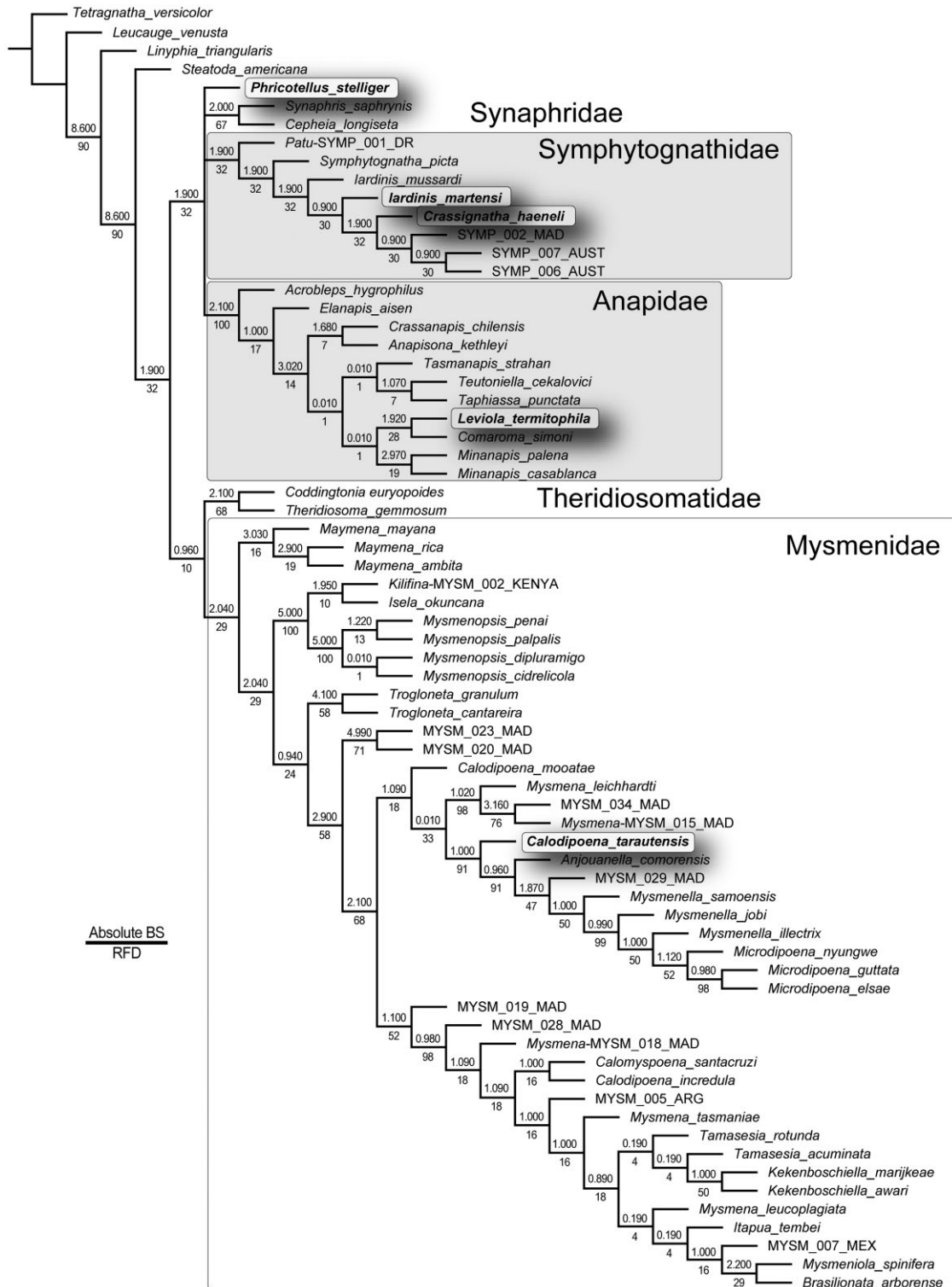


Figure 158. Strict consensus of 3835 most-parsimonious trees (MPTs) that resulted from the analysis of the morphological data set including only discrete characters. See tree statistics in Table 6. Numbers before and after the slash above and below each node indicate absolute symmetric frequencies (SFq) and frequency differences (GC) for the common nodes between the analysis of the discrete partition and the complete data set, respectively. Family codes used for unidentified species are as follows: MYSM, Mysmenidae; SYMP, Symphytognathidae; TSMD, Theridiosomatidae.



Downloaded from https://academic.oup.com/zoolinmean/article/173/3/527/2449763 by guest on 19 April 2024

Figure 159. Strict consensus of the three most-parsimonious trees (MPTs) that resulted from the analysis of the morphological data set including all taxa. The five taxa represented by 78% or more missing data are in bold. See tree statistics in Table 6. Numbers above and below each node indicate absolute Bremer support (BS) and relative BS (RFD) values, respectively. Family codes used for unidentified species are as follows: MYSM, Mysmenidae; SYMP, Symphytognathidae; TSM, Theridiosomatidae.

ejaculatory duct. Although found in other spider families (e.g. in some theridiids, linyphiids, cyatholipids, and agelenids), the pars pendula is an ambiguously optimized synapomorphy for Mysmeninae (ambiguously optimizes at its node because of missing information on the basal clade of this group), and it is secondarily absent in MYSM-005-ARG (*Mysmena*).

Tegular conductor: As in most symphytognathoids, most mysmenids have a conductor. Mysmenid conductor is distinctly voluminous and membranous, and originates subterminally from the tegulum, close to the embolic base (Figs 17A, 18D, 27A, B, 30E, 36C, 41D, 63B, D). This structure has been named 'bulbal shield' (e.g. Baert, 1984a; Schütt, 2003), and other than the embolus, it appears to be the only tegular sclerite. In mysmenids, the conductor often embraces and even covers the embolic base (Figs 41C, 43A, B). In some species there is a groove on the conductor surface housing the basal portion of the exposed embolus (Figs 36B, C, 47E); however, a groove housing the distal portion of embolus is absent in the tegular conductor of mysmenids, and the tip of the embolus is instead housed by one of the two conductors on the cymbium (see above). Within symphytognathoids, the occurrence of a tegular conductor is symplesiomorphic and widespread, with few independent losses of this sclerite occurring in anapids, symphytognathids, and mysmenids. Within Mysmenidae, the conductor is lost two times: in the clade that includes *Maymena* and Mysmenopsinae, and in *Mysmena* MYSM-005-ARG (Figs 4A, 10E, 28D).

Spermatic duct trajectory (SDT; refer to Fig. 127 and characters 220–228): As with most of the aforementioned palpal features, there does not seem to be a consistent pattern in the trajectory of the spermatic duct across the family, although there is some regularity within clades. The spermatic duct usually travels clockwise from the fundus (in left palp). If a switchback (SB) occurs, it alters this direction to travel counterclockwise. Usually, a counter-switch also occurs to return the duct trajectory to its original clockwise direction. Therefore, when SBs are present, they usually occur in pairs of switchbacks. The trajectory of the spermatic duct in *Trogloneta* differs from all other mysmenids in that the pair of switchbacks that occur before the spermatic duct completes one loop from the fundus (i.e. SB I and II, see Fig. 127) are absent, therefore the trajectory is completely spiralling or has one complete loop before the 'second' pair of switchbacks (SB III and IV) occurs (Fig. 131E, F). Although the general arrangement of the spermatic duct in all other mysmenid species examined in this study (except *Trogloneta*) is not necessarily similar among clades, all

have the first pair of switchbacks on their trajectories (SB I and II; Figs 131I, 132B, D).

The position of switchback I (SB I) varies within Mysmenidae also. A distal SB I (apart from basal fundus, on the opposite area of the bulb) occurs in most mysmenines, most *Maymena*, and in *Isela okuncana* (Figs 131H, I, 132B, E, 133A, B, 134B, C). A basal SB I that does not reach the distal part of the bulb can occur in other mysmenines, however (Figs 133H, I, 134F–H); whereas in most mysmenopsines and *Maymena mayana* the SB I occurs close to the fundus, after the spermatic duct has reached the distal wall of the bulb (i.e. 'beyond distal'; Fig. 131C, G, J).

In most mysmenids, the portions of spermatic duct forming the SB I are divergent, and SB II occurs relatively close to SB I (Figs 131B, H, J, 133A, B, 134D–G). In *Microdipoena* and most *Mysmena* species, the portions of spermatic duct comprising SB I run close to each other, and the SB II occurs close to the midpoint between SB I and the fundus, or even closer to the fundus (Figs 131I, 132B–D, 133D, E, 134A–C).

The plesiomorphic condition in Mysmenidae is to have two or more ascending loops in the last portion of the coiling reservoir before entering the embolus. This occurs basally within Mysmeninae (Figs 133D, E, 134E, H). Within the family, the number of loops decreases independently in distal clades (no loops or less than one entire loop, Figs 131B, E, H, I, 132F, 133A, B, 138C, G, 139E; or about one and one and a half loops, Figs 131D, 139C).

A pair of switchbacks (SB III and IV) can occur either after SB II, or if SB I and II are absent, after a complete loop of the spermatic duct (e.g. as in *Symphytognatha picta*; Fig. 139C). In this data set, an absence of pairs of extra switches (i.e. SB III and IV) is plesiomorphic for both symphytognathoids and Mysmenidae (Figs 131D, E, J, 133A, B, D, E, H, I, 134E). Switchbacks III and IV evolve independently in *Microdipoena*, *Mysmena* MYSM-007-MEX, *Isela okuncana*, and *Trogloneta cantareira* (Figs 131F, H, 132B–E). Furthermore, a distinct trajectory of the spermatic duct where several pairs of switchbacks occur evolved convergently in the mysmenines MYSM-020-MAD and MYSM-023-MAD (Figs 134F–H).

Epigynum (refer to characters 59–87)

Mysmenids are entelegyne spiders. That is, they have fertilization ducts leading from the spermathecae to the *uterus externus* and copulatory ducts connecting external openings to the spermathecae (e.g. Wiehle, 1967; Uhl, 2002). No comparative study of mysmenid female genitalia has ever been performed. In most female mysmenids, particularly mysmenines, the ducts and sometimes even the spermathecae are extremely membranous, almost invisible under light

microscopy. A few authors describing mysmenid species have published detailed illustrations and have attempted to identify the different components of female genitalia in as much detail as possible (e.g. Kraus, 1967; Loksa, 1973; Thaler, 1975; Baert, 1984a, b, 1986, 1988; Snazell, 1986; Baert & Murphy, 1987). Given the membranous and almost undetectable nature of mysmenid female genitalia, the interpretation of these structures is often difficult. Furthermore, the great diversity of mysmenid female genitalic morphology (see below) makes diagnosis of the family a challenging task if only based on this system of characters. Our interpretations and homology statements of female genitalic structures are based on light and SEM microscopy data.

External genitalia

The epigynum, as a sclerotized modification of the cuticle, is absent in most of the members of the subfamily Mysmeninae. In addition, the copulatory openings are located within the epigastric furrow (i.e. the epigynal area containing the copulatory openings is hidden within it; Fig. 24A). This latter trait has convergently evolved in most anapids. All representatives of Mysmeninae here examined have a membranous atrium (Figs 59H, 129A, E, G, 130B). The atrium has been defined as a 'widened cavity into the copulatory ducts' (Sierwald, 1989: 2), and can occur independently of the location (external or internal) of the copulatory openings. In most mysmenids, however, the seemingly epigynal area located centrally between the copulatory openings (here regarded as the 'dorsal plate' *sensu* Millidge, 1984; 'middle field' on Sierwald, 1989) is projecting, i.e. it is exposed or protruding from the epigastric furrow (Figs 11B, C, 12D, E, 37C, 42C, 44A, 49D, 67A, B). The dorsal plate is secondarily internal (i.e. neither exposed nor projecting) in Mysmenopsinae, *Maymena rica*, *Microdipoena*, and few other mysmenines (e.g. Fig. 24B).

Trogloneta, *Maymena*, Mysmenopsinae, and the mysmenine MYSM-023-MAD have a modified copulatory area or epigynum in the form of a sclerotized plate or a protruding modification of the cuticle, usually bearing setae and the copulatory openings (Figs 5A, B, 11B, C, 12D, E, 49D, E, 59H, 61A, 67A, B, 140D, I, 141G, H, 142C). The copulatory openings are exposed caudally (i.e. posteriorly) in the epigynal area (Figs 49D, 59H, 61B). A sclerotized external atrium is present in a few *Mysmenopsis* species (e.g. Fig. 59H). On the other hand, in most Mysmeninae the epigynal area is weakly modified or even absent (i.e. the cuticle in this area is similar to surrounding abdominal cuticle), and it is usually translucent (spermathecae can be observed beneath it; Figs 14C, 37A, 52F, 141D). Although seemingly widespread among araneoids (Levi & Levi, 1962; Millidge, 1984; Scharff & Coddington, 1997; Griswold,

2001), the ventral scape of most mysmenines is unique within symphytognathoids (Figs 24B, 29C, 31G, 37C, 42C, 129E).

Internal genitalia

Copulatory ducts: Within Mysmenidae, the copulatory ducts show varying degrees of sclerotization and width. In *Maymena* and most Mysmenopsinae the copulatory ducts are short, relatively sclerotized, narrow, and of invariable diameter (Figs 11D, 37D, 128A, D, G, 129G). In *Trogloneta* the walls of the distal portion of the long copulatory ducts are rather smooth, relatively sclerotized, and uniform in diameter; however, the proximal portion of the ducts of *Trogloneta* is highly membranous and has a larger diameter than the distal part (Figs 64A, 128F). In the aforementioned taxa (i.e. *Trogloneta*, *Maymena*, and Mysmenopsinae), the trajectory of the copulatory ducts is in most cases recognizable. Conversely, the copulatory ducts of Mysmeninae differ from all other mysmenids (with the exception of a few taxa). The walls of the ducts are extremely membranous, imperceptible under light microscopy, and are of uneven diameter. These irregular membranous ducts follow a convoluted and long trajectory of unclear course. The ducts seem to extend ventrally and anteriorly to the spermathecae, although without a definite pattern (Figs 18G, 27D, 129A, C, E, H, 130B). In some species the ducts can be subtly more sclerotized and definite, and a coiled trajectory can be observed (Figs 37D, 129G). The increase in the diameter of the proximal portion of the copulatory ducts (i.e. the first half of the ducts from the copulatory openings) has been termed 'bursae' by Schütt (2003: character 77), although it is not clear from that study whether the increase in diameter refers to the copulatory ducts or to the membranous atrium (see above).

Within Mysmeninae, there is a particular turn occurring proximally in the convoluted and membranous copulatory ducts, seemingly originating close to the internal atrium, but immediately before becoming widened and convoluted. This duct turn is characterized by a subtle but consistent sclerotization. This feature occurs in *Microdipoena*, and also evolved independently in two clades within *Mysmena* and in MYSM-029-MAD (Figs 129A, B, 130A).

A convoluted trajectory of the copulatory ducts characterizes Mysmenidae, although the ducts can vary greatly in terms of sclerotization and diameter. Straight ducts evolved independently twice: once in the clade comprising *Maymena* and Mysmenopsinae and once in *Mysmena* MYSM-034-MAD. Although rare in the current mysmenid taxon sample, coiled and more distinct copulatory ducts of mysmenines (as in Figs 37D, 129G) appear to be more common than represented here (e.g. Lopardo, Dupérré & Paquin, 2008; Miller *et al.*, 2009; L. Lopardo, A. Janzen, C. Griswold & P. Michalik,

unpubl. data). These distinct ducts might represent a plesiomorphic but intermediate condition (i.e. between sclerotized and fully membranous ducts) in the evolution of convoluted and highly membranous copulatory ducts, and might help in elucidating our current interpretation of their trajectory, as well as their identification.

Spermathecae and accessory glands: Most mysmenids have one sperm-storage compartment in each spermatheca (e.g. Fig. 33A). *Trogloneta* and some anapids have two pairs of compartments in each spermatheca (Fig. 128F). The spermathecae are usually defined by a thick sclerotized wall (Figs 129A, 130B), although exceptions occur (e.g. in mysmenine MYSM-023-MAD and a few anapids; Figs 49A, 130D).

Ovoid spermathecae are plesiomorphic for both symphytognathoids and Mysmenidae. Nevertheless, the diversity of spermathecal shapes within Mysmenidae is immense, seemingly following no particular phylogenetic pattern, not even at the genus level. Spermathecae can be ovoid (Figs 11D, 18G, 37D, 128D, 129A, G), C- or cup-shaped (Figs 27D,E, 42D, 128E, 130C), coiled within the same spermathecal structure (Figs 33A, B, 51D, 129C, 130B, G), tubuliform (as one large tube, sometimes like tracheoles; Figs 5D, 49A, 128A, C, 130D), clavate (Figs 12C, 128B), or even irregular (although consistent within each species), where no particular shape can be defined (Fig. 129D).

An additional paired structure occurs in the internal genitalia of *Trogloneta*, the mysmenine MYSM-029-MAD, *Mysmena* MYSM-005-ARG, *Microdipoena*, and the anapid *Tasmanapis*. This structure resembles either an apodeme or a glandular structure, and appears related to the copulatory ducts or the spermathecae (Figs 22B, 27D, 29A, 64A, 129B, E, H, 130A, F). It is better observed by SEM, although it can be distinguished in transparent preparations of the vulva by a higher degree of sclerotization, comparable with that of the spermathecae (Figs 129B, E, H, 130A, F; see also Brescovit & Lopardo, 2008: fig. 6C–E). Whether these structures are functional glands, muscle attachment points, or perform other functions remains unknown. They are regarded here as accessory glands.

Fertilization ducts: The morphology of fertilization ducts is also variable within the family. Fertilization ducts were identified in Mysmenidae by discerning the ducts connected to and from the spermathecae, and, with the help of SEM, an attempt was made to follow the trajectory of these ducts. Usually fertilization ducts are located either dorsal to or on the central internal lateral side of the spermathecae. As a convention, when the genital system was mainly composed by membranes, highly developed and convoluted copulatory

ducts were first identified, and then fertilization ducts were distinguished by elimination. The degree of sclerotization of the fertilization ducts appears highly homoplastic. Weakly sclerotized fertilization ducts with a distinguishable wall are plesiomorphic for Mysmenidae (although ambiguously optimized), and occur in *Isela*, mysmenine MYSM-023-MAD, and most *Mysmena* (Figs 42D, 49A, 128A, 129G); however, membranous, translucent, and almost imperceptible fertilization ducts also occur within the family, in *Trogloneta*, most *Mysmenopsis*, and all members of *Microdipoena* (Figs 18G, 27D, 51D, 60H, 64A, 128F, 136D).

Small, short fertilization ducts providing a direct connection between the spermathecae and the *uterus externus* (usually in straight fashion and unmodified) are plesiomorphic and widespread within Mysmenidae (Figs 42D, 49A, 64A, 128A, F). Large, long fertilization ducts, most often longer than the size of the spermathecae, might be provided with modifications or expansions (Figs 11D, 18G, 27D, 51D, 60H, 92F, 129G, 136D). They occur independently in most *Maymena*, most *Mysmenopsis*, most species of *Microdipoena*, and few *Mysmena*.

Spinneret silk gland spigot morphology (refer to characters 304–340)

The spinning organs of Mysmenidae have been described for a few species, including the kleptoparasitic *Isela okuncana* (Griswold, 1985), an undescribed *Isela* from Cameroon, *Mysmenopsis penai*, the Australian *Mysmena tasmaniae* and *M. leichhardti* (Lopardo & Michalik, 2013) and *Maymena mayana* (Griswold *et al.*, 1998). Recently, the gland spigot patterns of *Trogloneta cantareira* (Brescovit & Lopardo, 2008) and several Chinese mysmenids (*Mysmena*, *Gaoligonga*, *Chanea*, and *Maymena*, Miller *et al.*, 2009) were also described. The data in the aforementioned works suggest that mysmenids have the typical symphytognathoid and higher araneoid silk gland spigot conformation on the anterior lateral and the posterior median spinnerets (ALS and PMS, respectively): few ALS piriform gland spigots, few aciniform gland spigots on posterior (median and lateral) spinnerets, a furrow between major ampullate and piriform fields, and reduced piriform bases. In this study we examined in detail the spinneret gland spigot conformation of 30 mysmenid species. In the following section, the general arrangement of mysmenid spinneret gland spigots is described. Exceptions, singular features, and synapomorphies for the main mysmenid clades are noted below. See Appendix 2 for an explanation of cuticular textures.

In general, the colulus is fleshy and usually relatively large, bearing three or less setae (Figs 24E, 33C, 56D, 59I). On the anterior lateral spinnerets, a glabrous tuberculate intersegmental cuticle occurs (Figs 6A,

16B, 23A, C, 33F, 52B, 61C). The major ampullate gland spigot is accompanied by a nubbin and a tartipore (Figs 6B, 23A, C, 61C). The base of the piriform gland spigots is reduced (Figs 6B, 52B, 61C), and the cuticle surrounding those piriform gland spigots can be either fingerprint (in Mysmeninae and most Mysmenopsinae) or rugose (in *Maymena*, *Trogloneta*, and the *Isela* representative *Kilifina*-MYSM-002-KENYA; Fig. 6B). Two aciniform, one posterior minor ampullate, and (in females) one cylindrical gland spigot occur on the posterior median spinnerets (Figs 11F, 33D, 58F). The minor ampullate can be accompanied by a tartipore, a tartipore plus a nubbin, or by none of these. The posterior lateral spinnerets bear two cylindrical gland spigots, where both (Figs 11G, H, 13F, 67D) or only the posterior spigot is peripheral to the spinning field (the anterior spigot on the edge of the field; Figs 23B, 37B, 58H), and some aciniform gland spigots. The triad (the assemblage of one flagelliform and two aggregate gland spigots producing sticky silk in araneoids) is present in most female mysmenids (Figs 11G, 23B, 37B, 52C, 67D), as is usually the case in Araneoidea. Some exceptions occur, however (see below). Both aggregate and flagelliform gland spigots are similar in size (Figs 13F, G, 37B, 52C). In most species, the triad on males is vestigial, were remnants of previously functional gland spigots can be observed (Figs 23E, 33H). In some species, the triad is retained in adult males (Fig. 13G; this change is ambiguously optimized at the base of Mysmenidae).

The spinnerets of mysmenids differ from that of all other families represented in this data set by the presence of a lobe on the intersegmental groove of the ALS (Figs 23A, C, G, H, 52B). This lobe is also present within Anapidae, although with high homoplasy. Mysmenids also differ from other families in the separation of the major ampullate and piriform fields by a subtle (shallow) groove (Figs 13C, 23C, 33F, 52B, 61C, 64C), where the connection between both fields is distinctly evident proximally within the ALS segment (ambiguously occurring in Theridiosomatidae). Finally by the characteristic shape of a seta on the major ampullate field, with either one or two rows of long 'branches' (Figs 6A, 23F, 33F, 52B, 61C).

Trogloneta is the only symphytognathoid so far examined with minute but distinguishable colulus (Figs 64D, 67F, 68C; as opposed to the remnant colulus of *Patu*, see character 317). An additional anterior discrete cluster of cuticular protuberances of unknown function also occurs in the ALS of *Trogloneta* (Figs 64C, 66F). Other attributes occurring in *Trogloneta*, although not exclusive to this genus, include: a rugose cuticle on the piriform field on ALS (Fig. 64C); minor ampullate gland spigot accompanied solely by a tartipore on PMS; both PLS cylindrical gland spigots equally large and larger than the flagelliform gland spigot

(Fig. 67D); and triad spigots retained in adult males (at least in *T. granulum*).

In *Maymena*, the shape of the seta on the major ampullate field has a distinct single row of long 'branches' (Figs 11E, 13C, 16B); in other mysmenids, two rows occur. The PMS minor ampullate gland spigot is accompanied by a nubbin and a tartipore (Fig. 11F). The following features occur independently in both *Maymena* and Mysmeninae, and were not observed in any other taxa examined in this data set: an anterior distinctly flat spatulate modified seta on PLS (Figs 11G,H, 13E) and aciniform gland spigots of different shape in both the posterior spinnerets (median and lateral, Figs 11F, G, 13F, G; see character 304). Other attributes occurring in *Maymena*, although not exclusive of the genus, include: rugose cuticle on piriform field on ALS (Figs 11E, 16B), and both PLS cylindrical gland spigots equally large and larger than the flagelliform gland spigot (Figs 11G, H, 13F). Triad spigots are retained in adult males of *M. mayana* (Fig. 13G), but this retention appears autapomorphic for this species rather than a generic condition, given that the triad is vestigial in at least *M. rica*.

In Mysmenopsinae the adult male aggregate gland spigots are absent, and those of the females are distinctly absent as well (see below). Other spinneret features of this subfamily include: a fingerprint cuticle on ALS piriform field; PMS minor ampullate gland spigot accompanied by neither nubbin nor tartipore (Figs 6C, F, 58F, 61D); and both PLS cylindrical gland spigots slim as other gland spigots (not larger) and subequal to flagelliform gland spigot (Fig. 58H). In *Mysmenopsis*, the colulus bears four or more setae (Figs 56D, 59I). Although both aggregate gland spigots are absent in males and females, the flagelliform gland spigot in the representatives of *Mysmenopsis* studied has been retained, and seems to be functional in both sexes (Fig. 58G, H). In *Isela* both flagelliform and aggregate gland spigots are distinctly absent in both sexes (Fig. 6D, G).

Finally, the subfamily Mysmeninae shares with *Maymena* the anterior distinctly flat spatulate modified seta on PLS (Figs 23B, E, 33G, H, 37B, 52C) and aciniform gland spigots of different shape in both posterior spinnerets (median and lateral, Figs 23D, 33D, 37B; see character 304). These two features evolved independently in the two clades. Other features occurring in mysmenines include a fingerprint cuticle on ALS piriform field (Figs 23C, 52B); PMS minor ampullate gland spigot accompanied solely by a tartipore (Figs 19F, 23D, 33D); both PLS cylindrical gland spigots slim as other gland spigots (not larger) and subequal to flagelliform gland spigot (Figs 23B, 37B, E, 52C); and vestigial triad in males (Fig. 23E), independently functional in *Mysmena* MYSM-005-ARG and *Mysmena tasmaniae*.

Other morphological features of Mysmenidae

Clasping spines

The males of all mysmenids except *Maymena mayana* have a prolateral metatarsal clasping spine (macroseta) on leg I (e.g. Fig. 34C). The phylogenetic hypothesis from the total-evidence analysis agrees with the morphological hypothesis from this study and with previous studies that have suggested this macroseta as a synapomorphy (or diagnostic) for the family (Thaler, 1975; Platnick & Shadab, 1978; Brignoli, 1980; Griswold, 1985; Wunderlich, 1995; Griswold *et al.*, 1998; Schütt, 2003). Although some members of Anapidae have a clasping structure on the first legs, these structures are not spines (macrosetae) but spurs (short and stout seta), and can occur in both sexes. The clasping spines of mysmenids are sexually dimorphic, occurring in males, are unique for the family, and might be involved in mating behaviour (Schütt, 2003). The widespread condition is a medial and straight metatarsal clasping spine (Figs 34C, 42H, 45H, 65C), but the spine can be basal (e.g. *Maymena*; Figs 16G, 141K), apical (few *Mysmenopsis* and mysmenines species; Figs 50H, 59B, 143C, 144A), twisted (*Isela* and *Microdipoena*; Figs 3B, 8B, C, 26C, 140E, F, 141K, L, 142N), or strongly curved proximally and accompanied by adjacent strong setae (most *Mysmenopsis*; Figs 54D, 57I, 59B). Additional apical tibial clasping spines can also be found in some mysmenids, as is the case of one tibial clasping spine occurring in all *Maymena* species (except *M. mayana*) and in Mysmenopsinae (Figs 3A, 8D, 16G, 54C, 59B, 62E, F, 140E, J, K); or two clasping spines in *Mysmenopsis dipluramigo* (Fig. 140H) and *Microdipoena* (Figs 26C, 27I, 57F, G, 141L, O).

Femoral spot or other femoral structures

The femoral spot has been previously suggested as diagnostic or synapomorphic for the family (Thaler, 1975; Platnick & Shadab, 1978; Brignoli, 1980; Griswold, 1985; Wunderlich, 1995; Griswold *et al.*, 1998; Schütt, 2003), as this cuticular structure is unique to mysmenids. The results of our study corroborate this hypothesis. The adult females of all mysmenid species have either a sclerotized spot (Figs 34A, 39D, 140G, 141C, 143N) or a cuticular projection (Fig. 57A, E) on the apical ventral surface of at least femur I, although a few exceptions occur (e.g. *Mysmena* MYSM-005-ARG and a few *Mysmenopsis* species). The femoral structure of most female mysmenids occurs in both femora I and II (symplesiomorphic in this data set, Figs 141C, 142B). The occurrence of this feature only on femur I is convergent in *Trogloneta*, *Mysmenopsis* (when present), and a number of times within *Mysmena* (Fig. 140G).

The femoral sclerotization (i.e. spot) was first described by Marples (1955) for *Tamasesia* (= *Mysmena*). Its function remains unknown. The absence of pores

in its surface indicates that we should rule out a glandular function. It has been suggested that the spot could be a '... functionless remnant of an unknown structure, because it shows a great variability in size and shape among specimens and can be differently pronounced on the two first femora of a single specimen. It is too large to be the socket of a former spine and apart from this there is no space for a large spine so close to the patella ...' (Schütt, 2003: 143). Based on the results of the combined analysis, the spot originates at the node of Mysmenidae, becomes a femoral projection in *Mysmenopsis*, and is lost distally in some species. Whether the femoral spot actually has a function (e.g. a behavioural function), or is just a remnant of a functional structure, remains an unsolved puzzle.

All femoral structures are absent in juvenile mysmenids (which argues against the remnant hypothesis), although they can sometimes be perceived in subadult stages. The femoral projection occurs only in females of some species of *Mysmenopsis*. The femoral spot, however, can also occur on males (Fig. 21A). Male femoral spots evolved ambiguously in *Trogloneta* and *Maymena*, independently in *Microdipoena* [excluding its basal species *M.* (= *Mysmenella*) *samoensis*], and in two instances within *Mysmena*. In contrast with females, most mysmenid males have the femoral spot (when present) only on femur I (Fig. 141O), although in two cases the spot occurs in both femora I and II (*Maymena ambita* and *Mysmena tasmaniae*; Fig. 140M).

Prolateral row of modified setae in the male first leg tarsi

First observed and described as a ventral row of modified setae by Thaler (1975, 1995) for males of *Trogloneta granulum* and *Mysmeniola spinifera* (respectively), this prolateral row of modified setae (see below) is an ambiguously optimized synapomorphy for Mysmenidae. As is the case of most morphological features within Mysmenidae, and even though this row of modified setae occurs in all examined species, the particular details of this feature differ among clades. The modified setae are usually shorter than the surrounding tarsal setae, and can be slimmer and curved or stouter and straight. These modified setae can also be distributed along the entire length of the tarsus or just on the distal half. In Mysmeninae, the setae are slimmer and the row occupies the distal half of the tarsus (except in *Mysmeniola*, see below; Figs 26A, 34D, 45I, 50F). In *Maymena rica* and in *Mysmeniola spinifera* the setae are also slimmer but the row is distributed all along the segment (Fig. 16H). *Trogloneta* and *Isela* both have stout setae distributed along the tarsus (Figs 8F, 65D, 68A). And lastly, *Mysmenopsis* also have stout setae but, as in Mysmeninae, the row occupies the distal half of the tarsus (Figs 54G, 59D). Although the function of this row of modified setae remains unknown, the

fact that these setae are found only in the males suggests that it may be involved in mating behaviour.

Other morphological features of Mysmenids

Size of the tarsal organ opening on leg I: A large opening of the tarsal organ (i.e. subequal or larger than setal sockets) evolved independently in Mysmenidae and Anapidae (see Figs 26E, 39C, 48F, 50D, 73B, 83E, 95I, 101E, respectively). An opening distinctly smaller than setal sockets is the plesiomorphic condition in symphytognathoids. Within Mysmenidae, the tarsal organ opening becomes secondarily small in Mysmenopsinae, with a reversal in *Mysmenopsis palpalis* (Figs 3F, 54F, 62H).

Distinctly thick distal promarginal curved seta on chelicerae: Most taxa in this data set have a particularly distinct curved seta located distally at the promarginal edge of chelicerae, near the fang base. This seta differs from surrounding promarginal setae by its thickness and/or serration. Although a distinctly curved seta can also occur on the cheliceral retromargin of some araneomorph spiders (see Griswold *et al.*, 2005, character 34), retromarginal setae of the taxon sample examined in this study do not differ from surrounding setae (e.g. Fig. 7J). Within symphytognathoids, the distinctly curved promarginal seta is lost in Synaphridae and most Symphytognathidae (Figs 108E, 118E, 122A; the optimization of this character under parsimony is ambiguous). All examined mysmenid representatives have a uniquely thicker distal promarginal curved seta (Figs 19E, 25E, 38H, 48B), except *Maymena*. In some mysmenids this seta is equally serrated as surrounding seta, which is the plesiomorphic condition for the family; however, the thicker seta is strongly serrated on one side independently in Mysmeninae and most Mysmenopsinae (Figs 19E, 38H, 42E, 48B).

Intermediate sternum posterior margin: Pointed and truncate sternal margins are quite distinct in the taxa represented here, although the systematic value of this character has been questioned because of imprecision in shape definition, reliability of observation, homoplasy, and possible influence of overall body proportions on sternum shape (Coddington, 1986a; Griswold *et al.*, 1998; Schütt, 2003). A truncate sternum is a synapomorphy of symphytognathoids, occurring in all families except Mysmenidae. In Mysmenidae, an intermediate condition between pointed and truncate posterior sternal margin is consistently found (Figs 2C, 7C, 25B, 35C, 46A, 59G, 140B, 143B, I); however, an ambiguously optimized reversal to pointed posterior sternum occurs in *Maymena* (Fig. 141F), and two independent instances of truncate sternum occur within mysmenines (Fig. 143O).

Sparse imbricate cuticular pattern on carapace border: Almost all mysmenids here examined have a typical cuticle pattern on the carapace lateral edges that was not observed in other taxa. It consists of slender (i.e. not prominent) ridges running mostly parallel with each other and with the edge of the carapace, delimiting elongated scales (Fig. 50A). A smooth cuticle is widespread in both outgroup taxa and symphytognathoids (Figs 118A, B, 121B, E). Within Mysmenidae, a smooth cuticle is secondarily and independently present in *Maymena mayana* and the mysmenine MYSM-019-MAD.

Cheliceral fang furrow denticles: Minute denticles in the cheliceral fang furrow (Figs 7G, 15H, 48B) occur in almost all mysmenids studied (e.g. Forster, 1959; Brignoli, 1974; Thaler, 1975; absent in *Microdipoena jobi*; Platnick & Shadab, 1978; Griswold *et al.*, 1998; Schütt, 2003), and have been proposed as synapomorphic for the family (Platnick & Shadab, 1978). Although not unique for symphytognathoids (cheliceral denticles have been reported at least in nesticids, Wiehle, 1963; uloborids, Peters, 1982; and araneids and nephilids, Hormiga, Eberhard & Coddington, 1995), similar denticles also occur in Theridiosomatidae and some anapids (Coddington, 1986a; see also Schütt, 2003). Within symphytognathoids, denticles are an ambiguously optimized synapomorphy for both Theridiosomatidae and Mysmenidae.

Anterior median eyes on protruded area: Another particular feature shared between mysmenids and theridiosomatids is the arrangement of the anterior median eyes. Character optimization under parsimony for this feature is ambiguous. Both sexes of mysmenids (except *Trogloneta*, see below) and theridiosomatids have a depression around the anterior median eyes defining a protruded area (Figs 15B, D, 25C, 46D, E, 59C). This area is clearly protruded, not just smoothly raised from the rest of the carapace, and can be best observed with SEM and in frontal view. In *Trogloneta*, males have all eyes in a tubercle or a narrow elevation of the ocular area (Figs 63G, H, 66A).

THE BIGGER PICTURE: SYMPHYTOGNATHOID SILK GLAND SPIGOT CONFORMATION AND EVOLUTIONARY IMPLICATIONS

The spinneret silk gland spigots of symphytognathoids have been studied at varying levels of detail by a number of arachnologists (Forster & Platnick, 1984; Griswold, 1985; Coddington, 1986a; Platnick *et al.*, 1991; Griswold *et al.*, 1998; Schütt, 2000, 2003; Ramírez, Lopardo & Platnick, 2004; Lopardo & Hormiga, 2007, 2008; Lopardo *et al.*, 2007; Brescovit & Lopardo, 2008;

Miller *et al.*, 2009; Rix & Harvey, 2010). In general, most symphytognathoids have the typical higher ('derived') araneoid silk gland spigot conformation, consisting of anterior lateral spinnerets (ALSs) with a field of piriform gland spigots (Pis) of reduced bases and one peripheral major ampullate gland spigot (MAP), accompanied by a nubbin and a tartipore in both sexes, with the MAP and Pi fields separated by a groove. The female posterior median spinnerets (PMSs) have aciniform gland spigots (ACs), one posterior minor ampullate gland spigot (mAP), and one or two cylindrical gland spigots (CYs; cylindrical gland spigots are absent in males). The female posterior lateral spinnerets (PLSs) have a triplet of two aggregate (AGs) and one flagelliform (FL) gland spigots, several aciniform gland spigots (between one and ten), and two CY gland spigots (Coddington, 1989; Griswold *et al.*, 1998, 2005). Typical symphytognathoid gland spigot conformations differ from that of derived araneoids in the decrease in number of the multiple gland spigots, however: i.e. fewer Pis on ALS and fewer ACs on both PMS and PLS; a groove with varying degrees of depth between MAP and Pi fields; mAP gland spigots accompanied by a nubbin and a tartipore, just a tartipore, or no gland spigot remnant at all; and in some symphytognathoids, the triplet can be present in males (this study, but see also Griswold *et al.*, 1998; Schütt, 2003).

The evolutionary pattern of the spinneret features described in characters 304–340 fits and supports the family-level phylogenetic hypothesis that results from the total-evidence analysis (e.g. 24 out of 29 informative characters have retention index higher than 60%). Besides the typical araneoid gland spigot arrangement, the general symphytognathoid spinneret and gland spigot conformation is as follows. The colulus is fleshy and relatively large, bearing three or less setae (Figs 33C, 49F, 68C, 88F). The colulus becomes reduced in *Trogloneta* (Figs 64D, 67F, 68C), and is lost in Symphytognathidae (Figs 117F, 120C). A reversal to four or more colular setae occurred in *Mysmenopsis* (Fig. 56D).

ANTERIOR LATERAL SPINNERETS (ALSs)

Commonly in Araneoidea, the furrow between MAP and Pi fields on the ALS is deep, conspicuously separating the fields, which appear as two distinct distal segments. Within symphytognathoids, this condition occurs in the clade comprising Anapidae plus Symphytognathidae (Figs 75A, B, 103B, 113A). Alternatively, MAP and Pi fields are separated by a subtle or shallow groove in Mysmenidae and Theridiosomatidae, where the connection between both fields is distinctly evident basally (Figs 6A, 13C, 33F, 61C). As previously reported, no distinct separation between the fields occurs in Synaphridae (Fig. 107G),

i.e. no deep furrow can be observed, as in other non-araneoid spiders (Lopardo *et al.*, 2007).

The shape of the single seta located on the MAP field also differs within symphytognathoids. The ancestral condition, occurring in Synaphridae and the non-symphytognathoid outgroup representatives (Fig. 107G; with a reversal in *Taphiassa*, see Fig. 94E), is a seta similar to surrounding setae on ALS (i.e. smooth or similarly serrated). A seta with a row (or two, as in *Tasmanapis*) of minute branches is synapomorphic for the clade comprising Anapidae plus Symphytognathidae (Figs 89C, 103B, 113A), reversed in *Taphiassa*. Two rows of long branches in the MAP seta evolved independently from the ancestral condition in most Mysmenidae (Figs 6B, 23F, 33F, 52B; changing to one row of long branches in *Maymena*, see Figs 11E, 13C, 16B) and Theridiosomatidae. The function of this seta is unknown, but its shape appears to be distinct among symphytognathoid families or groups of families.

Glabrous tuberculate intersegmental cuticle is the ancestral and widespread cuticular pattern in symphytognathoids, occurring in other outgroup taxa as well (Figs 6A, 23C, 66F, 75A; see Appendix 2 for an explanation of cuticular textures). This cuticular pattern might represent at least a common pattern for Araneoidea. Fingerprint cuticle is synapomorphic for Symphytognathidae (Fig. 113A). Smooth cuticle is independently synapomorphic for Synaphridae, convergent in *Taphiassa* (Fig. 94A, E). The cuticle pattern within the Pi field also differs among symphytognathoid families or groups of them. This cuticle around Pi optimizes ambiguously at the base of symphytognathoids, because of a diversity of patterns both within symphytognathoids but also among the non-symphytognathoid outgroup representatives. Smooth cuticle occurs in the clade comprising Anapidae, Symphytognathidae, and Synaphridae (Figs 75A, 94A, 100A, 103A), but also in the Linyphiidae and Theridiidae representatives. Rugose cuticular pattern (just one ring around Pi gland spigots) occurs in the Tetragnathidae representatives, in Theridiosomatidae, and in the mysmenids *Trogloneta*, *Maymena*, and *Isela* sp. (*Kilifina-MYSM-002-KENYA*) (Figs 16B, 125D). Fingerprint pattern (i.e. concentric rings around Pi), occurs only within symphytognathoids, in Mysmeninae, and most Mysmenopsinae (see above; Figs 6B, 23A,C, 33E, 61C).

Although the function of this structure is unknown, the cuticular lobe on the ALS intersegmental groove is synapomorphic of Mysmenidae (Figs 23C, G, H, 33F, 52B), with homoplasy in the anapids *Acrobleps*, *Elanapis*, *Teutoniella*, and *Comaroma* (Fig. 103A).

POSTERIOR MEDIAN SPINNERETS (PMSs)

There appears to be a tendency within symphytognathoids towards a decrease in number of PMS

aciniform (AC) gland spigots. Three ACs occur in Theridiosomatidae (Fig. 123E) and most outgroup taxa in this matrix (except Theridiidae, with one AC). A change to two ACs occurs at the base of symphytognathoids excluding Theridiosomatidae (i.e. in the ANTS clade; Figs 6C, 11F, 13D, 19F, 33D, 61D), and a further change to one AC occurs in the Anapidae plus Symphytognathidae clade (Figs 75D, 78D, 82G, 94B, F, 103C, E, 114A), with a secondary reversal to two ACs in *Crassanapis*.

Variation in combinations of nubbin and tartipore accompanying the mAP gland spigot is not exclusive to Symphytognathidae. The nubbin and tartipore are secondarily and independently absent in the anapid *Teutoniella* and in the synaphrid *Cepheia* (see Fig. 103C, E). Although the evolution of these structures is ambiguously optimized, the common araneoid condition (mAP accompanied by nubbin plus tartipore) occurs in tetragnathid representatives on this data set, the theridiosomatid *Coddingtonia euryopoides* (TSM-D-002-THAI), Symphytognathidae, most Anapidae (except the distal clade comprising *Taphiassa* and *Comaroma*), and *Maymena* (Figs 11F, 75D, 88G, 113C, 122E, 125C). An mAP gland spigot accompanied only by a tartipore occurs in *Theridiosoma gemmosum*, *Trogloneta*, and Mysmeninae (Figs 19F, 23D, 33D, 123E), whereas an mAP alone occurs in *Linyphia*, *Steatoda*, Mysmenopsinae, and the distal anapid clade comprising *Taphiassa* plus *Comaroma* (Figs 6C, F, 58F, 61D, 78E, 82G, 94B, F).

POSTERIOR LATERAL SPINNERETS (PLSS)

The PLSSs in most taxa in our data set, both symphytognathoids and outgroup taxa, bear two cylindrical gland spigots (CYs), where both or only the posterior one is peripheral to the spinning field (the anterior one on the edge of the field; Figs 13F, 45F, 58H, 65A, 78H, 103F, 113D, 123F). The loss of one PLS CY occurred independently in *Cepheia* and our exemplar *Taphiassa* (Fig. 94F), although other *Taphiassa* species do possess both PLS CY gland spigots (see Rix & Harvey, 2010: fig. 162E). Ancestrally, both CY gland spigots are equally large and larger than the flagelliform gland spigot, a condition found in most outgroup taxa (except *Linyphia*, see below), and also in Theridiosomatidae, Synaphridae, *Maymena*, and *Trogloneta* (Figs 11G, H, 13F, 67D, 94F, 123F). Huge posterior CY gland spigot, much larger than the anterior one (both still larger than FL) diagnoses the clade comprising Anapidae plus Symphytognathidae, with a reversal in *Taphiassa* (but not in all congeners; Rix & Harvey, 2010) (Figs 75E, 78H, 89D, 100C, 103F, 113D, 114B). The presence of such enlarged CY gland spigots defined the so-called 'enlarged basal cylindrical gland' (EbCY) clade of Rix & Harvey (2010: 11), which in-

cludes Anapidae and Symphytognathidae, and also 'teutoniellids' and Micropholcommatidae *sensu* Rix & Harvey (2010). An enlarged posterior CY gland spigot also occurs independently in *Linyphia* as well as in other araneoids not studied here (e.g. Álvarez-Padilla *et al.*, 2009). Slim CY gland spigots, subequal to FL, evolved independently in Mysmeninae and Mysmenopsinae (Figs 23B, 37B, E).

The number of PLS AC gland spigots varies across families, and it appears uncorrelated, or weakly correlated, with size. For example, even though largest symphytognathoids such as theridiosomatids have between seven and 12 PLS AC gland spigots, and Mysmenidae have between four and ten (tiniest mysmenids have four ACs), the large anapid genus *Crassanapis* has only two ACs (anapids have between one and four ACs), whereas the smallest symphytognathoids, the minute Symphytognathidae, consistently have three ACs on their PLS. That body size is a poor predictor of the quantity of aciniform gland spigots is also suggested by other comparative studies of araneoid gland spigot morphology (e.g. Hormiga, 1994, 2000).

Finally, the triad (or triplet, the assemblage of one FL and two AG gland spigots producing the viscid sticky silk of araneoids) is present in most female symphytognathoids, as is usually the case in araneoids (Figs 13F, 23B, 58H, 67D, 75G, 78H, 103F, 113D, 123F), although as mentioned above, exceptions occur. In symphytognathoids, both AGs and FL gland spigots are similar in size (Figs 13G, 75F, 78H, 100D), except Theridiosomatidae (Fig. 123F). This observation is not applicable to Synaphridae, as only one gland spigot from the triad has been retained (Lopardo *et al.*, 2007). In most species, the triad is vestigial on males, and remnants of previously functional gland spigots from the subadult stage can often be observed (Figs 23E, 33H). In some species, the triad is retained in adult males. A complete and seemingly functional triad is retained in males of the clade comprising Anapidae plus Symphytognathidae (except *Taphiassa*, see below), *Trogloneta*, *Maymena mayana*, *Mysmena leichhardti*, and *Mysmena* species MYSM-005-ARG (Figs 75F, 82H, 103D, 117G; see also Forster & Platnick, 1984; Schütt, 2000). In Synaphridae, one triad gland spigot is retained in the adult males (Lopardo *et al.*, 2007). In *Mysmenopsis* and *Taphiassa*, the triad is partially lost in both sexes (or put differently, partially lost in females and partially gained in males), as the FL gland spigot appears as the only (and presumably functional) triad spigot (Figs 53H, 58G, H, 94D, F). Homology with FL is tentative though, as no remnant of aggregate gland spigots remains in the PLS (e.g. as in other males of mysmenids; Fig. 23E). The complete triad is further lost in *Isela*, where neither a functional or remnant FL nor an AG is present in either sex (Fig. 6D,G).

The absence of complete or partial PLS triad on Mysmenopsinae and the concomitant loss of the ability to spin sticky silk has been proposed as a result of the kleptoparasitic lifestyle of the members of this clade (Griswold *et al.*, 1998; see also Lopardo *et al.*, 2011). Our study supports this latter hypothesis. Accordingly, partial loss of the triad in both sexes of the micropholcommatine *Taphiassa punctata*, where only a seemingly functional FL gland spigot occurs, could therefore be indicative of the inability of this species to build typical capture webs, or at least webs with sticky silk. Unfortunately, the natural history of this species remains unknown. Conversely, females of the mysmenid *Maymena rica*, which have been reported as occasional kleptoparasite of *Tengella* webs (Eberhard *et al.*, 1993), have a completely functional triad (vestigial on males) and build the typical three-dimensional webs of many *Maymena* species (see Eberhard, 1987: fig. 11). Given the ability of *M. rica* to build capture webs, the alleged kleptoparasitic behaviour of this species is suspected to be accidental (Eberhard *et al.*, 1993).

As mentioned by Griswold *et al.* (1998), it appears that within Araneoidea the evolution of single pairs of glands remains relatively constant, whereas the multiple glands evolve towards a decrease in number. Even though reduction in size is a tempting explanation for most features observed in these minute spiders, subtle differences in the spinning organs as well as respiratory arrangements observed indicate that some other factors might act in concert to promote such diversification (L. Lopardo, P. Michalik & G. Hormiga, unpubl. data). Schütt (2003) convincingly argued that morphological characters thought to relate to miniaturization might after all provide phylogenetic information, in the sense that they are the result of common ancestry rather than mere convergences linked with smallness. Her discussion on the systematic value of these characters focused on whether other small-sized spiders also show these reductions, and whether spiders with similar morphologies are similarly small. Characters discussed by Schütt (2003) include eye number, female pedipalp, metatarsi length, and respiratory system. The male PLS triad was present in all symphytognathoid species included in her data set; however, the much more extensive taxon sample of our data set shows that the male triad is actually absent in several species of Mysmenidae, particularly the minute Mysmeninae, and also in Theridiosomatidae, therefore validating the argument that the male triad retention is not necessarily a consequence of smallness (Hormiga, 2002; Ramírez *et al.*, 2004).

As with respiratory system arrangements (L. Lopardo, P. Michalik & G. Hormiga, unpubl. data), no evident correlated pattern of evolution is perceived among these minute families. Regarding silk gland spigot confor-

mation, one would expect similarly arranged gland spigots in species building similar webs (see Lopardo *et al.*, 2011, for a review and phylogenetic implications regarding symphytognathoid web architectures). Similar webs are built by *Maymena* and most anapids; however, the silk gland spigot arrangement of *Maymena* resembles that of Mysmeninae rather than that of Anapidae. Accordingly, webs of *Elanapis* and, to a certain extent, *Tasmanapis* resemble the typical Symphytognathidae web; however, both Anapidae and Symphytognathidae have similar silk gland spigot arrays, yet the webs of most anapids have different web architectures.

CONCLUSION

This study presents the first comparative morphological review of mysmenid spiders and their close relatives, and explores the phylogenetic signal of the morphological data partition. The phylogenetic hypothesis based exclusively on morphological data re-delimits Mysmenidae, placing it as sister to Theridiosomatidae, a sister relationship recovered in only one recent phylogenetic study (Fig. 153, see also Fig. 151B; Lopardo & Hormiga, 2008). In addition, Synaphridae are hypothesized to be sister of Anapidae + Symphytognathidae. Our results support the placement of Micropholcommatinae as a subfamily of Anapidae, as it has been previously proposed (Forster, 1959; Brignoli, 1970; Schütt, 2003; Lopardo & Hormiga, 2008; but see Forster & Platnick, 1984; Platnick *et al.*, 1991; Rix *et al.*, 2008; Rix & Harvey, 2010). Recognition of micropholcommatines at the family rank would have the undesirable consequence of rendering Anapidae paraphyletic. Future research should test our hypothesis of Anapidae monophyly with an expanded selection of both anapid and micropholcommatine exemplars. A significant outcome of our comparative review is the entelegyne condition of the family Anapidae and the mysmenid genus *Trogloneta*: presence of fertilization ducts was observed in all examined anapids and in the *Trogloneta* representatives, suggesting an entelegyne (rather than haplogyne, as previously proposed; Platnick & Forster, 1989; see also Brescovit & Lopardo, 2008; Lopardo & Hormiga, 2008) internal genitalic conformation for the family.

A redefined monophyletic Mysmenidae are here diagnosed not only by the three traditional synapomorphies (femoral spot, clasping spines, and 'modified' cymbium), but also by more than 15 new synapomorphies (both unambiguous and ambiguously optimized) here proposed, related to various character systems. Our phylogenetic circumscription of Mysmenidae comprises the removal of at least three

genera. Obscure and/or little-known taxa examined in the present study include: *Calodipoena tarautensis* (placed in Mysmeninae); *Iardinis* (transferred to Symphytognathidae); the peculiar *Leviola* (transferred to Zodariidae); and *Phricotelus* (classified as 'Araneoidea incertae sedis' until specimens become available for a thorough morphological study, and its placement can be more rigorously tested). This study also concurs with the transfer of *Crassignatha* to Symphytognathidae by Miller *et al.* (2009).

The morphological character matrix presented here is part of a larger combined analysis of symphytognathoids. The phylogenetic hypothesis resulting from the total evidence analysis (which combines morphological, behavioural, and nucleotide sequence data) provides a comparative framework to study the evolution and diversification of mysmenids and their relatives, and the ultimate test of all hypothesis of synapomorphy. In light of the cladograms resulting from the total evidence analyses we have discussed the evolution of male and female genitalia, spinneret silk gland spigot morphology, leg structures, and other somatic features. For example, mysmenid male palps have distinct cymbial structures, including a paracymbium and a tegular conductor. The median apophysis or any other tegular sclerites are absent. The diversity of arrangements related to palpal structures and spinneret silk gland spigots is great within the family, although each particular arrangement seems characteristic at a higher level (genus, or sometimes subfamily). In addition, we have also discussed the evolutionary implications of the comparative spinneret spigot conformations within symphytognathoids.

This study is a first step towards a more thorough assessment of comparative morphology and evolutionary hypotheses of Mysmenidae and symphytognathoids (see also Rix & Harvey, 2010). We also hope to encourage researchers to pursue larger and more rigorous studies on these minute but extremely complex and amazing animals. Much more work remains to be done. The richness and diversity of this group remains largely undiscovered and numerous new species await description. This in turn will provide a broader spectrum of morphological variation and will hopefully facilitate our understanding of the evolution of the different character systems reported here. Furthermore, histological sections, micro computed tomography scanning, and other techniques are needed to explore the internal anatomy of mysmenids, which still remain poorly understood.

ACKNOWLEDGEMENTS

This work is part of a PhD thesis at The George Washington University (GWU) by the senior author. L.L. wishes to thank her dissertation committee members

(Gonzalo Giribet, Charles E. Griswold, James M. Clark, Diana L. Lipscomb, and Marc W. Allard) for their support, critical reading, comments, and suggestions that greatly improved her work. Special thanks go to Fernando Álvarez-Padilla for kindly sharing his unpublished SEM images and other morphological information from his own research, to Peter Michalik for translating otherwise obscure spider papers in German, and to Christian Kropf, Jaromir Hajer, Mark Harvey, and Charles E. Griswold for supplying inaccessible papers. Several friends and colleagues joined us in field trips around the world. We are grateful to Charles Griswold, Martín J. Ramírez, Robert Raven, Nikolaj Scharff, Diana Silva-Dávila, Lisa Joy Boutin, and Tamás Szüts (Australia); Cristian J. Grismado, Ana Quaglino, Luis Piacentini, and Gonzalo Rubio (Argentina); Fernando Álvarez-Padilla and José Luis Castelo-Calvillo (Mexico); and Dimitar S. Dimitrov (USA). The field trip to Misiones (Argentina) was funded by the Cosmos Club Foundation Program of Grants-In-Aid to Young Scholars (to L.L.) and the NSF-AToL spider project. We further thank the authorities at the Administración de Parques Nacionales (APN, Argentina) and Ministerio de Ecología, R.N.R y Turismo de la Provincia de Misiones (Misiones, Argentina) for collecting permits in protected areas, the park rangers for assistance in the field, and Martín J. Ramírez for logistic help. The field trip to Mexico was funded by the NSF-PEET grant (see below). We also thank Tila Pérez, G. Montiel and the IBUNAM staff (Mexico) for logistic support and resources, and the Álvarez-Padilla family for their hospitality. The Australian field trip was funded by the NSF-AToL spider project and the NSF-PEET grant. We further thank Robert Raven (QM) for logistic help, and the Parks and Wildlife Service (Department of Primary Industries, Water and Environment, Tasmania, Australia) and the Department of Conservation and Land Management (Western Australia) for spider-collecting permits. Mark Harvey (Western Australian Museum, Perth) and Lisa Joy Boutin (Queen Victoria Museum and Art Gallery, Launceston, Australia) provided valuable help for our fieldwork in Western Australia and Tasmania, respectively. We would also like to thank the Sheridan School and their staff at the Sheridan School Mountain Campus (Virginia, USA) for allowing us to collect at their property. For specimen collection and donation, we are immensely grateful to Jaromir Hajer (Department of Biology, University J.E. Purkinje, Ustí nad Labem, Czech Republic), Richard Hoffman (Virginia Museum of Natural History, VMNH, Martinsville, VA, USA), Christian Kropf (Department of Invertebrates, Natural History Museum Bern, Switzerland), Antonio Melic (Zaragoza, Spain), Martín J. Ramírez (Museo Argentino de Ciencias Naturales 'Bernardino Rivadavia', MACN-Ar, Buenos Aires, Argentina), and Robert Raven (Queensland Museum, QM,

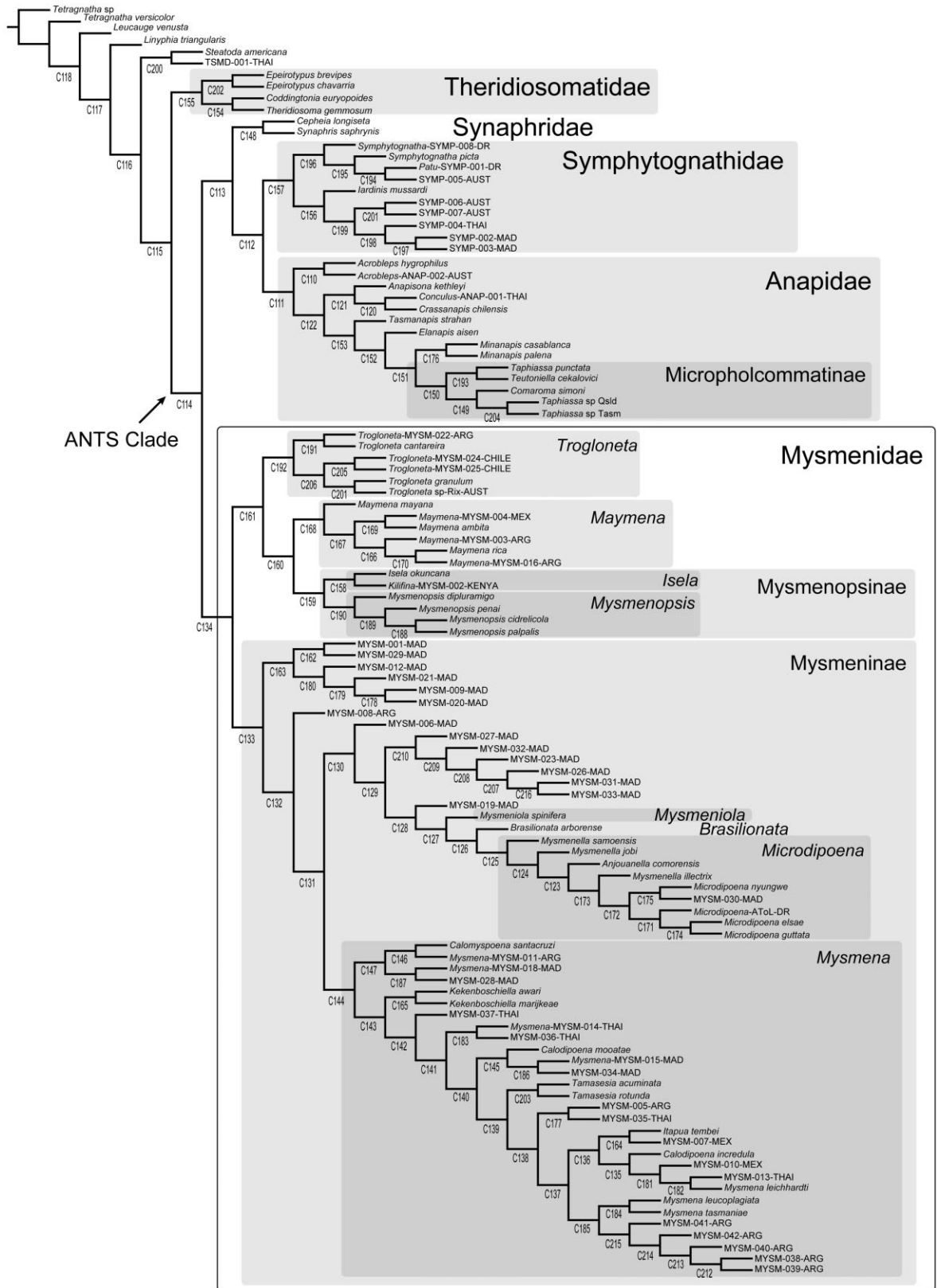


Figure 160. Phylogenetic hypothesis rendered by the complete morphological and molecular data set analysed under equal-weights parsimony using the dynamic homology criterion. Cladogram taken from Lopardo *et al.* (2011: fig. 12). Numbers below each node indicate node numbers. Note that the micropholcommatine *Taphiassa punctata* and the theridiosomatid *Coddingtonia eurypoides* were referred to as *Parapua punctata* and TSM-D-002-THAI (respectively) in Lopardo *et al.* (2011). Family codes used for unidentified species are as follows: ANAP, Anapidae; MYSM, Mysmenidae; SYMP, Symphytognathidae; TSM-D, Theridiosomatidae.

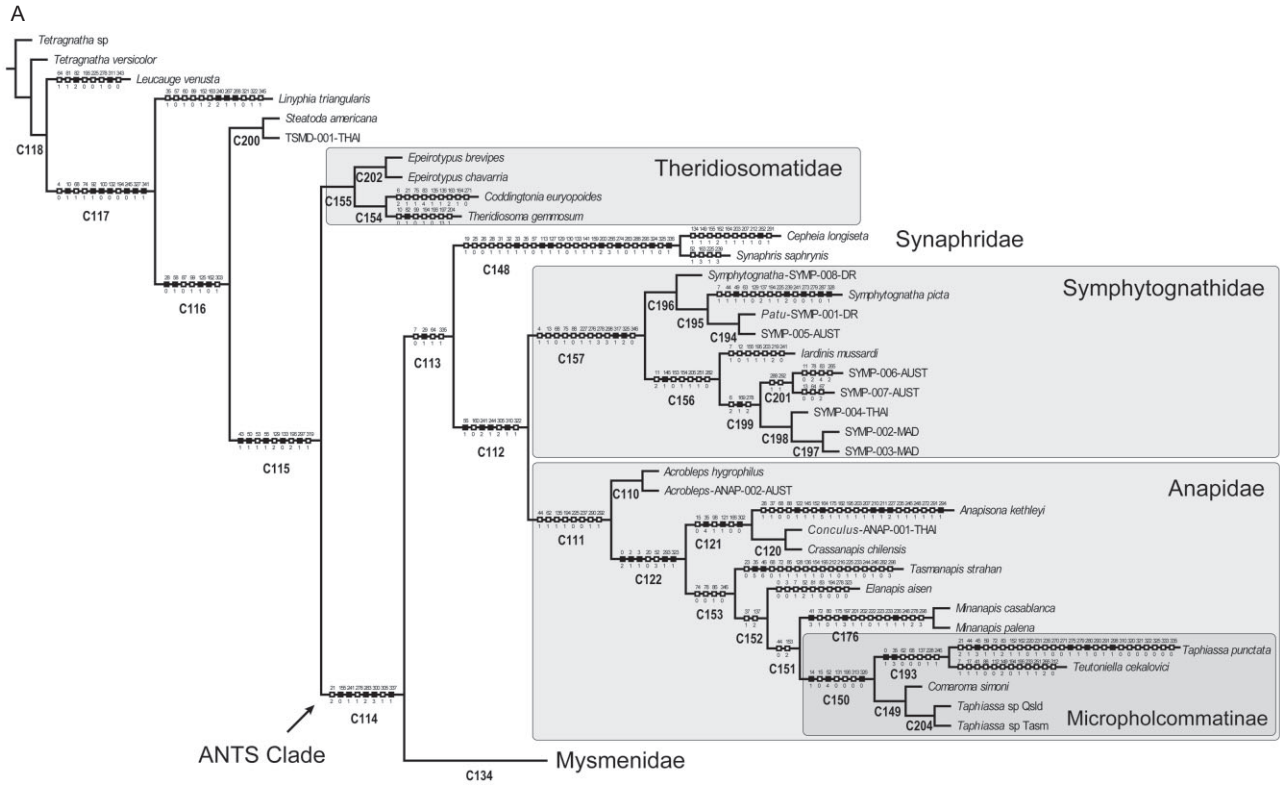
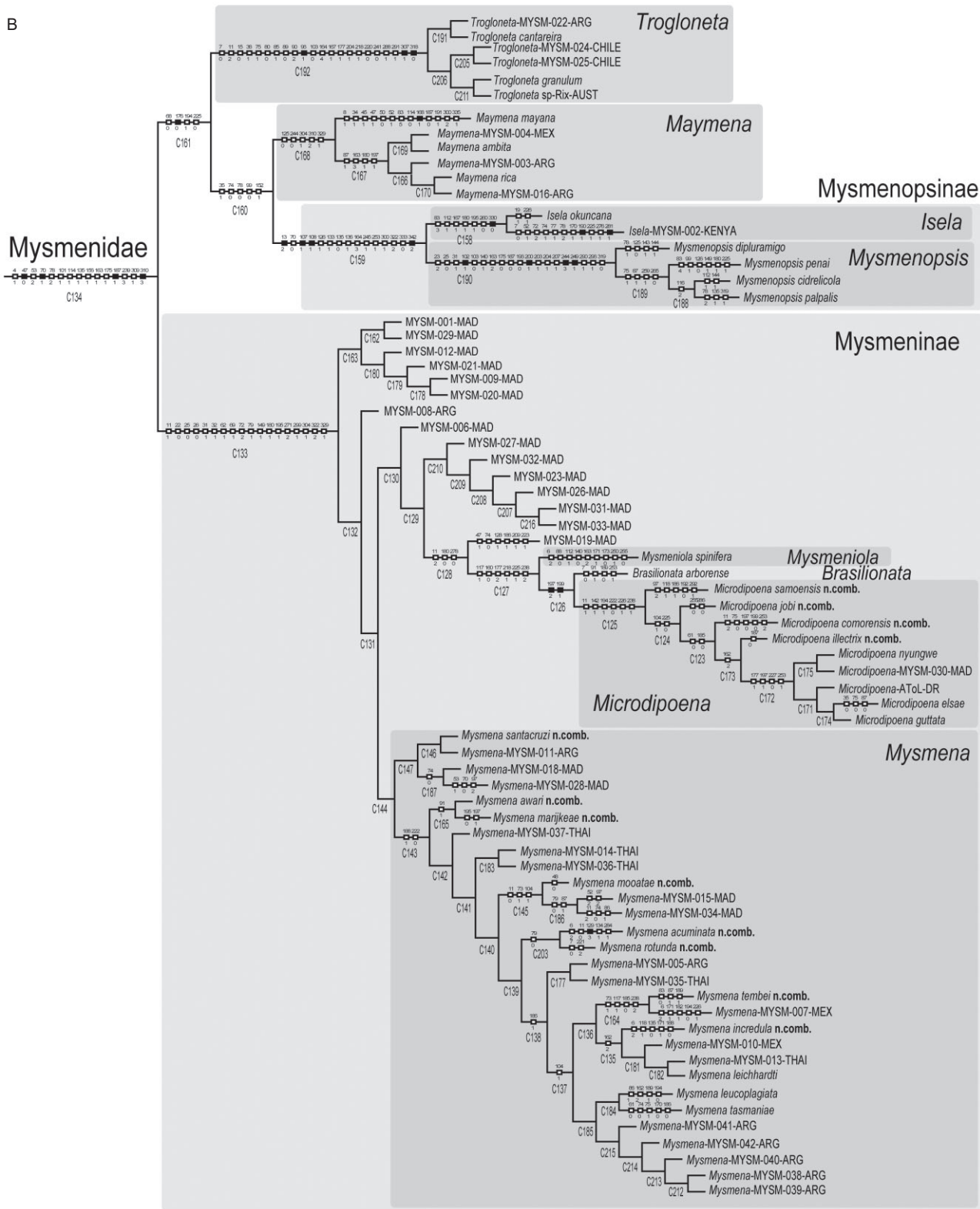


Figure 161. Hypothesis of relationships within Mysmenidae, taken from the results of the combined analysis from Lopardo *et al.* (2011) (see Fig. 160). New taxonomic (i.e. generic) status as proposed in our study is assigned to each representative; new combinations are emphasized in bold. Unambiguous morphological character optimizations are shown for every branch in the tree. Numbers below each node indicate node numbers. Empty and filled boxes represent homoplasious and non-homoplasious transformations, respectively. Major clades representing taxonomic decisions discussed in the text are highlighted in grey boxes.

Brisbane, Australia). Our thanks extend to the following curators and assistants for kindly loaning precious type and non-type material (in alphabetical order): Abigail Blair (Otago Museum, OMNZ, Dunedin, New Zealand), Alistair Ramsdale (Bernice P. Bishop Museum, BPBM, Hawaii, USA), Ansie Dippenaar-Schoeman (Plant Protection Research Institute, PPRI, Queenswood, South Africa), Antonio D. Brescovit (Instituto Butantan, IB, São Paulo, Brazil), Charles Griswold (California Academy of Sciences, CAS, San Francisco, CA, USA), Christine Rollard and Elise-Anne Leguin (Muséum National d'Histoire Naturelle, MNHN, Paris, France), Cristina Scioscia and Martín J. Ramírez (MACN-Ar), Debbie Jennings (Natal Museum, NMSA, Pietermar-

itzburg, South Africa), Diana Silva-Dávila (Museo de Historia Natural, Universidad Nacional Mayor de San Marcos, MUSM, Lima, Perú), Gonzalo Giribet and Laura Leibesperger (Museum of Comparative Zoology, Harvard University, MCZ, Cambridge, MA, USA), Graham Milledge (Australian Museum, AMS, Sydney, Australia), Hieronymus Dastych (Zoologisches Institut und Museum, Universität Hamburg, ZMH, Germany), Janet Beccaloni (The Natural History Museum, BMNH, London, UK), John Marris (Lincoln University, LUNZ, Canterbury, New Zealand), Jonathan Coddington (National Museum of Natural History, Smithsonian Institution, USNM, Washington DC, USA), Jürgen Gruber (Naturhistorisches Museum, NMW, Vienna, Austria),



Downloaded from https://academic.oup.com/iob/advance-article/doi/10.1093/iob/obz017/549763 by guest on 19 April 2024

Figure 161. Continued

Leon Baert (Institut Royal des Sciences Naturelles, IRSN, Brussels, Belgium), Lisa Joy Boutin (Queen Victoria Museum and Art Gallery, QVM, Launceston, Australia), Nikolaj Scharff (Zoological Museum, University of Copenhagen, ZMUC, Denmark), Norman Platnick and Lou Sorkin (American Museum of Natural History, AMNH, New York, USA), Pablo Goloboff (Instituto Miguel Lillo, IML, Tucumán, Argentina), Peter J. Schwendinger (Museum d'Histoire naturelle, MHNG, Geneve, Switzerland), Peter Jäger and Julia Altmann (Natur-Museum und Forschung-Institut, Senckenberg, SMF, Frankfurt am Main, Germany), Phil Sirvid (Museum of New Zealand Te Papa Tongarewa, MONZ, Wellington, New Zealand), Robert Raven (QM), Rowley Snazell (personal collection, RGS, UK), Rudy Jocque (Musée Royal Afrique Centrale, MRAC, Tervuren, Belgium), Seppo Koponen (Zoological Museum, University of Turku, ZMUT, Finland), and Torbjörn Kronstedt (Naturhistoriska Riksmuseet, NRS, Stockholm, Sweden). L.L. immensely thanks Gonzalo Giribet, Martín J. Ramírez, Fernando Álvarez-Padilla, Dimitar S. Dimitrov, Ligia R. Benavides Silva, Matjaž Kuntner, Jeremy A. Miller, Ingi Agnarsson, Anahita Shaya, Anastasia Kondakova, Vanessa Degrassi, Joana Zanol P. Silva, Vinita Gowda, Maria del Rosario Castañeda, Alexandra Herrera Martínez, Claudio D. Gutman, her family, friends, and Peter for their continuous support, encouragement, advice, and help. We are grateful to Gabriele Uhl for her support. Michael G. Rix, associate editor Ingi Agnarsson, and an anonymous reviewer are greatly thanked for their useful comments and critical reading of the article. Funding for this research has been provided by grants from the US National Science Foundation (DEB-0328644, DEB 1144492 and DEB 114417) to G.H. and Gonzalo Giribet, by a Weintraub Fellowship and a Research Enhancement Fund from The George Washington University (to GH), and by a BSF AToL grant (EAR-0228699) to W. Wheeler, J. Coddington, G. Hormiga, L. Prendini, and P. Sierwald.

REFERENCES

- Agnarsson I. 2004.** Morphological phylogeny of cobweb spiders and their relatives (Araneae, Araneoidea, Theridiidae). *Zoological Journal of the Linnean Society* **141**: 447–626.
- Agnarsson I, Coddington J, May-Collado LJ. 2007.** Elongated pedicellate setae: a putative sensory system and synapomorphy of spiders. *Journal of Arachnology* **35**: 411–426.
- Álvarez-Padilla F, Dimitrov D, Giribet G, Hormiga G. 2009.** Phylogenetic relationships of the spider family Tetragnathidae (Araneae, Araneoidea) based on morphological and DNA sequence data. *Cladistics* **25**: 109–146.
- Álvarez-Padilla F, Hormiga G. 2008.** A protocol for digesting internal soft tissues and mounting spiders for scanning electron microscopy. *Journal of Arachnology* **35**: 538–542.
- Baert L. 1982.** Spiders (Araneae) from Papua New Guinea III. Mysmenidae (Symphytognathoidea). *Bulletin of the British Arachnological Society* **5**: 303–308.
- Baert L. 1984a.** Spiders (Araneae) from Papua New Guinea. IV. Ochyroceratidae, Telemidae, Hadrotarsidae and Mysmenidae. *Indo-Malayan Zoology* **2**: 225–244.
- Baert L. 1984b.** Mysmenidae and Hadrotarsidae from the Neotropical Guaraní zoogeographical province (Paraguay and south Brasil) (Araneae). *Revue Suisse De Zoologie* **91**: 603–616.
- Baert L. 1985.** Telemidae, Mysmenidae and Ochyroceratidae from Cameroon (Araneae): scientific report of the Belgian Mount Cameroon Expeditions 1981 and 1983 (no. 13). *Biolog Jaarb Dodonaea* **53**: 44–57.
- Baert L. 1986.** Mysmenidae from the Comoro Islands (Araneae). *Revue de Zoologie Africaine* **100**: 265–267.
- Baert L. 1988.** The Ochyroceratidae and Mysmenidae from Sulawesi (Araneae). *Indo-Malayan Zoology* **5**: 9–22.
- Baert L. 1989.** Mysmenidae from Rwanda (Araneae). *Revue de Zoologie Africaine* **103**: 29–33.
- Baert L. 1990.** Mysmenidae (Araneae) from Peru. *Bulletin de l'Institut Royal des Sciences Naturelles de Belgique Entomologie* **60**: 5–18.
- Baert L, Maelfait J-P. 1983.** Spiders of the Galápagos Islands. I. Mysmenidae (Araneae). *Bulletin of the British Arachnological Society* **6**: 102–108.
- Baert L, Murphy J. 1987.** *Kilifia inquilina*, a new mysmenid spider from Kenya (Araneae, Mysmenidae). *Bulletin of the British Arachnological Society* **7**: 194–196.
- Baert L, Murphy J. 1992.** *Kilifina*, new generic name for *Kilifia*, preoccupied (Araneae, Mysmenidae). *Bulletin of the British Arachnological Society* **9**: 104.
- Banks N. 1895.** A list of the spiders of Long Island; with descriptions of new species. *Journal of the New York Entomological Society* **3**: 76–93.
- Barrows W. 1940.** New and rare spiders from the Great Smoky Mountain National Park region. *Ohio Journal of Science* **40**: 130–138.
- Bertkau P. 1889.** Interessante Tiere aus der Umgebung von Bonn. *Verhandlungen des Naturhistorischen Vereins der Preussischen Rheinlande und Westfalens* **46**: 69–82.
- Bishop S, Crosby C. 1926.** Notes on the spiders of the southeastern United States with descriptions of new species. *Journal of the Elisha Mitchell Scientific Society* **41**: 163–212.
- de Bivort BL, Clouse RM, Giribet G. 2010.** A morphometrics-based phylogeny of the temperate Gondwanan mite harvestmen (Opiliones, Cyphophthalmi, Pettalidae). *Journal of Zoological Systematics and Evolutionary Research* **48**: 294–309.
- Blackledge T, Scharff N, Coddington J, Szüts T, Wenzel J, Hayashi C, Agnarsson I. 2009.** Reconstructing web evolution and spider diversification in the molecular era. *Proceedings of the National Academy of Sciences of the United States of America* **106**: 5229–5234.
- Bond JE, Garrison NL, Hamilton CA, Godwin RL, Hedin M, Agnarsson I. 2014.** Phylogenomics resolves a spider

- backbone phylogeny and rejects a prevailing paradigm for orb web evolution. *Current Biology* **24**: 1765–1771. <http://dx.doi.org/10.1016/j.cub.2014.06.034>.
- Bremer K. 1988.** The limits of amino acid sequence data in angiosperm phylogenetic reconstruction. *Evolution* **42**: 795–803.
- Bremer K. 1994.** Branch support and tree stability. *Cladistics* **10**: 295–304.
- Brescovit A, Lopardo L. 2008.** The first record on the spider genus *Trogloneta* Simon in the southern hemisphere (Araneae, Mysmenidae), with descriptions of three new species from Brazil and remarks on the morphology. *Acta Zoologica (Stockholm)* **89**: 93–106.
- Breuss W. 2001.** Bemerkenswerte Spinnen aus Vorarlberg (Österreich) – I (Arachnida: Araneae: Lycosidae, Theridiidae, Mysmenidae, Gnaphosidae, Salticidae). *Berichte des Naturwissenschaftlich – Medizinischen Vereins in Innsbruck* **88**.
- Brignoli P. 1970.** Contribution à la connaissance des Symphytognathidae paléarctiques (Arachnida, Araneae). *Bulletin du Museum National d'Histoire Naturelle, Paris* **41**: 1403–1420.
- Brignoli P. 1974.** Notes on spiders, mainly cave-dwelling, of southern Mexico and Guatemala (Araneae). *Quaderni dell'Accademia Nazionale dei Lincei* **171**: 195–238.
- Brignoli P. 1978.** Spinnen aus Nepal, IV. Drei neue Symphytognathidae (Arachnida: Araneae). *Senckenbergiana Biologica* **59**: 247–252.
- Brignoli P. 1980.** On few Mysmenidae from the Oriental and Australian regions (Araneae). *Revue Suisse De Zoologie* **87**: 727–738.
- Brignoli P. 1981.** Spiders from the Philippines IV. A new *Ogulnius* and notes on some other Oriental and Japanese Theridiosomatidae (Araneae). *Acta Arachnologica, Tokyo* **30**: 9–19.
- Brignoli P. 1983.** *A catalogue of the Araneae described between 1940 and 1981*. Manchester: Manchester Univ. Press.
- Bryant E. 1940.** Cuban spiders in the Museum of Comparative Zoology. *Bulletin of the Museum of Comparative Zoology, Harvard* **86**: 247–554.
- Carico J. 1977.** A simple dusting device for coating orb webs for field photography. *Bulletin of the British Arachnological Society* **4**: 100.
- Chamberlin RV, Ivie W. 1938.** Araneida from Yucatan. *Publications, Carnegie Institution of Washington* **491**: 123–136.
- Chickering A. 1960.** The female of *Lucarachne beebey* Gertsch (Araneae: Symphytognathidae). *Psyche (Cambridge, Massachusetts)* **67**: 95–97.
- Clerck C. 1757.** *Svenska spindlar, uti sina hufvud-slågter indelte samt under några och sextio särskildte arter beskrefne och med illuminerade figurer uplyste*. Stockholm: Stockholmiae, Literis Laur. Salvii.
- Clouse RM, de Bivort BL, Giribet G. 2009.** A phylogenetic analysis for the South-east Asian mite harvestman family Stylocellidae (Opiliones, Cyphophthalmi) – a combined analysis using morphometric and molecular data. *Invertebrate Systematics* **23**: 515–529.
- Coddington J. 1986a.** The genera of the spider family Theridiosomatidae. *Smithsonian Contributions to Zoology* **422**: 1–96.
- Coddington J. 1986b.** The monophyletic origin of the orb web. In: Shear WA, ed. *Spider webs, behavior and evolution*. Redwood City, CA: Stanford University Press, 319–363.
- Coddington J. 1989.** Spinneret silk spigot morphology: evidence for the monophyly of orbweaving spiders, Cyrtophorinae (Araneae), and the group Theridiidae plus Nesticidae. *Journal of Arachnology* **17**: 71–95.
- Coddington J. 1990.** Ontogeny and homology in the male palpus of orb-weaving spiders and their relatives, with comments on phylogeny (Araneoclauda: Araneoidea, Deinopoidea). *Smithsonian Contributions to Zoology* **496**: 1–52.
- Coddington J, Scharff N. 1994.** Problems with zero-length branches. *Cladistics* **10**: 415–423.
- Comstock JH. 1910.** The palpi of male spiders. *Annals of the Entomological Society of America* **3**: 161–185.
- Coyle F, Meigs T. 1989.** Two new species of kleptoparasitic *Mysmenopsis* (Araneae, Mysmenidae) from Jamaica. *Journal of Arachnology* **17**: 59–70.
- Dahl F. 1901.** Nachtrag zur Uebersicht der Zoropsiden. *Sitzungsberichte der Gesellschaft Naturforschender Freunde zu Berlin* **1901**: 244–255.
- Davies V. 1985.** Araneomorphae (in part). *Zoological Catalogue of Australia* **3**: 49–125.
- Dimitrov D, Benavides L, Giribet G, Arnedo MA, Griswold CE, Scharff N, Hormiga G. 2013.** Squeezing the last drops of the lemon: molecular phylogeny of Orbiculariae (Araneae). In: *19th International Congress of Arachnology, Abstract Book*. Taiwan: Kenting National Park.
- Dimitrov D, Lopardo L, Giribet G, Arnedo MA, Álvarez-Padilla F, Hormiga G. 2012.** Tangled in a sparse spider web: single origin of orb weavers and their spinning work unravelled by denser taxonomic sampling. *Proceeding of the Royal Society B* **279**: 1341–1350.
- Dingerkus G, Uhler L. 1977.** Enzyme clearing of alcian blue stained whole small vertebrates for demonstration of cartilage. *Stain Technology* **52**: 229–232.
- Dippenaar-Schoeman A, Jocqué R. 1997.** Family Zodariidae. In: *African spiders: an identification manual*. (Handbook, PPRI). Pretoria. (9): 392p.
- Dunlop JA, Penney D, Jekel D. 2014.** A summary list of fossil spiders and their relatives. In: Platnick NI, ed. *The world spider catalog, version 14.5*. New York: American Museum of Natural History, 1–75. Available at: <http://research.amnh.org/entomology/spiders/catalog/index.html>
- Eberhard W. 1976.** Photography of orb webs in the field. *Bulletin of the British Arachnological Society* **3**: 200–204.
- Eberhard W. 1987.** Orb webs and construction behavior in Anapidae, Symphytognathidae, and Mysmenidae. *Journal of Arachnology* **14**: 339–356.
- Eberhard W, Platnick NI, Schuh R. 1993.** Natural history and systematics of arthropod symbionts (Araneae; Hemiptera; Diptera) inhabiting webs of the spider *Tengella radiata* (Araneae, Tengellidae). *American Museum Novitates* **3065**: 1–17.

- Emerton JH. 1882.** New England spiders of the family Theridiidae. *Transactions of the Connecticut Academy of Arts and Sciences* **6**: 1–86.
- Fage L. 1931.** Araneae, 5e série, précédée d'un essai sur l'évolution souterraine et son déterminisme. *Biospeologica (expér; LAZ)* **71**: 91–291.
- Farris J. 1990.** Phenetics in camouflage. *Cladistics* **6**: 91–100.
- Farris J. 1997.** The future of phylogeny reconstruction. *Zoologica Scripta* **26**: 303–311.
- Farris J, Albert V, Källersjö M, Lipscomb D, Kluge A. 1996.** Parsimony jackknifing outperforms neighbor-joining. *Cladistics* **12**: 99–124.
- Felsenstein J. 1985.** Confidence limits on phylogenies: an approach using the bootstrap. *Evolution* **39**: 783–791.
- Fernández R, Hormiga G, Giribet G. 2014.** Phylogenomic analysis of spiders reveals nonmonophyly of orb weavers. *Current Biology* **24**: 1772–1777. <http://dx.doi.org/10.1016/j.cub.2014.06.035>.
- Fitch WM. 1971.** Toward defining the course of evolution: minimum change for a specific tree topology. *Systematic Zoology* **20**: 406–416.
- Forster R. 1959.** The spiders of the family Symphytognathidae. *Transactions of the Royal Society of New Zealand* **86**: 269–329.
- Forster R. 1977.** Fam. Symphytognathidae. In: *La faune terrestre de l'île de Saïte-Hélène IV. Annales du Musée Royal de l'Afrique Centrale (Zoologique, Sn)* **220**: 129–131.
- Forster R. 1980.** Evolution of the tarsal organ, the respiratory system, and the female genitalia in spiders. In: Gruber J, ed. *Proceedings of the 8th International Congress of Arachnology*. Vienna: Egermann H, 269–284.
- Forster R, Platnick NI. 1977.** A review of the spider family Symphytognathidae (Arachnida, Araneae). *American Museum Novitates* **2619**: 1–29.
- Forster R, Platnick NI. 1984.** A review of the archaeid spiders and their relatives, with notes on the limits of the superfamily Palpimanoidea (Arachnida, Araneae). *Bulletin of the American Museum of Natural History* **178**: 1–106.
- Gertsch WJ. 1941.** Report on some arachnids from Barro Colorado Island, Canal Zone. *American Museum Novitates* **1146**: 1–14.
- Gertsch W. 1960a.** Descriptions of American spiders of the family Symphytognathidae. *American Museum Novitates* **1981**: 1–40.
- Gertsch W. 1960b.** The *fulva* group of the spider genus *Steatoda* (Araneae, Theridiidae). *American Museum Novitates* **1982**: 1–48.
- Gertsch W. 1971.** A report on some Mexican cave spiders. *Bulletin of the Association for Mexican Cave Studies* **4**: 47–111.
- Gertsch W, Davis L. 1936.** New spiders from Texas. *American Museum Novitates* **881**: 1–21.
- Giribet G. 2003.** Stability in phylogenetic formulations and its relationship to nodal support. *Systematic Biology* **42**: 554–564.
- Giribet G, Edgecombe G. 2006.** Conflict between datasets and phylogeny of centipedes: an analysis based on seven genes and morphology. *Proceedings of the Royal Society B* **273**: 531–538.
- Goloboff PA. 1993.** Estimating character weights during tree search. *Cladistics* **9**: 83–91.
- Goloboff PA, Farris J. 2001.** Methods for quick consensus estimation. *Cladistics* **17**: S26–S34.
- Goloboff PA, Farris J, Källersjö M, Oxelman B, Ramírez MJ, Szumik C. 2003a.** Improvements to resampling measures of group support. *Cladistics* **19**: 324–332.
- Goloboff PA, Farris J, Nixon K. 2003b.** T.N.T.: tree analysis using new technology. Version 1.1 (August, 2008). Willi Hennig Society Edition. Available at: <http://www.zmuc.dk/public/phylogeny>
- Goloboff PA, Farris J, Nixon K. 2008.** TNT, a free program for phylogenetic analysis. *Cladistics* **24**: 774–786.
- Goloboff PA, Mattoni C, Quinteros A. 2006.** Continuous characters analyzed as such. *Cladistics* **22**: 589–601.
- González-José R, Escapa I, Neves W, Cúneo R, Pucciarelli H. 2008.** Cladistic analysis of continuous modularized traits provides phylogenetic signals in *Homo* evolution. *Nature* **453**: 775–778.
- Griswold CE. 1985.** *Isele okuncana*, a new genus and species of kleptoparasitic spider from southern Africa (Araneae: Mysmenidae). *Annals of the Natal Museum* **27**: 207–217.
- Griswold CE. 2001.** A monograph of the living world genera and Afrotropical species of cyatholipid spiders (Araneae, Orbicularia, Araneioidea, Cyatholipidae). *Memoirs of the California Academy of Sciences* **26**: 1–251.
- Griswold CE, Coddington J, Hormiga G, Scharff N. 1998.** Phylogeny of the orb-web building spiders (Araneae, Orbicularia: Deinopoidea, Araneioidea). *Zoological Journal of the Linnean Society* **123**: 1–99.
- Griswold CE, Ramírez MJ, Coddington J, Platnick NI. 2005.** Atlas of phylogenetic data for entelegyne spiders (Araneae, Araneomorphae, Entelegynae), with comments on their phylogeny. *Proceedings of the California Academy of Sciences 4th Series* (56, Suppl. II): 1–324.
- Griswold CE, Yan H-M. 2003.** On the Egg-guarding Behavior of a Chinese Symphytognathid Spider of the Genus *Patu* Marples, 1951 (Araneae, Araneioidea, Symphytognathidae). *Proceedings of the California Academy of Sciences* **54**: 356–360.
- Gruia M. 1977.** Sur quelques Theridiidae et Symphytognathidae (Aranea) recueillis par la deuxième expédition biospéologique cubano-roumaine à Cuba. *Rés Expédition Biospéologique Cubano-Roumaine, Cuba* **2**: 159–163.
- Hajer J. 2000.** Web of *Trogloneta granulum* Simon (Araneae, Mysmenidae). *Bulletin of the British Arachnological Society* **11**: 333–338.
- Hajer J. 2002.** The spinning activity of the spider *Trogloneta granulum* Simon, 1922 (Araneae, Mysmenidae). *Acta Universitatis Purkynianae Studia Biologica* **VI**: 21–38.
- Hajer J, Reháková D. 2003.** Spinning activity of the spider *Trogloneta granulum* (Araneae, Mysmenidae): web, cocoon, cocoon handling behaviour, draglines and attachment discs. *Zoology* **106**: 223–231.

- Harris R. 1979.** A glossary of surface sculpturing. *Occasional Papers in Entomology* **28**: 1–31.
- Harvey MS. 1992.** A new species of *Symphytognatha* Hickman (Araneae: Symphytognathidae) from Western Australia. *Records of the Western Australian Museum* **15**: 685–689.
- Heimer S, Nentwig W. 1991.** *Spinnen Mitteleuropas: Ein Bestimmungsbuch*. Berlin: Verlag Paul Parey.
- Hickman VV. 1931.** A new family of spiders. *Proceedings of the Zoological Society of London (B)* **1931**: 1321–1328.
- Hickman VV. 1944.** On some new Australian Apneumonomorphae with notes on their respiratory system. *Papers and Proceedings of the Royal Society of Tasmania* **1943**: 179–195.
- Hickman VV. 1945.** A new group of apneumone spiders. *Transactions of the Connecticut Academy of Arts and Sciences* **36**: 135–157.
- Hickman V. 1979.** Some Tasmanian spiders of the families Oonopidae, Anapidae and Mysmenidae. *Papers and Proceedings of the Royal Society of Tasmania* **113**: 53–79.
- Hormiga G. 1994.** Cladistics and the comparative morphology of linyphiid spiders and their relatives (Araneae, Araneoidea, Linyphiidae). *Zoological Journal of the Linnean Society* **111**: 1–71.
- Hormiga G. 1999.** Cephalothoracic sulci in linyphiid spiders (Araneae, Araneoidea, Linyphiidae). *Journal of Arachnology* **27**: 94–102.
- Hormiga G. 2000.** Higher level phylogenetics of erigonine spiders (Araneae, Linyphiidae, Erigoninae). *Smithsonian Contributions to Zoology* **609**: 1–160.
- Hormiga G. 2002.** *Orsonwelles*, a new genus of giant linyphiid spiders (Araneae) from the Hawaiian Islands. *Invertebrate Systematics* **16**: 369–448.
- Hormiga G, Álvarez-Padilla F, Benjamin S. 2007.** First records of extant Hispaniolan spiders of the families Mysmenidae, Symphytognathidae and Ochyroceratidae (Araneae), including a new species of *Ochyrocera*. *American Museum Novitates* **3577**: 1–21.
- Hormiga G, Eberhard W, Coddington J. 1995.** Web-construction behaviour in Australian *Phonognatha* and the phylogeny of nephiline and tetragnathid spiders (Araneae: Tetragnathidae). *Australian Journal of Zoology* **43**: 313–364.
- Hormiga G, Griswold CE. 2014.** Systematics, Phylogeny and Evolution of Orb-weaving Spiders. *Annual Review of Entomology* **59**: 487–512.
- Hormiga G, Scharff N, Coddington J. 2000.** The Phylogenetic Basis of Sexual Size Dimorphism in Orb-Weaving Spiders (Araneae, Orbiculariae). *Systematic Biology* **49**: 435–462.
- Humphries C. 2002.** Homology, characters and continuous variables. In: MacLeod N, Forey P, eds. *Morphology, shape and phylogeny*. London: Taylor and Francis, 8–26.
- Jocqué R. 1987.** Descriptions of new genera and species of African Zodariinae with a revision of the genus *Heradida* (Araneae, Zodariidae). *Revue de Zoologie Africaine* **101**: 143–163.
- Jocqué R. 1991.** A generic revision of the spider family Zodariidae (Araneae). *Bulletin of the American Museum of Natural History* **201**: 1–160.
- Jocqué R, Dippenaar-Schoeman A. 2006.** *Spider families of the world*. Tervuren: Musée Royal de l'Afrique Central.
- Kasal P. 1982.** *Theridion antusi* sp.n. and *Mysmena jobi* from Czechoslovakia (Araneida, Theridiidae and Symphytognathidae). *Acta entomologica Bohemoslovaca* **79**: 73–76.
- Kaston B. 1978.** *How to know the spiders, 3rd edn*. Dubuque, IA: Brown WC.
- Koch CL. 1838.** *Die Arachniden*. Nürnberg In: der C.H. Zeh'schen Buchhandlung, Vierter Band, 109–144, Funfter Band, 1–124.
- Koch L. 1877.** Verzeichniss der bei Nürnberg bis jetzt beobachteten Arachniden (mit Ausschluss der Ixodiden und Acariden) und Beschreibungen von neuen, hier vorkommenden Arten. *Abhandlungen der Naturhistorischen Gesellschaft zu Nürnberg* **6**: 113–198.
- Kraus O. 1955.** Spinnen aus El Salvador (Arachnoidea, Araneae). *Abhandlungen der senckenbergisch-naturforschenden Gesellschaft* **493**: 1–112.
- Kraus O. 1967.** Zur Spinnenfauna Deutschlands, II. *Mysmena jobi* n. sp, eine Symphytognathide in Mitteleuropa (Arachnida: Araneae: Symphytognathidae). *Senckenbergiana Biologica* **48**: 387–399.
- Kropf C. 1990.** Web construction and prey capture of *Comaroma simoni* Bertkau (Araneae). *Acta Zoologica Fennica* **190**: 229–233.
- Labarque FM, Griswold CE. 2014.** New ray spiders from Southeast Asia: the new Philippine genus *Tagalogonia* gen. nov. and continental genus *Coddingtonia* Miller, Griswold and Yin, 2009 (Araneae: Theridiosomatidae), with comments on their intergeneric relationships. California Academy of Sciences Special Publication, The Coral Triangle: The 2011 Hearst Philippine Biodiversity Expedition, 406–26.
- Lee Y, Yoo J, Lee D, Kim J. 2004.** Ground dwelling spiders. *Korean Arachnology* **20**: 97–115.
- Levi H. 1956.** The spider genus *Mysmena* in the Americas (Araneae, Theridiidae). *American Museum Novitates* **1801**: 1–13.
- Levi H. 1961.** Evolutionary trends in the development of palpal sclerites in the spider family theridiidae. *Journal of Morphology* **108**: 1–9.
- Levi H. 1967.** Adaptations of respiratory systems of spiders. *Evolution* **21**: 571–583.
- Levi H. 1972.** Taxonomic-nomenclatural notes on misplaced theridiid spiders (Araneae: Theridiidae), with observations on *Anelosimus*. *Transactions of the American Microscopical Society* **91**: 533–538.
- Levi H, Kirber W. 1976.** On the evolution of tracheae in Arachnids. *Bulletin of the British Arachnological Society* **3**: 187–188.
- Levi H, Levi L. 1962.** The genera of the spider family Theridiidae. *Bulletin of the Museum of Comparative Zoology, Harvard* **127**: 1–71.
- Lin Y, Li S. 2008.** Mysmenid spiders of China (Araneae: Mysmenidae). *Annales Zoologici (Warszawa)* **58**: 487–520.
- Linnaeus C. 1758.** *Systema naturae per regna tria naturae, secundum classes, ordines, genera, species cum characteribus*

- differentiis, synonymis, locis. Editio decima, reformata.* Holmiae: Impensis Direct. Laurentii Salvii, 821 (Araneae, 619–624).
- Loksa I. 1973.** On the morphology and systematical position of *Mysmena leucoplagiata* (Simon, 1879) (Araneae: Symphytognathidae). *Acta Zoologica Academiae Scientiarum Hungaricae* **19**: 283–287.
- Lopardo L. 2005.** Phylogenetic revision of the spider genus *Negayan* (Araneae, Anyphaenidae, Amaurobioidinae). *Zoologica Scripta* **34**: 245–277.
- Lopardo L, Coddington J. 2005.** Chapter 40: Mysmenidae. In: Ubick D, Cushing P, Paquin P, eds. *Spiders of North America: an identification manual*. Poughkeepsie, NY: American Arachnology Society, 175–177.
- Lopardo L, Dupérré N, Paquin P. 2008.** Expanding horizons . . . The first report of the genus *Mysmena* (Araneae, Mysmenidae) from continental North America, with the description of a new species. *Zootaxa* **1718**: 36–44.
- Lopardo L, Giribet G, Hormiga G. 2011.** Morphology to the rescue: molecular data and the signal of morphological characters in combined phylogenetic analyses – a case study from mysmenid spiders (Araneae, Mysmenidae), with comments on the evolution of web architecture. *Cladistics* **27**: 278–330.
- Lopardo L, Hormiga G. 2007.** On the Synaphrid Spider *Cepheia longiseta* (Simon 1881) (Araneae, Synaphridae). *American Museum Novitates* **3575**: 1–18.
- Lopardo L, Hormiga G. 2008.** Phylogenetic placement of the Tasmanian spider *Acrobleps hygrophilus* (Araneae, Anapidae) with comments on the evolution of the capture web in Araneoidea. *Cladistics* **24**: 1–33.
- Lopardo L, Hormiga G, Melic A. 2007.** Spinneret spigot morphology in synaphrid spiders (Araneae, Synaphridae), with comments on the systematics of the family and description of a new species of *Synaphris* Simon 1894 from Spain. *American Museum Novitates* **3556**: 1–26.
- Lopardo L, Michalik P. 2013.** First description of a mysmenid spider species from mainland Australia and new data for *Mysmena tasmaniae* Hickman 1979 (Araneae, Mysmenidae). *Memoirs of the Queensland Museum/Nature* **58**: 381–396.
- Maddison WP. 1993.** Missing data versus missing characters in phylogenetic analysis. *Systematic Biology* **42**: 576–581.
- Maddison WP, Maddison D. 2007.** Mesquite: a modular system for evolutionary analysis. Version 2.01 (build j28). Available at: <http://mesquiteproject.org>
- Marples B. 1955.** Spiders from western Samoa. *Journal of the Linnean Society of London (Zoology)* **42**: 453–504.
- Marusik Y, Gnelitsa V, Kovblyuk M. 2005.** A new species of *Synaphris* (Araneae, Synaphridae) from Ukraine. *Bulletin of the British Arachnological Society* **13**: 125–130.
- Miller F. 1970.** Spinnenarten der Unterfamilie Micryphantinae und der Familie Theridiidae aus Angola. *Publicações Culturais da Companhia de Diamantes de Angola* **82**: 75–166.
- Miller JA. 2007.** Synaphridae of Madagascar (Araneae: Araneoidea): a new family record for the Afrotropical region. *Proceedings of the California Academy of Sciences* **58**: 21–48.
- Miller JA, Carmichael A, Ramírez MJ, Spagna J, Haddad CR, Rezáč M, Johannesen J, Král J, Wang X-P, Griswold CE. 2010.** Phylogeny of entelegyne spiders: affinities of the family Penestomidae (NEW RANK), generic phylogeny of Eresidae, and asymmetric rates of change in spinning organ evolution (Araneae, Araneoidea, Entelegynae). *Molecular Phylogenetics and Evolution* **55**: 786–804.
- Miller JA, Griswold CE, Yin C. 2009.** The symphytognathoid spiders of the Gaoligongshan, Yunnan, China (Araneae: Araneoidea): systematics and diversity of micro-orbweavers. *ZooKeys* **11**: 9–195.
- Millidge AF. 1984.** The taxonomy of the Linyphiidae, based chiefly on the epigynal and tracheal characters (Araneae: Linyphiidae). *Bulletin of the British Arachnological Society* **6**: 229–267.
- Müller H-G. 1987.** Spiders from Colombia V. A new *Mysmenopsis* from the Ciénaga Grande de Santa Marta, northern Colombia (Araneida: Mysmenidae). *Bulletin of the British Arachnological Society* **7**: 185.
- Namkung J. 2002.** *The spiders of Korea, 1st edn.* Seoul: Kyo-Hak Publishing Co.
- Namkung J. 2003.** *The spiders of Korea, 2nd edn.* Seoul: Kyo-Hak Publishing Co.
- Namkung J, Lee K. 1987.** A new record spider of the genus *Mysmenella* Brignoli, 1980 (Araneae: Mysmenidae) from Korea. *Korean Arachnology* **3**: 45–49.
- Nixon K. 1999a.** The parsimony ratchet, a new method for rapid parsimony analysis. *Cladistics* **15**: 407–414.
- Nixon K. 1999b.** WINCLADA, program and documentation. Available at: <http://www.cladistics.com>
- Ono H. 2007.** Eight new species of the families Hahniidae, Theridiidae, Linyphiidae and Anapidae (Arachida, Araneae) from Japan. *Bulletin of the National Science Museum, Tokyo* **33**: 153–173.
- Ono H, Chang Y, Tso I. 2007.** Three new spiders of the families Theridiidae and Anapidae (Araneae) from southern Taiwan. *Memoirs of the National Science Museum, Tokyo* **44**: 71–82.
- Penney D. 2000.** Miocene spiders in Dominican amber (Oonopidae, Mysmenidae). *Palaeontology* **43**: 343–357.
- Peters H. 1982.** Wie spinnen der Familie Uloboridae ihre beute einspinnen und verzehren. *Verhandlungen des Naturwissenschaftlichen Vereins in Hamburg* **25**: 147–167.
- Petrunkévitch A. 1928.** Systema Araneorum. *Transactions of the Connecticut Academy of Arts and Sciences* **29**: 1–270.
- Petrunkévitch A. 1971.** Chiapas amber spiders, II. *University of California Publications in Entomology* **63**: 1–44.
- Platnick NI. 2014.** The world spider catalog, version 14.5. American Museum of Natural History. Available at: <http://research.amnh.org/entomology/spiders/catalog/index.html>
- Platnick NI, Coddington J, Forster R, Griswold CE. 1991.** Spinneret Morphology and the Phylogeny of Haplogyne Spiders (Araneae, Araneomorphae). *American Museum Novitates* **3016**: 1–73.
- Platnick NI, Forster R. 1986.** On *Teutoniella*, an American Genus of the Spider Family Micropholcommatidae (Araneae, Palpimanoidea). *American Museum Novitates* **2854**: 1–23.

- Platnick NI, Forster R. 1987.** On the first American spiders of the subfamily Sternodinae (Araneae, Malkaridae). *American Museum Novitates* **2894**: 1–12.
- Platnick NI, Forster R. 1989.** A revision of the temperate South American and Australasian spiders of the family Anapidae (Araneae, Araneoidea). *Bulletin of the American Museum of Natural History* **190**: 1–139.
- Platnick NI, Shadab M. 1978.** A review of the spider genus *Mysmenopsis* (Araneae, Mysmenidae). *American Museum Novitates* **2661**: 1–22.
- Platnick NI, Shadab MU. 1979.** A review of the spider genera *Anapisona* and *Pseudanapis* (Araneae, Anapidae). *American Museum Novitates* **2672**: 1–20.
- Prendini L. 2001.** Species or supraspecific taxa as terminals in cladistic analysis? Groundplans versus exemplars revisited. *Systematic Biology* **50**: 290–300.
- Purcell W. 1909.** Development and origin of respiratory organs in Araneae. *Quarterly Journal of Microscopical Science* **54**: 1–110.
- Rae T. 1998.** The logical basis for the use of continuous characters in phylogenetic systematics. *Cladistics* **14**: 221–228.
- Ramírez MJ. 2000.** Respiratory system morphology and the phylogeny of haplogyne spiders (Araneae, Araneomorphae). *Journal of Arachnology* **28**: 149–157.
- Ramírez MJ, Lopardo L, Platnick NI. 2004.** Notes on Chilean anapids and their webs (Araneae, Anapidae). *American Museum Novitates* **3428**: 1–13.
- Rix MG. 2008.** A new species of *Micropholcomma* (Araneae: Araneoidea: Micropholcommatidae) from Western Australia. *Records of the Western Australian Museum* **24**: 343–348.
- Rix MG, Harvey MS. 2010.** The spider family Micropholcommatidae (Arachnida, Araneae, Araneoidea): a relimitation and revision at the generic level. *ZooKeys* **36**: 1–321.
- Rix MG, Harvey MS, Roberts J. 2008.** Molecular phylogenetics of the spider family Micropholcommatidae (Arachnida: Araneae) using nuclear rRNA genes (18S and 28S). *Molecular Phylogenetics and Evolution* **46**: 1031–1048.
- Rix MG, Harvey MS, Roberts JD. 2010.** A revision of the tricellin spider genus *Raveniella* (Araneae: Araneoidea: Micropholcommatidae): exploring patterns of phylogeny and biogeography in an Australian biodiversity hotspot. *Invertebrate Systematics* **24**: 209–237.
- Roberts M. 1978.** Contributions à l'étude de la faune terrestre des îles granitiques de l'archipel des Séchelles (Mission PL G Benoit – J J Van Mol 1972) Theridiidae, Mysmenidae and gen *Theridiosoma* (Araneidae) (Araneae). *Revue de Zoologie Africaine* **92**: 902–939.
- Saaristo M. 1978.** Spiders (Arachnida, Araneae) from the Seychelle islands, with notes on taxonomy. *Annales Zoologici Fennici* **15**: 99–126.
- Scharff N, Coddington J. 1997.** A phylogenetic analysis of the orb-weaving spider family Araneidae (Arachnida, Araneae). *Zoological Journal of the Linnean Society* **120**: 355–434.
- Schütt K. 2000.** The limits of the Araneoidea (Arachnida: Araneae). *Australian Journal of Zoology* **48**: 135–153.
- Schütt K. 2002.** The limits and phylogeny of the Araneoidea (Arachnida, Araneae). Unpublished D. Phil. Thesis, University of Berlin.
- Schütt K. 2003.** Phylogeny of Symphytognathidae s.l. (Araneae, Araneoidea). *Zoologica Scripta* **32**: 129–151.
- Shinkai E. 1977.** Spiders of Tokyo III. *Acta Arachnologica, Tokyo* **27**: 321–336.
- Sierwald P. 1989.** Morphology and Ontogeny of Female Copulatory Organs in American Pisauridae, with Special Reference to Homologous Features (Arachnida: Araneae). *Smithsonian Contributions to Zoology* **484**: 1–24.
- Simon E. 1879.** Arachnides nouveau de France, d'Espagne et d'Algérie. Premier mémoire. *Bulletin de la Société Zoologique de France* **4**: 251–263.
- Simon E. 1880.** Matériaux pour servir à une faun arachnologique de la Nouvelle Calédonie. *Annales de la Société Entomologique de Belgique* **23**(C.R.): 164–175.
- Simon E. 1881.** Les arachnides de France. *Paris* **5**: 1–180.
- Simon E. 1893.** Histoire naturelle des araignées. *Paris* **1**: 257–488.
- Simon E. 1894.** *Histoire naturelle des araignées*. Paris. 1: 489–760.
- Simon E. 1895a.** *Histoire naturelle des araignées*. Paris. 1: 761–1084.
- Simon E. 1895b.** Etudes arachnologiques. 26e XLI Descriptions d'espèces et de genres nouveaux de l'ordre des Araneae. *Annales de la Société Entomologique de France* **64**: 131–160.
- Simon E. 1897.** On the spiders of the island of St Vincent, III. *Proceedings of the Zoological Society of London* **1897**: 860–890.
- Simon E. 1899.** Contribution à la faune de Sumatra. Arachnides recueillis par M J L Weyers, à Sumatra (Deuxième mémoire). *Annales de la Société Entomologique de Belgique* **43**: 78–125.
- Simon E. 1903.** Descriptions d'arachnides nouveaux. *Annales de la Société Entomologique de Belgique* **47**: 21–39.
- Simon E. 1922.** Description de deux arachnides cavernicoles du midi de la France. *Bulletin de la Société Entomologique de France* **1922**: 199–200.
- Simon E. 1926.** *Les arachnides de France. Synopsis générale et catalogue des espèces françaises de l'ordre des Araneae; 2e partie*. Paris. 6: 309–532.
- Snazell R. 1986.** A new *Mysmena* (Araneae: Mysmenidae) from Spain. *Bulletin of the British Arachnological Society* **7**: 62–64.
- Strong E, Lipscomb D. 1999.** Character coding and inapplicable data. *Cladistics* **15**: 363–371.
- Sundevall CJ. 1833.** *Conspectus Arachnidum. Londini Gothorum*, 1–39.
- Thaler K. 1975.** *Trogloneta granulum* Simon, eine weitere Reliktart der Nordostalpen (Arachnida, Aranei, 'Symphytognathidae'). *Revue Suisse De Zoologie* **82**: 283–291.
- Thaler K. 1995.** *Mysmeniola spinifera* n.gen. n.sp., eine merkwürdige Kleinspinne aus Venezuela (Arachnida, Araneae: Mysmenidae). *Mitteilungen der Schweizerischen Entomologischen Gesellschaft* **68**: 429–433.

- Thaler K, Noflatscher M-T. 1990.** Neue und bemerkenswerte Spinnenfunde in Südtirol (Arachnida: Aranei). *Veröffentlichungen des Museum Ferdinandeum in Innsbruck* **69**: 169–190.
- Thiele K. 1993.** The Holy Grail of the perfect character: the cladistic treatment of morphometric data. *Cladistics* **9**: 275–304.
- Trotta A. 2005.** Introduzione al ragni italiani (Arachnida Araneae). *Memorie della Società Entomologica Italiana* **83**: 3–178.
- Uhl G. 2002.** Female genital morphology and sperm priority patterns in spiders (Araneae). In: Toft S, Scharff N, eds. *European arachnology 2000*. Aarhus: Aarhus University Press, 145–156.
- Walckenaer CA. 1841.** *Histoire naturelle des Insects. Aptères*. Paris **2**: 1–549.
- Wheeler W. 1995.** Sequence alignment, parameter sensitivity, and the phylogenetic analysis of molecular data. *Systematic Biology* **44**: 321–331.
- Wiehle H. 1963.** Über *Nesticus borutzkyi* Reimoser (Arach., Araneae). *Senckenbergiana Biologica* **44**: 431–435.
- Wiehle H. 1967.** Meta, -eine semientelegyne Gattung der Araneae (Arach.). *Senckenbergiana Biologica* **48**: 183–196.
- Wiens J. 2001.** Character analysis in morphological phylogenetics: problems and solutions. *Systematic Biology* **50**: 689–699.
- Wood HM, Griswold CE, Gillespie RG. 2012.** Phylogenetic placement of pelican spiders (Archaeidae, Araneae), with insight into evolution of the ‘neck’ and predatory behaviors of the superfamily Palpimanoidea. *Cladistics* **28**: 598–626.
- Wood HM, Matzke NJ, Gillespie RG, Griswold CE. 2013.** Treating fossils as terminal taxa in divergence time estimation reveals ancient vicariance patterns in the palpimanoid spiders. *Systematic Biology* **62**: 264–284.
- Wunderlich J. 1978.** Zu Taxonomie und Synonymie der Taxa Hadrotarsidae, *Lucarachne* Bryant 1940 und *Flegia* CL Koch & Berendt 1854 (Arachnida: Araneida: Theridiidae). *Zoologische Beiträge* **24**: 25–31.
- Wunderlich J. 1980a.** Sternal-organe der Theridiosomatidae – eine bisher übersehene Autapomorphie (Arachnida: Araneae). *Verhandlungen des Naturwissenschaftlichen Vereins in Hamburg* **23**: 255–257.
- Wunderlich J. 1980b.** Über europäische Symphytognathidae (Arach: Araneae). *Verhandlungen des Naturwissenschaftlichen Vereins in Hamburg* **23**: 259–273.
- Wunderlich J. 1986.** Die Beziehungen fossiler und rezenter Radnetzspinnen-Verwandter (überfamilie Araneoidea. In: Meyer Q, ed. *Spinnenfauna gestern und heute: Fossile Spinnen in Bernstein und ihre heute lebenden Verwandten*. Wiesbaden: Quelle & Meyer, 93–135.
- Wunderlich J. 1987.** *Die Spinnen der Kanarischen Inseln und Madeiras: adaptive radiation, biogeographie, revisionen und neubeschreibungen*. Langen: Verlag T.
- Wunderlich J. 1995.** Drei bisher unbekannte Arten und Gattungen der Familie Anapidae (s.l.) aus Süd-Afrika, Brasilien und Malaysia (Arachnida: Araneae). *Beiträge zur Araneologie* **4**: 543–551.
- Wunderlich J. 1998.** Beschreibung der ersten fossilen Spinnen der Unterfamilien Mysmeninae (Anapidae) und Erigoninae (Linyphiidae) im Dominikanischen Bernstein (Arachnida: Araneae). *Entomologische Zeitschrift, Frankfurt am Main* **108**: 363–367.
- Wunderlich J. 2004.** The fossil spiders of the family Anapidae s. l. (Aeaneae) [sic] in Baltic, Dominican and Mexican amber and their extant relatives, with the description of the new subfamily Comarominae. *Beiträge zur Araneologie* **3**: 1020–1111.
- Wunderlich J. 2008.** On extant and fossil (Eocene) European comb-footed spiders (Araneae: Theridiidae), with notes on their subfamilies, and with descriptions of new taxa. *Beiträge zur Araneologie* **5**: 140–469.
- Wunderlich J. 2011.** Some subrecent spiders (Araneae) in copal from Madagascar. *Beiträge zur Araneologie* **6**: 445–460.
- Yin C, Peng X, Bao Y. 2004.** A new species of the genus *Mysmenella* from China (Araneae, Mysmenidae). *Acta Zootaxonomica Sinica* **29**: 80–82.

APPENDIX 1

List of specimens examined. The generic assignment of unidentified mysmenid species (in parentheses after the identification code) is based on the phylogenetic hypothesis from the total-evidence analysis of Lopardo *et al.* (2011) (see Fig. 161B).

ANAPIDAE

Acrobleps hygrophilus

Australia: Tasmania; (SW of Hobart), Myrtle Gully (?), The Cascades, 13.xii.1945, under stone at side of creek, in fern gullies, manual, V.V. Hickman, ♂ holotype (MYSM-0147); ♀ allotype (MYSM-0148) (AMS); 10.iv.1961, 2♀ ♂ sub♂ (AMS, MYSM-0149); in fern gullies, 13.xii.1945, ♀ 4♂ 4sub♂ (AMS, MYSM-0150); Cascades Myrtle Gully, 13.xii.1945, V.V. Hickman, 1sub♂ (AMS-KS 30738, sub♂ SEM); Lake St. Clair NP. LSC-SFT, Flood Creek, 42°10'02"S, 146°11'35"E, (AGD 66), 16.ii.2004, buttongrass moorland, Pitfall: 3, –42.16722, 146.19306 (coll. M. Driessen), ♂ (GWU, gift from QM, MYSM-0085, ♂ SEM); Cradle Mountain-Lake St. Clair N.P., near Waldheim cabins, 22.6km 202° SWS Moina, 3.iii.2006, *Nothofagus* forest, S41°38'28.5" E145°56'26.5", 926 m, G. Hormiga, L. Lopardo, ♂ (GWU, 95% ethanol, LL-AU-02, LLS-088, ♂ sequenced); 3–5.iii.2006, 4♀ ♂ (GWU, MYSM-0179, ♀ SEM); manual, ♀ (GWU, MYSM-0181); 12♀ 6♂ sub♂ 1 juv (GWU, MYSM-0180, ♂♀ SEM, ♂♀ composite, ♀ genital drawing); Newall Creek, Franklin-Gordon Wild Rivers N.P., 9.57 km 177° S Queenstown, 14.iii.2006, *Nothofagus* rainforest, manual, 159 m, G. Hormiga, L. Lopardo, ♀ (GWU, MYSM-0182).

Anapisona kethleyi

Mexico: Chiapas, Ocosingo, Monumento Natural Bonampak, 16°43'32.5" N, 91°04'43.4" W, EPE07 207 m. 26.x–2.xi.2005. F. Alvarez, L. Lopardo & J. Castelo leg (BONA-01; 28.x.2005) ♂♀ 3sub♂ 1juv (♂ R1-f28-31, ♂♀ composite, ♂ genitalic drawing); sub♂ (80% ethanol, LLS-064, sequenced); sub♂ (R3-f13-16, SEM); ♀ (SEM, genitalic drawing); ♂ (SEM) (GWU/MCZ).

Comaroma simoni

Austria: Carinthia, Weissensee, Kleiner Silbergraben, 1150 m asl; July 7, 1991; C. Komposch leg., ♂♀ (GWU, Kropf donation, ♂ SEM, ♂♀ composite, ♂ genitalic drawing); no data, H. Franz leg, slg. H. Wiehle, ♀ (SMF 11456/5, SEM).

Crassanapis chilensis

Argentina: P. Nac. Lanín, Lago Queñi, 15.ii.96, Ramírez, 3♂ 2♀ 4juvs (MACN-Ar 10382, ♂♀ composite, ♂ genitalic drawing).

Chile: Región X (Los Lagos): Osorno Prov.: Parque Nacional Puyehue, 12.xii.2000–2.i.2001, J. Miller, I. Agnarsson, Alvarez, J. Coddington, G. Hormiga, Aguas Calientes, 40°44'0"S 72°18'45"W, 450 m, forest, (pitfall 515T1, 15 Dec 2000), 27♂ 5♀ (USNM, 75% ethanol, LLS-006, ♂ sequenced); Berlese, ♀ (USNM, 75% ethanol, LLS-007, ♀ SEM, ♀ sequenced); Antillanca road, 40°46'30"S, 72°12'00"W, 1000 m, ♀ (USNM, genitalic drawing); *Nothofagus pumilio* forest (pitfall 512T3, 29.Dec.2000), ♀ (USNM, SEM); ♂ (USNM, SEM).

Elanapis aisen

Argentina: Neuquén Prov.: P. Nac. Nahuel Huapi, Puerto Blest, 10.i.1998, Ramírez, 4♂ 2♀ 8juv (MACN-Ar 10380, ♂♀ SEM, ♂ composite, ♂♀ genitalic drawing).

Chile: Reg. X: Llanquihue, PN Alerce Andino, Correntoso, sendero 'Huillifoten', bosque humedo, 135 m, S41°27'53.0" W72°38'43.4", 3.ii.05, MJ Ramírez & F Labarque, ♀ (MACN-Ar, ♀ SEM, ♀ composite).

Minanapis casablanca

Chile: Región X (Los Lagos): Osorno Prov.: Parque Nacional Puyehue: Antillanca, 12.xii.2000–2.i.2001, J. Miller, I. Agnarsson, Alvarez, J. Coddington, G. Hormiga, 40°46'30"S, 72°12'00"W, 1150 m, *Nothofagus pumilio* forest, (pitfall 58T1, 2 Jan 2001) 6♂ 3♀ (USNM, 75% ethanol, LLS-002(♀), LLS-001(♂), ♂♀ SEM, ♂♀ composite, ♂ genitalic drawing, ♂♀ sequenced); 700 m, forest (pitfall 513T1, 18 Dec 2000) ♀ (USNM, SEM); 40°46'30"S, 72°11'30"W, 1050–1350 m, alpine meadow,

(pitfall 57T1, 12–15 Dec 2000), 4♀ (USNM, 75% ethanol, LLS-008, genitalic drawing, sequenced).

Minanapis palena

Chile: Región X (Los Lagos): Osorno Prov.: Parque Nacional Puyehue, J. Miller, I. Agnarsson, Alvarez, J. Coddington, G. Hormiga, 12.xii.2000–2.i.2001, 40°46'30"S 72°12'00"W, 700 m, (pitfall 513T1, 29 Dec 2000), 19♂ 13♀ 2juv (USNM, ♂♀ SEM, ♂ composite, ♀ genitalic drawing); Aguas Calientes, 40°44'0"S 72°18'45"W, 450 m, forest, Berlese, ♂♀ [USNM, 75% ethanol, LLS-004(♂), LLS-005(♀), ♂♀ sequenced].

Taphiassa punctata

New Zealand: South Island, Canterbury, Lincoln, Vortis suction sample, ARG McLachland, 22.x.1994, in grazed pasture, ♀ (LUNZ, MYSM-0057, composite); 30.v.1994, in grass under pine shelterbelt, 2♂ (LUNZ, MYSM-0055, SEM, composite, genitalic drawing); 22.xi.1995, in long grass under Eucalyptus trees, ♂ (LUNZ, MYSM-0056); 15.iv.1996, in grass under shelterbelt beside dairy pasture, ♂ (LUNZ, MYSM-0054); 15.v.1996, in long grass beside sheep pasture, ♀ (LUNZ, MYSM-0058, SEM, genitalic drawing).

Tasmanapis strahan

Australia: Tasmania: Franklin-Gordon Wild Rivers N.P., *Nothofagus* rainforest, Nelson Falls, 15.0km 089° E Queenstown, S42°06'13.9" E145°44'10.0", 338 m, 9.iii.2006, Ramírez, Griswold, Hormiga, Lopardo, Scharff, Silva, Boutin, Szüts, ♀ (MACN-Ar 11536, SEM, composite); Newall Creek, 9.57km 177° S Queenstown, S42°09'37.1" E145°32'20.1", 159 m, 10.iii.2006, G. Hormiga, L. Lopardo, ♂ (GWU, ♂♀ SEM, ♂ composite, ♂♀ genitalic drawing).

Teutoniella cekalovici

Chile: Concepcion Province: Estero Nonquen, 90 m, 16.xi.1981, N.I. Platnick & R.T. Schuh, conc. berlese, modified forest, floor litter, ♂♀ (AMNH, ♂♀ SEM, ♂♀ composite, ♂♀ genitalic drawing).

LINYPHIIDAE

Linyphia triangularis

Denmark: Hestehaven, Ronde, 22 km NE of Arhus, 56°17.46' N 10°28.50' E, 30-viii-1994, Bjorn, Christiansen, Coddington, Griswold, Hormiga, Krat, Langemark, Scharff & Sorensen leg., ♂♀ (USNM, several of both sexes, ♂♀ composite).

MYSMENIDAE

Anjouanella comorensis

Comoros: Anjouan, Sentier Hombo-N'Thindi, 3.xii.1983, Leaf litter, Litiere, tamisage, 600, R Jocque, 600 m, ♂

holotype (MRAC, MYSM-0151, composite); 900 m, 3♀ paratypes (MRAC, MYSM-0152, ♀ composite).

Brasilionata arborens

Brazil: Amazonas Central(?), near Manaus, Taruma Mirim, IX, 10–24.ix.1991, tree trap, U. Irmiler leg., ♂ holotype (AMNH, MYSM-0153, composite, genitalic drawing).

Calodipoena incredula

Panama: Cerro Galera, S. Heimer col., xii.1983, ♂ (MHNG, MYSM-0159); i.1984, 2♀ 6♂ 1 juv (MHNG, MYSM-0156, ♂♀ SEM); Colon, near Gamboa, S. Heimer col., xi.1983, ♂♀ (MHNG, MYSM-0157); i.1984, 4♀ ♂ (MHNG, MYSM-0158, ♀ SEM); vi.1983, ♂♀ (MHNG, MYSM-0160, ♂♀ composite); ii.1984, ♂ (MHNG, MYSM-0161). *USA*: Texas, Cameron Co., Palm Grove, 16.iii.1936, Cornell University Coll., 4♀ ♂ (AMNH, MYSM-0164).

Calodipoena mooatae

Sulawesi (Indonesia): Sulawesi Utara, Gunung (Mount) Mooat, Danau (Lake) Mooat, 29.x.1985, primary rain forest, 1050 m, R. Bosman & J. Van Stalle, ♀ holotype (IRSN, Cel. 064 BV, MYSM-0162, composite); S. de Kotamobago, 30.x.1985, primary rain forest, 1000 m, R. Bosman & J. Van Stalle, ♀ paratype (IRSN, MYSM-0163).

Calodipoena tarautensis

Sulawesi (Indonesia): Sulawesi Utara, Dumoga Bone National Park, Toraut, 27.x.1985, Grassland, 200 m, R. Bosman & J. Van Stalle, ♀ paratype (IRSN, MYSM-0165, composite, genitalic drawing).

Calomyspoena santacruzii

Ecuador: Galapagos Islands, Isla Isabela, Volcan Sierra Negra, 23.iii.1982, stems of grass clumps, manual, 160 m, L. Baert & J.-P. Maelfait, ♂ paratype 1 juv (IRSN, MYSM-0166, ♂ composite); Isla Santa Cruz, Caseta Occidente, 17–18.iii.1982, stems of grass clumps, manual, 170 m, L. Baert & J.-P. Maelfait, 3♀ paratype 1 juv (IRSN, MYSM-0167, ♀ composite).

Iardinis martensi

Nepal: Ost-Nepal: Jiri bei Those, 1800–2000 m, Martens leg., i.1970; Brignoli det. 1977, ‘male holotype’ (SMF-29597, female anapid found in vial, no male holotype, composite).

Iardinis mussardi

India: INDE (Madras): Madurai, 2.xi.1972, leg. C. Besuchet/I. Löbl (In 72/4), ♂ holotype (MHNG, composite, genitalic drawing).

Isela okuncana

South Africa: KwaZulu Natal, Mhlopheni Nature Reserve, 6Km SE Muden, 11.vi.1984, in sheet web of *Allothete*

teretis, 900 m, –29.02, 30.21, CE Griswold & T Meikle, ♂♀ paratypes (CAS, MYSM-0014); 3.ii.1984, 2♀ (CAS, MYSM-0015); 10Km SE of Muden, 2800ft, 29°01'12"S 030°12'36"E, 3–4.ii.1984, T&C Griswold, PMC Croeser, 6♂ 3♀ 1sub♂ (CAS, MYSM-0016, ♂♀ SEM, ♂♀ composite, ♂♀ genitalic drawing).

Itapua tembei

Paraguay: Itapua Prov., Salto Tembey, 1.xi.1982, Manhart *et al.* col, ♂ holotype (MHNG I.G.: 26619 (Py-82/20); A.LB 1200, Index 35, Arachn. Mod. II; composite); ♀ paratype (MHNG I.G.: 26619 (Py-20/82); A.LB 1200, Index 35, Arachn. Mod. II; SEM, composite).

Kekenboschiella awari

Papua New Guinea: Awar air strip, 18.vi.1982, P. Grootaert, ♂ paratype (IRSN-KBIN IG 26480 (1350) A.L.B. 1211, composite, genitalic drawing).

Kekenboschiella marijkeae

Papua New Guinea: Beri Village (Berlese #165), 27.v.1978, Y. Von Goethem, ♂ holotype (IRSN-KBIN IG 25848/1, composite, genitalic drawing); Bogia (?) (Berlese #227), 05.vi.1978, Y. Von Goethem, ♀ allotype (IRSN-KBIN IG 25848/2, composite).

Kilifina inquilina

Kenya: Kilifi, 9.viii.1980, JA Murphy, ♀ paratype (IRSN); Betty's Garden, 8.ix.1977, JA Murphy, ♂ paratype (IRSN); no collector, 16.ix.1977, ♀♂ paratypes (MRAC 174.634).

Maymena ambita

USA: Missouri, Rolla, Dry Fork Cr., H. Exline-Frizzell, 7.vii.1951, ♀ (CAS, composite); Virginia, Stafford Co., Falmouth, mixed deciduous forest, 27.vi.1978, H,L&F Levi, ♂ (MCZ 51259, SEM, composite, genitalic drawing); Alabama: Blount Co., Firelighter Cave #1, 33°54'N 86°47'W, 3.ix.2004, col. P. Paquin, J. Miller, N. Dupérré, D. Caudle, 2♀ (USNM, 95% ethanol, LLS-079–080, sequenced); Madison Co., Aladdin Cave, Sharp's Cave, AF Archer, 1.xii.1939, ♀ (AMNH, SEM); Tuscaloosa Co., Tuscaloosa, River Rd & Guild Woodo Rd, hollow logs, 4.vii.1981, J Coddington, 1sub♀ 1juv (MCZ 51256, SEM); ♀ (MCZ 51254, genitalic drawing).

Maymena mayana

Guatemala: Alta Vera Paz, Gruta de Lanquin, 6.ii.1980, B.-V. Roth, 4♀ ♂ (CAS, ♂♀ SEM).

Mexico: Veracruz, Municipio de Atoyac, Grutas de Atoyac, 18.9215°N 96.7653°W, A. Gluesenkamp C. Savvas P. Sprouse E. Gonzalez O. Francke, 22.ix.2004, 460 m, in cave, 5♀ 2♂ (AMNH, AGG 951, ATOL, 95% etOH, ♂ SEM); Tabasco, 2.4 km E of Teapa, Grutas de Cocona,

ca. 92°56'W 17°33'N, 7.vii.1983, W. Maddison, 83–098, ca. 250ft. ♀ 4♂ (MCZ 51264, ♂♀ genitalic drawing, composite).

Maymena rica

Costa Rica: Heredia, Organization for Tropical Studies field station at Finca La Selva, near Puerto Viejo, on West River Road, 13.i.1982, J. Coddington, ♂ holotype (MCZ 22902, composite); ♀ allotype (MCZ 24973, composite); general, 10.i.1982, J. Coddington, 4♂ 2♀ (MCZ 53351, ♂♀ SEM, ♂ genitalic drawing); West River Road at OTS, 10.i.1982, J. Coddington, ♀ (MCZ 53358, genitalic drawing).

Microdipoena elsae

Seychelles: Mahe near La Misère, ~600 m elevation, 30.x.1975, M. Saaristo leg., ♂ holotype (ZMTU, AA 0.045, composite); ♀ allotype (ZMTU, AA 0.046, composite); ♂♀ (ZMTU, AA 0.273, ♂♀ SEM, ♂♀ genitalic drawing); Big Sister Island, no specific locality, 10.ix.1975, M. Muhlenberg, ♀ (MRAC, MYSM-0063).

Comoros: Grande Comore, Boboni, sentier (path) Kartala, 24.xi.1983, tamisage (shifting), 1000 m, R Jocque, ♂ (MRAC, MYSM-0064).

Congo (DRC): Nord Kivu, PNA, sect. Tshiaberimu, riv. Musavaki, affl. Talya Nord, 15–21.iv.1955, 2720, PVanschuytbroeck RFonteyn, ♀ (MRAC, MYSM-0084).

Microdipoena guttata

USA: Several syntypes in vial with no label (MCZ, presumably from New York, Long Island, under dead leaves in dry woods Levi, 1956). *Alabama*: Blount Co., Rickle Cave, 32°27'N 83°41'W, 3.ix.2004, col. P. Paquin, J. Miller, N. Dupérré, D. Caudle ♂♀ (USNM, 95% ethanol, LLS-077, ♀ sequenced); Firelighter Cave #1, 33°54'N 86°47'W, 3.ix.2004, col. P. Paquin, J. Miller, N. Dupérré, D. Caudle, ♂ (USNM, 95% ethanol, LLS-078, ♂ sequenced); *Florida*, Alachua Co., Forest nr Devil's Millhopper, Gainesville, 1.viii.1994, from 3-D orb webs, C.E. Griswold, 17♀ 2♂ 2 juvs (CAS, MYSM-0025, ♂ genitalic drawing); *Ohio*, Champaign Co., no specific data, 26.i.1974, cedar bog – wood, K Menders, 1 juv (MCZ, MYSM-0029); *Warren Co.*, Camp Kern, 17.vii.1980, Beech forest – leaf litter, Tom Bultman, ♂ (MCZ, MYSM-0030); ♂ (MCZ, MYSM-0031); *Tennessee*, Sullivan Co., Warrior's Path State Park, 16.vi.1991, mixed hardwoods, 36.53333, -82.48333, C.E. Griswold, 2♀ ♂ (CAS, MYSM-0026); *Virginia*, Suffolk Co., South Quay, 6mi SSE Franklin, 100 m N Canal, 6.viii-16.ix.2003, SM Roble DFPF, ♂ (VMNH, MYSM-0168); *Page Co.* Rileyville, Sheridan School Mtn. Campus N38°43'49.2": W 78°22'58.8", 300 m, 29.vii.2006,

L. Lopardo, D. Dimitrov, ♂♀ (MCZ, several specimens, ♂♀ SEM, ♀ genitalic drawing).

Comoros: Mayotte, Majimbini, maison de la Convalescence, ruines, 21.ii.1998, forest, sieved litter, R Jocque, 2♂ (MRAC, MYSM-0067, ♂ SEM).

Congo (DRC): Nord Kivu, PNA, sect. Tshiaberimu, riv. Talya Nord, aff. g. de la Semliki, 26.iii.1954, 2340, PVanschuytbroeck HSynave, ♂ (MRAC, MYSM-0083).

Côte d'Ivoire: Appouesso, forêt classée de la Bossematié, station 5B, 2.i.1995, forest, pitfall, R Jocque & RG Tanoh, ♂ (MRAC, MYSM-0069); station 4F, 29.i.1995, forest, pitfall, R Jocque & RG Tanoh, ♂ (MRAC, MYSM-0071); rain forest, pitfall traps, R Jocque & N Séabé, station A,C,F, 1.xii.1994, 4♀ 2♂ (MRAC, MYSM-0073); station B 9-1-0, 29.xi.1993, 2♂ (MRAC, MYSM-0074); station B,C,D,F, 19.ix.1994, 6♂ (MRAC, MYSM-0076, ♂ SEM).

Microdipoena nyungwe

Rwanda: Forêt de Nyungwe, 7,5 km S de Pindura, rivière Nyungwe, 1850 m, litière de forêt, tamisage, Jocqué, Nsengimana & Michiels, 9.xi.1985, ♂ holotype (MRAC 164.921).

Tanzania: Tanga, E. Usambara Mtns., Amani, forest, 5°5.7'S 38°38'E, 950 m, 27.x-9.xi.1995, Griswold, Scharff, Ubick, ♂♀ (ZMUC 5599, ♂♀ SEM, ♂♀ composite, ♂♀ genitalic drawing).

Madagascar: Fianarantsoa: Forêt d'Atsirakambiaty, 7.6 km 285° WNW Itremo, 22°35'36"S, 46°33'48"E, 1550 m, 22–26.i.2003, montane rainforest, general collecting day spiders, Fisher, Griswold *et al.*, BLF7156, 10♀ 4♂ 13juv (CASENT 9017312, ♂♀ SEM, ♀ genitalic drawing). Mahajanga: Parc National d'Ankarafantsika, Forêt de Tsimaloto, 18.3 km 46° NE de Tsaramandroso, 2–8.iv.2001, 16°13'41"S, 46°8'37"E, elev 135 m, tropical dry forest, EF19 sifted litter, Fisher, Griswold *et al.*, BLF3599, 12♀ 4♂ 11juv (CASENT 9007648, 75% ethanol, LLS-036(♂)-037(♀), ♂♀ sequenced); Parc National Tsingy de Bemaraha, 3.4 km 93°E Bekopaka, Tombeau Vazimba, 6–10.XI.2001, 19°8'31"S, 44°49'41"E, elev. 50 m, tropical dry forest, EF19 sifted litter (leaf mold, rotten wood), B.L. Fisher *et al.* BLF4232, ♂ (CASENT 9008782). Antsiranana: Nosy Be, Parc National de Lokobe, 4.95 km 125°ESE Hellville, 13°24'56"S, 048°18'27.3"E, elev 0–200 m, lowland rainforest, 13–16.ii.2003, D. Andriamalala, D. Silva, C. Griswold, H. Ratsirarson, General collecting, day BLF7999, ♀ (CASENT 9005495); ♀ (CASENT 9005496); Reserve Speciale d'Ambre, 3.5 km 235°SW Sakaramy, 26–31.i.2001, 12°28'8"S, 49°14'32"E, Elev.

325 m, tropical dry forest, EF22 pitfall trap, general coll. Day, Fisher, Griswold *et al.*, BLF2655, 3♂♀ (CASENT 9006768); J.J. Rafanomezantsoa *et al.*, JJR0115, 2♀ 2♂ (CASENT 9004613); Montagne des Français, 7.2 km, 142° SE Antsiranana (= Diego Suarez), 12°19'22"S, 49°20'17"E, Elev 180 m, 22–28.ii.2001, tropical dry forest, EF19 sifted litter, Fisher, Griswold *et al.*, BLF3128, ♀ (CASENT 9007145). Toamasina: Res. Analamazaotra, Parc National Andasibe, 23 road km E Moramanga, 18°56'38"S, 48°25'3"E, 18°56'38.2"S, 48°25'03.2"E, elev 960 m, 16–18.i.2003, general collecting day, rainforest, C. Griswold, D. Silva, D. Andriamalala, BLF7993, ♂ juv (CASENT 9018286); Toliara: Parc National de Zombitse, 19.8 km 84° E Sakaraha, 22°50'36"S, 44°42'36"E, el. 770 m, 5–9.ii.2003, dry forest on sandy soil, general collecting day spiders, Fisher, Griswold *et al.*, BLF7512, ♂ (CASENT 9005786). Antananarivo: R.S. d'Ambohitantely, Forêt d'Ambohitantely, primary forest, ca. 20.9 km 72° NE d'Ankazobe, 18°13'30.3"S, 47°16'44"E, Elev. 1574 m, montane rainforest, Ludd/raking, 19.iii.2003, D. Andriamalala, D. Silva, *et al.*, DSD0037, 4♀ ♂ 12juv (CASENT 9014984).

Kilifina-MYSM-002-KENYA (*Isela*)

Kenya: Coastal Prov., Kilifi (?), 20 Km S Malindi, Kilifi, nr. Gede, 16.xi.1992, on diplurids webs, –3.33333, 40.01667, V&B Roth, 4♀ 2 juvs (CAS, MYSM-0018); Kwale, 30 Km S Mombasa, 12.xi.1992, on diplurids webs, –4.16667, 39.66667, V&B Roth, ♀ 2♂ 1 juv (CAS, MYSM-0019); 3♀ 5♂ (CAS, MYSM-0021); 39°40'E 4°10'S, 8♀ 7♂ 2 juvs (CAS, MYSM-0020, ♂♀ SEM, ♂♀ composite, ♂♀ genitalic drawing). Tsavo, Taita Discovery Center, gala camp, 29.iii.2000, wet area with dd trees, R Jocque, ♀ (MRAC, MYSM-0062).

MYSM-005-ARG (*Mysmena*)

Argentina: Misiones, San Pedro, P. Prov. Cruce Caballero, 13–16.i.2005, CC-Salto, manual, –26.46667, –53.96667, Grismado, Lopardo, Piacentini, Quaglino, Rubio, 2♀ (MACN-Ar, MYSM-0088); ♀ (MACN-Ar, MYSM-0093); ♀ (MACN-Ar, MYSM-0095); ♂ (MACN-Ar, MYSM-0096); 6♀ (MACN-Ar, MYSM-0104); ♂ (MACN-Ar, MYSM-0107); 26°28'00"S, 053°58'00"W, ♀ (MACN-Ar, 95% ethanol, MYSM-0173, LLS-069, sequenced). P.N. Iguazu: Sendero Macuco y Picadas aledañas, 18–21.i.2005, manual (coll. Grismado, Lopardo, Piacentini, Quaglino, Rubio), 25°40'43"S, 054°26'57"W, ♂ (MACN-Ar, MYSM-0099, ♂ composite); 5♀ (MACN-Ar, MYSM-0100, ♀ composite); 2♂ 3♀ 1 juv (MACN-Ar, MYSM-0101, ♂♀ SEM, ♂♀ genitalic drawing); ♀ (MACN-Ar, 95% ethanol, MYSM-0172, LLS-068, ♀ sequenced); –25.67861, –54.44917, 1 juv (MACN-Ar, MYSM-0102); 3♀ 3 juv (MACN-Ar, MYSM-0103); sendero macuco, 8–15 Feb 1995, manual, M.J. Ramírez, ♀ (MACN-Ar, MYSM-0123); RN 101, 6Km E seccional

Yacuy, 14–16 Dec 1999, manual, M.J. Ramírez y L. Lopardo, 2♀ (MACN-Ar, MYSM-0126); area Cataratas, 11–16 Dec 1999, manual, M.J. Ramírez y L. Lopardo, 2♀ (MACN-Ar, MYSM-0133).

MYSM-007-MEX (*Mysmena*)

Mexico: Chiapas, Ocosingo, Monumento Natural Bonampak, 16°43' 32.5" N, 91°04' 43.4" W, EPE07 207 m. 26.x–2.xi.2005. F. Alvarez, L. Lopardo & J. Castelo leg (BONA-01; 28.x.2005), 6♀ 3♂ 1sub♀ (GWU, 80% ethanol, LLS-066, ♀ SEM, ♂♀ genitalic drawing, ♀ sequenced); Arroyo Nayte Loc 1, Sierra de la Cojolita, 16°47' 36.2" N, 91°02' 35.3" W EPE06, 202 m. 26.x–2.xi.2005. F. Alvarez, L. Lopardo & J. Castelo leg. (NAYTE-01; 27.x.2005), ♂ (GWU/MCZ, composite); ♀ (GWU/MCZ, R2:f13-21, composite); ♂ (GWU/MCZ, R2-f6-12, SEM); Ejido Nueva Argentina, Laguna Miramar, Reserva de la Biósfera Montes Azules, 16°23' 36.2" N, 91°14' 29.6" W, EPE07 150 m. 23–25.x.2005. F. Alvarez, L. Lopardo & J. Castelo leg (MIRA-01; 23.x.2005), ♀ (GWU/MCZ, R1-f10-14, SEM).

Mysmena-MYSM-015-MAD (*Mysmena*)

Madagascar: Antananarivo: R.S. d'Ambohitantely, Forêt d'Ambohitantely, primary forest, ca. 20.9 km 72° NE d'Ankazobe, 18°13'30.3"S, 47°16'44"E, Elev. 1574 m, montane rainforest, General coll., 20–21.iii.2003, Ldd, D.Andriamalala, D.Silva, *et al.*, DSD0040, 15♀ 13♂ 5juv (CASENT 9015033, 75% ethanol, LLS-020(♂), LLS-021(♀), ♂♀ SEM, ♂♀ composite, ♀ genitalic drawing, ♂♀ sequenced).

Mysmena-MYSM-018-MAD (*Mysmena*)

Madagascar: Mahajanga: Parc National Tsingy de Bemaraha, 3.4 km 93°E Bekopaka, Tombeau Vazimba, 6–10.XI.2001, 19°8'31"S, 44°49'41"E, elev. 50 m, tropical dry forest, EF19 sifted litter (leaf mold, rotten wood), B.L. Fisher *et al.* BLF4232, ♂♀ (CASENT 9008782, several specimens, ♂♀ SEM, ♂♀ composite); Antsiranana: Reserve Speciale d'Ambre, 3.5 km 235°SW Sakaramy, 26–31.i.2001, 12°28'8"S, 49°14'32"E, Elev. 325 m, tropical dry forest, general coll. Day, J.J. Rafanomezantsoa *et al.*, JJR0115, 3♀ 3♂ 3juv, 2♀ ♂ 2juv, 2♀ 2♂ 3juv, 4♀ 2♂ 2juv, 59♀ 25♂, 14♀ 3♂ 7juv, ♂ 3♀, ♀ 3♂ (CASENT 9004612, 75% ethanol, LLS-038(♂), LLS-039(♀), ♂♀ sequenced).

MYSM-019-MAD (*Mysmeninae*)

Madagascar: Mahajanga: Réserve d'Ankoririka, 10.6km 13° NE de Tsaramandroso, 9–14.iv.2001, 16°16'2"S, 46°2'55"E, Elev 210 m, tropical dry forest, EF22 pitfall trap, Fisher, Griswold *et al.*, BLF3662, ♀ (CASENT 9007770, composite). Toliara: Forêt de Mite, 20.7 km 29° WNW Tongobory, 23°31'27"S, 44°7'17"E, el. 75 m, 27.ii–3.iii.2002, gallery forest, ER27 pitfall trap, coll. B.L.Fisher *et al.*, BLF5848, 1♀ 4♂, 1♀ 2♂ (CASENT

9014427, 75% ethanol, LLS-034(♂), LLS-035(♀), ♂♀ SEM, ♂ composite, ♂♀ genitalic drawing, ♂(♀ sequenced).

MYSM-020-MAD (Mysmeninae)

Madagascar: Toamasina: Res. Analamazaotra, Parc National Andasibe, 23 road km E Moramanga, 18°56'38"S, 48°25'3"E, el 960 m, 16–18.i.2003, general collecting day, rainforest, C. Griswold, D. Silva, D. Andriamalala, BLF7993, 6♂ (CASENT 9018285, 75% ethanol, LLS-016, ♂ SEM, ♂ composite, ♂ genitalic drawing, ♂ sequenced).

MYSM-023-MAD (Mysmeninae)

Madagascar: Antananarivo: 3 km 41° NE Andranomay, 11.5 km 147° SSE Anjozorobe, 5–13.xii.2000, 18°28'24"S, 47°57'36"E, Elev. 1300 m, montane rainforest, general collecting, Griswold *et al.*, BLF2543, 26♀ 17♂ 6juv, 2♀, 24♀, 1♂ 1juv (CASENT 9004228, 75% ethanol, LLS-033(♀), LLS-032(♂), ♂♀ SEM, ♂♀ composite, ♂♀ genitalic drawing, ♂♀ sequenced).

MYSM-028-MAD (Mysmena)

Madagascar: Antsiranana: Reserve Speciale d'Ambre, 3.5 km 235°SW Sakaramy, 26–31.i.2001, 12°28'8"S, 49°14'32"E, Elev. 325 m, tropical dry forest, general coll. Day, J.J. Rafanomezantsoa *et al.*, JJR0115 (CAS), 5♀ (CASENT 9004610, 75% ethanol, LLS-025, ♀ SEM, ♀ composite, ♀ sequenced).

MYSM-029-MAD (Mysmeninae)

Madagascar: Antsiranana: Nosy Be, Parc National de Lokobe, 4.95 km 125°ESE Hellville, 13°24'56"S, 048°18'27.3"E, elev 0–200 m, lowland rainforest, 13–16.ii.2003, D. Andriamalala, C. Griswold, H. Ratsirarson, D. Silva; General collecting, day BLF7999, ♀♀ (CASENT 9005464, 75% ethanol, LLS-027, ♀ SEM, ♀ composite, ♀ genitalic drawing, ♀ sequenced).

MYSM-034-MAD (Mysmena)

Madagascar: Antsiranana: Nosy Be, Parc National de Lokobe, 4.95 km 125°ESE Hellville, 13°24'56"S, 048°18'27.3"E, elev 0–200 m, lowland rainforest, 13–16.ii.2003, D. Andriamalala, C. Griswold, H. Ratsirarson, D. Silva; General collecting, day BLF7999, 7♀ (CASENT 9005464, 75% ethanol, LLS-031, ♀ SEM, ♀ composite, ♀ sequenced).

Mysmena leichhardti (as Mysmena-MYSM-017-AUST in Lopardo et al., 2011)

Australia: Queensland: Atherton Plateau, Rose Gums Wilderness Retreat, waterfall trail, around waterfall, rainforest, S17°18'51.1" E145°42'08.6", 770 m, 15.iii.2006, G. Hormiga, L. Lopardo, ♂♀ (GWU, many specimens, ATOL sequence: ARAGH000063 (GH0154), 95%

ethanol, LL-AU-13, LLS-062, ♂♀ SEM, ♂♀ composite, ♂♀ genitalic drawing, ♀ sequenced).

Mysmena leucoplagiata

France: Gallia merid., (Hierzu G. Mikro-Pràp.), ♀ type (MNHN AR 10982, composite); ♂ type (MNHN AR 10979, composite, genitalic drawing).

Mysmena tasmaniae

Australia: Tasmania: Maxwell River Valley, SW Tasmania, 42°38'S 145°54'E, 5.i.1978, L. Hill *et al.* ♂ holotype (AMS KS 2711), ♀ allotype (AMS KS 9625); SW Tasmania, 31.i.1977, L. Hill *et al.* ♂ (AMS KS 34486, SEM, genitalic drawing); Newall Creek, Franklin-Gordon Wild Rivers N.P., 9.57km 177° S Queenstown, *Nothofagus* rainforest, S42°09'37.1" E145°32'20.1", 159 m, 10.iii.2006, G. Hormiga, L. Lopardo, 2♂ ~10♀ (GWU, ♂♀ SEM, ♂♀ composite, ♀ genitalic drawing); Cradle Mountain-Lake St. Clair N.P., near Waldheim cabins, 22.6 km 202° SWS Moina, *Nothofagus* forest, S41°38'28.5" E145°56'26.5", 926 m, 5.iii.2006, G. Hormiga, L. Lopardo, sub♂ (GWU, ATOL seq ARAGH000062 (GH0153), 95% ethanol, LL-AU-04, LLS-061, sequenced); Lottah Road, 25.1km 284° WNW St Helens, disturbed *Nothofagus* forest, S41°13'04.0" E147°59'06.2", 550 m, 7.iii.2006, G. Hormiga, L. Lopardo, ♀ (GWU, 95% ethanol, LL-AU-xx, LLS-089, sequenced).

Mysmenella illectrix

Philippines: Manila, E Simon, no date, ♂ holotype (MNHN 11461, AR 10983).

Northern Mariana Islands: SAIPAN, As Lito. (Site#101), 15 07 35 N, 145 43 30 E, 60 m asl, 09.2001–02.2002, E. Benjamin leg., ♂ (ZMTU, composite, genitalic drawing).

Mysmenella jobi

Germany: Mainz-Gonsenheim, Gonsenheimer Wald, V. Job leg, 20.iv.1967, ♂ holotype (SMF 12958, genitalic drawing); v–vii.1967, pitfall trap, ♀ paratype (SMF 12959, genitalic drawing).

France: No locality data, ♂ (MNHN AR 10984, composite, misidentified specimen: '3036 *Mysmena leucoplagiata*, ♂ type (?) – Gall.merid. – Dresco rev.').

Italy: Sudtirolo, Guntschna, 470 m, b. Bozen.; D.F. Noflatscher, 1988, ♀ (NMW 14995, composite).

Mysmenella samoensis

Samoa: Upolu, under stones and vegetation, 1974, BJ Marples, ♂♀ syntypes (BMNH 1974.159, ♂♀ SEM, ♂♀ composite, ♂♀ genitalic drawing).

Mysmeniola spinifera

Venezuela: San Carlos de Rio Negro, Amazonas-Regenwald, 110 m, Bodenfalle Kübelböck, 21–28.i.1980, ♂ holotype (MHNG, composite, genitalic drawing).

Mysmenopsis cidrelicola

Venezuela: Colonia Tovar, E Simon(?), 1895(?), ♂ lectotype (presumably) and 2♂ paralectotypes (presumably, MNHN AR-2407, ♂ SEM, ♂ composite, ♂ genitalic drawing).

Mysmenopsis dipluramigo

Colombia: Chocó, Km 15 carretera Quibdó-Yuto, 24.iv.1984, Kleptoparasites of *Uruchus* – Dipluridae, 85 m, N. Paz S., 4♀ ♂ (MCZ 51286, MYSM-0040).

Panama: Bayano Region, upper Rio Maje, 11.vi.1976, in webs of Dipluridae sp., L. Kirkendal, ♂♀ (MCZ 51287, MYSM-0039); Coclé, 5 mi. SO. of El Valle, 11.i.1958, AM Chickering, 2♀ (MCZ 51286, MYSM-0041); 9♀ 4♂ 2 juvs (MCZ 51292, MYSM-0043, ♂♀ SEM, ♂♀ composite, ♂♀ genitalic drawing); El Valle, vii.1936, AM Chickering, ♂ (MCZ 51288, MYSM-0042).

Mysmenopsis femoralis

Saint Vincent: British West Indies, 2 ♀ syntypes (BMNH BM 1897.9.18.461–464); 2 ♀ (possibly syntypes, MNHN AR 1062).

Mysmenopsis palpalis

Honduras: Copán, H Peters, 9.ix.1951, ♂ holotype (SMF 8700/1); 3♂ 7♀ paratypes (SMF 8701).

Guatemala: Alta Verapaz, Lanquin nr Gruta, 5.ii.1980, V&B Roth, ♂ (CAS, MYSM-0022).

Mexico: Chiapas, Tapachula, viii.1909, no collector, ♂♀ (MCZ 51294, MYSM-0036); Veracruz, La Buena Ventura, 7-?-09?, ♂♀ (AMNH, ♂♀ SEM, ♂♀ composite).

Mysmenopsis penai

Ecuador: Napo, Coca, Río Napo, v.1965, L. Peña, ♂ holotype (MCZ).

Colombia: Amazonas, Rio Pira and Apaporis, 00°25'00"S, 070°15'00"W, 7–16.ii.1989 (coll. V&B Roth), 11♀ 2♂ 1sub♂ (CAS, MYSM-0023, ♂♀ SEM, ♂♀ composite, ♂ genitalic drawing).

Phricotelus stelliger

Sri Lanka: Ins. Taprobane/Ceylan, ♀ type (MNHN AR 1068, composite, genitalic drawing).

Tamasesia acuminata

Samoa: Upolu, at 1500 ft. from epiphytes in forest, col. BJ Marples, ♂♀ syntypes (BMNH 1974.192, ♀ SEM, ♂ composite); Upolu (same data as types? no other label in vial), ♀ (AMNH, composite).

Tamasesia rotunda

Samoa: Upolu, under stones, col. BJ Marples, ♂♀ syntypes (BMNH 1974.194, ♀ SEM, ♂ composite, ♂ genitalic drawing); Upolu (same data as types? no other label in vial), ♀ (AMNH, composite).

Trogloneta cantareira

Brazil: Sao Paulo, Cotia, Reserva do Morro Alto, 18–28.vi.2002, Equipe Biota col., ♂♀ (USNM, ex IBSP 59785, MYSM-0169, ♂♀ SEM, ♂ genitalic drawing); ♀ (USNM, ex IBSP 59786, MYSM-0170, ♀ SEM).

Trogloneta granulum

France: Dépt du Lot: Grotte de la Finou, com. et cant. de Livernon, lectotypes designated by Brignoli (1970) (MNHN AR 10974, 25370, one presumably juvenile in vial, no ♂ or ♀).

Czech Republic: South Bohemia (Jihočeský Kraj), Blanský Les Protected Landscape Area, Vysoká Běta, 780–790 m, 5.ix.2006, J. Hajer, V. Růžička, ♂♀ (GWU, J. Hajer donation, ♂♀ SEM, ♂♀ composite, ♂♀ genitalic drawing).

Austria: Styria: Ennstaler Alpen, Gesäuse, 700 m, 2.x.1973, K. Thaler, 2♀ (NMW 4529).

SYMPHYTOGNATHIDAE

Patu-SYMP-001-DR

Dominican Republic: Barahona Prov., Paraíso, Reserva Natural Cachote, cloud forest and secondary growth. N 18°05'54.8": W 71°11'22.0", 1220 m, 6–9.IV.2005. G. Hormiga, F. Alvarez & S. Benjamin, 44♀ 7♂ (GWU/MCZ, 80% ethanol, LLS-083, ♂♀ SEM, ♂♀ composite, ♀ sequenced).

SYMP-002-MAD

Madagascar: Mahajanga: Réserve d'Ankoririka, 10.6km 13° NE de Tsaramandroso, 9–14.iv.2001, 16°16'2"S, 46°2'55"E, Elev 210 m, tropical dry forest, EF19 sifted litter, Fisher, Griswold *et al.*, BLF3664, 6♀ 9♂ 6juv (CASENT 9007800, 75% ethanol, LLS-009(♂), LLS-010(♀), ♂♀ SEM, ♂♀ composite, ♂♀ sequenced).

SYMP-006-AUST

Australia: Queensland: Atherton Plateau, Rose Gums Wilderness Retreat, waterfall trail, around waterfall, rainforest, S17°18'51.1" E145°42'08.6", 770 m, 15.iii.2006, G. Hormiga, L. Lopardo, 2♀, ♀, ♀, ♂ sub♂, ♀, ♀, ♂ (GWU, 95% ethanol, LL-AU-11, LLS-087, ♂♀ SEM, ♂[R4.f15-19,24] ♀[R6.f3-9] composite, ♀ genitalic drawing, ♀ sequenced).

SYMP-007-AUST

Australia: Queensland: Atherton Plateau, Rose Gums Wilderness Retreat, waterfall trail, around waterfall, rainforest, S17°18'51.1" E145°42'08.6", 770 m, 15.iii.2006, G. Hormiga, L. Lopardo, 3♀ (GWU, 95% ethanol, LL-AU-12, LLS-084, SEM, composite, sequenced).

Symphytognatha picta

Australia: Western Australia: Tinglewood, near cabins, 6.98km 5° N Walpole, disturbed eucalypt forest, S34°54'51.0" E116°43'50.9", 185 m, 24.ii.2006, G. Hormiga, L. Lopardo, ♂ (GWU, ATOL seq ARAGH000064 (GH0155), 95% ethanol, LL-AU-01, LLS-063, composite, genitalic drawing, sequenced); Giant Red Tingle Tree, Walpole-Nornalup N.P., 5.29km 104° ESE Walpole, eucalypt forest, S34°58'57.3" E116°47'23.3", 87 m, 25.ii.2006, C.E. Griswold, ♂ (GWU, OZCG-02, SEM).

SYNAPHRIDAE

Cepheia longiseta

France: Gallia; coll. Simon; 4538, b.849, 14♀ 18♂ 3 juv paralectotypes (MNHN-AR1059, MYSM-0171, ♂♀ SEM, ♂♀ composite, ♂♀ genitalic drawing); Banyuls, no collector, ♂ sub♂ (MNHN, MYSM-0177).

Italy: South Tirol, Bolzano Province, Bolzano/Guntschna (= Guncinà), 27.vi.1988, 470, Noflatscher, 2♀ ♂ (NMW 14994, MYSM-0176). No locality data, no collector, ♂ (MNHN, MYSM-0178).

Synaphris saphrynis

Spain: Toledo, Huecas, 29.v.2003, Antonio Melic, 5739B-AM, 30T-395937, ♂ holotype (MNCN) 7♂ paratypes (MCNC, AMNH, MCZ, CAS, MYSM-0027, ♂ SEM, ♂ composite).

TETRAGNATHIDAE

Leucauge venusta

USA: District of Columbia, near Rock Creek Park, 18.v.2007, Lopardo, Dimitrov, Álvarez-Padilla, ♂♀ (GWU, composite).

Tetragnatha versicolor

USA: Georgia: Rabun Co., Ellicott Rock Wilderness Area, 1 km SW Ellicott Rock, cove hardwood for., 750–

800 m., 22.v.1993, 34°59' 46"N 83°06' 54"W, Bond, Dellinger, Dobyns, Hour 1, R. site 2, beating, day, ♀ (USNM, composite); Hour 6, R. site 3, beating, day, ♂ (USNM, composite).

THERIDIIDAE

Steatoda americana

USA: West Virginia, Berkeley County, Sleepy Creek Hunt & Fish Area, 6–13.VI.1986, Third hill Mtn. Oak-Pine Forest. P.J. Martinat unbaited pitfall trap 4 NEW N.E., 4♂ (USNM, composite); pitfall trap 5 NEW N.W., ♀ (USNM, composite).

THERIDIOSOMATIDAE

Theridiosoma gemmosum

USA: District of Columbia, near Rock Creek Park, 18.v.2007, Lopardo, Dimitrov, Álvarez-Padilla, ♀ (GWU, several specimens), ♀ (SEM), ♀ (composite).

Coddingtonia euryopoides

Thailand: Chiang Mai Prov., Doi Inthanon NP, cloud forest, Kew Mae Pan Nature trail, N 18°33'19.9"; E 98°28'56.4", 2170 m, 4–5.X.2003, ATOL Expedition 2003, 5♀ ♂ (USNM, ♂♀ SEM, ♀ composite); 2sub♂ (USNM, 95% ethanol, LLS-043, sub♂ sequenced); 1 ha. inventory, ca. 500 m from checkpoint at intersect. rd. summit/Mae Chaem, wet primary forest, N 18°31'47.9"; E 98°30'9.0", ca. 1800 m, 6–7.X.2003, ATOL Expedition 2003, ♀ (USNM, 95% ethanol, LLS-052, ♀ genitalic drawing, ♀ sequenced).

APPENDIX 2: MORPHOLOGICAL CHARACTERS

This appendix provides definitions and illustrations for almost all morphological and behavioural characters and states scored in the current morphological data set, with a brief discussion of their evolution within symphytognathoids as optimized on the preferred working hypothesis of relationships based on the total-evidence analysis of Lopardo *et al.* (2011) (see Figs 160, 161) (for a detailed report on Mysmenidae character evolution, see the Discussion in the main text). Almost all character states refer to at least one image as explanation. Usually more than one image was used in order to show morphological diversity among different groups for traits (i.e. character states) that were considered homologous and scored as being the same. Given the large number of images presented, a compromise between visual and written definitions was made, where images were preferred over long written descriptions. In this manner, character and state descriptions are highly succinct, whereas character and

state names are as descriptive as possible. Lengthy explanations are provided only when the images lack details, and/or when the original characters are missing a proper definition. All characters are referred to their original statements (except for new characters) in the abbreviated format (see below), followed by the original character number (note that reference to original statements does not necessarily mean character authorship). Characters from the literature have been taken from: Griswold *et al.* (1998), hereafter G98; Schütt (2002), S02; Schütt (2003), S03; Agnarsson (2004), A04; and Griswold *et al.* (2005), G05. Most of the characters taken from the literature have been reinterpreted here to accommodate symphytognathoid morphological variation and diversity. These changes in character and state names or interpretations are not indicated. Information for behavioural characters is scarce and has been mostly taken from the literature. Each morphological character set (continuous and discrete) is numbered independently of the other. Seven continuous characters were scored for abdomen (character 0), legs (characters 1–4), and spinnerets (characters 5–6). Discrete characters (a total number of 350) covering most of somatic and some internal morphology were scored as follows (Fig. 152): abdomen (including respiratory system), characters 0–33 (total 34); general body, character 34; cephalothorax, characters 35–54 (total 20); egg sacs, character 55; epiandrous fusules, characters 56–58 (total three); epigynum (internal and external female genitalia), characters 59–87 (total 29); eyes, characters 88–96 (total nine); legs, characters 97–150 (total 54); male palp: characters 151–261 (total 111); mouthparts: characters 262–296 (total 35); palp (female), characters 297–303 (total seven); spinnerets, characters 304–340 (total 37); web building (and other behavioural characters), characters 341–349 (total nine). All discrete characters are treated as non-additive or unordered, all continuous characters are treated as additive or ordered (for an explanation, see Material and methods). Node or clade numbers from the phylogenetic hypothesis based on morphological data (Fig. 153) begin with ‘M’; nodes from the combined total-evidence hypothesis (Figs 160, 161) begin with ‘C’.

CUTICLE

The details of the cuticular surface of the study taxa are in the majority of cases not visible with standard light microscopy. Therefore, cuticular patterns can only be studied under SEM. The cuticle texture shows an immense diversity, not only across families but also within them. The observed heterogeneity also occurs within and between the different regions of the body (carapace, sternum, legs, and spinnerets). For example, to account for such a diversity of patterns, the carapace was virtually divided into four regions showing

different combinations of cuticle textures: clypeus, anterior dorsal carapace, posterior dorsal carapace, and lateral margins. The following list of cuticular textures is an attempt to enclose such diversity into scorable states, although not all textures are present (or look the same) in all regions of the body (see each cuticle description). Names and descriptions of cuticular patterns follow the illustrated glossary of Harris (1979).

Imbricate (cf. squamate, scaly): Slender ridges delimiting partly overlapping ‘scales’ or small irregular areas: In the abdomen, the ridges may also be relatively parallel, in a strigulate manner that resembles the fingerprint cuticular pattern (see below), although in the latter the ridges are markedly elevated (compare Figs 86D, 20E, C). This cuticular pattern was observed on: abdomen (character 4, Fig. 86D), carapace (character 35, Fig. 15D; character 45, Fig. 13B); sternum (character 52, Fig. 111B); legs (character 97, Figs 21H, I, 34B, 65E, H); and posterior spinnerets (character 326, Figs 11G, 19F, 89D).

Fingerprint (cf. ridged, finely strigulate): Conflected elevated ridges running parallel with each other and producing a fingerprint pattern. In the piriform field of the ALS, this type of cuticle shows a fingerprint pattern around the piriform spigots, creating nearly concentric rings surrounding their bases. This cuticular pattern was observed on: abdomen (character 4, Fig. 20E, C); intersegmental cuticle on ALS (character 325, Fig. 113A); and piriform field on ALS (character 308, Figs 6B, 23A, C, 33E, 61C).

Smooth unsculptured surface: No evident ridges or other structures. In some cases subtle grooves, scales, or some other non-prominent cuticle pattern can be observed, but not as definite or evident as the other cuticular patterns. This unsculptured cuticle was observed on: carapace (character 35, Fig. 38D; character 45, Figs 72A, 85A; character 46, Fig. 50A; character 47, Figs 118A, B, 121B, E); sternum (character 52, Figs 112E, H, 121C, G); legs (character 97, Figs 80C, 119F, H); posterior spinnerets (character 326, Figs 78F, 82H, 94C, D); intersegmental cuticle on ALS (character 325, Fig. 94A, E); and piriform field on ALS (character 308, Figs 75A, 94A, 100A, 103A).

Imbricate–fingerprint: An imbricate pattern of slender wavy ridges delimiting scales. Within the scales, lower and shorter ridges are arranged in a fingerprint fashion. This cuticular pattern was observed on: carapace (character 35, Fig. 54A; character 45, Fig. 64F, I; character 46, Fig. 64E, F); and sternum (character 52, Figs 19D, 64H).

Punctate (cf. *pitted*, *foveate*): Large rounded pits interspersed. The pits do not house setal bases. This cuticular pattern was observed on: carapace (characters 35, 45, 46, and 47: Fig. 96A, E); and sternum (character 52, Figs 96B, E, 97A).

Rugose (cf. *irregular*, *asperous*, *bumpy*): Not a regular pattern. In the piriform field of the ALS, this type of cuticle shows a distinct ring around the Pi bases and granulate pattern surrounding these rings. This rugose cuticular pattern was observed on: carapace (character 35, Fig. 77A; character 45, Fig. 85A; character 46, Fig. 85A, F); sternum (character 52, Figs 99G, 118F); and piriform field on ALS (character 308, Figs 16B, 113B, 125D).

Prominent imbricate (cf. *alveolate*): Prominent (i.e. highly elevated, more marked) ridges delimiting regular, deep, angular 'scale-like' cavities. The ridges are not parallel. This cuticular pattern was observed only on carapace (character 35, Fig. 99E; character 46, Fig. 99D; character 47, Figs 91A, G, 99B).

Glabrous tuberculate: Densely covered or furnished with rounded, projecting lobes not related to setae. This cuticular pattern was observed on: carapace (character 46, Fig. 72A, D); sternum (character 52, *Linyphia*); and intersegmental cuticle on ALS (character 325, Figs 6A, 23C, 66F, 75A).

Sparse imbricate: This cuticular pattern occurs only on the borders of the carapace, and it consists of slender (i.e. not prominent) ridges, running mostly parallel with each other and with the edge of the carapace, and delimiting elongated scales (character 47, Fig. 50A).

Hirsute tuberculate-punctate: This cuticular pattern consists of scattered fine pits surrounding a row of sparse tubercles, each bearing a strong seta. These elevated setal bases were scored as carapace tubercles by Schütt (2002: characters 13, 14). This cuticle occurs only on the borders of the carapace (character 47, Fig. 82A).

Fatiscent (cf. *imbricate-smooth*): This cuticular pattern, observed only on legs, does not fit the definition of either imbricate or smooth cuticle (both also observed on legs), but instead presents an intermediate condition. As this cuticular pattern has been consistently observed across taxa, it is considered as a distinct kind of cuticle (i.e. a distinct state), otherwise only possibly scored as a polymorphism, therefore losing its potential phylogenetic information (character 97, Figs 73D, 87B, 93F).

CONTINUOUS CHARACTERS

The following continuous characters are based on measurements taken from only one specimen and assumed to be representative of the species, although when available, several specimens of each species were superficially examined in order to ensure constancy in the measurements (for details of measurements, refer to Material and methods). The choice of a more objective approach in the treatment of continuous characters (i.e. as such) was preferred after evaluating subjectivity of character state definitions in the original discrete character statements (see information at the end of each character explanation, see also Fig. 155A–G). Only ratio characters (i.e. not direct measurements) or counts were scored as continuous. Characters based on counts were treated as continuous (i.e. additive) only when comprising more than five states, otherwise they were treated as discrete characters. All measurements were arbitrarily taken from females, and in most of the cases no sexual dimorphism was observed in the measured variables.

0. Shape opisthosoma, lateral view (female, see Fig. 155A): range of measurements: 1.0–2.8 ($N = 55$). The shape of the female opisthosoma is here defined as the ratio length/height (L/H), where length is defined as the distance from the base of the spinnerets (spinnerets not included in the measurements) to their opposite side (i.e. if the spinnerets are ventral, then length is the distance to the highest point of the abdomen; if the spinnerets are posterior, then length is the distance to the anterior point). The perpendicular section to the length is taken as the height. Under this definition, it is assumed that, as discussed in character 5 (see below), the pedicel might shift positions across taxa. As this shift in position of the pedicel is related to a shift in the general orientation of the abdomen (where the spinnerets become ventral), then the 'length' orientation is also shifted to become perpendicular in some taxa, and can therefore be mistaken as height. Thus, the lengths (and consequently the heights) as defined here are assumed to be homologous, regardless of their orientation. In taxa with globular abdomens (where the height, length, and width are similar) and presenting bumps, those bumps are ignored in the measurements, and as an approximation, the height is taken to be similar to the width. The ratio measured in this character provides a tentative notion in an attempt to define abdominal shape, given that the shape of the abdomen may vary because of physiological conditions of the specimen at time of fixation, and whether the L/H ratio remains the same in live and fixed specimens is unknown. (S02 – 89; original states and definitions, 'oval or rectangular and long', 'subtriangular or globular and high').

1. Legs I and IV relative size (female, see Fig. 155B): range of measurements: 0.86–1.71 ($N = 53$). The relative length of leg IV is taken as the ratio of the lengths of leg I/leg IV. The total length of legs is, in most of the examined taxa, taken as the sum of the lengths of femur, tibia, metatarsus, and tarsus (except when the lengths were taken from literature). The ratio of the legs is assumed to be similar irrespective of the length of the patella (S02 – 61; S03 – 27; A04 – 184, 185; original states and definitions, S02 – 61 and S03 – 27: ‘longer’, ‘subequal’, ‘shorter’; A04 – 184, 185; ‘leg IV 3rd longest’, ‘leg IV 2nd longest’, and ‘leg IV longest’).
2. Metatarsus–tarsus relative size (female, see Fig. 155C): range of measurements: 0.45–3.2 ($N = 57$). This character is defined as the ratio of the lengths of metatarsus I/tarsus I. The lengths of these segments were taken from female leg I, and it appears relatively constant across all legs and sexes. Exceptions occur, as in *Mysmeniola spinifera* (scored as ‘?’), as only males are known, where the metatarsus I is subequal to tarsus I (ratio = 0.81), but metatarsus IV is shorter than tarsus IV (ratio = 0.55); and in *Leviola termitophila* (only known from females), where the metatarsus I is subequal to tarsus I (ratio = 1.03, scored), but metatarsus IV is longer than tarsus IV (ratio = 1.39) (S02 – 64; S03 – 29; original states and definitions, ‘Mt >> Ta’, ‘subequal’, ‘Mt << Ta’).
3. Femur–metatarsus relative size (female, see Fig. 155D): range of measurements: 1.03–3.16 ($N = 53$). As for continuous character 2, this character represents the ratio between the lengths of femur I/metatarsus I. (A04 – 186; original states and definitions: ‘metatarsus longer’, ‘metatarsus shorter’).
4. Tibia–metatarsus relative size (female, see Fig. 155E): range of measurements: 0.93–2.39 ($N = 55$). As in the previous two characters, this character represents the ratio of the lengths of tibia I/metatarsus I. (A04 – 187; original states and definitions: ‘metatarsus longer’, ‘metatarsus shorter’).
5. PLS AC spigot number (see Fig. 155F): range of measurements: 1–22 ($N = 48$). The range in the number of AC spigots on the PLS of the representatives of this data set appears large enough to be lumped into just two character states (A04 – 211; original states: ‘five or more’, ‘four or less’).
6. ALS Pi spigot number (see Fig. 155G): range of measurements, 4–65 ($N = 48$). The largest number of piriform spigots on the ALS occurring in the specimens studied was about 100. Instead, the maximum number was scored as 65, which is the upper limit of state value for continuous characters in the program TNT (Goloboff *et al.*, 2003b, 2008) (A04 – 205; original states and definitions: ‘large, over 40 spigots’, ‘small, less than 35 spigots’).

DISCRETE CHARACTERS

Abdomen

0. Male dorsal surface: (0) soft or coriaceous (Fig. 140E); (1) scattered with sclerotized spots (Fig. 146C); (2) with a scutum (Fig. 145F). Male dorsal abdominal scutum is a synapomorphy of clade C122 within Anapidae, changing to sclerotized spots in the micropholcommatine representatives (clade C193) (S02 – 91; S03 – 41; G98 – 47; A04 – 166).
1. Female dorsal surface: (0) soft or coriaceous (Figs 142D, 146D); (1) scattered with sclerotized spots (Fig. 145H); (2) with a scutum (Fig. 145M). Female dorsal sclerotized spots on abdomen optimize ambiguously at the base of anapid clade C122. A dorsal scutum is synapomorphic of *Minanapis* (clade C176) (S02 – 92; S03 – 42).
2. Male ventral surface: (0) soft or coriaceous (Fig. 141L); (1) with epigastric scutum (Fig. 145O). Synapomorphy of clade C122 within Anapidae (S02 – 93; S03 – 43).
3. Female ventral surface: (0) soft or coriaceous (Fig. 141H); (1) epigastric scutum (Fig. 145I). Synapomorphy of clade C122 within Anapidae (S02 – 94; S03 – 44).
4. Abdominal cuticle pattern: (0) imbricate (Fig. 86D); (1) fingerprint (Fig. 20E, C). The abdominal cuticle was observed on the sides of the abdomen in representatives with dorsal scutum. Only two cuticle patterns are present in the abdomen. Fingerprint abdominal cuticle arises convergently in Mysmenidae and Symphytognathidae (S02 – 104; S03 – 46).
5. Pedicel location: (0) anterior (Figs 144G, J, 146F); (1) central (Figs 11A, 16C, 31F, 87E, 140N); (2) intermediate (Figs 82E, 107C, 145G, 146D). The states of this character can be observed from lateral view in the entire specimen (e.g. Figs 140N, 144G, J, 145G, 146D, F), or from either lateral or ventral view in the dissected abdomen (e.g. Figs 2G, 5C, 16C, 31F, 39A, 72E, 82E, 87E, 107C). An anterior pedicel (state 0) entails posteriorly located spinnerets, whereas the central (state 1) pedicel is located distinctly in the centre of the abdomen when observed from ventral view (as in Figs 2G, 5C, 16C, 31F, 39A, 72E, 87E) and the spinnerets are located ventrally in a seemingly vertical abdomen (e.g. Fig. 140N). An intermediate pedicel (state 2) is usually located in between the positions on the previous states, but it does not, in a consistent manner, fit into any of them, as in ventral view, it is neither central nor completely anterior (Figs 82E, 107C, 144D, E, 145G, 146D). The position where the pedicel inserts in the abdomen seems to have changed from anterior

- towards central (i.e. ventral) in most symphytognathoids. A central pedicel is located closer to the epigastric groove and the spinnerets than to the anterior border. This condition appears to affect the relative position of the abdomen, where the spinnerets point ventrally and the anterior portion of the abdomen points dorsally (see discussion of characters 140 and 201 in Agnarsson, 2004). An alternative modification of potentially similar consequences could be a shift in the spinnerets relative position (from posterior to ventral). As both transitions could be equally possible and scoring either one of them accounts for the same variation observed, here we interpret this modification as a shift in the pedicel location, and assume that the same change has occurred across all the observed taxa. A central pedicel (state 1) optimizes ambiguously at the base of symphytognathoids (clade C115) (A04 – 140).
6. Abdominal humps: (0) abdomen smooth, without humps (Figs 140O, 146E); (1) with paired dorsal humps (Figs 16C, 141B); (2) with a dorsal-posterior single hump (Figs 142D, 143J–L, 144B, 146J–L). When present, the dorsal single hump (state 2) shows a high degree of protrusion between species, although consistent within a species. Species with a subtle posterior bulge were scored as smooth (state 0, e.g. *Microdipoena comorensis*, Fig. 141J, K). A pair of dorsal humps (state 1) is an autapomorphy of *Maymena rica* (S02 – 90; G98 – 46; A04 – 142).
 7. Abdominal dorsal colour pattern (in alcohol): (0) absent, uniform or unpigmented (Figs 144L, 143H); (1) present (Figs 140L, 141B, 142F). Homoplastic character (S02 – 99; A04 – 143).
 8. Abdominal dorsal colour pattern: (0) symmetrical bilateral pattern as white spots, blotches, or transversal lines (Figs 140L, 141B, 142F, 144C); (1) distinct central band (Fig. 141E). Only applicable to taxa with abdominal dorsal colour pattern. Within symphytognathoids, a central band is autapomorphic for *Maymena mayana* (A04 – 144).
 9. Abdominal central band: (0) dark with white edge (Fig. 144F, I); (1) light with dark edge (Fig. 141E). Only applicable to taxa with abdominal central dorsal band (A04 – 145).
 10. Abdominal dorsal pigment: (0) silver (Fig. 144F); (1) non-reflective, whitish (Fig. 140L); (2) dark (Fig. 144C). Only applicable to taxa with abdominal dorsal colour pattern. Within symphytognathoids, silver and black patterns are autapomorphies of *Theridiosoma gemmosum* and *Iardinis mussardi*, respectively (A04 – 146).
 11. Abdominal ventral colour pattern: (0) uniform, no clear pattern (Figs 140A, B, 145A, B, 146D); (1) with distinct white or lighter ring, restricted to surrounding the spinnerets (Figs 142J, L, 143A, B, G, I, L); (2) ventral abdominal area lighter (Figs 141K, L, 143D, E). Uniform ventral abdomen (state 0) presents the same coloration pattern as dorsally, including no change in coloration (Fig. 145A, B) as well as no change in the irregular pattern of dots (Fig. 140A, B). A distinct white ring (state 1) encircles the spinnerets posteriorly from the epigastric furrow area (Fig. 143I), but can also extend dorsally, beyond the anal tubercle (Fig. 143A, B). State 2 includes a distinctly lighter ventral abdomen, and/or a whitish extended coloration on the posterior abdomen. Greatly homoplastic, although ambiguously optimized and homoplastic, a white ring around the spinnerets (state 1) occurs only within Mysmenidae. A ventral lighter area (state 2) evolved convergently in *Trogloneta*, node C156 within Symphytognathidae, and a few other taxa.
 12. Sigilla: (0) conspicuous, deep, contrastingly colored (Fig. 146C); (1) inconspicuous, superficial (Fig. 143H). In some spiders with sclerotized dorsal abdomen (i.e. scutum), the sigilla is visible through the scutum (e.g. Fig. 145N). Conspicuous sigilla optimizes ambiguously at the base of Anapidae (A04 – 167).
 13. Opisthosoma vestiture: (0) uniform thin and short setae (Figs 31F, 39A, 72E, 141A); (1) uniform thick setae (Fig. 146A, B, J); (2) long and thick setae interspersed among shorter and thinner setae (Figs 2G, 5C, 140A). The abdomen of most symphytognathids is covered by distinctly thick and long setae (state 1), whereas in most kleptoparasitic mysmenids the setae arrangement is a mixture of both short and thin, and longer thicker setae, especially anteriorly (state 2). The abdomen of most anapids and non-kleptoparasitic mysmenids is covered by short and thin setae (state 0). *Steatoda* (state 1) presents thick setae covering the abdomen, although not as long as the characteristic setae of symphytognathids (S03 – 45).
 14. Strong setae with plates at base: (0) absent (Fig. 20A); (1) present (Figs 78A, 103G, I). There is no original definition of this character; the only statement including some clarification was its character name. Therefore, it was not clear what the meanings of the states were exactly, or the location of these bases. If these setal bases are scored according to the thickness of the setae they bear, then this character would not be independent of character 13 (opisthosoma vestiture). Independently of the type of seta borne, stronger (i.e. more evident, salient) setal bases with an apparent homogeneous distribution are observed in *Comaroma*, *Teutoniella*, and in some degree in *Taphiassa* (i.e. clade C150) (S02 – 97).

15. Abdominal suprapedicellate nubbins: (0) absent (Fig. 78A); (1) present (Figs 20E, 69C, D, 87G). These presumably stridulatory nubbins located on the anterior abdominal area above the pedicel were first described by Agnarsson (2004: character 149), who suggested that they were synapomorphic for Araneoidea. These nubbins seem absent in *Trogloneta*, Micropholcommatinae, the anapid clade C121, and some other mysmenids and theridiosomatids.
16. Stridulatory pick row (SPR): (0) absent (Fig. 20D, E); (1) present (see Agnarsson, 2004: fig. 72A, B). The presence of rows of modified setal bases as stridulatory picks is autapomorphic for Theridiidae in this data set (A04 – 150).
17. Suprapedicellate proprioceptors: (0) absent (Figs 72F, 78A, 87G); (1) present (Figs 20D, E, 24C, F, 35E, 113G). Agnarsson (2004) defined two characters (his characters 163 and 164) concerning the position of these presumed proprioceptors surrounding the pedicel area ('elongated pedicellate setae' of Agnarsson, Coddington & May-Collado 2007), which appear to be a synapomorphy of spiders. The positions were originally described as '11 o'clock' (i.e. dorsal) and '4 o'clock' (i.e. ventrolateral), but the relative position of these modified setae was later standardized to fit into one of six paired sectors (S1–S6) (Agnarsson *et al.*, 2007: fig. 1). In these previous studies, no symphytognathoid representative was studied. Most symphytognathoids present at least one pair of elongated setae that fit neither the 11 nor the 4 o'clock states, and fit between sectors S2 and S3. Therefore, the positional homology of individual setae for symphytognathoids remains ambiguous, although consistent within this group. Because of this ambiguity, only the presence of elongated pedicellate setae is scored here. The absence of proprioceptors occurs in at least *Cepheia* and most anapids, and is optimized ambiguously at the base of the clade containing Anapidae, Symphytognathidae, and Synaphridae.
18. Abdominal suprapedicellate apodemes: (0) distinctly disc-like, strongly rugose; (1) inconspicuous (Fig. 82E), weakly rugose (Figs 53G, 72F), or smooth (Figs 20E, 24C). As in theridiids, all symphytognathoids have weak suprapedicellate apodemes (A04 – 165).
19. Booklungs cover: (0) present (Figs 20D, 39A, 103G); (1) absent (Figs 2H, 107A, 115F, 117A). Although homoplastic within this data set, the absence of booklungs covers is synapomorphic for Synaphridae and a putative synapomorphy for clade C199 within Symphytognathidae (S03 – 47).
20. Booklungs cover cuticle: (0) smooth (Figs 86C, 93C, 97G, 103H); (1) imbricate (Figs 20B, 39B, 67E). Within symphytognathoids, smooth cuticle is synapomorphic for a clade comprising all anapids except its basal genus *Acrobleps* (node C122) (S02 – 100; G98 – 49).
21. Anterior respiratory system: (0) booklungs with more than 20 leaves (Fig. 123A); (1) booklungs with less than 15 leaves (Figs 67C, 79A, 85B); (2) tracheae (Figs 33A, 60H, 114C, 120E). The distinction between booklungs and 'reduced' booklungs is defined here as a clear difference in the number of leaves, where usually state 0 includes more than 20 leaves, whereas state 1 includes 15 or less, usually seven or eight leaves (for the taxa in this data set). In the few cases where the anterior respiratory system consisted of a combination of reduced booklungs plus tracheae, it was coded as polymorphic (states 1 and 2). In *Tasmanapis strahan*, *Kilifina*-MYSM-002-KENYA, and *Maymenarica*, the scoring of characters related to the anterior respiratory system was based on the reduced booklungs, not the tracheae. Conversely, in *Mysmenopsis dipluramigo* and *M. penai*, scoring was based on the predominant tracheal system (see L. Lopardo, P. Michalik & G. Hormiga, unpubl. data). Anterior tracheae evolved from booklungs in the ANTS clade (node C114), changing distally into reduced booklungs within anapids (ambiguously optimized). Within Mysmenidae, the evolution of both tracheae and reduced booklungs optimize as ambiguous in node C161 (i.e. all mysmenids except Mysmeninae) (S02 – 101; S03 – 48; G98 – 48).
22. Anterior tracheae: (0) restricted to opisthosoma (Fig. 33A); (1) extending into prosoma (Fig. 120E). Scoring of state 1 was based on preparations of digested abdomens and subsequent observations of the anterior tracheae actually entering into the pedicel. If tracheae were not observed entering the pedicel, state 0 was scored instead. Tracheae restricted to opisthosoma evolved in Mysmeninae (with some reversals) and convergently in *Acrobleps* (S03 – 49).
23. Anterior atria: (0) unconnected (Fig. 79A); (1) interconnected by transverse duct (Figs 33A, 123A); (2) connected by membranous duct (Fig. 60H). A transverse duct connecting both atria has the appearance of a more rigid tube (state 1). In contrast, a membranous connection between atria (state 2) lacks the tube-like form and seems flattened or irregular. A highly homoplastic character (S03 – 50).
24. Posterior respiratory system: (0) present (Figs 5E, 78B, 85C, 110F); (1) absent (Figs 114C, 117F, 120E). In cases where neither SEM nor light microscopy observations for the inner respiratory structures were available, an external posterior spiracle (observed in SEM preparations of non-digested abdomens) was taken as indicative for the presence of a posterior respiratory system. As far as

- observed in these minute spiders, taxa with posterior spiracle possess posterior tracheae, and vice versa. Similarly, taxa without a posterior spiracle lack posterior tracheae and vice versa. This way, the posterior respiratory system of *Taphiassa punctata* has been scored as present based on the presence of a posterior single spiracle (Fig. 97H), although the internal tracheae were not directly observed or were suggested to be absent (Forster, 1959 – 301; and Platnick & Forster, 1986 – 7). The posterior respiratory system has been lost at least once (i.e. it is ambiguously optimized), and it is absent in most Symphytognathidae and in *Acrobleps* (S03 – 51; G05 – 61).
25. Posterior spiracle: (0) wide spiracular opening (Figs 24E, 59I); (1) narrow spiracle (Figs 64D, 78B, 97H). A wide spiracle opening consists of two distant spiracular openings exteriorly connected by a thin ridge, and is usually almost as wide or wider than the spinnerets, whereas a narrow spiracle consists of a single central opening. Wide posterior spiracle originated three times, and is synapomorphic for *Mysmenopsis*, Mysmeninae, and Synaphridae (S02 – 102; S03 – 52; G98 – 50; G05 – 60).
 26. Posterior spiracle opening: (0) advanced, midway between the spinnerets and epigastric groove (Fig. 24A, E); (1) adjacent to the spinnerets (Figs 11A, 59I, 64D, 78B). An advanced posterior spiracle is convergently synapomorphic for Mysmeninae and Synaphridae (S02 – 103; S03 – 53).
 27. Median structures of posterior respiratory system (as either tracheae or third entapophyses): (0) present (Figs 29B, 64B, 85C); (1) absent (Fig. 60G). The third abdominal entapophyses are muscular apodemes located between the posterior respiratory structures (i.e. lateral tracheae) in spiders. These apodemes have developed into median tracheae in the Entelegynae (and convergently in austrochiline spiders, see character 28; Purcell, 1909; Forster, 1980; Ramírez, 2000). The third entapophyses have been lost in at least some *Mysmenopsis* species. In these cases, there appeared to be no evidence of these structures, and the lateral tracheae (although connected through an intertracheal duct) are well separated from each other and arising at each end of the wide posterior spiracle (Fig. 60G). In Synaphridae, two bundles of posterior tracheae (each containing both lateral and median tracheae) arise from a deep, flat, membranous atrium, with an intertracheal U-shaped duct connecting them. In this latter family the two tracheal bundles arise centrally and relatively closer to each other than in *Mysmenopsis*, and therefore it is here assumed that the median tracheae are present and arising together with their correspondent lateral tracheae in a branched fashion (G05 – 63).
 28. Median structure of posterior respiratory system: (0) apodemes, non-tubular (third entapophyses; Figs 64B, 85C); (1) tubular (median tracheae; Figs 5E, 110F). Third apodemal entapophyses are distinguished here as short fibrous structures that seemingly lack a lumen and have a clear muscular attachment point at their tips (e.g. Fig. 85C). Median tubes similar to, and as long as, lateral tracheae are considered here as functional median tracheae (see e.g. Fig. 5E), and are synapomorphic for *Isela*, convergent in Synaphridae and *Anapisona kethleyi* (G05 – 63).
 29. Posterior median tracheae: (0) single tubes (unbranched; Fig. 5E); (1) branching into several tracheoles (Fig. 110F). Branching posterior tracheae optimizes at the base of the clade comprising anapids, symphytognathids, and synaphrids (i.e. node C113) (G05 – 64).
 30. Posterior median tracheae: (0) restricted to abdomen (Fig. 5E); (1) extending into prosoma (Fig. 110F). Median tracheae extending into prosoma is an ambiguously optimized synapomorphy of Synaphridae.
 31. Posterior lateral tracheae: (0) single tubes (unbranched, Figs 5E, 85C); (1) branching into several tracheoles (Figs 33A, 60G, 110F). Branching lateral tracheae are synapomorphic for Mysmeninae, *Mysmenopsis*, and Synaphridae (G05 – 62).
 32. Posterior lateral tracheae: (0) restricted to abdomen (Figs 5E, 60G, 85C); (1) extending into prosoma (Figs 37D, 110F). Lateral tracheae extending into prosoma is convergently synapomorphic for Mysmeninae and Synaphridae.
 33. Posterior respiratory system arrangement: (0) median and lateral structures separated, resulting in four trunks usually arising independently from the posterior spiracle (Fig. 85C); (1) median and lateral structures sharing a common basal trunk, resulting in two bundles arising from the atrium (Fig. 110F); (2) median structures (usually as minute apodemes) surrounded by lateral tracheae (Fig. 29B); (3) a single median apodemal structure and two lateral tracheae, resulting in three trunks arising from the posterior spiracle (Fig. 64B). The *Kilifina* representative (*Kilifina*-MYSM-002-KENYA; Fig. 5E, F) has a pair of long median tracheae each arising from the same location as the lateral tracheae, but as the median and lateral tracheae do not share a common trunk, as in the characteristic arrangement of synaphrids (see Fig. 110F), *Kilifina* was coded as having state 2. This character applies only to taxa with posterior median structures. Four independent median and lateral structures (state 0) is a widespread condition in spiders (e.g. Purcell, 1909; Forster,

1980; Ramírez, 2000), and therefore resulted symplesiomorphic in this data set, occurring also in all anapids examined here (*Comaroma*, *Crassanapis*, *Elanapis*, *Minanapis*, and *Tasmanapis*), including the micropholcommatine representatives (*Teutoniella*), theridiosomatids, and all examined *Maymena* species (see L. Lopardo, P. Michalik & G. Hormiga, unpubl. data). Two bundles of median and lateral tracheae (state 1) are synapomorphic for Synaphridae, a single median structure (state 3) is (ambiguously) autapomorphic within *Trogloneta* and Symphytognathidae, and an arrangement of lateral tracheae surrounding a minute median apodeme is a putative synapomorphy of Mysmeninae.

Body

34. Body length: (0) medium, 5.0–8.0 mm; (1) small, 2.5–4.0 mm; (2) minute, < 2.0 mm. This character represents the length of adult spiders, although a justification for the delimitations of the states as originally defined was not provided. Nevertheless, the character provides a general notion of size, and each representative in this data set falls into one of the three distinct states here delimited. All species scored are monomorphic, or are assumed as such when only one sex is known. The length of adult *Trogloneta cantareira* was described mistakenly as larger than 2 mm (Brescovit & Lopardo, 2008), but the actual length is about 1 mm (compare scale bars on their figs 1A, B, 3A, B). All symphytognathoids studied here are minute, except the small *Maymena mayana*. Synapomorphy of symphytognathoids, although ambiguously optimized because of the small size of *Steatoda* (S02 – 2; S03 – 1).

Cephalothorax

35. Clypeus cuticle: (0) smooth (Fig. 38D); (1) imbricate (Fig. 15D); (2) imbricate–fingerprint (Fig. 54A); (3) punctate (Fig. 96E); (4) rugose (Fig. 77A); (5) prominent imbricate (Fig. 99E). Smooth clypeal cuticle is the plesiomorphic condition; imbricate clypei are highly homoplastic in this data set. Punctate clypeus is synapomorphic for the micropholcommatine representatives (node C193), whereas rugose clypeus is a synapomorphy of node C121 within Anapidae. A prominent imbricate clypeal cuticle is an autapomorphy of *Tasmanapis*, whereas imbricate–fingerprint cuticle is autapomorphic of *Mysmenopsis cidrelicola*.

36. Carapace dorsal view (female): (0) anteriorly narrowed (Figs 15C, 72A, 104C); (1) round, circular, subequal (i.e. ocular area not narrowed; Figs 108A,

146E). This character is based on the general shape of female carapace, not on measurements or ratios. The shape of the male carapace in dorsal view is usually the same as females, except when carapace dimorphism is present (see character 38). Dimorphic male carapace is mostly circular in dorsal view because of the elevation of the ocular area. Carapace with narrowed ocular area (state 0) is not necessarily longer than wide and shapes can vary from oval (Figs 104C, 142E), to triangular (Figs 15C, 141B), to even pear-shaped (Figs 72A, 145H). Autapomorphy of *Cepheia* (S02 – 4; S03 – 13.2; G05 – 29; A04 – 126).

37. Outline carapace lateral (pars cephalica elevation; female): (0) not elevated, height is less than half carapace length (Figs 38C, 99B, 143M, 145E); (1) elevated, height is more than half carapace length (Figs 91A, 112A, 145M, 146G). This character describes the height of the female carapace. See character 38 for height dimorphism. High carapace occurs in few clades within Anapidae and Symphytognathidae (S02 – 5; S03 – 2; G05 – 31; A04 – 124).
38. Carapace height dimorphism: (0) absent, both sexes with same height (compare Figs 2A and B, 15A and B); (1) present, male higher than female (compare Figs 27F and G, 63G and 64E, 112A and B, 141M and N). This character accounts for difference in height between males and females. Absent dimorphism include species in which both sexes present the same height on either elevated or not elevated carapaces. In dimorphic species, the male carapace is always the highest (and never *vice versa*). Dimorphic carapaces have evolved independently in many instances in the taxa studied.
39. Cephalic carapace transition: (0) smooth (Figs 7B, 38C); (1) cervical groove, U-shaped constriction separating cephalic from thoracic region of the carapace (Figs 72A, 91A, 99B, D). A cervical groove optimizes ambiguously at the base of node C122 within Anapidae (S02 – 6; S03 – 3).
40. Carapace hairiness: (0) sparsely or patchily hirsute (Fig. 50A); (1) uniformly hirsute (e.g. *Steatoda*, see Agnarsson, 2004: fig. 71D; and *Tetragnatha*) (A04 – 127).
41. Carapace pars stridens (pedicel area): (0) irregular (Fig. 15E); (1) regular parallel ridges (Fig. 104C); (2) elevated setal bases (Fig. 82B); (3) minute dorsal bumps (Fig. 89A). This character represents carapace structures on and around the pedicel area that presumably interact with the correspondent area on the abdomen, although the existence of a stridulatory mechanism between these two areas is unknown. Irregular pedicel area (state 0) includes areas with no structures (i.e. smooth) as well as any irregular cuticular pattern (Fig. 15E).

- Regular parallel ridges (state 1) comprise ridges lateral to the pedicel (e.g. in theridiids, as defined in the original character), as well as parallel ridges around the pedicel, as in *Teutoniella* (Fig. 104C). Elevated setal bases are an autapomorphy of *Comaroma*, minute dorsal bumps occur in *Minanapis* (A04 – 128).
42. Carapace pars stridens: (0) separate, i.e. two lateral patches (Agnarsson, 2004: fig. 71F); (1) continuous or central (Fig. 82B). Applies only to taxa with modified pars stridens (character 41, states 1, 2, and 3) (A04 – 129).
 43. Fovea: (0) present (Fig. 144F, I); (1) absent (Fig. 141E). The absence of a distinct apodemal groove on the thoracic region of the carapace is a synapomorphy of symphytognathoids (S02 – 11; S03 – 7).
 44. Pore bearing prosomal depression: (0) absent (Fig. 19C); (1) present (Figs 72C, 77I, 86A, E). Pore-bearing depressions on the anterolateral margins of the carapace have been proposed as an anapid synapomorphy (Platnick & Forster, 1989); however, these glandular depressions are not found in all anapids and are not unique to Anapidae (Platnick & Forster, 1989; Schütt, 2003). In this data set the anapids *Minanapis* (Fig. 91B) and *Comaroma* lack these depressions, whereas *Taphiassa* (Micropholcommatinae) has similar cuticular excavations (Fig. 96D, G; see also Schütt, 2003). These depressions have been reported to also occur in malkarids (Platnick & Forster, 1987) and in some linyphiids (Hormiga, 1999; and references therein). The depressions in *Elanapis aisen* (Fig. 88A, B) are weakly excavated and appear similar to those found in *Symphytognatha picta* (scored here as present; Fig. 121A, F). The pore-bearing depressions in *S. picta*, although weak, represent the first report of these pits in non-anapid symphytognathoids. In some cases, when the anterolateral ‘corners’ of the carapace bear no conspicuous glandular areas, some minute depressions might occur on a separate sclerite adjacent to the pedipalp, as in the Australian anapid genus *Maxanapis* (Platnick & Forster, 1989 – 95, figs 271, 272; see also Rix *et al.*, 2008 – 1044). In *Teutoniella* these hidden cuticular depressions occur at least between coxae II and III, but are presumably distributed between all leg and palpal coxae (Fig. 104A, H). As homology of this serial feature with the carapace excavations is dubious, *Teutoniella* was scored as absent. The pore-bearing depressions are a synapomorphy of Anapidae (with a reversal in node C151 and a regain in *Taphiassa*), and an autapomorphy of *Symphytognatha picta* (S02 – 15; S03 – 8).
 45. Cuticle pattern on anterior (dorsal) carapace: (0) smooth (Figs 72A, 85A); (1) imbricate (Fig. 13B); (2) imbricate–fingerprint (Fig. 64F, I); (3) punctate (Fig. 96A, E); (4) rugose (*Steatoda*). Putative synapomorphy of symphytognathoids, although most taxa in this data set have smooth cuticle anteriorly on the carapace. Within symphytognathoids, punctate anterior cuticle is an autapomorphy of *Taphiassa*, imbricate–fingerprint cuticle is an autapomorphy of *Trogloneta cantareira*, and imbricate cuticle is an autapomorphy of *Maymena mayana* (S02 – 12; S03 – 6; A04 – 123).
 46. Cuticle pattern on posterior (dorsal) carapace: (0) smooth (Fig. 50A); (1) imbricate (*Linyphia* and *Tetragnatha*); (2) imbricate–fingerprint (Fig. 64E, F); (3) punctate (Fig. 96A, E); (4) glabrous tuberculate (Fig. 72A, D); (5) rugose (Fig. 85A, F); (6) prominent imbricate (Fig. 99D). Potential synapomorphy of symphytognathoids, although most taxa in this data set have smooth cuticle posteriorly on the carapace (state 0). Within symphytognathoids, a glabrous tuberculate cuticle pattern (state 4) is an ambiguously optimized synapomorphy of the anapid clade C122; however, within this clade, punctate posterior cuticle pattern (state 3) is an autapomorphy of *Taphiassa*, rugose cuticle (state 5) is an autapomorphy of *Crassanapis*, and prominent imbricate cuticle (state 6) is an autapomorphy of *Tasmanapis* (S02 – 12; S03 – 6; A04 – 123).
 47. Cuticle pattern on carapace edge: (0) sparse imbricate (Fig. 50A); (1) smooth (Figs 118A, B, 121B, E); (2) prominent imbricate (Figs 91A, G, 99B); (3) hirsute tuberculate–punctate (Fig. 82A); (4) punctate (Fig. 96E). Sparse imbricate cuticle pattern is a synapomorphy of Mysmenidae. A diversity of cuticular patterns on the lateral borders of the carapace has evolved within Anapidae.
 48. Carapace coloration: (0) uniform (Figs 140O, 142M, 144C, 145H, 146C); (1) radial pattern (Figs 140L, 143K). Although highly homoplastic and of ambiguous optimization, a radial pattern of carapace coloration occurs in theridiosomatids and in most mysmenids (A04 – 125).
 49. Sternum shape: (0) scutiform, wider anteriorly, tapering posteriorly (Figs 59G, 91D, 108B); (1) rectangular, anterior, and posterior width similar (Figs 121C, 146I). Autapomorphy of *Symphytognatha picta* (S03 – 13.1).
 50. Lateral sternum profile: (0) flat (Fig. 13A); (1) domed (Figs 15B, 19B, 72C, 96C). The sternum of *Anapisona kethleyi* appears flat but is actually anteriorly bulged (Fig. 72C), and is here scored as domed, although it might represent a different character condition. Domed sternum is a synapomorphy of symphytognathoids, with a reversal to flat in *Maymena mayana* (S03 – 13).
 51. Sternal pits: (0) absent (Fig. 35D); (1) present (Figs 123D, 125A). A (potential) synapomorphy of

Theridiosomatidae (see also Wunderlich, 1980a; Coddington, 1986a) (S03 – 10.3; G98 – 42).

52. Sternum cuticle: (0) imbricate–fingerprint (Figs 19D, 64H); (1) imbricate (Fig. 111B); (2) smooth (Figs 112E, H, 121C, G); (3) rugose (Figs 99G, 118F); (4) punctate (Figs 96B, E, 97A); (5) glabrous tuberculate (*Linyphia*). An imbricate–fingerprint cuticle pattern on the sternum is a potential synapomorphy for Mysmenidae. Rugose and punctate cuticle patterns occur within Anapidae.
53. Sternum posterior margin (in ventral view): (0) pointed (Figs 141F, 144H); (1) truncate (Figs 70B, 87A, 91D, 96B, 99C, 112E, 121C, 143O, 144K); (2) intermediate (Figs 2C, 7C, 25B, 35C, 46A, 59G, 140B, C, 143B). Pointed and truncate sternal margins are quite distinct in the taxa represented here, and these character states were more objectively defined by Griswold *et al.* (1998). Nevertheless, a spectrum from one extreme condition to the other is found, particularly in mysmenids. The systematic value of this character has already been questioned (Coddington, 1986a; Griswold *et al.*, 1998; Schütt, 2003). Even though the homology statement is compromised in state 2, no means were found to quantify the varying shapes of the posterior margins of the sternum, and therefore a first attempt is made here to accommodate those intermediate conformations. A truncate sternum optimizes as a synapomorphy of symphytognathoids (occurring in theridiosomatids, anapids, symphytognathids, and synaphrids), whereas an intermediate margin is synapomorphic of Mysmenidae, with a few reversals (S02 – 29; S03 – 11; G98 – 43).
54. Sternum–carapace junction: (0) junction free, pleura exposed (Figs 2A, 13A, 19C, 146F); (1) joined by ‘strips’ leaving the pleura partly visible, or posterior carapace fused with sternum (i.e. between coxae II–IV; Figs 72C, 91C, 145G); (2) one unit, pleura not visible, carapace and sternum completely fused (Figs 96E, H, 99B, 101A, 146B). The different degrees of junction between carapace and sternum occur within Anapidae (in clade C122), but the details of their evolution are ambiguous (S02 – 30; S03 – 12).

Eggsacs

55. Egg sac doubly attached: (0) absent, one thread; (1) present, double attachment (Figs 147B, 149A,B). Based on its presence in Mysmenidae, Theridiosomatidae, and Anapidae, Griswold *et al.* (1998) proposed the double attachment of egg sacs as a synapomorphy of symphytognathoids. Griswold & Yan (2003) reported the same behaviour for an undescribed *Patu* species (Symphytognathidae) from China. The symphytognathid egg sacs were at-

tached to frame lines on the periphery of the webs, attached to the web by one or a few silken lines, with the females hanging close to them. We have also observed similar behaviour in an undescribed symphytognathid from Australia (SYMP-006-AUST; Fig. 149A, B). Double attachment optimizes as a synapomorphy of symphytognathoids, as previously proposed. Females of the kleptoparasitic mysmenid species *Isela okuncana* carry the egg sac attached to the spinnerets, supported by the fourth legs (Griswold, 1985: 216) (G98 – 91).

Epiandrous fusules

56. Epiandrous fusules: (0) present (Fig. 20F, G); (1) absent (Fig. 100G, H). The loss of epiandrous fusules is synapomorphic of Symphytognathidae plus Anapidae, with a regain in *Comaroma* (G05 – 66; A04 – 168).
57. Epiandrous fusule distribution: (0) dispersed in a row (Figs 12B, 16A, 110G); (1) grouped in two bunches or pair of sockets (Figs 24D, 35F, 48A, 56E, 82F). When only two epiandrous fusules are present (e.g. in *Cepheia*; Fig. 107E), they were considered dispersed (state 0), given that no group of spigots is evident on either side. Dispersed spigots occur independently in synaphrids and within Mysmenidae, (ambiguously optimized) in *Maymena* and *Isela* (G05 – 67; A04 – 169).
58. Epiandrous fusule pair number: (0) more than ten; (1) eight or fewer (Figs 24D, 48A). More than ten epiandrous fusules occur in outgroup taxa *Linyphia triangularis* (see Agnarsson, 2004: fig. 3C), *Leucauge venusta*, and *Tetragnatha versicolor* (A04 – 170).

Epigynum

59. Epigynal area: (0) weak or absent (Figs 14C, 37A, 52F, 141I); (1) modified copulatory area (Figs 5A, B, 11B, C, 12D, F, 49D, E, 59H, 61A, 67A, B, 140D, I, 141G, H, 142C). The epigynal area is considered as weak or even ‘absent’ (state 0) if the cuticle in this area does not differ from the surrounding abdominal cuticle, and/or is usually translucent so that the spermathecae can be observed beneath it. A sclerotized plate or any protruding structure of the cuticle (state 1) usually bearing setae and the copulatory openings is here defined as a ‘true epigynum’. The loss of epigynum is ambiguously optimized within symphytognathoids: within Mysmenidae (in Mysmeninae), and in the clade comprising Synaphridae, Symphytognathidae, and Anapidae, with one regain in each of the latter two families (S02 – 146; S03 – 74; G05 – 131; A04 – 2).
60. Ventral scapus: (0) absent (Figs 14C, 56C); (1) present (Figs 24B, 29C, 31G, 37C, 42C, 129E). A scapus is

- a finger-like, usually membranous, epigynal projection that appears to be widespread among araneoids (Millidge, 1984; Scharff & Coddington, 1997; Agnarsson, 2004). In mysmenids, the scapus is a putative synapomorphy of the mysmenine clade C132 (S02 – 147; S03 – 75; A04 – 1).
61. Scapus: (0) subtle projection (Figs 24B, 42C); (1) longer than wide (Figs 29C, 31G, 129E). The relative length of the scapus is taken here as the relationship between its length and width. A very short scapus (state 0) is usually weakly projecting and wider than long. A longer scapus, the plesiomorphic condition for this data set, is distinctly longer than wide, although absolute length is not considered here. Short scapus occurs in mysmenids, in clade C123 within *Microdipoena*, and is gained several times within *Mysmena* (S02 – 147; S03 – 75; A04 – 1).
 62. External copulatory openings: (0) copulatory openings exposed in the epigynal area (Figs 59H, 107A, 115G); (1) copulatory openings concealed, within the epigastric furrow (i.e. the epigynal area containing the copulatory openings is hidden within the epigastric furrow; Fig. 24A). Internal copulatory openings occur independently as synapomorphies of Anapidae (with a reversal in the micropholcommatine representatives) and of Mysmeninae (S03 – 76).
 63. External copulatory openings number: (0) two (Figs 59H, 107A, B, 115G); (1) one, wide (Fig. 49D) (S03 – 76).
 64. Copulatory openings position: (0) caudal (posterior) or under a dorsal modified area (Figs 49D, 59H, 61B); (1) ventral (Figs 107A, 115G). Within symphytognathoids and when present, ventral copulatory openings are synapomorphic of the clade containing Anapidae, Symphytognathidae, and Synaphridae (node C113), with one reversal (A04 – 4).
 65. Copulatory openings shape: (0) wide, open (Fig. 107B); (1) narrow slits (Fig. 115G). Applicable to few taxa only, highly homoplastic (A04 – 5).
 66. Strong setae on epigynal area: (0) absent, similar setae on epigynal area and remaining abdomen (Figs 107A, 115G); (1) present, distinctly stronger than abdominal setae (Fig. 59H). Autapomorphy of *Mysmenopsis palpalis*.
 67. Epigynal area elevation: (0) flat, not elevated (Fig. 115G); (1) elevated ventrally (Figs 5B, 49D, 107A); (2) elevated ventral and posteriorly (Fig. 59H). Ambiguously optimized within symphytognathoids (S02 – 146; S03 – 74; G05 – 131; A04 – 2).
 68. Atrium: (0) absent (Figs 115G, 128A, F); (1) present (Figs 59H, 107A, B, 129A, E, G, 130B). The atrium, a 'widened cavity into the copulatory ducts' (Sierwald, 1989 – 2) can occur independently of the position of the copulatory openings. In our analysis an atrium leading to the copulatory openings is the plesiomorphic condition. Atria are lost independently within symphytognathoids: in Symphytognathidae, the mysmenid clade C161 (with some reversals), and in several anapids.
 69. Cuticle of atrium: (0) sclerotized, or as sclerotized as surrounding abdominal cuticle (Figs 59H, 107A, B); (1) membranous, translucent (Figs 129A, E, G, 130B). Membranous atrium is synapomorphic for Mysmeninae and a putative synapomorphy of Anapidae, ambiguously optimized because of the absence of atrium in Symphytognathidae.
 70. Dorsal plate: (0) internal, not exposed nor projecting (Figs 24B, 115G); (1) projecting, exposed, or protruding from epigastric furrow (Figs 11B, C, 12D, F, 37C, 42C, 44A, 49D, 67A, B). Regardless of the location of the copulatory openings, a wide dorsal plate (Millidge, 1984; 'middle field' of Sierwald, 1989) is, in some taxa, projecting so that it is exposed through the epigastric furrow. A projecting median plate is a synapomorphy of Mysmenidae, although with some reversions within the family.
 71. Female genitalia: (0) haplogyne (fertilization ducts absent); (1) entelegyne (with separate copulatory and fertilization ducts). The absence of fertilization ducts occurs only in *Tetragnatha versicolor* and *Comaroma simoni*. Although it had been suggested that *Trogloneta* could be haplogyne (Brescovit & Lopardo, 2008), our data shows that is not, as it has both separate copulatory and fertilization ducts (see Figs 64A, 67C, 128F). *Acrobleps*, as well as other anapid genera examined in detail here (except for *Comaroma*) seem to have both copulatory and fertilization ducts, and are postulated in the present study to be entelegyne (Figs 69E, 85B, D, 87D, 92F, 136A–E) (S02 – 149; S03 – 79; G98 – 24; G05 – 130).
 72. Proximal region of copulatory ducts (CD): (0) with smooth uniform (even) walls, ducts of increased diameter (when compared with the distal half of the CD; Figs 64A, 128F, 136B, E); (1) narrow ducts, diameter as in the distal half of CD (Figs 11D, 37D, 128D, G, 129G, 136D, 137C, E); (2) uneven (irregular) membranous ducts (Figs 18G, 27D, 128C, 129A, C, E, H, 130B). The increase in the diameter of the proximal portion (i.e. the first half of the ducts from the copulatory openings) of the copulatory ducts has been termed 'bursae' by Schütt (2003: character 77). An increased diameter of uniform walls (state 0) refers to wide ducts with rather smooth or regular walls, whereas membranous convoluted ducts (state 2) refer to a complex and usually extremely membranous (almost imperceptible) proximal portion of the ducts. Ducts

with uniform diameter (regardless of width) present no widening from the copulatory openings to the spermathecae. The latter condition (state 1) is widespread among symphytognathoids and even within Araneomorphae (L. Lopardo & G. Hormiga, pers. observ.), although ambiguously optimized here. An increased diameter of uniform walls (state 0) occurs in *Trogloneta* as well as theridiosomatids and many anapid representatives. Irregular copulatory ducts occur in most mysmenines and in the *Isela* representative *Isela*-MYSM-002-KENYA (S03 – 77).

73. Proximal turn of CD: (0) sclerotized as the rest of CD (Fig. 130B, G); (1) distinctly sclerotized (Figs 129A, B, 130A). There is a particular turn of the proximal membranous copulatory ducts in mysmenids, from the internal atrium, and immediately before becoming widened and convoluted, that is characterized by a subtle sclerotization. Only applicable to taxa with membranous internal atrium and copulatory ducts. This distinct sclerotization occurs convergently within Mysmeninae, in *Microdipoena*, and in several other mysmenine nodes.
74. Copulatory duct length: (0) short, length equal or shorter than the size of the spermathecae (Figs 128A, 130G, 136D, F); (1) long, length at least two times the size of spermathecae (Figs 129A, 130B, 136B, 137D) (S02 – 148; S03 – 78; G05 – 134; A04 – 8).
75. Copulatory duct–spermatheca junction: (0) posterior (Figs 128A, D, 129A, B, 136B, D, 137C); (1) lateral or anterior (Figs 18G, 27D, 42D, 51D, 129A, B, F, 130C, E). In most of the taxa here examined the copulatory ducts connect with the spermathecae posteriorly. Lateral or anterior junction is greatly homoplastic, occurring in Symphytognathidae, *Trogloneta*, *Mysmenopsis*, several mysmenines, and within theridiosomatids (A04 – 7).
76. Copulatory duct loops relative to spermathecae: (0) apart (Figs 37D, 124A, 129G, 136B, 137D); (1) copulatory ducts encircling spermathecae (Figs 107D, 120E, F, 137A, B). Only applicable to taxa with coiled copulatory ducts (see character 78, state 1). Encircling copulatory ducts occur in Synaphridae and Symphytognathidae, although homology of this condition is dubious because of ambiguous optimization (A04 – 9).
77. Copulatory ducts diverticulum: (0) absent (Figs 128A, F, G, 129G); (1) present (Figs 49A, 129C, 130D, G). A ventral membranous pouch diverting from the initial portion of the CD seems to be present in some mysmenids. This character is difficult to assess because of the membranous and translucent nature of most ducts in many mysmenids. Nevertheless, this diverticulum appears to have evolved distally within Mysmenidae.
78. Copulatory ducts trajectory: (0) straight (Figs 128A, E, 137C); (1) coiled (Figs 37D, 129G, 136B); (2) convoluted, switches but not coiled (Figs 18G, 22A, B, 27D, E, 42D, 49A, 51D, 67C, 136C). Homoplastic. Coiled copulatory ducts are plesiomorphic in symphytognathoids. Convoluted ducts are synapomorphic for Mysmenidae, although straight ducts occur in the mysmenid node C160, and also in node C153 within anapids.
79. Distal half of copulatory ducts: (0) sclerotized distinct duct; (1) membranous. A CD with proximal walls of increased diameter (character 71, state 0), can be followed distally by either a typical sclerotized copulatory duct (e.g. Figs 128F, 136C), or a membranous duct (e.g. Fig. 136B). Narrow CDs with constant diameter (character 71, state 1) remain as sclerotized ducts (state 0 of this character, e.g. Figs 128A, B, D, G, 129G, 137C), and CDs with membranous uneven ducts (character 71, state 2) remain as membranous (state 1 of this character, e.g. Figs 129A, B, C, 130A–G). Ambiguously optimized at the base of Anapidae, membranous distal ducts are synapomorphic for Mysmeninae, although reversals occur in clades C186 and C203.
80. Spermathecae compartment number: (0) two sperm-storage compartments per spermatheca (Figs 128F, 135C, 136C); (1) one compartment (Figs 33A, 136B, 137C). Two compartments evolve independently in the spermathecae of *Trogloneta*, *Minanapis*, and *Crassanapis* (S02 – 150; G98 – 26; A04 – 10).
81. Spermathecae wall: (0) defined by a thick, well-sclerotized wall (Figs 129A, 130B, 136B, 137C); (1) membranous, weakly sclerotized wall (Figs 49A, 87D, 130D, 136E). Membranous spermathecae evolved independently in the mysmenine MYSM-023-MAD and the anapid *Elanapis* (S02 – 151; G05 – 133).
82. Spermathecae: (0) separate (Figs 33A, 129A, 130B, 136B, 137C); (1) connate, fused along the midline, sharing median wall (Fig. 123A); (2) touching (*Leucauge venusta*). Originally proposed as a diagnostic feature of Theridiosomatidae (Coddington, 1986a), connate spermathecae is here an autapomorphy of *Theridiosoma gemmosum* (S03 – 79.1; G98 – 25).
83. Spermathecal shape: (0) ovoid (Figs 11D, 18G, 37D, 128D, 129A, G, 136B); (1) C- or cup-shaped (Figs 27D, E, 42D, 128E, 130C); (2) coiled within the same spermathecal structure (Figs 33A, B, 51D, 129C, 130B, G, 137C); (3) tubuliform, one large tube, sometimes like tracheoles (Figs 5D, 49A, 128A, C, 130D); (4) irregular, no particular shape

- (Figs 117B, 129D, 137E); (5) clavate (Figs 12C, 87D, 128B, 136E). We have attempted to homologize the variety of spermathecal shapes in as few states as possible to avoid the proliferation of similar shapes with no grouping information. Although there was ambiguous optimization within the outgroups, ovoid spermathecae is the plesiomorphic shape in symphytognathoids and Mysmenidae. Within Mysmenidae, spermathecal shape is homoplastic and mostly ambiguously optimized (A04 – 11).
84. Tubuliform spermathecae: (0) relatively straight (Figs 49A, 130D); (1) coiled (Figs 5D, 128A, C). Applies only to taxa with tubuliform spermathecae (character 83, state 3).
 85. Accessory glands: (0) absent; (1) present (Figs 22B, 27D, E, 29A, 64A, 98A, 129B, E, H, 130A, F, 136F). In the internal genitalia of the mysmenids, *Trogloneta*, *Microdipoena*, *Mysmena*-MYSM-005-ARG, the mysmenine MYSM-029-MAD, as well as in the anapid *Tasmanapis*, there is an additional paired structure that resembles either a muscular apodeme or a glandular structure. This structure, probably related to the copulatory ducts or the spermathecae, is better observed under SEM, although it can be distinguished in transparent preparations of the vulva by a higher degree of sclerotization, comparable with that of the spermathecae (Figs 129B, E, H, 130A, F, 136F; see also Brescovit & Lopardo, 2008: fig. 6C–E). Whether these structures are functional glands, muscle attachment points, or perform other functions remains unknown. As the appearance of these structures seems consistent with a glandular function, they are regarded here as accessory glands. Given the absence of palpimanoids in our data set (for which this character was originally established), the homology of the palpimanoid glands with these accessory glands of symphytognathoids remains to be tested (S02 – 152).
 86. Fertilization duct sclerotization: (0) weakly sclerotized but with a distinguishable wall (Figs 42D, 49A, 51D, 128A, 129G); (1) membranous, translucent, almost imperceptible (Figs 18G, 27D, E, 60H, 64A, 128F, 136D). Highly homoplastic (A04 – 13).
 87. Fertilization ducts: (0) small, shorter than spermathecae length (Figs 42D, 49A, 64A, 128A, F); (1) large, longer than spermathecae length (Figs 11D, 14E, 18G, 27D, E, 51D, 60H, 92F, 129G, 136D). Short fertilization ducts provide a direct connection between the spermathecae to the uterus externus, usually in a straight fashion and without modifications. Long fertilization ducts can have modifications or expansions. Long fertilization ducts optimize ambiguously at the base of the Symphytognathidae plus Anapidae node (most symphytognathids have short ducts). Within Mysmenidae, long ducts originated independently six times.
- ### Eyes
88. Anterior median eyes (AME): (0) absent (Figs 77B, 104F, 112C, D, 120A, 142M, 145C, D, 146H); (1) present (Figs 35B, 99E). Anterior median eyes are absent in all Symphytognathidae studied here (including *Crassignatha* and *Iardinis*), in some anapids, and in the mysmenid *Mysmeniola* (S02 – 20; S03 – 9; G98 – 27).
 89. AME size: (0) minute (Figs 67G, 99E); (1) same as others (Fig. 35B); (2) largest (at least two times ALE). Minute eyes (state 0) are distinctly smaller than any other eyes, and are characteristic of all eight-eyed anapids (although ambiguously optimized because of the loss of AME in Symphytognathidae) and *Trogloneta*. Similar AMEs (state 1) can encompass subtly larger eyes, but differences in size are subtle. Largest eyes (state 2) refer to eyes two times larger than ALE, as reported for the misplaced zodariid *Leviola* (see Miller, 1970; S02 – 20; S03 – 9; G98 – 27; A04 – 104).
 90. Eyes elevation (male): (0) AME flush with carapace (Figs 91H, 96C); (1) AME on protruded area (Figs 15B, D, 25C, 46D, E, 59C); (2) all eyes on tubercle (Figs 63G, H, 66A). Anterior median eyes level with carapace (state 0) occurring in all non-symphytognathoid representatives, as well as in all eight-eyed anapids (including *Taphiassa*). Both male and female mysmenids (except *Trogloneta*) and theridiosomatids have a groove or depression around the AME that to some extent delimits a protruded area (state 1, ambiguously optimized, potentially synapomorphic for Theridiosomatidae and for Mysmenidae). This area is clearly protruded, not just smoothly raised from the rest of the carapace, and is best observed in frontal view using SEM. Males of *Acrobleps* and *Trogloneta* species have all eyes in a tubercle or a narrow elevation of the ocular area (state 2) (S02 – 21; A04 – 103).
 91. Distance between AME: (0) AME close (Figs 25C, 35B, 99E); (1) AME separate (Fig. 142K). The original character states considered the distance between AME in relation to the distance between AME and their correspondent ALE. As the size of AME can differ across taxa, and at the same time this difference in size can affect their relative distance to the ALE, the same AME diameters were used as a criterion to define the distance between AME. Here, close AME (state 0) refers to AME separated by about one or less their diameter. On the other

hand, distant AME (state 1) refers to AME separated by two or more their diameter, and in this data set it evolves independently in *Brasilionata* and node C165 within *Mysmena* (*M. awari* and *M. marijkeae*). AME separation is similar in both sexes, except for a few species in which males have distant AME (state 1) and females have close AME (state 0). Sexually dimorphic taxa were scored as 'polymorphic' and include *Mysmena incredula* (Fig. 35A, B), *M. tembei* (Fig. 142H, I), *M. santacruzii*, and *Mysmena*-MYSM-005-ARG (S02 – 26).

92. AME-ALE separation (females): (0) distant; (1) close (Figs 35B, 99E). The original character states considered the distance between AME and ALE in relation to the AME diameter. As explained in Character 91, the difference in dimensions of the AME with respect to other eyes in some taxa could distort the relative distances, and consequently potentially alter state assignation. Therefore, AME-ALE separation was measured as proportional to the number of ALE diameters between them. This way, distant anterior median and lateral eyes (state 0) are eyes separated by more than two ALE diameters, whereas close eyes (state 1) are separated by less than two ALE diameters. Distant AME-ALE occurs in the tetragnathid representatives *Leucauge venusta* and *Tetragnatha versicolor* (A04 – 105).
93. Secondary eyes tapetum: (0) present; (1) absent. Loss of tapeta (state 1) is autapomorphic for *Tetragnatha versicolor*, although detailed information is missing for most of the taxa. Our scoring was taken from (Griswold *et al.*, 1998: character 28) (S02 – 27; G98 – 28; G05 – 47).
94. Lateral eyes (male): (0) juxtaposed (Fig. 72C); (1) separate. Separate lateral eyes are autapomorphic for *Tetragnatha versicolor* (S02 – 23; S03 – 10.1; G98 – 30; A04 – 102).
95. Lateral eyes: (0) level with carapace (Figs 69A, 82C); (1) common elevation (Figs 46D, 77B, 104E). Level lateral eyes occur independently in *Acrobleps*, *Comaroma*, *Tetragnatha versicolor*, and presumably *Leviola* (S02 – 24; S03 – 10).
96. PME separation: (0) PME close (Figs 15F, 77C); (1) PME separated (Fig. 67H). Close PME (state 0) defined as distance between PME less or equal to the distance between PME-PLA, occur in most of the examined taxa. Separate PME (state 1) have a distance of separation greater than with their correspondent PLA, and are synapomorphic for *Trogloneta*. Separated eyes are also presumably found in the zodariid *Leviola* (S03 – 10.2).

Legs

97. Leg cuticle texture: (0) smooth (Figs 80C, 119F, H); (1) imbricate (Figs 21H, I, 34B, 65E, H); (2)

fatiscent (Figs 73D, 87B, 93F). Imbricate leg cuticle is the widespread condition in the taxa comprising this data set. Fatiscent leg cuticle evolves convergently in several mysmenids, and is a putative synapomorphy of Anapidae (ambiguously optimized because of the fatiscent leg cuticle of *Synaphris*). Smooth leg cuticle is an ambiguously optimized synapomorphy of Symphytognathidae (S02 – 85; G05 – 10).

98. Ventral elevated setal bases on femur I (male): (0) absent (Figs 42G, 93E); (1) present (Figs 74E, 84A, B, D, 145K). Schütt's (2003) original definition of this character did not specify which side of the femur it was referring to, or whether the tubercles were just cuticular protrusions or setal bases. Here, the character is redefined to score ventral elevated setal bases on femur I, a synapomorphy of anapid clade C121. In *Steatoda* the bases are seemingly present and in all legs (S03 – 32.2).
99. Femoral macrosetae: (0) present (Figs 16D, 57B, 141A, D, 144F, J); (1) absent (Figs 21C, E, 42F, 45G). Most of the taxa in this data set lack spines or strong macrosetae. Macrosetae are considered here as distinct spines and also as setae that are stronger than most of the setae covering the legs, like those macrosetae located distally on the dorsal patellae. Within symphytognathoids, femoral macrosetae occur convergently on the clade including *Maymena* and Mysmenopsinae (i.e. node C160, with a reversal in *Mysmenopsis penai*) and in *Theridiosoma gemmosum* (S02 – 67; S03 – 33; G98 – 59; A04 – 183).
100. Fe IV trichobothria: (0) absent; (1) present. Femoral trichobothria are restricted to the tetragnathid representatives of this data set (S02 – 76; G98 – 58; G05 – 1).
101. Female femur I ventro-apical area ('femoral spot or projection'): (0) cuticle unmodified, as the rest of the femur (Figs 74F, 144J); (1) cuticle with either a sclerotized spot or a projection (Figs 34A, 39D, 57A, E, 140G, 141C, 143N). With just a few exceptions (*Mysmena*-MYSM-005-ARG, *Mysmenopsis penai*, and *M. palpalis* in this data set), most mysmenid species have either a sclerotized spot or a cuticular projection on the apical ventral surface of at least femur I. This so called 'femoral spot' is a synapomorphy of Mysmenidae (see character 102) (S03 – 32; G98 – 56).
102. Female femur I structure: (0) femoral spot (Fig. 34A); (1) femoral projection (Fig. 57E). A femoral projection is a synapomorphy of *Mysmenopsis*, although lost in some species (see character 101) (S03 – 32; G98 – 56).
103. Location of female femoral structure: (0) femur I only (Fig. 140G); (1) femora I and II (Figs 141C,

- 142B). The femoral structure of most female mysmenids occurs in both femora I and II. The occurrence of this feature only on femur I is convergent in *Trogloneta* and *Mysmenopsis* (when present), *Mysmena*-MYSM-007-MEX, *M. incredula*, and *M. santacruzii* (S03 – 32.1).
104. Femur I ventro-apical sclerotized spot on males: (0) absent; (1) present (Fig. 21A). A distal ventral femoral structure on males is not as widespread within mysmenids as it is for females. A sclerotized spot in males, however, occurs independently in several relatively large groups within Mysmenidae: *Maymena* and *Trogloneta* (ambiguously optimized at their bases because of an absence of spot in mysmenopsine males), node C124 within *Microdipoena*, and nodes C137 and C145 within *Mysmena*.
105. Location of sclerotized spot on males: (0) femur I only (Fig. 141O); (1) femora I and II (Fig. 140M). Contrary to females, most mysmenid males have the femoral spot (when present) only on femur I, only in two occasions the spot occurs in both femora I and II (*Maymena ambita* and *Mysmena tasmaniae*).
106. Stridulatory field on retrolateral femur IV: (0) absent (Fig. 39F); (1) present (Fig. 105F, H). This modified field was observed only in females of *Teutoniella cekalovici*. It is presumably stridulatory, as is usually suspected in any area with modified cuticle, especially on leg segments. Autapomorphy of *Teutoniella*.
107. Stridulatory field on proteral femur IV: (0) absent (Fig. 34E); (1) present (Figs 9A–C, 54H, 59F). Synapomorphy of Mysmenopsinae.
108. Stridulatory field on retrolateral femur I (female): (0) absent (Fig. 29D); (1) present (Figs 3C, 57B–D). This presumably stridulatory field was observed and scored at least in females, although it can also be present in some males. Synapomorphy of Mysmenopsinae.
109. Modified area on proteral femur I: (0) absent; (1) present (compare Figs 116A, C, 119A,B). The cuticle on dorsal femur I can be weakly or more distinctly modified (when compared with the retrolateral cuticle) in some members of Symphytognathidae (putative synapomorphy).
110. Metatarsi preening setae: (0) ventral and dorsal setae identical (Figs 29F, 74B, 119C); (1) ventral setae strongly serrated (Figs 83B, C, 93G, I). Metatarsal preening setae are defined here as ventral setae that are more strongly serrated than the dorsal setae. They usually occur in both sexes in all metatarsi, not only on metatarsi III and IV. Whether these specialized setae actually perform a preening function is not known. The distribution of these setae along the metatarsi can be lengthwise (e.g. in *Comaroma*) or distal (e.g. *Minanapis*). The presumed zodariid genus *Leviola* has been reported to have a preening comb not only in all metatarsi, but also in all tibiae and tarsi (Miller, 1970 – 156), and is here scored as present (state 1). In *Teutoniella*, at least on metatarsus IV, the ventral setae appear less serrated than the dorsal setae (Fig. 105G), and is here scored as absent (state 0) (S02 – 73; G05 – 19).
111. Metatarsus I trichobothrium: (0) absent; (1) present. Absence of trichobothria on metatarsus I is an autapomorphy of *Tetragnatha versicolor* (S02 – 77; S03 – 35.5; G05 – 5).
112. Metatarsus I trichobothrium position: (0) proximal, at or within the proximal third (0.33) of metatarsus (Figs 26D, 39E, 105E); (1) median, within the middle third (usually at midpoint) of metatarsus (0.5) (Figs 8A, 95H, 101F); (2) distal, within distal third (*Leviola*). Ambiguously optimized, proximal metatarsal trichobothrium occurs in Mysmenidae (with few distal reversals), Theridiosomatidae, some Symphytognathidae, and *Teutoniella* (A04 – 189).
113. Metatarsus III trichobothrium: (0) present (Fig. 21G); (1) absent (Fig. 109D). Absence of trichobothrium on metatarsus III is a synapomorphy of Synaphridae (A04 – 190).
114. Metatarsus I proteral clasp structure on males: (0) absent (Figs 90F, 125F); (1) present (Figs 3A, 16G, 26C, 42H, 45H, 59B, 74D, 140C, 141G, K, 142N). These metatarsal clasp structures are a synapomorphy of Mysmenidae (absent in *Maymena mayana*). Similar structures have independently evolved in some anapids (S03 – 35.3; G98 – 57; G05 – 22).
115. Metatarsus I proteral clasp structure form (males): (0) spur (Figs 74D, 101F, H, 145D, L); (1) clasp spine (Figs 3A, B, 8C, 26C, 57I, 140C, 141K, 142G). Clasp spines are mostly proteral and spurs appear to be proteral–ventral. Nevertheless, these two types of modified setae arise from a cuticular socket and have been considered as homologous in a previous study (see Lopardo & Hormiga, 2008 – 28, character 57). Here, clasp spurs and spines are also regarded as homologous, and spurs are hereafter referred to as ‘proteral’. Clasp spurs occur in Anapidae. All male mysmenids, except *Maymena mayana*, have a proteral clasp spine on the first metatarsus (S03 – 35.3; G98 – 57; G05 – 22).
116. Metatarsus I proteral clasp structure position (males): (0) basal, extremely proximal or on basal third of metatarsus (Figs 16G, 141K); (1) medial, on middle third of metatarsus, including its borders (Figs 8A, 26C, D, 140C, 142G, N); (2) apical, beyond middle third (i.e. on distal third)

- of metatarsus (Figs 50H, 59B, 143C, 144A). Ambiguously optimizing at the basal node of Mysmenidae, basal clasping spine is a putative synapomorphy of *Maymena*. Medial spine occurs in the majority of mysmenids. Apical clasping spines evolve independently on several occasions (S03 – 35.4).
117. Metatarsus I prolateral clasping spine shape (males): (0) relatively straight or weakly curved (Figs 16G, 34C, 62E, 65C, 68B); (1) twisted (proximally straight and curved at middle angle, Figs 3B, 8B, C, 26C, 140E, F, 141K, L, 142N); (2) strongly curved proximally (Figs 54D, 57I, 59B). This character applies only to the shape of the metatarsal clasping spines. Twisted spine is synapomorphic of mysmenid nodes C127 and C164, and ambiguously optimized in *Isela*. Most *Mysmenopsis* representatives have strongly curved metatarsal clasping spines, although optimization is ambiguous because of straight spine of *Mysmenopsis penai*.
 118. Metatarsus I distal spine or stronger setae near to clasping spine (males): (0) absent (Fig. 62E); (1) present (Fig. 34C). Applicable only to metatarsal clasping spines. A stronger seta located close to the clasping spine occurs independently in two mysmenids (*Mysmena incredula* and *Microdipoena samoensis*).
 119. Metatarsus I proximal row of between five and eight spines or strong setae near clasping spine (males): (0) absent (Fig. 62E); (1) present (Figs 57H, 59B, 140H, J). Applicable only to taxa with metatarsal clasping spines. Ambiguously optimized synapomorphy of *Mysmenopsis*.
 120. Metatarsus I clasping spur number (males): (0) one (Fig. 145L); (1) two (Figs 74D, 101F, 145C, D). Applicable only to metatarsal clasping spurs.
 121. Metatarsus I apical prolateral spur (females): (0) absent (Fig. 89F); (1) present (Figs 74G, 84C, E). An apical spur on metatarsus I occurs in males but also in females of *Anapisona kethleyi* and *Crassanapis chilensis* (node C121).
 122. Metatarsus I apical retrolateral spur (males): (0) absent; (1) present (Fig. 73A). Males of *Anapisona kethleyi* have not only two spurs prolaterally on the first metatarsus but also one distal retrolateral spur.
 123. Metatarsus II prolateral clasping spine (males): (0) absent; (1) present. The presence of a second clasping spine on metatarsus II of males is an autapomorphy of *Mysmena santacruzii* (Baert & Maelfait, 1983 – 104).
 124. Patella dorsal macrosetae: (0) present (Figs 21D, 56A, 65B, 89G, 101D); (1) absent (Figs 80B, 83D, 109C). Dorsal distal patellar macrosetae (i.e. stronger setae) is independently lost (state 1) in *Comaroma* and *Cepheia* (S02 – 68; S03 – 34).
 125. Leg spination: (0) three or more macrosetae dorsally on tibiae, or macrosetae present also on femora, metatarsi, and/or ventral tibiae (Figs 140H, M, 141C, 144E, J); (1) ‘reduced’, only one or two macrosetae dorsally on tibiae, none on femora, metatarsi, and/or ventral tibiae (Figs 140E, 142E, 145G, K). ‘Reduced’ leg spination occurs in most symphytognathoids. When strong spines also occur, they are scored here as state 0. ‘Strong’ spination is synapomorphic for *Maymena*, convergent in *Mysmenopsis dipluramigo* (G05 – 21).
 126. Leg I (females): (0) with femur as wide as the other legs’ femora (Figs 140N, 145G, 146A); (1) femur two times as wide as the other legs’ femora (Figs 140A, D, G, 145J). This character was scored for females to avoid dependency of characters, as stronger leg I can be sexually dimorphic (i.e. stronger legs in males but not females, see character 128). Strong legs are a synapomorphy of Mysmenopsinae, also convergently occurring in *Crassanapis* (S02 – 63; G98 – 55; A04 – 182).
 127. Metatarsus–tarsus joint: (0) both segment tips with same width as rest of the segments (straight, square), i.e. not constricted (Figs 12G, 21B, 39J, 62G, 101B); (1) both segment tips constricted (Figs 109A, 111G); (2) tarsal tip constricted, metatarsal tip straight or square (Fig. 80A). Constriction of both metatarsus and tarsus optimizes here as a synapomorphy of Synaphridae.
 128. Leg I dimorphism: (0) absent (Figs 140D, E, M, N, 146A, B); (1) present, male leg I stronger or longer (Figs 143D, F, 144D, E, 145E, F, J, K). Leg dimorphism occurs independently on few species (S03 – 30).
 129. Tarsus I superior claws: (0) with comb of perpendicular long teeth (five or more separated teeth), teeth equally long or increasing in length (Figs 80D, E, 95F, G, 122G); (1) with a distinct row of four or more teeth of distally increasing length, oriented forward and usually touching (teeth can be short; Figs 3E, 12F, 56B, 109E, 111H); (2) with a row of between one and three short teeth oriented forward (Figs 26B, 52D, 65F, 69F, 70F, 73C, 123G); (3) smooth, teeth absent. Smooth paired claws (state 3) are autapomorphic of *Mysmena acuminata* (Marples, 1955). Paired claws with few short teeth (state 2) occur in most symphytognathoids and can be considered as a synapomorphy for the group. Claws with four or more teeth of decreasing length (state 1) are synapomorphic (and secondarily gained) for Mysmenopsinae (S02 – 81; S03 – 37).
 130. Tarsus IV median claw (male): (0) short, at most subequal than superior claws (Figs 83F, 95E); (1) long and strong, as superior claws (*Tetragnatha*);

- (2) long and slender (Figs 34F, 48G, 88I, 101G, 122H). Long and slender median claw IV in males (state 2) is a potential synapomorphy of symphytognathoids. Synaphridae has short median claw (state 0) (S02 – 82; S03 – 38; G98 – 63; A04 – 199).
131. Tarsus IV median claw (female): (0) short, at most subequal to superior claws (Figs 16F, 80F); (1) long and slender (Figs 9E, 12H, 123H); (2) minute (*Leviola*). Long and slender median claw IV in females (state 1) is a potential synapomorphy of symphytognathoids, with a reversal in *Maymena rica* and node C150 within Anapidae (A04 – 200).
132. Sustentaculum: (0) absent (Fig. 48G); (1) present. A sustentaculum occurs in the tetragnathid representatives of this data set (S02 – 84; G98 – 64).
133. Tarsal organ position: (0) proximal, by the junction with metatarsus (Figs 39C, H, 50D, E, 119D, 125G); (1) median, on the middle third of tarsus (Figs 8E, 54E, 56F). The position of the tarsal organ is constant in all legs in most examined taxa, except for (at least) *Isela okuncana* and *Taphiassa*, where the tarsal organ is medial on tarsus I, but basal on tarsus IV, and were scored here as polymorphic. Basal tarsal organ is a synapomorphy of symphytognathoids, with a reversal in Synaphridae and Mysmenopsinae (S03 – 39).
134. Shape of tarsal organ pocket: (0) domed (Figs 9D, 26E, 48F, 50D, 54F, 73B, 95I, 101E); (1) flat (Figs 109B, 119D). Scored for leg I. Some taxa have an intermediate shape of the capsulate tarsal organ (e.g. Figs 46G, 116E), where it is not clearly domed but is neither flat. These dubious situations were scored as ‘?’. Flat tarsal organ occur in *Cepheia* (Synaphridae), independently in *Mysmena* MYSM-007-MEX and *M. acuminata* (Mysmenidae), and ambiguously within Symphytognathidae (S03 – 40).
135. Size of tarsal organ opening: (0) distinctly smaller than setal sockets (Figs 3F, 54F, 62H, 109B, 119D); (1) subequal or larger than setal sockets (Figs 26E, 39C, 48F, 50D, 73B, 83E, 95I, 101E). This character was scored only for leg I, as the tarsal organ opening on leg IV is usually smaller than setal sockets. Small opening is the plesiomorphic condition; occurring in Synaphridae, most symphytognathids, and *Theridiosoma gemmosum*. Larger opening is independently synapomorphic for Anapidae and Mysmenidae (with a reversal in Mysmenopsinae and *Mysmena incredula*) (A04 – 198).
136. Shape of tarsal organ opening: (0) round (Figs 26E, 48F, 73B, 95I, 119D); (1) teardrop (Figs 3F, 9D, 62H, 101E, 125G). Within Mysmenidae, the teardrop tarsal organ opening is a synapomorphy of Mysmenopsinae. This shape of the opening also occurs independently in a few other symphytognathoids.
137. Tarsus IV ventral setae: (0) same as dorsal setae (Figs 3D, 26F, 39I, 74C); (1) serrated tarsal comb (i.e. theridiid comb); (2) sparse strongly serrated bristles (not a comb) (Figs 80G, 84F, 93H). The genus *Leviola* has been reported to have a serrated setae not only in all metatarsi (preening comb, see character 110), but also in all tibiae and tarsi (Miller, 1970 – 156), and is here scored as present (state 2). In *Isela okuncana*, both ventral and dorsal setae are serrated (Fig. 3D), and it is therefore scored as state 0. *Trogloneta* (Fig. 65G) and the symphytognathid SYMP-006-AUST (Fig. 119G) have weakly serrated ventral setae, but stronger than dorsal setae (although not ‘strongly serrated’), and therefore were scored as polymorphic (states 0 and 2). Strongly serrated ventral setae occur in Theridiosomatidae, some anapids, and *Symphytognatha picta* (S03 – 36; G98 – 62; G05 – 25; A04 – 193).
138. Tarsus I prolateral row of modified setae (male): (0) absent (Figs 74A, 89E); (1) present (Figs 16H, 34D, 59D, 65D). First observed and described as a ventral row of modified setae by Thaler (1975, 1995) for *Trogloneta granulum* and *Mysmeniola spinifera*, this prolateral row of modified setae (see below) is a potential synapomorphy for Mysmenidae.
139. Tarsus I prolateral row, type of setae (male): (0) shorter than surrounding setae, slim and curved (Figs 16H, 26A, 34D, 45I, 50F); (1) shorter, but stout and straight (Figs 8F, 54G, 59D, 65D, 68A). Applicable only to taxa with prolateral row of modified setae. Ambiguous optimization. Stout setae occur in *Trogloneta* and Mysmenopsinae, whereas slim setae are present in *Maymena* and Mysmeninae.
140. Tarsus I prolateral row of setae distribution (male): (0) along tarsus (Figs 8F, 16H, 65D, 68A); (1) distal half of tarsus (Figs 26A, 34D, 45I, 50F, 54G, 59D). Ambiguous optimization. Setal row along tarsus occurs in *Maymena*, *Trogloneta*, and *Isela*, and independently in *Mysmeniola*. Distal row is present convergently in *Mysmenopsis* and Mysmeninae.
141. Tibia dorsal macrosetae: (0) present (Figs 9F, 39G, 73E, 90E, 101C, 119H); (1) absent (Figs 80H, 83A, 111F). Generally at least one macrosetae, similar to that of the distal patella, is present on the dorsal tibiae. Tibial macrosetae are lost independently (state 1) in *Comaroma* and Synaphridae (S02 – 69; S03 – 35).
142. Tibia I prolateral apical clasping spine on males: (0) absent (Figs 45H, 90E, 143L); (1) present (Figs 3A, 26C, 140E, J, K, 141K, L, O). In addition to the prolateral metatarsal clasping spine,

some male mysmenids also have one or two prolateral clasping spines on tibia I. Tibial clasping spines evolved convergently within Mysmenidae: in *Microdipoena*, and ambiguously optimized at node C160 (*Maymena* + Mysmenopsinae, ambiguous because of its absence in *M. mayana*) (S03 – 35.1).

143. Tibia I prolateral apical clasping spines number (males): (0) one (Figs 3A, 8D, 16G, 54C, 59B, 62E, F, 140E, J, K); (1) two (Figs 26C, 27I, 57F, G, 140H, 141L, O). Only applicable to taxa with tibial clasping spines. Basal mysmenids (i.e. *Maymena* and Mysmenopsinae) have one tibial clasping spine (except for *Mysmenopsis dipluramigo*), whereas distal mysmenids (i.e. *Microdipoena*) have two spines.
144. Row of between two and five stout setae basal to tibial clasping spines (males): (0) absent (Figs 3A, 21F, 59B, 62E, 140E); (1) present (Figs 54C, 57G, J, 140H, J, K). Additional to the tibial clasping spine, stout setae occur in two instances within *Mysmenopsis*.
145. Tibia I prolateral median clasping structure on males: (0) absent (Fig. 21F); (1) present (Figs 16G, 73A). A median clasping structure occurs independently in *Maymena rica* and in *Anapisona*.
146. Ventral apical clasping spine on tibia II (males): (0) absent; (1) present (Figs 116B, D, 119H–J). A ventral clasping spine on tibia II of males occurs within symphytognathids (node C156), including taxa previously placed in Mysmenidae as *Iardinis mussardi* and *Crassignatha*.
147. Tibia I ventral paired setae with protruded bases (males): (0) absent (Fig. 70D); (1) present (Figs 48C–E, 50G). Evolves independently within Mysmenidae, in the Malagasy species MYSM-020-MAD and MYSM-023-MAD.
148. Ventral–prolateral row of short spines on tibia II: (0) absent; (1) present (Fig. 70E). Autapomorphy of *Acrobleps*.
149. Tibia III–IV trichobothrial length: (0) short, length equal or less than two times tibia diameter (Figs 84G, 90B, 93D); (1) median, length between more-than-two but less-than-three tibia diameters (Figs 26G, 29E, 39G, 73F, 88H); (2) long, length equal or more than three times tibia diameter (Figs 16E, 68D, 113H, 116F, 119E). As the trichobothria on the same tibial segment may differ in length, this character was scored based on the longest of them. Although long trichobothria on tibia III and IV (state 2) was proposed as a synapomorphy of Theridiosomatidae (Coddington, 1986a; Griswold *et al.*, 1998), here long trichobothria is also found in some anapids, micropholcommatids, mysmenids, and symphytognathids as well. Although highly homoplastic, short-length

trichobothria appear to be the ancestral state in symphytognathoids (S03 – 35.2; G98 – 61).

150. Tibia IV trichobothrial shaft: (0) smooth or serrated (Figs 16E, 113H); (1) distinctly plumose (Figs 90B, 93D). Plumose trichobothrial shaft is ambiguously optimized within Anapidae because of its occurrence in *Elanapis* and *Minanapis*.

Male palp

151. Bulb–cymbium lock mechanism (B–C lock): (0) absent; (1) present. B–C lock mechanism is an autapomorphy of *Steatoda* in this data set (A04 – 31; G98 – 12).
152. Conductor: (0) present (Figs 18D, 81B, 88D, 102A, 110A, 117D, 124F); (1) absent (Figs 4A, 10E, 28D, 76A, 95A, 113F). A convention discussed in Griswold *et al.* (1998) and followed here, contemplates that when only one sclerotized tegular sclerite occurs in the male palp (in addition to the embolus), which cannot be homologized to any of the palpal sclerites because of its uncertain structure and/or origin, it is regarded as the conductor. If two or more sclerites are present, then the one that originates closer to, or with a clear interaction with the embolus, is regarded as the conductor, the second is referred to as the MA, etc. Some mysmenids have a voluminous and membranous structure of the tegulum, which appears to originate close to the embolic base (Fig. 18D). This structure has been named ‘bulbal shield’ (e.g. Baert, 1984a; Schütt, 2003), and besides the embolus, it appears to be the only structure of the bulb. This structure often embraces and/or covers the embolic base, sometimes even a groove housing the embolus can occur. Even though the general structure of this feature is distinctive in most mysmenids (when present), it is regarded as a conductor here based on its origin and association with the embolus. Also, this homology statement avoids the proliferation of taxon-specific terms, otherwise of untestable homology. Here, the occurrence of conductor is symplesiomorphic and widespread, with independent losses of this sclerite occurring within symphytognathoids in anapids, symphytognathids, and mysmenids. Within Mysmenidae, the conductor is lost two times: in the node comprising *Maymena* and Mysmenopsinae (node C160), and in MYSM-005-ARG (G98 – 14; G05 – 118; A04 – 62; S03 – 69.2).
153. Conductor shape: (0) single, simple (Figs 102A, 117D, 124B); (1) bifid or with apophysis (i.e. two main peaks; Figs 88D, 106C, 110A, 122C); (2) complex, three or more peaks (Figs 81B, 86G, 92B, 114E); (3) globose and voluminous membrane

- (Figs 17A, B, D, 18D, E, 27A, B, 30A, E, 36C, 41D, 63A, D). A simple conductor is the plesiomorphic condition of symphytognathoids, occurring also in Theridiosomatidae. Bifid conductor optimizes as a putative synapomorphy of clade C113 (Synaphridae + Anapidae + Symphytognathidae), with ambiguously optimized distal transitions (to both simple and complex conductors) in Symphytognathidae and Anapidae. A voluminous and membranous conductor is a putative synapomorphy of Mysmenidae (S02 – 141; S03 – 72; G98 – 15; G05 – 121).
154. Conductor size: (0) large, about half the size or length of bulb, or larger (Figs 88D, 102A, 106D); (1) small, considerably smaller than half the size of the bulb (Figs 114E, 117D). Small conductor occurs independently in *Tasmanapis* and the symphytognathid node C156 (S02 – 142).
 155. Conductor position (origin): (0) subterminal, medial on ventral view (Figs 81B, 88D); (1) terminal, originating on the apical border of tegulum (Fig. 106C). Subterminal conductor is synapomorphic for the ANTS clade, with a reversal in *Cepheia longiseta* and *Iardinis mussardi* (G05 – 119; A04 – 69).
 156. Conductor distal groove: (0) with a groove for the distal portion of the embolus (Figs 106C, 117D, 124F); (1) entire, without groove (Figs 81C, 114E). A groove for the distal embolus is lost independently in Mysmenidae, in some anapids, and in a few symphytognathids (A04 – 64).
 157. Conductor tip sclerotization: (0) like base (Figs 138C, 139D); (1) more than base (Figs 138B, 139B,C). Ambiguously optimized. A sclerotized distal conductor occurs in Synaphridae, *Symphytognatha*, and *Crassanapis* (A04 – 67).
 158. Conductor apical portion: (0) width subequal to base (Figs 81C, 88D); (1) at least a portion is larger than the base width (Figs 86F, 124B). Ambiguously optimized. A large conductor occurs in *Microdipoena*, *Crassanapis*, theridiosomatids, and *Cepheia*. Subequal conductor occurs in *Synaphris*, symphytognathids, and most anapids. In most mysmenids this condition is unknown (i.e. scored as '?') (A04 – 63).
 159. Conductor surface: (0) smooth (Fig. 124B); (1) with small ridges or other cuticular structures (Figs 102A, D, 106D, 117D, E). Ridged conductor occurs independently in *Trogloneta*, *Teutoniella*, SYMP-006-AUST, and Synaphridae (A04 – 65).
 160. Conductor groove housing proximal and/or median embolus: (0) entire, without a groove (Figs 17A, B, D, 27A, B, 88D, 110A); (1) with a groove housing the proximal and/or median portions of the embolus (Figs 36B, C, 47E, 92B, 106D). Grooved conductor housing the embolus proximally is plesiomorphic for symphytognathoids.
- Entire conductor evolved independently three times: in *Trogloneta*, in the mysmenine clade C127, and in the clade comprising Symphytognathidae plus Anapidae (A04 – 68).
161. Conductor (C) and embolus (E) interaction: (0) separate, no association (Figs 63A, D, 81C, 114E); (1) conductor embraces embolus (Figs 41C, 43A, B, 86G, 117D). An association between C and E (state 1) is regarded as present when the C embraces the E completely or at least partially (e.g. in a groove), or when both C and E appear associated (usually adjacent through some length of the embolus). Although the presence of a distal or a basal groove on the conductor (characters 159 and 164 respectively) constrains the scoring of state 1 in this character, its absence is unspecific about the association between the two sclerites. A separate conductor occurs independently in *Trogloneta*, *Comaroma*, and a few symphytognathids (S02 – 143; S03 – 73; G98 – 19; G05 – 120).
 162. Cymbium and bulb size relative to carapace: (0) medium, about half size of carapace in lateral view (Figs 27F, 66A, 118B, 121B, 141K); (1) small, about one-fifth the size of carapace in lateral view (Figs 2B, 96D, 140E, 141D, 144D, G); (2) large, as large as prosoma (Figs 19B, 108G, 142A). The relative size of the male palp (i.e. excluding the palpal tibia) of the mysmenid genera *Isela* and *Mysmenopsis* was scored as small, as the large tibia is not taken into account for the general size of the palp. Although small male palps are common in spiders, medium-sized palps are widespread within symphytognathoids, becoming secondarily small in Mysmenopsinae (ambiguous optimization because of its small size in *Maymena mayana*). Huge male palps evolve independently in Theridiosomatidae, *Cepheia*, node C173 within *Microdipoena*, and twice distally within *Mysmena* (S03 – 61).
 163. Cymbium orientation: (0) dorsal, prolateral–dorsal (Figs 90A, 104D); (1) ventral, prolateral–ventral (Figs 38A, B, 42B, 66A); (2) strictly prolateral (Figs 50B, 115B, C); (3) retrolateral–dorsal (Figs 15B, 76B, 111A). Dorsal cymbia is the plesiomorphic condition for this data set. A ventral cymbium is a synapomorphy of Mysmenidae, further changing to prolateral in some taxa within the family, including *Mysmenopsis*. Retrolateral cymbium occurs in clade C167 within *Maymena*, and in *Synaphris* (S03 – 66; G98 – 2).
 164. Cymbium shape in dorsal view: (0) oval, longer than wide, cup-shaped, length of cymbium about 1.5 width or more (Figs 10A, 14A, 28B, 71E); (1) curved thin stripe without median constriction, length about five times cymbial width

- (Figs 106E, 124D); (2) curved thin stripe with median constriction (*Tetragnatha versicolor*); (3) as long as wide (Figs 1A, 4C, 22F, 30D, 41B, 55B); (4) distinctly flat and tapering distally with irregular edges (Figs 63C, 113E, 117C); (5) about two times wider than long (Fig. 76B). The cymbia of some symphytognathoids are usually modified compared with the typical cymbium of spiders, which is round to oval in dorsal view (see, e.g. Griswold *et al.*, 1998, figs 16A, 18F). This is especially so in mysmenids. The various morphologies of the cymbia (in dorsal view) were roughly accommodated into the different states proposed here. The general outline of the cymbium does not take into account any other structure considered by other characters (e.g. cymbial conductors, apophyses, paracymbia, expansions, etc). In this data set, an oval cymbium is the plesiomorphic and also widespread condition in symphytognathoids. A cymbium as long as wide (state 3) occurs independently only in Mysmenopsinae and most Mysmeninae (node C131), whereas a distinctly flat and tapering cymbium (state 4) occurs in *Trogloneta* and convergently in some symphytognathids (S03 – 65.2; G98 – 4, 5; A04 – 21).
165. Cymbium tip: (0) blunt (Figs 71B, 102D, 110B); (1) with distinct distal tip (Figs 55B, 58B, 114D). Not applicable in species with cymbial conductor. A distinct cymbial distal end is an ambiguously optimized synapomorphy of *Mysmenopsis*, convergent in some symphytognathids (S03 – 65.3).
166. Cymbial tarsal organ: (0) present (Figs 4I, 76J, 102F); (1) absent. Although homoplastic and optimizing ambiguously, an apparent loss of the cymbial tarsal organ occurred at the base of the clade comprising anapids, symphytognathids, and synaphrids.
167. Location of cymbial tarsal organ: (0) external (Figs 10I, J, 44D, 58C, 76A, J, 102F); (1) internal (Figs 4I, 40B, C, 63B, F). An internal tarsal organ optimizes as convergent for *Trogloneta*, *Isela*, and the mysmenines *Mysmena*-MSM-015-MAD and MYSM-020-MAD.
168. Cymbium dorsobasal margin: (0) entire (Fig. 10A); (1) strongly incised (Fig. 12A). Incised dorsobasal cymbial margin is an autapomorphy of *Maymena mayana*, although an uncertain condition is also found in *Trogloneta* (Fig. 66B) (A04 – 23).
169. Cymbial prolateral distal salience: (0) absent (Fig. 113E); (1) present (Figs 114E, 117C). Synapomorphy of the symphytognathid clade C199 (A04 – 24).
170. Cymbial prolateral basal expansion: (0) absent (Figs 10B, C, 55A); (1) present (Figs 4B, 27A, 30B, C, 36C, 47B, 66D, 110E). This character was originally named ‘prolateral basal paracymbium’ by Schütt (2003). The term ‘paracymbium’ has been proposed for the classical araneoid retrolateral process on the cymbium (e.g. Comstock, 1910; Coddington, 1986b, 1990; Griswold *et al.*, 1998, and references therein). In order to avoid misinterpretations, the prolateral structure examined in this character is simply referred to as ‘prolateral basal expansion’. This expansion surrounds the bulb ventrally in varying degrees (see next characters), and occurs in theridiosomatids and most mysmenids. Ambiguous optimization. Absent in *Maymena* and most mysmenopsines (S03 – 69.1).
171. Cymbial prolateral basal expansion size: (0) small, from a subtle expansion to covering (surrounding) half the bulb (Figs 4B, 27A, 36C, 47B, 66D, 110E); (1) large, surrounds the bulb ending close to the paracymbium on the retrolateral side (Figs 30A, B, 32A–C). An expansion surrounding the bulb evolves convergently in *Mysmena incredula*, *Mysmeniola spinifera*, and MYSM-007-MEX (S03 – 69.1).
172. Cymbial prolateral basal expansion setal pattern at tip: (0) no setae (Figs 4B, 27A, 36C, 47B, 66D, 110E); (1) setae present (Figs 31A, 32F). Only applicable in species with prolateral basal expansion. Within Mysmenidae, the presence of setae at the distal end of this expansion occurs in clade C138 within *Mysmena*, and also in *Mysmeniola* and clade C172 within *Microdipoena* (ambiguous optimization).
173. Cymbial prolateral basal expansion setae at tip: (0) minute, almost imperceptible (Figs 30A, 31A); (1) half the length of surrounding cymbial setae (Figs 18E, 32B, F). Only applicable in species with prolateral basal expansion. Minute setae occur independently in *Mysmeniola* and MYSM-007-MEX.
174. Stout short spines on cymbial prolateral basal expansion, below cymbial groove: (0) absent (Fig. 18E); (1) present (Fig. 32F). Autapomorphy of *Mysmena incredula*.
175. Primary cymbial conductor (CyC1): (0) absent (Figs 53D, 60D, 81C, 117C); (1) present (Figs 4G, 10C, 14B, D, 22F,G, 27A–C, 30F, 47C, 63C). Up to two apical cymbial grooves seemingly interacting with the distal portion of the embolus can occur on male cymbia. Both structures are here considered cymbial conductors. The ‘primary cymbial conductor’ (CyC1) is located internally (i.e. closer to the bulb) and, when present, can bear the cymbial fold (CyF). The ‘secondary cymbial conductor’ (CyC2) is external, located on the edge or dorsally on the cymbium (Figs 30F, 31C, 43C). The primary cymbial conductor is a

- synapomorphy of Mysmenidae, with a secondary loss in *Mysmenopsis*. An internal conductor can also occur in some anapids (*Anapisona* and *Minanapis* in this data set).
176. Primary cymbial conductor position: (0) prolateral–apical (Figs 4G, 10G, 14B, 63B, C); (1) retrolateral–apical (Fig. 76A); (2) strictly apical (Figs 22F, 27A, 30F, 41D, 43C, 47E, 92B). All cymbial conductors are located apically on the cymbium, but they differ on how far they extend into the margin of the cymbium. A prolateral CyC1 (state 0, synapomorphy of the clade C161 comprising *Trogloneta*, *Maymena*, and Mysmenopsinae) runs along about half or the entire prolateral edge of the cymbium, ending apically. In *Trogloneta* the longitudinal axis of the cymbium is at an angle relative to the axis of the pedipalp (displaced prolaterally) and the conductor is in prolateral position (Fig. 63C). *Anapisona* has a retrolateral primary conductor (state 1). The apical conductor (state 2, optimizing as the ancestral state for symphytognathoids) does not extend to either side of the cymbium.
177. Primary cymbial conductor apical end: (0) pointed, or extending vertically (Figs 4G, 30F, 40B, 43C, 47C, 76A); (1) blunt, extending transversally (Figs 22F, G, 63B, C, 92A,B); (2) irregular, expansions prolateral, retrolateral, and apically (Fig. 27A–C); (3) square apical end, apical cymbium bent over ventrally (Fig. 10D, G). Blunt (transversal, state 1) primary conductor occurs in *Trogloneta*, *Microdipoena* s.s. (i.e. node C172), and *Minanapis*. Most mysmenids have a pointed (state 0) cymbial conductor, which changed to apically irregular (state 2) in clade C127 and in *Mysmena santacruzii*. The primary cymbial conductor of *Maymena ambita* is apically square (state 3), with the apical cymbium bent over the ventral side. A similar cymbial arrangement is also found on the other *Maymena* representatives in this data set, although the cymbial conductor is also apically pointed, and was therefore scored as polymorphic.
178. Prolateral setal pattern on primary cymbial conductor: (0) setae as in the rest of cymbium (Figs 4F, G, 10G, H, 14B, D, 22C, 40A, 43C, 92A); (1) with one or two setae distinctly thicker than surrounding setae (Figs 28G, 30F, 31B). Distinct prolateral setae occur independently in MYSM-005-ARG and MYSM-007-MEX.
179. Shape of blunt primary cymbial conductor: (0) half circle (Fig. 63B, C); (1) spiral, one loop (Fig. 22C); (2) subtle depression (Fig. 92A, B). This character applies only to taxa with blunt primary cymbial conductor (character 177, state 1). This character optimizes ambiguously because of the few representatives with blunt primary cymbial conductor. Spiral conductor occurs in *Microdipoena* s.s. (node C172), half-circle shaped conductor in *Trogloneta*, and a subtle depression occurs in *Minanapis*.
180. Secondary (external) cymbial conductor (CyC2): (0) absent (Figs 22F, 63C); (1) present (Figs 4F, G, 10G, I, 31C, 40A, 43C, 60D, 71F). See character 175. Highly homoplastic. Within Mysmenidae, a secondary cymbial conductor occurs independently in most *Maymena* (node C167), in *Isela*, *Mysmenopsis penai*, and in Mysmeninae (becoming secondarily absent within the latter at node C128). An external conductor also occurs independently in *Acrobleps*, *Patu*-SYMP-001-DR, and *Tetragnatha versicolor*.
181. Secondary cymbial conductor position: (0) prolateral–apical (Fig. 4F–H); (1) apical (Figs 10E, 14B, 31C, 40A, 43C, 47C); (2) retrolateral–apical (Figs 60D, 71F). See character 176. Most mysmenids have an apical secondary conductor (state 1), which is the plesiomorphic condition for Mysmenidae (and the entire data set). Prolateral secondary conductor occurs in *Isela*; retrolateral conductor in *Mysmenopsis penai*.
182. Retrolateral apical setal pattern: (0) setae as in the rest of cymbium (Figs 14B, 40A, E, 60D); (1) with one or two setae distinctly thicker than surrounding setae (Figs 47D, 76H). Thicker setae are present convergently in the mysmenids MYSM-020-MAD, MYSM-023-MAD, MYSM-007-MEX, and in the anapid *Anapisona*.
183. Retrolateral apical modified seta/ae: (0) distally serrated and extremely thick single seta, four times thicker than surrounding setae (mysmenines, Figs 31D, 47D, 49C); (1) two smooth thick setae, about two times thicker than surrounding setae (*Anapisona*, Fig. 76H).
184. Cymbial conductor housing embolus (mostly SEM observation): (0) primary cymbial conductor (Fig. 14D); (1) secondary cymbial conductor (Figs 4G, H, 30F, 47C). Applies to taxa with two cymbial conductors, because of logical dependency when only one conductor occurs. Homoplastic. Embolus fitting on the secondary cymbial conductor is the ancestral condition for Mysmenidae. Embolus fitting on the primary conductor evolves independently in *Maymena* and in two clades within Mysmeninae (nodes C129 and C184).
185. Dorsal cymbial process (CyP): (0) absent (Fig. 22F, G); (1) present (Figs 4C–F, J, 43C, 45A). In most mysmenids there is a process, often pointed, on the dorsal surface of the cymbium. Homoplastic. The cymbial process is a potential synapomorphy of Mysmenidae, although secondarily lost in some clades.

186. Dorsal cymbial process position: (0) apical, retrolateral to cymbial tip (Figs 1A, E, 4C, D, 40F, 51A, 63C, 133G, 134G); (1) basal prolateral, at distal ending of cymbial groove (Figs 45A, 132D, E); (2) apical, prolateral to cymbial tip (Fig. 43C, D). Apical retrolateral process is the plesiomorphic form within Mysmenidae. High homoplasy.
187. Cymbial fold (CyF): (0) absent (Fig. 60D); (1) present (Figs 4G, 18E). Whereas the external cuticle of the cymbium is usually hirsute, the internal one is glabrous (see e.g. Figs 86G, 102D). In some mysmenids, although the delimitation of external and internal cuticle appears clear, the internal cuticle of the tip of the cymbium bears setae (and can bear the tarsal organ as well), and it frequently appears flattened against the outer cuticle. The internal cuticle is also usually modified into a primary cymbial conductor. This suggests that it might be formed as an extension ('fold') of the external cuticle. This condition is different from a folded tip of the cymbium, where the same external cuticle is bent inwards, ventrally (compare Figs 36B, 47B and Figs 10E, G, H, 14B). The cymbial fold is a synapomorphy of Mysmenidae, secondarily and independently lost in *Maymena mayana*, *Mysmenopsis*, and *Microdipoena illectrix*.
188. Row of setae on cymbial fold (CyFs): (0) absent (Figs 10G, 63C, F); (1) present (Figs 4G, 43E). A distinct row of setae can be present on the cymbial fold, usually associated with the primary cymbial conductor. Fold setae arise independently in *Isela*, node C143 within *Mysmena*, and node C126 (*Brasilionata* + *Microdipoena*).
189. Setal size of row on cymbial fold: (0) row setae similar to surrounding setae on tip of cymbium (Figs 40D, 43E); (1) row of minute setae (Figs 4G, 17A, 18E, 22C, 132A, D, 134A). A row of minute setae is the plesiomorphic setal size, changing to the size of surrounding setae on clade C140 within *Mysmena*, and *Brasilionata*.
190. Process on cymbial fold (CyPF): (0) absent (Fig. 1C); (1) present (Figs 4G, J). Autapomorphy of the *Isela* representative *Isela*-MYSM-002-KENYA.
191. Cymbial groove (CyG): (0) absent (Figs 1A, 4C, D, 10A, 41B); (1) present (Figs 22F, 30C, 36E). A dorsal diagonal furrow of varying depth can occur on the cymbium of some mysmenids. The groove is present in most mysmenines (ambiguous optimization), independently occurring in *Maymena mayana*.
192. Cymbial groove depth: (0) a shallow and wide irregular depression on dorsal cuticle (Figs 36E, 51A, B); (1) a narrow and deep furrow (Figs 18E, 22F, 28B, 30B, C, 45A, 134D). Narrow and deep groove on dorsal cymbium occurs in most mysmenines, independently reverting to shallow in *Microdipoena samoensis*, *Mysmena tasmaniae*, and *Mysmena*-MYSM-015-MAD (occurring convergently in *Maymena mayana*).
193. Cymbial groove position/length: (0) short/apical, restricted to the apical half of the dorsal cymbium (Figs 36E, 45A); (1) long/median, extending into prolateral cymbial expansion (Figs 18E, 22F, 28B, C, 30A, C). The position and the length of the cymbial groove appear to be correlated: apical grooves are always shorter than medial or basal grooves. The latter are longer, extending sometimes into the prolateral basal expansion of the cymbium. These two conditions are combined into a single character to avoid putative character dependency. Long groove is synapomorphic of clade C138 within *Mysmena*, and is ambiguously optimized at the base of node C127 (*Mysmeniola* + *Brasilionata* + *Microdipoena*) because of the short groove in *Microdipoena samoensis*.
194. Embolus width: (0) thin, filiform, most length of embolus as thin as tip (Figs 47B, 86G, 106D, 134F, G); (1) thick, usually flattened, most of length of embolus thicker than tip (even though tip might be thin; Figs 10E, 27A, B, 28D, 36B, 63B, E, 71C, 132B, D). Highly homoplastic. Thick embolus is a synapomorphy for *Microdipoena*, for the clade comprising Mysmenopsinae, *Trogloneta*, and *Maymena* (node C161), and independently for Anapidae (S02 – 139; A04 – 92).
195. Embolus curvature: (0) straight, irregular, or weakly curved (less than one loop; Figs 10E, 28D, E, 60F, 86G, 92B, 131A); (1) coiled, one loop or more (Figs 4H, 27A, 47A, B, 71C, 131H, 132D, E, 134G). A straight embolus is the plesiomorphic and widespread condition on this data set. Coiled embolus occurs independently in *Isela* and Mysmeninae, the latter with a few reversals (S02 – 140; S03 – 71).
196. Embolus length: (0) short, shorter than bulb length (Figs 60F, 81C, 131A–C); (1) medium, about bulb length (Fig. 28D); (2) long, much longer than bulb length (Figs 4A, 10E, 27A, 63E, 71C, 86G, 132E). Long embolus is synapomorphic of symphytognathoids, with some reversions to either short or medium embolus (S02 – 139; S03 – 71; A04 – 91).
197. Embolus tip: (0) without modifications, usually tapering (Figs 1D, 36B, 60F, 63B, C, 88E); (1) with distal apophysis (Figs 10H, 18F, 81E); (2) with distal irregular membrane (Figs 27A–C); (3) thickened tip (Fig. 92E). Absence of structure on the embolus is the widespread condition on most taxa in this data set. A distal apophysis on the embolus

- evolved independently from emboli without structures in a clade within *Maymena* (node C167), in *Trogloneta granulum*, in *Comaroma*, and in *Mysmena marijkeae*. The distal apophysis of *Microdipoena s.s.* (node C172), however, evolved from an embolic distal membrane (optimizing at the base of node C126). Thickened tip of the embolus is synapomorphic for *Minanapis* (A04 – 88).
198. Shape of embolic distal apophysis: (0) single, pointed (Figs 18F, 81E); (1) complex, flat (Fig. 10H). This character applies only to taxa with a distal embolic apophysis (character 197, state 1). Ambiguous optimization. Complex, usually flat embolic apophysis occurs in *Trogloneta* and *Maymena*, whereas a single pointed apophysis occurs within Mysmeninae.
 199. Coiling direction of embolus: (0) embolus coiling in a single direction (Figs 4H, 10H, 28D, E, 36B, 47B, 71C); (1) apical switch in the coiling direction (Figs 18C, D, F, 27C, 132B, D, E). An apical switch of the embolus is characteristic of *Microdipoena* and *Brasilionata* (clade C126), with a secondary loss in *Microdipoena comorensis*.
 200. Embolus origin: (0) retrolateral–ventral or ventral (Figs 10E, 63E); (1) apical (Figs 55G, 60F, 131A–C); (2) prolateral–ventral (Fig. 106D). Prolateral origin of embolus (state 2) is a synapomorphy of Synaphridae, whereas an embolus originating apically (state 1) is synapomorphic of *Mysmenopsis* (A04 – 89).
 201. Embolus surface: (0) smooth (Figs 10H, 18F, 27C, 60F, 71C); (1) ridged (Figs 28F, 32G, 40F, 92C). This character considers only the exposed part of the embolus (e.g. in the case of mysmenids), and is usually observable by means of SEM. Highly homoplastic (A04 – 90).
 202. Embolus rim: (0) entire (Figs 18F, 60F, 63E); (1) deeply grooved (Figs 10H, 28C, 71A, 92D). Usually applicable (and observable) in taxa with thick embolus. Grooved embolus occurs independently in MYSM-005-ARG, *Maymena*, and the anapids *Minanapis* and *Acrobleps* (A04 – 95).
 203. Embolic base: (0) smooth, as embolus (Figs 10E, 71A, 86G); (1) lobed, weakly or irregularly projected (Figs 60F, 76G, 81C, 106D, 131A). Within Mysmenidae, a lobed embolic base is synapomorphic of *Mysmenopsis*. Lobed bases arise convergently also in Theridiosomatidae, and a few other symphytognathoids (A04 – 98).
 204. Embolic basal apophysis: (0) absent (Figs 10E, 28D, 71A, 81C, 106D); (1) present, sclerotized basal apophysis as large as embolus (i.e. the embolus appears bifid; Figs 55G, 60F, 63E, 66E, 131A). A basal embolic apophysis arises independently in *Mysmenopsis*, *Trogloneta*, and *Theridiosoma gemmosum* (A04 – 96).
 205. Embolic membranous basal expansion: (0) absent (Figs 10E, 28D, 60F, 71A, 86G, 106D, 131A, H); (1) present (Figs 81C, 110A, 114E). An embolic basal expansion is present in *Synaphris*, as well as independently in other anapids and symphytognathids (A04 – 99).
 206. Embolus inserted piece: (0) entire (Figs 1D, 10G,H, 32G, 36B, 60F, 63B, 71A, 86G, 92D); (1) with potential break-off point (Fig. 18C, D, F). Although no details from behaviour are available and broken emboli were not observed in either males or females, the embolus in *Microdipoena s.s.* (node C172) species have a clear constriction, which is assumed here to be a detaching point (A04 – 100).
 207. Embolus–tegulum junction: (0) fixed, smooth transition (Figs 10E, 71A, 86G, 131H–J); (1) membranous, flexible (Figs 55G, 60F, 81C, 106D). Membranous junction (state 1) was scored when there was a clear division (such as a furrow) between the embolus and tegulum. A fixed embolus appears as a putative synapomorphy of symphytognathoids. A flexible junction is a synapomorphy of *Mysmenopsis*, evolving independently in *Cepheia*, *Anapisona*, and *Comaroma* (G98 – 22; A04 – 97).
 208. Pars pendula: (0) absent (Figs 131A, F, H, I, 133B, 138B–D); (1) present (Figs 32H, 36B, 132C–F, 133C). In some mysmenids the embolus has a membrane along part of its median trajectory that contains the spermatic duct before entering to the embolus. This membrane holding the spermatic duct was termed ‘pars pendula’ (Comstock, 1910). Therefore, the spermatic duct enters the embolus not at its origin but more distally, also meaning that the embolus as a sclerite is actually longer than the portion containing the ejaculatory duct. The pars pendula is a putative synapomorphy of Mysmeninae, ambiguously optimizes at its node because of missing information on the basal clade of this group. Within mysmenines, the pars pendula is absent in MYSM-005-ARG (A04 – 93).
 209. Pars pendula apophysis: (0) absent; (1) present (Figs 32H, 44C, 45E). An apophysis on the pars pendula occurs three times independently within Mysmeninae.
 210. Male palpal femur distal dorsal apophysis: (0) absent (Figs 86G, 91F); (1) present (Fig. 76A, F). A distal dorsal apophysis on the male palpal femur is an autapomorphy of *Anapisona*.
 211. Male palpal femur outline: (0) straight (Figs 86G, 91F); (1) curved, right angle towards palp (Fig. 76A, F). A curved male palpal femur is an autapomorphy of *Anapisona*.
 212. Median apophysis: (0) absent; (1) present (Figs 81B, C, 86F, G, 98D, 102D, 106A, 114E, 124B). Although absent in most taxa in this data set (including Mysmenidae), the median

- apophysis optimizes ambiguously at the base of symphytognathoids because of its presence in the theridiid *Steatoda*, and in Theridiosomatidae. Within symphytognathoids, the median apophysis evolves convergently in *Cepheia*, the symphytognathid SYMP-002-MAD, and in some anapids (S02 – 144; S03 – 70; G98 – 16; G05 – 123; A04 – 71).
213. Median apophysis shape: (0) single (Figs 81C, F, 106G, 124E); (1) with two or more processes or lobed base (Figs 86I, 98D, 102D–F, 114F). Ambiguous optimization. Applies only to taxa with median apophysis (G05 – 124).
214. Median apophysis–tegulum attachment: (0) membranous, flexible (Fig. 102E); (1) fused, fixed, smooth transition (Fig. 81F). Applies only to taxa with median apophysis. Applicable only to a few taxa (G05 – 125; A04 – 73).
215. Median apophysis and sperm duct: (0) sperm duct loop not inside MA (Figs 138H, 139A, D); (1) sperm duct loop inside MA (Fig. 138B, E). Coddington (1990) initially observed that the sperm duct may loop inside the theridiid tegular apophysis (TTA). In a morphological comparative study of Theridiidae, Agnarsson (2004) proposed that some of the TTA assigned by Coddington were actually MA, and therefore the character related to the inclusion of the sperm duct (character 72) refers to such sclerites. Applies only to taxa with median apophysis. Applicable only to a few taxa (A04 – 72).
216. Apophysis on median apophysis: (0) absent, entire (Fig. 98D); (1) with a pointed apophysis (Figs 86I, 102E, F, 106G, 124E). Applies only to taxa with median apophysis. Applicable only to a few taxa (A04 – 76).
217. Median apophysis distal tip: (0) entire (Fig. 98D); (1) hooded (*Steatoda*). Applies only to taxa with median apophysis. Applicable only to a few taxa (A04 – 78).
218. Tegular groove housing the embolus: (0) absent (Figs 28C, 36C); (1) present (Figs 27A, B, 63E, 66C, 113F). A tegular groove occurs independently in *Trogloneta*, the mysmenid clade comprising *Microdipoena*, *Mysmeniola*, and *Brasilionata* (clade C127), and in the symphytognathid *Patu*-SYMP-001-DR (G05 – 117; A04 – 47).
219. Reservoir (SD): (0) more or less tapering from fundus towards ejaculatory duct (Figs 131A, H, 132B, D); (1) wide (*Tetragnatha*); (2) extremely narrow (Fig. 134F, G). An extremely narrow reservoir evolves independently in the mysmenids MYSM-020-MAD and MYSM-023-MAD, convergent also in *Iardinis mussardi* (G98 – 13).
- its variation. He identified consistent portions of the trajectory (such as loops and switchbacks) and proposed a set of characters where these regions were homologized. Such an approach had been previously used in theridiosomatids (Coddington, 1986a), and the homology statements provided in these studies were phylogenetically informative. The following set of nine characters code consistent regions of the SDT within symphytognathoids (Fig. 127). Several characters originally proposed by Agnarsson (2004) are modified or replaced by new ones to accommodate the diversity of trajectories within symphytognathoids. *Iardinis mussardi* was not scored for any character related to SDT (except character 228, other characters were scored as ‘?’), as its trajectory is extremely complex and it does not seem possible to homologize it objectively (see Fig. 135A, B).
220. SDT, switchback I (SB I) and SB II: (0) absent, spiral (Figs 131E, F, 138G, H, 139C, E); (1) present (Figs 131I, 132B, D). The switchbacks here referred to as SB I and SB II are considered as absent if the SDT is completely spiralling (e.g. Fig. 139E), or when the duct completes at least one entire loop before switching direction (e.g. Fig. 139C). Both switches occur relatively close to each other and seem to be dependent; therefore, they are scored in a single character. The occurrence of this pair of switches is the ancestral condition for symphytognathoids, lost in *Trogloneta*, and independently in all synaphrid and symphytognathid representatives in this data set, and in some anapids (ambiguous optimization) (A04 – 51).
221. SDT, SB I position: (0) distal, apart from basal fundus, on opposite area of bulb (Figs 131H, I, 132B, D, 133A, B, 134B, C, 138A); (1) ‘beyond distal’, i.e. basal or close to fundus, but after passing through the distalmost wall of the bulb (Figs 131C, G, J, 138C, D, 139A); (2) medial or basal (i.e. ‘before-distal’), close to fundus, not reaching the apical wall of the bulb (Figs 133H, I, 134F–H). Ambiguous optimization. In most mysmenids, in *Theridiosoma*, and in *Crassanapis*, the SB I occurs distally on the bulb (state 0). A basal SB I not reaching the distal part of the bulb (state 2) occurs ambiguously in MYSM-020-MAD and MYSM-023-MAD, independently occurring also in *Mysmena rotunda*. Most mysmenopsines, *Maymena mayana*, and most anapids have an SB I occurring close to the fundus, after the spermatid duct reached the distal wall of the bulb (i.e. ‘beyond distal’, state 1).
222. SDT, SB I arrangement: (0) parallel, close switch; the portions of the spermatid duct before and after switch SB I run close to each other, and SB II occurs near midpoint between SB I and the fundus,

Spermatid duct trajectory (SDT)

Agnarsson (2004: characters 51–61) studied the trajectory of the SD in theridiids and attempted to code

- or closer to fundus (the portion of the duct comprising the 'right angle' of SB I – see character 223 – is not taken into account in this duct arrangement; Figs 131I, 132B–D, 133D, E, 134A–C, 138A); (1) divergent, open; the portions of the spermatic duct of SB I diverge, and SB II occurs distally, relatively close to SB I (Figs 131B, H, J, 133A, B, 134D, E, H, 139A). This character only scores the arrangement of the portions of the spermatic duct involved in the SB I, because SB II is always divergent (i.e. it is an open switch). Within Mysmenidae, a parallel SB I evolved independently from a divergent switchback in *Microdipoena*, in clade C143 within *Mysmena*, and in *Maymena ambita*.
223. SDT, SB I distally bending in right angle: (0) absent (Figs 131C, G–I, 132B, D, 133H, I, 134D); (1) present (Figs 133D–F, 134A, B, E, 138F). The portions of the spermatic duct constituting SB I can bend together distally in a near right angle before the SB I occurs. This angled SB I is a putative synapomorphy of *Mysmena*, occurring convergently in MYSM-019-MAD. A similar sort of angled SB I occurs independently in *Minanapis*.
224. SDT, SB I distal right angle arrangement: (0) closed, portions of the duct run relatively parallel (i.e. close to each other; Figs 133F, 134A, C, 138F); (1) open, circular (Figs 133D, E, 134B, E). Ambiguous optimization.
225. SDT, number of ascending loops before entering the embolus, after the most distal SB (either II or IV): (0) no loops, or less than one (Figs 131B, E, H, I, 132F, 133A, B, 138C, G, 139E); (1) between one and 1.5 loops (Figs 131D, 139C); (2) two or more than two loops (Figs 133D, E, 134E, H). This character refers to the last portion of the coiling reservoir before entering the embolus; it reports the number of ascending loops (i.e. towards the embolus) occurring after the last switch (i.e. SB IV when present, or SB II if SB IV is absent). This portion of the trajectory is regarded as tentative homologous based on position (i.e. the portion 'nearest to the embolus'), despite the fact that it might be situated after different (i.e. non-homologous) switches in different taxa. If both SB II and SB IV are absent, then it reports the number of loops in the entire spiral, here assumed homologous also. Highly homoplasious. Two or more loops (state 2) in the spermatic duct before entering the embolus is the plesiomorphic condition, changing convergently to less than one loop (state 0) in the mysmenid clade C161 (Mysmenopsinae, *Trogloneta*, *Maymena*), in Anapidae, and in Theridiosomatidae. Within Mysmeninae, the number of loops gradually decreases in the clade comprising *Mysmeniola*, *Brasilionata*, and *Microdipoena* (C127; change to state 1; distally changing to state 0 in clade C124 within *Microdipoena*). Ambiguous pattern within *Mysmena*.
226. SDT, extra switchbacks after SB II: (0) absent, no further switches (Figs 131D, E, J, 133A, B, D, E, H, I, 134E, 138C); (1) one pair of switches (SB III and IV, Figs 131F, H, 132B–E, 138G, 139C); (2) more than one pair, usually several pairs of switches (Figs 134F–H, 138A, B). The direction of the spermatic duct trajectory is usually clockwise from the fundus (in left palp). If a switchback occurs, it alters this direction to counterclockwise. Usually, a counter-switch also occurs to return the duct trajectory to its original clockwise direction. Therefore, when SBs are present, they usually occur in pairs of switchbacks, as is the case with SB I and II or, as in this character, SB III and IV. SB III and IV can occur either after SB II or, if SB I and II are absent, after a complete loop of the spermatic duct (e.g. as in *Symphytognatha picta*; Fig. 139C). In this data set, the absence of pairs of extra switches (state 0) is the plesiomorphic condition. Highly homoplasious. Within Mysmenidae, one extra pair of switchbacks (i.e. SB III and IV, state 1) evolves independently in *Microdipoena*, *Trogloneta cantareira*, *Isela okuncana*, and the *Mysmena* MYSM-007-MEX. Several pairs of switchbacks (state 2) occur convergently in the mysmenines MYSM-020-MAD and MYSM-023-MAD.
227. SDT, loops before extra switches III and IV: (0) absent (Figs 131H, 132B, 134F, G, 138A, B, 139A); (1) one loop (Figs 131F, 132E, F, 138D, 139C); (2) more than one loop (Fig. 138G). This character refers to loops before SB III, when either both pairs of switchbacks occur (SB I–IV) or only the pair SB III–IV. Specifically, this character applies only to taxa with SB III. When no switchback is present in the SDT, the number of ascending loops is accounted for in character 225, and here scored as inapplicable. Although scarce taxa were scored, the absence of these loops is the ancestral condition. One loop (state 1) occurs within *Microdipoena*, and independently in *Trogloneta cantareira*, *Symphytognathidae*, and *Comaroma*. Two or more loops (state 2) are autapomorphic for *Anapisona*.
228. SDT, constriction near embolus: (0) relatively gradual (Fig. 138G); (1) spermatic duct narrows abruptly before entering embolus (Fig. 139A, E). A sudden narrowing of the spermatic duct occurs independently in *Acroleps*, *Steatoda*, and the micropholcommatine representatives (A04 – 61).
229. Alveolar place of attachment of basal haematodocha: (0) central and basal (Figs 32D,

- 41E, 45D, 49B, 51C); (1) prolateral (*Steatoda*). Only observed in few specimens with available expanded palps. A prolateral attachment of the bulb is an autapomorphy of *Steatoda* (A04 – 41).
230. Additional tegular processes: (0) absent; (1) present. An additional tegular sclerite (i.e. TTA) is autapomorphic of *Steatoda* (S02 – 145; G98 – 18; G05 – 126; A04 – 80).
231. Apical retrolateral patellar apophysis: (0) absent (Figs 98E, 102B); (1) present (Figs 71H, 76I, 95D). The retrolateral apophysis on the anapid *Elanapis* is here considered an apical patellar apophysis, given that the male palpal tibia and patella are fused. Ambiguously optimized synapomorphy of Anapidae, although highly homoplastic within the family (S02 – 130; S03 – 62).
232. Size of apical retrolateral patellar apophysis: (0) minute, distinguishable with SEM (Fig. 71H); (1) large (Figs 76I, 86H, 95D). Applicable to taxa with apical retrolateral patellar apophysis. Minute apical retrolateral apophysis is an autapomorphy of *Acrobleps* (S03 – 62.1).
233. Subapical retrolateral patellar apophysis: (0) absent (Fig. 76I); (1) present (Figs 71H, 90C, 98E, 102B). This apophysis occurs within Anapidae, evolving independently four times in *Acrobleps*, *Tasmanapis*, *Minanapis*, and *Teutoniella* (S03 – 63).
234. Size of subapical retrolateral patellar apophysis: (0) minute, distinguishable with SEM (Fig. 71H); (1) large (Figs 98E, 102B). Minute subapical retrolateral apophysis is an autapomorphy of *Acrobleps*.
235. Apical prolateral patellar apophysis: (0) absent (Fig. 71D); (1) present (Figs 76C, 95D). A prolateral apical patellar apophysis occurs independently in *Anapisona* and *Taphiassa*.
236. Setae with large bases on retrolateral patella: (0) absent (Figs 76I, 86H, 98E); (1) present (Fig. 90C). Synapomorphy of *Minanapis*.
237. Retrolateral paracymbium (PC): (0) absent (Figs 71F, 92A); (1) present (Figs 27B, 60C, 81B, 122D, 124C). A retrolateral paracymbium occurs in most taxa examined here. This cymbial structure has been lost independently on several occasions: in two mysmenids (*Maymena rica*, *Isela*-MYSM-002-KENYA), *Steatoda* (theridiids), one symphytognathid (SYMP-006-AUST), and in Anapidae. Although the loss of the paracymbium optimizes here as synapomorphic for Anapidae, it has been secondarily regained in *Comaroma* (S02 – 136; S03 – 67; G98 – 7; G05 – 112; A04 – 29).
238. Paracymbium size: (0) large, width of PC about one-third or more the length of cymbium, or extremely long PC (e.g. as in *Tetragnatha*) (Figs 28E, 32A, 36A, 41B, E, 47A, 63A, 122D); (1) small, width of PC about one-tenth of cymbium and short (Figs 10F, 17C, 22G, 27B, 53C, 60C, 81E); (2) intermediate, not as narrow or as wide (Fig. 30E). An objective definition of the size of the PC was not provided in Schütt's description of this character. The size of the paracymbium is difficult to define, especially in taxa with a fixed junction of the PC to the cymbium, as is the case in Mysmenidae. Here, a tentative definition is provided, taking into account the width and/or length of the PC compared with the total length of the cymbium. Greatly homoplastic. A small paracymbium (state 1) is plesiomorphic in this data set. A large paracymbium (state 0) is a potential synapomorphy of Mysmenidae (ambiguously optimized because of the small paracymbium of *Mysmenopsis* and *Maymena ambita*). Within Mysmeninae, there seems to be a tendency in decreasing size of the paracymbium in the lineage comprising *Microdipoena* (large paracymbium changes to intermediate – state 2 – in node C127, and distally to small – state 1 – in *Microdipoena*) (S02 – 137).
239. Paracymbium shape: (0) hook shaped, thick (i.e. not flat), short distinct process, usually as long as wide (Figs 53D, 60D, 81E, 124C); (1) long, more than five times its width (*Tetragnatha*); (2) massive (Fig. 122C, D); (3) flat and rounded, uniform transition with cymbium (i.e. flat extension of cymbial edge; Figs 18B, 22G, 27B, 30E, 32A, 36A, 45B, 63A). A hook-shaped paracymbium (state 0) is the plesiomorphic shape. Massive and long paracymbia are autapomorphies of *Symphytognatha picta* and *Tetragnatha versicolor*, respectively, a flat, rounded paracymbium evolved independently as synapomorphic for Mysmenidae, but also in *Iardinis mussardi* and in *Synaphris*. Within Mysmenidae, the paracymbium becomes secondarily hook-shaped in *Mysmenopsis* (ambiguously optimized because of the absence of paracymbium in *Isela*) (S02 – 137; G98 – 9; A04 – 30).
240. Paracymbium attachment: (0) integral, fixed (Figs 27B, 60D, 81E, 122C, D); (1) flexible, moveable or separated, free (*Tetragnatha*); (2) intersegmental (*Linyphia*) (S02 – 138; S03 – 67.1; G98 – 8).
241. Paracymbium position: (0) basal (Figs 63A, 122D, 124C); (1) medial (Figs 10F, 17C, 30E, 36A, 53F, 110C); (2) apical (Fig. 81B). Apical PC (state 2) does not take into account the typical bulb-cymbium lock of theridiids, as these features might not be homologous, and such interaction of the distal PC of *Comaroma* (and some symphytognathids) with its bulb seems absent (see also A04 – 29). Although originally defined as a retrolateral basal process (i.e. the plesiomorphic position in this data set), a medial paracymbium

- optimizes as a synapomorphy of the ANTS clade, further becoming distal at node C112 (Anapidae + Symphytognathidae). Basal paracymbia therefore occurs in Theridiosomatidae, and it evolves secondarily in *Trogloneta*, *Symphytognatha picta*, and *Iardinis mussardi* (S03 – 68; G98 – 11).
242. Process in Paracymbium: (0) absent (Figs 63A, 81E); (1) present (Fig. 124C). Synapomorphy of Theridiosomatidae (G98 – 10).
243. Paracymbium–bulb interaction: (0) absent (Figs 17C, D, 27B, 81E); (1) present, paracymbium bent inwards and seemingly interacting with a tegular groove (Figs 53F, 55F, 58D, 60D). The interaction considered in this character is tentative. The paracymbium is bent inwards and appears to interact with a tegular groove located dorsally on the bulb. This dorsal tegular groove does not appear to have a ‘conductor’ function related to the embolus (see character 218), and the paracymbium–bulb interaction as a locking mechanism is not evident, as in the case of theridiids (A04 – 29). As a homology statement of this interaction acting as a locking mechanism (as present in Theridiidae) is dubious, they were scored as separate characters. This interaction is an ambiguously optimized synapomorphy of *Mysmenopsis*.
244. Male palpal tibia shape: (0) cylindrical (Figs 10A, 81D, 98B, C); (1) flat (Figs 91F, 95C, D, 102C); (2) broad distally (Figs 4A, D, 17D, 28A, 30E, 32E, 38A, 42A, 47B, 63C); (3) globose (Figs 55A, C, 58A, 60A). Flat tibia (state 1) is flattened from the base, and usually has an irregular (i.e. not circular) distal outline. Cylindrical tibia (state 0) is distally as wide as basally or less than two times its basal width. Those tibiae flattened or protruding only distally (i.e. with a cylindrical base) are considered cylindrical. A broad tibia (state 2) is wide distally, usually more than two times its basal width, and usually have a circular distal outline; it optimizes as the plesiomorphic condition in this data set, occurring in the theridiid *Steatoda*, in Theridiosomatidae, Synsphyridae, and most mysmenids (Mysmeninae, *Isela*, and *Trogloneta*). A cylindrical tibia is synapomorphic for *Maymena* in this data set, although convergent in *Comaroma* and *Tasmanapis*. Flat tibia optimizes as a synapomorphy of the clade comprising Symphytognathidae plus Anapidae. A globose tibia is a synapomorphy of *Mysmenopsis* (S02 – 131, 132; S03 – 65; A04 – 14).
245. Male palpal tibia size: (0) small, shorter than cymbium, i.e. less than one-tenth the size of carapace in lateral view (Figs 10A, 27A, B, 30D, 47B, 63B, C, 71D, 106C, 110E); (1) large, equal, or larger than cymbium, i.e. about one-fifth the size of carapace in lateral view (Figs 1A, 4A, 55A, C). Within symphytognathoids, a large tibia is synapomorphic for Mysmenopsinae (S02 – 131, 132; S03 – 65; A04 – 14).
246. Male palpal tibial retrolateral apophysis: (0) absent (Figs 28A, 38A, 42A, 45C, 47B, 55D); (1) present (Figs 76E, 95B, 98C, 102C). Within symphytognathoids, a retrolateral apophysis on the male palpal tibia evolves independently three times within Anapidae: in *Anapisona*, *Tasmanapis*, and the micropholcommatine representatives (RTA; S02 – 133; S03 – 65.1; G05 – 105).
247. Male palpal tibial retrolateral apophysis position: (0) apical (Figs 95B, 98C, 102C); (1) basal (Fig. 76E). A basal retrolateral apophysis is an autapomorphy of *Anapisona* (S02 – 133; S03 – 65.1; G05 – 105).
248. Male palpal tibia dorsal process: (0) absent (Figs 4E, 17D, 81D, 110D); (1) present (Figs 76D, 90C). A dorsal process (or apophysis) on the male palpal tibia occurs independently in the anapid genera *Anapisona* and *Minanapis* (DTA; S02 – 134; G05 – 108).
249. Male palpal tibial apical hollow area: (0) absent (Figs 1A, 32A); (1) present (Figs 53A, 58A, 60A). The hollow area is a sort of excavation located distally on ventral (sometimes ventral–retrolateral) tibia, usually bearing spurs. Synapomorphy of *Mysmenopsis* (VTA; G05 – 107).
250. Male palpal tibia prolateral apical process: (0) absent (Figs 76D, 110E); (1) present (Fig. 71D). This distal prolateral apophysis occurs independently in *Acrobleps* and in *Mysmeniola* (PTA; G05 – 111).
251. Male palpal tibia small prolateral basal process: (0) absent (Figs 76D, 110E); (1) present (Figs 71D, 102C). A small basal prolateral tibial apophysis occurs convergently in a clade within Symphytognathidae (clade C156), and in the anapids *Acrobleps*, and *Teutoniella*.
252. Male palpal tibia distal setae: (0) as in the rest of the tibia (Figs 22D, 30A, 36D, 41A, 47B, 76D, 110D); (1) spine-like or strong setae (Figs 1A, B, 4A, E); (2) spur (Figs 53E, 55H, 58E, 60B, 71G). Tibial spurs occur independently in *Acrobleps* and as an ambiguously optimized synapomorphy for *Mysmenopsis*. Strong tibial distal spines are a putative synapomorphy of *Isela* (G98 – 1).
253. Male palpal tibial rim: (0) uniform or only subtly asymmetric, similar tibial length on all sides (Figs 27F, 30A, E, 38A, 42A, 44B, 45C, 47B, 63C); (1) scoop-shaped, sudden strong and asymmetrical protrusion on one side (Figs 1A, 4A, 18A, 19A, 25A, 53B, 55A, C, 58A); (2) uniformly protruding, smooth transition between sides of different length (Figs 10D, K, 106B, 110E).

Not applicable in taxa with flat palpal tibia (character 244, state 1). Highly homoplastic. Scoop-shaped tibia is an ambiguously optimized synapomorphy of Mysmenopsinae, convergently synapomorphic for *Brasilionata* and *Microdipoena s.s.* (node C172) (A04 – 15).

254. Number of spurs on hollow area: (0) four or less (Figs 53E, 55H, I, 71G); (1) five or more (Figs 58E, 60B, E). Applicable only to taxa with palpal tibial apical hollow area (character 249, state 1). Five or more spurs occur in *Mysmenopsis penai* and *M. palpalis* (ambiguous optimization).
255. Male palpal tibial rim setal conformation: (0) irregular, few dispersed short setae (Figs 63C, 66A, 81D, 95C, 98C, 102C, 106F, 110D); (1) rim setae longer and arranged distally in a row or two (Figs 4E, 10D, 18A, 32E, 36D, 42B, 45C, 53B, 55C). Putative synapomorphy of Mysmenidae; optimizes ambiguously at its base because of the irregular setal conformation (state 0) in *Trogloneta*. Secondarily irregular in *Maymena rica*, *Mysmeniola spinifera*, and *Microdipoena jobi* (A04 – 16).
256. Male palpal tibial rim orientation: (0) dorsal (Figs 10C, D, 17B, 19A, 25A, 55A, 71E, 76D, 98C, 115A); (1) ventral (Fig. 30D); (2) prolateral (Fig. 95C); (3) retrolateral (Figs 106B, 110E). This character refers to the orientation where the protruding or flat tibia leans on the palp. Not applicable for taxa with uniform tibia (character 253, state 0). Ambiguously optimized at the node of symphytognathoids, the widespread condition is a dorsal rim. Synaphrid rim is retrolateral as in *Steatoda*. Prolateral rim occurs in *Trogloneta granulum* and in clade C151 within Anapidae. A ventral rim is a putative synapomorphy of *Mysmena* (A04 – 17).
257. Male palpal tibia retrolateral–dorsal trichobothria: (0) present (Figs 53B, 81A); (1) absent (Figs 4E, 30B, 41A, 71E, 95D, 102C). Loss of retrolateral trichobothria is a potential synapomorphy of the ANTS clade, ambiguously optimized because of the presence of such trichobothria in *Trogloneta*, *Mysmenopsis*, and *Maymena mayana* (A04 – 18).
258. Number of tibial retrolateral–dorsal trichobothria: (0) three or more (tetragnathids); (1) two (Figs 53B, 55C); (2) one (Fig. 81A). When present, one trichobothrium (state 2) is the plesiomorphic number within symphytognathoids. Two trichobothria (state 1) is an ambiguously optimized synapomorphy of *Mysmenopsis* (A04 – 18).
259. Male palpal tibia dorsal, prolateral–dorsal trichobothria: (0) present (Figs 4E, 110D); (1) absent (Figs 22D, 30A, E, 53B, 71E, 81D). Loss of prolateral trichobothria is a potential synapomorphy of the ANTS clade, ambiguously

optimized because of the presence of such trichobothria in *Maymena*, *Isela*, *Mysmenopsis dipluramigo*, and Synaphridae (A04 – 19).

260. Number of tibial dorsal prolateral–dorsal trichobothria: (0) two or more (Figs 1B, 4E); (1) one (Figs 10B, 55E, 106F, 110D). Two trichobothria are synapomorphic for *Isela* (A04 – 19).
261. Male palpal tibia–patella: (0) separate as two distinct segments (Figs 25A, 28A, 38A, 42A, 66A); (1) fused into one single segment (Figs 90C, 91F, 115A). A presumable fusion of the two palpal segments has occurred in the anapids *Elanapis* and *Minanapis* (ambiguous optimization), and independently in the symphytognathid SYMP-002-MAD.

Mouthparts

262. Cheliceral paturon length: (0) short, not nearly reaching tip of endites (Fig. 108C, H); (1) reaching tip of endites, or nearly so (Figs 2A, 82A); (2) long, more than four times longer than wide, beyond tip of endites (*Linyphia*, *Tetragnatha*). Short paturon is an autapomorphy of *Cepheia* in this data set (S02 – 31; G98 – 35; G05 – 36; A04 – 117).
263. Cheliceral length dimorphism: (0) absent, chelicerae subequal (Fig. 2A, B); (1) present, male chelicerae much longer (*Linyphia*, *Tetragnatha*) (S02 – 32; S03 – 14.1; G98 – 33; A04 – 113).
264. Chelicerae: (0) free (Figs 31E, 79B); (1) basally fused (Fig. 112G); (2) fused almost entire length (Fig. 121B, D). The chelicerae of some mysmenids have a dubious fusion at their base, which was first observed and reported by Schütt (2003: character 14). This basal subtle fusion was reported as occurring in *Trogloneta*, although absent in *Microdipoena*. Both genera as well as other mysmenid species have a similar cheliceral condition (compare Schütt, 2003: fig. 3C with Figs 25D, 46B, 46F in this study). Symphytognathid fused chelicerae are difficult to discern under light microscopy, because of the suture between the two chelicerae, which is observable even in taxa with completely fused chelicerae (e.g. *Symphytognatha picta*, see Fig. 146H). Nevertheless, under SEM observation, those chelicerae have an evident connection; the suture is no longer observable (see Figs 112G, 121B). Mysmenid chelicerae, on the other hand, appear separate under light microscopy, but are neither distinctly separate nor basally fused under SEM. As all chelicerae are proximally connected by a membrane, SEM images are sometimes misleading, and the chelicerae appear fused basally. The removal of one chelicera as a test for the fused condition is sometimes

- impractical in minute taxa where the fusion is subtle. Given this dubious condition in some mysmenids, they were scored here as '?'. In this data set, completely fused chelicerae are autapomorphic for *Symphytognatha picta*, whereas basally fused chelicerae are an autapomorphy of *Patu-SYMP-001-DR* (S02 – 33; S03 – 14; G98 – 38; G05 – 38).
265. Cheliceral outline: (0) evenly outlined, cylindrical or conical (Figs 52A, 59A, 66G); (1) constricted basally, i.e. salient anteriorly (Figs 7A, 70A, 91E, 111D); (2) distinctly doomed or with a distinct knob (at least on males, Figs 72B, 99A, 104B, 118D). This character is better observed in an anterolateral view. The scoring of this character is tentative, given that on occasion the spider can be fixed with the cheliceral base not exposed (i.e. retracted behind the clypeus), therefore covering the actual outline. Greatly homoplastic, this character optimizes ambiguously at the node of, and within, symphytognathoids (S02 – 35, 36; A04 – 115).
266. Cheliceral direction: (0) vertical (Fig. 2B); (1) oblique frontal (*Tetragnatha*). Oblique chelicerae are an autapomorphy of *Tetragnatha* (S02 – 34).
267. Male retrolateral stridulatory ridges: (0) absent (Figs 96F, 121E); (1) present (*Linyphia*). Autapomorphy of *Linyphia* (S02 – 38; S03 – 14.2; G98 – 37; G05 – 45; A04 – 114).
268. Female retrolateral stridulatory ridges: (0) absent (Fig. 99F); (1) present (*Linyphia*). Autapomorphy of *Linyphia* (S02 – 39).
269. Distal promarginal curved seta: (0) absent (Figs 108E, 118E, 122A); (1) present (Figs 19E, 79D, 97D). This character refers to a particularly distinct curved seta located distally at the promarginal edge of the chelicerae, near the fang base. Curved setae can occur on the chelicerae retromargin as well, although not different from the surrounding setae (e.g. Fig. 7J). The original character (G05 – 34) considered a distinct thicker seta on the retromargin. Here, representatives in this data set have distinct seta on the promargin. For retromarginal setae, see character 283. Within symphytognathoids, this particular seta is present in most taxa, but is ambiguously lost in Synaphridae and Symphytognathidae (G05 – 34).
270. Distal promarginal curved seta size: (0) minute, thinner than surrounding setae (Figs 15G, 97D); (1) as other setae (Figs 13I, 79D, 87F, 105D); (2) distinctly thicker than surrounding setae (Figs 19E, 25E, 38H, 48B). Optimizing ambiguously at the node of symphytognathoids, a thick seta (state 2) is a putative synapomorphy of Mysmenidae.
271. Serration of distal promarginal curved seta: (0) smooth, weakly serrated (Fig. 97D); (1) serrated as other setae, or plumose (Figs 79D, 87F, 105D); (2) strongly serrated on one side (Figs 19E, 38H, 42E, 48B). Similar serration as surrounding setae (state 1) is the plesiomorphic state in symphytognathoids. Smooth seta occurs independently in *Taphiassa* and *Coddingtonia*. Strong serration is a synapomorphy of Mysmeninae, and a putative independent synapomorphy of Mysmenopsinae.
272. Cheliceral lateral condyle-boss: (0) absent (Figs 90A, 99A); (1) present (Fig. 77A, F). Within symphytognathoids, autapomorphy of *Anapisona* (S02 – 37; G05 – 43; A04 – 122).
273. Median lamella: (0) present (Fig. 122A, B); (1) absent (Figs 97D, 115E). As discussed in Lopardo *et al.* (2007 – 19) and as defined by Kaston (1978 – 269), here the cheliceral lamella is interpreted as 'a triangular plate on the promargin of the cheliceral fang furrow in some spiders, resembling a broad tooth, and forms a kind of chela with the fang'. Autapomorphy of *Symphytognatha picta* (S02 – 41).
274. Cheliceral keel ending in single promarginal tooth: (0) absent (Fig. 7E); (1) present (Fig. 108D). As discussed in Lopardo *et al.* (2007 – 19), this cheliceral structure has been defined as a distinct sclerotized ridge on the inner side of the paturon over almost the entire length (Schütt, 2003 – 141). As the strong promarginal tooth is considered as part of the keel, it is not applicable in promarginal teeth characters, and the fang furrow in taxa with keel is also considered absent, and therefore all related characters are scored as inapplicable. Synapomorphy of Synaphridae (S02 – 42; S03 – 14.3).
275. Promargin of furrow: (0) with teeth (Figs 7F, 120D); (1) smooth (Fig. 97D). Smooth cheliceral promargin is an autapomorphy of *Taphiassa* (S02 – 46; S03 – 14.5; G05 – 39; A04 – 106).
276. Promargin cheliceral teeth origin: (0) distinct, sessile (Figs 13I, 77G, 123C); (1) common base, raised plate (Figs 7H, 88C, 120D, 122B). Promarginal teeth on a common plate evolved independently in Symphytognathidae, *Isela-MYSM-002-KENYA*, and ambiguously in *Elanapis* and *Minanapis* (S03 – 16; G98 – 36).
277. Promargin cheliceral teeth shape: (0) blunt (Figs 7G, 13J, 123C); (1) pointed, sharp (Fig. 120D). Sharp promarginal teeth are an ambiguously optimized synapomorphy for a clade within Symphytognathidae (node C199) (A04 – 107).
278. Promargin cheliceral teeth number: (0) four or more (Figs 7F, 88C, 123C); (1) three (Figs 15H, 77G, 82D); (2) two (Figs 2F, 120D); (3) one

- (Fig. 122A). Four or more promarginal teeth are the plesiomorphic teeth number for symphytognathoids. Although homoplastic, three teeth are synapomorphic for the ANTS clade. Within Mysmenidae, four or more teeth are secondarily gained in *Isela*-MYSM-002-KENYA and in the mysmenine clade C128, whereas two teeth occur independently in *Trogloneta granulorum* and *Isela okuncana* (A04 – 108).
279. Cheliceral setal teeth: (0) absent (Fig. 7F); (1) present (Figs 97B, 122B). A modified tooth-like seta (peg teeth?) evolved independently in *Taphiassa* and *Symphytognatha* (S02 – 46; S03 – 18; G05 – 41).
280. Cheliceral gland mound: (0) absent (Fig. 7F); (1) present (Fig. 97F). Autapomorphy of *Taphiassa punctata* (S02 – 49; S03 – 19; G05 – 42).
281. Cheliceral promarginal proximal tooth: (0) subequal to adjacent teeth (Figs 19E, 123B); (1) larger than adjacent teeth (Fig. 7G). A larger proximal tooth is an autapomorphy of *Isela*-MYSM-002-KENYA (A04 – 109).
282. Retromargin of furrow: (0) smooth; (1) with teeth (Fig. 15I). Within symphytognathoids, a smooth cheliceral retromargin occurs in *Mysmenopsis*, *Tasmanapis*, and the symphytognathid clade C156 (S02 – 47; S03 – 15; G05 – 39; A04 – 110).
283. Retromarginal distal cheliceral setae: (0) scarce or absent (Fig. 111E); (1) serrated setae, similar as surrounding cheliceral setae, not curved (Fig. 123C); (2) row of curved plumose setae (Figs 7G, 50C, 62D). Serrated setae (i.e. as the surrounding setae) are the plesiomorphic condition in this data set. A row of plumose and curved setae (state 2) is a synapomorphy of the ANTS clade, becoming scarce in Synaphridae (G05 – 34).
284. Cheliceral retromargin teeth number: (0) four or more (Fig. 15I); (1) three; (2) two (Fig. 50C); (3) one (Fig. 7I). Ambiguously optimized (A04 – 111).
285. Cheliceral fang length: (0) subequal, shorter than paturon (Fig. 7E); (1) long, nearly as long as paturon (*Linyphia* and *Tetragnatha*). Cheliceral length was mostly related to the paturon (instead of cheliceral groove), as those taxa with long fangs can have long cheliceral grooves as well (e.g. *Tetragnatha*) (S02 – 43; G98 – 34; A04 – 119).
286. Denticles in furrow: (0) absent; (1) present (Figs 7G, 15H, , 48B). The cheliceral denticles optimize ambiguously at the base of both symphytognathoids and the ANTS clade, because of their presence (and therefore potential synapomorphies) in Mysmenidae and Theridiosomatidae. A secondary loss occurs in *Microdipoena jobi* (S02 – 48; S03 – 17; G05 – 39; A04 – 112).
287. Labium width: (0) wide, about half sternum width (Fig. 121G); (1) narrow, one-third sternum width (Figs 19D, 99G). A wide labium is an autapomorphy of *Symphytognatha picta* (S02 – 57; S03 – 25.2; G98 – 41).
288. Labium shape: (0) square, subrectangular (Figs 2D, 7D, 59E, 85E, 97C); (1) triangular or pointed anteriorly (Figs 63I, 111E, , 118C, , 120B). A triangular labium evolved independently in the mysmenids *Trogloneta* and *Mysmena tasmaniae*, in Synaphridae, and twice within Symphytognathidae (S02 – 58; A04 – 136).
289. Mouthparts setae: (0) abundant (Figs 87F, 93B, 97C, 105C); (1) scarce (Figs 49H, 111C, 118C). This character refers to the number of maxillary and labral setae that converge at the tip of the mouthparts. Although the states proposed here lack a quantitative precise definition (e.g. number of setae on a delimited surface), both conditions are distinct enough to identify (see Figures referred to on each state). Scarce setae evolved in Synaphridae and Symphytognathidae (ambiguously optimized), and a few mysmenid taxa.
290. Labium distal margin: (0) straight or convex (Figs 2D, 7D, 63I, 97C, 111E, 120B); (1) concave or notched (Figs 54B, 59E, 85E, 105C). A concave labial margin is convergently synapomorphic of *Mysmenopsis* and Anapidae (secondarily straight in *Taphiassa*) (S02 – 59; S03 – 25).
291. Labium distal margin: (0) rebordered, swollen distally, with an irregular and flattened basal cuticle connecting labium and sternum (Figs 19D, 54B, 59E, 85E, 99H, 120B); (1) not swollen, distal and basal cuticle similar (Figs 63I, 66H, 97C, 121G). A non-rebordered labium occurs independently in *Trogloneta*, *Cepheia*, *Taphiassa*, *Anapisona*, and clade C195 within Symphytognathidae (S02 – 60; S03 – 25.1; A04 – 134).
292. Labium–sternum connection: (0) separated (Figs 49H, 54B, 56G, 63I, 108F, 111E, 112F); (1) one unit (Figs 27H, 85E, 89B, 97C, 105C, 120B). Separate labium (state 0) refers to a visible seam, subtle narrow groove, or suture between sternum and the base of the labium. A labium fused to sternum (state 1) lacks a groove or suture, and the sternal and labial cuticles appear continuous. The irregular basal cuticle of the rebordered labium can, in SEM observations, appear as a wide groove, misleading the scoring of the separation of the labium. Fused labium is a synapomorphy of Anapidae, convergent distally on Symphytognathidae (clade C201) and in *Microdipoena samoensis* (S02 – 56; S03 – 24; A04 – 135).
293. Labral spur: (0) absent (Figs 25F, 38F, 46C, 62C, 70C, 79F, 90D); (1) present (Figs 77E, 86B,

- 97E, 100F, 104G). For a detailed discussion on the problem of the labral spur, see Miller *et al.* (2009). This labral sclerite was considered as present (state 1) when there is at least a subtle protrusion occurring at the base of the labral flap. Micropholcommatines have a weak but protruding labral sclerite compared with those anapids (or other symphytognathoids) lacking spur (e.g. *Acrobleps* or *Comaroma*), and were scored here as 'present' (state 1). *Minanapis* species have a flap with salencies, but it is not protruding and was therefore considered as absent (state 0) in this data set. The labral spur is synapomorphic for Anapidae excluding its basal genus *Acrobleps* (i.e. node C122), and is secondarily lost in *Comaroma* and *Minanapis* (ambiguous optimization) (S02 – 51; S03 – 20; G98 – 40).
294. Labral spur projection: (0) subtle but distinct elevation (Figs 86B, 97E, 100F, 104G); (1) greatly projecting (Fig. 77E). A distinctly protruding labral spur is, in this taxon sample, an autapomorphy of *Anapisona* (S02 – 51; S03 – 20; G98 – 40).
295. Maxillary inner and distal border: (0) sclerotized as the remaining maxilla (Figs 27H, 49H, 59E); (1) membranous (Figs 115D, 120B, 121H). A membranous maxillary border occurs in some symphytognathids and is a putative synapomorphy of the family.
296. Maxillary setae: (0) mostly serrated/plumose setae, relatively absent clavate setae (Figs 87F, 105C); (1) mostly clavate setae, relatively absent plumose setae (Figs 54B, 62B, 125B). The maxillary setae are composed of at least two types of seta: serrated and clavate. This character accounts for the relative proportion of each type of seta. A higher proportion of serrated setae on the maxilla is the widespread condition for this data set, and is therefore ancestral for symphytognathoids. A higher proportion of clavate setae occurs independently in *Mysmenopsis*, Synaphridae, *Comaroma*, and *Coddingtonia*.

Palp female

297. Palpal claw: (0) present (tetragnathids, linyphiids, theridiids, and *Leviola*); (1) absent (Figs 22E, 69B, 79C, 93A, 108C). Absent claws were also scored for taxa with reduced palp. Synapomorphy of symphytognathoids (S02 – 55; G98 – 53; A04 – 176).
298. Female palp segment composition: (0) 'cx+5', coxa and five segments (Figs 38C, 72B, 104B, 108C); (1) 'cx+4', coxa and four segments (*Taphiassa*); (2) 'cx + nub', coxa and nubbin (*Acrobleps hygrophilus*, Fig. 69B); (3) coxa (Figs 91B, 93A, 100E, 118A). In most symphytognathoids, the female palp has all six segments, lacking only the palpal claw; however, a complete reduction of the palp (where only the coxa is present, state 3) is synapomorphic of Symphytognathidae. Within Anapidae, the reduction of the female palp occurs as independent events from the five-segmented palp: in *Taphiassa* (state 1), *Acrobleps* (state 2), and *Minanapis* and *Tasmanapis* (state 3, convergent with Symphytognathidae) (S03 – 23; G98 – 52).
299. Palpal tibial trichobothria (female): (0) present (Figs 2E, 13H, 64G); (1) absent (Figs 38E, 52E). Loss of female palpal trichobothria is synapomorphic for Mysmeninae and ambiguously optimized at the base of Anapidae (excluding its basal genus *Acrobleps*), although secondarily gained in *Comaroma* (A04 – 179).
300. Palpal tibial trichobothria number (female): (0) numerous, more than six (tetragnathids); (1) between three and five (Figs 2E, 62A); (2) two (Figs 13H, 125E); (3) one (Figs 64G, 79E). Applicable only to taxa with palpal trichobothria (character 299, state 0). One female palpal trichobothrium (state 3) optimizes as synapomorphic for the ANTS clade, reverting to two (state 2) in *Maymena mayana*, and between three and five (state 1) in Mysmenopsinae. Two palpal trichobothria (state 2) is the ancestral condition for symphytognathoids, occurring in *Steatoda* and Theridiosomatidae (A04 – 179).
301. Palpal tarsal setae (female): (0) strongly serrated (*Steatoda* and *Leviola*); (1) serrated as other setae (Figs 22E, 79C, 105B) (A04 – 180).
302. Female palpal tarsal organ location: (0) basal, i.e. proximal (Figs 77D, H, 85G); (1) medial–distal (Figs 22E, 38G, 79C, 105B). A proximal female palpal tarsal organ is a synapomorphy of the anapid clade C121 (*Anapisona*, *Conculus*, and *Crassanapis*).
303. Female palpal tarsus macrosetae: (0) present (Figs 2A, 13A, 15A, 79C); (1) absent (Figs 77D, 105A, B, 108C). Given that the taxa in this data set usually possess reduced macrosetae instead of strong spines (see character 125), female palpal tarsus macrosetae were scored as present (state 0) if occurring dorsally and/or ventrally. Female palpal macrosetae are ambiguously optimized at the base of node C160 (*Maymena* plus Mysmenopsinae), evolving convergently in *Comaroma* (A04 – 181).

Spinnerets

304. PS aciniform spigots: (0) same size and shape, uniform (Figs 6D, 61D, 75G, 94F, 113D, 123E, F); (1) two shapes (Figs 13D, 19F, 33D, 37B, E). All symphytognathoids have the typical araneoid spigot arrangement in both lateral and median

- posterior spinnerets (see Griswold *et al.*, 1998); however, there is one spigot located close to other aciniform spigots in the posterior spinnerets that cannot be assigned to any of the described functional araneoid spigots. When compared with other aciniform spigots, this spigot has a relatively thinner shaft and a marked ring around its base. Based on its location, it is tentatively assigned here to the aciniform gland spigot group. Although this character scores the presence of varying shapes within aciniform spigots, it does not state which of the shapes is the plesiomorphic condition in symphytognathoids. Moreover, this character could also be defined in terms of presence or absence of an additional aciniform spigot of different shape. Scoring such alternative definition is, however, identical. Aciniform spigots of different shape occur within Mysmenidae, convergently in *Maymena*, and in Mysmeninae.
305. PMS Aciniform spigots number: (0) three (Fig. 123E); (1) two (Figs 6C, 11F, 13D, 19F, 33D, 61D); (2) one (Figs 75D, 78D, 82G, 94B, F, 103C, E, 114A). Three aciniform glands are the ancestral condition for symphytognathoids (present in the outgroup and Theridiosomatidae). Within symphytognathoids, a reduction in AC spigot number occurs. Two AC spigots are synapomorphic for the ANTS clade (occurring in Mysmenidae and *Cepheia*). One AC spigot optimizes at the base of clade C112 (Anapidae plus Symphytognathidae), reverting to two in *Crassanapis* (S02 – 116; G05 – 84; A04 – 222).
306. ALS major ampullate–piriform (MAP–Pi) field separation: (0) no distinct separation between MAP and piriform field (Fig. 107G); (1) MAP and piriform field conspicuously separated by deep furrow, appearing as two distinct distal segments (Figs 75A, B, 103B, 113A); (2) MAP and piriform field separated by a subtle or shallow furrow (connection between both fields is distinctly evident basally; Figs 6A, 13C, 33F, 61C). Ambiguously optimized, a shallow furrow between the MAP and the piriform fields occurs in Mysmenidae and Theridiosomatidae, whereas an absence of furrow between the fields is a synapomorphy of Synaphridae (S03 – 54.2; G05 – 77).
307. ALS third additional anterior (spinning?) field: (0) absent (Figs 61C, 75A); (1) present (Figs 64C, 66F). Synapomorphy of *Trogloneta* (S03 – 54.3).
308. ALS cuticle on piriform field: (0) smooth (Figs 75A, 94A, 100A, 103A); (1) fingerprint (with concentric rings around Pi; Figs 6B, 23A, C, 33E, 61C); (2) rugose (just one ring around Pi; Figs 16B, 113B, 125D). Ambiguously optimization. Within symphytognathoids, smooth cuticle on the piriform field is a putative synapomorphy of the clade comprising Synaphridae, Anapidae, and Symphytognathidae (clade C113). A rugose cuticle occurs in *Trogloneta*, *Maymena*, and Theridiosomatidae. Within Mysmenidae, a fingerprint cuticle optimizes ambiguously at the base of Mysmeninae and of Mysmenopsinae.
309. ALS lobe on intersegmental groove: (0) absent (Figs 75A, 94A, 113A); (1) present (Figs 23C, G, H, 33F, 52B, 103A). Synapomorphy of Mysmenidae. This lobe is convergently present in some representatives of Anapidae, although in this family the lobe is homoplastic and ambiguously optimized.
310. ALS seta on major ampullate field: (0) as other setae surrounding the spinning field, i.e. smooth or similarly serrated (Figs 94E, 107G); (1) with a row (or two, as in *Tasmanapis*) of minute ‘branches’ (Figs 89C, 103B, 113A); (2) with a row of long ‘branches’ (Figs 11E, 13C, 16B); (3) with two rows of long ‘branches’ (Figs 6B, 23F, 33F, 52B). The ancestral condition in symphytognathoids, occurring in the outgroup, in Synaphridae, and convergently in *Taphiassa* is a seta similar to the surrounding setae on the ALS (state 0). Two rows of long branches are a synapomorphy of Mysmenidae. One row of long branches in the MAP seta is synapomorphic for *Maymena*, convergently evolving in Theridiosomatidae. A seta with a row of minute branches (state 1) is a synapomorphy of the clade comprising Anapidae plus Symphytognathidae (node C112, with a reversal in *Taphiassa*).
311. ALS middle fold: (0) present (*Leucauge*); (1) absent (Figs 33C, 78B, 97H). *Leucauge venusta* seems to have a subtle fold, which appears like a relict of a middle segment (L. Lopardo & G. Hormiga, pers. observ.). This character scores this fold, although its homology with a third segment remains unknown (S02 – 108; G05 – 75).
312. PMS minor ampullate (mAP): (0) absent (Fig. 103C, E); (1) present (Figs 6C, 19F, 125C). A loss of the mAP spigot occurred independently in *Cepheia* and *Teutoniella* (S02 – 113; G05 – 81).
313. PMS mAP tartipore and nubbin: (0) mAP only (Figs 6C, F, 58F, 61D, 78E, 82G, 94B, F); (1) mAP plus tartipore (Figs 19F, 23D, 33D, 123E); (2) mAP plus tartipore and nubbin (Figs 11F, 75D, 88G, 113C, 122E, 125C). The presence of a tartipore, or a nubbin plus tartipore accompanying the minor ampullate spigot optimizes ambiguously at the base of symphytognathoids, therefore, a pattern of loss of the nubbin, or the nubbin plus tartipore, is unclear. Within symphytognathoids, the presence of a nubbin and a tartipore occurs in symphytognathids, most anapids, *Coddingtonia*, and *Maymena*. The loss of the mAP nubbin

- (although not the tartipore) optimizes ambiguously as a potential synapomorphy for *Trogloneta* and for Mysmeninae. The complete loss of both the nubbin and the tartipore is ambiguously optimized in Mysmenopsinae, independently occurring in the anapid subfamily Micropholcommatinae (clade C150). (S02 – 115; S03 – 55; G98 – 71; A04 – 220).
314. PMS mAP shaft: (0) proximal diameter of shaft narrower than distal spigot base, shaft usually cylindrical and longer than wide (although it can be short; Figs 6C, F, 33D, 58F, 75C, 78D, 100B); (1) width of proximal shaft as wide as apical spigot base, shaft as long as wide (Figs 49G, 113C, 125C). This character optimizes ambiguously at the symphytognathoid node. A wide mAP base and shaft occur on Theridiosomatidae, independently in the symphytognathid clade C195, and the mysmenids *Mysmena leichhardti*, MYSM-020-MAD, and MYSM-023-MAD (S03 – 56).
315. PMS mAP spigot shaft length: (0) short, subequal to CY shaft (Figs 6C, 61D, 75D, 94F, 114A, 123E); (1) clearly longer than any CY shaft (*Linyphia* and *Steatoda*) (A04 – 223).
316. Major ampullate tartipores: (0) absent (Fig. 78C); (1) present (Fig. 23F). Absence of tartipores on MAP field (state 0) is an autapomorphy of *Comaroma* (G05 – 70).
317. Anterior median spinnerets (AMS): (0) colulus (Figs 33C, 49F, 68C, 88F); (1) absent (Figs 117F, 120C). The absence of colulus is synapomorphic for Symphytognathidae. The genus *Patu* has been reported to have an extremely minute colulus (e.g. in *Patu digua*; see Griswold *et al.*, 1998, fig. 37A), suggesting that the absence of colulus might be synapomorphic for at least a clade within Symphytognathidae. The cuticle in the colular area of the *Patu* representative in this data set (*Patu*-SYMP-001-DR) has a slit and bears two setae, although there is no evidence of protruding colulus (image not shown), and it is here considered as absent (S02 – 106; S03 – 54; G98 – 66; G05 – 71; A04 – 172).
318. Colulus size: (0) minute, about one-eighth width of ALS (Figs 64D, 67F, 68C); (1) large, fleshy, width about one-quarter width of ALS (Figs 33C, 49F, 88F). Minute colulus is a synapomorphy of *Trogloneta* (S02 – 107; S03 – 54; G98 – 65; A04 – 172, 173).
319. Colular setae number: (0) four or more (Fig. 56D); (1) three or less (Figs 67F, 78B). Three or less setae on colulus are synapomorphic of symphytognathoids. Within Mysmenidae, four or more colular setae are a synapomorphy of *Mysmenopsis* (with a reversal in *M. palpalis*) (G98 – 65; A04 – 175).
320. PLS Cylindrical (CY) spigot number: (0) one (Fig. 94F); (1) two (Figs 13F, 45F, 58H, 65A, 78H, 103F, 113D, 123F). Although usually one or two CY spigots occur on the PLS, in a few instances three CY can occur, as anomalies on one of the PLS (e.g. compare both PLS of *Comaroma*; Fig. 78G and H). These anomalies are not taken into account when scoring. One cylindrical gland spigot on the posterior lateral spinnerets evolved independently in *Cepheia* and *Taphiassa* (S02 – 119; G98 – 74; A04 – 210).
321. PLS anterior CY position: (0) below FL, on spinning field (Fig. 94F; also *Linyphia*); (1) peripheral, or above FL if on spinning field (Figs 58H, 78H, 113D, 123F). This character refers to the anterior CY spigot, i.e. the CY spigot closer to the ALS (as both spigots are usually mesal). When two CY spigots are present, the posterior one is always peripheral. A cylindrical spigot located on the spinning field (i.e. state 0, not peripheral) occurs independently in *Taphiassa* and *Linyphia* (G98 – 76).
322. PLS CY relative size: (0) both CY equally large and larger than FL (Figs 11G, H, 13F, 67D, 94F, 123F); (1) posterior CY huge, larger than anterior CY (both larger than FL; Figs 75E, 78H, 89D, 100C, 103F, 113D, 114B); (2) all slim as other spigots, not larger, but subequal to FL (Figs 23B, 37B, E). Slim cylindrical spigots (state 2) are convergent synapomorphies of Mysmenopsinae and Mysmeninae. A huge posterior cylindrical spigot (state 1) is a synapomorphy of Anapidae plus Symphytognathidae (node C112, reverting to state 0 in *Taphiassa*).
323. Sclerotized ring around spinnerets: (0) absent (Figs 6E, 59I, 107F, 117F, 140F); (1) present (Figs 78B, 97H, 145F, 146B). Partial sclerotized ring (heavily sclerotized cuticle not completely surrounding spinnerets) are considered present (e.g. in *Crassanapis*), whereas extremely weakly sclerotized rings were considered absent (e.g. in *Elanapis*). Synapomorphy of the anapid clade C122, with a reversal in *Elanapis* (S02 – 96; A04 – 202).
324. PLS distal segment: (0) short conical, as distal ALS segment (Figs 33C, 97H, 145F, 146B); (1) long cylindrical, distal PLS segment two times longer than distal ALS segment, usually visible on dorsal view (Figs 107F, 146E, F). Synapomorphy of Synaphridae (S03 – 54.1).
325. ALS intersegmental cuticle: (0) smooth (Fig. 94A, E); (1) glabrous tuberculate (Figs 6A, 23C, 66F, 75A); (2) fingerprint (Fig. 113A). A glabrous tuberculate cuticle (state 1) is the ancestral and widespread cuticular pattern in symphytognathoids, occurring in the outgroup taxa as well.

- A fingerprint cuticle (state 2) optimizes as a synapomorphy of Symphytognathidae. Smooth cuticle (state 0) is synapomorphic for Synaphridae, convergent in *Taphiassa*.
326. PS cuticle on spigot bases: (0) smooth (Figs 78F, 82H, 94C, D); (1) imbricate (Figs 11G, 23B, E, 89D). Scored for both PMS and PLS. Smooth cuticle is synapomorphic of the anapid subfamily Micropholcommatinae (clade C150) (G05 – 69).
327. ALS Pi spigot bases: (0) large (tetragnathids); (1) 'reduced' (Figs 33F, 75A) (S02 – 110; G98 – 69; A04 – 204).
328. PLS posterior setae: (0) slender setae (Figs 23B, 123F); (1) posterior row of clavate setae (Fig. 122F). The setae on the posterior distal border of the PLS of the symphytognathid SYMP-006-AUST appear subtly thicker than the surrounding setae (see Fig. 117G), but are not considered similar to the clavate setae of *Symphytognatha picta*, and were therefore scored as slender (state 0). Autapomorphy of *Symphytognatha picta* (S03 – 60.1).
329. PLS anterior flat spatulate modified seta: (0) absent or serrated seta (Figs 6B, 65A, 87C, 94D, 123F); (1) present (Figs 11H, 23B, E, 33G, H, 52C). The anterior distal border of the PLS of *Anapisona kethleyi* has a distinct seta, although it is not spatulate and therefore scored as serrated (state 0; see Fig. 75G). This particular seta evolved convergently within Mysmenidae, in *Maymena*, and in Mysmeninae (secondarily lost in *Mysmena rotunda*).
330. FL spigot in female: (0) absent (Fig. 6D); (1) present (Figs 13F, 23B, 58H, 67D, 75G, 78H, 94F, 103F, 113D, 123F). The female flagelliform spigot is lost in the mysmenid genus *Isela* (S02 – 125; G98 – 77; A04 – 212).
331. FL in male: (0) absent (Figs 6G, 23E); (1) present (Figs 53H, 58G, 75F, 82H, 94D, 103D, 117G). An apparently functional male flagelliform spigot occurs in *Mysmenopsis*, *Maymena mayana*, *Trogloneta granulum*, the clade C112 (comprising symphytognathids and anapids), and independently in some mysmenines. As a result of the homoplasy of this character, it optimizes ambiguously for symphytognathoids (S02 – 126; S03 – 58; A04 – 219).
332. FL spigot shaft: (0) straight (Figs 6D, 67D, 75G); (1) shaft curved (Figs 78F, H, 82H). Curved FL shaft is an autapomorphy of *Comaroma* (S03 – 59).
333. AG spigots in female: (0) absent (Figs 6D, 58H, 94F); (1) present (Figs 75G, 123F). The female aggregate spigots are lost in the kleptoparasitic mysmenids Mysmenopsinae, and independently in *Taphiassa* (S02 – 127; G98 – 78; G05 – 95).
334. AG spigot number in female: (0) two (Figs 13E, F, 23B, 75G, 87C, 113D, 123F); (1) one (*Cepheia*). One female aggregate spigot is an autapomorphy of *Cepheia* (A04 – 213).
335. AG spigots in male: (0) absent (Figs 6G, 23E, 33H, 58G, 94D); (1) present (Fig. 103D). Functional male aggregate spigots occur independently in *Maymena mayana*, *Trogloneta granulum*, a few mysmenines, and clade C113 (synaphrids, symphytognathids, and anapids) (S02 – 129; S03 – 58; A04 – 219).
336. AG spigot number in male: (0) two (Figs 13G, 75F, 82H, 100D, 103D); (1) one (synaphrids).
337. AG spigots: (0) broader than FL (Fig. 123F); (1) as FL (Figs 13F, G, 75F, 78H, 100D); (2) extremely large, huge (*Steatoda*). The aggregate spigots of *Theridiosoma gemmosum* are broader than the flagelliform spigot (state 0, ancestral state for symphytognathoids). Slim aggregate spigots (state 1) are a synapomorphy of the ANTS clade (S03 – 60; G98 – 78).
338. Anterior AG spigot shape: (0) round (Fig. 23B); (1) flattened (*Steatoda*). In order to score the shape of the single AG spigot of synaphrids, it was randomly assigned as posterior, and therefore scored under character 339. Autapomorphy of *Steatoda* (A04 – 215).
339. Posterior AG spigot shape: (0) round (Fig. 23B); (1) flattened (*Steatoda*). In order to score the shape of the single AG spigot of synaphrids, it was randomly considered as posterior, and therefore scored in this character. Autapomorphy of *Steatoda* (A04 – 216).
340. PLS aggregate gland form: (0) entire (*Linyphia* and *Tetragnatha*); (1) lobed (*Steatoda*). The scarce knowledge on the form of the aggregate gland was taken from A04 – 217, and was available for only three (outgroup) taxa.

Behavioural characters

341. Web posture: (0) legs I and II extended (tetragnathids); (1) legs I and II flexed (Fig. 147B) (G98 – 81).
342. Predatory strategy: (0) catching web; (1) free hunters (*Leviola*); (2) kleptoparasites (*Isela* and most *Mysmenopsis* species). Under this taxon sample, kleptoparasitism is a synapomorphy of Mysmenopsinae (S02 – 153; A04 – 224).
343. Wrap-bite attack: (0) present (*Steatoda* and *Leucauge*); (1) absent, bite first (G98 – 92; G05 – 154; A04 – 228).
344. R radii lengthened: (0) absent; (1) present. Only scored in five taxa. Lengthened radii are an ambiguously optimized synapomorphy of symphytognathoids, although it was only

- observed in theridiosomatids and mysmenids (G98 – 84).
345. Web architecture: (0) orb (Figs 147A, 148A, B, 149A); (1) sheet (*Linyphia*, *Trogloneta granulum*, and *Synaphris saphrynis*); (2) cobweb (*Steatoda* and *Comaroma*). The web of *Comaroma* has been reported by Kropf (1990) as an irregular three-dimensional web with long threads containing sticky silk at their distal end (i.e. at place of attachment to substrate), which is consistent with the description of the typical theridiid web (e.g. Griswold *et al.*, 1998, and references therein; Agnarsson, 2004) and was scored as such. As discussed by Griswold *et al.* (1998) and Lopardo & Hormiga (2008), the homologies involving web architectures and behaviours for the so-called ‘sheet web’ remain unsolved. Sheet webs encompass an enormous diversity of web architectures. Only three taxa in this data set are considered to be sheet-web weavers (see above). Even though homology statements in the behavioural and architectural aspects are compromised, the web of *Trogloneta granulum* was nevertheless considered and scored here as a sheet web (see detailed discussion on Lopardo *et al.*, 2011). The orb web is the plesiomorphic web in this data set; all other webs evolve independently on each taxon (S02 – 154; S03 – 80; G98 – 80; G05 – 142, 143; A04 – 225).
346. Orb web frame: Out of the plane radii (APR) on final web: (0) absent, two-dimensional (Figs 148A, 149C, D); (1) present, three-dimensional (Figs 147A, D, 148C, D). Retention of radii extending out of the orb web plane is a putative synapomorphy of symphytognathoids, reverting to bidimensional final webs independently in Symphytognathidae, and the anapid distal clade C153 (G98 – 82).
347. APR on final web: (0) above the plane (Figs 147D, E, 148B–D); (1) above and below the plane (Fig. 147A, B). APR oriented above and below the orb plane is an ambiguously optimized synapomorphy of Mysmeninae (clade C133).
348. Post-SS hub loops: (0) absent; (1) present. Only scored in six taxa. Post sticky silk hub loops are an ambiguously optimized synapomorphy of symphytognathoids, although it was only observed in theridiosomatids and mysmenids (G98 – 88).
349. Hub: (0) closed; (1) open. Only scored in six taxa. Closed hub is an ambiguously optimized synapomorphy of symphytognathoids, although (as in character 348) it was only observed in theridiosomatids and mysmenids (G98 – 90).

APPENDIX 3

Abbreviations used in text and figures.

A04	Agnarsson (2004)
AC	aciniform (gland spigot/s)
AG	aggregate (gland spigot)
AGs	aggregate (gland spigots)
ALS	anterior lateral spinnerets
AME	anterior median eyes
ANTS	anterior tracheal system
Atr	atrium
BS	Bremer support
C	tegular (bulbal) conductor
CD	copulatory ducts
CI	consistency index
CO	copulatory openings
CY	cylindrical (gland spigot/s)
Cy	cymbium
CyC1	primary (internal) cymbial conductor
CyC2	secondary (external) cymbial conductor
CyF	cymbial fold
CyFs	setae on cymbial fold
CyG	cymbial groove
CyP	cymbial process
CyPF	cymbial fold process
E	embolus
Eap	embolar (distal) apophysis
EB	embolar base
Ebap	embolar basal apophysis
F	fundus
FD	fertilization ducts
fe	femur
FL	flagelliform (gland spigot)
G05	Griswold <i>et al.</i> (2005)
G98	Griswold <i>et al.</i> (1998)
GC	frequency differences
gl	accessory gland
I	spermatic duct switchback I (drawing)
II	spermatic duct switchback II (drawing)
III	spermatic duct switchback III (drawing)
IV	spermatic duct switchback IV (drawing)
MA	median apophysis
MAP	major ampullate (gland spigot)
mAP	minor ampullate (gland spigot)
MPT	most-parsimonious tree/s
mt	metatarsus
n	nubbin
pa	patella
PC	paracymbium
Pi	piriform (gland spigot/s)
PLS	posterior lateral spinnerets
PME	posterior median eyes
PMS	posterior median spinnerets
pp	pars pendula
RAS	random-addition sequences
RFD	relative Bremer support, or relative fit difference
RI	retention index
S	spermatheca/e
S02	Schütt (2002)
S03	Schütt (2003)
SB	spermatic duct switchback
SD	spermatic duct
SDT	spermatic duct trajectory
SEM	scanning electron microscopy
SFq	symmetric resampling frequencies
Sp	spiracle
t	tartipore
T	tegulum
ta	tarsus
TBR	tree bisection and reconnection branch swapping
TC	tegular conductor
ti	tibia
to	tarsal organ

APPENDIX 4

Table A1. List of synapomorphic changes common to the three most parsimonious cladograms from the analysis of the morphological data

Taxon name/node number	All trees	Some trees			
<i>Acrobleps hygrophilus</i>	Character 22: 1 → 0 Character 90: 0 → 2 Character 180: 0 → 1 Character 233: 0 → 1 Character 252: 0 → 2 Character 346: 0 → 1	Character 24: 0 → 1 Character 95: 1 → 0 Character 195: 0 → 1 Character 250: 0 → 1 Character 278: 0 → 2	Character 38: 0 → 1 Character 152: 0 → 1 Character 228: 0 → 1 Character 251: 0 → 1 Character 298: 0 → 2	Character 202: 0 → 1	
<i>Anapisona kethleyi</i>	Character 21: 1 → 2 Character 88: 1 → 0 Character 152: 0 → 1 Character 182: 0 → 1 Character 207: 0 → 1 Character 220: 1 → 0 Character 248: 0 → 1 Character 294: 0 → 1	Character 28: 0 → 1 Character 122: 0 → 1 Character 164: 0 → 5 Character 195: 0 → 1 Character 210: 0 → 1 Character 235: 0 → 1 Character 272: 0 → 1	Character 68: 1 → 0 Character 145: 0 → 1 Character 175: 0 → 1 Character 203: 0 → 1 Character 211: 0 → 1 Character 246: 0 → 1 Character 291: 0 → 1	Character 1: 1 → 0	Character 79: 0 → 1
<i>Anjouanella comorensis</i>	Character 11: 1 → 2 Character 199: 1 → 0	Character 75: 1 → 0 Character 253: 0 → 2	Character 197: 2 → 0		
<i>Brasilionata arborensis</i>	Character 7: 1 → 0				
<i>Calodipoena incredula</i>	Character 38: 0 → 1 Character 162: 0 → 2	Character 104: 0 → 1 Character 222: 1 → 0	Character 118: 0 → 1		
<i>Calodipoena mooatae</i>	Character 48: 1 → 0				
<i>Calomyspoena santacruzii</i>	Character 123: 0 → 1	Character 177: 0 → 2	Character 186: 1 → 2		
<i>Cepheia longiseta</i>	Character 134: 0 → 1 Character 162: 0 → 2 Character 207: 0 → 1 Character 291: 0 → 1	Character 149: 0 → 1 Character 164: 0 → 1 Character 212: 0 → 1	Character 158: 0 → 1 Character 203: 0 → 1 Character 262: 1 → 0		
<i>Coddingtonia euryopoides</i>	Character 6: 0 → 2 Character 75: 0 → 1 Character 163: 0 → 2	Character 21: 0 → 1 Character 83: 0 → 4 Character 164: 0 → 1	Character 52: 0 → 1 Character 136: 0 → 1 Character 271: 1 → 0		
<i>Comaroma simony</i>	Character 5: 1 → 2 Character 56: 1 → 0 Character 97: 2 → 0 Character 127: 0 → 2 Character 161: 1 → 0 Character 207: 0 → 1 Character 237: 0 → 1 Character 284: 23 → 1 Character 299: 1 → 0 Character 332: 0 → 1	Character 23: 1 → 0 Character 71: 1 → 0 Character 110: 0 → 1 Character 136: 0 → 1 Character 197: 0 → 1 Character 213: 1 → 0 Character 244: 1 → 0 Character 293: 1 → 0 Character 303: 1 → 0	Character 41: 0 → 2 Character 95: 1 → 0 Character 124: 0 → 1 Character 141: 0 → 1 Character 203: 0 → 1 Character 214: 0 → 1 Character 257: 1 → 0 Character 296: 0 → 1 Character 316: 1 → 0	Character 46: 4 → 0	Character 215: 0 → 1
<i>Crassanapis chilensis</i>	Character 7: 0 → 1 Character 97: 2 → 0 Character 128: 0 → 1	Character 46: 4 → 5 Character 120: 1 → 0 Character 305: 2 → 1	Character 80: 1 → 0 Character 126: 0 → 1	Character 38: 0 → 1 Character 194: 1 → 0	Character 78: 1 → 2 Character 226: 1 → 2
<i>Elanapis aisen</i>	Character 7: 0 → 1 Character 83: 0 → 5 Character 276: 0 → 1	Character 11: 0 → 2 Character 150: 0 → 1	Character 81: 0 → 1 Character 261: 0 → 1	Character 86: 0 → 1	
<i>Iardinis mussardi</i>	Character 12: 1 → 0 Character 203: 0 → 1	Character 155: 0 → 1 Character 219: 0 → 2	Character 195: 0 → 1		
<i>Isela okuncana</i>	Character 19: 0 → 1	Character 67: 1 → 0	Character 226: 0 → 1		
<i>Itapua tembei</i>	Character 83: 2 → 0				
<i>Kekenboschiella awari</i>	Character 224: 0 → 1	Character 284: 1 → 2			
<i>Kekenboschiella marijkeae</i>	Character 195: 1 → 0	Character 197: 0 → 1			
<i>Leucauge venusta</i>	Character 64: 0 → 1 Character 196: 1 → 0 Character 311: 1 → 0	Character 81: 0 → 1 Character 225: 2 → 0 Character 343: 1 → 0	Character 82: 0 → 2 Character 278: 0 → 1		
<i>Linyphia triangularis</i>	Character 52: 2 → 5 Character 89: 1 → 0 Character 240: 0 → 2 Character 321: 1 → 0	Character 57: 1 → 0 Character 152: 0 → 1 Character 267: 0 → 1 Character 322: 0 → 1	Character 60: 0 → 1 Character 163: 0 → 2 Character 268: 0 → 1 Character 345: 0 → 1		
<i>Maymena ambita</i>	Character 4: 1 → 0 Character 222: 1 → 0	Character 7: 1 → 0	Character 105: 0 → 1		

Table A1. Continued

Taxon name/node number	All trees	Some trees	
<i>Maymena mayana</i>	Character 8: 0 → 1 Character 50: 1 → 0 Character 129: 2 → 1 Character 191: 0 → 1	Character 34: 2 → 1 Character 52: 0 → 1 Character 162: 0 → 1 Character 221: 0 → 1	Character 45: 0 → 1 Character 83: 0 → 5 Character 168: 0 → 1
<i>Maymena rica</i>	Character 6: 0 → 1 Character 21: 0 → 12 Character 70: 1 → 0 Character 145: 0 → 1	Character 12: 1 → 0 Character 23: 1 → 2 Character 83: 0 → 1 Character 201: 0 → 1	Character 17: 1 → 0 Character 59: 1 → 0 Character 131: 1 → 0 Character 237: 1 → 0
<i>Microdipoena elsae</i>	Character 35: 1 → 0	Character 75: 1 → 0	Character 87: 1 → 0
<i>Microdipoena guttata</i>	No autapomorphies:		
<i>Microdipoena nyungwe</i>	Character 48: 1 → 0		
<i>Minanapis Casablanca</i>	No autapomorphies:		
<i>Minanapis palena</i>	No autapomorphies:		
<i>Kilifna</i> -MYSM-002-KENYA	Character 7: 1 → 0 Character 190: 0 → 1 Character 281: 0 → 1	Character 52: 0 → 1 Character 225: 0 → 1 Character 308: 1 → 2	Character 77: 0 → 1 Character 276: 0 → 1
MYSM-005-ARG	Character 7: 1 → 0 Character 74: 1 → 0 Character 152: 0 → 1 Character 195: 1 → 0 Character 225: 2 → 0	Character 15: 1 → 0 Character 85: 0 → 1 Character 164: 3 → 0 Character 196: 2 → 1 Character 335: 0 → 1	Character 22: 0 → 1 Character 101: 1 → 0 Character 178: 0 → 1 Character 202: 0 → 1
MYSM-007-MEX	Character 6: 0 → 2 Character 171: 0 → 1 Character 189: 1 → 0	Character 103: 1 → 0 Character 178: 0 → 1 Character 226: 0 → 1	Character 134: 0 → 1 Character 182: 0 → 1
<i>Mysmena</i> -MYSM-015-MAD	Character 52: 0 → 2	Character 97: 1 → 2	
<i>Mysmena</i> -MYSM-018-MAD	Character 38: 0 → 1 Character 47: 0 → 1 Character 289: 0 → 1	Character 149: 0 → 1 Character 48: 1 → 0	Character 170: 1 → 0 Character 265: 0 → 1
MYSM-020-MAD	Character 48: 1 → 0	Character 164: 3 → 0	
MYSM-023-MAD	Character 23: 1 → 2 Character 184: 1 → 0	Character 97: 1 → 2 Character 265: 0 → 1	Character 163: 1 → 2 Character 289: 0 → 1
MYSM-028-MAD	Character 53: 2 → 1	Character 97: 1 → 2	
MYSM-029-MAD	Character 35: 1 → 0	Character 60: 1 → 0	Character 70: 0 → 1
MYSM-034-MAD	Character 11: 0 → 2	Character 74: 1 → 0	Character 86: 0 → 1
<i>Mysmena leichhardtii</i>	Character 38: 0 → 1 Character 191: 1 → 0	Character 162: 0 → 2 Character 224: 0 → 1	Character 186: 0 → 2 Character 314: 0 → 1
<i>Mysmena leucoplagiata</i>	Character 116: 1 → 2	Character 117: 1 → 0	Character 162: 0 → 2
<i>Mysmena tasmaniae</i>	Character 23: 1 → 2 Character 105: 0 → 1 Character 184: 1 → 0	Character 74: 1 → 0 Character 116: 1 → 2 Character 288: 0 → 1	Character 83: 1 → 2 Character 170: 1 → 0
<i>Mysmenella illectrix</i>	Character 187: 1 → 0		
<i>Mysmenella jobi</i>	Character 255: 1 → 0	Character 286: 1 → 0	
<i>Mysmenella samoensis</i>	Character 48: 1 → 0	Character 292: 0 → 1	
<i>Mysmeniola spinifera</i>	Character 6: 0 → 2 Character 112: 0 → 1	Character 48: 1 → 0 Character 163: 1 → 2	Character 88: 1 → 0 Character 250: 0 → 1
<i>Mysmenopsis cidrelicola</i>	Character 35: 1 → 2	Character 112: 0 → 1	Character 116: 1 → 2
<i>Mysmenopsis dipluramigo</i>	Character 125: 1 → 0 Character 265: 0 → 1	Character 143: 0 → 1	Character 259: 1 → 0
<i>Mysmenopsis palpalis</i>	Character 35: 1 → 0 Character 116: 1 → 2	Character 66: 0 → 1 Character 135: 0 → 1	Character 67: 1 → 2
<i>Mysmenopsis penai</i>	Character 83: 0 → 4 Character 271: 2 → 1	Character 99: 0 → 1	Character 126: 1 → 0
<i>Steatoda americana</i>	Character 12: 1 → 0 Character 20: 1 → 0 Character 47: 1 → 3 Character 137: 0 → 1 Character 203: 0 → 1 Character 228: 0 → 1 Character 237: 1 → 0 Character 278: 0 → 3 Character 301: 1 → 0 Character 343: 1 → 0	Character 13: 0 → 1 Character 40: 0 → 1 Character 52: 2 → 3 Character 151: 0 → 1 Character 208: 0 → 1 Character 229: 0 → 1 Character 255: 0 → 1 Character 282: 1 → 0 Character 338: 0 → 1 Character 345: 0 → 2	Character 16: 0 → 1 Character 41: 0 → 1 Character 98: 0 → 1 Character 161: 1 → 0 Character 212: 0 → 1 Character 230: 0 → 1 Character 271: 1 → 0 Character 291: 0 → 1 Character 339: 0 → 1

Table A1. Continued

Taxon name/node number	All trees	Some trees			
<i>Patu</i> -SYMP-001-DR	Character 38: 0 → 1 Character 86: 0 → 1 Character 165: 0 → 1 Character 185: 0 → 1 Character 218: 0 → 1	Character 74: 1 → 0 Character 152: 0 → 1 Character 170: 0 → 1 Character 195: 0 → 1 Character 288: 0 → 1	Character 78: 1 → 0 Character 164: 0 → 4 Character 180: 0 → 1 Character 201: 0 → 1		
SYMP-002-MAD	Character 74: 1 → 0	Character 153: 0 → 2	Character 261: 0 → 1		
SYMP-006-AUST	Character 11: 2 → 0 Character 265: 1 → 2	Character 78: 1 → 2 Character 295: 1 → 0	Character 83: 0 → 4		
SYMP-007-AUST	Character 13: 1 → 0	Character 64: 1 → 0	Character 67: 0 → 2		
<i>Symphytognatha picta</i>	Character 44: 0 → 1 Character 129: 2 → 0 Character 194: 0 → 1 Character 287: 1 → 0	Character 49: 0 → 1 Character 137: 0 → 2 Character 273: 1 → 0 Character 328: 0 → 1	Character 63: 0 → 1 Character 157: 0 → 1 Character 279: 0 → 1		
<i>Synaphris saphrynis</i>	Character 52: 2 → 1 Character 225: 2 → 1	Character 163: 0 → 3 Character 239: 0 → 3	Character 170: 0 → 1		
<i>Tamasesia acuminata</i>	Character 6: 0 → 2	Character 11: 1 → 0			
<i>Tamasesia rotunda</i>	Character 7: 1 → 0 Character 223: 1 → 0	Character 83: 2 → 5	Character 221: 0 → 2		
<i>Tasmanapis strahan</i>	Character 11: 0 → 2 Character 46: 4 → 6 Character 128: 0 → 1 Character 220: 1 → 0 Character 246: 0 → 1	Character 23: 1 → 0 Character 68: 1 → 0 Character 136: 0 → 1 Character 225: 0 → 1	Character 35: 0 → 5 Character 85: 0 → 1 Character 154: 0 → 1 Character 244: 1 → 0		
<i>Taphiassa punctata</i>	Character 21: 1 → 2 Character 72: 0 → 1 Character 162: 0 → 1 Character 270: 1 → 0 Character 279: 0 → 1 Character 291: 0 → 1 Character 320: 1 → 0 Character 325: 1 → 0	Character 45: 0 → 3 Character 83: 0 → 2 Character 220: 1 → 0 Character 271: 1 → 0 Character 280: 0 → 1 Character 298: 0 → 1 Character 321: 1 → 0 Character 333: 1 → 0	Character 59: 0 → 1 Character 152: 0 → 1 Character 235: 0 → 1 Character 275: 0 → 1 Character 290: 1 → 0 Character 310: 1 → 0 Character 322: 1 → 0 Character 335: 1 → 0	Character 46: 4 → 3 Character 226: 1 → 0 Character 309: 1 → 0	Character 166: 0 → 1 Character 231: 0 → 1
<i>Tetraghnatha versicolor</i>	No autapomorphies:				
<i>Teutoniella cekalovici</i>	Character 7: 0 → 1 Character 88: 1 → 0 Character 194: 1 → 0 Character 251: 0 → 1	Character 17: 0 → 1 Character 112: 1 → 0 Character 196: 0 → 1 Character 312: 1 → 0	Character 41: 0 → 1 Character 149: 1 → 2 Character 233: 0 → 1	Character 54: 2 → 0	
<i>Theridiosoma gemmosum</i>	Character 10: 1 → 0 Character 196: 2 → 0	Character 82: 0 → 1 Character 197: 0 → 13	Character 99: 1 → 0 Character 204: 0 → 1		
<i>Trogloneta cantareira</i>	Character 313: 2 → 1 Character 6: 0 → 2 Character 226: 0 → 1	Character 45: 0 → 2	Character 46: 0 → 12		
<i>Trogloneta granulum</i>	Character 149: 0 → 2 Character 225: 0 → 1	Character 196: 2 → 0 Character 278: 1 → 2	Character 197: 0 → 1		
Node M66	Character 44: 0 → 1 Character 237: 1 → 0	Character 62: 0 → 1 Character 290: 0 → 1	Character 225: 2 → 0 Character 292: 0 → 1	Character 231: 0 → 1	Character 309: 0 → 1
Node M67	Character 56: 0 → 1 Character 259: 0 → 1	Character 160: 1 → 0 Character 310: 0 → 1	Character 244: 2 → 1 Character 322: 0 → 1		
Node M68	Character 7: 1 → 0 Character 59: 1 → 0 Character 257: 0 → 1	Character 21: 0 → 2 Character 64: 0 → 1	Character 29: 0 → 1 Character 153: 0 → 1		
Node M69	Character 43: 0 → 1 Character 196: 1 → 2	Character 50: 0 → 1 Character 297: 0 → 1	Character 55: 0 → 1 Character 319: 0 → 1		
Node M70	Character 28: 1 → 0 Character 99: 0 → 1 Character 303: 0 → 1	Character 58: 0 → 1 Character 125: 0 → 1	Character 87: 1 → 0 Character 162: 1 → 0		
Node M71	Character 4: 1 → 0 Character 74: 0 → 1 Character 132: 1 → 0 Character 308: 2 → 0	Character 10: 0 → 1 Character 92: 0 → 1 Character 194: 1 → 0 Character 327: 0 → 1	Character 68: 0 → 1 Character 100: 1 → 0 Character 245: 1 → 0 Character 341: 0 → 1		
Node M72	No synapomorphies				
Node M73	Character 35: 0 → 4	Character 98: 0 → 1	Character 121: 0 → 1	Character 114: 0 → 1 Character 346: 0 → 1	Character 302: 1 → 0
Node M74	Character 0: 0 → 2 Character 323: 0 → 1	Character 3: 0 → 1	Character 278: 0 → 1	Character 1: 0 → 1 Character 52: 2 → 3 Character 153: 1 → 2	Character 46: 0 → 4 Character 54: 0 → 12

Table A1. *Continued*

Taxon name/node number	All trees	Some trees			
Node M75	Character 2: 0 → 1 Character 293: 0 → 1	Character 20: 1 → 0	Character 21: 2 → 1		
Node M76	Character 14: 0 → 1 Character 326: 1 → 0	Character 131: 1 → 0	Character 313: 2 → 0	Character 52: 3 → 4	Character 196: 2 → 0
Node M77	Character 1: 1 → 2 Character 110: 0 → 1 Character 175: 0 → 1 Character 261: 0 → 1 Character 293: 1 → 0	Character 41: 0 → 3 Character 150: 0 → 1 Character 236: 0 → 1 Character 276: 0 → 1	Character 80: 1 → 0 Character 160: 0 → 1 Character 248: 0 → 1 Character 278: 1 → 2	Character 44: 1 → 0	Character 256: 0 → 2
Node M78	Character 72: 0 → 1	Character 233: 0 → 1	Character 298: 0 → 3	Character 38: 0 → 1	Character 86: 0 → 1
Node M79	Character 0: 2 → 1 Character 68: 1 → 0	Character 35: 0 → 3 Character 228: 0 → 1	Character 62: 1 → 0 Character 246: 0 → 1		
Node M80	Character 61: 1 → 0	Character 185: 1 → 0			
Node M81	Character 104: 0 → 1	Character 225: 1 → 0	Character 278: 1 → 0		
Node M82	Character 142: 0 → 1 Character 238: 2 → 1	Character 194: 0 → 1	Character 226: 0 → 1		
Node M83	Character 160: 1 → 0 Character 223: 1 → 0	Character 177: 0 → 2	Character 218: 0 → 1		
Node M84	Character 184: 1 → 0				
Node M85	Character 87: 0 → 1				
Node M86	Character 38: 0 → 1 Character 225: 2 → 1	Character 73: 0 → 1	Character 117: 0 → 1		
Node M87	Character 188: 0 → 1	Character 222: 1 → 0			
Node M88	Character 83: 1 → 2	Character 223: 0 → 1			
Node M89	Character 172: 0 → 1	Character 192: 0 → 1	Character 193: 0 → 1		
Node M90	Character 59: 1 → 0 Character 67: 1 → 0	Character 60: 0 → 1 Character 191: 0 → 1	Character 62: 0 → 1		
Node M91	Character 22: 1 → 0 Character 69: 0 → 1 Character 225: 0 → 2 Character 329: 0 → 1	Character 26: 1 → 0 Character 79: 0 → 1 Character 299: 0 → 1	Character 32: 0 → 1 Character 176: 0 → 2 Character 304: 0 → 1		
Node M92	Character 271: 1 → 2	Character 308: 2 → 1	Character 322: 0 → 2		
Node M93	Character 167: 0 → 1 Character 270: 01 → 2 Character 313: 2 → 1	Character 185: 0 → 1 Character 284: 0 → 2	Character 259: 0 → 1 Character 310: 2 → 3		
Node M94	Character 4: 0 → 1 Character 175: 0 → 1 Character 309: 0 → 1	Character 101: 0 → 1 Character 239: 0 → 3	Character 163: 0 → 1 Character 278: 0 → 1		
Node M95	Character 52: 2 → 0 Character 158: 0 → 1 Character 306: 1 → 2 Character 346: 0 → 1	Character 90: 0 → 1 Character 225: 2 → 0 Character 308: 0 → 2	Character 112: 1 → 0 Character 286: 0 → 1 Character 310: 0 → 2		
Node M96	Character 11: 1 → 2	Character 222: 0 → 1			
Node M97	Character 6: 0 → 2	Character 103: 1 → 0			
Node M98	Character 11: 1 → 2	Character 209: 0 → 1	Character 224: 0 → 1		
Node M99	Character 11: 1 → 0	Character 73: 0 → 1			
Node M100	Character 35: 1 → 0 Character 189: 1 → 0	Character 104: 0 → 1 Character 222: 1 → 0	Character 188: 0 → 1		
Node M101	Character 11: 0 → 2 Character 154: 0 → 1 Character 282: 1 → 0	Character 146: 0 → 1 Character 205: 0 → 1	Character 153: 1 → 0 Character 251: 0 → 1		
Node M102	Character 24: 0 → 1 Character 269: 1 → 0 Character 295: 0 → 1	Character 134: 0 → 1 Character 278: 0 → 3	Character 238: 1 → 0 Character 289: 0 → 1		
Node M103	Character 4: 0 → 1 Character 75: 0 → 1 Character 226: 0 → 1 Character 317: 0 → 1	Character 13: 0 → 1 Character 88: 1 → 0 Character 276: 0 → 1 Character 325: 1 → 2	Character 68: 1 → 0 Character 112: 1 → 0 Character 298: 0 → 3		
Node M104	Character 57: 1 → 0 Character 260: 1 → 0	Character 112: 0 → 1 Character 265: 0 → 1	Character 259: 1 → 0 Character 330: 1 → 0		
Node M105	Character 13: 0 → 2 Character 107: 0 → 1 Character 129: 2 → 1 Character 136: 0 → 1 Character 162: 0 → 1 Character 333: 1 → 0	Character 70: 1 → 0 Character 108: 0 → 1 Character 133: 0 → 1 Character 142: 0 → 1 Character 245: 0 → 1 Character 342: 0 → 2	Character 99: 1 → 0 Character 126: 0 → 1 Character 135: 1 → 0 Character 152: 0 → 1 Character 313: 1 → 0		

Table A1. *Continued*

Taxon name/node number	All trees	Some trees	
Node M106	Character 91: 0 → 1		
Node M107	Character 284: 3 → 1		
Node M108	Character 79: 1 → 0		
Node M109	Character 87: 0 → 1	Character 142: 0 → 1	Character 163: 1 → 3
	Character 180: 0 → 1	Character 197: 0 → 1	Character 257: 0 → 1
Node M110	Character 57: 1 → 0	Character 74: 1 → 0	Character 99: 1 → 0
	Character 125: 1 → 0	Character 152: 0 → 1	Character 244: 2 → 0
	Character 303: 1 → 0	Character 304: 0 → 1	Character 329: 0 → 1
Node M111	Character 60: 1 → 0		
Node M112	Character 177: 2 → 1	Character 197: 2 → 1	Character 227: 1 → 0
	Character 253: 0 → 1		
Node M113	Character 162: 0 → 2		
Node M114	Character 79: 1 → 0	Character 83: 1 → 0	Character 87: 0 → 1
Node M115	Character 75: 0 → 1	Character 223: 0 → 1	
Node M116	Character 74: 1 → 0	Character 193: 1 → 0	
Node M118	Character 116: 1 → 2	Character 147: 0 → 1	Character 182: 0 → 1
	Character 194: 1 → 0	Character 219: 0 → 2	Character 221: 0 → 2
	Character 226: 0 → 2	Character 314: 0 → 1	
Node M119	Character 97: 1 → 2		
Node M120	Character 15: 1 → 0	Character 144: 0 → 1	
Node M121	Character 23: 1 → 2	Character 163: 1 → 2	Character 167: 1 → 0
	Character 175: 1 → 0	Character 187: 1 → 0	Character 196: 2 → 0
	Character 200: 0 → 1	Character 203: 0 → 1	Character 204: 0 → 1
	Character 207: 0 → 1	Character 244: 2 → 3	Character 249: 0 → 1
	Character 282: 1 → 0	Character 290: 0 → 1	Character 296: 0 → 1
Node M122	Character 75: 0 → 1	Character 86: 0 → 1	Character 87: 0 → 1
	Character 101: 1 → 0	Character 254: 0 → 1	
Node M123	Character 7: 1 → 0	Character 15: 1 → 0	Character 38: 0 → 1
	Character 75: 0 → 1	Character 80: 1 → 0	Character 85: 0 → 1
	Character 89: 1 → 0	Character 90: 1 → 2	Character 96: 0 → 1
	Character 103: 1 → 0	Character 159: 0 → 1	Character 160: 1 → 0
	Character 161: 1 → 0	Character 204: 0 → 1	Character 218: 0 → 1
	Character 220: 1 → 0	Character 288: 0 → 1	Character 291: 0 → 1
	Character 307: 0 → 1	Character 318: 1 → 0	
Node M124	Character 6: 0 → 2	Character 169: 0 → 1	Character 278: 3 → 2
Node M125	Character 112: 0 → 1	Character 288: 0 → 1	Character 292: 0 → 1
Node M126	Character 19: 0 → 1	Character 25: 1 → 0	Character 26: 1 → 0
	Character 28: 0 → 1	Character 31: 0 → 1	Character 32: 0 → 1
	Character 33: 0 → 1	Character 57: 1 → 0	Character 113: 0 → 1
	Character 127: 0 → 1	Character 141: 0 → 1	Character 157: 0 → 1
	Character 159: 0 → 1	Character 200: 0 → 2	Character 269: 1 → 0
	Character 274: 0 → 1	Character 288: 0 → 1	Character 289: 0 → 1
	Character 296: 0 → 1	Character 306: 1 → 0	Character 324: 0 → 1
	Character 325: 1 → 0	Character 336: 0 → 1	
Node M127	Character 51: 0 → 1	Character 137: 0 → 2	Character 149: 0 → 2
	Character 162: 0 → 2	Character 203: 0 → 1	Character 212: 0 → 1
	Character 242: 0 → 1		

Discrete characters (node numbers refer to nodes in consensus on Fig. 153). Only nodes with changes are listed.

Table A2. List of synapomorphic changes common to the three most parsimonious cladograms from the analysis of the morphological data

Taxon name/Node number	All trees	Some trees
<i>Acrobleps hygrophilus</i>	Character 0: 1.300–1.500 → 1.600 Character 2: 0.590–0.820 → 0.510 Character 3: 1.930–2.370 → 2.780 Character 4: 1.500–1.760 → 2.090	
<i>Anapisona kethleyi</i>	Character 0: 1.300–1.500 → 1.200 Character 1: 1.170 → 1.310 Character 5: 2.000 → 3.000 Character 6: 11.000 → 13.000	
<i>Anjouanella comorensis</i>	Character 0: 1.100 → 1.000 Character 1: 1.150–1.190 → 1.200	
<i>Brasilionata arborensis</i>	No autapomorphies	
<i>Calodipoena incredula</i>	Character 2: 0.870–0.900 → 0.790 Character 3: 1.830–1.900 → 1.970	
<i>Calodipoena mooatae</i>	Character 0: 1.200–1.300 → 1.400 Character 1: 1.200 → 1.230 Character 2: 0.910–0.950 → 0.960	
<i>Calomyspoena santacruzii</i>	Character 1: 1.200–1.210 → 1.160 Character 3: 1.830–1.900 → 1.780	
<i>Cepheia longiseta</i>	No autapomorphies	
<i>Coddingtonia euryopoides</i>	Character 3: 1.650–1.700 → 1.860 Character 4: 1.160 → 1.150 Character 5: 5.000 → 4.000	
<i>Comaroma simony</i>	Character 0: 1.300–1.500 → 1.800 Character 1: 1.120–1.170 → 0.950 Character 2: 0.590–0.820 → 0.990 Character 3: 1.930–2.370 → 1.660 Character 4: 1.500–1.760 → 1.370 Character 5: 2.000 → 1.000	
<i>Crassanapis chilensis</i>	Character 2: 0.590–0.690 → 0.450	
<i>Elanapis aisen</i>		Character 6: 9.000–10.000 → 11.000
<i>Iardinis mussardi</i>	No autapomorphies	
<i>Isela okuncana</i>	Character 6: 11.000 → 10.000	
<i>Itapua tembei</i>	Character 1: 1.090–1.130 → 1.040 Character 2: 0.830 → 0.760 Character 5: 4.000 → 3.000 Character 6: 9.000 → 7.000	
<i>Kekenboschiella awari</i>	No autapomorphies	
<i>Kekenboschiella marijkeae</i>	Character 0: 1.100 → 1.200	
<i>Leucauge venusta</i>	No autapomorphies	
<i>Linyphia triangularis</i>	Character 3: 1.110 → 1.030 Character 4: 1.050 → 0.930	
<i>Maymena ambita</i>	Character 0: 1.300 → 1.200 Character 1: 1.460–1.500 → 1.710 Character 2: 1.120–1.210 → 1.220	
<i>Maymena mayana</i>	Character 3: 1.650–1.700 → 1.510 Character 5: 7.000 → 10.000 Character 6: 14.000–16.000 → 22.000	
<i>Maymena rica</i>	Character 2: 1.120–1.210 → 1.080 Character 4: 1.440 → 1.450	
<i>Microdipoena elsae</i>	Character 1: 1.190 → 1.270 Character 4: 1.180–1.200 → 1.260	
<i>Microdipoena guttata</i>	Character 2: 0.890 → 0.860	

Table A2. Continued

Taxon name/Node number	All trees	Some trees
<i>Microdipoena nyungwe</i>	Character 2: 0.890 → 0.900 Character 3: 1.840–1.940 → 1.670 Character 4: 1.180–1.200 → 1.150 Character 6: 11.000 → 12.000	
<i>Minanapis Casablanca</i>	Character 4: 1.610 → 1.570	
<i>Minanapis palena</i>	Character 1: 1.000 → 0.970 Character 3: 2.140 → 1.990	
<i>Kilifina</i> -MYSM-002-KENYA	Character 6: 11.000 → 12.000	
MYSM-005-ARG	Character 1: 1.200 → 1.100 Character 2: 0.870–0.900 → 0.840 Character 6: 9.000 → 7.000	
MYSM-007-MEX	Character 0: 1.100 → 1.000 Character 4: 1.210–1.230 → 1.190	
<i>Mysmena</i> -MYSM-015-MAD	Character 1: 1.200 → 1.090 Character 2: 0.910 → 0.850 Character 4: 1.150 → 1.060 Character 5: 4.000 → 3.000	
<i>Mysmena</i> -MYSM-018-MAD	Character 1: 1.240 → 1.330 Character 2: 0.870–0.900 → 0.860 Character 3: 1.870–1.900 → 2.009 Character 6: 9.000 → 8.000	
MYSM-019-MAD	Character 4: 1.370–1.440 → 1.560 Character 6: 10.000 → 11.000	
MYSM-020-MAD	Character 0: 1.200–1.300 → 1.500	
MYSM-023-MAD	Character 0: 1.200–1.300 → 1.000	
MYSM-028-MAD	Character 2: 0.980 → 1.040	
MYSM-029-MAD	Character 2: 0.830 → 0.790 Character 3: 1.800 → 1.610	
MYSM-034-MAD	Character 3: 1.820 → 1.690	
<i>Mysmena leichhardti</i>	Character 3: 1.830 → 1.700 Character 6: 9.000 → 10.000	
<i>Mysmena leucoplagiata</i>	Character 3: 1.840–2.000 → 2.160 Character 4: 1.210–1.230 → 1.320	
<i>Mysmena tasmaniae</i>	Character 4: 1.170–1.230 → 1.280 Character 6: 9.000 → 7.000	
<i>Mysmenella illectrix</i>	No autapomorphies:	
<i>Mysmenella jobi</i>	Character 4: 1.200–1.230 → 1.250	
<i>Mysmenella samoensis</i>	Character 1: 1.170 → 1.210 Character 2: 0.830 → 1.020 Character 4: 1.200 → 1.190 Character 5: 5.000 → 6.000	
<i>Mysmeniola spinifera</i>	Character 0: 1.300 → 1.400	
<i>Mysmenopsis cidrelicola</i>	Character 1: 1.200 → 1.100 Character 2: 1.050–1.060 → 0.920	
<i>Mysmenopsis dipluramigo</i>	Character 1: 1.200 → 1.210 Character 2: 1.050–1.060 → 1.100 Character 3: 1.670–1.700 → 2.060 Character 4: 1.350 → 1.530	
<i>Mysmenopsis palpalis</i>	Character 2: 1.060 → 1.250 Character 4: 1.130 → 1.040	
<i>Mysmenopsis penai</i>	Character 1: 1.200 → 1.310 Character 3: 1.590 → 1.390	
<i>Steatoda Americana</i>	Character 1: 1.170–1.200 → 1.020	
<i>Patu</i> -SYMP-001-DR	Character 1: 1.170 → 1.250	

Table A2. *Continued*

Taxon name/Node number	All trees	Some trees
SYMP-002-MAD	Character 6: 8.000 → 5.000	
SYMP-006-AUST	Character 3: 2.009 → 2.050 Character 4: 1.370 → 1.390	
SYMP-007-AUST	Character 2: 0.810 → 0.800	
<i>Symphytognatha picta</i>	Character 1: 1.110–1.170 → 0.950 Character 2: 0.810–0.830 → 0.940 Character 4: 1.280 → 1.000	
<i>Synaphris saphrynis</i>	No autapomorphies:	
<i>Tamasesia acuminata</i>	No autapomorphies:	
<i>Tamasesia rotunda</i>	Character 2: 1.080 → 1.090 Character 3: 1.740 → 1.630	
<i>Taphiassa punctata</i>	Character 6: 6.000 → 5.000	
<i>Tasmanapis strahan</i>	Character 0: 1.300–1.500 → 1.200 Character 1: 1.120–1.170 → 1.280 Character 2: 0.590–0.690 → 0.480 Character 3: 1.930–2.370 → 3.160 Character 4: 1.500–1.760 → 2.390	
<i>Teutoniella cekalovici</i>	Character 2: 0.590–0.820 → 0.550 Character 3: 1.930–2.370 → 2.430 Character 4: 1.500–1.760 → 2.120	
<i>Theridiosoma gemmosum</i>	Character 1: 1.270 → 1.320 Character 2: 1.120–1.210 → 1.660 Character 3: 1.650–1.700 → 1.620 Character 5: 5.000 → 8.000 Character 6: 16.000 → 19.000	
<i>Trogloneta cantareira</i>	Character 3: 1.650–1.700 → 1.760	
<i>Trogloneta granulum</i>	Character 0: 1.300 → 1.400 Character 2: 1.110–1.210 → 1.220 Character 3: 1.650–1.700 → 1.550 Character 4: 1.210–1.320 → 0.960	
Node M66	Character 4: 1.280 → 1.500–1.760 Character 5: 3.000 → 2.000	Character 3: 1.810–1.930 → 2.140–2.370
Node M67	Character 2: 0.910 → 0.670–0.830 Character 3: 1.650–1.700 → 1.810–1.930 Character 4: 1.200 → 1.280	
Node M68	Character 2: 1.120–1.210 → 0.910 Character 6: 14.000–16.000 → 9.000	
Node M69	Character 0: 1.500 → 1.300 Character 2: 1.700 → 1.120–1.210 Character 3: 1.330 → 1.650–1.700 Character 4: 1.120 → 1.160–1.200 Character 6: 20.000 → 14.000–16.000	
Node M70	Character 2: 1.760 → 1.700 Character 3: 1.110 → 1.330 Character 4: 1.050 → 1.120 Character 5: 7.000 → 5.000 Character 6: 52.000 → 20.000	
Node M71	Character 0: 1.800 → 1.500 Character 2: 2.920 → 1.760 Character 5: 15.000 → 7.000 Character 6: 63.000 → 52.000	
Node M77	Character 1: 1.120–1.170 → 1.000 Character 5: 2.000 → 1.000	
Node M79	Character 6: 8.000–10.000 → 6.000	

Table A2. *Continued*

Taxon name/Node number	All trees	Some trees
Node M80	Character 2: 0.830 → 0.890	
Node M85	Character 2: 0.870 → 0.830	
Node M86	Character 1: 1.200–1.210 → 1.130	
Node M89	Character 0: 1.200–1.300 → 1.100	
Node M90	Character 5: 5.000 → 4.000	
	Character 6: 11.000 → 9.000	
Node M91	Character 2: 1.050–1.060 → 0.880–0.950	
	Character 3: 1.670–1.700 → 1.830–1.860	
Node M92	Character 2: 1.110–1.210 → 1.050–1.060	
Node M93	Character 6: 14.000–16.000 → 11.000	
Node M94	Character 4: 1.160–1.200 → 1.210–1.320	
Node M96	Character 0: 1.100 → 1.300	
Node M98	Character 4: 1.210–1.230 → 1.300–1.330	
	Character 5: 4.000 → 5.000	
Node M108	Character 1: 1.200–1.210 → 1.280	
	Character 2: 0.870–0.900 → 1.080	
	Character 3: 1.800–1.860 → 1.740	
Node M109	Character 4: 1.210–1.320 → 1.440	
Node M110	Character 1: 1.200–1.270 → 1.460–1.500	
	Character 5: 5.000 → 7.000	
Node M114	Character 3: 1.830 → 1.82	
	Character 4: 1.170–1.230 → 1.150	
Node M116	Character 0: 1.100 → 1.200	
	Character 1: 1.200–1.210 → 1.240	
	Character 4: 1.300–1.330 → 1.370–1.440	
Node M117	Character 2: 0.870–0.900 → 0.980	
	Character 6: 9.000 → 10.000	
Node M119	Character 3: 1.840–1.950 → 1.800	
Node M120	Character 4: 1.210–1.330 → 1.350	
Node M121	Character 5: 5.000 → 6.000	
Node M122	Character 3: 1.670–1.700 → 1.590	
	Character 4: 1.210–1.330 → 1.130	
Node M123	Character 1: 1.200 → 1.000	
Node M125	Character 0: 1.200 → 1.100	
	Character 3: 1.810–1.930 → 2.009	
	Character 4: 1.280 → 1.370	

Continuous characters (for node numbers, refer to nodes of consensus tree in Fig. 153). Only nodes with changes are listed.

APPENDIX 5

Mysmenid classification, phylogenetic relationships, and taxonomy (refer to Fig. 161B). Taxonomic or nomenclatural decisions regarding the composition, diagnoses, and circumscription of Mysmenidae, and its phylogenetic relationships to other araneoid lineages, are not based on the results from the morphological character partition alone. Instead, the following taxonomic decisions are based on the hypothesis of relationships and optimization of characters into the preferred optimal tree that results from the total evidence analysis using multiple sources of data (see Figs 160, 161; Lopardo *et al.*, 2011: fig. 12). Node or clade numbers from the phylogenetic hypothesis based on morphological data (Fig. 153) begin with 'M'; nodes from the combined total-evidence hypothesis (Figs 160, 161) begin with 'C'.

MAYMENA GERTSCH, 1960

(FIGS 10–16, 128B, D, E, 131I, J, 140M–O, 141A–I, 147D,E: CLADE C168)

Maymena Gertsch, 1960a: 30–38. Gertsch, 1971: 94–95. Brignoli, 1974: 224. Baert, 1990: 17. Platnick, in Eberhard, Platnick & Schuh, 1993: 11. Griswold *et al.*, 1998: 63.

Type species

Maymena mayana (Chamberlin & Ivie, 1938) by original designation, type material in MCZ, not examined.

Familial placement and composition

Transferred to Mysmenidae from Symphytognathidae by Forster & Platnick (1977). *Maymena* is closely related to Mysmenopsinae in our working phylogenetic hypothesis (Fig. 161B). Currently, *Maymena* comprises 13 described species (Platnick, 2014), and it is represented here by three described plus three undescribed species (the latter species scored only for molecular data): *M. mayana*, *M. ambita*, *M. rica*, *Maymena*-MYSM-003-ARG, *Maymena*-MYSM-004-MEX, and *Maymena*-MYSM-016-ARG.

Monophyly

Morphological synapomorphies of *Maymena* include: posterior lateral spinnerets with an anterior flat spatulate modified seta (Fig. 11H); aciniform gland spigots of the posterior spinnerets of two different shapes (Fig. 13D); seta on major ampullate field with one row of long 'branches' (Figs 11E, 13C, 16B); leg spination (i.e. macrosetae occurring on tibiae, femora, and metatarsi; Figs 140M, 141C); and males with cylindrical palpal tibia (Fig. 10A). Ambiguously optimized synapomorphies for *Maymena* include: males with a

femoral spot at least on femur I; metatarsal clasping spine particularly proximal (Fig. 16G); embolus rim deeply grooved (Fig. 10H); the primary cymbial conductor apically bent over the ventral side (Fig. 10D, G); epiandrous fusules dispersed in a row (Figs 12B, 16A); and macrosetae on female palpal tarsus (Figs 13A, 15A). *Maymena* is one of the few clades in this data set that is strongly supported and stable, and its monophyly is supported by most data partitions and parameter combinations. The genus is also supported by 125 molecular synapomorphies.

Diagnosis

Maymena shares with Mysmeninae the anterior flat spatulate modified seta on PLS and the aciniform gland spigots of two different shapes; with *Trogloneta* the presence of femoral spot on males; and with Mysmenopsinae the dispersed male epiandrous fusules, the macrosetae on female palpal tarsus, the leg spination, and the absence of tegular conductor (see also Gertsch, 1960a). *Maymena* differs from all other mysmenid genera by the combination of the aforementioned features, and by the presence of one row of long 'branches' on the major ampullate field seta, males with cylindrical palpal tibia, metatarsal clasping spine particularly proximal, seemingly interacting with the particularly distal tibial clasping spine in most species, and the male palpal morphology, with primary cymbial conductor apically bent over the ventral side. In addition, the respiratory arrangement distinguishes *Maymena* from other mysmenids. It consists of anterior booklungs and two long lateral tracheal tubes and two shorter median apodemes arising from a narrow posterior single spiracle (L. Lopardo, P. Michalik & G. Hormiga, unpubl. data; also Gertsch, 1960a).

TROGLONETA SIMON 1922

(FIGS 63, 64, 65B–H, 66–68, 128F, 131E, F, 142C: CLADE C192)

Trogloneta Simon, 1922: 200 (*Trogloneta*, *lapsus calami*). Simon, 1926: 313. Fage, 1931: 143. Gertsch, 1960a: 12. Levi & Levi, 1962: 64. Brignoli, 1970: 1409. Thaler, 1975: 284. Wunderlich, 1980b: 267. Brignoli, 1983: 380. Wunderlich, 1987: 139–140. Heimer & Nentwig, 1991: 306. Breuss, 2001: 187. Brescovit & Lopardo, 2008: 94–104.

Parogulnius Archer, 1953: 20. Gertsch, 1960a: 10 (synonymized with *Trogloneta*). Brignoli, 1970: 1410 (rejected synonymy, transfer to Theridiosomatidae). Coddington, 1986a: 6 (placed in Theridiosomatidae as *incertae sedis*). Lopardo & Coddington, 2005: 176 (suggested placement within Mysmenidae, no formal taxonomic action).

Type species

Trogloneta granulum Simon 1922 by original designation, type material in MNHN, examined.

Familial placement and composition

Transferred to Symphytognathidae from Theridiidae by Gertsch (1960a), and to Mysmenidae from Symphytognathidae by Forster & Platnick (1977). In the working phylogenetic hypothesis (Fig. 161B), *Trogloneta* is sister to the clade comprising *Maymena* plus Mysmenopsinae. Currently, *Trogloneta* includes nine described species (Platnick, 2014), and it is here represented by two described plus four undescribed species (the latter species have been scored for molecular data only): *T. granulum*, *T. cantareira*, *Trogloneta* sp.-Rix-AUST, *Trogloneta*-MYSM-022-ARG, *Trogloneta*-MYSM-024-CHILE, and *Trogloneta*-MYSM-025-CHILE).

Monophyly

Morphological synapomorphies of *Trogloneta* include: a third additional anterior field on ALS (Figs 64C, 66F); minute colulus (Figs 64D, 67F, 68C); minute AME (Fig. 67G); posterior median eyes separated (Fig. 67H); triangular labium, not swollen (Figs 63I, 66H); uniform coloration on dorsal abdomen, but distinctly lighter ventral abdomen, with whitish extended coloration posteriorly; no abdominal supra-pedicellate nubbins; lateral copulatory ducts–spermathecae junction; two sperm-storage compartments per spermatheca (Fig. 128F); accessory glands on vulva (Fig. 64A); female distal ventral sclerotized spot only on femur I; males with all eyes on tubercle (Figs 63G, H, 66A); carapace height dimorphism (i.e. male carapace higher than female, compare Figs 63G and 64E); bifid embolus (Figs 63E, 66E); tegular groove acting as conductor (Figs 63E, 66C); no switchbacks I and II on the spermatic duct (Fig. 131E, F); a flat and blunt primary cymbial conductor with a particular half circle shape (Fig. 63B, C), and particular cymbial shape, flat and tapering (Fig. 63C), with basal paracymbium (Fig. 63A), and with internal cymbial tarsal organ (Fig. 63B, F). Ambiguously optimized synapomorphies for *Trogloneta* include: anterior reduced booklungs (Fig. 67C); posterior respiratory system, with single median apodemal structure (Fig. 64B); epigynal area elevated ventrally and smooth uniform proximal copulatory ducts of increased diameter (Figs 64A, 128F); males with sclerotized femoral spot on femur I; shorter, but stout and straight setae comprising the tarsal prolateral row on leg I (Figs 65D, 68A); and tegular conductor neither with a proximal groove nor associated with embolus, and with a surface covered with small ridges (Fig. 63A, B, D). *Trogloneta* is also supported by 160 molecular synapomorphies.

Diagnosis

Trogloneta differs from all other mysmenid genera by the presence of a third additional anterior field on ALS; minute colulus (although it has been described as ‘large’ on the type species *T. granulum* by Thaler, 1975; but see figs 67F, 68C); minute AME; PME separated; posterior respiratory system with single median apodemal structure; triangular labium; two sperm-storage compartments per spermatheca; males with all eyes on tubercle; a basal paracymbium; a particular cymbial shape, flat and tapering, with a flat and blunt primary cymbial conductor with a particular half-circle shape; tegular conductor neither with a proximal groove nor associated with embolus, and with a surface covered with small ridges; and no switchbacks I and II on the spermatic duct. Although shared with a few other mysmenids, the following combination of features is unique for *Trogloneta*: distinctly lighter ventral abdomen, with whitish extended coloration posteriorly; carapace height dimorphism (male carapace higher than female); anterior booklungs reduced; females with distal ventral sclerotized spot only on femur I, epigynal area elevated ventrally, accessory glands on vulva, and smooth uniform proximal copulatory ducts of increased diameter; males with sclerotized femoral spot on femur I; shorter, but stout and straight setae comprising the tarsal prolateral row on leg I; bifid embolus; tegular groove acting as conductor; and internal cymbial tarsal organ. The taxonomic history and previous diagnostic features for *Trogloneta* have recently been reviewed by Brescovit & Lopardo (2008). Their proposed combination of features diagnostic for the genus is in agreement with those proposed in our study.

MYSMENOPSINAE SUBF. NOV.

(CLADE C159)

Mysmenopsinae comprises the kleptoparasitic genera *Isela* (including *Kilifina*, see below) and *Mysmenopsis*. This sister-taxon relationship has been previously proposed (Griswold, 1985). Although we lacked sequence data for the representatives of this clade, this seemingly stable group is strongly supported by the morphological partition.

Monophyly

Several synapomorphies support Mysmenopsinae: the kleptoparasitic predatory strategy; females without aggregate gland spigots on PLS (Figs 6D, 58H); with between three and five palpal tibial trichobothria (Figs 2E, 62A); and with a modified (stridulatory) field on retrolateral femur I (Figs 3C, 57B–D); both sexes also have a stridulatory field on prolateral femur IV (Figs 9A–C, 54H, 59F); strong leg I (Fig. 140A, D, G; secondary similar legs in *Mysmenopsis penai*); tarsal

organ located on the middle third of tarsus (Figs 8E, 54E, 56F), and with a teardrop-shaped opening distinctly smaller than setal sockets (Figs 3F, 9D, 54F, 62H); opisthosoma with long and thick setae interspersed among shorter and thinner setae (Fig. 140A); cylindrical gland spigots on PLS as slim as other spigots, subequal to flagelliform gland spigot; male palpal tibia with scoop-shaped rim (Figs 1A, 4A, 53B, 55A, C, 58A); large palpal tibia (i.e. about one-fifth the size of carapace in lateral view; Figs 1A, 4A, 55A, C); and cymbium as long as wide (Figs 1A, 4C, 55B). Ambiguously optimized synapomorphies for this clade include: shorter but stout and straight setae comprising the tarsal prolateral row on leg I (Figs 8F, 54G, 59D); strongly serrated distal promarginal curved seta on chelicerae; fingerprint cuticle on piriform field (Fig. 61C; rugose in *Kilifina*-MYSM-002-KENYA); minor ampullate (mAP) gland spigot without nubbins or tartipores (Figs 6C, G, 58F, 61D); males with palpal tibial bearing spine-like strong setae or spurs (Figs 1A, B, 4A, E, 53E, 55H, 58E, 60B); switchback I of spermatic duct close to fundus after passing through the distalmost wall of the bulb (Fig. 131C, G; distal in *Isela*); and metatarsal clasping spine twisted (Figs 3B, 8B, C, 140E, F) or strongly curved proximally (Figs 54D, 57I, 59B).

Diagnosis

Mysmenopsinae differs from the genera *Maymena*, *Trogloneta*, and the subfamily Mysmeninae by: their kleptoparasitic lifestyle; a stridulatory field on prolateral femur IV; strong leg I; tarsal organ located on the middle third of tarsus, and with a teardrop-shaped opening distinctly smaller than setal sockets; mAP gland spigot without nubbins or tartipores; opisthosoma with long and thick setae interspersed among shorter and thinner setae; females with between three and five palpal tibial trichobothria; without aggregate gland spigots on PLS; and with a modified (stridulatory) field on retrolateral femur I; and males with large palpal tibia bearing spine-like strong setae or spurs. The following combination of features is unique for Mysmenopsinae: females with narrow copulatory ducts of uniform diameter; males with metatarsal clasping spine twisted or strongly curved proximally; prolateral apical clasping spine on tibia I; shorter but stout and straight setae comprising the tarsal prolateral row on leg I; relatively small cymbium and bulb; palpal tibial with scoop-shaped rim; cymbium as long as wide; loss of tegular conductor; switchback I of spermatic duct close to fundus after passing through the distalmost wall of the bulb; both sexes also have femoral macrosetae; cylindrical gland spigots on PLS as slim as other spigots, subequal to flagelliform; strongly serrated distal promarginal curved seta on chelicerae; and fingerprint cuticle on piriform field.

ISELA GRISWOLD 1985

(FIGS 1–9, 128A, C, 131D, G, H, 140A–F;
CLADE C158)

Isela Griswold, 1985: 208.

Kilifina Baert & Murphy, 1992: 104 (replacement name for *Kilifina* Baert & Murphy, 1987: 194, preoccupied; type species by monotypy *Kilifina inquilina* Baert & Murphy, 1987, paratype material in IRSN and MRAC, examined). **New synonymy.**

Type species

Isela okuncana Griswold 1985 by original designation and monotypy, type material in NMSA and CAS, examined.

Synonymy justification

Both of these African monotypic genera share extremely peculiar male and female genitalia (see Figs 128A, C, 131D, G, H), form a clade in all morphological and combined analyses, and share several other morphological synapomorphies. The type material of both species have been examined as well as a third of undescribed species from Kenya, and the conformation of the genital morphology remains consistent across all of them.

Familial placement and composition

Isela is sister to *Mysmenopsis* within the subfamily Mysmenopsinae (Fig. 161B). Currently, and as defined here, the genus *Isela* comprises two species (*I. okuncana* and *I. inquilina* comb. nov.), and is here represented by one described plus one undescribed species: *I. okuncana* and *Kilifina*-MYSM-002-KENYA.

Synapomorphies

Morphological synapomorphies of *Isela* include: females with coiled tubuliform spermathecae (Figs 5D, 128A, C) and without flagelliform gland spigots (Fig. 6D); both sexes with median trichobothria on metatarsus I (Fig. 8A); and males with secondary external cymbial conductor (Fig. 4G); internal cymbial tarsal organ (Fig. 4I); coiled embolus (Figs 4H, 131H); and two or more prolateral tibial trichobothria on male palp (Figs 1B, 4E). Ambiguously optimized synapomorphies for this genus include: posterior respiratory system with median and single lateral tracheae (Fig. 5E); males with twisted metatarsal clasping spine (Figs 3B, 8B, C, 140E, F); epiandrous fusules dispersed in a row; palpal tibial bearing spine-like strong setae (Figs 1A, B, 4A, E); a prolateral apical secondary cymbial conductor (Fig. 4G, F); and a row of small setae on cymbial fold (Fig. 4G).

Diagnosis

Isela differs from all other mysmenid genera by the spine-like strong setae on male palpal tibial, a

secondary cymbial conductor located prolaterally–apically; females without flagelliform gland spigots and with coiled tubuliform spermathecae; posterior median and single lateral tracheae; and trichobothrium located medially on metatarsus I. In addition, the following combination of male features is unique for *Isela*: twisted metatarsal clasping spine; internal cymbial tarsal organ; a row of small setae on cymbial fold; coiled embolus; and epiandrous fusules dispersed in a row. Originally, *Isela* was diagnosed by the carapace depression separating the posterior median eyes (PME) from the anterior eye row (AER); the male palpal tibia large, cup-shaped, and with stout dorsoapical spines; by the morphology of cephalothorax; and by the general morphology of male and female genitalia (Griswold, 1985). Baert & Murphy (1987) also noted the general resemblance of *Kilifina* with *Isela* in terms of carapace morphology, the separation of the PME from the AER, and the swollen femora I, but stated that the differences between these two genera were based on the male palpal morphology, which were diagnostic for *Kilifina*. As the male and female genitalia of these two species are identical in their general morphology, the differences between them are here attributed to be at species, and not generic, level. Interestingly, the only diagnostic feature shared between the current and the previous diagnoses for *Isela* (including *Kilifina*) are the strong setae on the male palpal tibia. Remaining characteristics are shared in varying degrees with other mysmenid genera, and are not diagnostic of the genus.

MYSMENOPSIS SIMON 1897

(FIGS 53–62, 128G, 131A–C, 140G–L: CLADE C190)

Lucarachne Bryant, 1940: 350 (type *L. tibialis* Bryant, 1940). Kraus, 1955: 30. Forster, 1959: 328. Gertsch, 1960a: 28–29. Platnick & Shadab, 1978: 5 (synonymized to *Mysmenopsis*). Chickering, 1960: 95 (misidentification). Wunderlich, 1978: 29.

Mysmenopsis Simon, 1897: 865. Gertsch, 1960a: 23. Platnick & Shadab, 1978: 5–20 (revision of the genus). Müller, 1987: 185. Coyle & Meigs, 1989: 61–66. Baert, 1990: 5–17. Platnick, in Eberhard, Platnick & Schuh, 1993: 8. Jocqué & Dippenaar-Schoeman, 2006: 176.

Type species

Mysmenopsis femoralis Simon 1897 by original designation, syntype material in BMNH and MNHN, examined.

Familial placement and composition

Transferred to Symphytognathidae from Theridiidae by Gertsch (1960a), and to Mysmenidae from Symphytognathidae by Forster & Platnick (1977). Our working phylogenetic hypothesis places *Mysmenopsis* as sister to *Isela* within the subfamily Mysmenopsinae

(Fig. 161B). Currently, the genus *Mysmenopsis* comprises 27 described species (Platnick, 2014), and is here represented by four species: *M. dipluramigo*, *M. penai*, *M. cidrelicola*, and *M. palpalis*.

Monophyly

Morphological synapomorphies of *Mysmenopsis* include: anterior atria connected by membranous duct (Fig. 60H); posterior lateral tracheae branching into several tracheoles (Fig. 60G); wide posterior spiracular opening (Fig. 59I); distal labium concave (Figs 54B, 56G, 59E); relatively higher proportion of maxillary clavate setae (Fig. 62B); and four or more colular setae (Fig. 56D; three or less setae in *M. palpalis*, Fig. 59I); males with prolateral row of modified setae occupying only distal half of tarsus I (Figs 54G, 59D); with prolateral cymbium (Fig. 59A, G) without internal cymbial conductor and cymbial fold (CyC1 and CyF; Figs 53D, 55G, 60C, D, F); short apical bifid embolus of lobed or weakly projected embolic base and with membranous (flexible) embolus–tegulum junction (Figs 55G, 58D, 60D, F, 131A, C); globose palpal tibia (Figs 53A–C, 55A–E, 58A–B, 59A, 60A, 131A) with apical hollow area (Figs 53E, 55H, 58A, B, 60B, 131A–C); and females with a distal ventral femoral I projection (Figs 57A, B, E, 140G). Other *Mysmenopsis* species have either a femoral spot or no structure at all (Platnick & Shadab, 1978), although it is unclear whether the presence of the spot is plesiomorphic for the family or whether it represents a secondary gain. Ambiguously optimized synapomorphies for this clade include the following characters: cheliceral retromargin without teeth; absence of median structures of posterior respiratory system (Fig. 60G); male metatarsus I with proximal row of between five and eight spines (Fig. 57G, H; absent in *M. penai*); epiandrous fusules in two discrete clusters (Fig. 56E); males with flagelliform gland spigots (Figs 53H; 58G); cymbial tip without conductor grooves, but with a distinctly shaped tip (Fig. 58D) and with a hook-shaped paracymbium bent inwards and associated with a tegular groove (Figs 53D, F, 55F, 58D, 60D); male palpal tibial bearing spurs (Figs 53E, 55I, 58E, 60B, E) and with two retrolateral–dorsal trichobothria (Fig. 55E).

Diagnosis

Mysmenopsis differs from all other mysmenid genera in the following combination of features: the respiratory system consisting of anterior tracheae connected by a membranous duct and posterior lateral tracheae branching into several tracheoles, without median structures, arising from a wide posterior spiracular opening; the typical male palpal conformation, including a globose tibia with an apical hollow area bearing spurs and with two retrolateral–dorsal trichobothria, a prolateral cymbium without internal conductor grooves or cymbial fold, but with a distinct tip, and with a hook-shaped

paracymbium bent inwards and associated with a tegular groove, and a short apical bifid embolus. Also, a distal ventral projection on femur I occurs on females, males have a prolateral row of modified setae occupying the distal half of tarsus I, and a proximal row of between five and eight spines on metatarsus I (absent in *M. penai*); the epiandrous fusules are grouped into two clusters, both sexes retain only the flagelliform but not the aggregate spigots on the posterior lateral spinnerets; the labium is distally concave, a relatively higher proportion of maxillary clavate setae occurs in the mouthparts, and the colulus has four or more setae (three or less setae in *M. palpalis*). The taxonomic history and previous diagnostic features for *Mysmenopsis* have been reviewed by Platnick & Shadab (1978). Some of the previous diagnostic features proposed for this genus are also recovered here (see Simon, 1897; Bryant, 1940; Gertsch, 1960a; Platnick & Shadab, 1978).

MYSMENINAE PETRUNKEVITCH, 1928
(CLADE C133)

Composition

This morphologically distinct subfamily is circumscribed here to comprise the following genera: *Anjouanella*, *Brasilionata*, *Calodipoena*, *Calomyspoena*, *Itapua*, *Kekenboschiella*, *Microdipoena*, *Mysmena*, *Mysmenella*, *Mysmeniola*, and *Tamasesia* [Fig. 160, see below and refer to Fig. 161B for synonymies, see below for comments on recently erected Chinese genera not included in the analyses; see main text for the removal and suggested new familial status of *Crassignatha*, *Iardinis*, *Leviola*, and *Phricotelus*; see Miller *et al.* (2009) for the removal of *Crassignatha* based on morphology; and see Rix & Harvey (2010) for the transfer of *Taphiassa* to Micropholcommatinae and its synonymy with *Parapua*]. In our phylogenetic analyses, Mysmeninae included the following taxa: *Microdipoena*, *Mysmeniola*, *Brasilionata*, *Mysmena* (see below for total number of species and generic composition), and the following undescribed species (regarded here as Mysmeninae *incertae sedis*): MYSM-001-MAD, MYSM-006-MAD, MYSM-008-ARG, MYSM-009-MAD, MYSM-012-MAD, MYSM-019-MAD, MYSM-020-MAD, MYSM-021-MAD, MYSM-023-MAD, MYSM-026-MAD, MYSM-027-MAD, MYSM-029-MAD, MYSM-031-MAD, MYSM-032-MAD, and MYSM-033-MAD.

Monophyly

Relationships within Mysmeninae are unstable, except for a few taxa (see below). The following synapomorphies support Mysmeninae as we have circumscribed it: respiratory system with anterior tracheae restricted to opisthosoma (Fig. 37A; extending into pro-

soma in MYSM-005-ARG, MYSM-007-MEX, and *Microdipoena s.s.*); advanced and wide posterior spiracular opening located midway between the spinnerets and epigastric groove (Fig. 24A, E), connected to branched posterior lateral tracheae extending into prosoma (Fig. 22A, B); aciniform gland spigots of posterior spinnerets with two different outlines (Figs 19F, 33D, 37, B E); posterior lateral spinnerets with an anterior flat spatulate modified seta [Figs 23B, E, 33G, H, 52C; secondarily absent in *Mysmena* (= *Tamasesia*) *rotunda*], and slim cylindrical spigots (Figs 23B, 37B, E); palpal tibial trichobothria of females lacking (Figs 38E, 52E); female copulatory openings within the epigastric furrow (Fig. 24A; secondarily external in MYSM-023-MAD), membranous atrium (Figs 129A, E, G, 130B), and irregular membranous copulatory ducts (Figs 18G, 27D, 129A–C, E, H, 130A–G; distally sclerotized independently in two clades); males with coiled embolus (Figs 27A, 47A, B, 132D, E, 134G) and secondary (external) cymbial conductor (Figs 31C, 40A, 43C; secondarily absent in clade C128: *Microdipoena*, *Brasilionata*, *Mysmeniola*, and MYSM-019-MAD; Fig. 22F). Other synapomorphies include: abdomen with a whitish ventral ring surrounding the spinnerets (Figs 142J, L, 143A, B, G, I, L), trichobothria on tibia III and IV between two and three tibia diameters in length (Figs 26G, 29E, 39G; short trichobothria occurs independently within the group), and strongly serrated distal promarginal curved seta (Figs 19E, 38H, 42E, 48B). Ambiguously optimized synapomorphies for this clade include: a posterior tracheal arrangement consisting of lateral tracheae surrounding the minute median apodemes (Fig. 29B); fingerprint cuticular pattern on the piriform field (Figs 23A, C, 33E); flagelliform spigots absent in males (Fig. 23E; secondarily present in *Mysmena leichhardti* and MYSM-005-ARG); orb webs with a proliferation of out-of-plane radii both above and below the orb plane (Fig. 147A, B); males with prolateral row of slim setae occupying only distal half of tarsus I (Figs 16H, 26A, 34D, 45I, 50F; all along tarsus in *Mysmeniola spinifera*); cymbial prolateral basal expansion (Figs 27A, 30B, C, 36C, 47B); embolus with pars pendula (Figs 32H, 36B, 132C–F, 133C, secondarily absent in MYSM-005-ARG); palpal tibial rim setae longer and arranged distally in a row or two [Figs 18A, 32E, 36D, 42B, 45C; secondarily irregular in *Mysmeniola spinifera* and *Microdipoena* (= *Mysmenella*) *jobi*]; and females with weakly modified epigynal area (i.e. epigynum absent; Figs 14C, 37A, 52F; modified copulatory area in MYSM-023-MAD, Fig. 49D, E). A total of 163 molecular synapomorphies support this subfamily.

Diagnosis

Mysmeninae differs from all other mysmenid genera and subfamilies by the following unique combination

of features: the characteristic architecture of their orb webs with a proliferation of out-of-plane radii both above and below the orb plane; anterior tracheae restricted to opisthosoma (extending into prosoma in MYSM-005-ARG, MYSM-007-MEX, and *Microdipoena* s.s.), and an advanced and wide posterior spiracular opening located midway between the spinnerets and epigastric groove, connected to branched posterior lateral tracheae extending into prosoma and surrounding the minute median apodemes; anterior lateral spinnerets with fingerprint cuticular pattern on the piriform field, posterior spinnerets with aciniform gland spigots of two different outlines, and posterior lateral spinnerets with an anterior flat spatulate modified seta [as in *Maymena*, secondarily absent in *Mysmena* (= *Tamasesia*) *rotunda*], slim cylindrical spigots, and flagelliform spigots absent in males (secondarily present in males of *Mysmena leichhardti* and MYSM-005-ARG); females without epigynum and with the copulatory openings within the epigastric furrow (secondarily external in MYSM-023-MAD), a membranous internal atrium and irregular membranous copulatory ducts (distally sclerotized independently in two clades); males with secondary (external) cymbial conductor (secondarily absent in clade C128: *Microdipoena*, *Brasilionata*, *Mysmeniola*, and MYSM-019-MAD), cymbial prolateral basal expansion, coiled embolus with pars pendula (secondarily absent in MYSM-005-ARG), palpal tibial rim setae long and arranged distally in a row or two [secondarily irregular in *Mysmeniola spinifera* and *Microdipoena* (= *Mysmenella*) *jobi*], a prolateral row of slim setae occupying only distal half of tarsus I (all along tarsus in *Mysmeniola spinifera*); and also a strongly serrated distal promarginal curved seta, abdomen with a whitish ventral ring around the spinnerets, trichobothria on tibia III and IV of medium length.

MICRODIPOENA BANKS 1895

(FIGS 17–27, 129A, B, D–F, 132, 141J–O, 142A,B: CLADE C125)

Mysmena Simon, 1895b: 149. Bishop & Crosby, 1926: 177. Levi, 1956: 8. Forster, 1959: 306. Kraus, 1967: 392. Gruia, 1977: 162. Shinkai, 1977: 326. Roberts, 1978: 932. Wunderlich, 1980b: 267; 1986: 222. Kasal, 1982: 75. Heimer & Nentwig, 1991: 306.

Microdipoena Banks, 1895: 85. Saaristo, 1978: 124–125 (rejected synonymy to *Mysmena* by Bishop & Crosby, 1926: 177). Brignoli, 1980: 731 (rejected synonymy to *Mysmena* by Bishop & Crosby, 1926: 177). Baert, 1984b: 608; 1985: 51; 1989: 29.

Anjouanella Baert, 1986: 265 (type species by monotypy *A. comorensis* Baert, 1986, type material in MRAC, examined). **New synonymy.**

Mysmenella Brignoli, 1980: 731 (transfer from *Mysmena*, type *Mysmena illectrix* Simon, 1895b, type

material in MNHN, examined). Baert, 1984a: 240 (transfer from *Mysmena*); 1989: 32. Namkung & Lee, 1987: 46. Coddington, 1990: 19. Thaler & Noflatscher, 1990: 174. Namkung, 2002: 146; 2003: 148. Wunderlich, 2004: 1073 (considered a junior synonym of *Mysmena* Simon, 1894). Yin *et al.*, 2004: 80. Lee *et al.*, 2004: 100. Trotta, 2005: 170. Ono, 2007: 170. **New synonymy.**

Type species

Microdipoena guttata Banks, 1895 by original designation, type material in MCZ, examined.

Familial placement, composition, and re-circumscription

Our working phylogenetic hypothesis places *Microdipoena* sister to *Brasilionata* within the mysmenine clade C128, which also comprises *Mysmeniola* and MYSM-019-MAD. *Microdipoena* comprises four described species (Platnick, 2014) and under the current re-circumscription, 11 other described species are transferred here (a total of 15 described species). *Microdipoena* is here represented by seven described plus two undescribed species (Fig. 161B; the latter two species are scored only for molecular characters): *M. guttata*, *M. elsaie*, *M. nyungwe*, *M. samoensis* comb. nov. (from *Mysmenella*), *M. jobi* comb. nov. (from *Mysmenella*), *M. illectrix* comb. nov., *M. comorensis* comb. nov., *Microdipoena*-AToL-DR, and MYSM-030-MAD.

Monophyly, diagnosis, and synonymy justification

The following combination of morphological synapomorphies is unique and therefore diagnostic for *Microdipoena* (and are shared among all *Microdipoena* representatives, unless noted): abdomen with a whitish ventral ring around the spinnerets (Fig. 142A; except *Anjouanella*, with all ventral abdominal area lighter, Fig. 141J–L); males with two prolateral apical clasp spines on tibia I (Figs 26C, 27I, 141K, L, O), thick embolus with an apical switch in the coiling direction (Figs 18C, D, F, 27C, 132B, D, E; also in *Brasilionata*), and with either a distal apophysis (Fig. 18F) or a distal irregular membrane (Fig. 27A–C; except in *Anjouanella*, without modifications), spermatid duct switchback SB I parallel, with the portions of the spermatid duct before and after the switch SB I run close with each other and with one pair of extra switches (SB III and IV, Fig. 132B–E); and small paracymbium (Figs 17C, 22G, 27B). As most *Microdipoena* representatives in this data set were scored only for morphology, no molecular synapomorphies optimize at the node of this genus; however, its distal clade (clade C172), which includes the only sequenced species of this genus, is supported by 92 molecular synapomorphies. Previous diagnoses for *Microdipoena* s.s., *Mysmenella*, and *Anjouanella* are in

agreement with the current diagnosis of the enlarged *Microdipoena* (see e.g. Banks, 1895; Brignoli, 1980; Baert, 1986).

BRASILIONATA WUNDERLICH, 1995
FIGS 133G, 142O

Brasilionata Wunderlich, 1995: 545.

Type species

Brasilionata arborensis Wunderlich, 1995 by original designation and monotypy, holotype in AMNH, examined.

Familial placement and composition

Brasilionata is a member of the mysmeninae clade C128 (also comprising *Mysmeniola*, *Microdipoena*, and MYSM-019-MAD), and is sister to *Microdipoena* (Fig. 161B). *Brasilionata* is here represented by its type and only species *B. arborensis*.

Monophyly and diagnosis

This Brazilian monotypic genus is only known by the male holotype specimen, and it is diagnosed by the following combination of autapomorphies: male palpal tibial rim scoop-shaped, cymbial fold with row of setae similar to surrounding setae (i.e. not minute), embolus with an apical switch in the coiling direction as in *Microdipoena* (Fig. 133G), uniform abdominal dorsal colour pattern and anterior median eyes separate (Fig. 142O). There appears to be a subtle depression between the anterior median eyes, which could also be synapomorphic for the genus (Fig. 142O; see Wunderlich, 1995: fig. 10), although it has not been explicitly proposed as such in previous studies. *Brasilionata* has been previously diagnosed by somehow vague characters (Wunderlich, 1995), which when examined within a revisionary context can be assigned to any other mysmenid genus or are simply symplesiomorphies: lack of femoral spot on male, no trichobothrium on metatarsus IV, eight eyes equal in size, one metatarsal prolateral clasping spine, male palpal femur, patella and tibia without structures, cymbium long and distally slender, with a cymbial process, and embolus with apophysis. We could not find an embolic apophysis and instead we report a coiling switch of the distal part of the embolus.

MYSMENIOLA THALER, 1995
FIGS 134D, 142M, N

Mysmeniola Thaler, 1995: 429.

Type species

Mysmeniola spinifera Thaler, 1995 by original designation and monotypy, holotype in MHNG, examined.

Familial placement and composition

Our working phylogenetic hypothesis places *Mysmeniola* within the mysmenine clade C128 (*Brasilionata*,

Mysmeniola, *Microdipoena*, and MYSM-019-MAD), as sister to the clade including *Brasilionata* and *Microdipoena* (clade C126; Fig. 161B). *Mysmeniola* is here represented by its type and only species *M. spinifera*.

Monophyly and diagnosis

This singular Venezuelan monotypic genus, only known by males (see male palp drawing on Fig. 134D), is here diagnosed by the following combination of autapomorphies: six eyes (anterior median eyes absent; Fig. 142M); prolateral cymbium with a prolateral basal expansion surrounding the entire basal bulb and with minute setae at tip, male palpal tibia with prolateral apical process and irregular rim setal conformation, median trichobothrium on metatarsus I, tarsus I with prolateral row of setae distributed along tarsus, and minute but distinct dorsal–posterior abdominal hump (Fig. 142M, N). The presence of a cluster of strong setae at the base of the clypeus seems to be autapomorphic for the genus (see Fig. 142M; also Thaler, 1995: figs 1, 2). Previously proposed diagnostic features for *Mysmeniola* are in agreement with the diagnostic features suggested here.

MYSMENA SIMON, 1894

(FIGS 28–44, 51, 52, 65A, 129C, G, 130A–C, E, F, 133A–F, H, I, 134A–C, 142D–L, 143A–C, G–O, 144O, 147A, C: CLADE C144)

Mysmena Simon, 1894: 588. Bishop & Crosby 1926: 177 (synonymized *Microdipoena*). Levi, 1956: 3 (synonymized with *Calodipoena*, *Tamasesia*, and *Microdipoena*). Forster, 1959: 303–307; 1977: 129. Gertsch, 1960b: 13. Kraus, 1967: 388. Loksa, 1973: 283. Saaristo, 1978: 125 (rejected synonymy with *Microdipoena*). Hickman, 1979: 74. Brignoli, 1980: 729 (rejected synonymy with *Calodipoena*, *Tamasesia*, and *Microdipoena*). Wunderlich, 1980b: 267; 1986: 218. Davies, 1985: 91 (transfer to *Calodipoena* by Brignoli, 1983 rejected). Snazell, 1986: 62. Trotta, 2005: 170. Ono, in Ono, Chang & Tso, 2007: 73. Lopardo & Dupérré, in Lopardo *et al.*, 2008: 37.

Calodipoena Gertsch & Davis, 1936: 8 (type species by original designation *C. incredula* Gertsch & Davis, 1936, type material in AMNH, not examined). Brignoli, 1983: 376 (transfer from *Mysmena* because of alleged relationships with *C. incredula* Gertsch & Davis, 1936). **New synonymy.**

Itapua Baert, 1984b: 604 (type species by original designation and monotypy *I. tembei* Baert 1984, type material in MHNG, examined). **New synonymy.**

Calomyspoena Baert & Maelfait, 1983: 104 (type species by original designation and monotypy *C. santacruzii* Baert & Maelfait, 1983, type material in IRSN, examined). **New synonymy.**

Tamasesia Marples, 1955: 476 (type species by original designation *T. rotunda* Marples, 1955, type material in BMNH and MNHN, examined); Levi 1956: 3 (transfer from Tamasesiidae to Theridiidae, synonymized with *Mysmena*); Brignoli, 1980: 730 (transfer to Mysmenidae, rejected synonymy with *Mysmena*). **New synonymy.**

Kekenboschiella Baert, 1982: 303 (type species by original designation *K. marijkeae* Baert, 1982, type material in IRSN, examined). Baert 1984a: 230. **New synonymy.**

Type species

Mysmena leucoplagiata (Simon, 1879) by original designation, type material in MNHN, examined (see below, and also Kraus, 1967).

Synonymy justification

Relationships among and within mysmenine clades are highly unstable and poorly supported (see Results). Morphologically, these results are not surprising. In particular, homoplasy is widespread among the *Mysmena* representatives, and no notable synapomorphy characterizes this genus. The inclusion in the analysis of several undescribed mysmenid species with distinct and diverse morphology (especially genitalic morphology) might obscure relationships, producing an even more unstable pattern. In this case, although distinct undescribed species might possibly represent new genera (see comments below), to date the available data do not support such hypotheses. As circumscribed here, *Mysmena* includes a polyphyletic *Calodipoena*, the monotypic genera *Itapua* and *Calomyspoena*, and a (strictly) monophyletic *Tamasesia*, *Kekenboschiella*, and *Mysmena s.s.*, although the latter three genera are supported by just one (or none in the case of *Mysmena*) homoplastic character change, and no molecular transformations. In the absence of concise and unique diagnostic features for any of the aforementioned genera, we have re-circumscribed the genus *Mysmena* to avoid proliferation of monotypic genera and non-monophyletic taxa, losing phylogenetic information.

Familial placement, composition, and re-circumscription

Mysmena was transferred to Symphytognathidae from Theridiidae by Forster (1959), and to Mysmenidae from Symphytognathidae by Forster & Platnick (1977). In the proposed phylogenetic hypothesis, *Mysmena* comprises a large clade distally within the Mysmeninae lineage (Fig. 160; for synonymies and new combinations, refer to Fig. 161B). The re-circumscribed *Mysmena* comprises a total of 42 described species: 23 from

Mysmena, ten from *Calodipoena*, four from *Kekenboschiella*, three from *Tamasesia*, and one from each of the two monotypic genera *Calomyspoena* and *Itapua* (Platnick, 2014). *Mysmena* is here represented by 11 described plus 18 undescribed species (12 of the latter undescribed were species scored only for molecular data): *M. leucoplagiata*, *M. leichhardti*, *M. tasmaniae*, *M. mootae* comb. nov. (from *Calodipoena*), *M. incredula* comb. nov., *M. santacruzii* comb. nov., *M. tembei* comb. nov., *M. acuminata* comb. nov. (from *Tamasesia*), *M. rotunda* comb. nov., *M. awari* comb. nov. (from *Kekenboschiella*), *M. marijkeae* comb. nov., *Mysmena*-MYSM-011-ARG, *Mysmena*-MYSM-014-THAI, *Mysmena*-MYSM-(015 018)-MAD, MYSM-(005 038–042)-ARG, MYSM-(007 010)-MEX, MYSM-(013 035–037)-THAI, and MYSM-028-MAD.

Monophyly and diagnosis

Ambiguously optimized synapomorphies for *Mysmena*, shared by most of the taxa, include the spermatid duct switchback SB I distally bending at a right angle [Figs 133D–F, 134A, B, E; straight in *Mysmena*-MYSM-015-MAD, *Mysmena* (= *Tamasesia*) *rotunda* and MYSM-005-ARG, Fig. 133A, B, H, I], and the presence of a long ventral scapus (Figs 29C, 31G, 37C, 42C, 129C, G, 130B) and weakly sclerotized fertilization ducts, with a distinguishable wall (Figs 42D, 49A, 51D, 129C, G, 130A; independently membranous, translucent in *Itapua tembei*, *Mysmena leucoplagiata*, and MYSM-034-MAD). *Mysmena* monophyly is also supported by 265 molecular synapomorphies.

Because of its previous placement within Theridiidae, and its recurrent synonymies with *Calodipoena*, *Tamasesia*, and/or *Microdipoena*, the previous diagnoses of *Mysmena* include features that are currently considered synapomorphic for the subfamily Mysmeninae or even Mysmenidae (see e.g. Simon, 1894; Levi, 1956; Forster, 1959; Gertsch, 1960a; Kraus, 1967). Also, because of the mislabelling of the vial containing the type specimen of *Mysmena leucoplagiata*, which also included specimens of *Mysmenella jobi*, the diagnosis of *Mysmena* has been rather confusing and inaccurate (vial examined; see also Kraus, 1967). For example, the type species *Mysmena leucoplagiata* has been correctly redescribed by Kraus (1967) and Wunderlich (1980b), whereas *Mysmenella jobi* was mistakenly redescribed as *Mysmena leucoplagiata* by Levi (1956) and Loksa (1973). Furthermore, diagnostic features of the here-synonymized genera are also largely broad for the family or at least Mysmeninae (Gertsch & Davis, 1936; Marples, 1955; Baert, 1982, 1984a), except for a few diagnostic features of *Calomyspoena* (Baert & Maelfait, 1983).

OTHER MYSMENID GROUPS AND TAXA
FIGS 45–50, 129H, 130D, G, 134E–G, H,
143D–F, 144A

Molecular clades and taxa

No taxonomic action is taken for the remaining clades/taxa, given that they comprise undescribed species represented, in their majority, exclusively by molecular data. In this context, no morphological synapomorphies can be proposed to diagnose any of these clades/taxa. In addition, support for these clades is low. These taxa are regarded here as Mysmeninae *incertae sedis* (see also above). Clade C210 comprises only one taxon scored for morphology (MYSM-023-MAD), and is supported by only nine molecular synapomorphies. Clade C163 comprises two taxa scored for morphology (MYSM-029-MAD, with only female representatives; MYSM-020-MAD, with only male representatives) and is supported by 83 molecular synapomorphies, a relatively larger number. The remaining two taxa not grouping with other mysmenids in distinct clades (MYSM-006-MAD and MYSM-008-ARG) were not scored for morphology, but given their external morphology and their placement within Mysmeninae in our working hypothesis, they are regarded as such in the current study. MYSM-019-MAD is sister to the clade comprising the relatively well-defined mysmenid genera *Brasilionata*, *Mysmeniola*, and *Microdipoena*. Although not remarkably different from other mysmenid genera, this species possesses some highly homoplastic features and could represent a new genus, even if morphology alone places it as closely related to other *Mysmena* species.

Remarkable distinctive morphology

The following four undescribed mysmenids were scored for both morphological and molecular characters; however, morphologically these taxa differ from all other known mysmenids (both described and undescribed examined species, see Figs 28–31, 47–50, 129C, 130D, F, 133A–C, 134F–H, 143G–L, 144A). Individually, they most likely represent three different mysmenid genera, and the phylogenetic hypothesis based on the morphological partition alone places these taxa as either basal to major clades (MYSM-005-ARG and MYSM-007-MEX) or as a distinct well-defined, stable, and supported clade (MYSM-020-MAD and MYSM-023-MAD, see node M118 in Fig. 153). The combined total evidence analysis does not recover this hypothesis, however, splitting the morphologically robust clade

containing MYSM-020-MAD and MYSM-023-MAD, and placing the two other taxa within the undefined clade here referred to as *Mysmena*. Therefore no taxonomic decisions are taken in regard of these taxa, as more data are needed to more consistently resolve their phylogenetic placements.

CHINESE MYSMENID GENERA

In a recent study on Chinese symphytognathoids, Miller *et al.* (2009) described 17 new mysmenid species and four new genera. Six species were placed in *Mysmena*, two in *Maymena*, and nine species were assigned to the four new genera (*Simaoa*, *Gaoligonga*, *Mosu*, and the monotypic *Chanea*). Specimens of these four new genera were not available for examination when we were carrying out this project, and therefore they have not been included in our analyses. These Chinese species share most of the mysmenid diagnostic features, and therefore their placement within Mysmenidae seems conclusive; however, as the work was regional in scope and did not provide an exhaustive generic revision or an explicit phylogenetic justification for the erection of higher taxa, it is difficult to assess the monophyly of not only the new taxa, but the monophyly of more inclusive groups that may have been rendered paraphyletic by the erection of new genera. For example, the presence of strong clypeal setae in *Chanea*, which has also been observed and reported for *Mysmeniola* (Fig. 142M, N; Thaler, 1995; also L. Lopardo, pers. observ.), could suggest a close relationship between these two monotypic genera. *Simaoa* and *Gaoligonga* both build the typical mysmenine three-dimensional web, suggesting a close relationship with *Microdipoena* or *Mysmena*, or at least a placement within Mysmeninae. Therefore, although the new genera include species of remarkable morphology, not only at the genital level, their monophyly and their exact phylogenetic placement within the family has not been tested. Furthermore, the generic diagnoses and taxonomic justifications were based on combinations of features that have currently been found to be highly homoplastic within Mysmenid (e.g. cymbium enveloping the bulb, posterior abdominal tubercle, epigynal scapus, etc.). The instability of relationships within Mysmeninae, and the lack of unambiguous and consistent diagnostic traits for mysmenine genera, suggest that a more explicitly phylogenetic and monographic approach is needed to test the monophyly and circumscription of the new Chinese mysmenid genera.

Cover image

Right: Male palp from *Mysmena* sp. (*Mysmena*-MYSM-015-MAD, Mysmeninae, Mysmenidae) from Madagascar, SEM image. Top left: Male of *Microdipoena guttata* (Mysmeninae, Mysmenidae) from Comoros, composite image, lateral view (photo: Peter Michalik). Bottom left: Typical spherical mysmenid orbweb; *Mysmena leichhardti* female (Mysmeninae, Mysmenidae), from Australia, contrasted image.